Modelling for Control of Free Molecular Flow Processes

Dresscher, Martijn; Jayawardhana, Bayu; Scherpen, Jacquelien M.A.

[Link to publication in University of Groningen/UMCG research database](#)

Citation for published version (APA):
Dresscher, M., Jayawardhana, B., & Scherpen, J. M. A. (2016). Modelling for Control of Free Molecular Flow Processes. In R. Carloni, D. Jeltsema, & M. Lazar (Eds.), *35th Benelux Meeting on Systems and Control March 22 : 24, 2016 Soesterberg, The Netherlands : book of abstracts* (pp. 97). University of Twente.

35th Benelux Meeting

on

Systems and Control

March 22 – 24, 2016

Soesterberg, The Netherlands

Book of Abstracts

The 35th Benelux Meeting on Systems and Control is sponsored by

Raffaella Carloni, Dimitri Jeltsema, and Mircea Lazar (Eds.)
Book of Abstracts 35th Benelux Meeting on Systems and Control

Part 1

Programmatic Table of Contents

Tuesday, March 22, 2016

Plenary: P0   St. Janzaal
Welcome and Opening

Chair: Raffaella Carloni   11.25–11.30

Mini Course: P1   St. Janzaal
Data-driven model reduction - Part I
Athanasios Antoulas
Chair: Raffaella Carloni   11.30–12.30

Mini Course: P2   St. Janzaal
Data-driven model reduction - Part II
Athanasios Antoulas
Chair: Raffaella Carloni   13.45–14.45

TuE01   St. Janzaal
System Identification A
Chair: Paul Van den Hof   15.10-17.15

TuE01-1   15.10-15.35
2D Regularization for LTV systems using a single measurement: transient elimination and coping with large datasets 17
P.Z. Csurcsia   Vrije Universiteit Brussel
J. Schoukens   Vrije Universiteit Brussel
J. Lataire   Vrije Universiteit Brussel

TuE01-2   15.35-16.00
Inferring spectral properties of networks with local measurements 18
A. Mauroy   University of Luxembourg
J.M. Hendrickx   Université Catholique de Louvain

TuE01-3   16.00-16.25
Two case studies on optimal input design for simple Wiener systems: Pitfalls and challenges . . . 19
A. De Cock   Vrije Universiteit Brussel
J. Schoukens   Vrije Universiteit Brussel

TuE01-4   16.25-16.50
Fault diagnosis in a hydraulic pitch actuator based on frequency domain identification 20
S. Vasquez   Vrije Universiteit Brussel
M. Kinnaert   Université Libre de Bruxelles
R. Pintelon   Vrije Universiteit Brussel

TuE01-5   16.50-17.15
Weighted tensor decomposition for approximate decoupling of multivariate polynomials 21
G. Hollander   Vrije Universiteit Brussel
P. Dreesen   Vrije Universiteit Brussel
M. Ishteva   Vrije Universiteit Brussel
J. Schoukens

TuE02   Angola
System Theory A
Chair: Jan van Schuppen   15.10-17.15

TuE02-1   15.10-15.35
Event-triggered control systems under denial-of-service attacks 22
V. Dolk   Eindhoven University of Technology
P. Tesi   University of Groningen
C. De Persis   University of Groningenn
W.P.M.H. Heemels

TuE02-2   15.35-16.00
Bisimulation equivalence of DAE systems 23
N.Y. Megawati   University of Groningen
A. van der Schaft   University of Groningen

TuE02-3   16.00-16.25
Fault detection and isolation for systems defined over graphs 24
A.R.F. Everts   University of Groningen
P. Rapisarda   University of Southampton
M.K. Camlibel   University of Groningen

TuE02-4   16.25-16.50
Stabilization of planar slow-fast systems at non-hyperbolic points 25
H. Jardón-Kojakhmetov   University of Groningen
J.M.A. Scherpen   University of Groningen

TuE02-5   16.50-17.15
Model reference adaptive control of uncertain switched system with slow switching laws 26
S. Yuan   Delft University of Technology

TuE03   Botswana
Optimization A
Chair: Siep Weiland   15.10-17.15

TuE03-1   15.10-15.35
Optimization-based trajectory generation for overtaking on highways 27
I. Ballesteros Tolosana   Renault-CentraleSupelec
N. van Duijkeren   Katholieke Universiteit Leuven
J. Swevers   Katholieke Universiteit Leuven
S. Olaru

TuE03-2   15.35-16.00
Handling uncertainty in oil reservoir waterflooding using risk management tools 28
M. Mohsin Siraj   Eindhoven University of Technology
P.M.J. Van den Hof   Eindhoven University of Tech.
J.D. Jansen   Delft University of Technology

TuE03-3   16.00-16.25
Multi-objective iterative learning control 29
Tong Duy Son   Katholieke Universiteit Leuven
G. Pipeleers   Katholieke Universiteit Leuven
J. Swevers   Katholieke Universiteit Leuven

TuE03-4   16.25-16.50
Analysis of dynamic container terminal networks   30
R.T. Cahyono   University of Groningen
B. Jayawardhana   University of Groningen

TuE03-5   **16.50-17.15**

Quality-aware control of perishable goods in trans-
port networks 31
X. Lin   Delft University of Techonology
R.R. Negenborn   Delft University of Techonology
G. Lodewijks   Delft University of Techonology

TuE04   **Congo**
Nonlinear Control A
Chair: Bayu Jayawardhana   **15.10-17.15**

TuE04-1   **15.10-15.35**
Making stabilizing controllers track references for
constrained linear systems 32
V. Spinu   Eindhoven University of Technology
M. Lazar   Eindhoven University of Technology

TuE04-2   **15.35-16.00**
Stability and performance analysis of spatially in-
variant systems with networked communication . 33
S. Heijmans   Eindhoven University of Technology
N. Borgers   Eindhoven University of Technology
W.P.M.H. Heemels Eindhoven University of Technology

TuE04-3   **16.00-16.25**
Controller design for flow networks of switched
servers with setup times 34
E. Lefeber   Eindhoven University of Technology

TuE04-4   **16.25-16.50**
Stabilization with guaranteed safety via IDA-PBC 35
M. Zakiyullah Romdlony   University of Groningen
B. Jayawardhana   University of Groningen

TuE04-5   **16.50-17.15**
Practical optimal state regulation of distribution
networks with input constraints 36
T. Scholten   University of Groningen
C. De Persis   University of Groningen
P. Tesi   University of Groningen

TuE05   **Ghana**
Distributed Parameter Systems
Chair: Hans Zwart   **15.10-17.40**

TuE05-1   **15.10-15.35**
Stabilization of collocated systems by nonlinear
boundary control 37
H. Zwart   University of Twente
R. Curtain   University of Groningen

TuE05-2   **15.35-16.00**
Convergence analysis of a positive stabilization
scheme for a discretized diffusion system 38
J.N. Dehaye   University of Namur
J.J. Winkin   University of Namur

TuE05-3   **16.00-16.25**
Comparison of stabilization of piezoelectric Euler-
Bernoulli beam models 39
M.C. de Jong   University of Groningen
J.M.A. Scherpen   University of Groningen
K.A. Morris   University of Waterloo

TuE05-4   **16.25-16.50**
Thermal control in wafer scanners using high com-
plexity models 40
R.W.H. Merks   Eindhoven University of Technology
M.B.I. Habets   Eindhoven University of Technology
S. Weiland   Eindhoven University of Technology

TuE05-5   **16.50-17.15**
Continuous compliance compensation of position-
dependent flexible structures 41
N. Kontaras   Eindhoven University of Technology
M. Heertjes   Eindhoven University of Technology
H. Zwart   University of Twente

TuE05-6   **17.15-17.40**
Boundary information in a proper Petrov-
Galerkin projection for linear partial differential
equations 42
B. Tiemersma   Eindhoven University of Technology
E. Insuasty   Eindhoven University of Technology
S. Weiland   Eindhoven University of Technology

TuE06   **Tanzania**
Model Reduction
Chair: Jacquelien Scherpen   **15.10-17.15**

TuE06-1   **15.10-15.35**
Model order reduction of Li-ion batteries via POD
and DEIM 43
Z. Li   Eindhoven University of Technology
T. Donkers   Eindhoven University of Technology
D. Danilov   Eindhoven University of Technology
H.J. Bergveld

TuE06-2   **15.35-16.00**
On approximation of linear network systems . . 44
X. Cheng   University of Groningen
J. M.A. Scherpen   University of Groningen
Y. Kawano   Kyoto University

TuE06-3   **16.00-16.25**
Control of a flexible-joint manipulator with only
position measurements: a port-Hamiltonian ap-
proach 45
H. Jardón-Kojakhmetov   University of Groningen
M. Muñoz-Arias   University of Groningen
J. M.A. Scherpen   University of Groningen

TuE06-4   **16.25-16.50**
Coupled tensor decomposition: a step towards ro-
bust components 46
M.u Genicot   Université Catholique de Louvain
P.-A. Absil   Université Catholique de Louvain
R. Lambiotte   Universit de Namur
S. Sami

TuE06-5   **16.50-17.15**
Model reduction of networked systems by edge re-
moval 47
H.J. Jongsma   University of Groningen
H.L. Trentelman   University of Groningen
M.K. Camlibel   University of Groningen

Wednesday, March 23, 2016

Mini Course: P3   St. Janzaal
Data-driven model reduction - Part III
Athanasios Antoulas
Chair: Dimitri Jeltsema   8.30–9.30

Pleanary: P4   St. Janzaal
A control theoretic framework for power grids
Claudio De Persis
Chair: Dimitri Jeltsema   9:50–10.50

Event: E1   St. Janzaal
Meet the Experts

Chair: -   11:20–12.20

WeP01   St. Janzaal
System Identification B
Chair: Johan Schoukens   13.45-15.50

WeP01-1   13.45-14.10
Data driven dynamic measurements 48
G. Quintana-Carapia   Vrije Universiteit Brussel
I. Markovsky   Vrije Universiteit Brussel

WeP01-2   14.10-14.35
Regularized impulse response modeling using a filter interpretation 49
A. Marconato   Vrije Universiteit Brussel
M. Schoukens   Vrije Universiteit Brussel
J. Schoukens   Vrije Universiteit Brussel

WeP01-3   14.35-15.00
Accommodating temperature change in the identification of a nonlinear model of the Li-ion battery cell 50
R. Relan   Vrije Universiteit Brussel
K. Tiels   Vrije Universiteit Brussel
J.-M. Timmermans   Vrije Universiteit Brussel
J. Schoukens

WeP01-4   15.00-15.25
Identification for control of heavy-duty diesel engines via parametric and local parametric approaches 51
L.I. Huijben   Eindhoven University of Technology
T.A.C. van Keulen   Eindhoven University of Technology
T.A.E. Oomen   Eindhoven University of Technology

WeP01-5   15.25-15.50
Improved non-parametric identification of lightly damped mechanical systems 52
D. Verbeke   Vrije Universiteit Brussel

WeP02   Angola
Power Systems A
Chair: Dimitri Jeltsema   13.45-15.50

WeP02-1   13.45-14.10
Price-based control for electrical power distribution system 53
M. Jafarian   University of Groningen
J.M.A. Scherpen   University of Groningen
M. Aiello   University of Groningen

WeP02-2   14.10-14.35
A Communication-free master-slave microgrid with power sharing 54
P. Monshizadeh   University of Groningen
C. De Persis   University of Groningen
N. Monshizadeh   University of Groningen
A. van der Schaft

WeP02-3   14.35-15.00
Topological conditions on the stability of networked systems with damped and undamped nodes 55
F. Koerts   University of Groningen
M. B urger   University of Stuttgart
A. van der Schaft   University of Groningen
C. De Persis

WeP02-4   15.00-15.25
Coping with algebraic constraints in power networks 56
N. Monshizadeh   University of Groningen

WeP02-5   15.25-15.50
Preserving power network optimality in the presence of intermittent feedback measurements . . . 57
E. Weitenberg   University of Groningen
C. De Persis   University of Groningen
P. Tesi   University of Groningen

WeP03   Botswana
Optimization B
Chair: Julien Hendrickx   13.45-15.50

WeP03-1   13.45-14.10
A Scenario approach for probabilistic fault detection threshold design for uncertain nonlinear systems 58
V. Rostampour   Delft University of Technology
R. Ferrari   Delft University of Technology
R. Babuska   Delft University of Technology
T. Keviczky

WeP03-2   14.10-14.35
Design of an optimized gradient method for composite convex optimization 59
A.B. Taylor   Université Catholique de Louvain
F. Glineur   Université Catholique de Louvain
J.M. Hendrickx   Université Catholique de Louvain

WeP03-3   14.35-15.00
Approximate matrix geometric means 60
E.M. Massart   Université Catholique de Louvain
J.M. Hendrickx   Université Catholique de Louvain
P.-A. Absil   Université Catholique de Louvain

WeP03-4   **15.00-15.25**
Tensor methods for systems and control 61
M. Ishteva   Vrije Universiteit Brussel

WeP03-5   **15.25-15.50**
*Actuator management in Tokamaks using mixed
integer quadratic programming* 62
B. Maljaars   Eindhoven University of Technology
F. Felici   Eindhoven University of Technology

WeP04	**Congo**
Optimal Control	
Chair: Joseph Winkin	**13.45-15.50**

WeP04-1   **13.45-14.10**
*Optimal damping of harmonic signals with un-
known spectra* 63
Y.A. Kapitanyuk   University of Groningen
A.V. Proskurnikov   University of Groningen
M. Cao   University of Groningen

WeP04-2   **14.10-14.35**
*Remote sensing and control with performance
guarantees* 64
B. Asadi Khashooei   Eindhoven University of
Technology
D.J. Antunes   Eindhoven University of Technology
W.P.M.H. Heemels   Eindhoven University of Tech.

WeP04-3   **14.35-15.00**
*Aperiodic model predictive control: an event-
triggered strategy* 65
A. Sharifi Kolarijani   Delft University of Technology
T. Keviczky   Delft University of Technology

WeP04-4   **15.00-15.25**
*Online distributed motion planning for multi-
vehicle systems* 66
R. Van Parys   Katholieke Universiteit Leuven
G. Pipeleers   Katholieke Universiteit Leuven

WeP04-5   **15.25-15.50**
*Towards anticipative LPV tube model predictive
control* 67
J. Hanema   Eindhoven University of Technology
R. Toth   Eindhoven University of Technology
M. Lazar   Eindhoven University of Technology
S. Weiland

WeP05	**Ghana**
Modeling for Control A	
Chair: Maarten Steinbuch	**13.45-15.50**

WeP05-1   **13.45-14.10**
*Nonlinear vibrations phenomena of a tunable non-
linear spring characteristic* 68
K. Dekemele   University of Ghent
R. De Keyser   University of Ghent
M. Loccufier   University of Ghent

WeP05-2   **14.10-14.35**
*A time domain based MIMO waveform replication
algorithm* 69
S. Moten   Katholieke Universiteit Leuven
G. Pipeleers   Katholieke Universiteit Leuven
J. Swevers   Katholieke Universiteit Leuven

WeP05-3   **14.35-15.00**
*Combining probable trajectories in air traffic man-
agement* 70
F. Gonze   Université Catholique de Louvain
J. Boucquey   EUROCONTROL
R. M. Jungers   Université Catholique de Louvain

WeP05-4   **15.00-15.25**
*Plug-and-play control: integrating distributed
model predictive control in today's industry* . . . 71
P. Maelegheer   University of Ghent
C. Ionescu   University of Ghent
R. De Keyser   University of Ghent

WeP05-5   **15.25-15.50**
*Iterative pole-zero model updating using combined
sensitivities* 72
M. Dorosti   Eindhoven University of Technology
R. Fey   Eindhoven University of Technology
M. Heertjes   Eindhoven University of Technology
H. Nijmeijer

WeP06	**Tanzania**
Robotics A	
Chair: Raffaella Carloni	**13.45-15.50**

WeP06-1   **13.45-14.10**
*Hybrid trajectory tracking control for a robotic leg
performing hops* 73
M.W.L.M. Rijnen   Eindhoven University of Technology
A.T. van Rijn   Eindhoven University of Technology
H. Dallali   Michigan Technological University
A. Saccon, H. Nijmeijer

WeP06-2   **14.10-14.35**
*Bilateral human-robot control for semi-
autonomous UAV navigation* 74
H.W. Wopereis   University of Twente
M. Fumagalli   University of Twente
S. Stramigioli   University of Twente
R. Carloni

WeP06-3   **14.35-15.00**
*Experimental validation of path-following NMPC
applied to a serial-link robot manipulator* 75
N. van Duijkeren   Katholieke Universiteit Leuven
G. Pipeleers   Katholieke Universiteit Leuven
J. Swevers   Katholieke Universiteit Leuven

WeP06-4   **15.00-15.25**
*A variable stiffness robotic arm for the SHERPA
project* 76
E. Barrett   University of Twente
S. Stramigioli   University of Twente
R. Carloni   University of Twente

WeP06-5   **15.25-15.50**
Distributed control of autonomous agents with
sensor fusion methodologies   77
S. Cherlet   University of Ghent
C. Copot   University of Ghent
R. De Keyser   University of Ghent

WeE01	**St. Janzaal**
System Identification C	
Chair: Lars Grüne	**16.20-18.25**

WeE01-1   **16.20-16.45**
On the connection between different noise struc-
tures for LPV-SS models   78
P.B. Cox   Eindhoven University of Technology
R. Toth   Eindhoven University of Technology
P.M.J. van den Hof   Eindhoven University of Tech.

WeE01-2   **16.45-17.10**
State-space realization of coordinated linear
stochastic systems   79
M. Jozsa   University of Groningen
M. Petreczky   Ecole Centrale de Lille
M. Kanat Camlibel   University of Groningen

WeE01-3   **17.10-17.35**
Experimental evaluation of the combined global
and local LPV system identification approach . .   80
D. Turk   Katholieke Universiteit Leuven
J. Gillis   Katholieke Universiteit Leuven
G. Pipeleers   Katholieke Universiteit Leuven
Jan Swevers

WeE01-4   **17.35-18.00**
Maximum likelihood estimation of LPV-SS mod-
els: A Sequential Monte-Carlo approach   81
M.A.H. Darwish   Eindhoven University of Technology
S. Chitraganti   Amrita University
T.B. Sch on   Uppsala University
R.Toth, P.M.J. Van den Hof

WeE01-5   **18.00-18.25**
Using a polynomial decoupling algorithm for state-
space identification of a Bouc-Wen system   82
A. Fakhrizadeh Esfahani   Vrije Universiteit Brussel
P. Dreesen   Vrije Universiteit Brussel
J. Schoukens   Vrije Universiteit Brussel
K. Tiels

WeE02	**Angola**
Power Systems B	
Chair: Claudio de Persis	**16.20-18.25**

WeE02-1   **16.20-16.45**
Communication requirements for optimal fre-
quency regulation in power networks   83
S. Trip   University of Groningen
C. De Persis   University of Groningen

WeE02-2   **16.45-17.10**
Power balance of microgrids using min-max con-
trol of fuel cell cars   84
F.Alavi   Delft University of Technology
N. van de Wouw   Delft University of Technology
B. De Schutter   Delft University of Technology

WeE02-3   **17.10-17.35**
Distributed optimal control of smart energy grids
with congestion management   85
D. Bao Nguyen   University of Groningen
J.M.A. Scherpen   University of Groningen
W. Kramer   University of Groningen
F. Bliek, G.K.H. Larsen

WeE02-4   **17.35-18.00**
A port-Hamiltonian approach to optimal frequency
regulation in power grids   86
T. Stegink   University of Groningen
C. De Persis   University of Groningen
A. van der Schaft   University of Groningen

WeE02-5   **18.00-18.25**
Conservation of reactive energy in reactive time   87
D. Jeltsema   Delft University of Technology
G. Kaiser   Virginia Center for Signals and Waves

WeE03	**Botswana**
Games and Agent-Based Models A	
Chair: Anton Proskurnikov	**16.20-18.25**

WeE03-1   **16.20-16.45**
Government and central bank Interaction under
Uncertainty: A differential games approach . . .   88
J. Engwerda   Tilburg University
D. Mahmoudinia   Isfahan University
R. Dalali Isfahani   Isfahan University

WeE03-2   **16.45-17.10**
A local influence index for social networks   89
W.S. Rossi   University of Twente
P. Frasca   University of Twente

WeE03-3   **17.10-17.35**
Robust average consensus dynamics over wireless
networks   90
F. Acciani   University of Twente
G. Heijenk   University of Twente
P. Frasca   University of Twente

WeE03-4   **17.35-18.00**
Convergence of 2-strategy network games under
asynchronous best response dynamics   91
J. Riehl   University of Groningen
P. Ramazi   University of Groningen
M. Cao   University of Groningen

WeE03-5   **18.00-18.25**
Control of strategic interactions in finite heteroge-
neous populations under best-response update rule   92
P. Ramazi   University of Groningen
M. Cao   University of Groningen

WeE04   Congo
Modeling for Control B
Chair: Alessandro Saccon   **16.20-18.50**

WeE04-1   **16.20-16.45**
A novel approach to the model stable inversion for NMP systems 93
L. Jetto   UniversitaṔolitecnicadelleMarche
V. Orsini   UniversitaṔolitecnicadelleMarche
R. Romagnoli   UniversiteĹibredeBruxelles

WeE04-2   **16.45-17.10**
Resource utilization and quality-of-control trade-off for a composable platform 94
E.P. van Horssen   Eindhoven University of Technology
J.D. Valencia   Eindhoven University of Technology
D. Goswami   Eindhoven University of Technology
K.G.W. Goossens, W.P.M.H. Heemels

WeE04-3   **17.10-17.35**
Control oriented assessment of invertible non-linear models 95
R. Mohan   Eindhoven University of Technology
R. Gaasbeek   Eindhoven University of Technology
B. de Jager   Eindhoven University of Technology

WeE04-4   **17.35-18.00**
Synchronization Approached Through the Lens of Primitivity 96
F. Gonze   Université Catholique de Louvain
B. Gerencsér   Université Catholique de Louvain
R. M. Jungers   Université Catholique de Louvain

WeE04-5   **18.00-18.25**
Modelling for control of free molecular flow processes 97
M. Dresscher   University of Groningen
B. Jayawardhana   University of Groningen
J.M.A. Scherpen   University of Groningen

WeE04-6   **18.25-18.50**
Stochastic control of crop growth, a simulation study 98
S. van Mourik   Wageningen University
M. Vellekoop   University of Amsterdam
P. van Beveren   Wageningen University
B. van t́ Ooster, E. van Henten

WeE05   Ghana
Biochemical Engineering & Systems Biology
Chair: Paul van Dooren   **16.20-18.50**

WeE05-1   **16.20-16.45**
Dynamic metabolic flux convex analysis of hybridoma cell cultures 99
S. Fernandes de Sousa   University of Mons

WeE05-2   **16.45-17.10**
PHA production modeling with overflow dynamics 100
J. Oviedo   University of Mons
A. Vande Wouwer   University of Mons
A. Vargas   Universidad Nacional Autónoma de México

WeE05-3   **17.10-17.35**
Dynamic microorganism growth modelling for shelf life prediction: Application to cooked and brined shrimps 101
M. Aliou Diallo   Cheikh Anta Diop University
P. Bogaerts   Université Libre de Bruxelles

WeE05-4   **17.35-18.00**
Characterization of the visual space of butterfly eyes via a robotic scanner 102
A. Vargas-Delgado   University of Groningen
M. Munoz-Arias   University of Groningen
D. Stavenga   University of Groningen

WeE05-5   **18.00-18.25**
Reduced mathematical model of dengue virus replication whitin vero cell cultures 103
T. Abbate   University of Mons
L. Dewasme   University of Mons
A. Vande Wouwer   University of Mons

WeE05-6   **18.25-18.50**
Development of a biological culture simulator based on a simplified metabolic network and a constrained dynamic FBA 104
K. Mhallem Gziri   Université Libre de Bruxelles
A. Richelle   Université Libre de Bruxelles
P. Bogaerts   Université Libre de Bruxelles

WeE06   Tanzania
Observers
Chair: Pietro Tesi   **16.20-18.25**

WeE06-1   **16.20-16.45**
Impedance-based temperature estimation for Li-ion batteries 105
H.P.G.J. Beelen   Eindhoven University of Technology
M.C.F. Donkers   Eindhoven University of Technology
H.J. Bergveld   Eindhoven University of Technology

WeE06-2   **16.45-17.10**
Design of a robust Lipschitz observer - Experimental application 106
C. Feudijo   University of Mons
P. Bogaerts   University of Brussels
J.-S. Deschenes   Université du Quebec à Rimouski
A. Vande Wouwer

WeE06-3   **17.10-17.35**
On the model-based monitoring of industrial batch crystallizers 107
M. Porru   Eindhoven University of Technology
L. Ozkan   Eindhoven University of Technology

WeE06-4   **17.35-18.00**
Structured model-based observer design, application to plasma profile estimation in Tokamak . . 108
Benjamin Vincent   Université Catholique de Louvain
Denis Dochain   Université Catholique de Louvain
Laurent Lefévre   Université Grenoble Alpes

WeE06-5　　　　　　　　　　　　　　　**18.00-18.25**
Implementation of observers, controllers and su-
pervisory systems for tokamaks . . . .
T.C. Blanken　　　　　Eindhoven University of Technology
F. Felici　　　　　　　Eindhoven University of Technology

Thursday, March 24, 2016

Pleanary: P5　　　　　　　　　　　　**St. Janzaal**
Receding horizon control
Lars Grüne
Chair: Mircea Lazar　　　　　　　　　**8.30–9.30**

Receding horizon control . . . .
L. Grüne

Pleanary: P6　　　　　　　　　　　　**St. Janzaal**
Dissipativity and the turnpike property
Lars Grüne
Chair: Mircea Lazar　　　　　　　　**9.45–10.45**

Dissipativity and the turnpike property . . . . . .
L. Grüne

ThM01　　　　　　　　　　　　　　　**St. Janzaal**
System Identification D
Chair: Bram de Jager　　　　　　　**11.00-13.05**

ThM01-1　　　　　　　　　　　　　**11.00-11.25**
Noise-free signals make identification more diffi-
cult?! . . . .
H.H.M. Weerts　　　　Eindhoven University of Technology
P.M.J. Van den Hof　　　Eindhoven University of Tech.
A.G. Dankers　　　　　　　　　University of Calgary

ThM01-2　　　　　　　　　　　　　**11.25-11.50**
Data-driven modelling using symbolic regression　
D. Khandelwal　　　　Eindhoven University of Technology
R. Toth　　　　　　　Eindhoven University of Technology

ThM01-3　　　　　　　　　　　　　**11.50-12.15**
Identification of position-dependent mechanical
systems . . . .
R. de Rozario　　　　Eindhoven University of Technology
R. Voorhoeve　　　　Eindhoven University of Technology
W. Aangenent　　　　　　　　　ASML Veldhoven
T. Oomen

ThM01-4　　　　　　　　　　　　　**12.15-12.40**
Extrusion dynamic modeling: sensitivity analysis
and parameter identification . . . .
G. Jonathan　　　　　　　　　University of Mons

ThM01-5　　　　　　　　　　　　　**12.40-13.05**
Nonlinear identification of vortex-induced oscilla-
tors . . . .
J. Decuyper　　　　　　　　Vrije Universiteit Brussel
T. De Troyer　　　　　　　　Vrije Universiteit Brussel
M. Runacres　　　　　　　　Vrije Universiteit Brussel
K. Tiels, J. Schoukens

ThM02 — Optimal Control B — Angola

ThM02   **Angola**
Optimal Control B
Chair: Goele Pipeleers   **11.00-13.05**

ThM02-1   **11.00-11.25**
Real-time motion planning in the presence of moving obstacles 115
T. Mercy   Katholieke Universiteit Leuven
W. Van Loock   Katholieke Universiteit Leuven
G. Pipeleers   Katholieke Universiteit Leuven

ThM02-2   **11.25-11.50**
Receding horizon control for distributed energy management of a hybrid truck with auxiliaries . 116
T.C.J. Romijn   Eindhoven University of Technology
M.C.F. Donkers   Eindhoven University of Technology
S. Weiland   Eindhoven University of Technology
J.T.B.A. Kessels

ThM02-3   **11.50-12.15**
Model predictive control and wheel slip estimation for autonomous navigation of a tractor 117
A. De Preter   Katholieke Universiteit Leuven
G. Pipeleers   Katholieke Universiteit Leuven
J. Swevers   Katholieke Universiteit Leuven
J. Anthonis

ThM02-4   **12.15-12.40**
Thermal-aware workload scheduling in data centers 118
T. Van Damme   University of Groningen
C. De Persis   University of Groningen
P. Tesi   University of Groningen

ThM02-5   **12.40-13.05**
Characterization of the tracking error for OBF based MPC 119
A.A. Bachnas   Eindhoven University of Technology
S. Weiland   Eindhoven University of Technology
R. Toth   Eindhoven University of Technology

ThM03 — Mechanical Engineering A — Botswana

ThM03   **Botswana**
Mechanical Engineering A
Chair: Jan Swevers   **11.00-13.05**

ThM03-1   **11.00-11.25**
Feedforward control for flexible motion systems with a time-varying state-to-output map 120
Y. Kasemsinsup   Eindhoven University of Technology
S. Weiland   Eindhoven University of Technology
M. Heertjes   Eindhoven University of Technology
Hans Butler

ThM03-2   **11.25-11.50**
Multivariable fuel injection control in diesel combustion 121
X. Luo   Eindhoven University of Technology
B. de Jager   Eindhoven University of Technology
F. Willems   Eindhoven University of Technology

ThM03-3   **11.50-12.15**
Batch-to-batch rational feedforward tuning: From ;earning to identification approaches 122
L. Blanken   Eindhoven University of Technology
F. Boeren   Eindhoven University of Technology
D. Bruijnen   Philips Innovation Services
Tom Oomen

ThM03-4   **12.15-12.40**
Enhancing performance and cost-effectiveness in motion control via multi-rate sampling 123
J. van Zundert   Eindhoven University of Technology
T. Oomen   Eindhoven University of Technology
W. Aangenent   ASML
W.P.M.H. Heemels

ThM03-5   **12.40-13.05**
Dynamic event-triggered control with time regularization for linear systems 124
N. Borgers   Eindhoven University of Technology
V. Dolk   Eindhoven University of Technology
W.P.M.H. Heemels Einhoven University of Technology

ThM04 — Non-linear Control B — Congo

ThM04   **Congo**
Non-linear Control B
Chair: Mircea Lazar   **11.00-13.05**

ThM04-1   **11.00-11.25**
Robust constrained control of nonlinear systems: The explicit reference governor approach 125
M. Nicotra   Université Libre de Bruxelles
E. Garone   Université Libre de Bruxelles

ThM04-2   **11.25-11.50**
Sub-optimal extremum seeking 126
C. Labar   Université Libre de Bruxelles
E. Garone   Université Libre de Bruxelles

ThM04-3   **11.50-12.15**
Second-order reset elements for improved stage control design 127
L. Hazeleger   Eindhoven University of Technology
M.F. Heertjes   Eindhoven University of Technology
H. Nijmeijer   Eindhoven University of Technology

ThM04-4   **12.15-12.40**
Fraction-model-independent stability analysis for SMA-actuators 128
R. Gaasbeek   Eindhoven University of Technology

ThM04-5   **12.40-13.05**
Contraction-based control of physical systems . . 129
R. Reyes-Báez   University of Groningen
A. van der Schaft   University of Groningen
B. Jayawardhana   University of Groningen

ThM05 — Medical Applications — Ghana

ThM05   **Ghana**
Medical Applications
Chair: Athanasios Antoulas   **11.00-13.05**

ThM05-1   **11.00-11.25**
Testosterone regulation: A new mathematical model 130
H. Taghvaafrd   University of Groningen
A. V. Proskurnikov   University of Groningen
Ming Cao   University of Groningen

ThM05-2   **11.25-11.50**

Identifying a C-arc medical X-ray system: A 2D-LRM approach 131

A. van der Maas   Eindhoven University of Technology
R. van der Maas   Eindhoven University of Technology
R. Voorhoeve   Eindhoven University of Technology
T. Oomen

ThM05-3   **11.50-12.15**

Improving the selection of differentially expressed genes by spatiotemporal ICA 132

E. Renard   Université Catholique de Louvain
A.E. Teschendorff   University College London
P.-A. Absil   Université Catholique de Louvain
Emilie Renard

ThM05-4   **12.15-12.40**

Differentiable 2D Bézier interpolation on manifolds 133

P.-Y. Gousenbourger Université Catholique de Louvain
P.-A. Absil   Université Catholique de Louvain
P. Striewski   University of Muenster
Benedikt Wirth

ThM05-5   **12.40-13.05**

In-eye optical-coherence-tomography-based proximity control 134

Y. Douven   Eindhoven University of Technology
M. van de Molengraft   Eindhoven University of Tech.
M. Steinbuch   Eindhoven University of Technology

ThM06	**Tanzania**
Robotics B	
Chair: Dmitri Danilov	**11.00-13.05**

ThM06-1   **11.00-11.25**

Optimization-based iterative learning control for robotic manipulators 135

A. Steinhauser   Katholieke Universiteit Leuven
G. Pipeleers   Katholieke Universiteit Leuven
J. Swevers   Katholieke Universiteit Leuven

ThM06-2   **11.25-11.50**

A direct force-reflecting two-layer approach for stable bilateral teleoperation with time delays . . 136

D. Heck   Eindhoven University of Technology
A. Saccon   Eindhoven University of Technology
R. Beerens   Eindhoven University of Technology
H. Nijmeijer

ThM06-3   **11.50-12.15**

Task assignment for robotic networks with limited communication range 137

X. Bai   University of Groningen
M. Cao   University of Groningen

ThM06-4   **12.15-12.40**

Towards a navigation system for an autonomous UAV in indoor environment 138

T. Mac Thi   University of Ghent

ThM06-5   **12.40-13.05**

Formation feasibility of networked heterogenous systems with drift terms 139

Z. Sun   The Australian National University
B. Anderson   The Australian National University

ThP01	**St. Janzaal**
System Theory B	
Chair: Arjan van der Schaft	**14.00-16.05**

ThP01-1   **14.00-14.25**

Predictor-based controller design under denial-of-service 140

S. Feng   University of Groningen
P. Tesi   University of Groningen
Shuai Feng   University of Groningen

ThP01-2   **14.25-14.50**

Issues of carrier aggregation intermodulation distortions in LTE-Advanced System 141

L. Niyonkuru   Vrije Universiteit Brussel
L. Van Biesen   Vrije Universiteit Brussel
G. Vandersteen   Vrije Universiteit Brussel

ThP01-3   **14.50-15.15**

On stability and stabilization of nonlinear systems 142

A. Doban   Eindhoven University of Technology
M. Lazar   Eindhoven University of Technology

ThP01-4   **15.15-15.40**

Sampling-based stability verification 143

R. Bobiti   Eindhoven University of Technology
M. Lazar   Eindhoven University of Technology

ThP01-5   **15.40-16.05**

Characterizing the L2-gain of constrained switching systems using multiple storage functions . . . 144

M. Philippe   Université Catholique de Louvain
R. Essick   University of Illinois at Urbana Champaign
R. Jungers   Université Catholique de Louvain
Geir E. Dullerud

ThP02	**Angola**
Games and Agent-Based Models B	
Chair: Paolo Frasca	**14.00-15.40**

ThP02-1   **14.00-14.25**

Stability of matrix sets with common invariant oolyhedra 145

P.-Y. Chevalier   Université Catholique de Louvain
J. Hendrickx   Université Catholique de Louvain
R. Jungers   Université Catholique de Louvain

ThP02-2   **14.25-14.50**

Self-triggered coordination over a shared network under denial-of-service 146

D. Senejohnny   University of Groningen
P. Tesi   University of Groningen
C. De Persis   University of Groningen

ThP02-3   **14.50-15.15**

Aggregative game theoretic control for large populations of non-cooperative agents 147

S. Grammatico   Eindhoven University of Technology

ThP02-4   15.15-15.40

Bandicoot: an open-source Python toolbox to ana-
lyze mobile phone metadata   148
Y.-A. de Montjoye   Massachusetts Institute of Tech.
L. Rocher   Universit Catholique de Louvain
A.S. Pentland   Massachusetts Institute of Technology

ThP03	Botswana
Mechanical Engineering B	
Chair: Henk Nijmeijer	**14.00-16.05**

ThP03-1   14.00-14.25

Disturbance feedforward control for air mount sys-
tems with acoustic resonances   149
M. Beijen   Eindhoven University of Technology
M. Heertjes   Eindhoven University of Technology
H. Butler   Eindhoven University of Technology

ThP03-2   14.25-14.50

Huygens' Synchronization: Experiments, Model-
ing, and Local Stability Analysis   150
F.N. Hoogeboom   Eindhoven University of Technology
A.Y. Pogromsky   Eindhoven University of Technology
H. Nijmeijer   Eindhoven University of Technology

ThP03-3   14.50-15.15

Scheduled controller design for systems with vary-
ing sensor configurations: a frequency-domain ap-
proach   151
R. van der Weijst Eindhoven University of Technology
B. van Loon   Eindhoven University of Technology
M. Heertjes   Eindhoven University of Technology
W.P.M.H. Heemels

ThP03-4   15.15-15.40

SOC and SOH estimation for Li-ion battery, Part
I: SOC estimation   152
L.D. Couto   Université Libre de Bruxelles
J. Schorsch   Université Libre de Bruxelles
M. Nicotra   Université Libre de Bruxelles
M. Kinnaert

ThP03-5   15.40-16.05

An LTI control toolbox - simplifying feedback con-
troller design   153
M. Verbandt   Katholieke Universiteit Leuven
G. Pipeleers   Katholieke Universiteit Leuven
J. Swevers   Katholieke Universiteit Leuven

ThP04	Congo
Electro-Mechanical Engineering	
Chair: Tamas Keviczky	**14.00-15.40**

ThP04-1   14.00-14.25

Parasitic forces and torques compensation in iron-
less linear motors   154
T. Nguyen   Eindhoven University of Technology
M. Lazar   Eindhoven University of Technology
H. Butler   Eindhoven University of Technology

ThP04-2   14.25-14.50

Study on an extension of generalized repetitive
control to variable speed region based on Oppen-
heim's frequency transformation   155
M. Kanematsu   The University of Tokyo
H. Fujimoto   The University of Tokyo

ThP04-3   14.50-15.15

Nanometer-accurate planar actuation system
(NAPAS)   156
I. Proimadis   Eindhoven University of Technology
R. Toth   Eindhoven University of Technology

ThP04-4   15.15-15.40

SOC and SOH estimation for Li-ion battery, Part
II: SOH estimation   157
J. Schorsch   Université Libre de Bruxelles
L.D. Couto   Université Libre de Bruxelles
M. Kinnaert   Université Libre de Bruxelles

Event: E2	St. Janzaal
DISC Certificates & Best Thesis Award	
Chair: Henk Nijmeijer	**16.20–16.40**

Event: E3	St. Janzaal
Best Junior Presentation Award	
Chair: Award Committee	**16.40–16.55**

Event: E4	St. Janzaal
Closure	
Chair: Henk Nijmeijer & Martha Otte	**16.55**

Part 2

Contributed Lectures

2D Regularization for LTV systems using a single measurement: transient elimination and coping with large datasets

Péter Zoltán Csurcsia, Johan Schoukens, John Lataire

Vrije Universiteit Brussel, Pleinlaan 2, 1050 Elsene, Belgium

Email: `peter.zoltan.csurcsia@vub.ac.be`

1 Introduction and problem formulation

This abstract presents a methodology to obtain a nonparametric two-dimensional impulse response function (IRF) estimate $\hat{h}[t,\tau]$ of a linear time varying (LTV) system using 2D regularization. An example of an LTV IRF can be seen in Fig.1.a.

Unlike the linear time invariant systems where the IRF is unique, the time varying impulse response is not restricted to only one solution because the number of parameters is much higher than the number of data samples. The user can impose additional constraints to decrease this freedom. In the proposed case smoothness and exponential decaying are used over the system time t (direction of the impulse responses, referring to the behavior) and smoothing constraint is used over the global time τ (referring to the system memory). The excess degrees of freedom can be removed by 2D regularization using these constains [1][3]. A further issue is that a measurement of an LTV system cannot be usually repeated under the same conditions. Therefore it is needed to be able to estimate by using a single experiment with transient. Last but not least, when the 2D regularization is used, the computational time and the memory needs are quadratically growing with the number of samples and with the length of longest considered IRF. A simple method is developed to avoid the above-mentioned problem.

2 An example

In this Section a example is observed. A second order time varying low-pass filter is shown in Fig. 1.a. It is is noisless observed with transient. The filter is excited by a full band random phase multisine [2].

Fig. 1.b. illustrate the non-uniqness issues by showing the results of this Maximum Likelihood estimate. To decrease the degrees of freedom a special 2D regularization is used. Fig. 1.d. shows the results of the proposed method without transient elimination [3]. Fig. 1.c. shows the results of the proposed method with transient elimination [4].

3 Summary

In this work a powerful time domain estimation method is developed for smooth LTV systems. This technique is illustrative, flexible and user friendly. With respect to the system dynamics using the proposed method, it is possible 1)
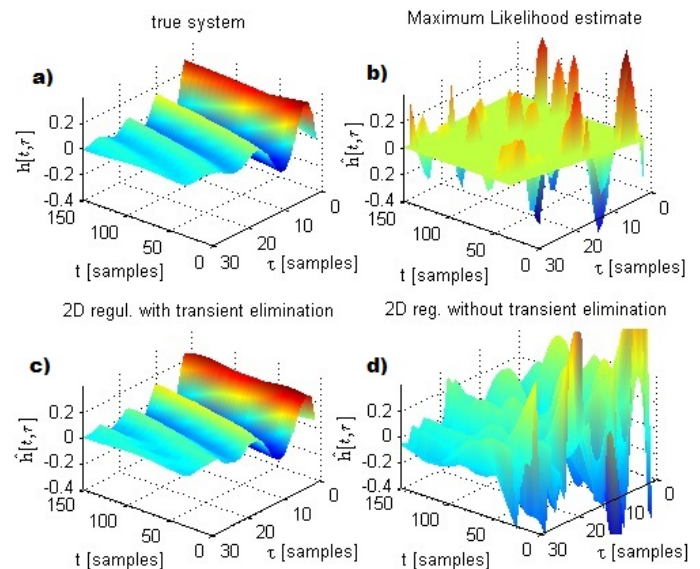
Figure 1: a) the true underlying system. It is noiseless observed with transient b) Maximum Likelihood estimate of the underlying system c) 2D regularized estimate using the transient elimination method d) 2D regularized estimate without using the transient elimination method

to decrease the effect of the disturbing noise 2) eliminate the undesired transient term 3) estimate from large datasets 4) estimate from a single experiment.

References

[1] G. Pillonetto, F. Dinuzzo, T. Chen, G. De Nicolao, and L. Ljung, "Kernel methods in system identification, machine learning and function estimation: A survey," Automatica, vol. 50, no. 3, pp. 657-682, 2014

[2] R. Pintelon, J. Schoukens: "System identification, a frequency domain approach, second edition" New Jersey, 2012

[3] P. Z. Csurcsia, J. Lataire: "Nonparametric Estimation of Time-varying Systems Using 2D Regularization ," IEEE Transactions on Instrumentation and Measurement, volume 65, issue 5, 2016, DOI: 10.1109/TIM.2015.2490918

[4] P. Z. Csurcsia: "Nonparametric identification of linear time-varying systems," PhD thesis, ISBN 978-94-6197-326-9, 2015, www.vubirelec.be

Inferring spectral properties of networks with local measurements

Alexandre Mauroy
Luxembourg Centre for Systems Biomedicine
University of Luxembourg
L-4367 Belvaux, Luxembourg
Email: alexandre.mauroy@uni.lu

Julien M. Hendrickx
ICTEAM Institute
Université catholique de Louvain, Belgium
B-1348 Louvain-la-Neuve, Belgium
Email: julien.hendrickx@uclouvain.be

1 Introduction

In natural and social sciences, it is often crucial to infer the structure of a network from measurements of its collective dynamics. While network identification has recently attracted considerable interest, the many methods proposed so far in dynamical systems theory require measuring all the units of the network, which is out of reach in large real systems. In contrast, we propose a method that focuses on the spectral properties of the network—instead of full topology—making possible the use of a few local measurements to uncover global topological properties. More details on this work can be found in [2].

2 Problem statement

We consider a set of n nonlinear dynamical units

$$\dot{x}_k = F(x_k) + G(x_k)u_k \in \mathbb{R}^m, \qquad k = 1, \dots, n$$

that interact in a network through a diffusive coupling $u_k = -\sum_{j=1}^{n} L_{kj} H(x_k)$, where L_{kj} are the entries of the Laplacian matrix L of the network. Assuming that the network dynamics converge to an equilibrium state, i.e. $\lim_{t\to\infty}[x_1(t)\cdots x_n(t)] = \lim_{t\to\infty} X(t) = X^*$, we address the following *spectral network identification* problem: infer the eigenvalues of L from $p \ll n$ measurements $f_l(X(t))$, $l = 1, \dots, p$, where the measurement functions f_l typically depend on a few number of states (possibly one).

3 Theoretical results

The measurements $f_l(X(t)) \equiv U^t f_l$ are related to the action of the so-called Koopman operator U^t. Using the Dynamic Mode Decomposition algorithm, one can extract from these measurements the spectrum of U^t [1]. In this work, we prove and characterize a bijection between the spectrum of the Koopman operator (which is measured) and the spectrum of the Laplacian matrix (which is inferred), thereby showing that the spectral network identification problem is feasible. For large networks, inferring every individual eigenvalue of the Laplacian matrix is out of reach. In this case, we show that one can estimate the spectral Laplacian moments $M_k(L) = \frac{1}{n}\text{trace}(L^k)$ instead, which are related to the distribution of vertex degrees. This approach is also well-suited to heterogeneous populations.

4 Applications

Through the spectral network identification framework, key global properties of the network can be inferred with a few local measurements. For instance, measuring only one vertex in a (directed, weighted) network, we can estimate the average number of connections with a good accuracy, even when the measured vertex is weakly connected to the rest of the network. This framework also provides a way to estimate the minimum and maximal vertex degree, through the estimation of the spectral radius and spectral gap in undirected networks. This can be used to detect efficiently the addition of a new vertex connected with an edge to a remote location in the network (see Figure).
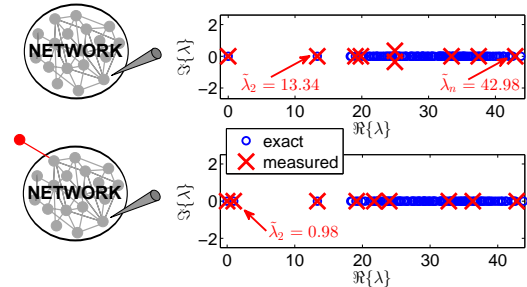
The present approach is also used successfully to measure whether two units influence each other indirectly, and thus belong to the same connected component of the network.

References

[1] C. W. ROWLEY, I. MEZIĆ, S. BAGHERI, P. SCHLATTER, AND D. S. HENNINGSON, *Spectral analysis of nonlinear flows*, Journal of Fluid Mechanics, 641 (2009), pp. 115–127.

[2] A. MAUROY AND J. HENDRICKX, *Spectral identification of networks using sparse measurements*, http://arxiv.org/abs/1601.04364

Acknowledgments

Two Case Studies on Optimal Input Design for simple Wiener Systems: Pitfalls and Challenges

Alexander De Cock and Johan Schoukens
Dept. of Fundamental Electricity and Instrumentation
Vrije Universiteit Brussel, Pleinlaan 2, 1050 Brussels
adecock@vub.ac.be, Johan.schoukens@vub.ac.be

1 Introduction

Optimal input design (OID) consists of finding the most informative input sequence out of the set of possible excitation signals. An input sequence is more informative if the derived estimated model has a lower model error, which depends on the model bias and variance. The set of possible excitation signals is often defined through constraints, which express the physical limitation of the measurement setup and a fixed value of the experiment cost.

2 Problem Statement

In this work, we evaluate the performance of different optimization strategies that compute the D-Optimal input design for two simple Wiener systems, which are depicted in figure 1. The first system is discreet and consists of a finite-impulse-response (FIR) filter followed by a static polynomial nonlinearity, while the second system consists of a continuous second order system (SoS) followed by a static polynomial nonlinearity.
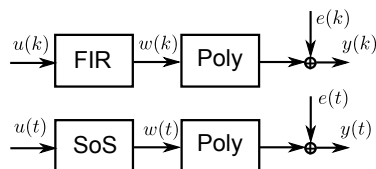
Figure 1: The two example systems

It is assumed that only the output measurements are corrupted by noise and that this noise is Gaussian, white, independently distributed. The set of possible excitation signals is restricted to signals that are periodic and band limited.

3 Solution Method

The first example system is part of a larger class of nonlinear systems called the nonlinear finite memory systems. For these systems a convex OID method is available that is numerically tractable if the memory of the system is short [3, 1, 2].
The second example system falls in the class of infinite memory nonlinear systems, which is a class of systems for which no general OID method is known. One way to approach the design problem is to approximate the infinite memory system with a finite memory system. However technical difficulties arise due to the memory length needed in order to get a good approximation.
We perform a brute force nonlinear optimization with respect to the samples of the input signal for both systems. Special care should be taken while choosing the optimization/design parameters (e.g. sampling time, signal duration, initial values, etc.) since small changes can have a high impact onto the design performance.

4 Results

From the experience obtained from these two case studies we derive generalizations for the class of systems to which the example systems belong. Special attention goes to guidelines to choose correct optimization/design parameters when brute force optimization is performed and techniques to extend the OID method presented in [3, 1, 2] in order to handle longer system memories.

5 Acknowledgments

References

[1]   A. De Cock, M. Gevers, and J. Schoukens. A preliminary study on optimal input design for nonlinear systems. In *Decision and Control (CDC), 2013 IEEE 52nd Annual Conference on*, pages 4931–4936, Dec 2013.

[2]   M. Forgione, X. Bombois, P.M.J. Van den Hof, and H. Hjalmarsson. Experiment design for parameter estimation in nonlinear systems based on multilevel excitation. 2014. Submitted to 2014 European Control Conference.

[3]   P.E. Valenzuela, C.R. Rojas, and H. Hjalmarsson. Optimal input design for non-linear dynamic systems: A graph theory approach. In *Decision and Control (CDC), 2013 IEEE 52nd Annual Conference on*, pages 5740–5745, Dec 2013.

Fault Diagnosis in a Hydraulic Pitch Actuator Based on Frequency Domain Identification

Sandra Vásquez[1,2], Michel Kinnaert[1] and Rik Pintelon[2]
[1]Deparment SAAS (ULB), [2]Department ELEC (VUB)
Email: savasque@vub.ac.be

1 Introduction

Wind turbines are equipped with condition monitoring systems that allow for a safer operation and a reduction of maintenance costs thanks to their feature of early detection of faults. Most of these systems are signal-based, however a model-based approach could enhance the performance, for example, by allowing a proper accommodation of faults through control adaptation. This project aims at designing a model-based fault diagnosis system with focus on the blade pitch system with hydraulic actuators, now that this system is characterized by a high failure rate. For this purpose, a physical model of the hydraulic pitch actuator [1] is analyzed. This model allows the simulation of different faults: abnormal bearing friction (due to damages on the pitch bearing) and high air/water content in cylinders (due to degradation of the hydraulic oil).

2 Results

This project proposes active fault detection and a system identification method that takes into account the effects produced by feedback, disturbances (like the pitching moment M_{p1} and the bearing friction moment M_{b1}), transients and the nonlinear nature of the pitch actuator. The proposed method (Fig. 1, 2) consists in applying a full random phase multisine (β_{pMS}) on top of the reference pitch angle (β_{prefPS}) and using frequency domain identification (the Local Polynomial Method and the Sample Maximum Likelihood estimator [2]) to obtain a continuous-time transfer function model of the pitch actuator ($G_{ML}(s)$). In this way, fault effects on the system are considered as a change in the model parameters and this information is used to devise a method for fault detection and isolation, which includes as well a first attempt for fault magnitude estimation (Fig. 3).

In addition, this work makes use of a wind turbine simulator based on the characteristics of a 1.25 MW real wind turbine (using the FAST/AeroDyn software). By means of this simulator, fictitious data representing the healthy/faulty operation of the pitch system can be generated. Also, the simulator allows testing the impact of the active fault detection on the operation of the wind turbine.

In conclusion, this project proves the feasibility and effectiveness of the proposed model-based fault diagnosis system. In fact, it is possible to detect and isolate faults in the
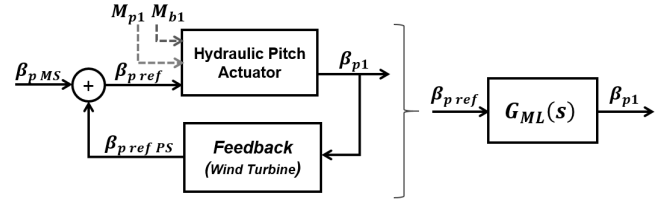
Figure 1: System Identification on hydraulic pitch actuator
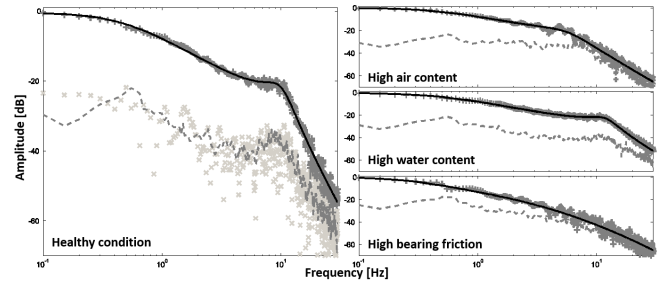
Figure 2: Frequency Response Functions (+:FRF, - -: $std(FRF)$) and Transfer Functions (–:TF, x: $Residuals$)

pitch actuator while maintaining a limited impact on the operation of the wind turbine. Future work includes the study of the effect of wind changes and the sensitivity to measurement noise.
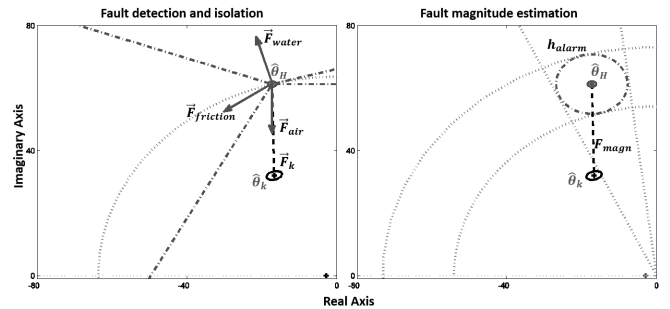
Figure 3: Fault detection, isolation and magnitude estimation (based on the complex poles of $G_{ML}(s)$)

3 References

[1] L. Rakoto, J. Schorsch, and M. Kinnaert, "Modelling hydraulic pitch actuator for wind turbine simulation under healthy and faulty conditions," 9th IFAC SAFEPROCESS Symposium. Paris, September 2015.
[2] R. Pintelon and J. Schoukens, System identication: A frequency domain approach. IEEE Press, 2012.

Weighted Tensor Decomposition for Approximate Decoupling of Multivariate Polynomials

Gabriel Hollander, Philippe Dreesen, Mariya Ishteva, Johan Schoukens
Dept. ELEC, Vrije Universiteit Brussel, Pleinlaan 2, 1050 Brussels, Belgium
gabriel.hollander@vub.ac.be

1 Introduction

In the field of system identification, one special type of nonlinear models are the so-called block-oriented models, consisting of linear time-invariant blocks and nonlinear static blocks. More specifically, this presentation will focus its attention on the parallel Wiener-Hammerstein models. When identifying these types of systems, a multiple-input-multiple-output polynomial should be decoupled, that was obtained from noisy measurements. In our work, an earlier developed decoupling algorithm with good results in the noiseless case is generalized to the noisy case.

2 Algorithm

Let $\mathbf{f}$ be a multivariate polynomial vector function under the influence of noise, whose coefficients are approximated and let $\Sigma_{\mathbf{f}}$ denote the covariance matrix on these coefficients. We wish to decouple this function by finding transformation matrices $\mathbf{V}$ and $\mathbf{W}$, such that $\mathbf{f}$ can be expressed as $\mathbf{f}(\mathbf{u}) = \mathbf{W} \cdot \mathbf{g}(\mathbf{V}^T \cdot \mathbf{u})$, where the internal vector function $\mathbf{g}$ is a set of r univariate functions: every component g_i of g is only dependent on one variable x_i, which is the i-th component of the internal variable $\mathbf{x} = \mathbf{V}^T \cdot \mathbf{u}$. Figure 1 shows a graphical representation of this decoupling procedure.

The earlier developed algorithm described in [1] uses first-order derivative information of f and involves the so-called Canonical Polyadic (CP) Decomposition of a tensor, which is, loosely speaking, a generalization of the singular value decomposition for two-dimensional matrices to multidimensional arrays of numbers, see [2]. In our work, a weight matrix based on the covariance matrix $\Sigma_{\mathbf{f}}$ is included during the CP decomposition.

This generalizes the CP decomposition to a Weighted CP decomposition, which takes the variances of and covariances between the elements of the tensor to be decomposed into account.

3 Conclusions

In the Wiener-Hammerstein identification setting, the model errors diminish using the weighted CP decomposition. The weighted decoupling gives results which are at least as good as the unweighted decoupling described in [1]. In the case where the unweighted decoupling does not give satisfactory results, the weighted decoupling diminishes model errors.

4 Acknowledgments

References

[1] P. Dreesen, M. Ishteva, J. Schoukens, *Decoupling Multivariate Polynomials in a Parallel Wiener-Hammerstein System Using First-Order Information*, SIAM Journal Matrix Analysis and Applications, 36(2),864–879, 2015.

[2] T. G. Kolda and B. W. Bader, *Tensor decompositions and applications*, SIAM Review, Vol. 51(3), 455–500, 2009

[3] G. Hollander, P. Dreesen, M. Ishteva, J. Schoukens, *Weighted tensor decomposition for approximate decoupling of multivariate polynomials*, arXiv:1601.07800
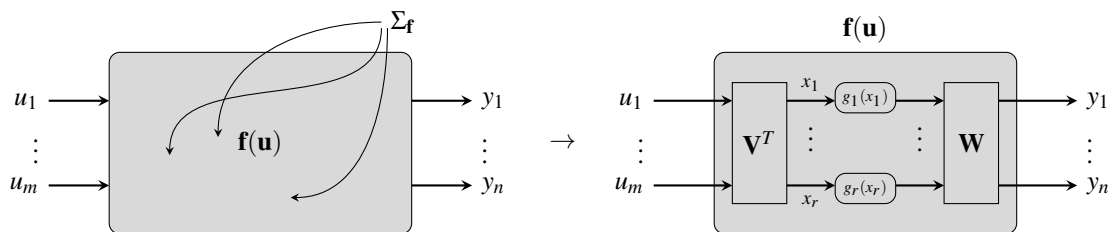
Figure 1: *Decoupling of the multivariate function $\mathbf{f}$ by taking the covariance matrix $\Sigma_{\mathbf{f}}$ into account.*

Event-triggered Control Systems under Denial-of-Service Attacks

V.S. Dolk*   P. Tesi**   C. De Persis**   W.P.M.H. Heemels*

*Department of Mechanical Engineering, Eindhoven University of Technology

P.O. Box 513, 5600MB Eindhoven, The Netherlands. Email: `v.s.dolk@tue.nl`

**Faculty of Mathematics and Natural Sciences, Eindhoven University of Technology, The Netherlands

1 Introduction

Due to the rapidly emerging field of *cyber-physical systems* (CPS) and, in particular, networked control systems (NCSs), there is a strong need for novel analysis and synthesis tools in control theory to guarantee safe and secure operation despite the presence of possible malicious attacks. One of the main concerns in NCSs regarding security are so-called *denial-of-service* (DoS) attacks. These DoS attacks, which are often induced by radio interference signals (also referred to as *jamming* signals), typically cause periods in time at which communication is not possible as illustrated in Figure 1. Besides this resilience requirement, the control strategy also needs to deal with inherent network-induced imperfections such as limited communication resources. In this work, we propose an *output-based*, *resource-aware* and *resilient* control approach that aims to reduce the utilization of communication resources while the desired stability and performance criteria are maintained.
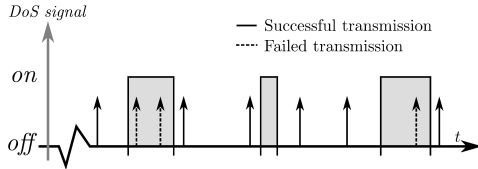
Figure 1: Schematic representation of a DoS sequence

2 Control Setup

The considered control setup consists of an interconnection of a continuous-time plant $\mathscr{P}$, a (dynamic) *output-based* controller $\mathscr{C}$ and a network $\mathscr{N}$ subject to disturbances and DoS attacks as depicted in Figure 2. Typically, the communication over the network $\mathscr{N}$ is packet-based which implies that the output measurements y can only be transmitted at discrete instants in time, *i.e.*, at times t_j, $j \in \mathbb{N}$, satisfying $0 \leqslant t_0 < t_1 < t_2 < \ldots$. When a transmission is attempted and no DoS attack is active, the value of $\hat{y}$ is updated/jumps according to $\hat{y}^+ = y$. Otherwise, when the DoS is active, the attempt fails and $\hat{y}$ can not be updated and then $\hat{y}^+ = \hat{y}$.

To deal with scarcity of the communication resources, we consider a *dynamic* event-triggering mechanism, see also [2], that takes the following form

$$t_{j+1} := \inf\{t > t_j + \tau_{miet} \mid \eta(t) < 0\},$$

for all $j \in \mathbb{N}$, where $\tau_{miet} \in \mathbb{R}_{\geqslant 0}$ is an (enforced) lower bound on the minimum inter-event time (MIET) and η a dynamical

variable. The evolution of the triggering variable η is given by

$$\dot{\eta} = \Psi(o, \eta), \; \eta^+ = \eta_0(o)$$

where o represents the information *locally* available at the ETM (see Figure 2) such as output $y \in \mathbb{R}^{n_y}$ and the transmission error $e := \hat{y} - y$.
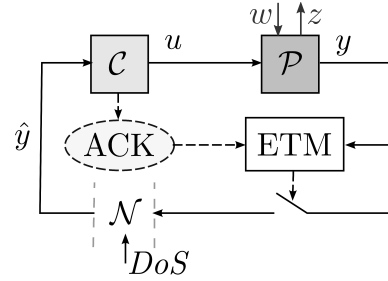
Figure 2: Schematic representation of the event-triggered NCS

Since in practice, the resources of the attacker are limited, it is reasonable to assume that the DoS attacks are constrained in terms of *frequency* and *duration*, see also [1]. To be more concrete, the *DoS frequency* and *DoS duration* constraints for given DoS parameters $\tau_D, \nu, \varsigma \in \mathbb{R}_{>0}$ and $T \in \mathbb{R}_{>1}$, are satisfied if for all $\tau, t \in \mathbb{R}_{\geqslant 0}$ with $t \geqslant \tau$

$$n(\tau, t) \leqslant \nu + \frac{t - \tau}{\tau_D} \text{ and } |\Xi(\tau, t)| \leqslant \varsigma + \frac{t - \tau}{T}, \quad (1)$$

respectively, where $n(\tau, t)$ denotes the number of DoS *off/on* transitions occurring on the interval $[\tau, t)$ and $|\Xi(\tau, t)|$ the total length of the DoS attacks active on the interval $[\tau, t)$.

3 Main Result

Given the system as described above with DoS parameters ν, τ_D, ς and T, if τ_{miet} and the functions Ψ, η_0 are well designed in the sense that they satisfy the conditions proposed in [3], then the resulting closed-loop system is UGES and, in the presence of disturbances, has a finite *peak-to-peak gain* and *energy-to-peak gain*.

References

[1]   C. De Persis, and P. Tesi, "Input-to-State Stabilizing Control Under Denial-of-Service," TAC, 60(11):2930-2944, 2015.

[2]   V.S. Dolk, D.P. Borgers and W.P.M.H. Heemels, "Dynamic Event-triggered Control: Tradeoffs Between Transmission Intervals and Performance," CDC, 2014, pp.2764-2769.

[3]   V.S. Dolk, P. Tesi, C. De Persis and W.P.M.H. Heemels, "Output-based Event-triggered Control Systems under Denial-of-Service Attacks," CDC, 2015.

Bisimulation equivalence of DAE systems

Noorma Yulia Megawati
Jan C. Willems Center for Systems and Control
University of Groningen
P.O.Box 407, 9700 AK Groningen
n.y.megawati@rug.nl

Arjan van der Schaft
Jan C. Willems Center for Systems and Control
University of Groningen
P.O.Box 407, 9700 AK Groningen
a.j.van.der.schaft@rug.nl

1 Introduction

Classical notions developed in systems and control theory for external equivalence are transfer matrix equality and state space equivalence. Within computer science the basic notion has been called *bisimulation relation* [1]. In particular, it has been shown how for linear systems a notion of bisimulation relation can be developed mimicking the notion of bisimulation relation for transition systems, and directly extending classical notions of transfer matrix equality and state space equivalence [2].

The present paper continues on these developments by extending the notion of bisimulation relation to general linear *differential-algebraic systems*. As in previous work on bisimulation theory for input-state-output systems [3], we explicitly allow for the possibility of 'non-determinism' in the sense that the state may evolve according to different time-trajectories for the same values of the external variables.

2 Main results

Consider two systems given by

$$\Sigma_i : \begin{array}{ll} E_i \dot{x}_i = & A_i x_i + B_i u_i + G_i d_i, \quad x_i \in \mathscr{X}_i, u_i \in \mathscr{U}, d_i \in \mathscr{D}_i \\ y_i = & C_i x_i, \qquad\qquad y_i \in \mathscr{Y}, i = 1, 2. \end{array} \tag{1}$$

where $E_i, A_i \in \mathbb{R}^{q_i \times n_i}$ and $B_i \in \mathbb{R}^{q_i \times m}, G_i \in \mathbb{R}^{q_i \times s_i}, C_i \in \mathbb{R}^{p \times n_i}$ for $i = 1, 2$, with $\mathscr{X}_i, \mathscr{D}_i, i = 1, 2$, the state space and disturbance spaces, and $\mathscr{U}, \mathscr{Y}$ the common input and output spaces. The *consistent subset* $\mathscr{V}_i^*$ for a system Σ_i is either empty or given as the maximal subspace $\mathscr{V}_i \subset \mathbb{R}^n$ satisfying

$$\begin{array}{ll} (i) & A_i \mathscr{V}_i \subset E_i \mathscr{V}_i + \mathscr{G}_i \\ (ii) & \operatorname{im} B_i \subset E_i \mathscr{V}_i + \mathscr{G}_i \end{array} \tag{2}$$

where $\mathscr{G}_i = \operatorname{im} G_i$. It follows that $\mathscr{V}_i^*$ equals the set of all initial conditions x_{0i} for which for every piecewise-continuous input function $u_i(\cdot)$ there exist a piecewise-continuous function $d_i(\cdot)$ and a continuous and piecewise-differentiable solution trajectory $x_i(\cdot)$ of Σ_i with $x(0i) = x_{0i}$.

The fundamental definition of bisimulation relation is given as follows.

Definition 2.1. *A subspace $\mathscr{R} \subset \mathscr{X}_1 \times \mathscr{X}_2$, with $\pi_i(\mathscr{R}) \subset \mathscr{V}_i^*, i = 1, 2$, is a bisimulation relation between two systems Σ_1 and Σ_2 with consistent subsets $\mathscr{V}_i^*, i = 1, 2$, if and only if*

for all pairs of initial conditions $(x_1, x_2) \in \mathscr{R}$ and any joint input function $u_1(\cdot) = u_2(\cdot) = u(\cdot) \in \mathfrak{U}$ the following properties hold:

1. *for every disturbance function $d_1(\cdot) \in \mathfrak{D}_1$ for which there exists a solution $x_1(\cdot)$ of Σ_1 (with $x_1(0) = x_1$) of Σ_1, there exists a disturbance function $d_2(\cdot) \in \mathfrak{D}_2$ such that the resulting solution trajectoriy $x_2(\cdot)$ of Σ_2 (with $x_2(0) = x_2$) satisfy*

$$(x_1(t), x_2(t)) \in \mathscr{R}, t \geq 0, \tag{3}$$

and conversely, for every disturbance function $d_2(\cdot)$ for which there exists a solution $x_2(\cdot)$ of Σ_2 (with $x_2(0) = x_2$) of Σ_2, there exists a disturbance function $d_1(\cdot)$ such that (3) holds.

2.

$$C_1 x_1(t) = C_2 x_2(t), t \geq 0. \tag{4}$$

Using the geometric notion of a *controlled invariant subspace*, a linear-algebraic characterization of a bisimulation relation is given. This also leads to an algorithm for computing the maximal bisimulation relation. We will also study the implication of adding the condition of *regularity* to the matrix pencil $sE - A$, and show how in this case bisimilarity reduces to equality of transfer matrices.

Furthermore, by developing a one-sided version of bisimulation relation, characterizations of simulation and abstraction are obtained. Moreover, it is shown how state space reduction is performed by computing the maximal bisimulation relation between the DAE system and itself.

References

[1] E.M. Clarke Jr., O. Grumberg, D.A. Peled, Model Checking, The MIT Press, Cambridge, Massachussets, 2002.

[2] A.J. van der Schaft, Equivalence of dynamical systems by bisimulation, *IEEE Transactions on Automatic Control*, vol. 49, 2004, pp 2160-2172.

[3] A.J. van der Schaft, Equivalence of hybrid dynamical system, *in Sixteenth International Symposium on Mathematical Theory of Networks and Systems*, Belgium, 2004.

Fault detection and isolation for systems defined over graphs

A.R.F. Everts[♭], P. Rapisarda[♯] and M.K. Camlibel[♭]

[♭]JBI for Mathematics and Computer Science, University of Groningen, The Netherlands

[♯]CSPC group, School of Electronics and Computer Science, University of Southampton, United Kingdom

a.r.f.everts@rug.nl, pr3@ecs.soton.ac.uk, m.k.camlibel@rug.nl

1 Introduction

Detecting and identifying faults in multi-agent systems is particularly relevant, given the absence of a centralized observer monitoring the whole network and the practical applications of such systems, where faults either in the agents or in the communication structure can have serious consequences.

In this work, we consider a class of linear dynamical systems defined by an undirected graph containing faulty vertices and observer vertices. Two disjoint sets of agents are identified in the network: those prone to failure (called "faulty") and those whose output is measurable (called "observer"). Faults such as total communication and biased sensing can be modelled in a straightforward way in this framework. Fault detection is performed by an unknown input observer, and stated in the geometric language of the pioneering work by M.-A. Massoumnia in [2], i.e. output separability of fault subspaces.

2 Problem statement

Let $G = (V,E)$ be a simple and connected graph with the vertex set

$$V = \{1, 2, \ldots, n\}.$$

Two subsets of V will play an important role in the sequel. We denote these sets by V_F (*faulty vertices*) and V_O (*observer vertices*), see for example Figure 1. For simplicity, we assume that these sets are disjoint and that the first q vertices are faulty and the last s are observer vertices.

We consider systems of the form

$$\dot{x} = Xx + Mf$$
$$y = Nx$$

where x is the state, f is the fault mode and y is the output vector. The matrices X, M and N are related to the given simple graph G and the pair (V_F, V_O) in the following sense. The matrices M and N are selection matrices that encode the faulty vertices and observer vertices respectively:

$$M = \begin{bmatrix} I_q \\ 0_{n-q,q} \end{bmatrix} \quad \text{and} \quad N = \begin{bmatrix} 0_{s,n-s} & I_s \end{bmatrix}.$$

The matrix X is assumed to be a *distance-information preserving* matrix with respect to the graph $G = (V,E)$, that is,

$$(X^k)_{i,j} \begin{cases} = 0 & \text{if } \text{dist}(i,j) > k, \\ \neq 0 & \text{if } \text{dist}(i,j) = k \end{cases}$$

for $k \geqslant 0$, where $\text{dist}(i,j)$ denotes the distance between vertices i and j in the graph.

The problem that we address in this work amounts to setting up an observer in order to detect if and which faults are active.

First we present a characterization of the smallest conditioned invariant subspaces that are generated by the faults. These subspaces play a major role in the analysis of fault detection as well as in the design of fault detectors. Based on this characterization, we present a graph-topological sufficient condition for the so-called output separability of these subspaces, which is the crux of the fault detection problem, for any distance-information preserving matrix X. This condition is based on the distances between faulty agents and observer vertices.

This work has been published in [1].
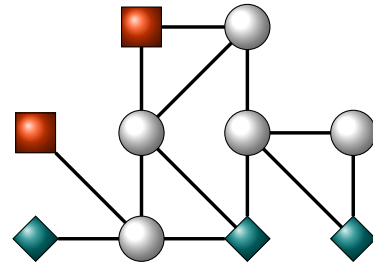
Figure 1: Graph with 10 vertices, including 2 faulty agents (squares) and 3 observer vertices (diamonds).

References

[1] P. Rapisarda, A.R.F. Everts and M.K. Camlibel, "Fault detection and isolation for systems defined over graphs", *Proc. of the 54th IEEE Conference on Decision and Control*, Osaka, Japan, 2015.

[2] M.-A. Massoumnia, "A geometric approach to the synthesis of failure detection filters", *IEEE Transactions on Automatic Control*, 31(9):839–846, 1986.

Stabilization of planar slow-fast systems at non-hyperbolic points

H. Jardón-Kojakhmetov and J.M.A. Scherpen

Engineering and Technology Institute (ENTEG), University of Groningen,

Groningen, The Netherlands.

{h.jardon.kojakhmetov, j.m.a.scherpen}@rug.nl

1 Abstract

We study a particular class of 'controlled' slow-fast systems of the form

$$\begin{aligned}
\dot{x} &= f(x,z,\varepsilon) + u(x,z,\varepsilon) \\
\varepsilon\dot{z} &= g(x,z,\varepsilon),
\end{aligned} \tag{1}$$

where $x \in \mathbb{R}$, $z \in \mathbb{R}$ and $\varepsilon > 0$ is a small parameter $\varepsilon \ll 1$. Note that due to the presence of ε, the variable z evolves much faster that x. Therefore, x and z are called the *slow* and the *fast* variable respectively. Open loop slow-fast systems (with $u = 0$) are frequently used to model phenomena with two time scales. For $\varepsilon > 0$ a new time $\tau = \frac{t}{\varepsilon}$ can be defined. In this way (1) is rewritten as

$$\begin{aligned}
x' &= \varepsilon f(x,z,\varepsilon) + \varepsilon u(x,z,\varepsilon) \\
z' &= g(x,z,\varepsilon),
\end{aligned} \tag{2}$$

where now the prime denotes the derivate with respect to τ. A first approach to study slow-fast systems is to analyze their limit when $\varepsilon \to 0$. An important ingredient in the analysis of slow-fast systems is the *critical manifold*, which is defined as the set of equilibrium points of (2) when $\varepsilon = 0$, this is

$$S = \left\{ (x,z) \in \mathbb{R}^2 \,|\, g(x,z,0) = 0 \right\}. \tag{3}$$

If the set S has only hyperbolic equilibria, it is called *normally hyperbolic*. It is known [2] that normally hyperbolic manifolds persist under small C^1-perturbations of the corresponding vector field. This hyperbolicity property has been the key factor in designing reduced controllers for slow-fast systems. Briefly speaking, one first constructs controllers for the limit ($\varepsilon \to 0$) systems of (1) and (2). Then, due to the persistence property it can be shown that small ε-perturbations of these reduced controllers can be used in combination to control a slow-fast system, see e.g. [5].

Contribution.

There are many phenomena in nature that are characterized by a rapid transition between stable states of the system. Examples can be found in: electric circuits (like the van der Pol oscillator), biology systems (like the heartbeat or the nerve impulse), ecology (predator-pray models), chemistry, and many others. The analysis of these rapid transitions and related behavior such as relaxation oscillations and/or canards has attracted a lot of interest due to its potential applications. Mathematically speaking, these phenomena occur at *non-hyperbolic points* of the slow-fast system. In a qualitative way, non-hyperbolic points are very sensitive to small changes in the slow variables. From the control point of view, since the strong property of hyperbolicity is lost, the classical approach of control design cannot be used anymore.

In our current research we apply a geometric tool called blow up [1] to stabilize planar slow-fast systems at non-hyperbolic points. Interestingly, the blow up technique provides a way to analyze a regular perturbation problem instead of a singular one. Moreover, we show that the blow up technique can be combined with Lyapunov based control design in order to stabilize non-hyperbolic points of slow-fast systems. Our results open a wide range of interesting mathematical extensions of existing theories, and motivate many potential applications of controllers for systems exhibiting fast transitions [3, 4].

References

[1] Dumortier, F. and Roussarie, R.H. (1996). *Canard Cycles and Center Manifolds*, volume 121. American Mathematical Society.

[2] Fenichel, N. (1979). Geometric singular perturbation theory. *JDE*, 53–98.

[3] Jardón-Kojakhmetov, H. and Scherpen, J.M.A. (2016). Stabilization of a planar slow-fast systems at a non-hyperbolic point. *Submitted to MTNS, 2016*.

[4] Jardón-Kojakhmetov, H. and Scherpen, J.M.A. (2016). Nonlinear adaptive stabilization of a planar slow-fast systems at a non-hyperbolic point. *Submitted to CDC, 2016*.

[5] Kokotovic, P.V. (1984). Applications of Singular Perturbation Techniques to Control Problems. *SIAM Review*, 26(4), 501–550.

Model reference adaptive control of uncertain switched system with slow switching laws

Shuai Yuan, Simone Baldi, and Bart De Schutter
Delft Center for Systems and Control
Delft University of Technology
2628 CD, Delft, The Netherlands
s.yuan-1@tudelft.nl

1 Introduction

Switched system is an important subclass of hybrid systems that consists of subsystems with continuous dynamics and a rule, called *switching law*, to regulate the switching behavior between them. Switched system appears in a wide range of applications, such as intelligent transportation systems, power electronics, and smart energy systems [1].There are mainly two time-constraint switching strategies: i.e., dwell time (DT) and average dwell time (ADT) [2]. In DT switching, the switching interval between two consecutive discontinuities of the switching law should be larger than a sufficiently large constant to guarantee the stability of the switched system. In ADT switching, the switching interval between two consecutive discontinuities of the switching law should be sufficiently large in an average sense. This means that very small intervals are allowed as soon as they are compensated by large intervals.

2 Problem formulation and methodology

Recently, a new time-constraint switching strategy has been proposed [3], which is called mode-dependent average dwell time (MDADT). It exploits information of every subsystem, such as the exponentially decreasing rate of its corresponding Lyapunov function, instead of information of all subsystems in the average dwell-time case. Some research has been conducted about MRAC of uncertain switched system. However, not much attention has been paid to the time-constraint switching laws for MRAC of uncertain switched system considering the information of subsystems. Moreover, in ADT and MDADT switching, short switching intervals might cause undesired behavior of the switched system. Therefore, it is relevant to address the following question: can we design a switching law that is less conservative than DT and that also avoids undesired transient behavior of the tracking error based on ADT and MDADT?

MRAC scheme for uncertain switched system is adopted based on a mode-dependent dwell time (MDDT) switching law. Similar with mode-dependent average dwell time, the main idea of MDDT is to design the switching law by exploiting the information of every subsystem. Furthermore, notice that the information of the next subsystem to be switched on is known in many practical problems, such

as the speeding up of an automobile power train [4]. To address these cases, we propose a new time-dependent switching scheme: mode-mode-dependent dwell-time (MMDDT). It not only exploits the information of the current subsystem but also of the next subsystem. This can allow less conservative switching laws than MDDT.

3 Conclusions and future work

Switching laws based on the mode-dependent dwell time and the mode-mode-dependent dwell time have been developed, which are less conservative than ones based on the dwell time. Globally uniformly ultimate boundedness of the closed-loop switched system based on the proposed methods can be guaranteed. Moreover, the upper bound and the ultimate bound of the tracking error have been proposed. Finally, numerical simulations demonstrate the effectiveness of the proposed model reference adaptive control methods. Future work will be focused on the extension of the results about the behavior of the tracking error introduced in this paper when the time-varying quadratic Lyapunov function is used.

References

[1]   D. Liberzon. *Switching in Systems and Control.* Birkhauser, Boston, 2003.

[2]   J. P. Hespanha and A. S. Morse. Stability of switched systems with average dwell-time. *Proc. 38th Conference on Decision and Control*, pages 2655–2660, 1999.

[3]   X. D. Zhao, L. Zhang, P. Shi, and M. Liu. Stability and stabilization of switched linear systems with mode-dependent average dwell time. *IEEE Transactions on Automatic Control*, 57(7):1809–1815, 2012.

[4]   X. Xu and P. J. Antsaklis. Optimal control of switched systems based on parameterization of the switched instants. *IEEE Transactions on Automatic Control*, 49(1):2–16, 2004.

Optimization-based trajectory generation for overtaking on highways

Iris Ballesteros Tolosana[1,3], Niels van Duijkeren[2], Jan Swevers[2], Sorin Olaru[3]

[1]Renault SAS, DEA-SAD5, Developtment of ADAS control laws, France

[2]Department of Mechanical Engineering, Division PMA, KU Leuven, Belgium

[3]Laboratory of Signals and Systems (L2S), Centrale-Supèlec, CNRS, Université de Paris-Saclay, France.

`iris.ballesteros-tolosana@renault.com`

1 Introduction

Automotive industry has focused its attention to Advanced Driving Assistance Systems (ADAS) in the recent years. Most of the car manufacturers are starting to incorporate this kind of controllers in order to improve the drivers experience. Progressively, these systems are evolving from passive warning signals to complex control systems that are able to take control over the vehicle dynamics, improving vehicles safety and comfort.

A crucial component that is needed for automated maneuvers such as lane changing or overtaking, is the trajectory generation algorithm. For safe operation, the algorithm needs to be sufficiently sophisticated to capture the real-time complexity of the problem along the maneuver. However, available computational resources and measurements are constrained by the typically low cost hardware utilized in passenger cars.

Maximizing the driver comfort is one of the main priorities of ADAS, alongside ensuring safety through collision avoidance and stabilizing the vehicle dynamics. Driver comfort is typically measured via the jerk levels perceived by the passengers, very sudden movements are to be avoided. A successful trajectory generator ought to effectively address these priorities. We discuss viable approaches for the trajectory generation problem for the specified scenario and compare their performance in a simulation study.
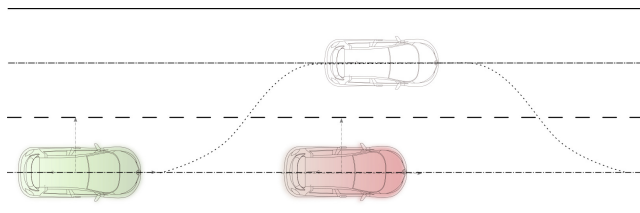
Figure 1: Overtaking maneuver scheme

2 Approaches

The trajectory generator is implemented following a Receding Horizon philosophy. The objective is to minimize jerk, which is a generally accepted approach to maximize driver comfort. Two candidate strategies are considered for a point-mass vehicle model driving a straight highway.

Firstly, a trapezoidal acceleration profile approach is considered. This kind of formulation allows to parameterize lateral jerk explicitly along the maneuver. Despite being a strategy in which collision avoidance constraints cannot be included, this approach seems considerably attractive because of its simplicity and low computational cost.

The second approach formulates the problem as a quadratic program formulation (QP), previously introduced in [2]. This kind of formulation is attractive since, efficient embedded solvers are available. The drawback of this approach is that the collision avoidance constraints are tedious to preprocess. There is a wide range of penalizing functions that can be formulated in order to generate minimum-jerk trajectories, as well as methods to solve the QP. In [3] a comparison between direct and in methods is presented; the quadratic cost function incorporates a minimal jerk objective and penalizes deviations from a desired terminal state, in order to enforce stability.

3 Validation

The generated trajectories from both approaches will be compared in a simulation environment using a vehicle model. Special attention is paid to driver comfort and safety, as well as the complexity of the algorithm. Finally, an important factor considered, is the difficulty of the tuning process for each algorithm, as this task consumes an considerable amount of time of the development process.

References

[1] N. Murgovski, J. Sjöberg "Predictive cruise control with autonomous overtaking," In proceedings of the 54th Annual Conference on Decision and Control (CDC), 2015.

[2] J. Nilsson "On Decision-Making and Control for Automated Highway Driving," Licentiate Thesis, Department of Signals and Systems, Chalmers University of Technology, 2014.

[3] C. Rathgeber, F. Winkler, X. Kang, S. Müller "Optimal Trajectories for Highly Automated Driving," *International Journal of Mechanical, Aerospace, Industrial, Mechatronic and Manufacturing Engineering*, vol. 9, no. 6, 2015.

Handling uncertainty in oil reservoir water-flooding using risk management tools

M. Mohsin Siraj and Paul M.J. Van den Hof
Electrical Engineering, Control Systems group
Eindhoven University of Technology
m.m.siraj,P.M.J.vandenhof@tue.nl

Jan Dirk Jansen
Department of Geoscience and Engineering
Delft University of Technology
J.D.Jansen@tudelft.nl

1 Introduction

Water-flooding involves the injection of water in an oil reservoir to increase oil production. Dynamic optimization of the water-flooding process has shown significant scope for improvement of the economic life-cycle performance of oil fields compared to a more conventional reactive strategy [1]. In these studies a financial measure, i.e., Net Present Value (NPV), is maximized. One of the key challenges in this model-based economic optimization is the high level of uncertainty arising from varying economic conditions and the limited knowledge of the model parameters. For improving robustness, different approaches, e.g., mean optimization (MO) or mean-variance optimization (MVO) have been proposed [3]. One of the drawbacks of the MVO approach is the symmetric nature of the variance and hence the reduction of the best cases. In this work, we focus only on the lower tail, i.e., the worst case(s) and aims to maximize the lower tail of the economic objective function without heavily compromising the best cases.

2 Robust optimization

In order to achieve asymmetric shaping of the NPV distribution, concepts from worst-case optimization and the theory of risk (a risk averse mean-CVaR optimization) are considered with respect to the given economic uncertainty.

2.1 Worst-case optimization (WCO)

WCO assumes that the uncertainty is known only within certain bounds and the robust solution is optimal for any realization of the uncertainty in the given set $\mathscr{U}$. Hence it focuses only on the worst-case in $\mathscr{U}$ and solves a max-min (or min-max) problem.

$$\max_{\mathbf{u}} \min_{\theta_i} J_i(\mathbf{u}, \theta_i) \tag{1}$$

where $\mathbf{u}$ is the control input, J_i is NPV and θ_i is the uncertainty ensemble.

2.2 Conditional Value-at-Risk

Conditional Value-at-Risk (CVaR) is a popular tool for managing risk in finance. CVaR indicates average of the β-tail of the worst cases of a distribution. It addresses the overly conservative solution of WCO by considering a class of worst cases. The mean-CVaR optimization (MCVaRO) is formulated as follows:

$$J_{\text{MCVaR}} = J_{\text{MO}} - \omega J_{\text{CVaR}} \tag{2}$$

where J_{MO} is the average NPV, J_{CVaR} is CVaR risk with given confidence level β and ω is the weighting on CVaR term. Objective (2) aims at maximizing the average NPV objective while minimizing the CVaR with a given ω [2].

3 Simulation examples

A scenario-based approach is used, where an ensemble of oil price scenarios characterizes the economic uncertainty. The MVO and MCVaRO strategies are applied to the uncertainty ensemble, a pdf is drawn on NPV points and compared in Fig. 1. It can be seen that MVO largely penalizes best cases in order to improve the worst cases compared to MCVaRO.

(a) MCVaRO   (b) MVO
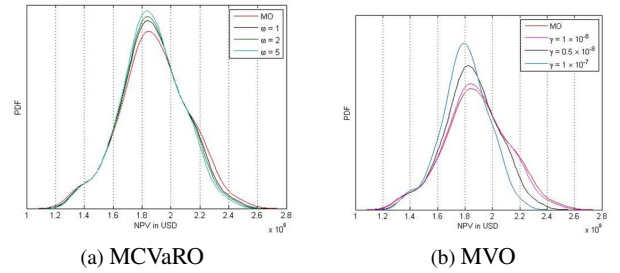
Figure 1: Results comparison for MVO and MCVaRO

4 Acknowledgements

References

[1] P.M.J. Van den Hof, J.D. Jansen and A.W. Heemink. *Recent developments in model-based optimization and control of subsurface flow in oil reservoirs*. Proc. 1st IFAC Workshop on Automatic Control in Offshore Oil and Gas Production. 2012, Trondheim, Norway, pp. 189-200.

[2] M.M. Siraj, P.M.J. Van den Hof and J.D. Jansen. *Risk management in oil reservoir water-flooding under economic uncertainty*. Proc. 54th IEEE Conference on Decision and Control, 2015, Osaka, Japan, pp. 7542-7547.

[3] M.M. Siraj, P.M.J. Van den Hof and J.D. Jansen. *Model and economic uncertainties in balancing short-term and long-term objectives in water-flooding optimization*. Proc. SPE Reservoir Simulation Symposium, 2015, Houston, TX, USA. SPE 173285-MS

Multi-objective Iterative Learning Control

Tong Duy Son, Goele Pipeleers and Jan Swevers

Division PMA, Department of Mechanical Engineering,

Katholieke Universiteit Leuven, Celestijnenlaan 300B, B-3001 Heverlee, Belgium

Email: `tong.duyson@kuleuven.be`

1 Introduction

Iterative learning control (ILC) is widely used in control applications to improve performance of repetitive processes [1]. The setup of a standard ILC is given by

$$u_{j+1}(k) = Q(\mathrm{q})\left[u_j(k) + L(\mathrm{q})e_j(k+1)\right],$$

where $u_j(k)$ is the ILC input signal and $e_j(k)$ is the error signal. The subscript j denotes the trial number. $Q(\mathrm{q})$ and $L(\mathrm{q})$ are known in ILC literature as the Q-filter and learning function, respectively. The choice of $Q(\mathrm{q})$ and $L(\mathrm{q})$ is the main issue in the design of an ILC algorithm.

This work presents a novel multi-objective iterative learning control (ILC) design approach that realizes an optimal trade-off between robust convergence, converged tracking performance, convergence speed, and input constraints. Linear time-invariant single-input single-output systems represented by parametric as well as nonparametric models are considered. The noncausal filter $Q(\mathrm{q})$ and learning function $L(\mathrm{q})$ are simultaneously optimized by solving a convex optimization problem.

2 Multi-objective ILC design

We consider a linear discrete-time system that is subjected to unstructured multiplicative uncertainty:

$$P_\Delta(\mathrm{q}) = \hat{P}(\mathrm{q})(1 + \Delta(\mathrm{q})W(\mathrm{q})), \quad \|\Delta(\mathrm{q})\|_\infty \le 1,$$

where $\hat{P}(\mathrm{q})$ is the nominal plant model and $W(\mathrm{q})$ is the uncertainty weight function.

Robust convergence [1]: The ILC system achieves robust convergence if:

$$|Q(\mathrm{q})[1 - L(\mathrm{q})P_\Delta(\mathrm{q})]| = \gamma^* < 1, \ \forall P_\Delta(\mathrm{q}).$$

And the smaller γ^*, the higher the convergence speed.

Robust performance [1]: The tracking performance of an ILC system is based on the asymptotic value of the error signal in the trial domain. Robust performance of ILC requires the tracking performance specifications to be met for all plants in the uncertainty set:

$$\left| W_{\mathrm{p}}(\mathrm{q}) \frac{1 - Q(\mathrm{q})}{1 - Q(\mathrm{q})[1 - L(\mathrm{q})P_\Delta(\mathrm{q})]} \right| \le 1, \ \forall P_\Delta(\mathrm{q}),$$

where $W_{\mathrm{p}}(\mathrm{q})$ is the performance weight selected by the designer.

The aforementioned ILC objectives are combined together into one constrained optimization problem for $Q(\mathrm{q})$ and $L(\mathrm{q})$:

$$
\begin{array}{ll}
\underset{Q(\mathrm{q}),\,L(\mathrm{q})}{\text{minimize}} & \text{convergence speed} \\
\text{subject to} & \text{robust convergence} \\
& \text{robust performance} \\
& \text{input constraint.}
\end{array}
$$

The main idea is to optimize the convergence speed considering given tracking performance specification, and taking into account robustness and input constraint. The problem is reformulated as a convex problem, guaranteeing an efficient and reliable computation of the global optimum and allowing straightforward computation of trade-off curves between different performance indices, e.g. as shown in Fig. 1 for the non-minimal phase system considered in the numerical validation of our multi-objective approach and comparison with a model-inversion based ILC design. These trade-off curves assist the control engineer in selecting the desired controller taking into account different objectives.
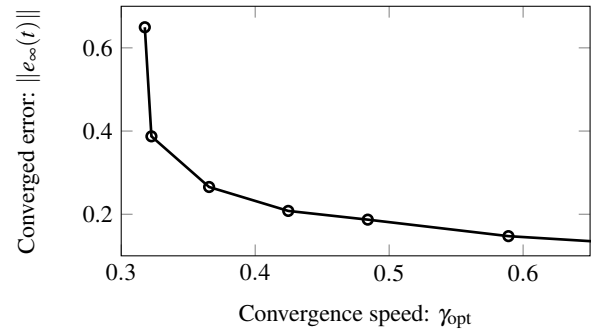
Figure 1: Trade-off curve: converged tracking error vs convergence speed

References

[1] D.A. Bristow, M. Tharayil, and A.G. Alleyne, "A survey of iterative learning control: A learning-based method for high-performance tracking control", *IEEE Control Systems Magazine*, vol. 26, no. 3, pp. 96–114, 2006.

Analysis of dynamic container terminal networks

R. T. Cahyono[1,2] and B. Jayawardhana[1]

[1]Faculty of Mathematics and Natural Sciences, Rijksuniversiteit Groningen
Nijenborgh 4 9747 AG, Groningen, the Netherlands
[2]Faculty of Industrial Technology, Institut Teknologi Bandung
Jalan Ganesha 10, Bandung, 40132, Indonesia
{r.tri.cahyono, b.jayawardhana}@rug.nl[1], rully@ti.itb.ac.id[2]

1 Introduction

The dynamical model that describes the operations of complex berthing process in a single container terminal has been developed, as discussed in [2]. It also proposes a model predictive control (MPC)-based numerical optimization strategy, as opposed to the traditional first-come first-served (FCFS) in allocating berth position and quay crane (QC) to the set of arriving ships.

2 Modeling framework

We apply the case to one of the projects of the Government of Indonesia, so-called "the sea highway", that consists of six major seaports, as can be seen in Figure 1. Every seaport has different number of berth positions and QCs. We define an arc or a link as the connection path between two seaports. The number of containers moved and the transportation cost also differs among each link. For instance, the number of containers transported is the biggest in the Tg. Priuk-Tg. Perak-Tg. Priuk link. The data of seaports' equipment, container demand, and transportation cost is obtained from [1]. Our goal is to apply the different strategy (FCFS or MPC) applied to each seaport in the network and analyse the behavior of each strategy.
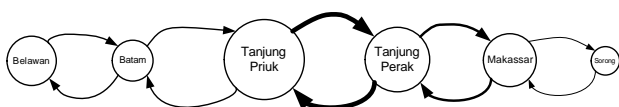
Figure 1: Six seaports of the "Indonesian sea highway". The diameter of each circle represents the size of the seaport, which directly relates to its number of berth positions and QCs. The directed arcs show the direction of container flows among seaports. The weigh of each arc represents the number of container flow between the particular two seaports.

3 Simulation results

A strategy of applying the MPC to all seaports may not be favorable to some of them, due to the fact that MPC allocation can lead dissatisfaction to their customers (ships). Hence, we try to apply the MPC strategy only to "important" links. The importance of each link is obtained from

Nagurney-Qiang (NQ) method, as cited in [3]. The result is presented in Table 1.

Table 1: Importance value of each link in the network based on Nagurney-Qiang method.

Link	Importance value	Rank of importance
Belawan-Batam-Belawan	0.085	3
Batam-Tg. Priuk-Batam	0.022	4
Tg. Priuk-Tg. Perak-Tg. Priuk	0.492	1
Tg. Perak-Makassar-Tg. Perak	0.398	2
Makassar-Sorong-Makassar	0.003	5

In Table 2, we can see the behavior of each strategy. The cost reduction is calculated from the traditional FCFS method. By applying MPC only to seaports in rank 1 and 2, its cost reduction does not much differ when compared to applying MPC to all seaports. We can further analyse that even by only applying MPC to seaports in rank 2, which has a relative big importance value, the cost reduction is still quite significant. This is an interesting behavior, that the optimal strategy can be wisely applied only to number of seaports instead to the entire seaports in the network.

Table 2: Network cost of each different strategy.

Scenario	Cost (Euro)
All seaports use FCFS	23,742,448
All seaports use MPC	20,292,606
Rank 1 & 2 use MPC, the rest use FCFS	20,695,268
Rank 1 use MPC, the rest use FCFS	21,245,822
Rank 2 use MPC, the rest use FCFS	21,791,657
Rank 3 use MPC, the rest use FCFS	23,432,178

References

[1]   The World Bank, State of Logistics Indonesia 2015.

[2]   R. T. Cahyono, E. J. Flonk, and B. Jayawardhana, "Dynamical modeling and predictive control of simultaneous berth and quay crane allocation," Preprint submitted.

[3]   A. Nagurney, Q. Qiang, and L. S. Nagurney, "Environmental impact assessment of transportation networks with degradable links in an era of climate change," Int. J. Sust. Transp., vol. 4, pp. 154–171, 2010.

Quality-aware control of perishable goods in transport networks

Xiao Lin, Rudy R. Negenborn and Gabriel Lodewijks
Maritime and Transport Technology, Delft University of Technology
Delft, The Netherlands
Email: {X.Lin, R.R.Negenborn, G.Lodewijks}@tudelft.nl

1 Introduction

Spoilage of fresh products can happen anytime due to the changing environmental conditions and the varying nature of perishables [1]. The transport of highly perishable goods is then critical for preserving the quality of products within supply chains. Food losses can be reduced via proper control strategies of logistics activities that use quality information of products. However, existing approaches do not consider product quality as an individual feature of each transport unit (e.g., a container) [2], ignoring the fact that the perishing feature can be different even for the same perishable product. We are therefore developing a modeling approach and a control strategy for perishables transport scheduling from a container perspective. We consider a number of containers that each needs to go through a series of transport stages (e.g. loading, shipping, etc.) before reaching their final destination. The control question is then at what time the containers should move from one transport stage to which next one, in order to have the highest quality at the destination. We also consider the handling time and the capacity for each stage due to efficiency and availability of handling equipments. Moreover, the quality of perishables can decrease at varying rates during the procedure of logistics.

2 System modeling and predictive control approach

A discrete time model of the perishables container transport process is proposed adopting a system and control perspective for logistic service providers. The containers are considered as dynamical components in the system, with state variables representing the stage they are in and the quality of the fresh products they carry. The stages they need to go through are represented by a directed graph $G = \{N, E\}$ for each container, with N the nodes representing possible stages and E the arcs representing possible transitions between stages. With each stage particular costs can be associated. Information of quality is considered as intrinsic attribute of each container and can be influenced in different ways in the different stages. The quality of the perishable goods is assumed to be non-negative. When entering a stage, the container is being handled by certain equipment. The handling time and capacity are limited by the equipment used in each stage. As a result the containers cannot move to the next stage before the handling is finished, and there can only be a maximum amount of containers being handled in a particular stage at the same time. The capacity and handling

time are hereby assumed to be static. It is moreover assumed that quality of the perishable goods in each container can be measured and that their quality decreases monotonically.

The controller measures the quality of fresh products in each container, and decides when and where to move the containers using a model predictive control philosophy: by solving an MIP problem with the objective of minimizing the total costs of all logistic activities and losses of quality for all containers.

3 Computational experiments and conclusions

To test the proposed approach, different scenarios are set up. We consider a particular transport system with three stages. Quality of perishable goods in each container can decrease at different rates. For comparison we apply a quality-unaware control strategy in which all containers are handled regardless of quality of the product they carry. The proposed control strategy shows that less costs can be achieved by proper scheduling the transport activity considering the information of quality. Therefore we can see the importance of involving quality information in perishables transport. As impacts of quality information in transport and logistics are being studied in more detail [3], more research is needed to further investigate the utilization of quality information in control strategies and interactions for different components of transport systems. This will enable a quality-oriented, intelligent transport system [4].

References

[1] M.A.J.S. van Boekel, 2008. "Kinetic modeling of food quality: a critical review." Comprehensive Reviews in Food Science and Food Safety 7(1): 144-158.

[2] A. Rong, R. Akkerman, and M. Grunow, 2011. "An optimization approach for managing fresh food quality throughout the supply chain." International Journal of Production Economics 131(1): 421-429.

[3] X. Lin, R.R. Negenborn, G. Lodewijks. "Quality-aware predictive scheduling of raw perishable material transports." In Proceedings of the 5th International Conference on Dynamics in Logistics (LDIC 2016), Bremen, Germany, 2016.

[4] X. Lin, R.R. Negenborn, and G. Lodewijks. "Survey on Operational Perishables Quality Control and Logistics." In Proceedings of the 6th International Conference on Computational Logistics. 398-421. Delft, The Netherlands, 2015.

Making stabilizing controllers track references for constrained linear systems

Veaceslav Spinu
Control Systems Group
Electrical Engineering Department
Eindhoven University of Technology
De Zaale, Flux building, Office 5.130
v.spinu@tue.nl

Mircea Lazar
Control Systems Group
Electrical Engineering Department
Eindhoven University of Technology
De Zaale, Flux building, Office 5.130
m.lazar@tue.nl

1 Available solutions and their limitations

Reference tracking under constraints is known to be difficult for classical control design methods. In last decades, Model Predictive Control (MPC) practically monopolized the constrained control applications. However, extension of the MPC to reference tracking with stability and recursive feasibility guarantees is not trivial, and in many cases too complex to implement. Reference governor approach [2] is a simpler solution to this problem, where a local stabilizing controller is designed disregarding constraints and wrapped into a reference adjustment loop. In this loop, an auxiliary reference trajectory is created which converges to the actual reference eventually, but ensures that the state and input trajectories satisfy constraints at all times. Although reference governors perform well for slowly varying references close to the nominal one, the performance close to constrains can be severely compromised.

Another constructive approach to constrained reference tracking by linear systems is proposed in [1]. There, the control action in the requested equilibrium state is interpolated with the control action in a suitably chosen state on the boundary of a positively invariant set for the system in the closed-loop with a nominal stabilizing controller. The interpolated control action ensures asymptotic convergence of the system state to the requested equilibrium which can be different from the nominal one. The downside of this approach is that the resulting control law is homogeneous for any given reference, and the nominal control action within the domain of attraction is not utilized, compromising the performance close to the equilibrium state.

2 Proposed approach

The control design method developed in this paper looks for inspiration to the reference governors and the method in [1], and provides a middle ground solution to the tracking problem, see [4] for the preliminary results. More exactly, the aim is to keep the locally optimal behavior of the reference governor, and enjoy high performance close to constrains where the method from [1] is more efficient. In this way, the tracking controller inherits the non-homogeneous nature of

stabilizing one and ensures asymptotic tracking of stepwise references without constraints violation.

Hereby, the method from [1] is extended via the reference governor approach to tracking references outside the domain of attraction of the initial stabilizing controller. Moreover, a new interpolation scheme is proposed which engages the states inside the domain of attraction, and consequently, passes the non-homogeneity property of the stabilizing controller to the tracking one.

Finally, the method is illustrated on the reference tracking problem in a synchronous buck power converter with two alternative designs for the stabilizing controller. The first design employs Hybrid Polytopic Partition (HPP) framework [3] and yields a discontinuous and non-homogeneous controller from a homogeneous control Lyapunov function. MPC is considered as an alternative with a non-homogeneous Lyapunov function for the nominal closed-loop system. Hence, the proposed approach is not limited by neither non-homogeneity of the stabilizing controller nor by the non-homogeneity of the Lyapunov function guaranteeing stability for the nominal closed-loop.

References

[1] F. Blanchini and S. Miani. Any domain of attraction for a linear constrained system is a tracking domain of attraction. *SIAM Journal on Control and Optimization*, 38(3):971–994, 2000.

[2] I. Kolmanovsky, E. Garone, and S. Di Cairano. Reference and command governors: A tutorial on their theory and automotive applications. In *American Control Conference*, pages 226–241, June 2014.

[3] V. Spinu and M. Lazar. Integration of real-time and stability constraints via hybrid polytopic partitions. In *Proceedings of IEEE Conference on Control Applications*, pages 226–233, Dubrovnik, Croatia, Oct. 2012.

[4] V. Spinu and M. Lazar. From non-homogeneous stabilizing control laws to tracking of constrained discrete-time linear systems. In *Proceedings of the 54th IEEE Conference on Decision and Control*, pages 264–269, Osaka, Japan, Dec. 2015.

Stability and Performance Analysis of Spatially Invariant Systems with Networked Communication

S.H.J. Heijmans, D.P. Borgers, and W.P.M.H. Heemels

Department of Mechanical Engineering, Eindhoven University of Technology

Eindhoven, 5600 MB The Netherlands

E-mail corresponding author: s.h.j.heijmans@tue.nl

1 Introduction

Many systems consist of interconnections of similar units or subsystems that only interact with their nearest neighbors [1]. One of the main underlying assumptions hereby often is that the communication between the subsystems is perfect, whereas in many applications this assumption does not hold. In such "networked" systems in which packet-based communication is used, network-induced artifacts such as time-varying transmission intervals (possibly due to packet losses or channel unavailability) are present next to scheduling protocols that determine which sensor, controller or actuator node is allowed to communicate at a transmission time. We study stability and performance for these networked systems by considering interconnections consisting of an infinite number of spatially invariant subsystems that use packet-based communication networks for the exchange of information.

2 A hybrid systems approach

We consider the system configuration as depicted in Fig. 1, consisting of an infinite number of subsystems or "basic building blocks" $\mathcal{P}(s)$ that are all identical and where the communication between the subsystems occurs via packet-based communication networks $\mathcal{N}(s)$ with $s \in \mathbb{Z}$, which captures the infinite spatial extent.
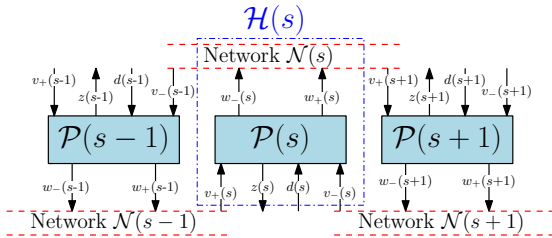
Figure 1: Infinite networked interconnection, where each plant $\mathcal{P}(s)$ has its own communication network $\mathcal{N}(s)$ to communicate with its neighbors, $s \in \mathbb{Z}$. The overall networked subsystem $\mathcal{H}(s)$ is the combination of the plant $\mathcal{P}(s)$ and its network $\mathcal{N}(s)$.

Inspired by [2], we can model each "networked" subsystem as a hybrid subsystem given by

$$\mathcal{H}(s): \begin{cases} \dot{\xi}(s) = F(\xi, d)(s), & \tau(s) \in [0, \tau_{mati}] \\ \xi^+(s) \in G(\xi(s)), & \tau(s) \in [\delta, \infty) \end{cases}, \quad (1)$$

where $\xi(s)$ is the state of the subsystem, $d(t, s)$ a (external) disturbance input, and $\tau(s)$ a timer, which is part of the state $\xi(s)$.

3 Stability and performance analysis

For the general setup of (1), *local* Lyapunov-based conditions (local in the sense that they only involve the *local* dynamics of one subsystem in the interconnection and information about the *local* communication network) are obtained, which lead to a bound on the maximally allowable transmission interval (MATI) τ_{mati} such that a *global* Lyapunov function guaranteeing UGES or $\mathcal{L}_p$-stability can be constructed for the overall *infinite-dimensional* interconnected system.

4 Example: A string of vehicles

We consider an infinite string of spatially invariant vehicles as in Fig. 2. To maintain a constant time headway h (time between the vehicles), wireless communication is used to transmit velocity, acceleration and jerk data from the vehicle at s to the following vehicle at $s + 1$.
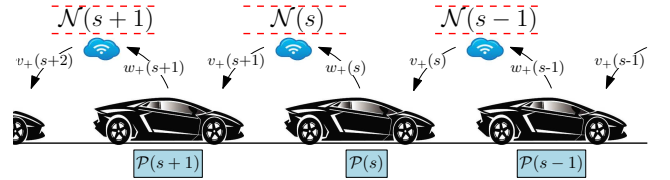
Figure 2: A string of vehicles.

Using the obtained stability analysis, values for τ_{mati} guaranteeing UGES of the infinite string are obtained. These are shown in Fig. 3 for various time headways.
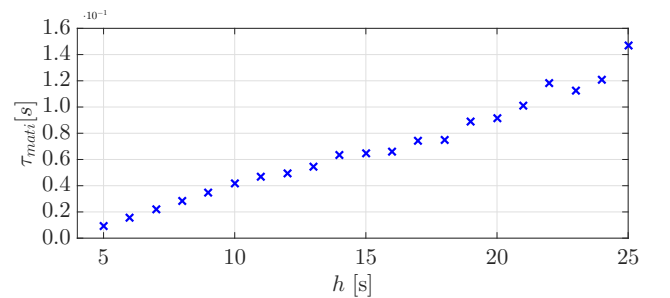
Figure 3: Upper bounds for τ_{mati} guaranteeing UGES.

References

[1]   R. D'Andrea and G.E. Dullerud (2003). Distributed control design for spatially interconnected systems. *IEEE Transactions on Automatic Control*, 48(9), 1478–1495.

[2]   Nešić, D. and Teel, A.R. (2004). Input-output stability properties of networked control systems. *IEEE Transactions on Automatic Control*, 49(10), 1650- 1667.

Controller design for flow networks of switched servers with setup times

Erjen Lefeber
Dynamics and Control Group
Department of Mechanical Engineering
Eindhoven University of Technology
A.A.J.Lefeber@tue.nl

1 Abstract

This work is concerned with the controller design for networks of switching servers with setup times, e.g. manufacturing systems or urban road networks (traffic light control). Control of these networks is difficult, since using controllers that are stable for a server in isolation might render the network unstable. Sofar, in literature, most people first propose a policy, and then study the resulting behavior of the network under this policy.

In this work we propose an entirely different way of looking at the problem of controlling a network of switching servers with setup times. Instead of starting from a policy and then analyzing the proposed policy, we start from a priori specified desired network behavior. Using this desired behavior for the network under consideration as a starting point, we look for a policy which guarantees convergence of the system towards this desired behavior.
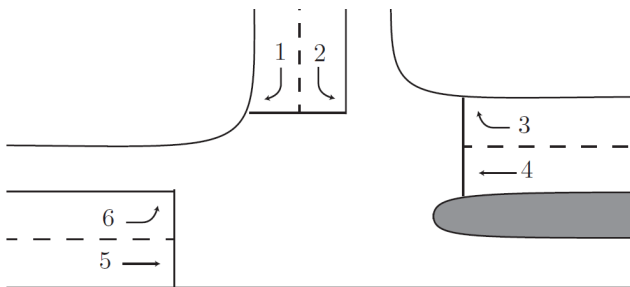
Figure 1: A T-junction

As an example consider the traffic light control of an isolated intersection, see Figure 1.

Before we develop a controller for this intersection we first determine an optimal periodic fixed time schedule using a novel group-based approach. By adding an objective function to the mathematical model of [1], we can obtain a mixed integer programming problem (MIP). Solving this MIP results in a periodic schedule as depicted in Figure 2.

Next step is to determine a controller which stabilizes the system towards this given optimal periodic orbit. The pro-
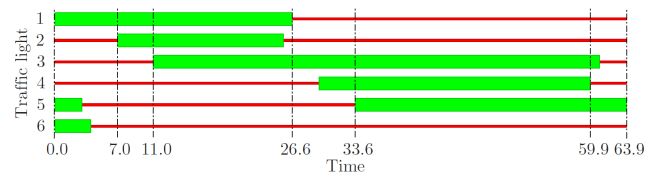
Figure 2: Optimal periodic schedule for the T-junction

posed controller periodically repeats the phases of the periodic orbit, where each phase is equipped with its phase control rule which determines when a phase ends. Such a phase control rule implies a dynamical operator which maps the state at the beginning of a phase to the state at the end of a phase. The monodromy operator is a similar map for the entire cycle. We propose phase control rules which are such that not only the optimal periodic orbit is a fixed point of the monodromy operator, but also all solutions converge to this fixed point. To that end we use the ideas presented in [2]. This approach can also be applied in a network setting for manufacturing systems where we have control over the service rate.

Future work consists of extending the optimization approach for determining optimal periodic behavior from an isolated intersection to a network of intersections. Also, we are looking for suitable phase control rules in case we have no control over the service rate, as typically is the case in the setting of traffic light control.

References

[1] P. Serafini and W. Ukovich. A mathematical model for periodic scheduling problems. *SIAM Journal on Discrete Mathematics*, 2(4):550–581, 1989.

[2] V. Feoktistova, A. Matveev, E. Lefeber, J.E. Rooda, Designs of optimal switching feedback decentralized control policies for fluid queueing networks, *Mathematics of Control, Signals, and Systems* 24, 477–503, 2012.

Stabilization with guaranteed safety via IDA-PBC

Muhammad Zakiyullah Romdlony
Engineering and Technology Institute Groningen
University of Groningen
Nijenborgh 4
9747 AG Groningen
The Netherlands
Email: M.Z.Romdlony@rug.nl

Bayu Jayawardhana
Engineering and Technology Institute Groningen
University of Groningen
Nijenborgh 4
9747 AG Groningen
The Netherlands
Email: B.Jayawardhana@rug.nl

1 Abstract

In this work, we study the problem of stabilization with guaranteed safety for affine nonlinear system. We extend the idea of IDA-PBC (Interconnection and Damping Assignment - Passivity-Based Control) technique to solve this problem. In particular, we show that the desired equilibrium of the closed-loop system is asymptotically stable and the state trajectories stay away from the given unsafe state.

2 Incorporating safety aspect into IDA-PBC

Energy is common notion that widely used in all domain of systems. One of the well-known energy-based controller is IDA-PBC (Interconnection and Damping Assignment - Passivity-Based Control). In IDA-PBC, the energy exchange between physical elements and the dissipated energy are encapsulated in the interconnection and damping matrices in the port-Hamiltonian framework.

We investigate the generalization of IDA-PBC to solve the problem of stabilization with guaranteed safety. Here, safety means that all admissible state trajectories do not violate system constraints or enter a set of unsafe states. The incorporation of safety aspect into the stabilization of the closed-loop system has been considered before in [2, 6, 4, 1, 5]. In [4, 1, 5], the well-known Control Lyapunov Function-based control method is combined with the Control Barrier Function-based control method which is proposed in [7] to solve the problem. The proposed control method in [4, 5] does not impose unboundedness of energy function on the boundary of the set of unsafe states as imposed in [2, 6].

We propose an energy-based method for solving this problem that offers a nice energy interpretation. The main approach behind our proposed method is to assign a desired energy function such that it has a minimum at the desired equilibrium point and has local maxima in the set of unsafe states. Thus with an appropriate interconnection and damping matrices, the closed-loop system will converge to the minima (that includes the desired one) while avoiding the region of concavity where the unsafe state belongs to. If the minimum is not unique, this approach results in local stability with guaranteed safety. To obtain the global result, we propose a hybrid control strategy that combines the global stability result of IDA-PBC with respect to the set of equilibria and another state-feedback controller that can steer the system from the set of undesired equilibria to the desired one.

References

[1] A. D. Ames, J. W. Grizzle, P. Tabuada,"Control Barrier Function based Quadratic Programs with Application to Adaptive Cruise Control," *IEEE Conf. on Dec. and Contr.*, Los Angeles, 2014.

[2] K. B. Ngo, et al,"Integrator backstepping using barrier functions for systems with multiple state constraints," *IEEE Conf. on Dec. and Contr. & Eur. Contr. Conf.*, pp. 8306-8312, Sevilla, 2005

[3] R. Ortega et.al. "Interconnection and Damping Assignment Passivity-Based Control of Port Controlled Hamiltonian Systems," *Automatica*, Vol. 38, pp. 585-596, 2002.

[4] M. Z. Romdlony & B. Jayawardhana, "Uniting Control Lyapunov and Barrier Function," *IEEE Conf. on Dec. and Contr.*, Los Angeles, pp. 2293-2298, 2014.

[5] M. Z. Romdlony & B. Jayawardhana, "Stabilization with Guaranteed Safety Using Control Lyapunov-Barrier Function," *Automatica*, vol. 66, pp. 39-47, 2016.

[6] K. P. Tee, S. S. Ge, E. H. Tay, "Barrier Lyapunov Functions for the Control of Output-Constrained Nonlinear Systems," *Automatica*, vol. 45, no. 4, pp. 918-927, 2009.

[7] P. Wieland & F. Allgöwer, "Constructive safety using control barrier functions," *IFAC Symp. Nonlin. Contr. Syst.*, pp. 473-478, Pretoria, 2007.

Practical optimal state regulation of distribution networks with input constraints

Tjardo Scholten
Department of ENTEG
University of Groningen
Nijenborgh 4
9747 AG Groningen
t.w.scholten@rug.nl

Claudio De Persis
Department of ENTEG
University of Groningen
Nijenborgh 4
9747 AG Groningen
c.de.persis@rug.nl

Pietro Tesi
Department of ENTEG
University of Groningen
Nijenborgh 4
9747 AG Groningen
p.tesi@rug.nl

We consider a network of physically interconnected dynamical systems for which the goal is to solve an optimal regulation problem in the presence of input saturation. Based on Lyapunov arguments we propose distributed controllers which guarantee global practical convergence to the desired optimal steady state.

1 Model

Inspired by [1], we consider a network of physically linked undamped dynamical systems which can be represented by a graph $\mathscr{G} = (\mathscr{E}, \mathscr{V})$, where $|\mathscr{E}| = m$ and $|\mathscr{V}| = n$. This graph is represented by a incidence matrix $B \in \mathbb{R}^{n \times m}$ and each node i has an input $(u_p)_i$ and a disturbance d_i, along with a state variable x_i, which may represent a storage level. The edges $\mathscr{E}$ represent transportation links, which interconnect the nodes, and we denote the flow on link j by $(u_e)_j$. The dynamic model is as follows:

$$\dot{x} = Bu_e + u_p + d$$
$$y = x - \bar{x},$$

where $x, u_p, y \in \mathbb{R}^n$, $u_e \in \mathbb{R}^m$ and $d \in \mathbb{R}^n$. The input u_p and the flow rates u_e are considered to be controllable inputs and the disturbance d is regarded as an unknown constant. Finally, we regard $\bar{x} \in \mathbb{R}^n$ as the desired setpoint for x.

2 Optimality

Building upon [2], we consider a control problem in which we desire that distributed controllers convergence to an optimal steady state. To this end we define the optimal steady state as the solution of an optimization problem. The cost function we consider is given by

$$C(u_p) = s + r^T u_p + \frac{1}{2} u_p^T Q u_p,$$

where $s \in \mathbb{R}$, $r \in \mathbb{R}^n$ and $Q \in \mathbb{R}^{n \times n}$. Furthermore we want the total disturbance to match the total input at steady state, *i.e.* $\mathbb{1}_n^T(u_p - d) = 0$. For this reason we consider the following optimization problem:

$$\underset{u_p}{\text{minimize}} \quad C(u_p)$$
$$\text{subject to} \quad \mathbb{1}_n^T(u_p + d) = 0.$$

This implies, after standard calculation, that the optimal steady state is characterized as

$$\bar{u}_p = -Q^{-1}\left(\mathbb{1}_n \frac{\mathbb{1}_n^T(d - Q^{-1}r)}{\mathbb{1}_n^T Q^{-1} \mathbb{1}_n} + r \right). \tag{1}$$

3 Main result

On top of optimality condition (1), we consider a heterogeneous saturation on both u_e and u_p. In particular, we enforce positivity constraints on the link flows, *i.e.* the network is restricted to unidirectional flows. This results in the following control problem:

Problem. *Design distributed controllers that regulate the flows on the edges u_e and input u_p at the nodes such that*

$$\lim_{t \to \infty} ||x - \bar{x}|| \le \varepsilon_1$$
$$\lim_{t \to \infty} ||u_p - \bar{u}_p|| \le \varepsilon_2,$$

for any given positive arbitrarily small numbers ε_1 and ε_2, where $\bar{u}_p$ is as in (1) and $\bar{x} \in \mathbb{R}^n$ is a given constant setpoint for x, and

$$u_p^- \le u_p \le u_p^+$$
$$0 \le u_e \le u_e^+,$$

for all $t \ge 0$.

We provide two distributed controllers, one that regulates the input on each node and one that controls the flows on the edges. Finally we provide sufficient conditions for global asymptotic practical stability based on Lyapunov arguments.

References

[1] J. Wei and A. van der Schaft, "Load balancing of dynamical distribution networks with flow constraints and unknown in/outflows," *Systems & Control Letters*, vol. 62, no. 11, pp. 1001–1008, 2013.

[2] S. Trip, M. Bürger, and C. De Persis, "An internal model approach to (optimal) frequency regulation in power grids with time-varying voltages," *Automatica*, vol. 64, pp. 240 – 253, 2016.

Stabilization of collocated systems by nonlinear boundary control

Hans Zwart

Department of Applied Mathematics,
University of Twente, P.O. Box 217, 7500AE Enschede,
The Netherlands
h.j.zwart@utwente.nl
and
Dynamics and Control,
Technische Universiteit Eindhoven,
P.O. Box 513
5600 MB EINDHOVEN,
H.J.Zwart@tue.nl

Ruth Curtain
Bernoulli Institute for Mathematics and Computer Science,
University of Groningen, P.O. Box 407, 9700AK Groningen,
The Netherlands
r.f.curtain@rug.nl

1 Abstract

A popular way of stabilizing beam-like models is to apply collocated control and measurement action. In many cases, by a suitable choice of an extended state space, even collocated systems with boundary control action can be formulated as systems with bounded control. This results in a state linear system $\Sigma(A, B, B^*, 0)$ on the state space Z, where A the infinitesimal generator of a contraction C_0-semigroup and $B \in \mathscr{L}(U, Z)$, U is another Hilbert space.

For the above class of systems we show that non-linear damping will result in a globally asymptotically closed loop system, provided that the linearized control law will ensure asymptotic stability.

To illustrate our approach we use an example of Slemrod [2]. It was motivated by the SCOLE-related model from Bailey and Hubbard [1] of one of the arms of a satellite, consisting of a central hub with four flexible beams attached to it.

References

[1]   T. Bailey and J.E. Hubbard. Distributed piezoelectric polymer active vibration control of a cantilever beam. *J. Guidance Control and Dynamics*, **8**, pp. 605-611, 1985.

[2]   M. Slemrod. Feedback stabilization of a linear control system in Hilbert space with an a priori bounded control dynamical systems, *Mathematics of Control, Signals and Systems*, **2**, pp. 265-285, 1989.

Convergence analysis of a positive stabilization scheme
for a discretized diffusion system

Jonathan N. Dehaye, Joseph J. Winkin
Namur Center for Complex Systems (naXys) and Department of Mathematics
University of Namur, 8 Rempart de la Vierge, B-5000 Namur, Belgium
Email: jonathan.dehaye@unamur.be, joseph.winkin@unamur.be

1 Framework

A pure diffusion system is discretized by means of the finite difference method. The resulting finite-dimensional system belongs to a class of systems for which it is possible to parameterize all positively stabilizing feedbacks. A feedback (row) matrix k is said to be positively stabilizing for such system if the resulting closed-loop system is positive and internally (exponentially) stable. The convergence of the feedback control scheme is then studied in order to extend the latter to the nominal system. The analysis involves positive control theory [1], consistency and stability study of the numerical scheme [2], and state space approach [3].

2 Main result

The considered pure diffusion system is described by the parabolic partial differential equation

$$\frac{\partial x}{\partial t} = D_a \frac{\partial^2 x}{\partial z^2}$$

with Neumann boundary conditions

$$\begin{cases} \frac{\partial x}{\partial z}(t,0) & = & u(t) \\ \frac{\partial x}{\partial z}(t,L) & = & 0 \end{cases}$$

where D_a is the axial dispersion coefficient, L is the domain length and u is the input. Discretizing the system by means of the finite difference method (with n discretization points z_i, $i = 1,...,n$) leads to a finite-dimensional approximating system. Both the nominal system and the discretized one are positive and unstable. First we parameterize the set of all (infinitely many) feedbacks that positively stabilize the approximating system, then we show the convergence of the finite difference scheme by use of a standard approach and, for a specific given feedback, by state space approach. This method leads to a positive and stable closed-loop PDE system with boundary control of state feedback type $u(t) = \kappa x(t,0)$.

3 Numerical simulations

The parameterization has been coded in MATLAB as an algorithm that provides the user with positively stabilizing feedbacks for the discretized system for a sufficiently small discretization step. The numerical results are dependent upon the choice of parameter values. For example, considering $L = 1$, $D_a = 1$ and $n = 21$ and choosing the all-ones eigenvector corresponding to the Frobenius unstable eigenvalue

$\lambda = 0$ as initial condition yields the state trajectories shown in Figure 1, which illustrate that the closed-loop system is positive and that it is stable unlike the open-loop system.
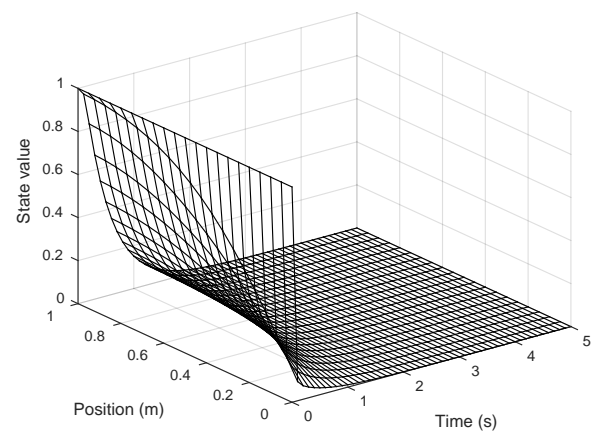
Figure 1: State trajectories in closed-loop

4 Perspectives

Next steps in this work are - among others - to find conditions so that the discretized feedback automatically converges to a positively stabilizing feedback for the nominal PDE system, to optimize the choice of a positively stabilizing feedback with respect to some given criterion, to design observer based compensators and to apply the results to a specific interesting application (bioreactor models, population dynamics models,...). These questions are currently under investigation.

References

[1]   J. N. DEHAYE and J. J. WINKIN. Parameterization of Positively Stabilizing Feedbacks for Single-Input Positive Systems. [Submitted].

[2]   P. J. FREY. The finite difference method, https://www.ljll.math.upmc.fr/frey/ftp/finite-differences.pdf. 2009. [Online; accessed 13-January-2016].

[3]   Z. EMIRSJLOW and S. TOWNLEY. From PDEs with boundary control to the abstract state equation with an unbounded input operator: A tutorial. *European Journal of Control*, 6:2749. 2000.

Comparison of Stabilization of Piezoelectric Euler-Bernoulli Beam Models

M.C. de Jong and J.M.A. Scherpen

Faculty of Mathematics and Natural Sciences, University of Groningen

{matthijs.de.jong, j.m.a.scherpen}@rug.nl

K.A. Morris

Department of Applied Mathematics, University of Waterloo

kmorris@uwaterloo.ca

1 Introduction

Piezoelectric materials are used in many control and sensing applications via a strip of piezoelectric material also known as a piezoelectric beam. Applications can be vibration control in (complex) mechanical structures and on-line measurement or compensation in high-precision technology for shape control of beams and surfaces. To manipulate or observe the electric-field of the beam, a plate capacitor can be used, see Fig. 1. The behavior of piezoelectric beams depends on the interaction between the electrical, magnetic and mechanical effects and is non trivial. Many different assumptions for the mechanical part of the beam and the electric-field can be used. For stabilization, and more generally, controller design, a finite-dimensional approximation must be used.

2 Approach

In this work the linear Euler-Bernoulli model [2] for the mechanical behavior is used with both the quasi-static electric-field assumption [4] and the dynamic electromagnetic-field assumption, described by both [6] and [8] in different frameworks. The abstracted mathematical models are put in the port-Hamiltonian (pH) framework [7]. Subsequently, the spatial-discretization procedure, described in [3], is applied for further analysis and results again in a pH-system.

3 Contribution

The contribution of this work is the investigation of the influence of the type of approximation on stabilization and controlled system performance. The obtained models are compared to other (pH) models, described in [1], [5], and [6] on the basis of different modeling assumptions and their influence on stabilization and controllability for the infinite- and finite-dimensional systems. The stability properties of the approximated linear pH-models are investigated and compared to the original infinite-dimensional model. The energy functions of the various models are also compared.
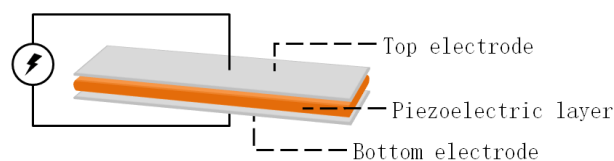
Figure 1: Piezoelectric beam depiction

References

[1]   T. Voß and J.M.A Scherpen, *Structure preserving port-Hamiltonian discretization of a 1-D inflatable space reflector*, Proc. of the European Control Conference, 2009

[2]   E. Carrera, G. Giunta, and M. Petrolo, *Beam Structures: Classical and Advanced Theories*, Wiley Series in Computational Mechanics Series, Wiley, 2011.

[3]   G. Golo, V. Talasila, A.J. van der Schaft, and B. Maschke, *Hamiltonian discretization of boundary control systems*, Automatica, vol 40, no. 5, pp 757 - 771, 2004.

[4]   A. H. Meitzler et al., *IEEE Standard on Piezo-electricity*, ANSI/IEEE Std 176-1987, 1988.

[5]   K.A. Morris and A.Ö. Özer, *Strong Stabilization of piezoelectric beams with magnetic effects*, Proc. of the Conference on Decision and Control, 2013.

[6]   K.A. Morris and A.Ö. Özer, *Modeling and Stabilizability of Voltage-Actuated Piezoelectric Beams with Magnetic Effects*, SIAM Journal on Control and Optimization, vol. 52, pp 23712398, 2014.

[7]   A.J. van der Schaft and D. Jeltsema, *Port-Hamiltonian Systems Theory: An Introductory Overview*, Foundations and Trends in Systems and Control, vol. 1, no. 2-3, pp. 173378, 2014.

[8]   T. Voß, *Port-Hamiltonian Modeling and Control of Piezoelectric Beams and Plates: Application to Inflatable Space Structures*, Ph.D. dissertation, FWN, RuG, Groningen, 2010.

Thermal control in wafer scanners using high complexity models

R.W.H. Merks[1]   M.B.I. Habets[1]   S. Weiland[1]
r.w.h.merks@tue.nl   m.b.i.habets@tue.nl   s.weiland@tue.nl

[1]Department of Electrical Engineering, Eindhoven University of Technology
P.O. Box 513, 5600 MB Eindhoven, The Netherlands

1 Introduction

The performance of ASML's wafer scanners is mainly measured in terms of speed and resolution. The company is therefore aiming at reducing feature sizes on chips, while at the same time increasing machine throughput. As a result error margins become smaller, while both the power and bandwidth of signals increase.

Thermally induced deformations of various components are a significant source of errors in wafer scanners [1] [2]. In practice, low complexity models are used for real time control purposes, because high complexity models are generally not fast enough. These low complexity models have a limited accuracy, which therefore limits the system performance. For this reason the use of high resolution, multiphysics models for control purposes is proposed.

2 Modeling of heat transfer and thermal expansion

Thermal diffusion is described by a partial differential equation, which can be described by an infinite dimensional system. A finite dimensional approximation of these systems can be created using the finite elements method. For linear thermal expansion the thermally induced deformations z can be modeled by a linear mapping of the temperature states T, which is described by $z = AT$. In order for these models to be accurate, generally $\gg 10^4$ states are required, which leads to slow and complex models. Because of this, these models are generally only used for simulation and analysis purposes [3].

3 Control based on low complexity models

Consider the system interconnection in Fig. 1. The plant is subject to disturbances d (e.g. heat fluxes), has inputs u (e.g. heater power set-points) and measured outputs y (e.g. measured temperatures). The deformations z cannot be measured continuously.

In general, low order lumped elements models are used in thermal control. These low order models describe thermal behavior relatively well, but lack the spatial resolution required to determine the resulting deformations z accurately. For this reason the control objective is defined on y, which can be measured accurately [3]. With this approach, some norm on the deformations $||z||$ is reduced by reducing $||T||$.
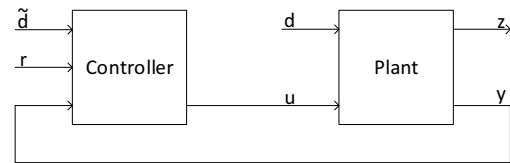
Figure 1: Assumed closed-loop system interconnection

4 The advantage of high complexity models

High complexity models on the other hand are capable of determining the deformations z accurately. Therefore, it is possible to reduce $||z|| = ||AT||$ directly. In this way the entire null space of A can be utilized instead of just working towards the trivial solution $||T|| = 0$. Moreover, in some cases it is desired to minimize a weighted norm of z. As a result, extra freedom in the control of the temperature states is introduced, which can be used to improve the controlled system performance.

5 Future Work

For control of thermally induced deformations, high complexity models can theoretically be used to increase the system performance. However, these models are generally not fast enough. Model reduction can be used to overcome this problem, but utilizing these reduced models for real time control is not trivial [2]. As a first step, model reduction for this type of systems will therefore be investigated. The aim is to develop an accurate thermo-mechanical model that is $5-10$ times faster than real time.

References

[1] M. Habets, R. Merks, S. Weiland, and W. Coene, "A multiphysics modeling approach for thermal aberration prediction and control in extreme ultraviolet lithography," in Imaging and Applied Optics 2015, 2015, p. AOM4B.2.

[2] C. Bikcora, S. Weiland, and W. M. J. Coene, "Reduced-order modeling of thermally induced deformations on reticles for extreme ultraviolet lithography," in American Control Conference (ACC), 2013, 2013, pp. 55425549.

[3] H. Thompson and K. Vogiatzis, "Heat balance and thermal management of the TMT Observatory," 2014, vol. 9150, p. 915012.

Continuous compliance compensation of position-dependent flexible structures

Nikolaos Kontaras
TU/e P.O. Box 513
5600 MB Eindhoven,
GEM-Z -01.144
The Netherlands
n.kontaras@tue.nl

Marcel Heertjes
TU/e, P.O. Box 513
5600 MB Eindhoven,
GEM-Z -01.144
The Netherlands
m.f.heertjes@tue.nl

Hans Zwart
UT, P.O. Box 217
7500 AE Enschede,
Zi - 3062
The Netherlands
h.j.zwart@utwente.nl/h.j.zwart@tue.nl

1 Abstract

The implementation of lightweight high-performance motion systems in lithography and other applications imposes lower requirements on actuators, amplifiers and cooling. However, the decreased stiffness of lightweight designs increases the effect of structural flexibilities especially when the point of interest is not at a fixed location. This is for example occurring when positioning a silicon wafer during exposure. The present work addresses the problem of compliance compensation in flexible structures, when the performance location is time-varying. The compliance is derived using the frequency domain representation of the solution of the partial differential equation (PDE) describing the structure, which yields its exact compliance function. The advantage is that an exact function at every position of the structure is obtained, without the need for interpolation.

During the production of silicon chips, a silicon wafer is placed on top of the wafer stage of the lithographic system. A source emanating extreme ultraviolet (EUV) light passes through the reticle stage containing the blueprint, and an optical column with projection lenses, before it exposes the photo-sensitive layers of the wafer's surface. Assuming that the wafer stage is a lightweight structure, i.e. its dynamics are dependent substantially on position, during exposure the time-varying performance location induces time-varying dynamics, which need to be compensated.

The contribution in this work is twofold. Firstly, it introduces a position-dependent compliance compensation method which accounts for the compliant part of the flexible dynamics in motion systems, including cases with a time-varying performance location, a situation met during wafer exposure. A second contribution is that the spatially continuous dynamics of the flexible structure (Euler-Bernoulli beam) is derived from a partial differential equation (PDE) describing this beam. The PDE representation is exploited to derive the position-dependent compliance function of the beam, which gives the exact compliance on every position. The method is validated in a continuous-time simulation environment, using a simulation model containing a single flexible mode, corrected to obtain the compliance of the original infinite-dimensional model.

References

[1] S.O. Reza Moheimani, Dunant Halim, Andrew J. Fleming, *Spatial Control of Vibration*, World Scientific, 2003.

[2] Leopold Herrmann, *Vibration of the Euler-Bernoulli Beam with Allowance for Dampings*, Proceedings of the World Congress on Engineering, 2008.

[3] Ruth Curtain, and Kirsten Morris, *Transfer Functions of Distributed Parameter Systems:A Tutorial*, Automatica, Volume 45, Issue 5, May 2009, Pages 1101-1116, ISSN 0005-1098.

[4] G. E. Moore, *Cramming more components on integrated circuits*, Electronics, vol. 38, no. 8, pp. 13, 1965.

[5] M. Boerlage, *MIMO jerk derivative feedforward for motion systems*, in American Control Conference, 2006, pp. 38923897.

[6] J. J. M. van de Wijdeven, *Iterative learning control design for uncertain and time-windowed systems*, Ph.D. dissertation, Eindhoven University of Technology, 2008.

[7] P. Lambrechts, M. Boerlage, and M. Steinbuch, *Trajectory planning and feedforward design for electromechanical motion system*, Control Engineering Practice, vol. 13, no. 2, pp. 145157, 2005.

[8] Michael Ronde, John van den Bulk, René van de Molengraft, and Maarten Steinbuch, *Feedforward for flexible systems with time-varying performance locations*, American Control Conference (ACC), 2013 , vol., no., pp.6033,6038, 17-19 June 2013.

[9] R.F. Curtain, and H.J. Zwart, *An Introduction to Infinite-dimensional Linear Systems Theory*, Berlin: Springer, Verlag, 1995.

Boundary information in a Proper Petrov-Galerkin projection for linear partial differential equations

Bart Tiemersma
Control Systems Group
Department of Electrical Engineering
Eindhoven University of Technology
b.j.m.tiemersma@student.tue.nl

Edwin Insuasty
Control Systems Group
Department of Electrical Engineering
Eindhoven University of Technology
e.g.insuasty.moreno@tue.nl

Siep Weiland
Control Systems Group
Department of Electrical Engineering
Eindhoven University of Technology
s.weiland@tue.nl

1 Introduction

In model order reduction, the Petrov-Galerkin projection [1] of linear partial differential equations (PDEs) faces two different problems. On the one hand, there is not a systematic methodology for the selection of the residual projection subspace. This fact has influenced the advent of a particular case of Petrov-Galerkin (the Galerkin-based projections) where the residual and the solution projection spaces are equual [2]. On the other hand, the Petrov-Galerkin projections lack of a systematic procedure for the inclusion of boundary information in the construction of the reduced order model.

In this work, we introduce new developments in both aspects. Firstly, we have introduced the concept of Proper Residual Projection for Petrov-Galerkin methods where the selection of the optimal residual projection is translated into an optimization problem. Secondly, Dirichlet and Neumann boundary conditions are included in the reduced order formulation by a successive application of the Gauss theorem. The methodologies have been tested for the projection of a parabolic PDE. For this application case, the numerical results indicates that the proper residual projection generates a stable reduced-order dynamical system that resembles accurately the behavior of the original PDE.

2 A proper residual projection

Here we select a residual projection space (*test space*) such that the residual seminorm of the projected (and finite dimensional) solution of the PDE onto the signal space is minimized. Let $R(u)$ be a residual operator and let the solution of a PDE u satisfy $R(u) = 0$. Let the projection of u into the signal space to be denoted by $u_h = \Phi a$. Then, we select a test space that minimizes the following cost function:

$$J(u_h) = \|u_h\|_R^2 = \|R(\Phi a)\|^2 \qquad (1)$$

A global minimum can be found by applying optimality conditions on the previous optimization problem.

3 Boundary conditions in the reduced order model

It is well understood that a weak formulation of PDEs, and an application of the Gauss theorem may naturally include the Neumann boundary conditions in the reduced-order formulation [3]. Neumann boundary conditions correspond to values of the vector field defined by the gradient of u at the boundaries, and as the Gauss theorem relates the divergence of a vector field inside a domain with the vector field itself at the boundary, the treatment of Neumann information in the reduced order formulation is straightforward. The case of Dirichlet boundary conditions is more delicate. However, with a proper algebraic modification, Dirichlet information can be treated as any other type of boundary condition in the weak formulation of the PDE.

4 Conclusions

We have proved that there exists a test space the minimize the residual norm of the signal projection, in addition we present a methodology to include Dirichlet and Neumann boundary conditions in the reduced order formulation. These results aim to establish a systematic methodology for system projections and model order reduction of linear PDEs.

References

[1]   A. Antoulas, *Approximation of Large-Scale Dynamical Systems*, Society for Industrial and Applied Mathematics (2005).

[2]   S. Brenner and L. Scott, *The Mathematical Theory of Finite Element Methods*, Springer, New York (2008).

[3]   H. Elman H., D. Silvester and A. Wathen, *Finite elements and fast iterative solvers: with applications in incompressible fluid dynamics*, Oxford University Press, London (2014).

Model Order Reduction of Li-ion Batteries via POD and DEIM

Zhi Li, Tijs Donkers, Dmitri Danilov, Henk Jan Bergveld
Control Systems group, Department of Electrical Engineering
Eindhoven University of Technology, P.O. Box 513, 5600 MB Eindhoven, Netherlands
Email: {Zhi.Li,M.C.F.Donkers,D.G.Danilov,H.J.Bergveld}@tue.nl

1 Introduction

Li-ion batteries are commonly employed in various applications owing to their high energy density and long service life. Li-ion battery models are used for analyzing batteries and enabling power control in applications. The Doyle-Fuller-Newman (DFN) model is a popular one, which represents relevant solid-state and electrolyte diffusion dynamics and accurately predicts current/voltage response. Unfortunately, solving the full DFN model requires significant computation time, which prohibits using it in real-time applications. The objective of the present work is to apply Model Order Reduction (MOR) techniques to obtain a Reduced-Order Model (ROM) for the DFN model. The ROM is expected to give considerable reduction in computation time, while preserving the accuracy of the input/output behavior.

2 Mathematical Modeling of the Lithium-ion Batteries

The DFN model is a physics-based electrochemical battery model, which is composed of several Partial Differential Equations (PDEs) describing the physics of the Li-ion concentrations and conservation of charge in both the solid and electrolyte phases along with the Butler-Volmer equation describing surface kinetic limitations [1]. Analytically solving this set of nonlinear PDEs is not possible. Still, spatial and temporal discretization methods, e.g., the finite-volume method and the Euler method, respectively, can be applied to obtain solutions by solving algebraic equations of the form:

$$Ax(t) + f(x(t)) = 0, \tag{1}$$

where $A \in R^{n \times n}$, $x(t) \in R^n$, and $f(\cdot)$ is a nonlinear function. The numerical solution can be obtained by solving (1) recursively. However, the discretized model generally contains a large number of states, leading to long computation time, which renders the model unsuited for real-time application. Therefore, MOR can be applied to reduce the order n in (1).

3 Model Order Reduction

The aim of MOR techniques is to generate a model of the system with $k \ll n$ states, while still accurately describing the behavior of the original system. Many MOR strategies are based on projecting the states of the original system onto a suitably selected reduced-order state space. Among available MORs, the Proper Orthogonal Decomposition (POD)

has been commonly used. By projecting (1) onto $V \in R^{n \times k}$ based on POD method, (1) becomes

$$V^T AVx(t) + V^T f(Vx(t)) = 0. \tag{2}$$

The term $V^T AVx(t)$ in (2) is now of low dimension. However, $f(Vx(t))$ still requires n function evaluations. The discrete empirical interpolation method (DEIM), therefore, is able to reduce the order of $f(Vx(t))$. The approximation from projecting $f(\tau)$ onto the subspace is of the form

$$f(\tau) \approx Uc(\tau), \tag{3}$$

where $U = [u_1, \ldots, u_m] \in R^{n \times m}$ and $c(\tau)$ is the corresponding coefficient vector. The coefficient vector $c(\tau)$ is obtained by the DEIM algorithm [2].

In this work, the POD and the DEIM approaches are combined and applied to the DFN model, leading to a model that has small computation time. Moreover, it is possible to trace key physical variables by backward projection. Several ROMs with different reductions k, m are obtained. In the original system, $n = 368$ is selected, which takes 795 s to run the simulation from SOC 100% to SOC 0%. In the POD-DEIM algorithm, $k = 2$ and $m = 4$ is finally selected, which takes only 17 s to run the simulation. Figure 1 illustrates behavior of full and ROM. The normalized root mean square error between the output voltage of original model and ROM is $1.9 \cdot 10^{-3}$.
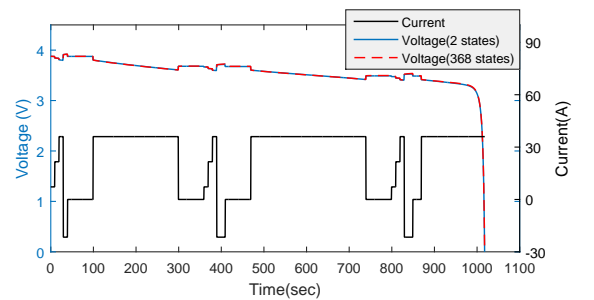
Figure 1: Full and reduced-order model simulation results

References

[1] K. Smith, C.D. Rahn, and C-Y. Wang, Control oriented 1D electrochemical model of lithium ion battery, Energ. Convers. Manage., 48, 2565–2578, 2007.

[2] S. Chaturantabut and D. C. Sorensen, Nonlinear model reduction via discrete empirical interpolation, SIAM J. Sci. Comput., 32, 2737–2764, 2010.

On Approximation of Linear Network Systems

Xiaodong Cheng, Jacquelien M.A. Scherpen
Faculty of Mathematics and Natural Science
University of Groningen
Nijenborgh 4, 9747 AG Groningen
The Netherlands
Email: {x.cheng,j.m.a.scherpen}@rug.nl

Yu Kawano
Graduate School of Informatics
Kyoto University
Sakyo-ku, Kyoto 606-8501
Japan
Email:ykawano@i.kyoto-u.ac.jp

Structure-preserving model reduction of network systems is investigated. The underlying system is defined on a connected undirected graph and given as

$$\begin{cases} M\dot{x} = -Lx + Bu, \\ y = x. \end{cases} \quad (1)$$

In the model, $L \in \mathbb{R}^{n \times n}$ is the so-called *graph Laplacian* associated with a connected undirected graph. $x \in \mathbb{R}^n$ and $M := \mathrm{diag}\,(m_1, m_2, \cdots, m_n) \in \mathbb{R}^{n \times n}$. $u \in \mathbb{R}$ is the external input. This kind of system can easily become a high dimensional system with a growing number of nodes. Therefore, one of the important issue concerns model reduction.

Note that the graph topology is uniquely determined by the structure of its Laplacian matrix [1]. Thus, it is crucial to preserve the properties of L in the reduced-order model. In [1], we propose a model reduction procedure using clustering-based projection

$$x(t) \approx P\hat{x}(t), \quad (2)$$

where $\hat{x} \in \mathbb{R}^r$ and $P \in \mathbb{R}^{n \times r}$. P is generated by the result of clustering. The main idea of such clustering process is first to evaluate how similar the behaviors of all nodes on the graph are in terms of the $\mathscr{H}_\infty$-norms of their difference transfer functions and then to recursively aggregate those nodes having closer behavior into a same cluster. This method allows for an insightful physical interpretation and the consensus property of the network system is preserved. The resulting reduced-order model can be written as

$$\begin{cases} \hat{M}\dot{\hat{x}} = -\hat{L}\hat{x} + \hat{B}u, \\ \hat{y} = P\hat{x}, \end{cases} \quad (3)$$

where, $\hat{M} := P^T M P$, $\hat{L} := P^T L P$, and $\hat{B} := P^T B$. Note that $\hat{M}$ is again a diagonal positive matrix and $\hat{L}$ is again a Laplacian matrix of a connected undirected graph with less number of vertices. Therefore, the network structure is preserved.

Moreover, we have the following theorem.

Theorem 1 *Consider a network system (1) and its reduced-order model (3) resulting from a arbitrary clustering P. Then, both systems reach consensus. Furthermore,*

$$\lim_{t \to \infty} y(t) = \lim_{t \to \infty} \hat{y}(t) = \frac{\mathbf{1}_n \mathbf{1}_n^T B}{\mathbf{1}_n^T M \mathbf{1}_n}. \quad (4)$$
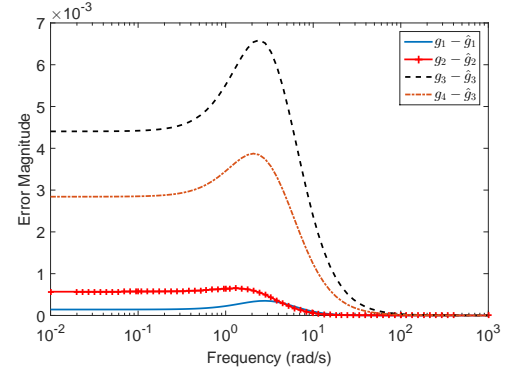
Figure 1: The magnitude of the approximation error.

where $\mathbf{1}_n$ denotes a n-entries vector of all ones. $y(t)$ and $\hat{y}(t)$ are the impulse responses of the systems $(sM + L)^{-1}B$ and $P(s\hat{M} + \hat{L})^{-1}\hat{B}$, respectively.

From above theorem, both the original and new systems converge to a same final value when $t \to \infty$ which implies that the reduced-order model preserves the consensus of the network.

Furthermore, the error of the model reduction is studied. Specifically, the explicit error of a one-step aggregation is presented and then the computable bounds on the error are derived. An illustrate example is shown in Fig. 1 where we consider a network system with four nodes. By one step clustering, the node 3 and 4 are aggregated which gives us a three-dimensional new system. let

$$\begin{bmatrix} g_1 & g_2 & g_3 & g_4 \end{bmatrix}^T = (sM + L)^{-1}B, \quad (5)$$

$$\begin{bmatrix} \hat{g}_1 & \hat{g}_2 & \hat{g}_3 \end{bmatrix}^T = (s\hat{M} + \hat{L})^{-1}\hat{B}. \quad (6)$$

We plot the approximation errors in Fig. 1.

Future work includes extension to second-order networks and to network systems with subsystems of higher-order linear dynamics.

References

[1]   X. Cheng, Y. Kawano, and J. M. A. Scherpen, "Graph structure-preserving model reduction of linear network systems," *Submitted*.

Control of a flexible-joint manipulator with only position measurements: a port-Hamiltonian approach

H. Jardón-Kojakhmetov*, M. Muñoz-Arias** and Jacquelien M.A. Scherpen*

*Engineering and Technology Institute (ENTEG), University of Groningen.

**School of Electronics Engineering, Costa Rica Institute of Technology, Cartago, Costa Rica.

{h.jardon.kojakhmetov, m.munoz.arias,j.m.a.scherpen}@rug.nl

1 Introduction

In this paper we study the tracking control problem of a flexible-joint robot. In particular, we are interested in controllers that only have access to position measurements. Although this setup is well known in the Lagrangian framework, e.g. [4], here we propose to use the port-Hamiltonian framework instead. We shall compare both methodologies and point out the advantages provided by the port-Hamiltonian formalism.

Remark 1. *One of our main contributions is to show that, as in the Lagrangian framework, model order reduction based on singular perturbations can also be used, in the port-Hamiltonian framework, to design controllers of flexible-joint robots. As it is expected and under some classical assumptions, the reduced order model of a (port-Hamiltonian modeled) flexible-joint robot results in a port-Hamiltonian model which coincides with that of a rigid robot.*

2 Preliminaries

A singularly perturbed ordinary differential equation is usually written as

$$\dot{x} = f(x,z,\varepsilon)$$
$$\varepsilon\dot{z} = g(x,z,\varepsilon), \tag{1}$$

where $x \in \mathbb{R}^m$, $z \in \mathbb{R}^n$ and $\varepsilon > 0$ is a small parameter $\varepsilon \ll 1$. Under the time rescaling $\tau = \frac{t}{\varepsilon}$, system (1) can be rewritten as

$$x' = \varepsilon f(x,z,\varepsilon)$$
$$z' = g(x,z,\varepsilon). \tag{2}$$

There are two reduced subsystems associated to (1) and (2) and are defined by taking the limit $\varepsilon \to 0$, these are

$$\dot{x} = f(x,z,0)$$
$$0 = g(x,z,0), \tag{3}$$

which corresponds to (1), and

$$x' = 0$$
$$z' = g(x,z,0), \tag{4}$$

which is related to (2). It is well known, e.g. [2, 3], that under the hyperbolicity condition $\left\|\frac{\partial g}{\partial z}\right\| \neq 0$, the dynamics

of (1) are ε-close to the dynamics provided by (3) and (4). In general terms, this implies that a control design strategy is to synthesize controllers u_0 for the reduced systems and therefore (1) can be controlled by a small perturbation $u_\varepsilon = u_0 + O(\varepsilon)$ of u_0.

3 Contribution

Modeling: we show that the port-Hamiltonian model of a flexible-joint robot can be written in the classical format of singular perturbations, that is

$$\dot{q}_s = f_s(q_s,q_f,p_s,p_f,u,\varepsilon)$$
$$\varepsilon\dot{q}_f = f_f(q_s,q_f,p_s,p_f,u,\varepsilon)$$
$$\dot{p}_s = g_s(q_s,q_f,p_s,p_f,u,\varepsilon)$$
$$\varepsilon\dot{p}_f = g_f(q_s,q_f,p_s,p_f,u,\varepsilon), \tag{5}$$

where (q_s,p_s) correspond to generalized coordinates of the slow subsystem (coinciding with a rigid robot), and (q_f,p_f) correspond to generalized coordinates of the fast subsystem, and u denotes the controller.

Model order reduction: due to the singular perturbation format of the port-Hamiltonian model, it is possible to obtain two reduced subsystems, one *slow* and one *fast*.

Controller synthesis: using persistence arguments from singular perturbation theory, e.g. [2], we can implement controllers based on rigid robots such as the ones in [1]. Such controllers would work on the flexible-joint robot, but they can be improved using the fast subsystem obtained in the model order reduction step.

References

[1] Dirksz, D.A. and Scherpen, J.M.A. (2013). On Tracking Control of Rigid-Joint Robots With Only Position Measurements. *IEEE Transactions on Control Systems Technology*, 21(4), 1510–1513.

[2] Fenichel, N. (1979). Geometric singular perturbation theory. *JDE*, 53–98.

[3] Kokotovic, P.V. (1984). Applications of Singular Perturbation Techniques to Control Problems. *SIAM Review*, 26(4), 501–550.

[4] Spong, M.W. (1987). Modeling and Control of Elastic Joint Robots. *Journal of Dynamic Systems, Measurement, and Control*, 109(4), 310.

Coupled Tensor Decomposition: a step towards robust components

Matthieu Genicot
ICTEAM Institute
Université Catholique de Louvain,
Avenue Georges Lemaître, 4,
B-1348 Louvain-la-Neuve, Belgium
Email: matthieu.genicot@uclouvain.be

Pierre-Antoine Absil
ICTEAM Institute
Université Catholique de Louvain,
Avenue Georges Lemaître, 4,
B-1348 Louvain-la-Neuve, Belgium
Email: absil@inma.ucl.ac.be

Renaud Lambiotte
Centre Namurois des Systèmes Complexes
Université de Namur
Rempart de la Vierge 8
B-5000 Namur, Belgium
Email: Renaud.Lambiotte@unamur.be

Saber Sami
Department of Clinical Neurosciences
University of Cambridge
Cambridge Biomedical Campus,
Cambridge CB3 0SZ, UK
Email: ssa42@medschl.cam.ac.uk

1 Introduction

The rush for data collection over the past decade has lead to an evolution of the way many datasets are represented. A flat matrix, limited to two dimensions, is no longer suitable in some applications where more complex abstractions are required. Social networks, biomedical, audio or imaging datasets, among others, now often have to deal with more than two dimensions. To better exploit the potential of these multi-dimensional datasets, higher-order tensors have naturally taken over matrices. Taking more than two dimensions into account makes the analysis of the tensors both more informative and more challenging than in the case of matrices.

Tensor factorization (i.e., tensor decomposition) has emerged as one of the key tools to investigate these datasets [1]. Generalizing the concept of matrix factorization, it aims to capture the underlying structure of the data by modelling the tensor as a sum of components. These components can be used for various purposes, from early visualization to latest classification task.

As a natural extension of individual tensor decomposition, the problem of decomposing two or more tensors conjointly is of great interest in many applications where more than one source of information is available. A joint analysis of different datasets that record similar phenomena has the potential to draw a more complete picture of the underlying structure of the data. An efficient gradient-based optimization approach to perform this coupled decomposition task with tensors of different orders was introduced by Acar et al. [2].

Among the many challenges arising when performing such coupled analysis, the difficulty to deal with the presence of both shared and unshared (i.e., dataset-specific) components among the datasets remains a concern. Because of the presence of the unshared sources, the results can be both in-consistent and largely dependent of the initialization, which calls for more robust methods.

2 Robust coupled tensor decomposition

In this work, a general framework, using the algorithm developed in [2], is built to extract more reliable components. We aim to tackle the lack of robustness in coupled tensor decomposition by comparing the components resulting from the individual decompositions and from the joint decomposition.

More specifically, individual decompositions are first performed (A) and the resulting components from both tensors are compared to detect similarities. Based on these similarity measures, some components are constrained to be shared and a joint decomposition is performed (B), initialized with the components extracted in (A). The differences between the components of (A) and of (B) are analysed, the number of components and the initializations for (A) are adapted and the process is repeated until convergence.

It results in both a more reliable and a more versatile joint decomposition method, with (i) a variable number of components, (ii) both shared and unshared components and (iii) components that are retrieved in both the individual and in the joint decompositions.

References

[1] A. Cichocki, D. Mandic, C. Caiafa, A.-H. Phan, G. Zhou, Q. Zhao, and L. De Lathauwer, *Tensor Decompositions for Signal Processing Applications*, IEEE Signal Processing Magazine, 2015

[2] E. Acar, T. Kolda and D. Dunlavy, *All-at-once Optimization for Coupled Matrix and Tensor Factorizations*, KDD Workshop on Mining and Learning with Graphs, 2011.

Model Reduction of Networked Systems by Edge Removal

H.J. Jongsma[1]
h.jongsma@rug.nl

H.L. Trentelman
h.l.trentelman@rug.nl

M.K. Camlibel
m.k.camlibel@rug.nl

Abstract

An increasing interest in complex networked systems has been observed in the past decade. Even with the availability of huge computational power and sophisticated tools for analysis, model reduction remains an important problem in the theory of networked systems. Here, the goal is to find systems of reduced complexity that closely approximate the behavior of the original complex network. The direct application of existing model reduction techniques for linear time invariant systems to these networked system destroys the interaction structure of the network. In this abstract we approximate *networked multi-agent systems* using model reduction techniques that remove certain edges from the network graph, preserving some of the network topology, and give expressions for the resulting approximation error.

In this abstract, the network is given by interconnected identical dynamical systems called *agents*. The the network graph is the *unweighted graph* $G = (V, \mathcal{E})$, with *agents* $V = \{1, 2, \ldots, n\}$ and edge set $\mathcal{E}$. While the edges are undirected, in this abstract we assign an arbitrary orientation to each edge. The set of *neighbors* of agent i is denoted N_i. Each agent is a symmetrical system and has state $x_i \in \mathbb{R}^p$, input u_i and output y_i in $\mathbb{R}^m$, and dynamics

$$\dot{x}_i = Ax_i + Bu_i, \quad y_i = B^T x_i$$

where u_i is the diffusive coupling given by $u_i = \sum_{j \in N_i} y_j - y_i$ and $A = A^T$. The overall network dynamics with state $x = \mathrm{col}(x_1, x_2, \ldots, x_n) \in \mathbb{R}^{np}$ is then given by

$$\dot{x} = (I \otimes A - L \otimes BB^T)x \qquad (1)$$

where L is the *Laplacian matrix* of the graph G. We assume that the system reaches consensus, or equivalently that the matrix $A - \lambda_i BB^T$ is Hurwitz for all nonzero eigenvalues λ_i for $i = 2, \ldots, n$ of L. To compare the system (1) to an approximating system, we assign a virtual input d and a virtual output z to the system. We obtain the following two-port consensus model:

$$\dot{x} = (I \otimes A - L \otimes BB^T)x + (I \otimes I)d, \quad z = (E^T \otimes I)x. \quad (2)$$

The output z represents the disagreement over every edge in the graph. Using ideas from [1], we will look at a *minimal representation* of system (2). First we choose a spanning tree $\mathcal{T}$ of G, then we look at the representation Σ given by

$$\dot{\xi} = (I \otimes A - L_e(I + TT^T) \otimes BB^T)\xi + (E_{\mathcal{T}}^T \otimes I)d, \ z = \xi, \ (3)$$

where $L_e = E_{\mathcal{T}}^T E_{\mathcal{T}}$ is a positive-definite matrix and $T = (E_{\mathcal{T}}^T E_{\mathcal{T}})^{-1} E_{\mathcal{T}}^T E_c$. The matrix $E_{\mathcal{T}}$ is the *incidence matrix* of $\mathcal{T}$ and the matrix E_c contains the columns of the incidence matrix E of G representing the edges that are not in $\mathcal{T}$, which close the cycles in G. The state $\xi \in \mathbb{R}^{|\mathcal{E}_{\mathcal{T}}|p}$ represents the disagreement along the edges in the edge set $\mathcal{E}_{\mathcal{T}}$ of the spanning tree $\mathcal{T}$. The matrix $L_e(I + TT^T)$ is called the *essential edge Laplacian* of G. Now, the goal is to approximate system Σ by a less complex system $\hat{\Sigma}$, whose network graph $\hat{G}$ is a subgraph of G. In this abstract, we restrict ourselves to the case that $\hat{G} = \mathcal{T}$. The system (3) is then approximated by system $\hat{\Sigma}$ given by

$$\dot{w} = (I \otimes A - L_e \otimes BB^T)w + (E_{\mathcal{T}}^T \otimes I)d, \ \hat{z} = w. \quad (4)$$

We assume that the unforced reduced model also reaches consensus, i.e. the matrix $A - \mu_i BB^T$ is Hurwitz for all eigenvalues μ_i $(i = 2, \ldots, n)$ of L_e. Note that the eigenvalues μ_i are exactly the nonzero eigenvalues of the Laplacian matrix of $\mathcal{T}$. Next, we can compute the *approximation error*, which is the H_2-norm of the error system that maps the input d to the error $z - \hat{z}$. An expression for the approximation error in the case that the original graph consists of a tree and a single extra edge, and hence $T = c \in \mathbb{R}^{|\mathcal{E}_{\mathcal{T}}|}$, is given in the following theorem.

Theorem. *Let Σ be a network consisting of a tree $\mathcal{T}$ and a single edge such that the graph has one cycle c. The absolute approximation error then satisfies*

$$||\Sigma - \hat{\Sigma}||_2^2$$
$$= \frac{1}{2} \sum_{i,j} (x_i^T c)^2 \frac{\lambda_i^2}{\sigma_{ij}^2} y_{ij}^T B \left(I + \sum_{k=2}^{n} \lambda_k (x_k^T c)^2 G_k(-\sigma_{ij})\right)^{-1} B^T y_{ij}$$
$$+ \frac{1}{2} \sum_{i=2}^{n} \left(1 - \frac{(v_i^T c)^2}{l(c)}\right) \mu_i \, \mathrm{tr} \, (\mu_i BB^T - A)^{-1}$$
$$- \frac{1}{2} \sum_{i=2}^{n} \lambda_i \, \mathrm{tr} \, (\lambda_i BB^T - A)^{-1}$$

where λ_i (μ_i) and x_i (v_i) are the e.v. and normalized eigenvectors of L_e ($[I + cc^T]^{\frac{1}{2}} L_e [I + cc^T]^{\frac{1}{2}}$), σ_{ij} and y_{ij} are the e.v. and normalized eigenvectors of $A - \lambda_i BB^T$, $l(c)$ is the length (number of edges) of the cycle c, and $G_k(s) = B^T(sI - A + \lambda_k BB^T)^{-1}B$.

References

[1] D. Zelazo *et al*, "Performance and design of cycles in consensus networks", *Sys. & Contr. Lett.*, vol. 62, no. 1, pp. 85-96, 2013.

[1] Johann Bernoulli Institute for Mathematics and Computer Science, University of Groningen, P.O. Box 407, 9700 AK Groningen, The Netherlands

Data driven dynamic measurements

Gustavo Quintana-Carapia and Ivan Markovsky
Department ELEC, Vrije Universiteit Brussel (VUB)
Email: `ivan.markovsky@vub.ac.be`

1 Introduction

Measurement techniques have fundamental speed and accuracy limitations. The speed and precision of a measurement device used in monitoring and control tasks determines the quality of the available data, which in turn limits the accuracy of models derived from the data. A method, called data driven fast measurement (DDFM), is proposed to overcome the hardware constraints. This method performs model free real-time processing of the signals measured.

2 Step input estimation problem

The metrology problem of a speeding up a measurement device is modeled as an input estimation problem for a dynamical system with step input. The step level is the unknown (to-be-measured) quantity, the output is the known (measured) quantity, and the input-output relation represents the unknown measurement process dynamics.

Problem: Given output observations

$$y = (y(1),\ldots,y(T)), \qquad y(t) \in \mathbb{R}^{\mathtt{p}},$$

of a stable linear time-invariant system with known dc-gain $G \in \mathbb{R}^{\mathtt{p} \times \mathtt{m}}$, generated by step input $u = \bar{u}s$, where s is the unit step function, find the input step value $\bar{u} \in \mathbb{R}^{\mathtt{m}}$.

3 Data driven fast measurement

A dynamic compensator performs on-line identification and model based design. The DDFM method is a model-free approach that bypasses the parameter identification and compensator design and finds directly the quantity of interest $\bar{u}$.

We assume that the unknown measurement process is a linear time-invariant system of order $\mathtt{n}$. The set $\mathscr{B}_{\mathtt{s}}$ of all output signal, generated by step inputs, is an autonomous system of order $\mathtt{n} + \mathtt{m}$, where $\mathtt{m}$ poles are at one.

Considering the unit difference operator Δ defined by

$$\Delta y(t) := y(t) - y(t-1).$$

The behavior $\Delta\mathscr{B}_{\mathtt{s}}$ is linear time-invariant autonomous of order $\mathtt{n}$ and $\mathscr{B}_{\mathtt{s}} = \Delta\mathscr{B}_{\mathtt{s}} + \bar{y}s$, for some $\bar{y} \in \mathbb{R}^{\mathtt{p}}$. Therefore, for any $y \in \mathscr{B}_{\mathtt{s}}$ that corresponds to a step input $\bar{u}s$, we have:

$$y = \bar{y}s + \Delta y, \text{ where } \bar{y} = G\bar{u} \text{ and } \Delta y \in \Delta\mathscr{B}_{\mathtt{s}} \qquad (1)$$

Using (1), we obtain the system of linear equations:

$$\left[\begin{bmatrix} G \\ \vdots \\ G \end{bmatrix} \quad \mathscr{H}(\Delta y)\right] \begin{bmatrix} \bar{u} \\ \ell \end{bmatrix} = \begin{bmatrix} y(\mathtt{n}+1) \\ \vdots \\ y(T) \end{bmatrix}, \qquad (2)$$

where $\mathscr{H}(\Delta y)$ is the block-Hankel matrix with $\mathtt{n}$ columns, constructed from Δy. The quantity of interest $\bar{u}$ is computed directly from the data by solving (2) recursively.

4 Practical implementation

The DDFM algorithm is implemented on a digital signal processor (NXT Lego brick). As a test bed we use temperature measurement. The estimation error $e := \bar{u} - \hat{u}$ is shown as a function of time. Here $\bar{u}$ is the steady state value and $\hat{u}$ is the current prediction of $\bar{u}$. The following methods are compared: 1) direct measurement of the sensor, 2) estimate of the measured quantity, obtained by the DDFM method, 3) estimate of the measured quantity, obtained by the Kalman filter, designed using on a model of the measurement processed, identified offline from the measured data.

The results of a particular experiment are shown below. Initially, the Kalman filter gives the best estimate but has bias. The DDFM method has slower response than the Kalman filter but has no bias and improves the raw measurement.
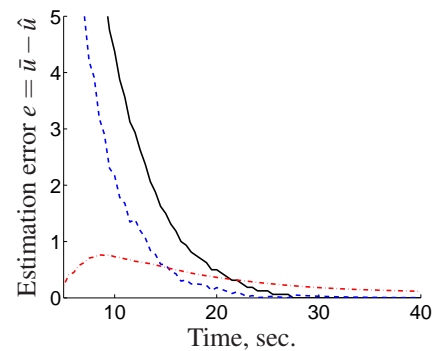
black—raw measurement, dashed—DDFM method, dashed dotted—Kalman filter

References

[1]   I. Markovsky, "An application of system identification in metrology," Control Eng. Prac., 43:85-93, 2015.

[2]   I. Markovsky, "Comparison of adaptive and model-free methods for dynamic measurement," IEEE Signal Proc. Letters, 22:1094-1097, 2015.

Regularized impulse response modeling using a filter interpretation

Anna Marconato, Maarten Schoukens, Johan Schoukens
Department ELEC
Vrije Universiteit Brussel
Pleinlaan 2, 1050 Brussels
Belgium
anna.marconato@vub.ac.be

1 Introduction

Kernel-based regularization techniques are constantly gaining attention in the identification world, due to their success in modeling the impulse response of linear systems, see e.g. [1]. In this work, instead, the problem of estimating a regularized impulse response model is studied from a different perspective [2]. The aim is to provide an intuitive interpretation of regularization problems from an engineering point of view.

2 Methodology

To achieve this, the estimation problem is analyzed focusing on the cost function. The main idea is to define the regularization matrix as a filtering operation on the estimated parameters before they enter the cost function. Since the regularization term can be seen as a penalty term on the model complexity, the regularization matrix should include the properties that one needs to penalize in order to get an accurate description of the system [2]. Figure 1 illustrates this idea on a band-pass system modeling example.

This filter-based approach is not only useful to get more insight about the existing kernel techniques from an engineering point of view, but can also be exploited to design new user-friendly regularization methods, by including the available prior information about the system, directly at the cost function level.

3 Results

The proposed approach allows one to deal in an effective way with low-pass, band-pass, and high-pass systems. Furthermore, the filter structure used to build the regularization term makes it also possible to model resonance systems by means of a flexible design algorithm. The effectiveness of the proposed approach is illustrated by means of Monte Carlo simulations on different modeling examples. The obtained results show that the filter-based approach outperforms the standard least squares method and the existing kernel-based regularization approaches in all the considered examples (see Figure 2 for the results on a band-pass system example), and offers an intuitive way to accurately model low-pass, band-pass, and high-pass systems [2].
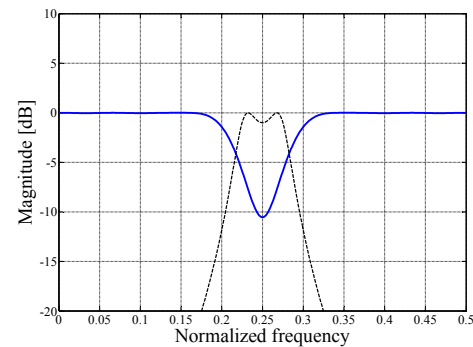
Figure 1: True system (dashed black line), and filter used to compensate for the system behaviour in the regularization term (solid blue line).
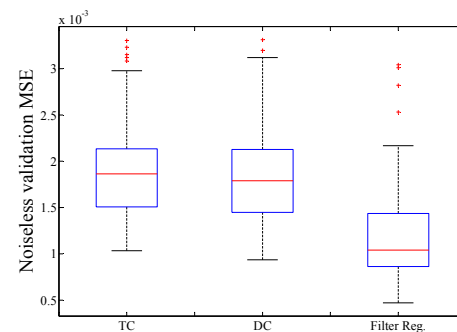
Figure 2: Validation error obtained with the filtering approach, compared with the state-of-the-art TC and DC kernels.

References

[1]   T. Chen, H. Ohlsson and L. Ljung, "On the estimation of transfer functions, regularizations and Gaussian processes - Revisited", Automatica, vol. 48, no. 8, pp. 1525-1535, 2012.

[2]   A. Marconato, M. Schoukens and J. Schoukens, "Filter interpretation of regularized impulse response modeling", submitted to the 15th European Control Conference (ECC 2016), Aalborg, Denmark, 2016.

Accommodating temperature change in the identification of a nonlinear model of the Li-ion battery cell

Rishi Relan[*], Koen Tiels[*], Jean-Marc Timmermans[**], Johan Schoukens[*]

Department ELEC[*], Department ETEC-MOBI[**], Vrije Universiteit Brussel

[rishi.relan@vub.ac.be]

1 Introduction

The success of the next generation systems, from consumer electronics, aerospace systems to the modern transportation systems rely on their energy consumption, efficiency and lifetime (both calendar life and cycling life). One of the most crucial (important) components and still one of the weakest links in such systems is the main energy storage component i.e. the battery or battery pack [1]. Lithium ion batteries (LiB) have gained acceptance into the consumer electronic, power grid, automotive and aerospace worlds as compared to other types of batteries because their high energy and high power density render them an excellent option for energy storage, particularly in hybrid and electric vehicles as well as an ideal candidate for a wide variety of applications. In order to develop a complete dynamic model of a lithium ion battery that is suitable for virtual-prototyping of portable battery-powered systems, accurate estimation of the state of charge (SOC) and state of health (SOH) is required, which in-turn depends on the quality of the models which are used for the estimation of these quantities. Temperature is known to have a significant impact on the performance, safety, and cycle lifetime of LiB [2–4]. In order to correctly predict (or simulate) the short-term electric response of a LiB cell , it is neccessary to accommodate the effect of temperature in the dynamic model of the LiB cell. In this paper, a data-driven polynomial nonlinear state-space (PNLSS) model structure is proposed, which can accommodate the effect of temperature change when the battery operates in the nonlinear regime of its electrical operation.

2 Nonlinear modelling

In order to identify the discrete-time nonlinear model for the battery, the polynomial nonlinear state-space model structure [5] is selected :

$$x(t+1) = Ax(t) + Bu(t) + E\zeta(t) \qquad (1)$$

$$y(t) = Cx(t) + Du(t) + F\eta(t) \qquad (2)$$

The coefficients of the linear terms in $x(t) \in \mathbb{R}^{n_a}$ and $u(t)$ are given by the matrices $A \in \mathbb{R}^{n_a \times n_a}$ and $B \in \mathbb{R}^{n_a \times n_u}$ in the state equation, $C \in \mathbb{R}^{n_y \times n_a}$ and $D \in \mathbb{R}^{n_y \times n_u}$ in the output equation. The vectors $\zeta(t) \in \mathbb{R}^{n_\zeta}$ and $\eta(t) \in \mathbb{R}^{n_\eta}$ contain nonlinear monomials in $x(t)$ and $u(t)$ of degree two up to a chosen degree P . The coefficients associated with these nonlinear terms are given by the matrices $E \in \mathbb{R}^{n_a \times n_\zeta}$

and $F \in \mathbb{R}^{n_y \times n_\eta}$. For the identification, a discrete-time linear model is fitted on non-parametric data and this linear discrete-time model was converted in to a state-space form before optimizing it to identify in least-square sense a nonlinear state-space model. Fig.1 shows a comparison between the response (output error) of a linear model and the PNLSS model (after accommodating the effect of temperature, a step change from $25° C$ to $40° C$) in the desired frequency band of interest with respect to the output measurement. It can be seen that the PNLSS model performs significantly better than the linear model in the frequency band of interest.
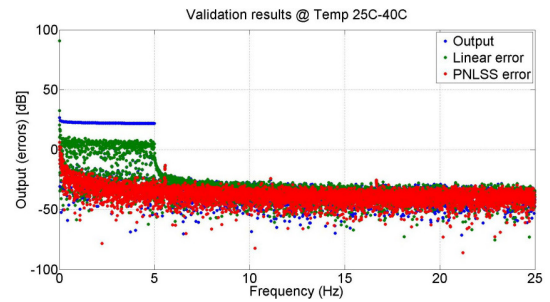
FIGURE 1: Output error comparison : Temperature dependent PNLSS model vs. Linear model

3 Acknowledgements

References

[1]   A. A. Franco, Ed., *Rechargeable Lithium Batteries : From Fundamentals to Applications*, ser. Woodhead Publishing Series in Energy. Woodhead Publishing, 2015.

[2]   F. Leng, C. M. Tan, and M. Pecht, "Effect of Temperature on the Aging rate of Li Ion Battery Operating above Room Temperature," *Scientific Reports*, vol. 5, p. 12967, Aug. 2015. [Online]. Available : http ://dx.doi.org/10.1038/srep12967 10.1038/srep12967

[3]   L. Saw, K. Somasundaram, Y. Ye, and A. Tay, "Electro-thermal analysis of lithium iron phosphate battery for electric vehicles," *Journal of Power Sources*, vol. 249, pp. 231 – 238, 2014.

[4]   C. Zhu, X. Li, L. Song, and L. Xiang, "Development of a theoretically based thermal model for lithium ion battery pack," *Journal of Power Sources*, vol. 223, pp. 155 – 164, 2013.

[5]   J. Paduart, L. Lauwers, J. Swevers, K. Smolders, J. Schoukens, and R. Pintelon, "Identification of nonlinear systems using polynomial nonlinear state space models," *Automatica*, vol. 46, no. 4, pp. 647 – 656, 2010.

Identification for Control of Heavy-Duty Diesel Engines via Parametric and Local Parametric Approaches

Lars Huijben[‡*], Thijs van Keulen[‡*] and Tom Oomen[‡]

[‡]TU/e, Dept. of Mech. Eng., Control Systems Technology group, The Netherlands.

[*]DAF Trucks N.V., Eindhoven, The Netherlands.

L.I.Huijben@student.tue.nl, T.A.C.v.Keulen@tue.nl and T.A.E.Oomen@tue.nl

1 Introduction

Heavy-duty diesel engine manufacturers are challenged to decrease fuel consumption while NO_x emissions are strictly regulated. Therefore, these engines are equipped with an increasing number of sensors and actuators, such as an exhaust gas recirculation (EGR) valve and a variable geometry turbine (VGT). This provides advanced means to control the combustion process. To systematically design such multivariable controllers, a model-based approach is pursued. The required models can be obtained through first-principles modeling or system identification [4]. However, first-principles models are often very complex, expensive, and inaccurate for high performance control design.

2 Approach

The approach considered in this research is based on a non-parametric model of the system, similar to [4], followed by a multivariable parametric model [3] fitted upon these measurements. Hence, an accurate model can be identified that is also suitable for model based control techniques. Furthermore, the local rational method (LRM) [1, 2] is employed to perform the non-parametric identification. Compared to classical spectral identification methods, the LRM has superior suppression of leakage (transient) errors and it contains noise averaging properties that are at least as good as time-domain windowing techniques [1].

3 Results

The engine dynamic behaviour is strongly varying at different operating points (engine speed, load, ambient conditions), which need to be identified independently. Consequently, the "fast" method adaptation of the LRM is applied to approximate the local dynamics as this method allows a full identification of the multivariable plant with a single experiment, leading to essential time reduction compared to other multivariable identification techniques. The LRM locally approximates the transient and the plant G by a rational function, shown in (1).

$$G(\omega_{k+r_E}) = \frac{N(\omega_{k+r_E})}{D(\omega_{k+r_E})} = \frac{\sum_{s=0}^{n_G} g_s(k) r_E^s}{1 + \sum_{s=1}^{n_D} d_s(k) r_E^s} \qquad (1)$$

This rational function, consisting of a polynomial numerator and denominator of order n_G and n_D respectively, estimates the response at frequency ω_k by a least squares fit through the local window r_E of adjoining excited frequencies. Figure 1 shows an LRM estimation based on three periods of

a 100s multisine, compared to a robust measurement consisting of 26 experiments of six 100s multisine periods each.
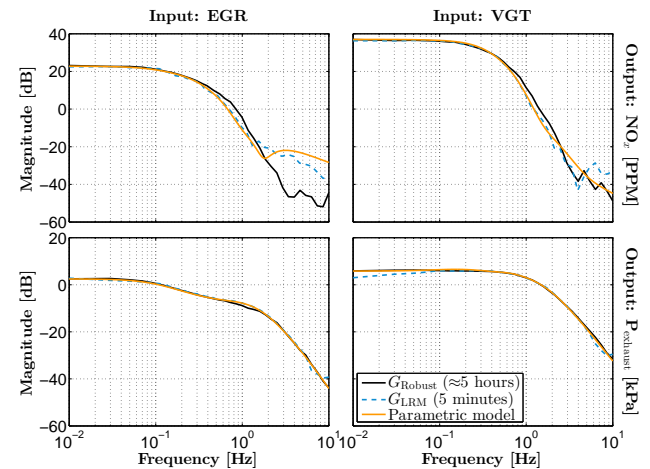
Figure 1: Magnitude bode plots of the LRM estimate, the robust estimate and the parametric model of the plant from EGR and VGT to NO_x and exhaust manifold pressure.

The LRM estimate is a close approximation of the robust benchmark, the covariances (not shown) are estimated with similar precision. A parametric modelling procedure [3] capable of identifying the common dynamics of the system is applied to the LRM estimation. The resulting parametric fit is shown in Figure 1 as well.

4 Future work

In future work, more control inputs will be included in the model such as fuel injection timing, quantity and pressure, extending the system size up to 6-by-6 elements. Furthermore, a broader range of operating points will be identified and a multivariable controller will be synthesized.

References

[1] J. Schoukens, G. Vandersteen, K. Barbé and R. Pintelon, *"Non-parametric Preprocessing in System Identification: a Powerful Tool"*, European Journal of Control (2009)3-4:260-274.

[2] T. McKelvey and G. Gurin, *"Non-parametric frequency response estimation using a local rational model"*, IFAC Symp. on Sys. Id., vol.16, part.1, pp.49-54, 2012.

[3] T. Oomen, R. van Herpen, S. Quist, M. van de Wal, O. Bosgra and M. Steinbuch, *"Connecting System Identification and Robust Control for Next-Generation Motion Control of a Wafer Stage"*, in *Control Systems Technology, IEEE Transactions on*, vol.22, no.1, pp.102-118, Jan. 2014.

[4] C. Criens, T. van Keulen, F. Willems and M. Steinbuch, *"A Control Oriented Multivirable Identification Procedure for Turbocharged Diesel Engines"*, Int. J. of Powertrains (accepted for publication).

The local polynomial method applied to a lightly damped mechanical MIMO system

Dieter Verbeke, Egon Geerardeyn, Johan Schoukens
Department of Electrical Engineering (ELEC)
University of Brussels (VUB)
1050, Brussels
dieter.verbeke@vub.ac.be

1 Introduction

This presentation discusses the estimation of nonparametric noise and frequency response matrix (FRM) models for multiple-input-multiple-output(MIMO) systems. [1] introduced the local polynomial method (LPM) for dynamic multivariable systems excited by arbitrary signals. [2] extended this work to MIMO systems excited by periodic signals in presence of both input and output noise (i.e. an errors-in-variables framework). The local polynomial methods result in a nonparametrical suppression of the noise and system transients (leakage errors) in the frequency response matrix and noise (co-)variance estimates. For lightly damped systems they can either significantly reduce the measurement time or, for a given experiment duration, significantly increase the frequency resolution of the FRM estimate. Although the objective is to apply the methodology to an experimental set-up, namely an active vibration isolation system (AVIS), the discussion here is limited to a series of simulations dealing with critical features.

2 The local polynomial method

The LPM builds on the assumption that the input-output discrete Fourier transform (DFT) spectra $U(k)$, $Y(k)$ of the input-output signals $u(t)$ and $y(t)$ are related as

$$U(k) = U_0(k) + N_U(k)$$
$$Y(k) = G(\Omega_k)U_0(k) + N_Y(k)$$

$$N_U(k) = H_U(k)E_U(k) + T_U(\Omega_k)$$
$$N_Y(k) = H_Y(k)E_U(k) + T_Y(\Omega_k)$$

$$T_Z(\Omega_{kP}) = \begin{bmatrix} T_Y(\Omega_{kP}) \\ T_U(\Omega_{kP}) \end{bmatrix},$$

where $\Omega = e^{-j\omega T_s}$ is the frequency variable in discrete time with $\Omega_k = 2\pi k f_s$, and $f_s = 1/T_s$ is the sampling frequency.

Both G, and T_Z are rational functions in Ω_k that can be approximated locally at DFT frequencies $kP+m$ for $k = 0, 1, ..., N/2 - 1$ and $m = 1, 2, ...P - 1$:

$$T_Z(\Omega_{kP+m}) = T_Z(\Omega_{kP}) + \sum_{r=1}^{R} t_r(k)m^r + \frac{1}{\sqrt{PN}}O(N_1^{-(R+1)})$$

with P the number of periods of the periodic signals, N the number of samples per period, and $N_1 = NP/m$.

3 Objectives

The simulations will provide insight into critical aspects of the methodoly for the particular case of a lightly damped mechanical MIMO system . This includes the design of appropriate input signals, and the choice of the parameters in the local polynomial method. Of particular interest is the impact these decision variables will have on the quality of the obtained FRF estimates around the resonance frequencies. As such, this work is the first stage in the process of using the LPM for the identification of the benchmark example of an industrial AVIS [3] with 8 inputs and 6 outputs..

Acknowledgement

References

[1] R. Pintelon, J. Schoukens, G. Vandersteen, K. Barbé, "Estimation of nonparametric noise and FRF models for multivariable systems - Part I: Theory," *Mechanical Systems and Signal Processing*, vol. 24, no. 3, pp.573-595, 2010.

[2] R. Pintelon, K. Barbé, G. Vandersteen, J. Schoukens, "Improved (non-) parametric identification of dynamic systems excited by periodic signals - the multivariate case," *Mechanical Systems and Signal Processing*, vol. 25, no. 8, pp.2892-2922, 2011.

[3] T. Oomen, R. van der Maas, C. Rojas and H. Hjalmarsson, "Iteratively learning the $\mathcal{H}_\infty$ norm of multivariable systems applied to model-error-modeling of a vibration isolation system," Proc. of the 2013 American Control Conference, Invited paper, Washington DC, USA, 2013.

Price-based control for electrical power distribution system

Matin Jafarian[1], Jacquelien Scherpen[1], and Marco Aiello[2]

ENTEG[1], Johann Bernoulli Institute for Mathematics and Computer Science[2],
Faculty of Mathematics and Natural Sciences,
Univerity of Groningen, The Netherlands
Email: {m.jafarian,j.m.a.scherpen,m.aiello}@rug.nl

1 Introduction

In the coming years, the exploitation of Renewable Energy Sources (RES), i.e. wind and solar sources, will increase significantly. Comparing to fossil-fuel sources, RES are produced and distributed in a more decentralized fashion and their availability mainly depends on the climate and weather conditions. As a result, the current energy systems are facing new challenges [2, 4]. For instance, the distribution network system should cope with the effects of RES in order to maintain the desired voltage levels and prevent the network bottlenecks which can occur as a result of a surplus of RES generation and/or high consumption. Dealing with these challenges, the price-based (market-based) approach provides a promising framework in which consumers and producers will be motivated, by means of economic incentives, to transform to controllable (price-elastic) components, which react to price signals to obtain and maintain the desired behavior of the grid [1, 3]. In this talk, we present a price-based mechanism for the distribution system in order to maintain the voltage at each bus within its desired bounds and to deal with (active power) congestion.

2 Price-based (optimal) control

We consider a radial distribution network composed of *n* buses and *m* branches and model the network as a connected, undirected graph with *n* nodes and *m* edges. The nodal active and reactive powers obey the AC power flow model

$$P_i = \sum_{j=1}^{n} V_i V_j Y_{ij} \cos(\delta_i - \delta_j - \theta_{ij}),$$
$$Q_i = \sum_{j=1}^{n} V_i V_j Y_{ij} \sin(\delta_i - \delta_j - \theta_{ij}), \qquad (1)$$

where $V_i \angle \delta_i$ and $Y_{ij} \angle \theta_{ij}$ are the complex voltage of bus i and the admittance between nodes i and j, respectively. We formulate our objective as a distributed optimal control problem with constraints on active, reactive power flows and the voltage bounds. The output of the optimal controller are the price signals. It is assumed that there is a network operator who communicates the price signals with the controllable units. Our current research is focused on designing the optimal price-based control algorithm and validating the algorithm by means of simulating a benchmark system. The case study is composed of a standard IEEE 37 distribution bus connected to price-elastic /-inelastic loads and a few distributed generation units (DG). Each DG unit is composed

of a RES production source together with an inverter and a storage system. For RES production, we consider a variable speed wind-turbine and a few PV systems. Figure 1 shows the physical model together with the controller.
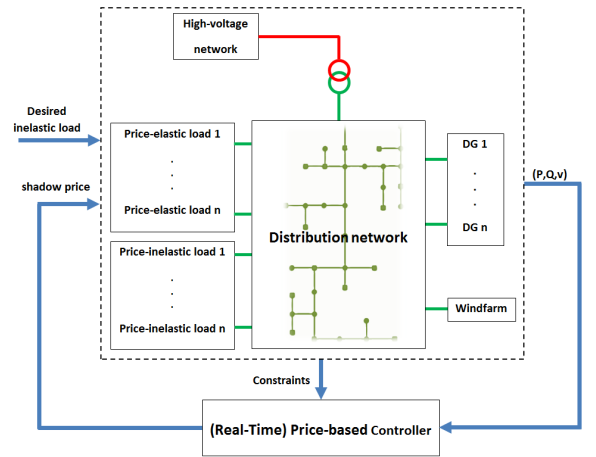
Figure 1: Price-based control scheme for the distribution grid.

3 Concluding remarks

This research is currently focused on designing a real-time price-based control for power distribution network. Next step is to use the controller output (shadow prices) in order to design time-varying network tariffs [1]. Moreover, one of the future avenues is to analyze and improve our design to provide a fault-tolerant structure for switching between grid-connected and islanded modes.

References

[1] Redesigning the electricity market to foster renewable energy: http://www.rug.nl/research/ceer/kennis/nworug.

[2] L. Fiorini. The integration of storage in hv grids: optimal use of renewable sources. 2015. Master Thesis, University of Pisa and University of Groningen.

[3] A. Jokić. Price-based optimal control of electrical power systems. 2007.

[4] J.M.A Scherpen. Distributed supply-demand balancing and the physics of smart energy systems. *European Journal of Control*, 2015.

A Communication-free Master-Slave Microgrid with Power Sharing

Pooya Monshizadeh   Claudio De Persis   Nima Monshizadeh   Arjan van der Schaft

University of Groningen
9712 CP Groningen
The Netherlands

{p.monshizadeh@rug.nl,c.de.persis@rug.nl,n.monshizadeh@rug.nl,a.j.van.der.schaft@rug.nl}

1 Introduction

A microgrid is a network of connected power sources and loads in a small area which can be seen as one entity within the wide area power system. Considering such a network as a building block of the power grid is mainly motivated by preventing blackouts. The microgrid is capable of disconnecting itself from the main grid in case of a fault in the main grid and reconnecting when the fault is resolved, and it typically includes synchronous generators, inverters, and loads. Inverters are divided into three categories. The first category, "Grid-forming" inverters, act as a voltage source with fixed frequency and amplitude. "Grid-feeding" inverters form the second category, working as current sources such that their voltage follow the frequency of the grid/microgrid. The third category contains sources that are designed to contribute to the regulation and stability of the microgrid, which are called "grid-supporting". This category includes both Voltage Source Inverters (VSI) and Current Source Inverters (CSI). Grid-supporting VSIs are capable of self-regulation and therefore the network consisting of these inverters synchronize in frequency [1]. These devices measure power they inject to the grid and determine the output voltage amplitude and frequency according to these measured values. Counter-wise, grid-supporting CSIs measure the voltage amplitude and frequency, in order to inject a desired amount of active and reactive power accordingly [3].

2 Problem Statement

A large number of articles have triggered deploying grid-supporting VSIs. These inverters generate their own frequencies and then synchronize in the steady state with a proportionally shared power. In the next step, generations are increased/decreased regarding to the increased/decreased load (secondary layer). We are looking for an alternative microgrid architecture that can fulfill all aims at once.

3 Solution Method

We propose a microgrid with a master-slave architecture in which a synchronous generator acts as the master and current source grid-supporting CSIs act as the slaves (Figure 1). Following its nature, such a network is synchronized at all times and stable under constant power loads [2].
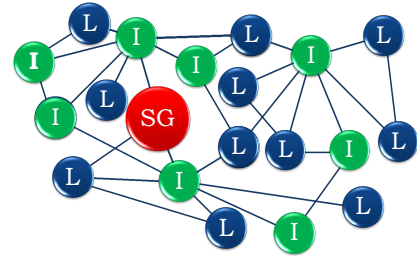
Figure 1: The proposed method applies to any topology of the microgrid power network graph. Synchronous Generator (SG) acts as the master, and Inverters (I) act as slaves. The dark blue nodes represent power loads (L).
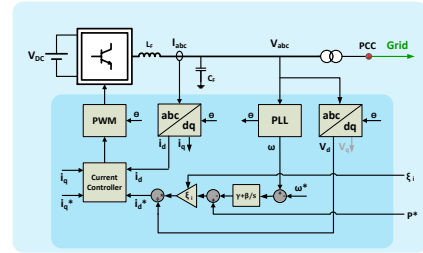
Figure 2: Implementation of the proposed inverter

4 Implementation

Figure 2 depicts the schematic of the proposed current source inverter. With such devices, frequency regulation and power sharing can be achieved without any communication.

References

[1] Nima Monshizadeh and Claudio De Persis. Output agreement in networks with unmatched disturbances and algebraic constraints. *CoRR*, abs/1504.03609, 2015.

[2] Pooya Monshizadeh, Claudio De Persis, Nima Monshizadeh, and Arjan van der Schaft. A communication-free master-slave microgrid with power sharing. *CoRR*, abs/1509.08847, 2015.

[3] J. Rocabert, A. Luna, F. Blaabjerg, and P. Rodriguez. Control of power converters in ac microgrids. *Power Electronics, IEEE Transactions on*, 27(11):4734–4749, Nov 2012.

Topological conditions on the stability of networked systems with damped and undamped nodes

Filip Koerts
University of Groningen
f.j.koerts@rug.nl

Arjan van der Schaft
University of Groningen
a.j.van.der.schaft@rug.nl

Claudio de Persis
University of Groningen
c.de.persis@rug.nl

Mathias Buerger
University of Stuttgart
mathias.buerger@ist.uni-stuttgart.de

1 Problem formulation

We consider a linear mass-spring-damper system with dynamics

$$M\ddot{s} = -R\dot{s} - BWB^T s + c,$$

where the system parameters are the diagonal positive definite matrices M and W of mass values and edge weights respectively, the positive-semidefinite matrix R with nonnegative resistance values and a constant input c. B represents the node-edge incidence matrix of the underlying graph $\mathscr{G}$. We assume that $\mathscr{G}$ is connected and there is at least one damped and one undamped node.

We say that the system reaches consensus if the velocity of the nodes converges to an agreement value in the long run, i.e. when $\lim_{t\to\infty} \dot{s}(t) \to \mathbb{1}\beta$ for some $\beta \in \mathbb{R}$. By defining node states $p = M\dot{s}$ and edge states $q = B^T s$, the consensus problem is shown to be equivalent to global asymptotic stability (GAS) of the closed-loop system of the node and edge systems induced by the state variables. After a linear shift of this system, the dynamics become independent of c.

Suppose that we only know the underlying damping graph, i.e. the incidence matrix B and the set of damped nodes, but do not know the system matrices W, M and R precisely. The *parameter independent stability* problem asks whether systems with a given underlying damping graph are GAS for all system parameters. In this case we say that the damping graph is parameter independent GAS, abbreviated PI-GAS.

The conceptual linear mass-spring-damper system that is used in this stability analysis allows for powerful applications such as power systems and multi-vehicle systems.

2 Results

The parameter independent stability problem is equivalent to the *richly balanced coloring problem*. In this graph coloring problem, damped nodes are colored black and $\mathscr{G}$ admits a richly balanced colored graph if the undamped nodes can be colored black, blue or red in such a way that (i) every black node b is balanced, i.e. either b has only black neighbors, or it has at least one red and at least one blue neighbor (in that case, b is richly balanced) and (ii) not all nodes in $\mathscr{G}$ are black. $\mathscr{G}$ is PI-GAS if and only if it there exists a richly balanced colored

graph of $\mathscr{G}$. By a reduction from the boolean satisfiability problem, the problem is shown to be NP-complete.

A sufficient condition for $\mathscr{G}$ being PI-GAS is that it satisfies the zero forcing property. This happens if $\mathscr{G}$ only consists of black nodes after repeatedly applying the blackening rule of selecting a black node that has precisely one white neighbor and coloring this white neighbor black. For the special case that $\mathscr{G}$ is a tree graph, the zero forcing property is also a necessary condition for PI-GAS.

Despite of the complexity of the problem, we can do better than a brute-force search on all nodes. For a given combination of colors of undamped nodes that are incident to a set of chords (i.e. an edge that does not belong to a certain spanning tree of $\mathscr{G}$), it can be verified in linear time if there exists a coloring of the remaining undamped nodes that creates a richly balanced colored graph. The proof for this relies on (i) two forcing rules that are necessary implications to balance a colored graph and (ii) a procedure to color all undamped nodes red or blue of a tree graph to which the zero forcing algorithm is applied. In this way, the parameter independent stability problem for networks with few fundamental cycles is easily solved.
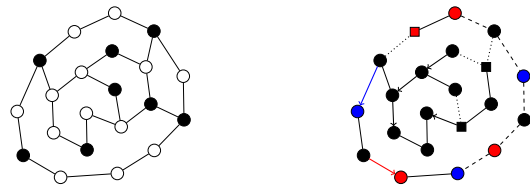
Figure 1: The figure on the left shows a damping graph where black and white nodes represent damped and undamped nodes, respectively. For the given combination of colors of the chord nodes (squares in the right figure), the chord node coloring algorithm colors the remaining undamped nodes such that a richly balanced colored graph is created.

References

[1]   F. Koerts, C. de Persis, A.J. van der Schaft, M. Bürger. "Topological conditions on the stability of networked systems with damped and undamped nodes", *2016 (journal paper, under construction)*,

Coping with Algebraic Constraints in Power Networks

Nima Monshizadeh   Claudio De Persis   Arjan J. van der Schaft   Jacquelien M.A. Scherpen

University of Groningen, The Netherlands

{n.monshizadeh@rug.nl, c.de.persis@rug.nl, a.j.van.der.schaft@rug.nl, j.m.a.scherpen@rug.nl}

1 Introduction

In the intuitive modelling of the power network, the generators and the loads are located at different subset of nodes. This corresponds to the so-called *structure preserving* model which is naturally expressed in terms of differential algebraic equations (DAE). The algebraic constraints in the structure preserving model are associated with the load dynamics.

Motivated by the fact the presence of the algebraic constraints hinders the analysis and control of power networks, several aggregated models are reported in the literature where each bus of the grid is associated with certain load and generation. The advantage of these aggregated models is mainly due to the fact that they are described by ordinary differential equations (ODE) which facilitates the analysis of the network. However, the explicit relationship between the aggregated model and the original structure preserved model is often missing, which restricts the validity and applicability of the results.

Aiming at simplified ODE description of the model together with respecting the heterogenous structure of the power network has endorsed the use of Kron reduced models; see e.g. [2]. In the Kron reduction method, the variables which are exclusive to the algebraic constraints are solved in terms of the rest of the variables. This results in a reduced graph, the (loopy) Laplaican matrix of which is the Schur complement of the (loopy) Laplaican matrix of the original graph. By construction, the Kron reduction technique restricts the class of the applicable load dynamics to linear loads.

The algebraic constraints can also be solved in the case of frequency dependent loads where the active power drawn by each load consists of a constant term and a frequency-dependent term [1],[3]. However, in the popular class of constant power loads, the algebraic constraints are "proper", meaning that they are not explicitly solvable.

In this talk, first we revisit the Kron reduction method for the linear case, where the Schur complement of the Laplacian matrix (which is again a Laplacian) naturally appears in the network dynamics. It turns out that the usual decomposition of the reduced Laplacian matrix leads to a state space realization which contains merely partial information of the original power network, and the frequency behavior of the loads is not visible. As a remedy for this problem, we introduce a new matrix, namely the projected pseudo incidence matrix, which yields a novel decomposition of the reduced Laplacian. Then, we derive reduced order models capturing the behavior of the original structure preserved model. Next, we turn our attention to the nonlinear case where the algebraic constraints are not readily solvable. Again by the use of the projected pseudo incidence matrix, we propose explicit reduced models expressed in terms of ordinary differential equations. We identify the loads embedded in the proposed reduced network by unveiling the conserved quantity of the system.

2 Main Result

We start with the differential algebraic system

$$\dot{\theta}_G = \omega_G \tag{1a}$$

$$M\dot{\omega}_G = -A\omega_G - B_G\Gamma\sin(B^T\theta) + u \tag{1b}$$

$$0 = -B_L\Gamma\sin(B^T\theta) + p \tag{1c}$$

and obtain the follwoing reduced model of ordinary differential equations:

$$\dot{\eta} = B_S^T(\eta)\omega_G \tag{2a}$$

$$M\dot{\omega}_G = -A\omega_G - B_G\Gamma\sin(\eta) + u. \tag{2b}$$

We show that under mild conditions, the systems above admit identical solutions. Here, θ_G is the vector of voltage angles, ω_G is the frequency, M_G denotes the angular momentum of the generators, A is diagonal and collects the damping coefficients, the matrix B denotes the incidence matrix of the graph of the power network and $B = \text{col}(B_G, B_L)$, Γ is a positive definite matrix, u is the control input and p is the vector of constant power loads.

References

[1] A.R. Bergen and D.J. Hill. A structure preserving model for power system stability analysis. *Power Apparatus and Systems, IEEE Transactions on*, (1):25–35, 1981.

[2] F. Dörfler and F. Bullo. Kron reduction of graphs with applications to electrical networks. *IEEE Transactions on Circuits and Systems I: Regular Papers*, 1(60):150–163, 2013.

[3] N. Monshizadeh and C. De Persis. Output agreement in networks with unmatched disturbances and algebraic constraints. *arXiv preprint arXiv:1504.03609*, 2015.

Preserving power network optimality in the presence of intermittent feedback measurements

Erik Weitenberg
University of Groningen
e.r.a.weitenberg@rug.nl

Claudio De Persis
University of Groningen
c.de.persis@rug.nl

Pietro Tesi
University of Groningen
p.tesi@rug.nl

We study the distributed optimal control of power networks under intermittent interruptions in communication, referred to hereafter as Denial of Service (DoS). Stability of the solutions under both DoS and non-DoS conditions can be achieved using suitable controllers. We characterize the duration of those DoS-intervals for which optimality of the solution achieved by the controllers is still guaranteed.

1 Introduction

During day-to-day operation of a power network, fluctuations occur in the power load and production at various places in the network. As a result, the frequency of power observed by the consumer can be different from its nominal value. This can damage sensitive electronics, and should therefore be avoided.

Traditionally, droop control and automatic generation control are used to retain power quality. More recently, distributed control schemes have been proposed [1], which provide for optimal regulation, meaning that more capable generators compensate for more load elsewhere in the network. Communication between the controllers is required to achieve this optimality.

2 Setting

We study power networks, modeled using second-order Kuramoto-like oscillators, given in vector form as

$$\dot{\eta} = B^\top \omega$$
$$\dot{\omega} = -A\omega - B\Gamma(\sin \eta) - u + d.$$

Here, η denotes the vector of differences of rotor angles on each edge and ω is the vector of frequency deviations at the generators. A and Γ are positive-definite diagonal matrices representing droop coefficients and susceptances of the power lines, respectively; B denotes the incidence matrix and d is the vector of loads at the generators. Control is possible by way of the power generation vector u. The control goal is then to steer the frequency deviation from the nominal frequency, denoted by ω, to 0 asymptotically.

The distributed controller proposed in [1] can be denoted by

$$\dot{\xi} = -\mathscr{L}_c \xi - Q^{-1}\omega$$
$$u = Q^{-1}\xi,$$

in which $\mathscr{L}_c$ is the Laplacian matrix of the communication graph, and Q denotes the diagonal, positive definite matrix associated with the quadratic cost of power generation at each node.

Previous work has shown already, using LaSalle–Lyapunov arguments, that the power network is locally asymptotically stable under suitable assumptions [1].

Economic optimality of the solution requires additionally that the control variable ξ converges to

$$\bar{\xi} = Q^{-1}\mathbf{1}\frac{\mathbf{1}^\top d}{\mathbf{1}^\top Q^{-1}\mathbf{1}},$$

which is the total power demand optimally divided among the generators. The steady state achieved by the controllers above is optimal in this sense.

3 Denial of Service

We consider the scenario in which, for various reasons, the communication network may not always be available. For example, natural disasters or adversarial intervention may disrupt the network at unpredictable times, for unknown durations. We model this condition, called Denial of Service, as a series of intervals during which $\mathscr{L}_c$ is replaced by the zero matrix.

In this work, we aim to relate the optimality of the solution to the availability of the communication network.

We derive a bound on the maximum total length of all DoS intervals for which we can still guarantee asymptotic convergence to the optimal solution.

References

[1] S. Trip, M. Bürger and C. De Persis. An internal model approach to frequency regulation in power grids. *Automatica*, 64:240–253, 2016.

[2] C. De Persis and P. Tesi. Input-to-state Stabilizing Control under Denial-of-Service. *Transactions on Automatic Control*, 27-03-2015.

[3] C. De Persis and P. Tesi. Resilient Control under Denial-Of-Service. *Proceedings of the 19th IFAC World Congress, 2014*, pp. 134–139.

A Scenario Approach for Probabilistic Fault Detection Threshold Design for Uncertain Nonlinear Systems

Vahab Rostampour, Riccardo M.G. Ferrari, Robert Babuška, and Tamás Keviczky

Delft Center for Systems and Control, Delft University of Technology
{v.rostampour, r.ferrari, r.babuska, t.keviczky}@tudelft.nl

Abstract

Advanced model-based fault diagnosis methods have emerged in important industrial sectors, such as aerospace, as fundamental tools for guaranteeing high operational readiness levels and reducing unneeded maintenance costs. A key problem to be solved for widespread industrial adoption is the development of robust methods providing satisfactory, and easy to tune performances in terms of the so-called *false positive* and *false negative* alarm ratios, with respect to true negative and true positive ones, respectively. A major culprit leading to false alarms are the unavoidable model and measurement uncertainties, which are dealt with by a careful choice of the residual generators, and by designing robust fault detection thresholds, that ideally are only exceeded in the presence of faults. In the case of linear systems, and under some conditions also for nonlinear systems [1], geometric approaches exist that can lead to residuals that are perfectly decoupled from the uncertainties, thus making the problem of threshold design trivial. For general nonlinear systems, thresholds are usually designed by assuming the existence of a known, static or dynamic upper bound on the uncertainties magnitude, thus obtaining a guarantee for zero false positive alarms by design. Such a powerful property often comes at the cost of very conservative thresholds, often leading to high false negative ratios, though some of these can be characterized by suitable detectability theorems. The key reason behind the conservativeness is that the uncertainty bounds must account also for large, but possibly rare values taken by the uncertainties. This problem in practical situations is exacerbated by the fact that tight dynamic bounds on the uncertainties are seldom known, thus leading to users choosing excessively high and static bounds in order to guarantee the worst case condition. This highlights the necessity of formulating stochastic variants of standard fault detection threshold problems, while ensuring performance guarantees by means of probabilistic designs.

This paper aims to relax the condition on the absence of false positives, by introducing fault detection thresholds with probabilistic, rather than deterministic, guarantees. This will lead in general to lower thresholds, which will allow better detectability of faults with small magnitudes, with only a marginal presence of false positive alarms due to the fact that very rare values of the uncertainties are excluded from the threshold design process. The probability of false positives,

as it will be shown, will be a tunable design parameter in the proposed procedure, so that a user may choose from the probabilistic metric space. Though the scientific literature already produced some works on fault detection thresholds with probabilistic guarantees (see [2, 3, 4, 5], etc), an innovative feature of the proposed approach is that the problem of guaranteeing a given probability of false positives, whilst minimizing the amount of false negatives, will be solved at the same time. We will in fact use a scenario approach in order to determine the optimal threshold as the solution of a chance-constrained optimization problem, which minimizes the probability of false negatives while respecting a user-set bound on the probability of false positives, for a given class of faults. An added advantage coming from the use of a scenario approach, with important practical implications, is that the requirements on the knowledge of tight (or probabilistic) bounds on the uncertainties is replaced by the requirement to hold a sufficiently high number of samples of the residual in healthy conditions, this number being in turn dependent on the given level of false positives and false negatives desired.

References

[1]   C. De Persis and A. Isidori, "A geometric approach to nonlinear fault detection and isolation," *IEEE Transaction on Automatic Control*, vol. 46, pp. 853–865, June 2001.

[2]   P. Mohajerin Esfahani and J. Lygeros, "A tractable fault detection and isolation approach for nonlinear systems with probabilistic performance," *IEEE Transaction on Automatic Control*, vol. PP, no. 99, pp. 1–1, 2015.

[3]   G. R. Marseglia, J. K. Scott, L. Magni, R. D. Braatz, and D. M. Raimondo, "A hybrid Stochastic-Deterministic approach for active fault diagnosis using scenario optimization," in *IFAC World Congress*, vol. 19, pp. 1102–1107, 2014.

[4]   F. Dabbene, D. Henrion, C. Lagoa, and P. Shcherbakov, "Randomized approximations of the image set of nonlinear mappings with applications to filtering," *IFAC Symposium on Robust Control Design*, vol. 48, no. 14, pp. 37–42, 2015.

[5]   F. Boem, R. M. G. Ferrari, T. Parisini, and M. M. Polycarpou, "Optimal topology for distributed fault detection of large-scale systems," *IFAC Symposium on Fault Detection, Supervision and Safety for Technical Processes*, vol. 48, no. 21, pp. 60–65, 2015.

Design of an optimized gradient method for composite convex optimization

Adrien B. Taylor, François Glineur, Julien M. Hendrickx

Institute of Information and Communication
Technologies, Electronics and Applied Mathematics
Université catholique de Louvain, Belgium

Email: {adrien.taylor, francois.glineur, julien.hendrickx}@uclouvain.be

1 Introduction

In this work, we exploit the *performance estimation* (PE) [2, 5, 6] methodology for doing algorithmic design. This methodology aims at automatically establishing exact bounds on the convergence of fixed-step first-order algorithms for convex optimization problems. In addition to its capability of improvement of existing bounds, this framework can be used for the development of improved methods.

Using the PE approach, we propose an extension of the optimized gradient method [3, 4], originally designed for smooth unconstrained convex optimization, for possibly handling constraints, or a proximal term. This new algorithm is very similar to a variant of the celebrated FISTA [1], but has a worst-case behaviour which is about twice better.

2 Composite convex optimization

We consider the following minimization problem, which we qualify as the *composite* convex optimization problem:

$$\min_{x \in \mathbb{R}^d} f(x) + h(x),$$

where both f and h are convex functions. In this setting, we assume that f is a smooth function whose gradient can be computed, while h is a possibly nonsmooth function for which we assume one can compute the following proximal operator (implicit gradient method):

$$\mathrm{prox}_{\lambda h}(y) = \operatorname*{argmin}_{x \in \mathbb{R}^d} \left\{ h(x) + \frac{1}{2\lambda} \|y - x\|_2^2 \right\}.$$

Note that when h is the indicator function of some convex set, the proximal operator performs a projection on that set, so that this class of problems includes constrained problems.

3 PE for composite convex optimization

In [5, 6], we adapt the PE approach [2] for obtaining the *exact* worst-case values for a class of first-order methods for composite convex optimization — whereas previous works focused on upper bounds [2, 3]. The idea is that given an algorithm of that class, one can generate the problem (that is, convex functions f and h) on which the given algorithm behaves the worst according to some chosen performance criteria (such as objective function accuracy, or distance to the solution).

This technique is applicable for the class of so-called *fixed-step linear gradient methods* [6], which basically includes the majority of existing first-order methods provided they use fixed step lengths, including classical gradient methods, accelerated variants (including variants for constrained problems), proximal gradient, conditional gradient, subgradient methods, etc.

4 Algorithmic design

Using the PE approach, it is therefore possible to obtain the exact worst-case behaviours of algorithms in the class of *fixed-step linear gradient methods*. This approach opens the door for tuning the algorithms in order to obtain *better performing methods*. As an example, this has been done analytically for fixed-step gradient methods for smooth unconstrained optimization in [2, 3] and resulted in the so-called optimized gradient method (OGM) — which is optimal for a weaker (relaxed) version of the PE approach.

Using PE for composite convex optimization, we propose a non-standard extension of OGM for the composite case. This extension has a worst-case behaviour which is about twice better than the celebrated fast iterative shrinkage-thresholding algorithm (FISTA) [1].

References
[1]   A. Beck, M. Teboulle. "A fast iterative shrinkage-thresholding algorithm for linear inverse problems." SIAM Journal on Imaging Sciences 2 (1), 183–202 (2009).

[2]   Y. Drori, M. Teboulle. "Performance of first-order methods for smooth convex minimization: a novel approach." Mathematical Programming 145.1-2 (2014).

[3]   D. Kim, J.A. Fessler. "Optimized first-order methods for smooth convex minimization." Mathematical Progamming (2015).

[4]   D. Kim, J.A. Fessler "On the convergence analysis of the optimized gradient methods." arXiv:1510.08573 (2015)

[5]   A.B. Taylor, J.M. Hendrickx, F. Glineur. "Smooth Strongly Convex Interpolation and Exact Worst-case Performance of First-order Methods." arXiv:1502.05666 (2015).

[6]   A.B. Taylor, J.M. Hendrickx, F. Glineur. "Exact Worst-case Performance of First-order Algorithms for Composite Convex Optimization." arXiv:1512.07516 (2015).

Approximate matrix geometric means[*]

Estelle M. Massart, Julien M. Hendrickx, P.-A. Absil

ICTEAM Institute, Université catholique de Louvain, B-1348 Louvain-la-Neuve, Belgium.

Email: { estelle.massart, julien.hendrickx, pa.absil } @uclouvain.be

1 Introduction

We consider the problem of efficiently averaging a set of N symmetric positive definite (SPD) matrices. This task appears in various applications, e.g., in medical imaging, mechanics (elasticity tensor estimation), video-tracking and radar detection. These two last applications justify the need to develop fast algorithms to solve this problem.

The geometric mean is usually preferred to the arithmetic mean for SPD matrices. However, the definition of the geometric mean of a set of SPD matrices is far from trivial. To be considered as a geometric mean, a matrix mean has to fulfill a list of criteria (usually refered to as the ALM list). This results in a unique definition of the 2-variable geometric mean, which corresponds to the center of the geodesic binding the two matrices (in the sense of the affine-invariant metric), but several definitions have been proposed for the geometric mean of more than two matrices. The most widespread multi-variable geometric mean is probably the Riemannian center of mass of the matrices (also termed Karcher mean).

The main shortcoming of these geometric means is that they are expensive to compute. Therefore, several approximate geometric means (operators satisfying most of the ALM properties) have been proposed in the literature, e.g., the CHEAP mean [1] and the Circular mean [2]. We propose here another family of approximate geometric means which all rely on a progressive merging method described next.

2 The Progressive Merging algorithm

The Progressive Merging algorithm consists in successively replacing couples of matrices by one matrix corresponding to their weighted geometric mean. The result of this algorithm, denoted here $PM(A_1, \ldots, A_N)$, is also termed "inductive mean" in the literature. The PM algorithm does not qualify as a geometric mean because it does not satisfy the ALM property of invariance under permutation. Moreover, we have observed empirically that it tends to overemphasize the last matrices in its argument list. Our proposed family of methods offers a framework to remedy these drawbacks.

3 Approximate matrix geometric means

The approximate geometric means that we propose fit in the following scheme. Given data matrices $A_1, \ldots, A_N$ in $\mathbb{P}_n$ (the set of SDP matrices of size n):

1. Consider a list $p = (p_1, \ldots, p_k)$ of permutations of $1, \ldots, N$.
2. Compute $B_i = PM(A_1, \ldots, A_N, p_i)$, $i = 1, \ldots, k$, where PM is the inductive mean.
3. Return $M(B_1, \ldots, B_k)$ where M is some matrix mean.

We investigate various ways to build the permutation list p, as well as several matrix means M. The resulting algorithms are named according to the pattern <p>-PM-<M>, where <p> indicates the permutation generation mechanism and <M> refers to the choice of M. For a more accurate description of our algorithms, see [3].

4 Performances analysis

We compare <p>-PM-<M> algorithms with state-of-the-art methods according to two criteria: distance to the Karcher mean and computation time. We observe that some of the algorithms we propose are nondominated, i.e., none of the other algorithms achieve both higher precision and lower computation time. We also notice that the advantage of the new algorithms becomes stronger when the size or the condition number of the data matrices gets large. It is also interesting to note that the <p>-PM-PM methods solely rely on the two-variable weighted geometric mean, a favorable situation towards an extension to sets other than $\mathbb{P}_n$.

We also prove that our estimate geometric means satisfy, depending on the choice of <p> and <M>, from seven to nine criteria among the ten criteria of the ALM list.

References

[1]   D.A. Bini, B. Iannazzo,"A note on computing matrix geometric means", Advances in Computational Mathematics, 35(2-4):175-192, 2011.

[2]   M. Palfia,"A multivariable extension of two-variable matrix means", SIAM Journal on Matrix Analysis and Applications, 32(2):385-393, 2011.

[3]   E.M. Massart, J.M. Hendrickx, P.-A. Absil, "Approximate matrix geometric means based on the inductive mean", http://sites.uclouvain.be/absil/2015.09 (preprint), 2015.

Tensor methods for systems and control

Mariya Ishteva
Department ELEC
Vrije Universiteit Brussel (VUB)
Pleinlaan 2, 1050 Brussels, Belgium
Email: mariya.ishteva@vub.ac.be

1 Introduction

Tensor decompositions are becoming increasingly popular in various scientific fields [4, 1], including signal processing, higher-order statistics, and chemometrics. This is due to their useful properties, namely, uniqueness and thus interpretability of the factors, ability to work with high-dimensional data directly, and ability to work with multiple data sets simultaneously (data fusion), among others.

Tensor methods are slowly entering the systems and control world [2, 5, 10] but their potential has not yet been fully utilized. We present an overview of re-occuring problems in systems and control where the powerful tensor techniques can be applied successfully, with the hope to increase their impact on the community.

2 Resolved problems

Often, a number of matrices are collected, mostly one matrix at a time instant, and their simultaneous diagonalization is required in order to proceed. Most of the diagonalizing techniques are based on orthogonal transformations; however, in many practical applications the required matrices are not necessarily orthogonal. This seemingly difficult problem is readily solved by the so-called canonical polyadic decomposition of the tensor build from the given matrices. We have recently used this equivalence for two totally different problems, namely for decoupling static nonlinearities in block-oriented system identification [2], and for calibration [7].

We briefly list a few more applications of tensors in systems and control. There is a one-to-one correspondence between homogeneous polynomials and symmetric tensors, which has been used in [8]. Hierarchical tensor decompositions are often used when numerically solving high-dimensional partial differential equations. Such decompositions are able to deal with the 'curse of dimensionality' [6, 3]. Further, data fusion techniques are particularly useful when having a number of (partially) related data sets. Tensors have also proven useful for sum-of-exponentials modeling and common dynamics estimation [5]. Higher-order singular value decomposition has been used for modeling linear parameter-varying systems, for data compression and for approximation of ND systems [10].

3 Final remarks

Tensor methods have a lot to offer to the systems and control community. Moreover, they can readily be used – there already exist a number of tensor toolboxes for MATLAB. Notably, the Tensorlab [9] has been developed in our network.

Acknowledgements

References

[1]   L. De Lathauwer. A survey of tensor methods. In *Proc. of the 2009 IEEE International Symposium on Circuits and Systems (ISCAS 2009)*, pages 2773–2776, Taipei, Taiwan, May 2009.

[2]   P. Dreesen, M. Ishteva, and J. Schoukens. Decoupling multivariate polynomials using first-order information and tensor decompositions. *SIAM J. Matrix Anal. Appl.*, 36(2):864–879, 2015.

[3]   L. Grasedyck. Hierarchical singular value decomposition of tensors. *SIAM J. Matrix Anal. Appl.*, 31(4):2029–2054, 2010.

[4]   T. G. Kolda and B. W. Bader. Tensor decompositions and applications. *SIAM Review*, 51(3):455–500, September 2009.

[5]   I. Markovsky, Otto Debals, and Lieven De Lathauwer. Sum-of-exponentials modeling and common dynamics estimation using tensorlab. Technical report, Vrije Univ. Brussel, 2015.

[6]   I. V. Oseledets. Tensor-train decomposition. *SIAM Journal on Scientific Computing*, 33:2295–2317, 2011.

[7]   Y. Rolain, M. Ishteva, E. Van Nechel, and F. Ferranti. Multi-line TRL revisited. In *Microwave Measurement Conference (ARFTG), 2015 85th*, pages 1–3, 2015.

[8]   M. Schoukens, K. Tiels, M. Ishteva, and J. Schoukens. Identification of parallel Wiener-Hammerstein systems with a decoupled static nonlinearity. In *The 19th World Congress of the International Federation of Automatic Control (IFAC WC 2014), Cape Town, South Africa*, 2014.

[9]   L. Sorber, M. Van Barel, and L. De Lathauwer. Tensorlab v2.0. Available online, January 2014, http://www.tensorlab.net/.

[10]   F. van Belzen and S. Weiland. A tensor decomposition approach to data compression and approximation of ND systems. *Multidimensional Systems and Signal Processing*, 23(1):209–236, 2012.

Actuator Management in Tokamaks using Mixed Integer Quadratic Programming

Bert Maljaars, Federico Felici
Eindhoven University of Technology
Department of Mechanical Engineering
P.O. Box 513, 5600 MB Eindhoven
The Netherlands
Email: (e.maljaars, f.felici)@tue.nl

Introduction

The tokamak is the furthest developed nuclear fusion device in which a ionized gas (plasma) is confined using magnetic fields. Such a tokamak requires a plasma control system (PCS) to help ensure that physics goals are met while remaining within operational and machine limits. Several control tasks need to be executed simultaneously which share a limited set of actuators. The priority of these control tasks and the availability of actuators may change suddenly due to events in plasma or hardware [1]. As such, actuator management is required to determine actuator requests to realize controller requests for a given actuator availability. Initial work on actuator management for the ASDEX-Upgrade tokamak was done using brute force computing [2]. In this work we propose a Mixed Integer Quadratic Programming (MIQP) approach to efficiently solve this actuator management problem.

Actuator management overview

In a tokamak, multiple distributed power sources are present to heat and drive current in the plasma. As an example, the Electron Cyclotron heating system for the future tokamak ITER uses electro-magnetic waves to locally heat and drive current in the plasma. This EC system consists of 24 sources that are connected to 11 steerable launchers that determine the deposition location in the plasma, where mechanical switches for each source determine connection options to launchers.

An overview of the actuator manager and its interfaces is given in Figure 1. Based on the provided controller requests with their corresponding priorities, and using the state of the actuators and the plasma, the actuator management block determines the source powers, launcher deposition locations and switch settings. The actuator management block uses an actuator availability description in terms of constraints and a performance measure (cost function) with penalties on e.g. error between requested and delivered power, launcher movements, and non-idle sources.
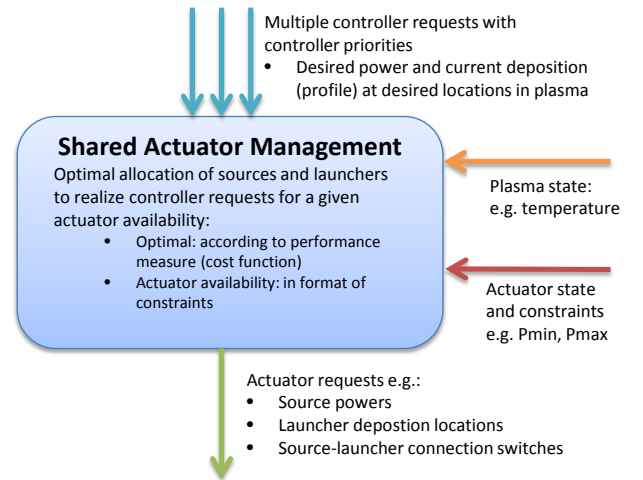
Figure 1: Overview of Shared Actuator Management.

MIQP-problem formulation

This actuator management problem with cost function and constraints can be formulated as a standard MIQP-problem:

$$
\begin{aligned}
\underset{z}{\text{minimize}} \quad & J(z) = z^T H z + f^T z, \\
\text{subject to} \quad & A_{ineq} z \leq b_{ineq}, \\
& A_{\text{eq}} z = b_{\text{eq}}, \\
& z_i \in \{0,1\}, \quad i \in \mathbb{I}^{n_b}
\end{aligned} \tag{1}
$$

where $\mathbb{I}^{n_b}$ is the set of indices corresponding to binary variables. These MIQP-problems can be solved efficiently using existing MIQP-solvers.

Results and conclusions

Results of representative test cases for the TCV tokamak and the future ITER tokamak show the potential of this MIQP-approach. The required computational time is compatible with (control) timescales of these tokamaks and scales favorable for increasing problem size compared to brute force computing [2].

References

[1]   D. Humphreys *et al*, Phys. Plasmas **22** 2 (2015)

[2]   C. J. Rapson *et al*, Fus. Eng. and Design **96-97** (2015)

Optimal damping of harmonic signals with unknown spectra

Yuri A. Kapitanyuk
ENTEG
University of Groningen
i.kapitaniuk@rug.nl

Anton V. Proskurnikov
ENTEG
University of Groningen
a.v.proskurnikov@rug.nl

Ming Cao
ENTEG
University of Groningen
m.cao@rug.nl

Most of the existing approaches to optimal damping and tracking of polyharmonic signals employ the performance indices that are independent of the control variable, as exemplified by the "cheap servomechanism problem" [1]. In the recent papers by V.A. Yakubovich and A.V. Proskurnikov, see e.g. [2, 3], another type of optimal linear-quadratic problems was considered where the cost functionals "penalize" the average powers of both state and control variables. For external signals with *known* spectrum the approach, elaborated in [2], allows to design a "universal controller", which delivers the optimal process independent of the signal's amplitudes (which can be uncertain). However, limitation of this result is the necessity to know the spectrum of the signal, which defines the coefficients of the controller. To overcome this limitation, we use the adaptive approach, complementing our systems with a frequency observer [4]. For simplicity, we confine ourselves to the case of uncertain sinusoidal signals $d(t) = a_0 + a_1 \sin(\omega t + \phi)$.

The Yakubovich "optimal universal" controllers

Given a linear *stable* plant with known coefficients

$$\dot{x}(t) = Ax(t) + Bu(t) + Ed(t), \quad y = Cx(t) + Dd(t), \quad (1)$$

in [2] a class of controllers (2) was proposed

$$N(p)u(t) = M(p)y(t), \quad p = d/dt, \quad (2)$$

that optimizes the quadratic performance index

$$J[x(\cdot), u(\cdot), d(\cdot)] = \overline{\lim_{T \to \infty}} \frac{1}{T} \int_0^T F[x(t), u(t), d(t)] dt, \quad (3)$$

for an *arbitrary* signal $d(t) = \sum_{j=1}^N d_j e^{i\omega_j t}$ with known ω_j. Here N, M are matrix polynomials and $\det N \neq 0$ and F is a quadratic form. The controller's coefficients are given by

$$M(p) = \delta(p)r_0(p), \; N(p) = M(p)CA_p^{-1}B + \rho(p)I_m,$$

where $A_p = pI_n - A$, $\delta(p) = \det A_p$, $r_0(p)$ is a matrix polynomial and $\rho(p)$ is a scalar Hurwitz polynomial, satisfying the *interpolation conditions* [2] with known matrices R_j

$$\delta(i\omega_j)r_0(i\omega_j)[D + CA_{i\omega_j}^{-1}E] = \rho(i\omega_j)R_j. \quad (4)$$

Here R_j depends on the plant (1), $\{\omega_j\}_{j=1}^N$ and the form F.

Adaptive optimal controller

Assume now that $d(t) = a_0 + a_1 \sin(\omega t + \phi)$, where a_i, ϕ, ω are uncertain. We consider a time-varying controller

$$\hat{M}(p, \hat{\omega}) = \delta(p)\hat{r}_0(p, \hat{\omega}), \; \hat{N}(p, \hat{\omega}) = \hat{M}(p, \hat{\omega})CA_p^{-1}B + \rho(p)I_m,$$

where $\hat{\omega}(t)$ is the output of the adaptive frequency estimator [4]. This estimator is designed as follows

$$\hat{\omega} = \sqrt{|\hat{\theta}|}, \; \hat{\theta} = \chi + k\dot{\xi}\ddot{\xi}, \; \dot{\chi} = -k\dot{\xi}^2\hat{\theta} - k\ddot{\theta}^2, \; k > 0 \quad (5)$$

$$(p + \lambda)^2\xi(t) = \lambda^2\tilde{y}(t), \quad \lambda > 0. \quad (6)$$

Here $\tilde{y}(s)$ is the "disturbance driven" part of the output, i.e.

$$\tilde{y}(t) = y(t) - W(p)u(t), \quad W(p) = C(pI - A)^{-1}B.$$

That estimator guarantees [4] that $|\omega - \hat{\omega}| \leq \rho_1 e^{-\beta_1 t}$, $\rho_1, \beta_1 > 0$, $\forall t \geq 0$.

Numerical example

As an example we present a simple task for the rejection of the harmonic signal in the linear plant

$$(p^2 + p + 1)y(p) = u(t) + d(t) \quad (7)$$

We simulate the behavior for the signal $d(t) = 3 + 5\sin\omega t$. Here $\omega = 2$ for $t < 25$, and then is switched to $\omega = 1.5$. The quadratic form is $F[x(\cdot), u(\cdot), d(\cdot)] = y^2 + 0.1u^2$.
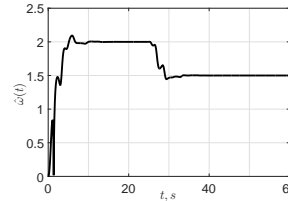
Figure 1: Frequency $\hat{\omega}(t)$ **Figure 2:** Output $y(t)$
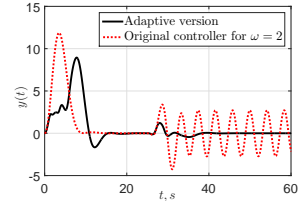
References

[1] Qiu, L. , Davison E.J., Performance Limitations of Non-minimum Phase Systems in the Servomechanism Problem// Automatica, 29(2), p.337-349, 1993

[2] Proskurnikov, A. V., Yakubovich, V. A., Universal controllers in model matching optimal control problems for unknown external signals// J. of Computer and Systems Science International, 51(2), p.214-227

[3] Proskurnikov, A. V., Universal controllers of V.A. Yakubovich: a systematic approach to LQR problems with uncertain external signals//IFAC-PapersOnLine 48(11), p.557562, 2015

[4] Bobtsov, A.A., Efimov, D., Pyrkin, A., Zolghadri, A., Switched Algorithm for Frequency Estimation with Noise Rejection//IEEE TAC, 57(9), p.2400-2404, 2012

Remote sensing and control with performance guarantees

B. Asadi Khashooei, D. J. Antunes, W. P. M. H. Heemels

Mechanical Engineering Dept., Eindhoven University of Technology, Eindhoven, The Netherlands

Emails: B.Asadi.Khashooei, D.Antunes, M.Heemels@tue.nl

1 Introduction

We consider a networked control system in which a remote controller queries the plant's sensors for measurement data and decides when to transmit control inputs to the plant's actuators. The goal is to keep transmissions to a minimum while guaranteeing that the closed-loop performance is within acceptable bounds.

2 Problem Formulation

We consider the remote control of a linear discrete-time system as depicted in Figure 1. The plant model is assumed to be given by

$$
\begin{aligned}
x_{k+1} &= Ax_k + B\hat{u}_k + v_k \\
\hat{y}_k &= Cx_k + r_k,
\end{aligned}
\tag{1}
$$

where $x_k \in \mathbb{R}^{n_x}$, $\hat{u}_k \in \mathbb{R}^{n_u}$ and $\hat{y}_k \in \mathbb{R}^{n_y}$ denote the state, the input, and the output, respectively and v_k and r_k denote the state disturbance and measurement noise at time $k \in \mathbb{N}_0$. We assume that the disturbance and noise processes are Gaussian zero-mean, independent sequences of random vectors with covariances Φ_v and Φ_r, respectively. The initial state is assumed to be either a Gaussian random variable with mean $\hat{x}_0$ and covariance Θ_0 or known in which case x_0 equals $\hat{x}_0$ and $\Theta_0 = 0$.

The transmissions in the networks are modeled by introducing $\sigma_k = (\beta_k, \gamma_k) \in \{0,1\}^2, k \in \mathbb{N}_0$, as a decision vector where $\beta_k = 1$ (or $\gamma_k = 1$) indicates the occurrence of a transmission through the network from sensor to controller (or from controller to actuator) at time k and $\beta_k = 0$ (or $\gamma_k = 0$) otherwise. We also consider that a standard zero-order hold device holds the most recently received value of the control action at the actuator side (in case no new control input is transmitted). Let u_k (or y_k) denote the sent (or received) value by the controller at time $k \in \mathbb{N}_0$ when a transmission occurs. We write $u_k = \emptyset$ (or $y_k = \emptyset$) to denote the case when at time $k \in \mathbb{N}_0$ no new values are transmitted. Moreover in order to control the plant, we consider the following cost to be minimized

$$
\lim_{N \to \infty} \frac{1}{N} \mathbb{E}\Big[\sum_{k=0}^{N-1} (x_k^T Q x_k + \hat{u}_k^T R \hat{u}_k) \Big]
\tag{2}
$$

where $Q \succ 0, R \succ 0$ are proper (positive definite) weighting matrices.

3 Proposed algorithm and results

The main result of the paper will be explained with the help of Figure 1. The event-triggering control block (ETC) consists of three functions of the information up to time k,
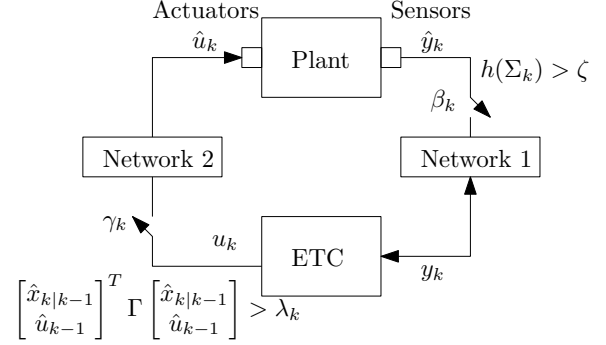
Figure 1: Overall setup and proposed policies: sensor query depends only on the Kalman filter covariance matrices Σ_k, while the control update transmissions are scheduled based on the Kalman filter state estimate $\hat{x}_{k|k-1}$, and the previously sent control input $\hat{u}_{k-1}$.

namely: (i) the estimator, which computes estimates of the state $\hat{x}_{k|k-1}$, (ii) the controller, which computes control actions, and (iii) the scheduler, which makes the transmission decisions. The proposed event-triggered control policies for sensor query and control input transmissions are derived using approximate dynamic programming (in particular, rollout techniques). This policy can be separated into an offline scheme for sensor query and an online scheme to schedule control input transmissions. In the online scheme determining the controller-to-actuator transmissions, the decisions are based on the state and control estimates, which are not known a priori and can be obtained via the time-varying Kalman filter. In the offline scheme for sensor query, transmissions are based on the covariances of the Kalman filter state estimates, which are known a priori. Interestingly, we can interpret this offline scheme as a policy in which transmissions occur when a function of the covariance of the Kalman filter exceeds a given threshold. The main advantage of our approach is that we can show that this event-triggered policy is stable (in a mean-square sense) and leads to performance guarantees in terms of the cost of all-time transmission policy (see [1] for details).

4 Acknowledgment

References

[1] B. Asadi Khashooei, D. J. Antunes, W. P. M. H. Heemels, "An event-triggered policy for remote sensing and control with performance guarantees," in Decision and Control (CDC), 2015 IEEE 54th Annual Conference on, December 2015, pp. 4830-4835.

Aperiodic Model Predictive Control: an Event-Triggered Strategy

Arman Sharifi Kolarijani　and　Tamas Keviczky

Delft Center for Systems and Control, Delft University of Technology

Email: {a.sharifikolarijani,t.keviczky}@tudelft.nl

1 Introduction

In networked control systems with bandwidth-limited communications, the application of traditional periodic sampling results into over-provisioning in communication components. To tackle this issue, researchers have proposed a new class of strategies, the so-called *event-driven control* (EDC) strategies. In these strategies, based on a desired notion of stability (and/or a measure of performance) the responsible entity for triggering is called the *triggering mechanism* (TM). EDC systems can be categorized into two subclasses: *event-triggered control* (ETC) and *self-triggered control* (STC). In ETC, the TM is an intelligent sensory system placed at the output of the system. In STC, the TM is encoded in the controller and determines the next triggering instant after each triggering event. Most of EDC strategies are called *emulation-based* techniques referring to the fact that the determination of the TM is based on an already synthesized controller for the plant [1].

Recently, researchers have been motivated to incorporate the processes of controller synthesis and TM design in a single framework. In this regard, the incorporation of model predictive control (MPC) and EDC is one of the directions that has been pursued. By doing so, the triggering mechanism enjoys not only characteristics of EDC but also interesting properties of MPC, such as synthesis of an optimization-based controller over a finite horizon and simultaneous treatment of state and input constraints [2].

2 Problem Setup

The problem we seek to tackle is the design of an event-triggering mechanism for a specific MPC problem. First, we introduce the specifications of the considered MPC problem. Then, we present a general framework of our approach to design an event-triggering mechanism.

Consider a continuous-time nonlinear system with bounded additive disturbance:

$$\dot{x}(t) = f(x(t), u(t)) + w(t) \qquad (1)$$

where $x(t) \in \mathscr{X} \subset \mathbb{R}^n$, $u(t) \in \mathscr{U} \subset \mathbb{R}^m$, and $w(t) \in \mathscr{W} \subset \mathbb{R}^n$ denote the state, input, and disturbance, respectively. Note that $\mathscr{X}$, $\mathscr{U}$, and $\mathscr{W}$ are compact convex sets. The nominal system is given by $\dot{\bar{x}} = f(\bar{x}(t), u(t))$. The finite horizon optimal control problem over the horizon T at the triggering instant t_s is given by:

$$\min_{u \in \mathscr{U}} J(\bar{x}(t_s), u(t)) = \min_{u \in \mathscr{U}} \int_{t_s}^{t_s+T} l(\bar{x}(s), u(s))ds + l_f(\bar{x}(t_s+T)),$$
$$(2)$$

subject to:

$$\begin{aligned}
\bar{x}(t) &\in \mathscr{X}(t), \; \forall t \in [t_s, t_s+T], \\
u(t) &\in \mathscr{U}, \; \forall t \in [t_s, t_s+T], \\
\bar{x}(t_s) &= x(t_s), \\
\bar{x}(t_s+T) &\in \mathscr{X}_f,
\end{aligned} \qquad (3)$$

where $J(\bar{x}(t_s), u(t))$ is the objective function, $l(\cdot, \cdot)$ and $l_f(\cdot)$ are the stage and terminal cost functions, $\mathscr{X}(t)$ is a time-dependent contractive set (to take into account the effect of w in the nominal system), and $\mathscr{X}_f$ is the terminal set (to guarantee the closed-loop stability). Consider $u^\star(t)$ and $\hat{x}(t)$ are the computed input and state trajectories by solving(2)-(3). Traditionally, (2)-(3) is solved with a fixed sampling period δ (i.e., $t_{s+1} - t_s = \delta > 0$, $s \in \mathbb{N}_{\geq 0}$) and the control action is given by $u(t) = u^\star(t_s)$, $\forall t \in [t_s, t_{s+1})$. The period δ is a pre-designed parameter based on the nonlinear system (1).

In this study, unlike the traditional MPC implementations, our main goal is to design a *time-varying sampling function* $\delta(x(t_s))$ (i.e., the triggering mechanism) rather than a fixed δ. In this regards, we consider the MPC problem with its sample-and-hold nature as a *sampled-data system* (i.e., the control action is updated in a sample-and-hold fashion). Such system can be viewed as a *retarded* (or *delayed*) *system* [3]. Following this line of reasoning, we intend to borrow the stability notions such as *Lyapunov-Razumikhin* or *Lyapunov-Krasovskii* to design the triggering mechanism as follows:

$$\delta(x(t_s)) := \min\{t > t_s \mid \alpha(\hat{x}(t), x(t)) > 0\}, \qquad (4)$$

where $\alpha(\cdot, \cdot)$ can be derived based on the notion of stability that will be used.

References

[1]   M. Heemels, K.H. Johansson, and P. Tabuada, "An introduction to event-triggered and self-triggered control," *in proc. IEEE 51st Annual Conference on Decision and Control*, pp. 3270-3285, 2012.

[2]   L. Grüne and J. Pannek, "Nonlinear Model Predictive Control: Theory and Algorithms," Springer, 2011.

[3]   J. Chen, K. Gu, and V. Kharitonov, "Stability of Time-Delay Systems," Springer, 2003.

Online distributed motion planning for multi-vehicle systems

Ruben Van Parys, Goele Pipeleers
KU Leuven, BE-3001 Heverlee, Belgium
Department of Mechanical Engineering, Division PMA
ruben.vanparys@kuleuven.be

1 Introduction

Networked multi-vehicle systems have received increasing attention over the last decades. Interesting application areas include surveillance, search and rescue, automated highway systems and cooperative transportation. This work presents a novel strategy for finding optimal input trajectories for vehicles to steer them from an initial location towards a desired destination. In doing so, interaction constraints between the agents, such as attaining a formation, avoiding collisions with each other or meeting at a destination position must be satisfied, while every vehicle should respect its local constraints. The computations for solving the problem are distributed among the agents by using the Alternating Direction Methods of Multipliers (ADMM). The algorithm is further formulated in an online fashion in order to cope with disturbances and variations in the environment.

2 Distributed formulation of the motion planning

The motion planning problem (1) for multi-vehicle systems searches for each vehicle's time-dependent trajectory $\mathbf{x}_i(\cdot)$. Optimal trajectories are obtained by minimizing the sum of all vehicle objectives J_i and are subject to local vehicle constraints, such as kinematic and dynamic limitations and collision avoidance constraints, described by a set $\mathscr{X}_i$. Each vehicle has several neighbors, denoted by the set $\mathscr{N}_i$ and an interaction constraint g_{ij} implies a relation between the trajectory $\mathbf{x}_i$ and $\mathbf{x}_j$ of respectively an agent i and its neighbor j.

$$
\begin{aligned}
\underset{\forall i:\, \mathbf{x}_i(\cdot)}{\text{minimize}} \quad & \sum_{i=1}^{N} J_i(\mathbf{x}_i) \\
\text{subject to} \quad & \mathbf{x}_i(t) \in \mathscr{X}_i \\
& g_{ij}(\mathbf{x}_i(t), \mathbf{x}_j(t)) = 0, \quad \forall j \in \mathscr{N}_i \\
& \forall t \in [0, T], \quad \forall i \in \{1, ..., N\}.
\end{aligned}
\tag{1}
$$

The trajectories are parameterized as splines as they allow a representation with a limited number of variables and enable guaranteed constraint satisfaction with a finite set of constraints [1]. The resulting optimization problem is decoupled using ADMM [2], which results in an iterative procedure where each iteration an agent only solves a local motion planning problem, considering its own constraints and objective. By communicating with its nearest neighbors, it is possible to incorporate the neighbors' intentions. This way, the ADMM iterations converge towards optimal motion trajectories where both the local vehicle constraints and the global cooperative constraints are satisfied.
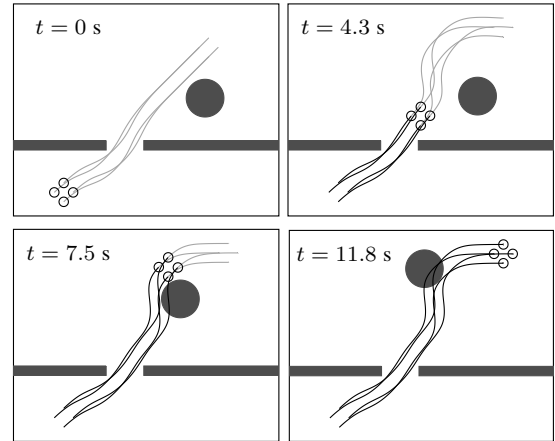
Figure 1: Motion trajectories for a formation of four holonomic vehicles in a dynamic environment. The circular obstacle starts moving at $t = 4\,\mathrm{s}$ with a velocity of $(-0.15, 0.15)$ m/s. As the updates proceed, the trajectories converge towards a new optimum. The average trajectory update time equals 47.15 ms.

3 Extension to real-time distributed motion planning

The algorithm is extended to a receding horizon formulation, such that the future part of the motion trajectories are reoptimized iteratively. The required update time and amount of inter-vehicle communication are reduced by performing only one ADMM iteration per trajectory update. In this way, the problem converges while the vehicles are heading towards their destination. Each update a new time horizon and a corresponding spline basis is defined. Because an ADMM iteration requires the information of trajectories of the previous iteration, their future part is first expressed in the new basis before introducing them to the next iteration.

4 Implementation and numerical validation

The proposed algorithm is implemented as part of a general spline-based motion planning toolbox, which facilitates the implementation and simulation of real-time motion planning problems. It is validated on numerical examples with linear as well as non-linear vehicle systems. Figure 1 considers a formation of holonomic vehicles in a dynamic environment.

References

[1]   W. Van Loock, G. Pipeleers, and J. Swevers, "B-spline parameterized optimal motion trajectories for robotic systems with guaranteed constraint satisfaction," *Mechanical Sciences*, vol. 6, no. 2, pp. 163–171, 2015.

[2]   S. Boyd, N. Parikh, E. Chu, B. Peleato, and J. Eckstein, "Distributed optimization and statistical learning via the alternating direction method of multipliers," *Foundations and Trends® in Machine Learning*, vol. 3, no. 1, pp. 1–122, 2011.

Towards anticipative LPV tube model predictive control

J. Hanema, R. Tóth, M. Lazar and S. Weiland
Control Systems Group, Department of Electrical Engineering,
Eindhoven University of Technology
P.O. Box 513, 5600 MB, The Netherlands
j.hanema@tue.nl

1 Introduction

Many practical systems (e.g., in high-precision motion applications) have operating-point dependent dynamics and are subject to constraints on their inputs, states, or outputs. For control design such dynamics can be represented by a linear parameter-varying (LPV) model, while constraints are handled using model predictive control (MPC). We consider the application of MPC to the LPV system

$$x(k + 1) = A\left(\theta(k)\right) x(k) + Bu(k), \; x(0) = x_0, \quad (1)$$

where $u : \mathbb{N} \to \mathbb{U} \subseteq \mathbb{R}^{n_u}$ is the input[1], $x : \mathbb{N} \to \mathbb{X} \subseteq \mathbb{R}^{n_x}$ is the state vector, and $\theta : \mathbb{N} \to \Theta \subseteq \mathbb{R}^{n_\theta}$ is the scheduling signal, which can be measured exactly. The sets $\mathbb{U}$ and $\mathbb{X}$ are the input- and state constraint sets. The set Θ is called the global scheduling set and it is known that $\forall k \in \mathbb{N} : \theta(k) \in \Theta_k \subseteq \Theta$. We call the sets Θ_k the scheduling subsets.

The addition of the time-varying scheduling subsets constitutes an extended setup in comparison to "classical" LPV MPC approaches, where it is assumed that $\theta(k) \in \Theta$ for all $k \in \mathbb{N}$. Through the sets Θ_k, we can include all available knowledge on how the scheduling variable might evolve in time. Examples include a tube around a nominal scheduling trajectory or known bounds on the rate of variation.

2 Anticipative LPV tube MPC

We have developed a tube MPC formulation for LPV systems (1) as an application of the general theory of [1].

Definition 1 (Constraint invariant tube). *A constraint invariant tube for the constraints* $(\mathbb{X}, \mathbb{U}) \subseteq \mathbb{R}^{n_x} \times \mathbb{R}^{n_u}$ *is defined as* $\mathbf{T}_N := (\{X_0, \dots, X_N\}, \{\Pi_0, \dots, \Pi_{N-1}\})$ *where* $X_i \subseteq \mathbb{R}^{n_x}, i \in \mathbb{N}_{[0,N]}$ *are sets and* $\Pi_i : \Theta_i \times X_i \to \mathbb{U}, i \in \mathbb{N}_{[0,N-1]}$ *are control laws. It holds that* $\forall x \in X_i, \forall \theta \in \Theta_i : A(\theta)x + B\Pi_i(\theta, x) \in X_{i+1} \cap \mathbb{X}$.

Instead of predicting the exact state evolution under the uncertainties, the controllers $\Pi_i, i \in \mathbb{N}_{[0,N-1]}$ guarantee that the state evolves inside a tube formed by the set sequence $X_i, i \in \mathbb{N}_{[0,N]}$ (Figure 1). On-line, we solve an optimization
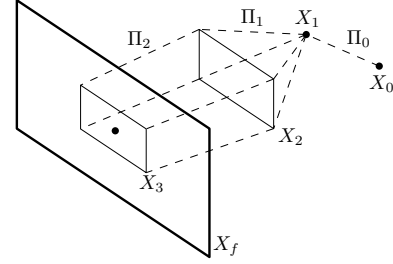
Figure 1: A two-dimensional tube with $N = 3$.

problem of the form

$$V(x_0) = \min_{\mathbf{T}_N} \; \sum_{i=0}^{N-1} \ell(X_i, \Pi_i) + V_f(X_N)$$
$$\text{s.t.} \quad \mathbf{T}_N \text{ satisfies Definition 1,}$$
$$X_0 = \{x_0\}, \; X_N \in \mathbb{X}_f, \quad (2)$$

where $\ell(\cdot, \cdot)$ is the stage cost representing a performance criterion, and $V_f(\cdot)$ and $\mathbb{X}_f$ are a terminal cost and -set selected to ensure asymptotic stability. The main challenge is to find parameterizations of the sets X_i and the control laws Π_i which are non-conservative but still lead to efficient computations. We choose tube cross-sections homothetic to a terminal set, gain-scheduled vertex controllers, and a worst-case linear stage cost. We assume that all $\Theta_i, i \in \mathbb{N}_{[0,N-1]}$ are polytopes and the dependency of A in (1) on θ is affine. Then, the on-line optimization problem is a linear program. The number of decision variables and constraints is linear in the prediction horizon N. It may, however, still be very large depending mainly on the complexity of the sets X_i. We are currently investigating alternative parameterizations of the control laws and cross-sections to achieve different trade-offs between control performance and computational complexity.

The approach is demonstrated on a simple example. It is shown how exploiting the available future knowledge of $\theta(k)$ – as described by the sets $\Theta_{k+i}, i \in \mathbb{N}_{[0,N-1]}$ – leads to improved control performance and larger domains of attraction.

References

[1] F. D. Brunner, M. Lazar, and F. Allgöwer, "An Explicit Solution to Constrained Stabilization via Polytopic Tubes," in *Proc. of the 52nd IEEE CDC*, 2013, pp. 7721–7727.

---

[1]Let $\mathbb{N}$ denote the set of nonnegative integers including zero.

Nonlinear vibrations phenomena of a tunable nonlinear spring characteristic

Kevin Dekemele, Robin De Keyser, Mia Loccufier
Department of Electrical Energy, Systems and Automation, Ghent University
Technologiepark 914, 9052 Zwijnaarde, Belgium
Email: Kevin.Dekemele@ugent.be

1 Introduction

Nonlinear vibrations occur in systems that have a nonlinear spring force. This system in the undamped case is:

$$m\ddot{x} + z(x) = F(t) \tag{1}$$

Previous research has focussed on spring forces expressed as polynomials, $z(x) = a_1 \cdot x + a_2 \cdot x^2 + a_3 \cdot x^3 + \ldots$. If $a_1 >> a_i$, the spring is called a weakly nonlinear. Semi-analytic techniques have shown the existence of sub and superharmonic resonances, as well bifurcations near these resonances ([1]). Other research focuses on $z(x) = ax^p$ for $p > 1$, often called strong nonlinear springs. Dependence of the free vibration frequency on initial energy is shown in ([2]). When harmonically excited, strongly nonlinear systems can vibrate significantly at any frequency, as long as the initial energy is above a certain threshold ([2]). The current study present a tunable spring element, first introduced in ([3]), for which $z(x)$ can be approximated as a polynomial in x through Taylor expansion. The polynomial coefficients are tunable to $a_1 >> a_i$ but also $a_1 \geq a_i$, increasing nonlinearity. With simulations, it is checked to what extend the approximated polynomial can predict nonlinear phenomena of the exact model.

2 Concept

The spring force is generated by the proposed string-pulley system, fig. 1a. Pulleys P1 and P3 are fixed, but P2 can move in the direction perpendicular to x. As the string is pulled at point M in the positive x direction, the tension in the string pushes down pulley $P2$ and the linear spring, which has stiffness k. A negative tension (pushing) will loosen the string from the pulleys, such that a positive displacement/force is required. The tension T in the string in function of x is:

$$T(x) = \frac{1}{2}k \cdot \frac{(h_0 - \sqrt{(L_0 - \frac{x}{2})^2 - l^2})(L_0 - \frac{x}{2})}{\sqrt{(L_0 - \frac{x}{2})^2 - l^2}} \tag{2}$$

with dimensions L_0, h_0 and l as indicated on fig. 1a.
To agree with the constraint of positive tension, two setups are concieved. In the first setup, fig. 1b, a mass m is attached to the string and moves forward and backward around a chosen working point (x_0, F_0). The second setup employs two spring elements, fig. 1c. By imposing an initial displacement x_0 on both elements, the tension in both strings is the
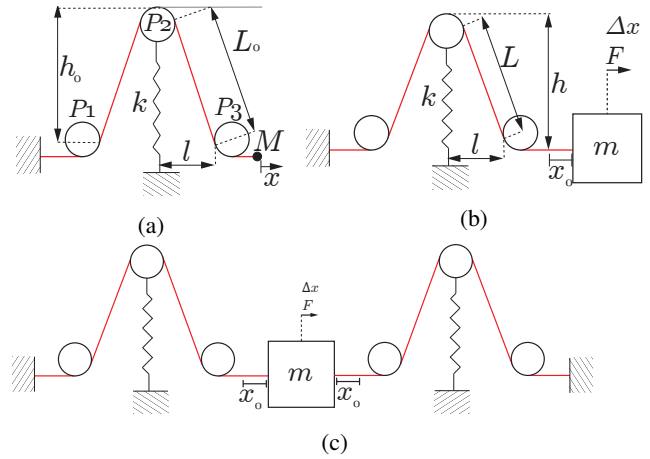
Figure 1: Nonlinear spring element in rest, (a) and with a connected mass and an initial displacement/force (b). Two elements allow for vibration around equilibrium Δx ([3])

same but opposite, creating an equilibrium position. A periodic force then acts on the mass. Series expansion of (2) reveals that the ratio L/h around an x_0 highly influences the coefficients of higher order terms for both setups. As the coefficients are tuned, different type of nonlinear phenomena occur for the approximate series, which are found in simulations of the exact system as well.

3 Conclusion

A nonlinear spring element is proposed which can be tuned to exhibit both weakly and strongly nonlinear vibration phenomena. In the future works, the role of the spring element on vibration absorption of a main system will be investigated.

References

[1]   A. H. Nayfeh and D. T. Mook, "Nonlinear oscillations," WHILEY-VCH, 1995.

[2]   F. Petit, et al. , "The Energy Thresholds of Nonlinear Vibration Absorbers", Nonlinear dynamics, 2013.

[3]   G. Tionietti et al., "Design and control of a variable stiffness actuator for safe and fast physical human/robot interaction", IEEE proceedings, 2005.

A time domain based MIMO waveform replication algorithm

Sikandar Moten, Goele Pipeleers and Jan Swevers
Department of Mechanical Engineering, KU Leuven
Celestijnenlaan 300 - bus 2420, 3001 Leuven, Belgium
sikandar.moten@kuleuven.be

1 Abstract

In automotive industry, service load simulation and component testing such as qualification tests, durability tests and endurance tests are an integral part of the overall design and development process of vehicles. A substantial amount of these tests is performed on multi-axial hydraulic test rigs in the laboratory [1]. The goal of these tests is to replicate real operating conditions in a lab environment. The existing state-of-the-art replication algorithm consists of two phases [1]: Identification of a non-parametric frequency domain model and its inverse, followed by an off-line frequency domain iterative learning control (ILC) phase. The update law transforms the error and drive signals to the frequency domain using a discrete fourier transform (DFT) and re-transforms back the updated drive signal to time domain using an inverse DFT. These transformations require considerable amount of time in between trials in case of long time waveforms. Unlike existing methods, this research proposes an online time domain based technique. The method combines adaptive inverse plant modeling and a time domain based update law, which help to accelerate the drive signal generation process.

2 Experimental Validation

First, the proposed algorithm learns itself how to control a specific system using adaptive inverse plant modeling and creates the first feedforward drive signal. Next, the use of ILC helps to improve the performance. The presentation will discuss an experimental validation of the proposed approach. A rear sub-frame of a car is used as the testing component. The goal is to replicate the target data with a spectral content between 5 and 50 Hz in the X and Z direction at a specified point on the frame i.e. top left corner. An industrial six degrees of freedom hydraulic CUBE^{TM} Shaker, also shown in Figure 1, is used to replicate the target data. The qualitative behaviour of the measured responses as compared to the target signals for X and Z axes are shown in Figure 2(a). In addition, the tracking and convergence behavior can be seen in Figure 2(b). Figure 2 shows that the algorithm is capable to precisely track the target signals.

In conclusion, we have proposed an online technique for the waveform replication which doesn't need to transform the time domain signals to frequency domain and back, and therefore requires minimal processing time in between trials
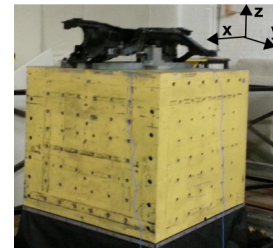
Figure 1: A rear sub-frame of a car mounted on CUBE shaker

irrespective of the length of the target signal.
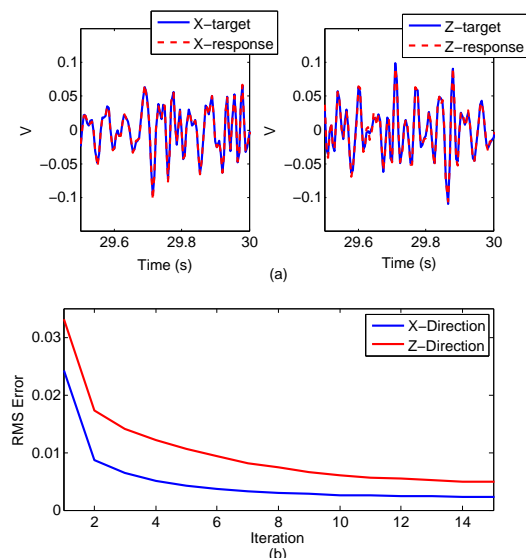
Figure 2: Response signals in comparison with reference target

3 Acknowledgement

References

[1]   J. De Cuyper. Linear feedback control for durability test rigs in the automotive industry. *PhD Thesis*, Katholieke Universiteit Leuven, 2006.

Combining Probable Trajectories in Air Traffic Management

François Gonze*   Jean Boucquey[†]   Raphaël M. Jungers[*1]

`francois.gonze@uclouvain.be`   `jean.boucquey@eurocontrol.int`   `raphael.jungers@uclouvain.be`

* ICTEAM Institute, UCLouvain, Louvain-la-Neuve, Belgium
[†] ATM/RDS/ATS, EUROCONTROL, Brussels, Belgium

Introduction

We introduce here the COPTRA project (COmbining Probable TRAjectories). COPTRA is an Air Traffic Management (ATM) project which aims at better predicting and controlling the uncertainty of air traffic situations in the European sky. The idea is to combine the available aircraft trajectory information and to generalize its use in Air Traffic Control (ATC) planning. This project has recently been presented for funding to the European Commission. It is currently in the negotiation phase, and could start in March 2016. COPTRA involves a consortium of 5 entities from three different countries: *CRIDA* (*Centro de Referencia Investigacion Desarrollo e innovacion ATM*), leader of the project, from Spain, *BR&TE* (*Boeing Research & Technology Europe*) from Spain, *ITU* (*Istanbul Teknik Universitesi*) from Turkey, *EUROCONTROL* (*European Organisation for the Safety of Air Navigation*), and the *UCLouvain* (*Université catholique de Louvain*) from Belgium. The project should last for two years.

1 The SESAR Framework

The Single European Sky ATM Research (SESAR) is a European programme aiming at completely overhaul European airspace and its air traffic management. SESAR involves numerous calls for projects, both for applied/industrial research, and for fundamental/exploratory research, see [1].

The COPTRA project has been presented at the *SESAR joint undertaking exploratory research H2020 call 1* (see [1]).

2 The Project

COPTRA aims at modeling and predicting uncertainty in plane trajectories by better combining available information. The project is divided in three parts. The first step is to define the air traffic situation uncertainty and a way of quantifying it. The second step is, based on the definition from the first step and on available data, to analyze how the uncertainties (in time and space) on the different flights combine with each other and propagate in the network of trajectories. This part is more detailed in the next section. The last step is

to integrate the new models and algorithms into the existing ATM planning tools and operations.
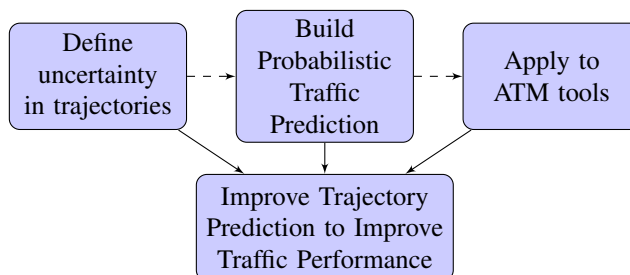
3 Modeling and analysis of the network of trajectories

The goal of this work package is to leverage tools from applied mathematics towards ATM applications. These tools range through various fields, from queuing theory (see [2]) to robust control, or large graphs and networks analysis. In particular, we will analyze how trajectories interact with each other by modeling them with a graph. We will apply recent techniques from large networks analysis (e.g. [3]) in order to quantify the propagation of uncertainty, detect critical trajectories, and develop decision making tools for air traffic controllers. The definition of the graph (vertices and edges) is part of the project, and numerous approaches are possible (relation between planes could for example be based on the fact that the two planes are in the control of the same air traffic controller at the same time, start from the same airport, etc.). Based on the analysis of this large network, we will investigate how robust control methods can be designed for optimizing aircraft trajectories.[2]

References

[1] SESAR Joint Undertaking, SESAR 2020 Exploratory Research: First Call for Research Projects V1.1, 24/03/2015, *http : //ec.europa.eu/research/participants/data/ref/h2020/ other/call_fiches/jtis/h2020 − call − doc − er − sesar − ju_en.pdf*.

[2] H. Chen and David D. Yao, Fundamentals of queueing networks: Performance, asymptotics, and optimization, Springer, 2010.

[3] V.D. Blondel, J.-L. Guillaume, R. Lambiotte and E. Lefebvre, Fast Unfolding of Communities in Large Networks, J. Stat. Mech, p. 10008, 2008.

[2]If you are interested in the project, please contact R. Jungers.

Plug-and-play control: integrating distributed model predictive control in today's industry

Pieter Maelegheer
DySC Technologiepark, 914
B-9052 Zwijnaarde (Gent)
Pieter.Maelegheer@Ugent.be

Clara Ionescu
DySC Technologiepark, 914
B-9052 Zwijnaarde (Gent)
ClaraMihaela.Ionescu@Ugent.be

Robin De Keyser
DySC Technologiepark, 914
B-9052 Zwijnaarde (Gent)
Robain.DeKeyser@Ugent.be

1 Introduction

Nowadays industrial processes, manufacturing systems and traffic networks consist increasingly of multiple independent yet interacting subsystems. Tackling such a large scale system with a centralised control structure is generally viewed as impractical, inflexible and unsuitable due to the presence of high coupling, constraints, nonlinearity and communication limitations. Hence, several control architectures have been developed and applied over the last four decades [1]. A first and most often applied structure is the decentralised approach where only local control is of importance, i.e. the local regulators have no knowledge of neighbouring regulators. This approach is rarely optimal and might lead to instabilities when the interactions are significant. In order to overcome these issues, one could consider the alternative of higher level control which coordinates the local regulators as with the hierarchical structure. Alas, the higher level control often becomes so complex that its hard to justify the advantages over a fully centralised approach [2]. Consequently the distributed control architecture with exchange of information among local regulators is increasing in popularity. Hereby the effects of the local actions are taken into account at a system-wide level such that the nearly optimal global performance can be achieved.

2 Plug-and-play distributed MPC

One of the control techniques which benefits from these developments is the model-based predictive control (MPC). This control methodology uses an online process model to calculate predictions of the future plant output and one or more cost functions in order to optimise future control actions with or without constraints. Due to the above, large-scale systems are more and more regulated using the MPC technique combined with a distributed architecture. In [3] an up-to-date overview of all the different published DMPC topologies is given. Besides the lower computational complexity and communication load w.r.t. the centralised approach, DMPC also allows us to add a plug and play feature to the large-scale system. This is particularly interesting since most large industrial processes are always live systems in the sense that they are subject to constant change in terms of instrumentation (sensors and actuators) and in terms of subsystems that are added or removed [4].

3 Goals

In this project we address the problem of scalability of a large scale system while taking into account both the local as the global constraints. Accordingly, this allows flexible adaptations to the large scale system. The ultimate goal is to combine the benefits of adaptive algorithms with that of MPC, leading to increased acceptance in the process industry. The long-term goal can be divided into two main objectives:

1. To develep a constrained DMPC scheme on a laboratory scale application consisting of n independent yet interacting subsystems. Hereby, stability, robustness and energy efficiency will be the guiding terms during this developing phase.

2. To optimise the obtained DMPC algorithm with a model-adapting property which will be able to obtain the most relevant model parameters from a control-point-of-view. Those essential parameters can vary due to changes in operating point and number of subsystems.

References

[1]   R. Scattolini. Architectures for distributed and hierarchical model predictive control–a review. *Journal of Process Control*, 19(5):723–731, 2009.

[2]   A. Dutta, C. Ionescu, and R. De Keyser. A pragmatic approach to distributed nonlinear model predictive control: Application to a hydrostatic drivetrain. *Optimal Control Applications and Methods*, 36(3):369–380, 2015.

[3]   R.R. Negenborn and J.M. Maestre. Distributed model predictive control: An overview and roadmap of future research opportunities. *Control Systems Magazine, IEEE*, 34(4):87–97, 2014.

[4]   J. Stoustrup. Plug & play control: Control technology towards new challenges. *European Journal of Control*, 15(3):311–330, 2009.

Iterative Pole-Zero Model Updating Using Combined Sensitivities

Masoud Dorosti, Rob Fey, Marcel Heertjes, and Henk Nijmeijer
Department of Mechanical Engineering, Eindhoven University of Technology
Eindhoven, The Netherlands
Email: m.dorosti@tue.nl

1 Introduction

A crucial step in the control of a high-tech system is having a very accurate dynamic model of the system from actuators to sensors and to the unmeasured performance variables. A (reduced) Finite Element (FE) dynamic model may be a good candidate apart from the fact that its accuracy is often limited to satisfy the control purpose. To improve the accuracy of the FE model, an Iterative Pole-Zero (IPZ) model updating procedure is proposed that updates poles and zeros of the system by updating the eigenvalues of the stiffness and/or damping matrix. Pole and zero estimates from measured Frequency Response Functions (FRFs) is deployed.

2 Case Study

Consider a 2D finite element model of an aluminum beam with 1 m length and 0.02 m thickness, see Figure 1. 12 Euler beam elements of equal size are used. Each element has two nodes and each node has two Degrees Of Freedom (DOFs): transversal (w) and rotational (r_x) displacement. Modal damping of 0.1% is added to all modes. The experimental structure differs from the original model where the 6th and 7th elements has 0.03 m thickness instead. Assume
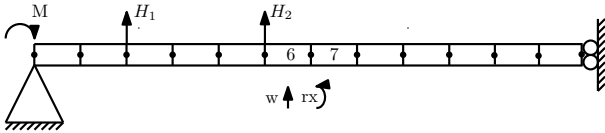
Figure 1: 2D aluminum beam system.

that a moment actuator is located on the left end, a displacement sensor is located on the transversal DOF of the third node (H_1), and the unmeasured performance variable is the transversal DOF of the sixth node (H_2). The poles (λ_p) of the original H_1 FRF is calculated via the eigenvalue problem

$$(\lambda_p^2 M_n + \lambda_p C_n + K_n)u_p = 0, \tag{1}$$

where M_n, C_n, K_n are mass, damping, and stiffness matrices and u_p is the eigenmode. The zeros (λ_z) are calculated via

$$(\lambda_z^2 M_s + \lambda_z C_s + K_s)u_z = 0, \tag{2}$$

where M_s, C_s, K_s are the substructure matrices derived from M_n, C_n, K_n by deleting the column and the row corresponding to the actuator and the sensor DOFs.

3 Iterative Pole-Zero Model Updating

If no information is available on possible locations of stiffness/damping errors in the model, it is proposed to use only a limited number of eigenvalues of the stiffness and damping matrix as generic parameters (θ) to be updated. IPZ model updating is a procedure which tries to minimize the following pole-zero error function iteratively (i) by updating the generic parameters.

$$\varepsilon_i = (\Delta r_i)^H W (\Delta r_i) \tag{3}$$

where $W > 0$ is diagonal weighting matrix and,

$$\Delta r_i = \begin{bmatrix} \lambda_p^e \\ \lambda_z^e \end{bmatrix} - \begin{bmatrix} \lambda_p^n \\ \lambda_z^n \end{bmatrix}_i - \begin{bmatrix} \frac{\partial \lambda_p^n}{\partial \theta_p} & \frac{\partial \lambda_p^n}{\partial \theta_z} \\ \frac{\partial \lambda_z^n}{\partial \theta_p} & \frac{\partial \lambda_z^n}{\partial \theta_z} \end{bmatrix}_i \begin{bmatrix} \Delta \theta_p \\ \Delta \theta_z \end{bmatrix}_i. \tag{4}$$

IPZ model updating without combined sensitivity is presented in [1].

4 Simulation Results and Conclusions

The IPZ model updating is performed on the original H_1 FRF by updating the first three complex-valued poles and zeros toward the measured poles and zeros from the experimental H_1 FRF. In Figure 2, the original, experimental, and updated H_1 and H_2 FRFs are shown. In contrast to the original H_1 FRF, the updated H_1 FRF matches very well with the experimental H_1 FRF. Furthermore, the updated unmeasured variable reflected by H_2 FRF also matches well with the experimental H_2 FRF in contrast to the original H_2 FRF.
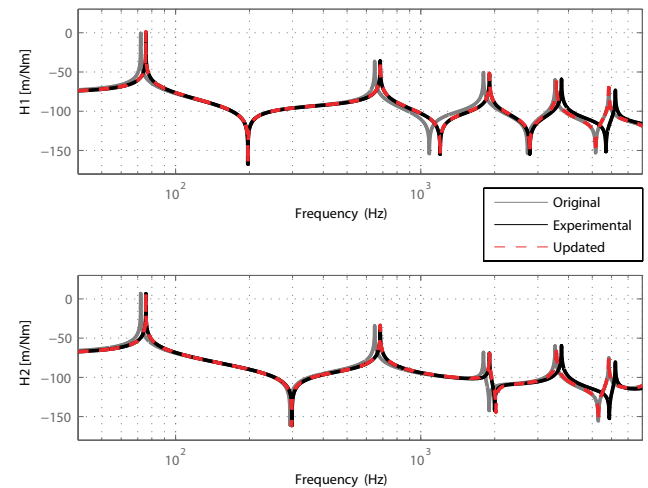
Figure 2: Original, experimental, and updated H_1 (top) and H_2 (bottom) FRFs after IPZ model updating.

References

[1] M. Dorosti et al, Iterative Pole-Zero Model Updating Using Generic Parameters, submitted to MSSP, 2015.

Hybrid trajectory tracking control
for a robotic leg performing hops

M.W.L.M. Rijnen, A.T. van Rijn,
A. Saccon, and H. Nijmeijer
Department of Mechanical Engineering
Eindhoven University of Technology
5600 MB Eindhoven, The Netherlands
m.w.l.m.rijnen@tue.nl

H. Dallali
Department of Mechanical Engineering
Michigan Technological University
MI 49931-1295 Houghton, USA

1 Introduction

We consider the trajectory tracking problem for robotic systems with unilateral constraints. Such systems can be modeled using the hybrid systems framework with continuous dynamics when in contact mode or in free motion and discrete dynamics describing transitions between the different modes. We focus in this work on a recently introduced hybrid trajectory tracking controller [1] and investigate if it is suitable for trajectories with changing state dimension due to evolution in different modes. In particular, we consider trajectory tracking of a hopping motion for a robotic leg.

2 Problem description

Consider the robotic leg depicted in Fig. 1 (cf. [2]). It consists of two links connected to each other and to two vertical sliders via revolute joints. An input torque τ can be applied to it at the 'knee'. When in mid-air (mode 1) the configuration of the robot can be captured by the two degrees of freedom (DOF) q_k and q_h (see Fig. 1), whereas when the leg is in contact with the ground (mode 2) the angle q_k suffices. The aim of this work is to investigate if the hybrid trajectory tracking controller, introduced in [1], can be used to track a hopping reference trajectory for the robotic leg where the number of DOF differs per mode. The control strategy is based on extending the reference trajectories before and after mode transitions to beyond the corresponding event time.
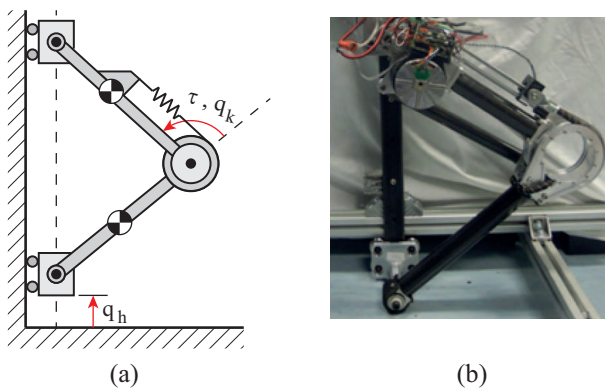
Figure 1: Schematic representation (a) and image (b) of the hopping robotic leg.

3 Results

As a reference trajectory, consider a continuing sequence of 0.1 m hops separated in time by 0.3 s contact periods, as illustrated in Fig. 2. Starting from a perturbed initial condition, the hybrid trajectory tracking controller is used to steer the system towards this reference. From Fig. 2 can be concluded that the controller indeed does so successfully.
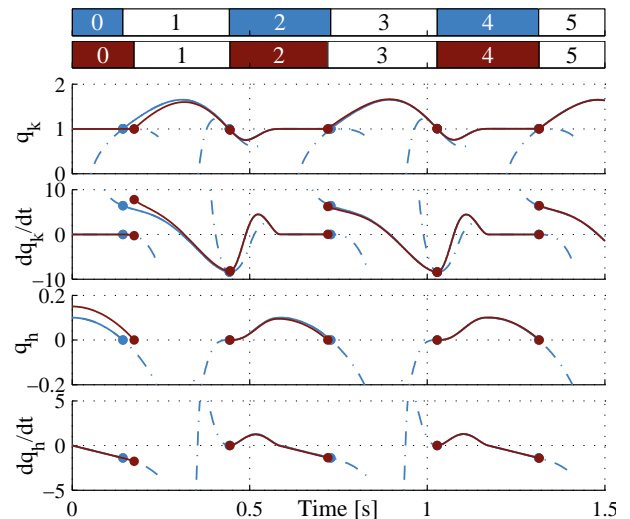
Figure 2: Resulting trajectory (dark red) in tracking a reference trajectory (light blue) with extensions (dashed) for the robotic leg in Fig. 1 with perturbed initial condition. The bars on top indicate the mode (in mid-air when colored and in contact when white) and counter j.

References

[1] A. Saccon, N. van de Wouw, H. Nijmeijer. Sensitivity analysis of hybrid systems with state jumps with application to trajectory tracking. *53rd IEEE Conference on Decision and Control (CDC)*, Dec. 15-17, 2014, Los Angeles, USA

[2] N.G. Tsagarakis, H. Dallali, F. Negrello, W. Roozing, G.A. Medrano-Cerda, D.G. Caldwell. Compliant antagonistic joint tuning for gravitational load cancellation and improved efficient mobility. *14th IEEE-RAS International Conference on Humanoid Robots*, Nov. 18-20, 2014, Madrid, Spain

Bilateral Human-Robot Control for Semi-Autonomous UAV Navigation[1]

Han W. Wopereis, Matteo Fumagalli, Stefano Stramigioli, and Raffaella Carloni
Faculty of Electrical Engineering, Mathematics and Computer Science, University of Twente, The Netherlands
{h.w.wopereis, m.fumagalli, s.stramigioli, r.carloni}@utwente.nl

1 Introduction

Thanks to their agility, Unmanned Aerial Vehicles (UAVs) are exemplary to be used in surveillance, inspection and search-and-rescue missions [1]. Although fully autonomous operation is often desirable, many complex tasks in dense terrains can only be accomplished if the UAV is supervised by a human operator. Teleoperation requires full attention of the operator, which is not cost-efficient, and can increase the duration of the operation as the time needed to perform a specific task depends linearly on the delay in the loop.

2 Semi-autonomous Control

This work proposes a semi-autonomous control architecture which can be classified as supervisory-control [2]. The control architecture is depicted in Figure 1 and is based on the classical bilateral teleoperation paradigm in which the human-operator operates a *Master device*, which consists of the *Human machine interface* and the *Master controller*, to interact with the *Slave device* via a communication channel. The *Slave device* consists of the *Slave controller*, which performs low-level control, and the *Slave robot* which represents the physical robot. The *Master device* receives a feedback on the state of the slave and/or on the environment.

Our approach extends the classical paradigm by inserting an autonomous controller between the *Master device* and the *Slave device*. The human operator can issue discrete commands to the autonomous controller and, when desired or needed by the mission, the human can overrule the autonomous controller's parameters. The autonomous controller translates these discrete signals into a continuous stream of setpoints.

A quadrotor UAV has to autonomously navigate a cluttered environment, while avoiding obstacles and paths that are narrower than a certain safety distance. The human operator is equipped with a non- invasive human-machine-interface that facilitates inertial and electro-myographic inputs so that the safety level can be overruled by interpreting the gestures of the human operator. Non-invasive haptic and graphical information are fed back during performing the mission.
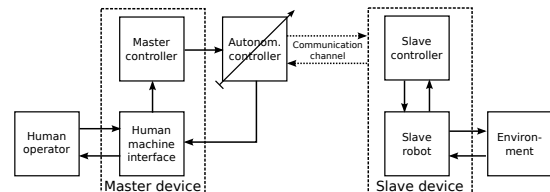
Figure 1: Overview of the semi-autonomous bilateral architecture.

3 Experiments

In the experiments, the task given to the operator was to guide the UAV through the opening without hitting the walls. The opening had a size of 0.7 m, which is slightly bigger than the UAV. The operator was able to set any target-location in the map and could alter the safety-distance r_s, which could be set to 12 discrete values between $0.62m$ and $0.31m$. This is accordance with the discrete output of the inertial measurement unit in the MYO armband. Figures 2 shows one of the successful trials.
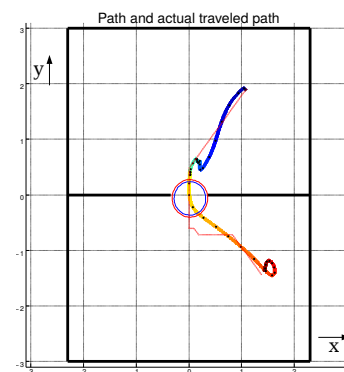
Figure 2: 2D visualization of the traveled path in one of the trials of the experiment.

References

[1] L. Marconi, et al., The SHERPA project: Smart collaboration between humans and ground-aerial robots for improving rescuing activities in alpine environments, *IEEE SSRR*, 2012.

[2] H.W. Wopereis, et al., Bilateral Human-Robot Control for Semi-Autonomous UAV Navigation, *IEEE IROS*, 2015.

Experimental validation of path-following NMPC applied to a serial-link robot manipulator

Niels van Duijkeren, Goele Pipeleers and Jan Swevers
KU Leuven, BE-3001 Leuven, Belgium
Department of Mechanical Engineering, Division PMA
Niels.vanDuijkeren@kuleuven.be

1 Introduction

In robotics, it is often the case that the essence of a given task is described by the path the end-effector should follow. Examples include the control of welding, gluing, assembly robots and CNC machines. Offline methods exist to generate a time-/energy-optimal trajectory aiming for tracking a given geometric path exactly, and recently an efficient convex reformulation of this problem has been derived [1]. These path planning methods generate a time-based reference signal that can readily be fed to joint angle controllers of the robotic system. Path following control concerns feedback laws that drive systems to follow a geometric path, while accounting for disturbances and model mismatch. In practice this means that the timing law (i.e., where to be when on the path) is introduced as control freedom. This enables control systems to trade off speed and path following accuracy. Predictive approaches to path following control are commonly referred to as model predictive path-following control (MPFC) techniques [2]. We introduce a control strategy related to MPFC employing a transformation of the prediction model system dynamics. Consequently, the geometric nature of path following is prominently present in the resulting problem formulation [3]. This presentation addresses practical challenges regarding the implementation of the control method, which are particularly about trading computation times against optimality of the control law.

2 Control approach

Let $\gamma(t)$ be a continuous, sufficiently smooth curve in three-dimensional Euclidean space $\Gamma = \{\gamma(s) \in \mathbb{R}^3 : s \in [0,l]\}$, parametrized by its arc length. Furthermore, let $p(t)$ be the position of the end effector in the inertial world frame, which can be calculated using the forward kinematics of the robot manipulator. Then the point on the path γ closest to $p(t)$ is $\gamma(s^\star)$, where $s^\star = \arg\min_s \frac{1}{2}\|r(s,t)\|_2^2$ for $r(s,t) = p(t) - \gamma(s)$. Via the necessary optimality conditions for $s^\star$ we obtain its time derivative [3],

$$\dot{s}(t) = \frac{v(t)^T \gamma'(s(t))}{1 - r(s(t),t)^T \gamma''(s(t))}. \tag{1}$$

Consider the state vector ξ; using the established representation for the dynamics of the position of the end-effector

Figure 1: Illustration of the writing experiment, executed by the ABB IRB120 industrial robot.

$p(t)$ with respect to the path (1), we perform a spatial transformation of the equations of motion:

$$\xi' := \frac{d\xi}{ds} = \frac{d\xi}{dt}\frac{dt}{ds} = \frac{1}{\dot{s}(t)}\dot{\xi}. \tag{2}$$

The resulting control law for a finite horizon least-squares integral objective $J(\xi, u, \dot{s})$, employing transformation (2), follows from solving:

$$\min_u \{J(\xi, u, \dot{s}) | \xi' = \frac{f(\xi, u)}{\dot{s}}, u \in \mathscr{U}, \xi \in \mathscr{X}\} \tag{3}$$

Here we consider a differentially flat model of the robot manipulator, meaning u represents the joint angle accelerations.

3 Experiments

The control approach is experimentally validated through a writing task executed by an industrial robot. Considered here is a six-DOF ABB IRB120 with an open joint angle trajectory controller, see Figure 1 for an illustration.

References

[1] D. Verscheure, B. Demeulenaere, J. Swevers, J. De Schutter, and M. Diehl, "Time-optimal path tracking for robots: A convex optimization approach," *IEEE Transactions on Automatic Control*, vol. 54, no. 10, pp. 2318–2327, 2009.

[2] T. Faulwasser and R. Findeisen, "Nonlinear model predictive control," in *Nonlinear Model Predictive Control*, pp. 67–85, 2009.

[3] N. van Duijkeren, R. Verschueren, G. Pipeleers, M. Diehl, and J. Swevers, "Path-following nmpc for serial-link robot manipulators using a path-parametric system reformulation." Submitted to the 2016 European Control Conference, 2016.

A Variable Stiffness Robotic Arm for the SHERPA Project[1]

E. Barrett, S. Stramigioli and R. Carloni

Faculty of Electrical Engineering, Mathematics and Computer Science, University of Twente, The Netherlands

{e.barrett, s.stramigioli, r.carloni}@utwente.nl

1 Introduction

The goal of SHERPA is to develop a mixed ground and aerial robotic platform to support search and rescue activities in a real-world hostile environment like the alpine scenario [1]. A key part of the robotic team is a ground rover that acts as a mobile base station for small unmanned aerial vehicles (UAVs). A robotic arm enables the rover to autonomously deploy and recover the UAVs during the mission, thus relieving the human operator from the need to recharge or look after the UAVs.

The SHERPA robotic arm must be able to interact with its environment in a safe and robust way, especially when performing dexterous grasping and docking maneuvers with the UAVs. The use of a mechanically variable compliance in the actuation of the arm is of core importance for the performance of the arm and for the accomplishment of the search and rescue activity.

2 The SHERPA arm

The SHERPA arm, shown in Figure 1 (left), is a seven DoF robotic arm with a reach of one meter, designed to manipulate an UAV in a adverse outdoor conditions. It is composed of a three DoF differentially actuated shoulder, a one DoF elbow joint that actuates two coupled axes, and a three DoF wrist, that is also differentially actuated. Finally it is equipped with a gripper, giving it one additional DoF to robustly lock into a custom interface on the UAV.

3 Variable Stiffness Modules

The SHERPA arm has several DoF with a variable mechanical compliance, namely in the shoulder and wrist joints. The differentially actuated wrist joint incorporates a 2-DoF variable stiffness mechanism, with a coupled compliance. This means that only one actuator is needed to change the stiffness of both DoF, resulting in a 2-DoF spherical output stiffness of the wrist.

The shoulder joint is also differentially actuated, but the variable stiffness mechanism is connected in series to the robot's DoF. However, both designs are based on a variable transmission achieved through moving the pivot point of a lever that is connected to the internal springs on one end, and
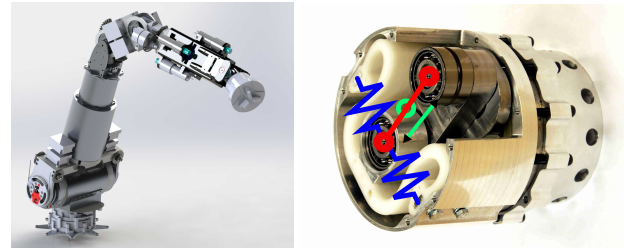
Figure 1: The SHERPA arm (left) and the variable stiffness module of the shoulder joint (right).

to the mechanism's output at the other. The key difference between the wrist and shoulder joints is that the shoulder is subject to much higher loads.

4 Elastic Energy Storage

Most variable stiffness mechanisms show a strong dependency of their achievable output deflection on their output stiffness, i.e. their passive deflection is limited for higher stiffnesses. This is often a particular feature of their working principle, but also a consequence of the limited energy storage capacity of their internal springs. A limited torque-deflection workspace limits the range of the output stiffness for large torques. This is particularly true for the highly loaded shoulder joint, shown in Figure 1(right).

A special Ω-shaped leaf spring has been designed to maximize the spring's energy capacity within the given design constraints, thus preserving the arm's capacity to adjust its stiffness, even under large loads. The spring's shape and thickness have been laid out such that it is as stiff as possible, while the stress remains below a permissible level. Distributing the stress as uniformly as possible maximizes the strain energy in the material.

References

[1]   L. Marconi, et al., The SHERPA project: Smart collaboration between humans and ground-aerial robots for improving rescuing activities in alpine environments, *IEEE SSRR*, 2012.

[2]   B. Vanderborght, et al., Variable impedance actuators: A review, *Robotics and Autonomous Systems*, vol. 61, no. 12, pp. 160-1614, 2013.

Distributed control of autonomous agents with sensor fusion methodologies

Simon Cherlet
DySC, Ghent University
Technology Park 914
B-9052 Zwijnaarde
Simon.Cherlet@UGent.be

Cosmin Copot
DySC, Ghent University
Technology Park 914
B-9052 Zwijnaarde
Cosmin.Copot@UGent.be

Robain De Keyser
DySC, Ghent University
Technology Park 914
B-9052 Zwijnaarde
Robain.DeKeyser@UGent.be

1 Introduction

Stimulated by a worldwide demand for ever larger productivity in crop harvesting, agricultural manufacturers have pushed the size and power of contemporary combine harvesters to its maximum. However this trend is now steadily saturating due to several considerations such as cost, complexity, maintenance issues, and road transportation restrictions. Because of these problems manufacturers have to come up with other ways of making future farming even more cost efficient.

Bearing in mind the current state-of-the-art in autonomous vehicles, beit ground or aerial [1, 2], it seems the time is right to introduce a novel approach to the aforementioned problem. Namely, instead of using one very large, ponderous combine harvester, multiple somewhat smaller harvesting machines could be applied in such a way that only one of them (the leader) is being controlled by an operator and the others follow autonomously in a certain, predefined pattern. And to obtain enhanced control performance local sensory data on each of the harvesters (e.g. GPS, computer vision...) could be fused with information gathered by a quadrotor overflying the formation from above [3, 4].

2 Distributed multi-agent coordination

Over time a lot of research has been done on coordinated control of multiple autonomous mobile robots [5]. From a control engineering perspective, the goal is to compute the inputs that drive the vehicles along trajectories which maintain relative positions as well as safe distances between each agent while performing a certain objective. In this regard model-based predictive control (MPC) has proven to be very promising due to its ability to handle complex, constrained multivariable systems easily and effectively. However, the computational effort required for the inherent optimization scales poorly with the size of the system and can become prohibitive for large systems. To address this computational issue when applying a centralised MPC architecture, attention has recently focused on distributed MPC (DMPC) where each subsystem (i.e. vehicle controller) solves its own smaller optimization problem taking into account information communicated by its neighbour [6].

3 Goals

This research project aims at developing a DMPC framework for formation control of multiple autonomous ground vehicles extended with aerial agents (e.g. quadrotor) acting as remote sensors. Since this is actually a networked control system the framework should be able to deal with communication delays and information drop outs. From a global perspective, two major objectives are targeted:

1. To develop and validate a constrained DMPC scheme on a laboratory scale application consisting of n autonomous ground vehicles and a quadrotor acting as a remote sensor.

2. To develop a methodology for instrumentation and for variable selection with the purpose of sensor fusion as an aid tool to improve global control.

References

[1] Tomás Lozano-Perez, Ingemar J Cox, and Gordon T Wilfong. *Autonomous robot vehicles*. Springer Science & Business Media, 2012.

[2] Kimon P Valavanis and George J Vachtsevanos. *Handbook of Unmanned Aerial Vehicles*. Springer, 2015.

[3] Andres Hernandez, Harold Murcia, Cosmin Copot, and Robin De Keyser. Towards the development of a smart flying sensor: Illustration in the field of precision agriculture. *Sensors*, 15(7):16688–16709, 2015.

[4] Jairo Andres Hernandez Naranjo, Harold Murcia, Cosmin Copot, and Robain De Keyser. Model predictive path-following control of an a.r. drone quadrotor. In *Memorias del XVI Congreso Latinoamericano de Control Automatico, Proceedings*, pages 618–623, 2014.

[5] Yongcan Cao, Wenwu Yu, Wei Ren, and Guanrong Chen. An overview of recent progress in the study of distributed multi-agent coordination. *Industrial Informatics, IEEE Transactions on*, 9(1):427–438, 2013.

[6] Hojjat A Izadi, Brandon W Gordon, and Youmin Zhang. Decentralized model predictive control for cooperative multiple vehicles subject to communication loss. *International Journal of Aerospace Engineering*, 2011, 2011.

On the Connection Between Different Noise Structures for LPV-SS Models[*]

P. B. Cox, R. Tóth, and P. M. J. Van den Hof

Control Systems Group

Eindhoven University of Technology

P.O. Box 513, 5600 MB Eindhoven, The Netherlands

p.b.cox@tue.nl

1 Introduction

Many chemical or physical processes exhibit parameter variations due to non-stationary or nonlinear behaviour, often dependent on measurable exogenous variables or measurable process states. These nonlinear parameter variations can be captured in the *linear parameter-varying* (LPV) modelling paradigm, which originates from the need of finding model structures, that are linear and low in complexity, but still allow to represent the nonlinear aspects of systems during control design. To achieve this, the LPV model class assumes a linear relation between the inputs and outputs of the system, however, the parameters of this relation are functions of a measurable, time-varying signal, the *scheduling variable p*, which expresses the current operating conditions, time-conditions, or nonlinearities of the plant.

2 LPV-SS models with general noise structure

Recasting nonlinear system descriptions as LPV representations can be accomplished in various forms, such as *state-space* (SS), *impulse response*, *kernel*, or *input-output* representations. For control purposes, LPV-SS representation forms are preferable, particularly with static and affine dependence on the scheduling signal. However, generally speaking, not all phenomena affecting the physical system at hand are captured in the original nonlinear model equations, therefore, a disturbance term is usually added to the state equation and output signal to represent unmodelled dynamics, environmental effects, measurement disturbances, etc. Hence, the LPV model should equivalently be equipped with an appropriate noise structure. Such an LPV-SS representation with general noise structure is given by

$$x_{t+1} = \mathcal{A}(p_t)x + \mathcal{B}(p_t)u + \mathcal{G}(p_t)w_t, \tag{1a}$$

$$y_t = \mathcal{C}(p_t)x + \mathcal{D}(p_t)u + \mathcal{H}(p_t)v_t, \tag{1b}$$

where subscript t is the discrete time, x is the state variable, y is the measured output signal, u denotes the input signal, w_t, v_t are assumed to be zero-mean noise processes satisfying $\begin{bmatrix} w_t \\ v_t \end{bmatrix} \sim \mathcal{N}\left(0, \begin{bmatrix} \mathcal{W} & \mathcal{S} \\ \mathcal{S}^\top & \mathcal{R} \end{bmatrix}\right)$ with covariance matrices $\mathcal{W}, \mathcal{S}, \mathcal{R}$, and $\mathcal{A}, \ldots, \mathcal{H}$ are affine functions in the scheduling signal, i.e, $\mathcal{A}(p_t) = A_0 + \sum_{i=1}^{n_p} A_i p_t^{[i]}$ with $p_t^{[i]}$ the i-th element in p_t. The system description (1) is capable of representing a large generality of noise scenarios, like its LTI or time-varying counterparts [1].

3 Connection to the innovation noise structure

In practice, the coefficients $\{A_i, \ldots, H_i\}_{i=0}^{n_p}$ of the model (1) are estimated from data, as their values are unknown. However, state-of-the-art LPV-SS identification approaches are designed for an innovation type of noise structure, e.g. [2]:

$$\check{x}_{t+1} = \mathcal{A}(p_t)\check{x}_t + \mathcal{B}(p_t)u_t + \mathcal{K}(p_t)\xi_t, \tag{2a}$$

$$y_t = \mathcal{C}(p_t)\check{x}_t + \mathcal{D}(p_t)u_t + \xi_t, \tag{2b}$$

where ξ_t is a zero-mean noise process satisfying $\xi_t \sim \mathcal{N}(0, \mathcal{Q})$ with covariance matrix $\mathcal{Q}$, and $\mathcal{K}$ is an affine function in the scheduling signal, similarly parameterized as $\mathcal{A}, \ldots, \mathcal{H}$ in (1). In the LTI case, i.e., for $\mathcal{A}(\cdot) = A, \ldots, \mathcal{H}(\cdot) = H, \mathcal{K}(\cdot) = K$, the innovation noise structure (2) is the optimal linear filter given (1) [1]. Hence, in this case, the innovation noise structure can represent the noise scenarios expressed by (1). As many LPV identification schemes are extensions from their LTI counterpart, the innovation noise structure is an obvious and popular choice.

Therefore, we will analyse the stochastic properties of (1)-(2) and their connection. We will show that: i) the matrix functions $\mathcal{K}, \mathcal{Q}$ should have rational and dynamic dependence on the scheduling signal for an equivalence between (1) and (2) governed by the Kalman filter equations; ii) in practical situations $\mathcal{K}(p_t, \ldots, p_{t-n_k})$ can be a good approximation due to the asymptotic convergence of the underlying filter. In addition, if it is assumed that this approximation is equal to the data-generating system then, for some cases, this system has an equivalent LPV-SS representation with affine and static dependency on the scheduling signal at the cost of additional states x, as will be demonstrated by an example. Hence, system (1) can possibly be captured in the innovation form (2), but at the cost of a non-state-minimal system. Consequently, LPV subspace identification schemes might loose their rank revealing properties.

References

[1] B. D. O. Anderson and J. B. Moore. *Optimal Filtering*. Prentice Hall, 1979.

[2] J. W. van Wingerden and M. Verhaegen. Subspace identification of bilinear and LPV systems for open- and closed-loop data. *Automatica*, 45(2):372–381, 2009.

State-space realization of coordinated linear stochastic systems

M. Józsa[1]
University of Groningen
m.jozsa@rug.nl

M. Petreczky
Signal et Automatique de Lille
mihaly.petreczky@ec-lille.fr

M. K. Camlibel
University of Groningen
m.k.camlibel@rug.nl

Introduction

A significant part of realization theory is the study of the relationship between a behaviour of an observed process and the structure of its state-space representation. In this abstract we consider noncausality conditions of a stochastic process and we show that these can be realized by a state-space representation having system matrices with a certain structure. More specifically, we give necessary and sufficient conditions for a process to be the output of a minimal coordinated linear stochastic system defined in [1]. Indeed, the realization of the process $\mathbf{y} = [\mathbf{y}_1^T, \ldots, \mathbf{y}_n^T]^T$ in Theorem 1 represents a coordinated system where $\mathbf{y}_n$ is the coordinator, communicating with the agents, $\mathbf{y}_i$'s $i \in \{1, \ldots, n-1\}$, who send no information to each other.

The results could be of interest for reverse engineering the network structure of state-space representations which arise in system biology and neuroscience. Also, it can be useful for structure preserving model reduction and for control design of coordinated systems.

The space of square-integrable random variables forms a Hilbert space, say H, with the covariance function as the inner product. We denote the Hilbert spaces generated by the one-dimensional components of the processes $\{\mathbf{z}(s)\}_{s=-\infty}^{\infty}, \{\mathbf{z}(s)\}_{s=-\infty}^{t-1}, \{\mathbf{z}(s)\}_{s=t}^{\infty}$ by $H^{\mathbf{z}}, H_{t-}^{\mathbf{z}}$ and $H_{t+}^{\mathbf{z}}$, respectively. The orthogonal projection of $A \subseteq H$ onto $B \subseteq H$ is written as $E_l[A|B] := \{E_l[a|B], a \in A\}$.[2] For closed subspaces $A, B, C \subseteq H$, we say that A and B have a *conditionally trivial intersection* with respect to C, denoted by $A \cap B | C = \{0\}$, if $\{a - E_l[a|C] \mid a \in A\} \cap \{b - E_l[b|C] \mid b \in B\} = \{0\}$, i.e. the intersection of the projections of A, B onto the orthogonal complement of C in H is the zero subspace.

We say that $\mathbf{y}_1$ is *Granger noncausal* for $\mathbf{y}_2$ (or equivalently, there is no feedback from $\mathbf{y}_1$ to $\mathbf{y}_2$) if for all $t, k \in \mathbb{Z}, k \geq 0$

$$E_l[\mathbf{y}_2(t+k) \mid H_{t-}^{\mathbf{y}_2}] = E_l[\mathbf{y}_2(t+k) \mid H_{t-}^{\mathbf{y}}].$$

Contribution

It is assumed that the processes are discrete-time zero mean wide-sense stationary processes with rational spectrum. We denote by $\sigma\mathbf{z}$ the time-shifted process satisfying $(\sigma\mathbf{z})(t) = \mathbf{z}(t+1)$. In the theorem below t takes values from the set of integers and i, j are the elements of $\{1, 2, \ldots, n-1\}, i \neq j$.

---

[1] Johann Bernoulli Institute for Mathematics and Computer Science, 9700 AK Groningen, The Netherlands

[2] For Gaussian processes the orthogonal projection is equivalent with the conditional expectation.

Theorem 1 *There exists a stochastic linear system for* $\mathbf{y} = [\mathbf{y}_1^T, \ldots, \mathbf{y}_n^T]^T$ *in forward innovation form, such that*

$$
\sigma \underbrace{\begin{bmatrix} \mathbf{x}_1 \\ \mathbf{x}_2 \\ \vdots \\ \mathbf{x}_{n-1} \\ \mathbf{x}_n \end{bmatrix}}_{\sigma\mathbf{x}} = \underbrace{\begin{bmatrix} A_{1,1} & 0 & \ldots & 0 & A_{1,n} \\ 0 & A_{2,2} & \ldots & 0 & A_{2,n} \\ \vdots & \vdots & \ddots & \vdots & \vdots \\ 0 & 0 & \ldots & A_{n-1,n-1} & A_{n-1,n} \\ 0 & 0 & \ldots & 0 & A_{n,n} \end{bmatrix}}_{A} \underbrace{\begin{bmatrix} \mathbf{x}_1 \\ \mathbf{x}_2 \\ \vdots \\ \mathbf{x}_{n-1} \\ \mathbf{x}_n \end{bmatrix}}_{\mathbf{x}}
$$

$$
+ \underbrace{\begin{bmatrix} K_{1,1} & 0 & \ldots & 0 & K_{1,n} \\ 0 & K_{2,2} & \ldots & 0 & K_{2,n} \\ \vdots & \vdots & \ddots & \vdots & \vdots \\ 0 & 0 & \ldots & K_{n-1,n-1} & K_{n-1,n} \\ 0 & 0 & \ldots & 0 & K_{n,n} \end{bmatrix}}_{K} \underbrace{\begin{bmatrix} \mathbf{e}_1 \\ \mathbf{e}_2 \\ \vdots \\ \mathbf{e}_{n-1} \\ \mathbf{e}_n \end{bmatrix}}_{\mathbf{e}}
$$

$$
\underbrace{\begin{bmatrix} \mathbf{y}_1 \\ \mathbf{y}_2 \\ \vdots \\ \mathbf{y}_{n-1} \\ \mathbf{y}_n \end{bmatrix}}_{\mathbf{y}} = \underbrace{\begin{bmatrix} C_{1,1} & 0 & \ldots & 0 & C_{1,n} \\ 0 & C_{2,2} & \ldots & 0 & C_{2,n} \\ \vdots & \vdots & \ddots & \vdots & \vdots \\ 0 & 0 & \ldots & C_{n-1,n-1} & C_{n-1,n} \\ 0 & 0 & \ldots & 0 & C_{n,n} \end{bmatrix}}_{C} \begin{bmatrix} \mathbf{x}_1 \\ \mathbf{x}_2 \\ \vdots \\ \mathbf{x}_{n-1} \\ \mathbf{x}_n \end{bmatrix} + \begin{bmatrix} \mathbf{e}_1 \\ \mathbf{e}_2 \\ \vdots \\ \mathbf{e}_{n-1} \\ \mathbf{e}_n \end{bmatrix}
$$

- $\mathbf{e}_i(t) = \mathbf{y}_i(t) - E_l[\mathbf{y}_i(t)|H_{t-}^{\mathbf{y}_i, \mathbf{y}_n}]$;

- $(A_{n,n}, G_{n,n})$ is controllable, $G_{n,n} := E[\mathbf{x}_n(t)\mathbf{y}_n^T(t-1)]$;

- defining $\Lambda_0^{\mathbf{y}_n} := E[\mathbf{y}_n(t)\mathbf{y}_n(t)^T]$, the matrix $P_{n,n} := E[\mathbf{x}_n(t)\mathbf{x}_n^T(t)]$ is the minimal positive definite solution of

$$\Sigma = A_{n,n}\Sigma A_{n,n}^T + (G_{n,n} - A_{n,n}\Sigma C_{n,n}^T)(\Lambda_0^{\mathbf{y}_n} - C_{n,n}\Sigma C_{n,n}^T)^{-1}(G_{n,n} - A_{n,n}\Sigma C_{n,n}^T)^T$$

if and only if

- $\mathbf{y}_i$ *is Granger noncausal for* $\mathbf{y}_n$;

- $\mathbf{y}_i$ *is Granger noncausal for* $[\mathbf{y}_j^T, \mathbf{y}_n^T]^T$.

In addition, if the realization above exists, then it is minimal if and only if

$$E_l[H_{t+}^{\mathbf{y}_i}|H_{t-}^{\mathbf{y}_i, \mathbf{y}_n}] \cap E_l[H_{t+}^{\mathbf{y}_j}|H_{t-}^{\mathbf{y}_j, \mathbf{y}_n}] \mid E_l[H_{t+}^{\mathbf{y}_n}|H_{t-}^{\mathbf{y}_n}] = \{0\}.$$

The proof of sufficiency of Theorem 1 is constructive, and it yields an algorithm to compute a minimal coordinated linear stochastic system. In the case when $n = 2$ Theorem 1 provides a characterization of Granger noncausality in terms of state-space representation.

References

[1] M. Józsa, M. Petreczky and M. K. Camlibel, "Towards realization theory of interconnected linear stochastic systems", submitted to the International Symposium on Mathematical Theory of Networks and Systems, Minneapolis, 2016.

Experimental evaluation of the combined global and local LPV system identification approach

Dora Turk, Joris Gillis, Goele Pipeleers and Jan Swevers
Department of Mechanical Engineering, KU Leuven, Belgium
Email: dora.turk@kuleuven.be

1 Abstract

This work focuses on identifying a linear parameter-varying (LPV) model of an XY-motion system by combining two seemingly antagonizing identification approaches. One extreme of the approach results in a model optimal - in terms of accuracy - under varying scheduling parameter conditions, while the other returns a model with optimal behavior for fixed scheduling parameter. Ideally, the combined approach retains advantages of the two extremes, with the possibility to emphasize one or the other (as shown in [1]). Practically, various difficulties may appear, one of which is overparameterization.

2 Experimental validation

2.1 Setup description

The system under test is a mechatronic XY-motion system (Fig.1), used for fast positioning of the end-effector. The system consists of two perpendicularly mounted linear stages and a flexible cantilever beam. The length of this beam is changed by the position of the Y-motor, such that system resonances and hence the dynamics of the XY-motion system in the X-direction depends on the position of the Y-motor [2]. The position of the Y-motor can thus be seen as a scheduling parameter of the system we aim to identify. The referent velocity for the X-motor is considered to be the system input, while the acceleration of the end-effector in the same direction represents the system output.

2.2 Identification procedure

The model to be identified is a fully-parameterized, discrete-time LPV model in the state-space form:

$$\begin{cases} x(t+1) = \mathscr{A}(p(t)) \cdot x(t) + \mathscr{B}(p(t)) \cdot u(t) \\ y(t) = \mathscr{C}(p(t)) \cdot x(t) + \mathscr{D}(p(t)) \cdot u(t), \end{cases} \quad (1)$$

where $x(t) \in \mathbb{R}^3$, $u(t) \in \mathbb{R}^1$, $y(t) \in \mathbb{R}^1$, $p(t) \in \mathbb{R}^1$, and

$$\mathscr{A}(p(t)) = A^{(0)} + \sum_{i=1}^{3} A^{(i)} p(t)^i. \quad (2)$$

The data gathered in an experiment where the system input and the scheduling parameter were simultaneously excited, are combined with four frequency response functions resulting from experiments with fixed scheduling parameter. All together forms a nonlinear least squares optimization problem, solved by the Levenberg-Marquardt algorithm.

2.3 Results

Figure 2 shows the parameter dependent frequency response function (FRF) of one of the identified LPV models. During the optimization, the model has been gaining on accuracy in the local and global sense, but only for the data points involved in the identification. The model FRF is experiencing undesirable bumps and folds in-between, which indicates the need for regularization.
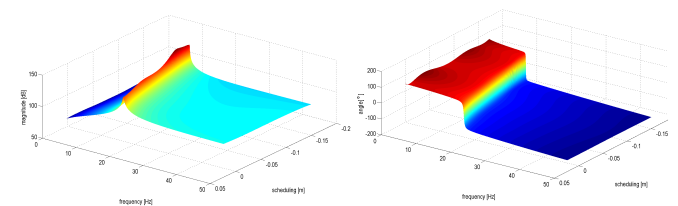
Figure 2: Magnitude (left) and phase response (right) of the obtained LPV model

References

[1]   Turk, D., Pipeleers, G., Swevers, J. (2015). A Combined Global and Local Identification Approach for LPV Systems. In *Proceedings of the 17th IFAC Symposium on System Identification, Beijing, China* 184 –189.

[2]   De Caigny, Jan 2009. *Contributions to the Modeling and Control of Linear Parameter-Varying Systems.* Ph.D thesis, KU Leuven.

Figure 1: XY-motion system

Maximum Likelihood Estimation of LPV-SS Models:
A Sequential Monte-Carlo Approach[1]

M. A. H. Darwish[a], S. Chitraganti[b], T. B. Schön[c], R. Tóth[a] and P. M. J. Van den Hof[a]

[a]Control Systems Group, Department of Electrical Engineering, Eindhoven University of Technology
[b]Department of Electronics and Communication Engineering, Amrita Vishwa Vidyapeetham, India
[c]Department of Information Technology, Uppsala University, Sweden
m.a.h.darwish@tue.nl

1 Introduction

A linear parameter-varying (LPV) model structure offers a flexible framework to capture non-stationary or nonlinear behaviour of physical or chemical processes in terms of a varying linear structure wherein the variation is related to a known (measurable) "scheduling" signal. Powerful control synthesis approaches are available for LPV models, however, the majority of these approaches presume that an LPV State-Space (SS) model with affine dependence on the scheduling variable is available. Therefore, the identification of such models from experimental data is a central topic in the LPV field. Among many choices, a Maximum Likelihood (ML) approach, that minimises the prediction error in a stochastic sense, enjoys well understood theoretical properties, e.g., strong consistency.

In the implementation of this concept, it is common to use gradient based search techniques, which are computationally expensive as they require the Jacobian of the cost function. Alternatively, an Expectation Maximisation (EM) algorithm can be used to compute such estimates, where the gradient of the likelihood function is not needed. The EM algorithm for the estimation of LPV-SS models with affine dependency has been developed in [1]. However, the developed approach can only handle the Gaussian noise case where Kalman filtering/smoothing can be easily applied. Although, the Gaussian assumption simplifies the estimation problem, it seems restrictive for many real-world applications.

Inspired by the approach introduced in [2], a particle EM algorithm is employed to tackle the estimation of LPV-SS models that are affected by both state and measurement noise, which are not necessarily Gaussian.

2 Particle Expectation Maximisation Algorithm for LPV-SS models

ML estimation involves maximising the joint density (Likelihood) $p_\theta(Y_N)$ of the observations Y_N, where θ is the unknown parameter vector. Equivalently,

$$\hat{\theta}_{ML} = \arg\min_\theta -L_\theta(Y_N),$$

where, $L_\theta(Y_N) = \log p_\theta(Y_N)$ is the log-likelihood. The EM algorithm, which is an iterative procedure specialised to compute an ML estimate for the unknown parameter vector θ, regards the state sequence X_N as missing data. In particular, it considers the "complete" log likelihood $L_\theta(X_N, Y_N)$ under the assumption that maximising it is easier than maximising the "incomplete" log likelihood, i.e., $L_\theta(Y_N)$. Then, an approximation $Q(\theta, \theta_k)$ of $L_\theta(X_N, Y_N)$ is formed, e.g., the minimum variance estimate of $L_\theta(X_N, Y_N)$ given the observations and an assumption θ_k of the true parameter value:

$$Q(\theta, \theta_k) = \mathbb{E}_{\theta_k}\{L_\theta(X_N, Y_N) \mid Y_N\},$$

where $\mathbb{E}$ is the expectation operator. It turns out that, by iteratively maximising $Q(\theta, \theta_k)$, non-decreasing values for $L_\theta(Y_N)$ are obtained. The EM algorithm consists of two steps:

1. (E) step, computation of $Q(\theta, \theta_k)$, which is the main challenge of implementing the EM algorithm as it involves the evaluation of the smoothed estimates of the states and the expectation with respect to it. For LPV-SS models with Gaussian noise, Kalman filtering/smoothing can be used [1]. However, The more general situation of non-Gaussian noise has not been addressed yet. In this work, a particle EM algorithm is employed, where a particle filter/smoother is employed to approximate the required state estimates.

2. (M) step, maximisation of $Q(\theta, \theta_k)$, where in the linear/Gaussian case, a closed form expression can be obtained for the maximiser of $Q(\theta, \theta_k)$. However, in the nonlinear/non-Gaussian case, a nonlinear optimisation problem is required to be solved to compute it.

In this work the formulation of the particle EM algorithm for LPV-SS models is given and the utility of the considered algorithm is assessed by a simulation example and experimentally by estimating an LPV-SS model of a DC motor with unbalanced disk.

References

[1]   A. Wills and B. Ninness, "System identification of linear parameter varying state-space models," in Linear parameter-varying system identification: new developments and trends, P. Lopes dos Santos, T. P. Azevedo Perdicoúlis, C. Novara, J. A. Ramos, and D. E. Rivera, Eds. World Scientific, 2011, ch. 11, pp. 295-316.

[2]   T. B. Schön, A. Wills, and B. Ninness. System identification of nonlinear state-space models. Automatica, 47(1):39-49, 2011.

Using a polynomial decoupling algorithm for state-space identification of a Bouc-Wen system

Alireza Fakhrizadeh Esfahani   Philippe Dreesen   Johan Schoukens
afakhriz@vub.ac.be   Philippe.Dreesen@vub.ac.be Johan.Schoukens@vub.ac.be
Koen Tiels
Koen.Tiels@vub.ac.be
Vrije Universiteit Brussel, Dept. ELEC

1 Introduction

The polynomial nonlinear state space (PNLSS) approach [1] is a powerful tool for modeling nonlinear systems. A PNLSS model consists of a discrete-time linear state space model, extended with polynomials in the state and the output equation:

$$x(t+1) = Ax(t) + Bu(t) + E\zeta(t) \tag{1}$$
$$y(t) = Cx(t) + Du(t) + F\eta(t) \tag{2}$$

where $\zeta(x(t), u(t))$ and $\eta(x(t), u(t))$ are both vectors with monomials in the states $x(t)$ and the inputs $u(t)$. The matrices E and F contain the polynomial coefficients. The PNLSS model is very flexible as it can capture many different types of nonlinear behavior, such as nonlinear feedback and hysteresis. This flexibility generally comes at the cost of a large number of parameters. Increasing the order of the polynomials for example leads to a combinatorial increase of the number of parameters due to the multivariate nature of the polynomials $E\zeta(x(t), u(t))$ and $F\eta(x(t), u(t))$. In this study, the PNLSS approach is used to model a Bouc-Wen hysteretic system. The multivariate polynomials $E\zeta(x(t), u(t))$ and $F\eta(x(t), u(t))$ are decoupled using the method in [2]. Like this, the nonlinearity in the PNLSS model is described in terms of univariate polynomials for which increasing their order is not so parameter expensive.

2 Methodology

The simulated data is extracted from the Bouc-Wen model with the equations:

$$m\ddot{y} + c\dot{y} + ky + z(y, \dot{y}) = u(t) \tag{3}$$
$$\dot{z} = \dot{y} - \alpha|\dot{y}|z - \beta\dot{y}|z| \tag{4}$$

where m is the mass, c is the damping coefficient, $y(t)$ is the measured output and $u(t)$ is the input force which is a random phase multisine. The parameters α and β are chosen equal to 5×10^4 and 0.8 respectively. In a first step, we estimate the best linear approximation (BLA) [3] of the system. A linear state-space model estimated on the BLA serves as an initial guess for the PNLSS model in (1) and (2), which is optimized using a Levenberg-Marquardt approach. In a second step, the multivariate polynomials $E\zeta(t)$ and $F\eta(t)$ are decoupled using the decomposition method in [2]:

$$E\zeta(x(t), u(t)) \approx W_x g\left(V^T \begin{bmatrix} x(t) \\ u(t) \end{bmatrix}\right) \tag{5}$$

$$F\eta(x(t), u(t)) \approx W_y g\left(V^T \begin{bmatrix} x(t) \\ u(t) \end{bmatrix}\right) \tag{6}$$
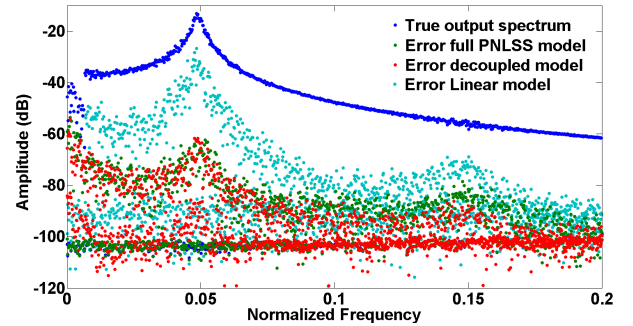
Figure 1: The validation output spectrum (in blue), the error of linear model (cyan) and the error of PNLSS (green) for 2nd and 3rd degree monomials of states and inputs in state updates ($F = 0$), and the error for the decoupled model with 11th degree polynomials (in red).

where the matrix V transforms the states and inputs in new variables $\xi = V^T \begin{bmatrix} x(t) & u(t) \end{bmatrix}^T$. The function g is a collection of univariate polynomials $g_i(\xi_i)$ for $i = 1, 2, \cdots, r$: $g(\xi) = \begin{bmatrix} g_1(\xi_1) & g_2(\xi_2) & \cdots & g_r(\xi_r) \end{bmatrix}^T$ that act as basis functions for the decoupled state-space model. The matrices W_x and W_y contain the corresponding basis function coefficients.

3 Results

The Bouc-Wen model is excited with a random phase multisine of 6.813 N in the standard deviation. The results for the PNLSS modelling is plotted in Figure 1 for the validation data.

4 Conclusion

A PNLSS model can capture the behavior of a Bouc-Wen system. A decoupled PNLSS model reaches a similar accuracy, but has less than two third of the number of parameters. The order of the polynomials in the decoupled model can also be increased without blowing up the number of parameters, as it is the case for the full PNLSS model.

References

[1]   J. P. Paduart, L. Lauwers, J. Swevers, K. Smolders, J. Schoukens, and R. Pintelon, "Identification of nonlinear systems using Polynomial Nonlinear State Space models," *Automatica* 46(4) 2010: 647-656.

[2]   Ph. Dreesen, M. Ishteva, and J. Schoukens, "Decoupling multivariate polynomials using first-order information and tensor decoupling," *SIAM Journal on Matrix Analysis and Applications* 36, pp. 864-879, 2015.

[3]   R. Pintelon, and J. Schoukens, "System Identification: a Frequency Domain Approach," John Wiley & Sons, 2012.

Communication requirements for optimal frequency regulation in power networks

Sebastian Trip
Engineering and Technology Institute Groningen
Faculty of Mathematics and Natural Sciences
University of Groningen
Nijenborgh 4, 9747 AG Groningen
the Netherlands
E-mail: s.trip@rug.nl

Claudio De Persis
Engineering and Technology Institute Groningen
Faculty of Mathematics and Natural Sciences
University of Groningen
Nijenborgh 4, 9747 AG Groningen
the Netherlands
E-mail: c.de.persis@rug.nl

1 Abstract

In order to guarantee reliable operation of the power network the frequency is tightly regulated around its nominal value, such as 50 Hz. Recently we proposed a novel distributed controller in [1] that controls power production such that the frequency is regulated in an economic efficient way. In order to obtain economic efficiency, the controller continuously utilizes a communication network. This work makes a first step in reducing these communication requirements.

2 Optimal frequency regulation

The dynamics of the network are described by the so called structure-preserving Bergen-Hill model. The dynamics at a generator bus are given by

$$
\begin{aligned}
\dot{\delta}_i &= \omega_{gi} \\
M_i \dot{\omega}_{gi} &= -D_{gi}\omega_{gi} \\
&\quad -\sum_{j \in \mathcal{N}_i} V_i V_j B_{ij}\sin(\delta_i - \delta_j) + u_{gi}.
\end{aligned}
\tag{1}
$$

The dynamics at a load bus are given by

$$
\begin{aligned}
\dot{\delta}_i &= \omega_{li} \\
0 &= -D_{li}\omega_{li} \\
&\quad -\sum_{j \in \mathcal{N}_i} V_i V_j B_{ij}\sin(\delta_i - \delta_j) - P_{li}.
\end{aligned}
\tag{2}
$$

Here, δ_i, ω_i are the voltage angle and frequency deviation respectively. The unknown demand is indicated by P_{li}, whereas u_{gi} is the controllable power generation. In [1] we proposed a distributed controller of the following form:

$$
\begin{aligned}
\dot{\theta}_i &= \sum_{j \in \mathcal{N}_i}[\theta_j - \theta_i] - q_i^{-1}\omega_i \\
u_{gi} &= q_i^{-1}\theta_i.
\end{aligned}
\tag{3}
$$

Exploiting an incremental passivity property of the power network, we proved asymptotic regulation of the frequency and that the steady state generation solves the following optimization problem

$$
\begin{aligned}
\min_{u_g} C(u_g) &= \min_{u_g} \sum_{i \in \mathcal{V}_g} \tfrac{1}{2} q_i u_{gi}^2 \\
\text{s.t.} \quad 0 &= \mathbf{1}_{n_g}^T u_g - \mathbf{1}_{n_l}^T P_l.
\end{aligned}
\tag{4}
$$

In other words, the proposed controller achieves frequency regulation in an economic efficient way.
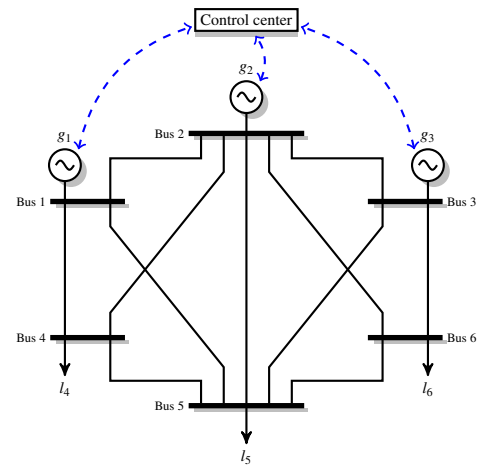
Figure 1: Diagram for the 6 bus power network model, consisting of 3 generator and 3 load buses. The communication links are represented by the dashed lines.

3 Communication constraints

The requirement of continuous exchange of information in (3) over a communication network makes the control structure above difficult to implement. In this work we discuss how we can relax this requirement, following similar arguments as in [2]. As a first step we consider a centralized control structure depicted in Figure 1. The control center samples at specific moments the different generators and broadcasts back a new control signal. We will present a possible control algorithm with discrete communication and prove that it indeed regulates the frequency and achieves economic efficiency.

References

[1] S. Trip, M. Bürger and C. De Persis, "An internal model approach to (optimal) frequency regulation in power grids," *Automatica*, vol. 64, pp. 240 - 253, 2016.

[2] C. De Persis and R. Postoyan, "A Lyapunov redesign of coordination algorithms for cyber-physical systems," *arXiv preprint arXiv:1404.0576*, 2014.

Power balance of microgrids using min-max control of fuel cell cars

Farid Alavi, Nathan van de Wouw, and Bart De Schutter
Delft Center for Systems and Control
Delft University of Technology
Mekelweg 2, 2628 CD Delft
The Netherlands
f.alavi@tudelft.nl

1 Introduction

The idea of using fuel cell cars for producing electricity is a relatively new concept in distributed power generation. In this paper, a parking lot for fuel cell cars is operated as a virtual power plant. We consider a scenario in which several fuel cell cars can exchange information with a central controller in the parking lot. In such a setting, the central controller can be employed, on the one hand, to manage the electricity production of fuel cell cars in order to balance the power production and consumption and, on the other hand, to minimize the operational costs. It is assumed that the controller plans the electricity production of fuel cell cars based on the prediction of the demand in the microgrid. The control method should be able to deal with the uncertainty due to the difference between the actual future electricity demand and its prediction.

2 Problem Statement

We consider a parking lot for fuel cell cars inside a microgrid connected to the power network. In this scenario, the power exchange between the microgrid and the power network is limited and the demand of electricity in the microgrid cannot be influenced. However, it is assumed that the demand profile for the next few hours can be predicted, e.g. based on historical data in combination with smart grid devices. We consider the difference between the actual and predicted electricity demand as an uncertainty in the system. The fuel cell cars are employed to guarantee the power balance in the microgrid. Hence, a control system is necessary in the parking lot in order to use all the fuel cell and batteries of the cars in such a way that the power production meets the expectations and also such that the operational cost of the microgrid is minimized. In this work, we design such a controller while considering the hybrid nature of the system.

3 Modeling and Control Strategy

The fuel cell and battery of the cars are modeled considering their operational costs. Two operation modes, on and off, are considered for the fuel cells and due to different behaviors in each mode, a hybrid model is developed for the fuel cells. A similar approach is adopted for the battery, taking into account its charging and discharging modes. Important factors in determining the operational costs of fuel cell devices are the cost of fuel (hydrogen) and the degradation of the device. In order to determine the fuel cost, the relation between the hydrogen consumption and the net power production is considered [1]. It is assumed that the degradation cost of a fuel cell is only associated with turning the fuel cell on or off. As a result, a hybrid piecewise affine (PWA) model for the fuel cell is developed. For the batteries of the cars, two operational modes, charging and discharging, are considered and a simplified PWA model of the battery [2] is used. The models of fuel cells and batteries are combined to form an overall system model in the mixed logical dynamical form. The control problem is formulated as a mixed integer linear programming (MILP) problem, where the cost is a function of the power generation and stored energy in each fuel cell car. The power generation of fuel cell cars is related to the actual electricity demand in the microgrid, due to the power balance constraint. Hence, the operational costs can also be written in terms of predicted demand and the uncertainty in its realization. The constraint set in the MILP problem consists of the physical constraints of each device and the power balance condition. A min-max control strategy is used to minimize the operational costs of the system considering the worst case realization of uncertainty. The complexity of the optimization problem is reduced by using special properties in the problem and as a result, the system is operated robustly in presence of uncertain electricity demand in the microgrid.

ACKNOWLEDGMENT

References

[1] P. Rodatz, G. Paganelli, A. Sciarretta, and L. Guzzella. Optimal power management of an experimental fuel cell/supercapacitor-powered hybrid vehicle. *Control Engineering Practice*, 13:41–53, 2005.

[2] A. Parisio, E. Rikos, and L. Glielmo. A model predictive control approach to microgrid operation optimization. *IEEE Transactions on Control Systems Technology*, 22(5):1813–1827, September 2014.

Distributed Optimal Control of Smart Energy Grids with Congestion Management*

D.B. Nguyen, J.M.A. Scherpen, and W. Kramer
University of Groningen
Nijenborgh 4, 9747 AG Groningen
E-mail: d.b.nguyen@rug.nl

F. Bliek and G.K.H. Larsen
DNV GL
Energieweg 17, 9743 AN Groningen

Introduction

One of the big challenges in the transition towards smart grids is how to deal with the intermittent nature of renewable energy resources such as wind or solar energy. For example, a prediction of the electricity supply and demand is typically made a day ahead, but the actual supply during operation can deviate from the plan since weather conditions influence the generation. The system needs to compensate for this deviation and minimize the economic costs associated with it. The problem can be addressed by demand response, in which households with flexible appliances – devices that are capable of moving their load in time – also play an active role in the balancing process [1].

Problem formulation

In this study, we assume that a day-ahead planning of the electricity load for a network of households has already been made. Then, given heat demands of the households, the objective is to fulfill that demand while keeping the electricity load as close to the day-ahead planning as possible (i.e., minimizing the prediction error). Each household is equipped with one flexible appliance, either a μCHP or a heat pump, connected to a heat buffer. The role of the Distribution System Operator (DSO) is considered as well, in order to avoid congestion over the distribution network. Our model is embedded in the hierarchical, market-based structure of the Universal Smart Energy Framework [3].

Approach

We express the prediction error $x_i[k]$ of household i as

$$x_i[k+1] = A_{ii}x_i[k] + \sum_{j \neq i} A_{ij}x_j[k] + u_i[k] + w_i[k] - \Delta\text{goal}_i[k],$$

where $u_i[k]$ is the change in flexible load, $w_i[k]$ is the change in fixed (inflexible) load, and $\mathbf{A} = (A_{ij})$ represents an information coupling between neighboring households. The goal function is introduced to steer the flexible appliances, and is a division of the day-ahead planning among the households proportional to their available flexibility. We propose

a receding horizon controller that solves the minimization of the prediction error in a distributed manner: each household contributes to the optimization process based only on local information exchange with their neighbors [2]. This distributed formulation is achieved *via* dual decomposition.

Results

The scenario with no congestion management is illustrated below. The upper figure depicts the aggregated loads, the lower figure details the loads of the individual appliances, with the convention of using negative sign for supply. The controlled load follows the day-ahead planning, however, it violates the DSO constraint at multiple time-steps.
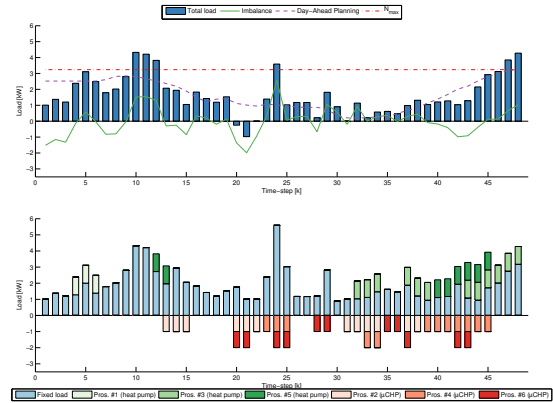
We show that our controller is able to solve these congestion points when the distribution network capacity limitations are also taken into account.

References

[1] D.B. Nguyen, D. Alkano, and J.M.A. Scherpen, "The Optimal Control Problem in Smart Energy Grids", in *Smart Grids from a Global Perspective: Bridging Old and New Energy Systems*, A. Beaulieu, J. de Wilde, and J.M.A. Scherpen, Eds. (n.p.): Springer, In press.

[2] D.B. Nguyen *et al.*, "Distributed Optimal Control and Congestion Management in the Universal Smart Energy Framework", Manuscript submitted for publication, 2015.

[3] Smart Energy Collective, "An Introduction to the Universal Smart Energy Framework", Arnhem, The Netherlands, 2014.

A port-Hamiltonian approach to optimal frequency regulation in power grids

Tjerk Stegink
Engineering and Technology Institute Groningen
Nijenborgh 9, 9747 AG Groningen
t.w.stegink@rug.nl

Claudio De Persis
Engineering and Technology Institute Groningen
Nijenborgh 4, 9747 AG Groningen
c.de.persis@rug.nl

Arjan van der Schaft
Johann Bernoulli Institute for Mathematics and Computer Science
P.O.Box 407, 9700 AK Groningen
a.j.van.der.schaft@rug.nl

1 Real-time dynamic pricing

Provisioning energy has become increasingly complicated due to several reasons, including the increased share of renewables. As a result, it is more difficult for traditional energy sources to match the supply with the demand. To alleviate some of these problems, we introduce a distributed real-time dynamic pricing scheme that encourages the consumers to change their usage when it is difficult for the generators and the network to match the demand.

In addition, real-time dynamic pricing allows for maximization of the *social welfare*. The objective here is to have producers and consumers to fairly share utilities and costs associated with the generation and consumption of power in an optimal manner. Simultaneously, the goal is to achieve zero frequency deviation w.r.t. to the nominal value (e.g. 50 Hz) in the physical power network.

However, existing dynamic pricing algorithms often neglect the physical dynamics of the grid, and focus merely on the economic part of the optimal supply-demand matching problem [1], [2]. Nevertheless, this coupling is essential for guaranteeing stability of both the frequency and the power market [3], [4], [5].

2 Primal-dual gradient method

A common method to solve an optimization problem (e.g. maximizing the social welfare) is the primal-dual gradient method. Also in power grids this is a commonly used approach to design optimal distributed controllers [3], [4], [5].

As shown in our previous work [6], the system obtained by applying a continuous time gradient method to an optimization problem admits a port-Hamiltonian representation. In this present work, we apply the primal-dual gradient method to the social welfare problem to obtain a distributed real-time dynamic pricing scheme [5]. In this price-based controller there is freedom in choosing a desired communication network.

The resulting system is then interconnected with the physical system in a *power-preserving* manner to obtain a closed-loop port-Hamiltonian system. The properties of the closed-loop system are exploited to prove both convergence to the set of optimal points (maximal social welfare) and regulation of the frequency.

2.1 Extensions

Finally, we show that the real-time pricing scheme also allows for many possible extensions such as including nodal power constraints (e.g. generator capacity limits) and line congestion into the social welfare problem [5].

References

[1]   A. Kiani and A. Annaswamy. "The effect of a smart meter on congestion and stability in a power market." In 49th *IEEE Conference on Decision and Control*, Atlanta, 2010.

[2]   M. Roozbehani, M. Dahleh, and S. Mitter. "On the stability of wholesale electricity markets under real-time pricing." In *49th IEEE Conference on Decision and Control (CDC)*, 2010, pp. 1911–1918.

[3]   N. Li, L. Chen, C. Zhao, and S. H. Low. "Connecting automatic generation control and economic dispatch from an optimization view." In *American Control Conference*. IEEE, 2014, pp. 735–740.

[4]   X. Zhang and A. Papachristodoulou. "A real-time control framework for smart power networks with star topology." In *American Control Conference (ACC)*, pages 5062–5067, 2013.

[5]   T.W. Stegink, C. De Persis, and A.J. van der Schaft. "A unifying energy-based approach to optimal frequency and market regulation in power grids." *arXiv preprint arXiv:1510.05420*, 2015.

[6]   T.W. Stegink, C. De Persis, and A.J. van der Schaft. "Port-hamiltonian formulation of the gradient method applied to smart grids." In *5th IFAC Workshop on Lagrangian and Hamiltonian Methods for Non Linear Control*, Lyon, France, July 2015.

Conservation of Reactive Energy in Reactive Time

Dimitri Jeltsema
Delft Institute of Applied Mathematics
Delft, The Netherlands
Email: d.jeltsema@tudelft.nl

Gerald Kaiser
Center for Signals and Waves
Portland, OR, USA
Email: kaiser@wavelets.com

Abstract

Electrical networks, and physical systems in general, are known to satisfy a power balance equation, which states that the rate of change of the stored energy in time equals the supplied power minus the power dissipated. Remarkably, when complex power is considered, there does not seem to exist a similar statement for the imaginary power, neither in the time-domain nor in the frequency-domain. Recently, in the context of electromagnetic fields, it has been shown that by complexifying the time axis, introducing the concept of reactive time, it is possible to setup an imaginary power balance in terms of the rate of change of reactive energy in reactive time. In this talk, these ideas are specialized to linear and time-invariant RLC networks. For non-sinusoidal waveforms it is shown that the rate of change of reactive energy in reactive time contains all the essential properties and features of the commonly accepted definition of reactive power under sinusoidal conditions. We believe that this provides an unambiguous and physically motivated resolution to the longstanding debate on how to generalize reactive power to non-sinusoidal waveforms.

Power Balance

Consider a single-phase generator transmitting energy to a load. Let $u(t)$ and $i(t)$ be the port voltage and current, then

$$\frac{\mathrm{d}}{\mathrm{d}t}w(t) = p(t) - p_d(t), \qquad (1)$$

where $w(t) = w_m(t) + w_e(t)$ represents the sum of the total stored magnetic and electric energies, $p(t) = u(t)i(t)$ is the instantaneous supplied power, and $p_d(t)$ the total instantaneous dissipated power. The power balance equation (1) holds regardless of the nature of the elements or the excitation and is consistent with the principle of conservation of energy.

Under sinusoidal conditions, and when the load is linear and time-invariant (LTI), the port voltage and current can be represented by phasors, which yields the complex power [1]

$$\underline{S} := \tfrac{1}{2}\underline{U}\,\underline{I}^* = P + jQ = P_d + j2\omega\left[W_m - W_e\right], \qquad (2)$$

where P_d represents the average power dissipated in the resistors and W_m and W_e represent the total average magnetic and electric energies, respectively.

Although it is trivial to relate the real part of (2) with the periodic average of (1), i.e.,

$$\frac{\mathrm{d}}{\mathrm{d}t}W = P - P_d,$$

which, since the total average energy $W = W_m + W_e$ is constant, reduces to $P = P_d$, there does *not* exists a power balance equation for the imaginary part in terms of a rate of change of reactive energy, at least not in the time-domain.

Energy and Power in the Time-Scale Domain

The contribution of this talk is two-fold. First, we show that (2) can be generalized to *arbitrary* waveforms by extending the phasors to their analytic time signals associated to the positive-frequency part of the voltage and current spectra. Consequently, the complex power generally becomes time-dependent [2] and reveals that, due to the non-exactness of the differential forms associated to its imaginary part, there cannot exists a potential function that represents reactive energy in time. Secondly, to resolve the non-exactness problem, we analytically continue the voltage and current to the complex *time-scale* domain via [3]

$$\left\{\underline{u}(t+js), \underline{i}(t+js)\right\} = \frac{1}{\pi}\int_0^\infty \left\{\hat{U}(\omega), \hat{I}(\omega)\right\}e^{j\omega(t+js)}\,\mathrm{d}\omega,$$

where $s > 0$ represents a time resolution scale, referred to as *reactive time*, measured in seconds-reactive [sr]. This naturally enables us to setup a reactive power balance

$$-\frac{\partial}{\partial s}\mathcal{X}(t,s) = \mathcal{Q}(t,s),$$

where $\mathcal{X}(t,s) := \mathcal{W}_m(t,s) - \mathcal{W}_e(t,s)$ represents the *scaled reactive energy* and $\mathcal{Q}(t,s)$ the *scaled reactive power*. This suggests that reactive energy is *not* conserved in regular time t, but in reactive time s, tracking its *leads* and *lags*.

References

[1]   C. A. Desoer and E. S. Kuh. *Basic Circuit Theory*. McGraw-Hill Book company, 1969.

[2]   D. Jeltsema. *Time-varying phasors and their application to power analysis*. Mathematical Control Theory I, Lecture Notes in Control and Information Sciences, Vol. 461, pp 51-72, 2015.

[3]   G. Kaiser, *Completing the complex Poynting theorem: Conservation of reactive energy in reactive time*, 2014. Available at http://arxiv.org/abs/1412.3850. Also *Conservation of reactive EM energy in reactive time*, in proc. IEEE AP-S Symposium on Antennas & Propagation and URSI CNC/USNC Joint Meeting, Vancouver, BC, July 2015.

Government and Central bank Interaction under Uncertainty: A Differential Games Approach

Jacob Engwerda, Tilburg University, The Netherlands, P.O. Box 90153, 5000 LE Tilburg
engwerda@uvt.nl
Davoud Mahmoudinia, Isfahan University
Rahim Dalali Isfahani, Isfahan University

1 Abstract

Today, debt stabilization in an uncertain environment is an important issue. In particular, the question how fiscal and monetary authorities should deal with this uncertainty is very important. Especially for some developing countries such as Iran, in which on average 60 percent of government revenues comes from oil, and consequently uncertainty about oil prices has a large effect on budget planning, this is an important question. For this reason, we extend in this paper the well-known debt stabilization game introduced by Tabellini [3]. We incorporate deterministic noise into that framework. We solve this extended game under a Non-cooperative, Cooperative and Stackelberg setting assuming a feedback information structure. The main result shows that under all three regimes, more active policies are used to track debt to its equilibrium level and this equilibrium level becomes smaller, the more fiscal and monetary authorities are concerned about noise. Furthermore, a fiscal leadership seems to be the best-response policy configuration if policymakers are confronted with much uncertainty.

Following the approach introduced by Tabellini [3] we consider next dynamics

$$\dot{d}(t) = (r - g)d(t) + f(t) - m(t) + w(t). \qquad (1)$$

In which d denotes government debt scaled to nominal income, f is the primary fiscal deficit scaled to nominal income and m is the growth rate of base money scaled to nominal income. Furthermore, r and g are real interest rate and growth rate of real income (per capita), respectively, and they are assumed to be exogenous and independent of time. $w(t)$ expresses the uncertainty present in the various variables and parameters in this model. This unknown disturbance can be government and central bank uncertainty about oil income, inflation, exchange rate, economic growth, and etc. Also, we assume that debt can not grow forever. Or, in game theoretic phrasing, the no Ponzi game condition holds. The inter-temporal loss function of fiscal and monetary authorities under uncertainty are (2) and (3), respectively.

$$L_F = \frac{1}{2}\int_0^\infty e^{-\rho t}\left\{ (f(t) - \bar{f})^2 + \varphi(m(t) - \bar{m})^2 \right.$$
$$\left. + \theta(d(t) - \bar{d})^2 - v_f w^2(t) \right\} dt, \qquad (2)$$

$$L_M = \frac{1}{2}\int_0^\infty e^{-\rho t}\left\{ (m(t) - \bar{m})^2 + \eta(f(t) - \bar{f})^2 \right.$$
$$\left. + \tau(d(t) - \bar{d})^2 - v_m w^2(t) \right\} dt. \qquad (3)$$

The two policymakers are trying to minimize their loss functions subject to the budget constraint (1). The parameter ρ in both loss functions indicates the discount rate and $\bar{f}$, $\bar{m}$ and $\bar{d}$ are the target levels for deficit, monetary base and debt, respectively. Using the concept of soft-constrained equilibria (see, e.g., Engwerda [2]) we derive these equilibria for this extended Tabellini model, under a Non-cooperative, a Cooperative and Stackelberg setting, respectively. Then, after finding the equilibrium actions, we simulate the model for Iran's economy and analyze the outcomes.

References

[1]   Engwerda, J.C., Mahmoudinia, D., R.D. Isfahani, 2016. Government and Central bank Interaction under Uncertainty: A Differential Games Approach. Submitted.

[2]   Engwerda, J.C., 2005. *LQ Dynamic Optimization and Differential Games*. John Wiley and Sons. Chichester.

[3]   Tabellini, G.,1986. Money, debt and deficits in a dynamic game. *Journal of Economic Dynamics and Control* 10, 427-442.

A "local" influence index for social networks

Wilbert Samuel Rossi
EWI-HS, University of Twente;
7522 NB Enschede, The Netherlands
w.s.rossi@utwente.nl

Paolo Frasca
EWI-HS, University of Twente;
7522 NB Enschede, The Netherlands
p.frasca@utwente.nl

1 Introduction

The identification of the most influential nodes is an important issue in the study of networks and dynamical processes on them. Different notions of centrality have been proposed, depending on the process and the control objective [1], [2], [3]. Inspired by [1], [4], [5] we consider an opinion dynamics model in a connected network containing stubborn agents. Regular agents update their opinion with a local consensus rule, under the possible influence of an external bias. Although the bias is just an extra stubborn agent, keeping the distinction has advantages during the analysis of the model. Taking the bias into account, we generalize the *Harmonic influence Centrality* (HIC) measure [1] to the *Local-HIC*: simulations show that the bias localizes the influence of each single stubborn on the network. These indexes are the basis to formulate an *Optimal Stubborn Placement Problem*, whose solution can be used in a greedy, sub-optimal algorithm to place further stubborn agents in the network [5]. A distributed Message Passing Algoritm (MPA) can estimate these indices. The MPA is exact on trees and convergent on regular networks [1]. We investigate the properties of the MPA associated to the *Local-HIC* and prove its convergence on any unicyclic graph (i.e. containing exactly one cycle). Similar techniques might extended the result to further topologies.

2 Electrical analogy and centralized computation

The opinion dynamics model has a useful electrical interpretation. Let $\mathscr{G} = (I, E)$ be the graph, Z the set of pre-existing stubborn agents held at null potential, $\ell \in I \setminus Z$ be the candidate stubborn agent held at potential one. Edges in E have unitary conductance, and there is a conductance $\gamma \geq 0$ between any node and a null reference potential representing the bias. The equilibrium electrical potentials of the remaining regular agents $R^\ell = I \setminus Z \setminus \{\ell\}$ correspond to their limiting opinions. The *Local*-HIC index $H_\gamma(\ell)$ of the candidate ℓ is the sum of all node potentials.

Let $A \in \{0,1\}^{I \times I}$ and $L \in \mathbb{R}^{I \times I}$ be the adjacency and Laplacian matrix of $\mathscr{G}$ respectively, $\mathbb{I}$ and $\mathbf{1}$ be the identity matrix and the all-one vector of appropriate size. For any $\gamma \geq 0$, the L-HIC of ℓ can be formally defined by

$$H_\gamma(\ell) := 1 + \mathbf{1}^\top (L_{R^\ell, R^\ell} + \gamma \mathbb{I})^{-1} A_{R^\ell, \{\ell\}}$$

where $A_{R^\ell, \{\ell\}}$ and L_{R^ℓ, R^ℓ} are the sub-matrices of A and L cor-

responding to the subsets of I.

Proposition 1. $H_\gamma(\ell)$ *is Lipschitz continuous for any* $\gamma \geq 0$.

We stress that $H_0(\ell)$ is the index described in [1]. Given Z, the Optimal Stubborn Placement Problem amounts at the identification of the most influential stubborn agent:

$$\ell_\gamma^* = \arg\max_{\ell \in I \setminus Z} H_\gamma(\ell).$$

3 Distributed computation and future directions

The electrical analogy allows the development of a MPA to estimate the L-HIC in a distributed and iterative fashion. With our formulation, we prove the following.

Proposition 2. *Let* $\gamma > 0$ *or* Z *be non-empty. The MPA converges on any finite connected unicyclic graph.*

The proof uses the properties of the MPA "message exchange" graph and the monotonicity of the message updates. We envision that this approach can be extended to prove the convergence of the MPA in further graph topologies.

References

[1] L. Vassio, F. Fagnani, P. Frasca, and A. Ozdaglar, "Message passing optimization of harmonic influence centrality," *Control of Network Systems, IEEE Transactions on*, vol. 1, no. 1, pp. 109–120, March 2014.

[2] D. Kempe, J. Kleinberg, and É. Tardos, "Maximizing the spread of influence through a social network," in *Proceedings of the ninth ACM SIGKDD international conference on Knowledge discovery and data mining*. ACM, 2003, pp. 137–146.

[3] E. Estrada and N. Hatano, "A vibrational approach to node centrality and vulnerability in complex networks," *Physica A: Statistical Mechanics and its Applications*, vol. 389, no. 17, pp. 3648 – 3660, 2010.

[4] D. Acemoglu, G. Como, F. Fagnani, and A. Ozdaglar, "Opinion fluctuations and disagreement in social networks," *Mathematics of Operations Research*, vol. 38, no. 1, pp. 1–27, 2013.

[5] E. Yildiz, A. Ozdaglar, D. Acemoglu, A. Saberi, and A. Scaglione, "Binary opinion dynamics with stubborn agents," *ACM Trans. Econ. Comput.*, vol. 1, no. 4, pp. 19:1–19:30, Dec. 2013.

Robust average consensus dynamics over wireless networks

Francesco Acciani
Department of
Applied Mathematics
University of Twente
Enschede, The Netherlands
f.acciani@utwente.nl

Geert Heijenk
Department of
Computer Science
University of Twente
Enschede, The Netherlands
geert.heijenk@utwente.nl

Paolo Frasca
Department of
Applied Mathematics
University of Twente
Enschede, The Netherlands
p.frasca@utwente.nl

1 Introduction

This work addresses the average consensus problem over wireless networks, with transmitter-based and link-based random communication losses. A novel methods is proposed to compensate for the information lost during communication due to packet collision over symmetric networks. Distributed consensus algorithms have been widely studied in the past decade, as they form the base for a large number of distributed algorithms . However, the assumption of a static network , i.e. all the links are reliable and fixed, is not realistic in a wireless scenario, as packets can be lost due to collisions. The presence of packet losses makes necessary to adopt a compensation method to achieve consensus, which might not be to the average of the nodes' initial states [1], [2].

2 Consensus and compensation

The standard distributed algorithm to achieve the averaging over a number n of nodes is described by

$$x_i(k+1) = \sum_{j=1}^{n} \bar{P}_{ij} x_j(k), \qquad (1)$$

where $\bar{P}$ is the matrix representing the weight of the network links, $\bar{P}_{ij} = 0$ if the nodes i and j are not connected. If $\bar{P}$ is *doubly stochastic* (i.e. $\bar{P}_{ij} \geq 0 \, \forall i, j$, $\bar{P} \mathbb{1} = \mathbb{1}$ and $\mathbb{1}^T \bar{P} = \mathbb{1}^T$) and the network is *strongly connected* and *aperiodic* then $\bar{P}$ solves the average consensus problem. In this work, aperiodicity and strong connectivity of the network are assumed as true. Moreover, we suppose that the communication is bidirectional and multicast: a message sent from one node is received by every neighbour. We assume that if a packet is lost, all the packets from the sending node are lost for the round when the collision happened, due to the shared nature of the physical medium. This leads to a node-based failure model: every node has a certain probability p to fail in the global communication with all the nodes in his neighbourhood at any given time. The network is supposed to be homogeneous, i.e. the failure probability is the same for every node. While the assumptions of node-based collisions and network homogeneity are not needed for the new compensation method to converge to the average of the network's

initial condition, they make the analytical estimation of the rate of convergence tractable.

3 Proposed solution

In presence of a communication failure, each node performs the compensation of packet loss according to the following update rule

$$x_i(k+1) = x_i(k) + f_i(k) \sum_{j=1}^{n} f_j(k) \bar{P}_{ij} (x_j(k) - x_i(k)) \quad (2)$$

where $f_i = 0$ if the node i was not able to communicate at time k, $f_i = 1$ otherwise, and $\mathbb{P}[f_i = 0] = p$. This leads to a dynamics described by

$$x(k+1) = P_n(k)x(k) \qquad (3)$$

where

$$P_n(k) = F(k)\bar{P}F(k) + I - diag(F(k)\bar{P}F(k)\mathbb{1}), \qquad (4)$$

which is doubly stochastic, provided the matrix $\bar{P}$ is symmetric. It can be shown that this (random) matrix solves the average consensus problem over bidirectional networks in a probabilistic sense. Furthermore, its rate of convergence can be estimated. Details are available in [3].

4 Conclusion

A novel approach to deal with packet losses over wireless networks was proposed, capable to achieve average consensus over unreliable symmetric networks. Current work is focusing on implementing and validating this compensation method via simulations on dedicated software.

References

[1] F. Fagnani and S. Zampieri, "Average consensus with packet drop communication," *SIAM Journal on Control and Optimization*, vol. 48, no. 1, pp. 102–133, 2009.

[2] K. Cai and H. Ishii, "Average consensus on general strongly connected digraphs," *Automatica*, vol. 48, no. 11, pp. 2750 – 2761, 2012.

[3] F. Acciani, P. Frasca, and G. Heijenk., "Robust average consensus dynamics over wireless networks," ECC, 2016.

Convergence of 2-Strategy Network Games under Asynchronous Best Response Dynamics

James Riehl
University of Groningen
j.r.riehl@rug.nl

Pouria Ramazi
University of Groningen
p.ramazi@rug.nl

Ming Cao
University of Groningen
m.cao@rug.nl

1 Abstract

The idea behind *best response dynamics* is simple: in a network of interacting agents, each agent takes the action that results in the best cumulative outcome against its neighbors. This framework is widely studied in a game theoretic context but its impact is broadened by the fact that when there are two available actions for each agent, it is equivalent to what is called a *linear threshold model*. This comes with an alternate yet also intuitive interpretation: if enough of my neighbors are taking action A, I will also take action A. The reverse is also possible: if too many of my neighbors are taking action A, I will switch to action B. We call agents that follow the first rule *coordinating agents*, and those that follow the second *anti-coordinating agents*. These switches may be considered voluntary as in changing a behavior, policy, or opinion, or involuntary as getting infected by virus or defaulting on a loan. Due to the wide applicability of this model, there has already been extensive research into the conditions under which action A will spread as well as the speed at which this may occur, *e.g.*[1][2]. However, although simple at first glance, the complexity of this model almost always necessitates some simplifying assumptions, whether on the number and characteristic of different thresholds, synchrony of the dynamics, or the structure of the underlying networks. **In this work, we find that every network consisting of all coordinating or all anti-coordinating agents with asynchronous updates will reach equilibrium in finite time, even if each agent has a different threshold/payoff matrix.** A mixture of agent types will not necessarily converge.

2 Model

Consider an undirected network $\mathbb{G} = (\mathcal{V}, \mathcal{E})$ where the nodes $\mathcal{V} = \{1, \ldots, n\}$ correspond to agents and each edge in the set $\mathcal{E} \subseteq \mathcal{V} \times \mathcal{V}$ represents a 2-player game between neighboring agents. Each agent $i \in \mathcal{V}$ can choose a strategy from a binary set $\mathcal{S} := \{A, B\}$ and receives payoffs from each game according to the matrix:

$$
\begin{array}{cc}
 & \begin{array}{cc} A & B \end{array} \\
\begin{array}{c} A \\ B \end{array} & \begin{pmatrix} a_i & b_i \\ c_i & d_i \end{pmatrix}.
\end{array} \tag{1}
$$

Let $x_i(t) \in \mathcal{S}$ denote the strategy (state) of agent i at time t, and denote the number of neighbors playing A and B at time t by $n_i^A(t)$ and $n_i^B(t)$. The total payoff to agent i at time t is accumulated over all neighbors and equal to $a_i n_i^A(t) + b_i n_i^B(t)$ when $x_i(t) = A$, or $c_i n_i^A(t) + d_i n_i^B(t)$ when $x_i(t) = B$. In asynchronous (myopic) best response dynamics, one agent at a time becomes active and chooses a single action to play against all neighbors. The active agent at time t, chosen at random, updates to the action that achieves the highest total payoff, *i.e.* is the best response, against the current actions of its neighbors. This rule can be expressed compactly as follows:

$$
x_i(t+1) = \begin{cases} A, & \text{if } \delta_i n_i^A(t) > \gamma_i \deg_i \\ B, & \text{if } \delta_i n_i^A(t) < \gamma_i \deg_i \\ z_i, & \text{if } \delta_i n_i^A(t) = \gamma_i \deg_i \end{cases} \tag{2}
$$

where $\delta_i := a_i - c_i + d_i - b_i$, $\gamma_i := d_i - b_i$, and $\deg_i$ denotes the degree of agent i. If A and B result in equal payoffs, both are best responses and we use z_i to indicate one of A, B or $x_i(t)$ for the equality case. Let $\tau_i = \frac{\gamma_i}{\delta_i}$ denote a threshold for agent i. When $\delta \neq 0$ and $\tau \in [0, 1]$, the sign of δ_i determines whether the agents are coordinating ($\delta_i > 0$) or anti-coordinating ($\delta_i < 0$). Otherwise there exists a dominant strategy and it can be shown that the model is equivalent to one in which $\tau \in \{0, 1\}$ and $z_i \in \{A, B\}$. An *equilibrium* of (2) is a state in which every agent satisfies the threshold required to maintain its current strategy.

3 Conclusions and Future Work

Our main result is that every network consisting of all coordinating or all anti-coordinating agents with asynchronous updates will reach an equilibrium in finite time. This holds for arbitrary networks and threshold distributions. The proof uses a potential function for the case of uniform thresholds and an augmented network to extend to the case of varying thresholds. In the future we plan to investigate convergence of the noisy best response dynamics as well as possibilities for using control to stabilize particular equilibrium states.

References

[1]   E. M. Adam, M. Dahleh, A. Ozdaglar, et al. On the behavior of threshold models over finite networks. In *51st IEEE Conference on Decision and Control*, 2012.

[2]   S. Morris. Contagion. *The Review of Economic Studies*, 67(1):57–78, 2000.

Control of Strategic Interactions in Finite Heterogeneous Populations under Best-Response Update Rule

Pouria Ramazi and Ming Cao
DTPA, University of Groningen, The Netherlands. Email: {p.ramazi, m.cao}@rug.nl

1 Introduction

One of the simple yet intelligent mechanisms that evolutionary game theory postulates to understand the evolution of cooperation, is the best-response update rule. Recently in [1], the convergence analysis of a finite, heterogeneous population of individuals playing matrix games has been performed where individuals have different payoff matrices and revise their strategies asynchronously according to the best response update rule. While modeling and analyzing such systems are the necessary steps towards understanding the evolution of cooperation, controlling them is an enticing goal. However, for most population dynamics, control of the strategic interactions under the best-response update rule is quite challenging, and it becomes even more complex in case of heterogeneous populations. The first question arises is what the control input is. One possible input would be the strategies of the agents. However, while it may be possible to set a robot to a desired strategy, it may be unrealistic to ask a company to always cooperate with other competing firms or to ask a person to always expose the same behavior in face of other members of a social group. The aim of this work is to control the population dynamics in [1] by shifting the types (payoff matrices) of the agents. Specifically, for a given population of known types of agents, we find how to change the types of the agents to have a desired number of cooperators in the long run.

2 The model

Consider a finite, well-mixed population of n agents that are participating in a population game evolving over time $t = 0, 1, \ldots$. Each agent chooses between cooperation (C) and defection (D). At each time step, an agent is randomly activated to update her choice according to how well she is doing when she plays her current strategy against the average population. More specifically, the four possible payoffs of an agent i, $i = 1, \ldots, n$, are summarized in the following payoff matrix

$$A_i = \begin{array}{c} C \\ D \end{array}\begin{pmatrix} R_i & S_i \\ T_i & P_i \end{pmatrix}, \qquad T_i > R_i > \max\{S_i, P_i\}.$$

Denote agent i's strategy vector at time t by $s_i(t)$, which is defined to be $[1\ 0]^T$ when agent i chooses to cooperate at t and $[0\ 1]^T$ otherwise. Let $x_C(t)$ denote the ratio of cooperators in the whole population at time t and define the *average*

population vector $s_C(t) = \begin{bmatrix} x_C(t) & 1 - x_C(t) \end{bmatrix}^T$. Then agent i's payoff at time t against the average population is calculated by $u_i(s_i(t), s_C(t)) = s_i(t)^T A_i s_C(t)$. When agent i is activated to update her strategy at time t, she follows the *(myopic) best-response update rule*: agent i sticks to her current choice of strategy if her alternative strategy does not give her a higher payoff, and otherwise she switches her strategy. Clearly the payoff matrices are critical for the strategy update dynamics. In this setup, A_i corresponds to either a prisoner's dilemma (PD) game, satisfying $P_i > S_i$ or a snowdrift (SD) game, satisfying $S_i > P_i$. We call each agent with a PD (resp. SD) payoff matrix a *PD type agent* (resp. *SD type agent*). The SD agents are further classified into $l > 0$ types $SD_1, \ldots, SD_l$ according to their different values of $\frac{S_i - P_i}{T_i - R_i + S_i - P_i}$. Then there are altogether $l + 1$ types among the n agents. Denote the agents' choices at time t by the vector $a(t) \in \{C, D\}^n$. Let n_{PD} denote the number of PD agents and n_{SD_j}, $j = 1, \ldots, l$, the number of SD$_j$ agents. Then the *type population* defined by $p = (n_{SD_1}, n_{SD_2}, \ldots, n_{SD_l}, n_{PD})^T$ belongs to the set $\mathscr{P}_n := \{p \in \mathbb{Z}_{\geq 0}^{l+1} \mid \sum_{i=1}^{l+1} p_i = n\}$. Given $p \in \mathscr{P}_n$ and $a(0)$, denote the number of cooperators in the population at time t by $n_C(p, a(0), t)$.

3 Controlling the number of cooperators

We start with defining the *reachable set* $\mathscr{D}_n$ to be the set of all the nonnegative integers r for which there exists a type population p so that under the update rule, the number of cooperators equals and remains r after some time τ, i.e., $\mathscr{D}_n := \{r \in \mathbb{Z}_{\geq 0} \mid \exists p \in \mathscr{P}_n : \forall a(0), (\exists \tau : n_C(p, a(0), t) = r \quad \forall t \geq \tau)\}$. After determining $\mathscr{D}_n$, we are able to find, for each $r \in \mathscr{D}_n$, the set of all feasible type-populations such that under the best response update rule, the number of cooperators equals r for all time greater than some constant τ, i.e., $\mathscr{F}(r, n) := \{p \in \mathscr{P}_n \mid \forall a(0), (\exists \tau : n_C(p, a(0), t) = r \quad \forall t \geq \tau)\}$. Then it leads to possible ways to change the types of the agents to have r cooperators in the long run. Finally, we clarify the minimum number of changes needed to set the number of cooperators to r at the final state.

References

[1]   P. Ramazi, and M. Cao, "Analysis and control of strategic interactions in finite heterogeneous populations under best-response update rule", *in Proc. IEEE Conf. Decision Control (CDC)*, Osaka, Japan, Dec. 2015.

A novel approach to the model stable inversion for NMP systems

L. Jetto and V. Orsini

Dip. di Ingegneria dell'Informazione

Universitá Politecnica delle Marche

Via Brecce Bianche 12, 60131 Ancona

Italy

Email: [l.jetto,v.orsini]@univpm.it

R. Romagnoli

Service d'Automatique et d'Analyse des Systèmes

Universitè Libre de Bruxelles (ULB)

50, av. F.D. Roosevelt,CP 165/55, 1050 Bruxelles

Belgium

Email: rromagno@ulb.ac.be

1 Introduction

A new method to achieve an accurate output tracking for nonminimum phase (NMP) linear systems with nonhyperbolic or near nonhyperbolic internal dynamics is presented [1]. The main challenge is given by the transient output tracking, thus a feedforward filter yielding the external reference trajectory $r(t)$ is designed. The aim is to find a stable $r(t)$ that solves the transient output tracking. Classical general approaches are based on the exact solution of the stable inversion [2]. The proposed method is called *pseudo-inversion* because it is formulated as an optimization problem whose solution is obtained through a least square algorithm. The new method overcomes the main limitations of classical methods [2] like pre-actuation, unfeasibility for nonhyperbolic and near-nonhyperbolic plants, numerical complications in the case of MIMO systems.

2 Preliminaries

The continuous-time least square problem

$$\min_f J(e) = \min_f \|Q^{1/2}e\|_2^2 = \min_f \int_0^T e(t)^T Q(t)e(t)dt, \quad (1)$$

$$e(t) \stackrel{\triangle}{=} b(t) - D(t)f \quad (2)$$

where $e(t)$ is the residual vector, $b(t)$ is the observation vector, $D(t)$ is the design matrix, $Q(t)$ is a positive definite weight matrix for each fixed $t \in [0,T]$ and f is the vector of model parameters. The norm functional $J(e)$ defines the squared weighted L_2 norm of $e(t), t \in [0,T]$. The solution is known to be given by

$$\hat{f} = \left(\int_0^T D(t)^T Q(t)D(t)dt \right)^{-1} \int_0^T D(t)^T Q(t)b(t)dt \quad (3)$$

provided the inverse exists.
Spline function $s(t)$

Over a time interval $T \stackrel{\triangle}{=} [a,b]$ composed of disjoint sub-intervals $T_l \stackrel{\triangle}{=} [t_l,t_{l+1})$, with $a = t_0 < \cdots < t_{\bar{l}+1} = b$, the restriction of $s(t)$ to each T_l is a polynomial $p_l(t)$ of a fixed order m such that

$$[p_l^{(m)}(t)]_{t=t_{l+1}} = [p_{l+1}^{(m)}(t)]_{t=t_{l+1}}, \quad (4)$$
$$l = 0, \cdots, \bar{l} - 1 \quad , \quad m = 0, \cdots, r-1,$$

where $[p_l^{(m)}(t)]$ is the m-th derivative of $p_l(t)$. The time instants $t_l, l = 0, \cdots, \bar{l}+1$ are called knot points of the spline.

3 Pseudo-Inversion

Let $\Sigma = (C, A, B)$ be a LTI, continuous time, possibly nonminimum phase and/or nonhyperbolic, asymptotically internally stable closed loop control system. The actual response of Σ is given by

$$y(t) = Ce^{At}x(0) + \int_0^t Ce^{A(t-\tau)}Br(\tau)d\tau \quad (5)$$

where $x \in \mathbb{R}^n, y \in \mathbb{R}^p$ and $r(t) \in \mathbb{R}^p$ represents the external reference input. By the existence of the steady-state of Σ, $r(t)$ can partitioned in a transient $r_t(t)$ and steady state $r_s(t)$ components where $r(t) = r_t(t)$, $t \in T_t \stackrel{\triangle}{=} [0, t_t]$ and $r(t) = r_s(t)$, $t \in (t_t, \infty)$. The problem is to find $r_t(t)$ minimizing the transient error $e_t(t) \stackrel{\triangle}{=} y_d(t) - y(t)$ subject to $r_t(t_t) = r_s(t_t)$. We define a minimization problem as in (1) replacing f and $e(t)$ with r_t and $e_t(t)$. The transient error is computed using the known desired output $y_d(t)$ and the actual response (5) where $r_t(\cdot)$ is replaced by a spline function $s(\cdot)$. I this way $e_t(t)$ assumes the same form of (2)

$$e_t(t) = \bar{z}(t) - \mathbf{G}(t)\tilde{\mathbf{S}} \quad (6)$$

where $\bar{z} = y_d(t) - Ce^{At}x(0)$ and $\hat{\mathbf{S}} = \left[S^{1^T}, \cdots, S^{\bar{l}^T} \right]^T$ represents the unknown spline polynomials coefficients. This is due to the fact that $\hat{\mathbf{S}}$ is time independent, thus we take it out from the sign of integral (5). Also the spline continuity constraints (4) can be rewritten into the same form of (6), thus defining an augmented measurement error $e_a(t) \stackrel{\triangle}{=} [e_t(t)^T \ e_c(t)^T]^T$ we can take into account (4) into the minimization problem. The new functional is obtained substituting $e_a(t)$ into (2), thus (1) can be minimized by (3). For sake of simplicity the solution presented here is referred to the SISO case, but the same structures and properties are maintained using an extended form that takes into account all p inputs.

References

[1]   L.Jetto, V. Orsini, R. Romagnoli, Accurate output tracking for non minimum phase non hyperbolic and near non-hyperbolic systems, European Journal of Control, Vol.20,No. 6, pp. 292-300, November 2014.

[2]   Q. Zou, S. Devasia, Preview-based stable-inversion for output tracking of linear systems, *Journal of Dynamic Systems, Measurement, and Control*, 1999, 121, (4), pp. 625-630.

Resource Utilization and Quality-of-Control Trade-off for a Composable Platform

E.P. van Horssen[†], J.D. Valencia[*], D. Goswami[*], K.G.W. Goossens[*], W.P.M.H. Heemels[†]
Control Systems Technology[†] and Electronic Systems[*] groups, Eindhoven University of Technology
P.O. Box 513, 5600 MB, Eindhoven   `e.p.v.horssen@tue.nl`

1 Introduction

Consolidation of multiple software applications into a single hardware platform allows for significant reduction in infrastructure and complexity of hardware management and maintenance. Hence, such embedded system implementations are a trend in cost-sensitive industries, such as automotive. The challenges in realizing this consolidation are; (i) the deployment of effective coexistence mechanisms, (ii) the allocation of (processing) resources among the applications, and (iii) the resource-aware implementation of the applications. In this context, we consider the design and implementation of a resource-aware feedback control application. For such an application, we assess the trade-off between the allocation of resources (resource utilization) and the performance of the control application (Quality-of-Control / QoC).

In this work, the coexistence of the applications is realized by the Composable and Predictable System on Chip (CompSOC) platform [1]. The physical processors, their interconnections, and memories are virtualized following Time-Division Multiplexing (TDM) policies allowing for independent interference-free application development.

In the platform, a fraction of the resources, in terms of several TDM slots of processor time, are allocated to the control application. Control strategies based on uniform sampling schemes are not applicable in this context or achieve unsatisfactory performance [2]. On the other hand, resource-aware implementation of feedback controllers often leads to an unpredictable sampling scheme [3]. This gives rise to the need for control design methodologies taking into account non-uniform sampling intervals resulting from a given resource allocation. One such methodology is presented.

2 Methodology

This work connects ideas from periodic control systems [4] to the TDM-based resource utilization on CompSOC. Our framework deals with three design considerations: the amount of allocated resources, the allocation pattern (e.g., contiguous or spread) and the (optimal) QoC. For a given TDM-based resource allocation, controller timing behaviour in the platform can be characterized by a *finite*, *known* and *periodic* set of sampling intervals (see Figure 1). Utilizing this timing behaviour, we show that the control design problem can be transformed, by a time-lifted reformulation, into a classical or periodic discrete-time Linear Quadratic Regu-
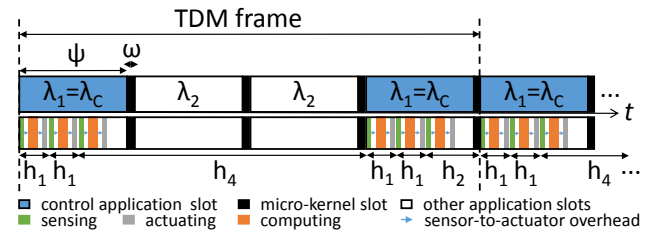
Figure 1: Resource utilization example for one TDM period.

lator (LQR) problem which can be efficiently solved to obtain the optimal QoC. Furthermore, we obtain an optimal periodic switched feedback controller. Since the design is explicit, the assessment of QoC can be done off-line. This allows the consideration of the QoC in the platform design. Hence, the proposed methodology facilitates a co-design framework for efficient resource-aware implementation of feedback controllers on TDM-based embedded platforms.

3 Discussion

We demonstrate how our design framework can be used to analyze the trade-off in a quantitative manner, thereby enabling educated designs of both the allocation pattern and the (optimal) feedback controller. Our method is validated both in simulation and experiments with a MIMO control example. For the studied case, we found that; (i) for a contiguous allocation pattern, an increased allocation amount provides a higher QoC, and (ii) for a given allocation, a contiguous allocation pattern outperforms a spread pattern.

References

[1] K. Goossens et al., "Virtual Execution Platforms for Mixed-time-criticality Systems: The CompSOC Architecture and Design Flow," *SIGBED Rev.*, vol. 10, no. 3, pp. 23–34, Oct. 2013.

[2] J. Valencia, D. Goswami, and K. Goossens, "Composable platform-aware embedded control systems on a multi-core architecture," in *Digital System Design (DSD), Euromicro Conference on*, 2015.

[3] W. Heemels, K. Johansson, and P. Tabuada, "An introduction to event-triggered and self-triggered control," in *IEEE Conference on Decision and Control (CDC) 2012, Hawaii, USA*, December 2012, pp. 3270–3285.

[4] S. Bittanti and P. Colaneri, *Periodic systems: filtering and control*. Springer Science & Business Media, 2008, vol. 5108985.

Control oriented assessment of invertible non-linear models

Rishi Mohan, Rolf Gaasbeek, Bram de Jager

Eindhoven University of Technology, Department of Mechanical Engineering, P.O. Box 513, 5600 MB Eindhoven, The Netherlands

Email: R.Mohan@tue.nl, R.I.Gaasbeek@tue.nl

1 Introduction

In a certain class of non-linear systems, the non-linearity can be characterized by a mathematical model which is invertible, i.e, the input-output mapping of the model can be reversed. These mathematical models are categorized as *invertible non-linear models*. One such non-linear phenomenon is hysteresis, which typically affects *smart material actuators* during actuation [1]. Smart material actuators convert non-mechanical input (electrical, magnetic or thermal power) to mechanical output and are widely used to develop micro/nano-positioning systems for various commercial applications [2]. However, the position control of these actuators is limited due to the presence of non-linear hysteresis.

2 Inverse-based Control

To mitigate the detrimental effects of non-linear hysteresis, inverse-based control architectures have been developed [3]. Considering an invertible hysteresis model (γ) is used to describe actuator hysteresis, the inverse-based approach utilizes an approximate inverse of this model to precompensate hysteresis. Primarily, this approach facilitates linear controller design by nullifying the hysteresis non-linearity [4]. As depicted in Figure 1, the approach combines inverse compensation in series with linear feedback control. The hysteresis inverse (γ^{-1}) is constructed to cancel non-linear hysteresis effects which permits the development of a linear controller (K). The controller is designed to handle the inversion error and linear dynamics of the resulting system ($G_l(s)$) after hysteresis compensation.
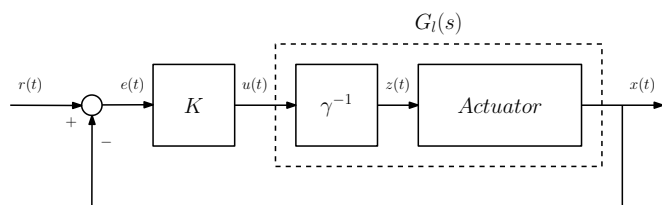
Figure 1: Inverse-based Control Architecture

3 Model Selection

The hysteresis inverse forms the core of the inverse-based approach. Consequently, selecting the appropriate hysteresis model is a critical task. In general, model selection for inverse compensation is based on the ability of a model to accurately predict the actuator's hysteresis behavior. An invertible model is selected to describe hysteresis behavior and is in turn inverted to achieve hysteresis compensation. It is assumed that the more accurate a hysteresis model, the better is its inverse in canceling out hysteresis. The individual effectiveness of the inverse model is either neglected or is not experimentally verified.

4 Control Oriented Model Assessment

In this work, a model assessment framework is proposed in order to evaluate the efficacy of inverse hysteresis models for inverse-based control. The framework comprises of estimating the best linear approximation (BLA) and the level of stochastic non-linear distortions present in the system [5] after application of the inverse. Quantifying the level of non-linear distortions provides a direct evaluation of the residual non-linearity remaining in the system after hysteresis cancellation. A greater level of distortion suggests poor performance of the inverse compensator. The proposed framework is not limited to smart material actuators and can be extended to invertible non-linear models in general. An added advantage of the approach is the insight obtained in the linear dynamics of the compensated system. The BLA of the compensated system provides a quantitative and qualitative account of the linear behavior of the system after compensation. From a control viewpoint, not only does this provide behavioral information of the plant to be controlled, this information is derived without explicit *apriori* knowledge of the system's linear dynamics.

References

[1]   X. Tan and J. S. Baras, "Adaptive identification and control of hysteresis in smart materials," *IEEE Transactions on Automatic Control*, vol. 50, no. 6, pp. 827–839, 2005.

[2]   M. Rakotondrabe, M. Al Janaideh, A. Bienaimé, and Q. Xu, "Introduction: Smart materials as essential base for actuators in micro/nanopositioning," in *Smart Materials-Based Actuators at the Micro/Nano-Scale*.   Springer, 2013, pp. 1–14.

[3]   H. Sayyaadi and M. R. Zakerzadeh, "Position control of shape memory alloy actuator based on the Generalized Prandtl–Ishlinskii inverse model," *Mechatronics*, vol. 22, no. 7, pp. 945–957, 2012.

[4]   P. Krejci and K. Kuhnen, "Inverse control of systems with hysteresis and creep," *IEEE Proceedings-Control Theory and Applications*, vol. 148, no. 3, pp. 185–192, 2001.

[5]   R. Pintelon and J. Schoukens, *System Identification: A frequency domain approach*.   John Wiley & Sons, 2012.

Synchronization Approached Through the Lens of Primitivity

François Gonze*   Balázs Gerencsér†   Raphaël M. Jungers*[1]

francois.gonze@uclouvain.be   gerencser.balazs@renyi.mta.hu   raphael.jungers@uclouvain.be

* ICTEAM Institute, UCLouvain, Louvain-la-Neuve, Belgium

† Alfréd Rényi Institute of Mathematics, Budapest, Hungary

Introduction

Because of its links with synchronization and reachability of consensus, primitivity has recently attracted attention in the engineering community. Moreover, it allows to approach the *Černý Conjecture*, one of the most famous open problems in automata theory. In this work, we tackle the problem of generating sets of large matrices with the primitivity property. We propose a methodology to generate such sets and show its performance on numerical experiments.

1 From primitive sets to synchronizing automata

In matrix theory, a set of matrices with nonnegative entries is called *primitive* if there exists a positive product of matrices of this set. If a binary matrix has no zero row and no zero column, we call it *NZRC*. Furthermore, a set of binary row-stochastic matrices (*letters*) is called a *synchronizing automaton* if there exists a product of matrices (*word*) of this set with a positive column. This product is called a *synchronizing word*.

Blondel et al. [1] showed how the length of a shortest positive product composed from a primitive set of NZRC matrices is linked with the length of synchronizing words:

Theorem 1 (Theorem 17 in [1]). *For any primitive set of NZRC matrices*

$$M = \{A_1, \dots, A_m\} \subset \{0,1\}^{n \times n}$$

there exist two synchronizing automata

$$M_B = \{B_1, \dots, B_t\}, M_C = \{C_1, \dots, C_u\},$$

such that

$$\forall 1 \leq s \leq t, \exists l \in \{1, \dots, m\} : B_s \leq A_l \text{ (entrywise)} \quad (1)$$

$$\forall 1 \leq s \leq u, \exists l \in \{1, \dots, m\} : C_s \leq A_l^\top \text{ (entrywise).} \quad (2)$$

Thus, for two synchronizing words w_B and w_C of M_B and M_C, we can obtain a positive product of matrices from M partly by choosing the matrices based on the majorating property ensured by (1) and (2). The length of the product is at most the sum of the lengths of these words plus $n-1$.

In the context of this theorem, the *Černý Conjecture*, which states that any synchronizing automaton of size n has a synchronizing word of length at most $(n-1)^2$ (see [2]), would

imply that any primitive set of NZRC matrices has a positive product of length at most $2(n-1)^2 + n - 1$, whereas any shortest positive product of higher length would provide a counterexample. This is why the constructive approach of primitive sets is really interesting. Also, an upper bound for the length of the shortest positive product of a set of NZRC matrices is obtained from the best proven bound of Černý Conjecture (see [1, 3]).

2 Construction of primitive sets of matrices

In order to generate primitive sets of NZRC matrices with long shortest primitive product, we need conditions guaranteeing primitivity, while minimizing the number of positive entries. The method we propose is to take two random permutation matrices, and to change a "0" entry into a "1". This construction guarantees primitivity with high probability if the size is a prime number, and a minimal number of positive entries. Indeed, primitivity is equivalent to the set being irreducible and having no block-permutation structure. First, a set of two random permutations is irreducible with high probability. In addition, a second theorem allow us to say that for prime numbers, there is either no block-permutation structure or that the blocks are of size 1:

Theorem 2. *If an irreducible set of permutation matrices has a block-permutation structure, then all the blocks have the same size.*

Since our construction is not compatible with blocks of size 1, the set must be primitive.

We compared the probability of being primitive and the length of the shortest product of the matrices obtained using this method with other random NZRC sets generation methods. For both tests, it appears that our method provides a substantial improvement.

References

[1]   V. D. Blondel, R. M. Jungers and A. Olshevsky, On primitivity of sets of matrices, Automatica, 61, 80-88, 2015.

[2]   M. V. Volkov, Synchronizing Automata and the Černý Conjecture, Proceedings of LATA'08, 11-27, Springer-Verlag, 2008.

[3]   F. Gonze, R. M. Jungers and A. N. Trahtman, A Note on a Recent Attempt to Improve the Pin-Frankl Bound, Discrete Mathematics and Theoretical Computer Science, 17, 307-308, 2015.

Modelling for Control of Free Molecular Flow Processes

M. Dresscher
Nijenborgh 4
9747 AG Groningen
m.dresscher@rug.nl

B. Jayawardhana
b.jayawardhana@rug.nl

J. M. A. Scherpen
j.m.a.scherpen@rug.nl

1 Abstract

Modelling of free molecular flow started in the early 20th century with a series of experiments performed by Knudsen. In his first paper in 1909 [1], Knudsen introduced two fundamental concepts: (i) a defining criterion for free molecular flow, now known as the Knudsen number and (ii) the first arguments for the validity of a cosine law for diffusion from rough surfaces, now known as the Knudsen cosine law. Knudsen formally introduced this cosine law in kinetic theory in 1915 [2]. During the following 75 years, many useful contributions were made based on these fundamental insights. This history of free molecular flow theory was nicely documented in the 1986 review by Steckelmacher [3]. Since then, modelling and simulation methods have been developed to predict the evolution of free molecular flow in industrial processes. A mathematical framework has been introduced by Cale and Raupp for simple geometries, like a cylinder [4]. For more complex geometries, Monte-Carlo analysis is often performed [5].

Thus the state of the art in the modelling of molecular flow is focussed on improving understanding of the evolution of gas flow in a system. This focus often results in computational models suitable for simulation purposes. A logical next step would be to use the insights gained from the modelling efforts so far to develop a modelling framework that allows for control design.

From a control perspective, deposition control in free molecular flow can be applied in the Chemical Vapour Deposition (CVD) processes such as Ultra-High Vacuum CVD (UHVCVD) and Atomic Layer Deposition (ALD). Both processes are used for deposition of thin layers, usually for semi-conductor or other microelectronics manufacturing. An overview of the modelling and control challenges in microelectronics manufacturing can be found in [6]. This paper highlights the challenges with real-time control in these processes due to restrictions on sensor placement. For this reason, state estimation gains importance. The state estimation can in turn be combined with reference generation and tracking through a controllable input and observable (possibly *exsitu*) output.

We present a modelling framework suitable for control design of the evolution of free molecular flow fluxes inside a geometry. Methods to obtain finite element migration probabilities, based on the Knudsen cosine law for rough, weakly adsorbing surfaces, are presented. The modelling framework further allows for incorporation of chamber leakage, sticking behaviour and external input. We illustrate the main results by implementing the modelling framework for a cylinder. The relevant finite element migration probabilities are obtained through Monte-Carlo simulation. The obtained results are then compared with analytical solutions available in literature. Finally, we show the control potential for linear sticking behaviour.

References

[1] M. Knudsen, "Die gesetze der molekularstrmung und der inneren reibungsstrmung der gase durch rhren," *Annalen der Physik*, vol. 28, pp. 75–130, 1909.

[2] ——, "The cosine law in the kinetic theory of gases," *Annalen der Physik*, vol. 48, pp. 1113–1121, 1915.

[3] W. Steckelmacher, "Knudsen flow 75 years on: the current state of the art for flow of rarefied gases in tubes and systems," *Reports on Progress in Physics*, vol. 49, no. 10, p. 1083, 1986.

[4] T. S. Cale and G. B. Raupp, "Free molecular transport and deposition in cylindrical features," *Journal of Vacuum Science & Technology B*, vol. 649, no. 8, 1990.

[5] R. Dorsman, C. R. Kleijn, J. F. M. Velthuis, J. P. Zijp, and A. M. B. V. Mol, "Zinc deposition experiments for validation of direct-simulation Monte Carlo calculations of rarefied internal gas flows," *Journal of Vacuum Science Technology A*, vol. 25, no. 3, 2007.

[6] T. F. Edgar, S. W. Butler, W. J. Campbell, C. Pfeiffer, C. Bode, S. B. Hwang, K. Balakrishnan, and J. Hahn, "Automatic control in microelectronics manufacturing: Practices, challenges, and possibilities," *Automatica*, vol. 36, no. 11, pp. 1567–1603, 2000.

Stochastic control of crop growth, a simulation study

Simon van Mourik
Farm Technology Group
Wageningen University
P.O. Box 16 6700 AA Wageningen
The Netherlands
simon.vanmourik@wur.nl

Michel Vellekoop
Faculty of Economics and Business
University of Amsterdam
The Netherlands
m.h.vellekoop@uva.nl

Peter van Beveren
Farm Technology Group
Wageningen University
The Netherlands
peter.vanbeveren@wur.nl

Bert van 't Ooster
Farm Technology Group
Wageningen University
The Netherlands
bert.vantooster@wur.nl

Eldert van Henten
Farm Technology Group
Wageningen University
The Netherlands
eldert.vanhenten@wur.nl

1 Introduction

In horticulture, the role of dynamics of crop growth response, and subsequently the optimal timing of climatic factors such as temperature, humidity, and carbon-dioxide concentration, has been generally recognized and studied [1, 2]. Model based control has focused mainly on deterministic approaches, with only few exceptions [3]. However, uncertainty and variability are important factors for the behavior of many biosystems. Studies in ecology [4] and systems biology [5, 6] demonstrate that ignoring or oversimplifying them may lead to severe prediction errors.

2 Material and methods

Our case study concerned lettuce growth control via temperature, inside a greenhouse. We used a simple lettuce growth model, with stochastic noise on the state, and a performance criterion consisting of revenue based on crop final weight, minus the heating costs. We tested three controllers: a controller with constant output, dynamic optimal open loop control, and stochastic optimal control via dynamic programming.

3 Results

Our preliminary results predict that taking uncertainty into account will result in substantial improvement of controller performance.

4 Discussion

The results demonstrate that uncertainty control for crop growth deserves attention. However, the predictions should be validated experimentally, and model refinement seems necessary. The model assumptions regarding climate dynamics, uncertainty modeling, and growth modeling at this moment are quite strong.

References

[1]   F. Tap, "Economics-based optimal control of greenhouse tomato crop production," Wageningen University, 2000.

[2]   G. van Straten et al., "Optimal control of greenhouse cultivation," CRC press, 2010.

[3]   T.G. Doeswijk, "Reducing prediction uncertainty of weather controlled systems," Wageningen University, 2007.

[4]   C. Loehle, "Control theory and the management of ecosystems," Journal of applied ecology 43, 957-966, 2006.

[5]   R.N. Gutenkunst et al., "Universally sloppy parameter sensitivities in systems biology models ," PLoS computational biology 3, e189, 2007.

[6]   S. van Mourik et al., "Prediction uncertainty assessment of a systems biology model requires a sample of the full probability distribution of its parameters ," PeerJ 2, e433, 2014.

Dynamic metabolic flux convex analysis of hybridoma cell cultures

Sofia Fernandes de Sousa[1], Georges Bastin[2],
Mario Jolicoeur [3] and Alain Vande Wouwer[1]

[1]Automatic Control Laboratory, University of Mons,
31 Boulevard Dolez, 7000 Mons, Belgium
(sofia.afonsofernandes and alain.vandewouwer@umons.ac.be)
[2]ICTEAM, Department of Mathematical Engineering, Catholic University of Louvain,
av. G. Lemaitre 4, B1348 Louvain-La-Neuve, Belgium
[3]Laboratory in Applied Metabolic Engineering, Department of Chemical Engineering,
Polytechnic University of Montreal
C.P 6079, Centre-ville Station, Montreal, Canada
(mario.jolicoeur@polymtl.ac)

1 Introduction

In recent years, dynamic metabolic flux analysis (DMFA) has been developed in order to evaluate the dynamic evolution of the metabolic fluxes [1]. Most of the proposed approaches are dedicated to exactly determined or overdetermined systems. When an underdetermined system is considered, the literature suggests the use of dynamic flux balance analysis (DFBA) [2]. However the main challenge of this approach is to determine an appropriate objective function, which remains valid over the whole culture.

In the present study, an alternative DMFA method is proposed, which is suitable for underdetermined systems, and does not require the definition of ad-hoc objective functions. The method is based on convex analysis, and builds upon the methodology introduced in [3]. Dynamic Metabolic Flux Convex Analysis (DMFCA) [4] allows the determination of bounded intervals for the fluxes using the available knowledge of the metabolic network and information provided by the time evolution of extracellular component concentrations. Smoothing splines and mass balance differential equations are used to estimate the time evolution of the uptake and excretion rates from the experimental data. The main advantage of the proposed procedure is that it does not require additional constraints or objective functions, and provides relatively narrow intervals for the intracellular metabolic fluxes (see figure 1).

DMFCA is applied to experimental data from hybridoma HB58 cell perfusion cultures, in order to investigate the influence of the operating mode (batch and perfusion) on the metabolic flux distribution.

Acknowledgements
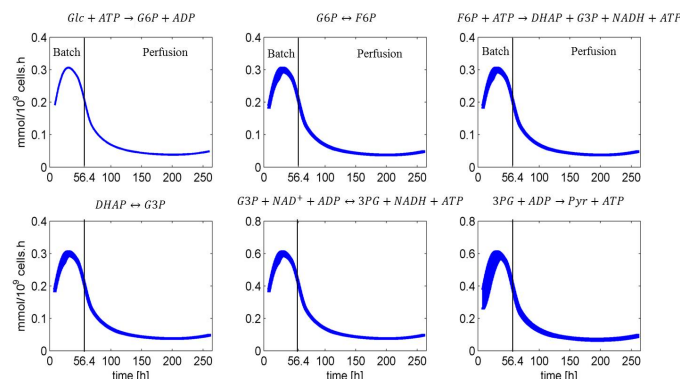
Figure 1: Dynamic evolution of glycolysis fluxes along culture time.

References

[1]   MR. Antoniewicz. Methods and advances in metabolic flux analysis: a mini-review. *J. Ind. Microbiol. Biotechnol*. 42:317325, 2015.

[2]   R. Mahadevan, JS. Edwards, FJ. Doyle. Dynamic Flux Balance Analysis of Diauxic Growth in Escherichia coli. *Biophys. J*. 83:13311340, 2002.

[3]   A. Provost and G. Bastin. Dynamic metabolic modelling under the balanced growth condition. *Journal of Process Control*, 14(7):717-728, 2004.

[4]   S. Fernandes de Sousa, G. Bastin, M. Jolicoeur and A. Vande Wouwer. Dynamic metabolic flux analysis using a convex analysis approach: Application to hybridoma cell cultures in perfusion. *Biotechnology and bioengineering*, 2015. doi:10.1002/bit.25879.

PHA production modeling with overflow dynamics

Julián Oviedo, Alain Vande Wouwer
Control Engineering Department
University of Mons
Bld Dolez 31, 7000 Mons
Belgium
Email: julian.oviedosantana@umons.ac.be

Alejandro Vargas
Instituto de Ingeniería
UNAM México
Blvd Juriquilla 3001
76230 Querétaro
México
Email: avargasc@iingen.unam.mx

1 Introduction

Polyhydroxyalkanoates (PHA) are a family of environment-friendly molecules with properties similar to polypropylene, thus making them proper bioplastics [1]. Producing PHA by means of pure cultures has been the main direction of research since the discovery of their producing bacteria almost 100 years ago. Nonetheless, their industrial scale-up has found hurdles mainly due to the high costs involving sterilization, costly substrates (e.g. glucose and volatile fatty acids), and production. Therefore attention has been focused towards mixed cultures. Being able to optimize mixed production would make feasible the competition with synthetic plastics, while offering lower environmental impact. In the present work we introduce a simple dynamic model of PHA production by mixed cultures, which describes the shift in metabolism through a controlled feeding strategy.

2 PHA modeling

Understanding the PHA dynamics is not an easy task and even though several models have been proposed in recent years, it remains an open subject. Research has shown consensus in the so-called "feast-famine regime" which basically accounts for short periods of substrate in excess (feast), and long periods of substrate limitation (famine). Intermittent periods of feast and famine, also addressed as *aerobic dynamic feeding*, are used as selective pressure on the microorganisms to select those capable of creating the metabolic change in the cultures.

However, it seems that the literature has focused mostly on microscopic (metabolic) aspects and therefore complex models. There is a lack of consideration of the operational bioreactor variables, especially the dissolved oxygen O. Oxygen plays a pivotal role as manipulated variable since it can control the accumulation of the biopolymer under aerobic conditions [4].

In this work it is assumed that the substrate consumption rate and/or the PHA production/consumption rates is/are linked to the oxygen consumption rate, as revealed by the observation of experimental data.

In fact oxygen concentration will be determinant of the respiratory capacity of the bacteria. According to this respiratory capacity, the substrate present in the culture medium can be scarce or in excess, and PHA can be produced in an overflow metabolism or consumed as an alternative substrate. This is the essence of the bottleneck assumption developed in [3], and exploited in extremum seeking in [2].

Inspired by these developments, this paper discusses a possible model structure, using the concept of overflow metabolism, presents simulation results and preliminary work on parameter estimation from experimental data, including sensitivity analysis.

3 Acknowledgment

References

[1] G. Braunegg, G. Lefebvre, and K.F. Genser, "Polyhydroxyalkanoates, biopolyesters from renewable resources: physiological and engineering aspects," Journal of Biotechnology, Vol 65(2), 127-161, 1998.

[2] L. Dewasme, B. Srinivasan, M. Perrier and A. Vande Wouwer, "Extremum-seeking algorithm design for fed-batch cultures of microorganisms with overflow metabolism," Journal of Process Control, Vol 21, 1092-1104, 2011.

[3] B. Sonnleitner, and O. Käppeli, "Growth of *Saccharomyces cerevisiae* is controlled by its limited respiratory capacity: Formulation and verification of a hypothesis," Biotechnology & Bioengineering, Vol 28(6), 927-937, 1986.

[4] A. Vargas, L. Montaño, and R. Amaya, "Enhanced polyhydroxyalkanoate production from organic wastes via process control," Bioresource technology, Vol 156, 248-255, 2014.

Dynamic microorganism growth modelling for shelf life prediction: Application to cooked and brined shrimps.

Mamadou Aliou Diallo
Mathematics-Informatics Department
Université Cheikh Anta Diop
Dakar, Sénégal
mamadou.aliou.diallo@ulb.ac.be

Philippe Bogaerts
3BIO-BioControl, Université Libre de Bruxelles,
Av. F. D. Roosevelt, 50 CP 165/61, B-1050 Brussels, Belgium
philippe.bogaerts@ulb.ac.be

1 Introduction

Predictive food microbiology is a very important research domain in food safety and quality. It is indeed of primary importance to predict growth of spoilage microorganisms to assure products safety and quality. Many strategies have been developed to extend products shelf life and to assure food safety and quality, e.g. environmental factors (such as temperature) control, cooking, brining, packaging, smoking, etc. [2]. Several methods have been proposed to develop models for shelf life prediction. One approach consists in estimating shelf life values by evaluating product off-flavor, aspect and texture and, subsequently, in building models correlating the shelf life estimates to environmental conditions like temperature [2]. Other models were developed by analyzing the effect of the growth of spoilage microorganisms on sensory quality of products [3].

In this contribution, the aim is to predict shelf-life in a two-step procedure. The first one consists of the identification and validation of a dynamical model which allows predicting spoilage microorganism growth at different storage temperatures. The second step consists in using that dynamical model for predicting shelf life as a function of the storage temperature by computing the elapsed time before the spoilage microorganism concentration reaches its admissible upper limit for ready-to-eat products.

2 Results

The 95% confidence intervals of the microorganism concentration time profiles were predicted by the developed model. Based on this latter and the admissible upper limit of *Listeria monocytogenes* in ready-to-eat products 100 cfu/g [2], shelf life and its associated confidence interval was predicted as a function of the storage temperature. The obtained predicted shelf lives were 42-53 days at 8°C, 9-11 days at 15°C and 3-4 days at 25°C. These results were compared to the ones of [2]. It turns out that the predicted values are in agreement with those estimated experimentally (with the largest difference at the storage temperature of 15°C). Note that, the approach presented here does not use experimental information on the shelf life.

3 Conclusion

The dynamic microorganism growth model proposed in this study uses the Baranyi's primary model [1] coupled with the secondary square root model and a sigmoidal function for describing the temperature dependency on, respectively, the maximum specific growth rate and the maximum cell density. The global predictive model and the associated uncertainty analysis allows the predictive determination of shelf life as a function of the storage temperature, based on the admissible upper limit of the microorganism concentration in ready-to-eat products. A case study concerning the growth of *Listeria monocytogenes* in cooked and brined warm water shrimps [2] is used for illustrating the methodology. This model could also be generalized for the secondary modelling of other influencing factors like pH, salt concentration, etc.

References

[1] Baranyi, J. and Roberts, T.A. (1994). A dynamic approach to predicting bacterial growth in food. International Journal of Food Microbiology, 23, 277-294.

[2] Dalgaard, P. and Jørgensen, L. V. (2000). Cooked and brined shrimps packed in a modified atmosphere have a shelf-life of $>$ 7 months at 0°C, but spoil in 4-6 days at 25°C. International Journal of Food Science and Technology, 35, 431-442.

[3] Dalcanton, F., Pérez-Rodríguez, F., Posada-Izquierdo, G.D., de Aragão, G.M.F. and García-Gimeno, R.M. (2013). Modelling growth of Lactobacillus plantarum and shelf life of vacuum-packaged cooked chopped pork at different temperatures. International Journal of Food Science and Technology, 48, 2580-2587.

Characterization of the visual space of butterfly eyes via a robotic scanner

Andrés Vargas-Delgado[1,2]   Mauricio Muñoz-Arias[1,2]   Doekele G. Stavenga[1]

[1]Faculty of Mathematics and Natural Sciences, University of Groningen, Nijenborgh 4, 9747 AG Groningen, the Netherlands

[2]School of Electronics, Costa Rica Institute of Technology, P.O. Box 159-7050, Cartago, Costa Rica

Email: `j.a.vargas.delgado@rug.nl`; `m.munoz.arias@rug.nl`; `d.g.stavenga@rug.nl`

1 Introduction

Nature has anticipated problems that research and development is aiming to solve. Understanding how the solution given by nature works is the appropriate path to reproduce its effectiveness in modern systems. Such is the case of the reduction of lens reflexions in modern optical systems by the "moth eye" principle [2], implemented nowadays in computer monitors, television screens and LCD displays. The research of a wider range of insect eyes becomes of interest in the current project. Among insects, butterflies have potential optical characteristics that can be exploited for modern artificial vision developments [7]. Characteristics such as *pseudopupils*, *deep pseudopupils* (DPP), and the separation of visual axes, i.e., *interommatidial angles* can been used to improve vision at low-light intensity [6, 7].

More recently, a state-of-the-art mechatronic system has been used for rapid evaluation of regional compound eye specializations [7]. Besides, a similar system also has been used to map the visual space of butterfly eyes [1, 5]. In [1] the design and implementation of an autofocusing algorithm for the robotic scanner has been done. Furthermore, the actuation of the robotic scanner via a microcontroller was designed and implemented in [5].

The main focus of this project is to improve the previous developments of the robotic scanner by completing an automatic scan of a butterfly eyes via the imaged-based vision servo control proposed initially by [3]. During the scanning process the system will focus on the aforementioned interommatidial angles. Furthermore, the data to be obtained with the scanner will create a 3D virtual image of the eye with local information about reflections and curvatures. Finally, the information will provide an insight into the way insects have solved problems related to vision.

2 Experimental setup

The experimental setup consists of a robotic scanner, which is a state-of-the-art mechatronic system, such as in [4]. The system is meant to simplify the data acquisition process of the visual properties of the butterflies. Subsequently, it is designed to obtain accurate information during the scanning process. Figure 1 shows a picture of the system at the Computational Physics Department, University of Groningen.
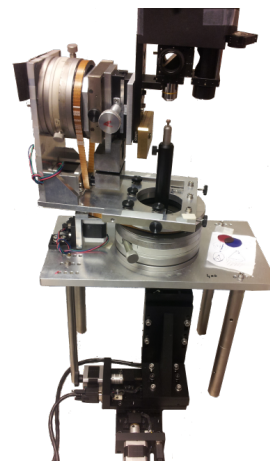
Figure 1: Robotic scanner at the University of Groningen [5].

References

[1]   Doornbos, G.J. (2015). Design and implementation of an autofocusing algorithm. University of Groningen, NL.

[2]   Lohmueller, T., Brunner, R., and Spatz, J.P. (2010). Improved properties of optical surfaces by following the example of the moth eye. *Biomimetics Learnings from Nature*, INTECH, pp 451–466.

[3]   Muñoz-Arias, M., Scherpen, J.M.A. and El-Hawwary, M. (2015). Imaged-based vision servo control using the port-Hamiltonian framework, *Workshop on LHMNLC*, Lyon, France, pp 105–110.

[4]   Siciliano, B. and Khatib, O. eds., (2008). Springer handbook of robotics. Springer Science & Business Media.

[5]   Spanier, T. (2015). The design and implementation of the full actuation for the five DoF robotic scanner. University of Groningen, NL.

[6]   Stavenga, D.G., Foletti, S., Palasantzas, G. and Arikawa, K. (2006). Light on the moth-eye corneal nipple array of butterflies. *Proceedings of the Royal Society of London B: Biological Sciences*, 273(1587), pp 661–667.

[7]   Stavenga, D.G. (2005). Modern optical tools for studying insect eyes. *Methods in insect sensory neuroscience*. Edited by TA Christensen. CRC Press, Florida, USA, pp 159–184.

Reduced mathematical model of dengue virus replication whitin vero cell cultures

Thomas Abbate, Laurent Dewasme and Alain Vande Wouwer

Automatic Control Laboratory

University of Mons

Bld Dolez 31, 7000 Mons

Belgium

Email: thomas.abbate@umons.ac.be

Introduction

Dengue is a mosquito-borne viral infection that develops in tropical and sub-tropical regions. Even though the World Health Organization indicates that about half of the world's population is currently at risk, no specific treatment nor vaccination against dengue exists. The elaboration of an effective vaccine would then constitute an important breakthrough. Efforts are therefore made to better understand the dengue virus amplification mechanisms that take place within mammalian cell cultures used to find a vaccine candidate. In this context, the present study proposes different state space models to describe the various population and metabolite dynamics encountered during vero cell culture and to provide information about critical culture parameters.

Contribution of this work

During the experiments, concentrations were adjusted using punctual medium renewals and/or direct injections of glucose and glutamine. This allows to consider the experiments as a series of batch processes and neglect environment-induced death. Moreover these adjustments prevent the concentrations from getting close to limiting/inhibiting levels. Nevertheless, even though the effect of serine on vero cell growth is not clearly demonstrated, concentrations measured in this work sometimes reach limiting levels according to Ursache et al.[3]. This study therefore investigates different scenarios where serine would become a limiting factor or not.

The proposed models are based on several reference models from the literature ([1], [2] and [3]) in which the virus amplification is represented as a function of the infected biomass. The current study considers alternative models based on the assumption that the infection kinetics is fast compared to cell growth and maintenance.

In all reference models, it is also assumed that, once infected, the cells are not able to replicate. This study therefore investigates this assumption as well as the case where viral particles are considered as a growth-inhibiting factor (see Table 1)

Parameter identification is performed based on experimental data. Best results are obtained when serine is not growth-

Case	X_r	μ_x
1	X_u	$\mu_{max} \cdot \frac{X_{max}-X}{X_{max}}$
2	X_u	$\mu_{max} \cdot \frac{Ser}{Ser+k_{ser}} \cdot \frac{X_{max}-X}{X_{max}}$
3	X	$\mu_{max} \cdot \frac{k_{v,i}}{Vir+k_{v,i}} \cdot \frac{X_{max}-X}{X_{max}}$
4	X	$\mu_{max} \frac{Ser}{Ser+k_{ser}} \cdot \frac{k_{v,i}}{Vir+k_{v,i}} \cdot \frac{X_{max}-X}{X_{max}}$

Table 1: Presentation of the different representations of the replicating biomass X_r and of the corresponding kinetic model formulations, i.e., the specific growth rate μ_x and the specific virus replication rate μ_v. X_u and X_i are respectively the uninfected and infected biomass and $X = X_i + X_u$.

limiting and infection does not cancel biomass replication. Sensitivity analysis is provided to support our conclusions and characterize the current operating conditions.

References

[1] L. Möhler, D. Flockerzi, H. Sann and U. Reichl. "Mathematical model of influenza A virus production in large-scale microcarrier culture", biotechnology and bioengineering, Vol. 90 (n1), p.46-58, 2005.

[2] J. Schulze-Horsel, M. Schulze G. Agalaridis, Y. Genzel, U. Reichl. "Infection dynamics and virus-induced apoptosis in cell culture-based influenza vaccine production-Flow cytometry and mathematical modeling". Vol 27(20), p.2712-2722, 2009.

[3] R. Ursache, Y. Thomassen, G. Van Eikenhorst, P. Verheijen and W. Bakker, Wilfried. "Mathematical model of adherent Vero cell growth and poliovirus production in animal component free medium" Springer, Biop. and biosys. eng., Vol.38(3), p.543-555, 2015.

Development of a biological culture simulator based on a simplified metabolic network and a constrained dynamic FBA

Khadija Mhallem Gziri, Anne Richelle and Philippe Bogaerts
Unit of Biomodelling and Bioprocesses
Université Libre de Bruxelles
Department of General Chemistry and Biosystems
Av. F.-D. Roosevelt 50 C.P. 165/61
B-1050 Brussels
kmhallem@ulb.ac.be; arichell@ulb.ac.be; Philippe.Bogaerts@ulb.ac.be

1 Abstract

To study the overflow metabolism in hybridoma cell cultures, a biological culture simulator based on a simplified metabolic network and a constrained dynamic Flux Balance Anyalysis (dFBA) is developed. It is legitimated by determining an objective function and linear constraints with a methodology going from a detailed Metabolic Flux Analysis (MFA) to FBA. The objective is to recover the admissible flux intervals obtained by the detailed MFA to enable a dynamic simulator construction. [1]

2 Introduction

The cells are used for decades in biopharmaceutical industries for their ability to biocatalyse substrates into products of interest such as viral vaccines. To mimic the cell, the constraint based modelling is applying constraints to the metabolic reactions. These later are based on the thermodynamic properties of the reactions or on regulatory mechanisms for instance. Indeed, the constraint based models are based on two main assumptions: the metabolic network can be translated into a stoichiometric matrix and a steady state assumption.[2, 3]

The cell cultures here studied are in overflow. This metabolism relates to an incomplete oxidation of the substrates despite aerobic conditions because of an energy supply abundance. It leads to organic byproducts that are often inhibitory for the growth cell. The overflow metabolism of mammalian cells is more complex than the one of the microbial cells. [1, 2]

The Flux Balance Analysis (FBA) is one constraint based modelling approach that overcomes the underdetermination problem (more reactions than metabolites). The solution space defined by the two previous cited hypotheses, can be reduced by applying additional constraints. But how to define objectively these additional constraints and introduce them in a dynamic simulator? [3]

3 Contribution

To define the additional constraints and to develop a biological culture simulator, data of two fed-batch cultures of hybridoma cell line HB-58 producing IgG1 monoclonal antibodies are used. They consist of measurements of the biomass, two substrates (glucose and glutamine) and three products concentrations (lactate, alanine and ammonia).

As already used in [2], the metabolic network used in this study, is constituted of glycolysis, glutaminolysis, TCA cycle, the pentose phosphate and the nucleotide synthesis pathways. Based on this network, the additional constraints have been defined by an analysis of the admissible flux intervals obtained with a limited FBA (using only inputs measurements) in reference to a detailed MFA (using inputs and outputs measurements). These constraints are presented as equations balancing reaction inputs and outputs and/or as inequalities carried out by flux signs : two inequality constraints for the fluxes corresponding to the substrates overflow defined by Monod lower bounds; one linear inequality implying two anaplerotic fluxes from glutamate to alphaketoglurate. Moreover, the objective cost function aiming at maximizing cell growth is also legitimated trough this comparaison of FBA and MFA results. Based on this dynamical FBA modelisation, a biological culture simulator able to predict the dynamics of biomass growth, substrate consumption and metabolites production has been constructed.

References

[1] Z. Amribt, H. Niu, P.Bogaerts, "Macroscopic modelling of overflow metabolism and model based optimization of hybridoma cell fed-batch cultures," A Biochemical Engineering Journal, vol. 70, pp. 196-209, 2013.

[2] A. Provost, G. Bastin, S. N. Agathos, Y.-J. Schneider, "Metabolic design of macroscopic bioreaction models: application to Chinese hamster ovary cells," Bioprocess and Biosystems Engineering, vol. 29, pp. 349-366, 2006.

[3] J.D. Orth, I. Thiele, B.O. Palsson, "What is flux balance analysis," Nature Biotechnology, vol. 28, pp. 245-248, 2010.

Impedance-based temperature estimation for Li-ion batteries[1]

H.P.G.J. Beelen, M.C.F. Donkers and H.J. Bergveld
Department of Electrical Engineering, Control Systems Group
Eindhoven University of Technology, P.O. Box 513, 5600 MB Eindhoven
Email: h.p.g.j.beelen@tue.nl, m.c.f.donkers@tue.nl, h.j.bergveld@tue.nl

1 Introduction

Due to properties such as high energy density, Lithium-ion (Li-ion) batteries are used in various applications such as battery packs in (hybrid) electric vehicles and in mobile phones. For safety and control purposes, monitoring the temperature of Li-ion batteries is of vital importance. A relatively new field of temperature estimation methods is based on Electrochemical Impedance Spectroscopy (EIS), where a temperature relation is inferred from the electrochemical battery impedance. An advantage of using EIS for temperature estimation is that no intrusive or surface-mounted temperature sensors are needed.

2 Impedance-Based Temperature Estimation

A number of studies have presented EIS-based temperature estimation methods [1-3]. It can be argued that these meth-
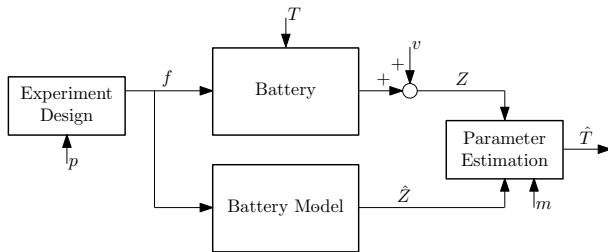
Figure 1: Top-level block diagram of measurement system [4].

ods can be broken down into two components [4], as depicted in Figure 1: experiment design, i.e. choosing excitation frequency f, and parameter estimation, i.e. estimating the battery temperature T with $\hat{T}$, given the measured battery impedance Z. The model of the battery impedance, $\hat{Z}$, is given by a function $\hat{g} : \mathbb{R}^3 \to \mathbb{C}$ which also depends on State-of-Charge (SoC):

$$\hat{Z} = \hat{g}(f, T, \text{SoC}). \qquad (1)$$

Furthermore, measurement noise v is taken to be complex-valued zero-mean Gaussian noise. By applying certain settings for experiment design and parameter estimation, p and m respectively, and by comparing the measured and modelled battery impedance, an estimate of the battery temperature can be computed. The settings p and m are different for all existing methods. Moreover, it is unclear which settings yield the most-accurate estimate.

3 Analysis, Comparison and Synthesis

In this work, we propose a framework, which jointly selects the settings p and m, for comparing and analysing existing methods. Besides analysis, the framework allows for synthesizing a more-accurate method. The basis for this framework is the estimator given by

$$\hat{T}(f, \alpha, Z) = \underset{T}{\text{argmin}}\, \alpha\, \bar{g}_1^2(f, T, Z) + (1-\alpha)\, \bar{g}_2^2(f, T, Z), \quad (2)$$

where $\alpha \in [0, 1]$ denotes a selector variable which allows weighting $\text{Re}(Z)$ and $\text{Im}(Z)$ when $\bar{g}_1$ and $\bar{g}_2$ are given by

$$\bar{g}_1(f, T, Z) = \text{Re}\big(\hat{g}(f, T) - Z\big) \qquad (3a)$$

$$\bar{g}_2(f, T, Z) = \text{Im}\big(\hat{g}(f, T) - Z\big). \qquad (3b)$$

4 Results

Results of the comparison are shown in Figure 2. Parameters for the newly synthesized method where selected using (2) in a Monte-Carlo approach. It can be seen that this proposed method yields the smallest MSE for all temperatures.
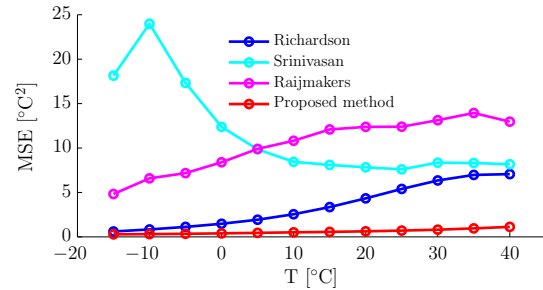
Figure 2: MSE for SoC = 40%

References

[1]   R. Richardson, "Battery internal temperature estimation by combined impedance and surface temperature measurement," Journal of Power Sources, vol. 265, pp. 254-261, 2014.

[2]   R. Srinivasan, B.G. Carkhuff, M.H. Butler, A.C. Baisden, "Instantaneous measurement of the internal temperature in lithium-ion rechargeable cells," Electrochimica Acta, vol. 56, no. 17, pp. 6198-6024, jul 2011.

[3]   L.H.J. Raijmakers, D.L. Danilov, J.P.M. van Lammeren, M.J.G. Lammers, P.H.L. Notten, "Sensorless battery temperature measurements based on electrochemical impedance spectroscopy," Journal of Power Sources, vol. 247, pp. 539-544, feb 2014.

[4]   H.P.G.J. Beelen, L.H.J. Raijmakers, M.C.F. Donkers, P.H.L. Notten, H.J. Bergveld, "An Improved Impedance-Based Temperature Estimation Method for Li-ion Batteries," IFAC-PapersOnLine, vol. 48, no. 15, pp. 383-388, 2015.

Design of a Robust Lipschitz Observer - Experimental application

Christian Feudjio [1], Philippe Bogaerts [2]

Jean-Sebastien Deschenes[3], Alain Vande Wouwer[1]

[1] Automatic Control Laboratory, University of Mons, Belgium

{Christian.FeudjioLetchindjio, Alain.VandeWouwer}@umons.ac.be

[2] 3BIO - Modeling and Control of Bioprocesses, University of Brussels, Belgium

[3] Universite du Quebec a Rimouski, Canada

Abstract

The culture of micro-algae in photo-bioreactors (PBR) has received a regain of interest in the last two decades in view of the multiple potential applications ranging from the production of biofuels to pigments, nutrients and wastewater treatment process [1]. For monitoring and advanced control purposes, measurements of the process states are mandatory. However it is often impractical to get the full array of measurements, and as a remedy, software sensors [2, 3] can be used to reconstruct on-line the evolution of unmeasured states by blending the predictive information of a dynamic process model with the measurement information of the available hardware sensors. In micro-algae cultures, it is impossible to measure on-line the microalgae internal quota, i.e., the content of the internal substrate pool.

The aim of this study is to investigate the use of Lipschitz observers and to propose a systematic procedure for the construction of the linear part of the model so as to ensure that the pair (A, C) is stable (with assigned dynamics) and observable.

The observer is tested both in simulation and real-life experiments with the culture of micro-algae Scenesdesmus obliquus.

Acknowledgements

References

[1] Y. Chisti, "Biodiesel from microalgae", Biotechnology Advances, (50) 291–300, 2007.

[2] Ph. Bogaerts, A. Vande Wouwer "Software Sensors for bioprocess", ISA transactions, (42) 547–558, 2003.

[3] G. Goffaux, A. Vande Wouwer, and O. Bernard,"Improving continuous–discrete interval observers with application to microalgae-based bioprocesses", Journal of Process Control, (19) 1182–1190, 2009.
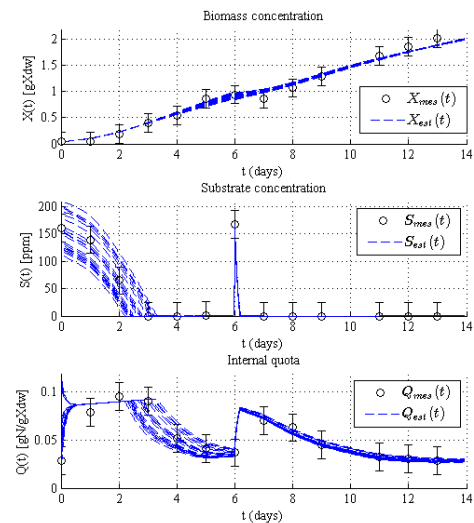
Figure 1: Estimation of Biomass (X), Substrate (S) and Internal Quota (Q) from various initial conditions using Biomass measurements
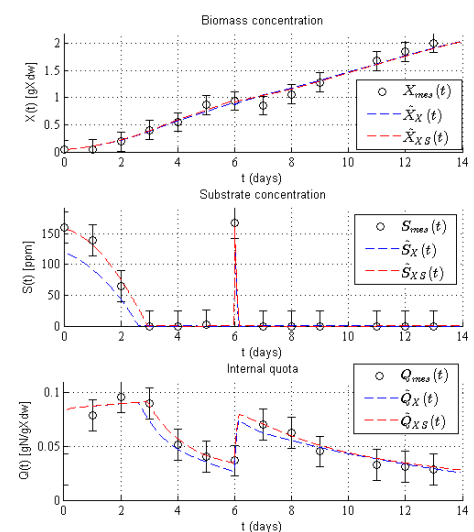
Figure 2: Estimation of Biomass (X), Substrate (S) and Internal Quota (Q) using Biomass measurements versus using both Biomass and Substrate measurements

On the model-based monitoring of industrial batch crystallizers

Marcella Porru
Dept. of Electrical Engineering, CS
Eindhoven University of Technology
De Zaale, 5612 AJ Eindhoven
The Netherlands
Email: m.porru@tue.nl

Leyla Özkan
Dept. of Electrical Engineering, CS
Eindhoven University of Technology
De Zaale, 5612 AJ Eindhoven
The Netherlands
Email: l.ozkan@tue.nl

1 Introduction

Crystallization is an important separation process to obtain high value-added chemicals in crystalline form from liquid solution in pharmaceutical, food and fine chemical industries. As most of the particulate processes, the quality of the solid product is determined by its particle size distribution (PSD). The achievement of the desired quality targets of the fine crystalline products relies on an efficient online process monitoring for separation supervision and control. However, hardware analyzers able to online measure the PSD and the solute concentration are rarely available, due to their costs [1]. These unmeasured process variables can be estimated by state estimators that combine information from the process model and secondary measurements. The problem of designing state observers for online monitoring the PSD evolution has been mostly addressed under the assumption that some PSD measurements were available (see [6] and literature therein), which is not likely in practice. This work proposes a methodology to asses the feasibility of using common measurements (e.g. temperature and liquid fraction) for estimation purposes based on local observability [2] and detectability [3] arguments. The results are supported using a data-derived technique, with data generated by a simulation model of the industrial crystallizer. Based on the results of the observability analysis, the structure of a state estimator is proposed.

2 Observability analysis for the batch crystallizer

The effectiveness of the process monitoring with state observers depends on the observability and detectability of the nonlinear model of the batch crystallization process. Since temperature and liquid-fraction measurements are commonly available in industry, the feasibility of observing the PSD and the solute concentration through these measurements is evaluated. To this end, the observation spaces are separately calculated for both measurements and the associated observability codistributions are analyzed. It was found that the concentration is distinguishable while the PSD is not. The results of the observability analysis are supported by using the measures of topological relevance (MTR) [5] on the self-organized map (SOM) [4], which is a data visualization technique offering the possibility to display and quantify similarities among the behavior of process

variable.

3 State detectors for online PSD monitoring

The previous results suggest to use a state detector where temperature and liquid-fraction measurements are used to correct the prediction of the temperature, solid concentration, crystallization volume and crystal production, while the PSD is inferred though the model in "open loop" fashion. Preliminary simulation results of the estimator functioning under the assumption of a crystallization process dominated by the crystal growth phenomena show that the estimator with the proposed structure is capable to give a better estimation than the model without corrections when the initial conditions are affected by uncertainties.

4 Acknowledgments

References

[1]   L.L. Simon et al. (2015) Assessment of recent process analytical technologies (PAT) trends: a multiauthor review, *Org. Process Res. Dev.*, 19, 3-61.

[2]   R. Hermann and A.J. Krener (1977) Nonlinear controllability and observability, *IEEE Trans. Autom. Control*, AC-22 (5), 728-740.

[3]   J. Alvarez and C. Fernandez (2009) Geometric estimation of nonlinear process systems, *J. Process Contr.*, 19, 247-260.

[4]   E. Alhoniemi, J. Hollmen, O. Simula, J. Vesanto (1999) Process monitoring and modelling using the self-organized map, *Integr. Comput. Aid. E.*, 6 (1), 3-14.

[5]   F. Corona, M. Mulas,R. Baratti, J.A. Romagnoli (2012) Data-derived analysis and inference for an industrial deethanizer, *Ind. Eng. Chem. Res.*, 51, 13732-13742.

[6]   A. Mesbah, A.E. Huesman , H.J. Kramer, P.M. Van den Hof (2011) A comparison of nonlinear observers for output feedback model-based control of seeded batch crystallization processes, *J. Process Contr.*, 21 (4), 652-666.

Structured Model-Based Observer Design, Application to Plasma Profile Estimation in Tokamak

Benjamin Vincent, Nicolas Hudon and Denis Dochain
ICTEAM, INMA
Université Catholique de Louvain
B-1348 Louvain-la-Neuve, Belgium
{benjamin.vincent,nicolas.hudon,denis.dochain}@uclouvain.be

Laurent Lefèvre
Univ. Grenoble Alpes, LCIS
F-26902, France
laurent.lefevre@lcis.grenoble-inp.fr

1 Abstract

A tokamak is a toroidal-shaped equipment responsible for the control of nuclear fusion reaction. It magnetically confines and heats up a plasma (to hundred million degrees Celsius). With ohmic and non-inductive heating sources, this ionized gas made of hydrogen isotopes satisfy Lawson criterion (and produce more energy than used). To reach the steady state operation, temperature and density plasma profiles must be controlled according to non-uniform profiles references.

In previous work, a one-dimensional structured plasma model has been derived for the electro-magnetic and thermal domains [1]. This model has the standard form of Port-Hamiltonian systems:

$$\begin{cases} \dot{x} & = & [J(x) - R(x)]\frac{\partial H}{\partial x}(x) + gu \\ y & = & g^{\top}\frac{\partial H}{\partial x}(x) \end{cases} \tag{1}$$

with $x \in \mathbb{R}^n$ the state variables, $u \in \mathbb{R}^m$ the input and $y \in \mathbb{R}^m$ the output denotes the exchanges with the environment. The total energy function $H(x) \in C^1(\mathbb{R}^n) \to \mathbb{R}^n$ is called the Hamiltonian function. The structured matrices $J(x) = -J(x)^{\top} \in \mathbb{R}^n \times \mathbb{R}^n$ and $R(x) = R(x)^{\top} \geq 0 \in \mathbb{R}^n \times \mathbb{R}^n$ are the interconnection and dissipative matrices, respectively. The skew-symmetric matrix represents the energy exchanges between the system physicals domains, and the symmetric matrix characterizes the system loss [2].
Port-Hamiltonian systems as presented in equation (1) satisfy the property of passivity since the energy function trajectories verify:

$$\frac{\partial H(x)}{\partial t} = -\frac{\partial^{\top} H(x)}{\partial x}R(x)\frac{\partial H(x)}{\partial x} + y^{\top}u \geq y^{\top}u \tag{2}$$

This balance equation implies that the system composition is limited to dissipative and conservative elements. This property is used to prove stability and to design control laws.

A physical interpretation rises from the Port-Hamiltonian formulation, and systems are seen as energy transformation

devices. Therefore, new state feedback control strategies based on the passivity property have been studied and successfully applied to plasma control [1]. The complete state is assumed to be completely measurable. In practice, only few of them are reachable by sensors. For example in the Tore Supra, an experimental tokamak only the temperature at the center of the plasma is available. To overcome this limitation, state observers must be implemented in the control loop to compute the complete temperature profile.

The objective is to present a model-based state observer design strategy for Port-Hamiltonian systems. The design approach is based on passivity, like in [3]. A new observer is detailed and an integral extension added to improve the observer robustness. Simulation results for the observation of thermal and magnetic plasma profiles will be presented.

2 Acknowledgement

References

[1] Ngoc Minh Trang Vu. *The Port-Hamiltonian approach for the modelling, reduction and control of plasmas dynamics in tokamaks*. PhD thesis, Laboratoire de Conception et d'Intégration des Systèmes (LCIS), 2014.

[2] Duindam, V., Macchelli, A., Stramigioli, S., and Bruyninckx, H. (2009). Modeling and Control of Complex Physical Systems: The Port-Hamiltonian Approach. *Springer Berlin Heidelberg*.

[3] Venkatraman, A. and Schaft, A. (2010). Full-order observer design for a class of port-Hamiltonian systems. *Automatica*, 46(3), 555–561.

Implementation of observers, controllers and supervisory systems for tokamaks

T.C. Blanken
Eindhoven University of Technology
Department of Mechanical Engineering
Control Systems Technology
P.O. Box 513, 5600 MB Eindhoven
The Netherlands
Email: t.c.blanken@tue.nl

F. Felici
Eindhoven University of Technology
Department of Mechanical Engineering
Control Systems Technology
P.O. Box 513, 5600 MB Eindhoven
The Netherlands
Email: f.felici@tue.nl

1 Introduction

Nuclear fusion is a viable option for clean and long-lasting energy on earth. The tokamak is a device that magnetically confines a plasma for production of power by controlled thermonuclear fusion. Development of a plasma control system (PCS) for future reactors is key for safe and reliable machine operation and production of electricity.

2 Real-time control challenges on tokamaks

Control of tokamak plasmas is needed to maintain the desired operating conditions, while suppressing magnetic instabilities and avoiding plasma disruptions. This poses several control tasks that need to be executed simultaneously in real time. However, only a limited set of actuators and sensors is available on future reactors.

A number of challenges need to be solved to ensure high-performance control of tokamak plasmas. First, the measurement systems in tokamaks have limited reliability and often do not measure the controlled quantities directly. Second, there is nonlinear coupling between many controlled quantities. Up to now, control design on tokamaks has rarely been extended beyond SISO control of the controlled quantities. Third, certain control tasks require the use of the same set of actuators, complicating simultaneous control of multiple quantities.

Solving these challenges requires a novel and consistent approach to the design of a plasma control system. Newly considered tasks include estimation of all plasma profiles (temperature, density, current density), and detection of physical events (magnetic instabilities) and machine events (measurement and actuator faults). On top of this, a supervisory system should coordinate and prioritize the control tasks to ensure proper operation of the reactor.

3 Development of real-time control algorithms

On TCV (*tokamak à configuration variable*) and the ASDEX-Upgrade tokamak, we are implementing and testing various components for the tasks described above. TCV is a flexible tokamak, well-suited for development of control systems. Recently, a new computer was installed in the real-time control network on which various control algorithms can be executed simultaneously in multiple threads on dedicated CPU's.

On both tokamaks, observers are implemented for estimation of the plasma profiles, based on the RAPTOR code [1], which solves the transport of temperature and magnetic flux in a tokamak plasma, and a plasma density evolution code [2, 3]. In the latter observer, a real-time detector is used to correct for errors in the density-related measurements [2, 3]. We aim to obtain reliable routine operation of the profile observers to provide signals of controlled variables in various operating regimes. Furthermore, feedback controllers for the average density, and temperature and current density profile are being implemented on TCV.

4 Future work

We extend the plasma control system (PCS) on currently operating tokamaks with observers and controllers for the plasma profiles. Other control components such as supervisors and actuator sharing management are still in early stages of design. Successful and routine operation of these systems after initial tests in the spring and summer of 2016 on TCV and ASDEX-Upgrade will justify the use of these components on PCSs on future nuclear fusion reactors.

References

[1]   F. Felici, M. de Baar and M. Steinbuch, "A dynamic state observer for real-time reconstruction of the tokamak plasma profile states and disturbances," American Control Conference, Portland, USA (2014).

[2]   T.C. Blanken, F. Felici, M. de Baar and W.P.M.H. Heemels, "Model-based reconstruction and feedback control of the plasma particle density in tokamaks," (to be submitted, 2016).

[3]   T.C. Blanken, F. Felici, M. de Baar and W.P.M.H. Heemels, "Modeling, observer design and robust control of the particle density in tokamak plasmas," Conference on Decision and Control, Osaka, Japan (2015).

Noise-free signals make identification more difficult?!

H.H.M. Weerts
Eindhoven University of Technology[1]
h.h.m.weerts@tue.nl

P.M.J. Van den Hof
Eindhoven University of Technology
p.m.j.vandenhof@tue.nl

A.G. Dankers
University of Calgary
Email: adankers@hifieng.com

1 Introduction

In dynamic network identification we would like to be able to model the full dynamics of a network on the basis of measured node variables, while treating all node variables in a symmetric way. To this end we employ basic techniques from multivariable prediction error identification. We might have node signals that are noise-free, see e.g. the classical closed-loop system with noise-free node u (Figure 1), and disturbed node y. In the classical multivariable system identification framework it is assumed that all measured (output) variables are noise disturbed, or in other words: the output noise process is of full rank. However this assumption does not comply with the full network in Figure 1. The noise-free signal u invalidates one of the assumptions of our methods. In the Joint-IO method nodes are treated symmetrically and the known r_u is replaced by an unknown stochastic process to work around the invalidated assumption.
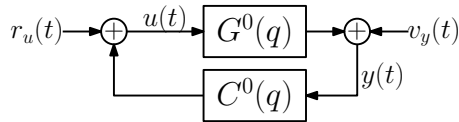
Figure 1: Closed-loop system with nodes u and y, noise process v_y and external excitation r_u.

Classical identification techniques are typically used to identify G_0 only, using a predictor that predicts $y(t)$ only. If we would like to extend this to identifying the full network, we have to predict not only $y(t)$ but also $u(t)$ at the same time and deal with a fully symmetric treatment of the node signals. When constructing a predictor for $w(t) := \begin{bmatrix} y(t) \\ u(t) \end{bmatrix}$ we will have to deal a rank reduced noise process $v(t) := \begin{bmatrix} v_y(t) \\ 0 \end{bmatrix}$. A key component in the reasoning behind predictors is that the noise process can be decomposed into a monic filter H and a white noise. This decomposition is unique only if the noise process is of full rank. The current rank reduced noise process v can not be decomposed in a unique way.

In [1] we formulate an identification method that can deal with this rank reduced noise process.

2 Identification

It is assumed that the parameterized prediction errors ε_y and ε_u have been defined. Suppose that the identification criterion of the form $\varepsilon_y^2 + \lambda \varepsilon_u^2$ is chosen. Then for maximum likelihood reasons we would like the weight λ to correspond to the inverse of the variance of the noise of u, however u is noise-free. We could interpret the noise-free situation as being noise with variance 0. The noise-free situation becomes problematic in the maximum likelihood reasoning. Instead we consider the limit of the variance going towards 0, then the weight λ goes towards infinity. The prediction error of u is infinitely more weighted than the prediction error of y. An equivalent identification criterion to this limit case is the constrained criterion

$$J = \left\{ \begin{array}{c} \arg\min_{\theta} \bar{\mathbb{E}}\, \varepsilon_y^2(t,\theta) \\ \text{subject to: } \varepsilon_u^2(t,\theta) = 0 \text{ for all } t \end{array} \right\}. \quad (1)$$

3 Analysis

Consistency of an identification method typically has the requirement that data is informative and that the model structure is identifiable. The properties identifiability and informativity together imply that one prediction error is related to one model, which guarantees uniqueness of the estimated model. These classical properties identifiability and informativity are related to the typical least squares identification criterion. We propose a different criterion, one that is constrained, hence a generalization of identifiability and informativity which takes the new criterion into account is needed. This new notion has to be a property which describes whether the criterion can distinguish between any two models in the model set.

References

[1] H.H.M. Weerts, P.M.J. Van den Hof, A.G. Dankers, "Identifiability of dynamic networks with part of the nodes noise-free", ALCOSP (Submitted), 2016.

[1]P.O. Box 513, 5600 MB Eindhoven, The Netherlands.

Data-Driven Modelling using Symbolic Regression

D. Khandelwal, R. Tóth

Control Systems Group

Department of Electrical Engineering

Eindhoven University of Technology

P.O. Box 513, 5600 MB, Eindhoven, The Netherlands

Email: D.Khandelwal@tue.nl

1 Introduction

This research aims at automating the process of system identification and control synthesis for complex systems by means of evolutionary symbolic tools that result in interpretable models and control laws, enabling compact and efficient controller implementations for cyber-physical systems. The work primarily focuses on building a new framework for computing data-driven models that incorporates symbolic regression analysis.

2 Symbolic Regression and System Identification

Symbolic regression is a novel evolutionary optimization technique that searches for analytical expressions that fit measured numerical data. Symbolic regression has gained much attention recently in the scientific community for its ability to find mathematical laws that explain observed physical phenomena automatically, without human intervention [1]. This has opened the path for the creation of a "robot scientist" where mathematical expressions are manipulated by a machine in a similar way as humans do. Symbolic regression has the potential to change many fields of science, in particular giving answers to many challenges of system identification and control.

The major handicap of the state-of-the-art of system identification is the selection a priori of an actual model class. This involves imposing assumptions on the structural relationships of the model, which requires vast experience from the user [2] and often leads to costly iterative processes to arrive at valid structural knowledge. For these reasons, system identification remains an arduous and challenging task.

The proposed scheme to incorporate symbolic methods in the process of system identification and controller synthesis is illustrated in Fig. 1. The numerical data from experiments (N), symbolic models (M), their properties (P) and the synthesized controller (C) form the chief components of the evolutionary scheme. Existing methods of identification, control and experiment design are viewed as operators that enable the evolution of these components. The symbolic plant models and the synthesized controllers constructed during the evolution process are evaluated using a user-define fitness criteria. The fitness scores are used to de-
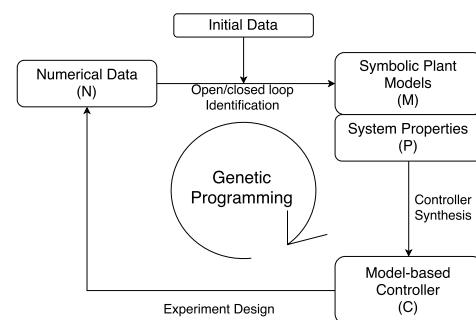
Figure 1: Proposed evolutionary scheme for identification and control

termine the pareto front of the genetic optimization process, which allows one to determine the best trade-off between model performance and complexity.

The primary focus of this research lies on the evolution of models M. These models are built from fundamental blocks such as noise structures, dynamic structures (shift operators), non-linearities, signal elements, and so on. Symbolic regression manipulates these basic blocks to find a solution in the model space that best explains the numerical data N, according to an appropriately defined cost function. Thus, this method of identification is not restricted by assumptions on the structure of the model, but by the parameterized blocks that a model can be built from. Additionally, parameterization of the components of a model allows this approach to be relevant for cyber-physical systems, which are typically characterized by logical operators in addition to the other components mentioned above.

The main objective of this project is to develop a novel software tool that automatically manipulates models in order to satisfy complex modeling or control objectives dictated by economical, performance and safety specifications.

References

[1]   M. Schmidt, H. Lipson. "*Distilling free-form natural laws from experimental data,*" Science, Vol. 324, 2009.

[2]   L. Ljung, "*System Identication: Theory for the user.*" Prentice Hall Information, 1987.

Identification of position-dependent mechanical systems

Robin de Rozario, Robbert Voorhoeve, Wouter Aangenent, Tom Oomen

Eindhoven University of Technology, Department of Mechanical Engineering, Control Systems Technology group

P.O. Box 513, 5600 MB Eindhoven, The Netherlands, Email: `r.d.rozario@student.tue.nl`

1 Background

Increasing accuracy and speed demands in precision applications lead to a situation where the flexible behavior of the system becomes relevant [1]. For instance, the internal deformations hamper the performance at the point of interest, which is typically not measured directly. Hence, ensuring satisfactory performance at this point can be achieved through control strategies that infer the point of interest from indirect measurements in conjunction with a model, e.g., through an observer. In general, these models are Linear Parameter Varying (LPV), since the point of interest is position-dependent. The aim of this research [2] is to develop mechanical models whose outputs are position-dependent.

2 Approach

The key step in the proposed approach is to use a local LPV identification [3] approach while exploiting physical properties of the class of mechanical systems. As such, a set of local frozen systems is estimated, where each frozen system represents a fixed mapping for a given position. The frozen systems are parametrized as modal mechanical systems,

$$\mathcal{L}[s^2 I + s D_m + \Omega^2]^{-1} \mathcal{R}, \tag{1}$$

$\mathcal{L} \in \mathbb{R}^{n_y \times n_m}$, $D_m, \Omega^2 \in \mathbb{R}^{n_m \times n_m}$, $\mathcal{R} \in \mathbb{R}^{n_m \times n_u}$, with n_y, n_m and n_u the number of outputs, mechanical modes and inputs, respectively. This nonlinear-in-the-parameters parametric model is identified from frequency response data by first estimating a Left Matrix Fraction Description (LMFD) using the Sanathanan-and-Koerner method, [4]. Then, possibly after refining this model using gradient-based techniques, this estimate is transformed to an initial estimate with the modal structure and is subsequently refined using a gradient-based approach.

The frozen system set is then interpolated to yield a system that is continuous in the position variable. By virtue of the mechanical system structure, the interpolation of the frozen systems is equivalent to the interpolation of the mode shapes of the system. Robust interpolation of these modes is achieved by using a basis-function expansion with optimal model order selection, or by using Thin Plate Splines with optimal smoothing, where optimality is defined with respect to a cross-validation measure [5].

3 Results

The developed method is successfully implemented numerically and a position-dependent model of the Over-Actuated-Test rig, a prototype next-generation wafer stage as shown in Figure 1, is estimated, thereby confirming that proposed the identification method is well-suited for practical applications.
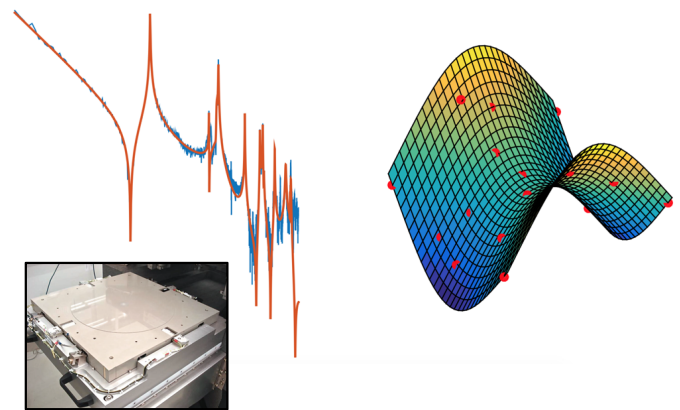
Figure 1: Lower left: OAT-chuck. Upper left: Modal model fit of one of the transfers of the OAT setup. Right: Experimental estimate of the second flexible mode of the OAT chuck.

4 Ongoing work

Further research focuses on controller synthesis using the obtained LPV-models in relation to inferential control, learning and robustness aspects.

References

[1] Oomen, T., Grassens, E., Hendriks, F., *Inferential Motion Control: Identification and Robust Control Framework for Positioning an Unmeasurable Point of Interest*, IEEE Transactions on Control Systems Technology, 23(4), 1602-1610, 2015.

[2] R. de Rozario, *Identifying Position-Dependent Mechanical Systems, a physics-based LPV approach, with application to a wafer stage*, M.Sc Thesis, Eindhoven University of Technology, 2015.

[3] De Caigny, J., Pintelon, R., Camino, J. F., & Swevers, J., *Interpolated modeling of LPV systems*, Control Systems Technology, IEEE Transactions on, 22(6), 2232-2246, 2014.

[4] Pintelon, R. and Schoukens, J. *System Identification: A Frequency Domain Approach*. IEEE Press, John Wiley & Sons, Hoboken, New Jersey, 2012.

[5] Craven, P., and Wahba, G., *Smoothing Noisy Data with Spline Functions, Estimating the Correct Degree of Smoothing by the Method of Generalized Cross-Validation*, Numerical Mathematics, vol. 31, pp. 377- 403, 1979.

Extrusion dynamic modeling: sensitivity analysis and parameter identification

J. Grimard, L. Dewasme, J. Thiry, F. Krier, B. Evrard, A. Vande Wouwer

Service d'Automatique, Université de Mons, Bd. Dolez 31, 7000 Mons - Belgique

jonathan.grimard@umons.ac.be, laurent.dewasme@umons.ac.be, alain.vandewouwer@umons.ac.be

1 Introduction

Hot-melt extrusion is a forming technique well established in the industry since the 19th century. This thermo-mechanical process implies the transformation of several solid materials into a specific uniform product conveyed through the extruder thanks to the screw rotation [Gerrens(1994)]. More and more forming processes use this technique and extruded products are numerous: metals, plastics, foods, drugs ...

In this work, a distributed parameter model is proposed to represent the extruder behavior for the mixing of a polymeric matrix and an active pharmaceutical ingredient for accurate quality control purpose. In the same spirit as [Kulshreshtha(1992)], this dynamic model is based on partial differential equations (PDEs) and on several assumptions such as the mono-dimension of the flow, the distinct boundaries between the different screw zones, constant melting product density and specific heat capacity, and negligible heat loss in the screw shafts.

Several transportation parameters can be inferred from experimental data and, according to [Choulak(2004)], residence time distribution (RTD) measurements contain sufficient information to identify the extruder operating parameters.

2 Dynamic modeling

PDE extrusion models are based on mass and energy balances involving the variations of variables such as the filling ratio, the pressure, the material temperature, the barrel temperature and the screw temperature. A classical extruder is composed of different screw elements with variable geometries defining zones which can be partially (solid conveying) or completely (melting) filled with materials. Consequently, two corresponding PDE systems are derived and an ordinary differential equation (ODE) is added to determine the position of a moving interface separating the zones.

3 Parameter identification: preliminary results

Model parameter identification focuses on the determination of the screw geometrical parameters and the material diffusion coefficient. To this end, a sensitivity analysis of the model outputs (die filling ratio, die pressure, die temperature and die tracer concentration) with respect to the unknown parameters is achieved. The residence time distribution appears to provide sufficient information, and 6 experiments with a pilot extruder at the University of Liege are achieved with different operating conditions. These experiments are divided in two sets, dedicated to direct and cross validations, respectively. Good results are obtained in direct validation (see figure 1), confirmed by a satisfactory predictive capability shown in cross-validation.
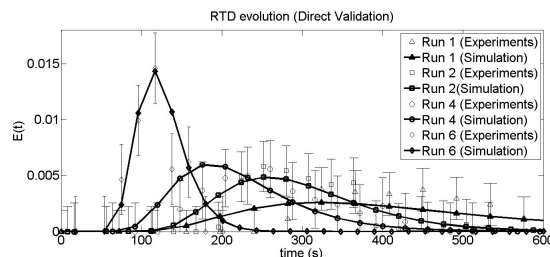
Figure 1: RTD evolutions for the Direct Validation

References

[Choulak(2004)] S. Choulak, F. Couenne, Y. Le Gorrec, C. Jallut, P. Cassagnau, A. Michel *Generic dynamic model for simulation and control of reactive extrusion*, Ind. Eng. Chem. Res., 43 (2004), pages 7373-7382

[Gerrens(1994)] H. Gerrens.*Handbuch der Technischen Polymerchemie.* Von A Echte. VCH Verlagsgesellschaft mbH,Weinheim. Chem. Ing. Tech. Volume 66, 239, 1994

[Kulshreshtha(1992)] M.K. Kulshreshtha, C. Zaror. *An unsteady state model for twin screw extruders.* Food and Bio-products Processing Volume 70, pages 21-28, 1992

Nonlinear identification of vortex-induced oscillators

Jan Decuyper[1,2]
jan.decuyper@vub.ac.be

Tim De Troyer[2]
tim.de.troyer@vub.ac.be

Mark Runacres[2]
mark.runacres@vub.ac.be

Koen Tiels[1]
koen.tiels@vub.ac.be

Johan Schoukens[1]
johan.schoukens@vub.ac.be

[1] VUB, ELEC, Pleinlaan 2, 1050 Brussels   [2] VUB, INDI, Pleinlaan 2, 1050 Brussels

1 Introduction

Vortex-induced vibrations (VIV) are a frequently found form of fluid-structure interaction. Due to flow instabilities, vortices are shed in the wake of the structure [3]. As a result, the structure is excited by an alternating lift force. Common examples are chimneys exposed to wind, or marine structures. When the frequency of vortex shedding approaches the natural frequency of the structure, a synchronization phenomenon kicks in, resulting in a resonance state and possibly harmful amplitudes.

2 A system identification approach

Despite a large body of research, a full physical comprehension of the complex dynamical system has yet to be achieved. For now, one has to rely on time-consuming CFD simulations to be able to predict the kinematics of the system with high fidelity. Constrained by computational cost, fast or even real-time predictions remain unattainable, notwithstanding the great advantage it would provide in many design and monitoring applications. What is lacking is an accurate, efficient model that comes at low computational cost. We believe system identification is especially well suited to provide such a model.

The inherent nonlinear nature of the relationship between oscillation and lift force, makes modelling a challenging task. The model must for instance be able to reproduce the autonomous oscillation of the lift force, even in the static non-excited case. Apart from this, also the typical phase-locking behaviour must be embedded in the model.

3 A Van der Pol test case

In this work a polynomial nonlinear state space (PNLSS) [2] model structure is used to estimate the device under test. The method was first successfully tested on a Van der Pol (VdP) oscillator. The VdP equation is a quite generic description of a nonlinear oscillator, frequently used to approximate VIV behaviour [1].

4 Modelling vortex-induced vibrations

The same method is then used on time series of the lift force on a circular cylinder performing a forced oscillation in a
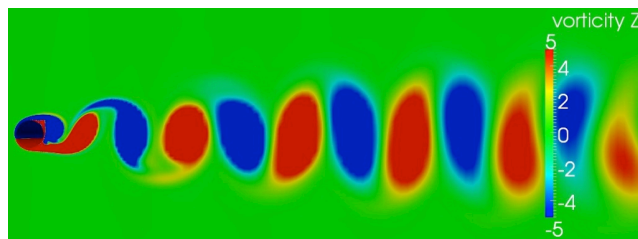
Figure 1: z-component of the vorticity, forced osc. with rel. amp. A/D = 0.2 and rel. freq. f/fSt = 1.1.

fluid stream. Data are generated via CFD simulations (figure 1). As excitation signals, i.e the displacement of the cylinder, a deliberate selection of rich multisines as well as monosines is used to explore the different operating regimes of the system. From random phase multisine realisations with a bandwidth centred around the Strouhal frequency (the natural vortex shedding frequency when unexcited) the Best Linear Approximation (BLA) of the transfer function is constructed. Next the linear model is extended towards a polynomial nonlinear model structure. Nonlinear optimization on a combined data set, representing distinct regimes, results in a good estimate of the underlying system. The predictions of the constructed model are in good agreement with the data.

5 Acknowledgement

References

[1]   R.E.D. Bishop, A.Y. Hassan, The lift and drag forces on a circular cylinder in a flowing fluid, Proceedings of the Royal Society Series A 277, 32?50, 1963.

[2]   J. Paduart, L. Lauwers, J. Swevers, K. Smolders, J. Schoukens, R. Pintelon, Identification of nonlinear systems using Polynomial Nonlinear State Space models, Automatica 46, 647-656, 2010.

[3]   M. M. Zdravkovich, Flow Around Circular Cylinders, Vol. 1: Fundamentals, Oxford University Press, 1991.

Real-time motion planning in the presence of moving obstacles

Tim Mercy, Wannes Van Loock and Goele Pipeleers
KU Leuven, BE-3001 Leuven, Belgium
Department of Mechanical Engineering, Division PMA
Tim.Mercy@kuleuven.be

1 Introduction

Reasons to automate processes vary widely, from relieving humans from repetitive tasks such as harvesting fields over improving accuracy in robotic surgery to increasing the speed of product assembly. For these purposes industry uses autonomous motion systems like robotic arms, autonomous guided vehicles and drones. Safe operation of any autonomous system demands a collision-free motion trajectory at every time instant. Since the environment is generally variable, real-time trajectory generation is required.

This abstract presents a method to calculate time-optimal motion trajectories for autonomous systems moving through an environment with both stationary and moving obstacles, by using numerical optimization. To transform this motion planning problem into a small dimensional optimization problem, suitable for a real-time implementation, the approach (i) uses a spline parameterization of the motion trajectory; and (ii) exploits spline properties to reduce the number of constraints [1]. By solving the resulting optimization problem with a receding horizon it is possible to deal with variations in the environment.

The method is experimentally validated on a *KUKA youBot*. The average solving time of the optimization problem in the experiments ($0.05s$) is sufficiently fast for correcting deviations from the initial trajectory.

2 Methodology

This abstract builds on [1], which uses a B-spline parameterization for the motion trajectory. This work only consideres static environments containing circular obstacles. The proposed method extends the approach with an efficient solution to include anti-collision constraints for convex obstacles, which is based on the separating hyperplane theorem [2]. Since both the system and the obstacles can move, the separating hyperplanes are allowed to be time-varying, by parameterizing them as a B-spline. Furthermore, the method takes into account the latest information about the (uncertain) environment by solving the problem with a receding horizon. The real-time motion planning provides implicit position feedback and only additional wheel velocity feedback is required to steer the system. Finally, the method accounts for obstacle movements by using a linear prediction of the obstacle position, which is based on the obstacle's measured velocity.

The resulting optimization problem contains initial and final conditions on the system's state, kinematic constraints, and anti-collision constraints, which are described by separating hyperplanes. The goal is to find the minimal motion time and determine the corresponding spline coefficients of the motion trajectory.

The developed method generates a time-optimal point-to-point trajectory which steers an autonomous motion system along circular and rectangular, stationary and moving obstacles. The method is included into a motion planning toolbox, which allows users to easily implement, solve and simulate motion planning problems for both single agent and multi-agent systems.

3 Results

Figure 1 shows a test result for a *youBot* which has to pass two stationary rectangular obstacles. Every cross denotes a new iteration of the method, every curve denotes a calculated trajectory. The average calculation time per iteration was $0.05s$, the maximum time was $0.45s$. This figure proves that feedforward velocity setpoints suffice for trajectory following and that no further control methods are necessary.
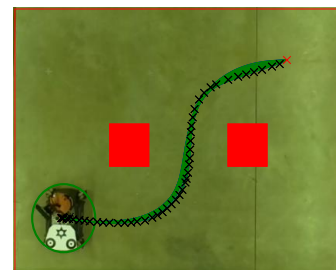
Figure 1: Time-optimal motion of the *youBot*

References

[1]   W. Van Loock, G. Pipeleers, and J. Swevers, "B-spline parameterized optimal motion trajectories for robotic systems with guaranteed constraint satisfaction," *Mechanical Sciences*, vol. 6, no. 2, pp. 163–171, 2015.

[2]   S. Boyd and L. Vandenberghe, *Convex Optimization*. Cambridge, UK: Cambridge University Press, 2004.

Receding Horizon Control for Distributed Energy Management of a Hybrid Truck with Auxiliaries

T.C.J. Romijn, M.C.F. Donkers, S. Weiland and J.T.B.A. Kessels
Department of Electrical Engineering, Control Systems Group
Eindhoven University, P.O. Box 513, 5600 MB Eindhoven
Email: T.C.J.Romijn@tue.nl, M.C.F.Donkers@tue.nl, S.Weiland@tue.nl, J.T.B.A.Kessels@tue.nl

1 Introduction

Hybrid vehicle technology requires an energy management strategy to optimally control the power flow between the internal combustion engine (ICE) and the electric machine (EM), such that the fuel consumption is minimized. Besides an electric machine, heavy-duty vehicles can also be equipped with a refrigerated semi-trailer and many other auxiliaries with the interesting property of having a flexible power demand and/or the ability of storing energy (see Fig. 1). Including these components in the energy management strategy, yields a complete vehicle energy management (CVEM) and is attractive for reducing fuel consumption. The computational complexity however, increases with the number of components added to the CVEM and real-time implementation requires a new approach to solve the energy management problem [2].
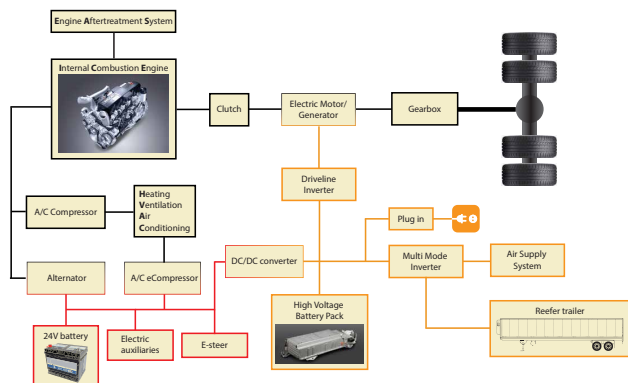
Figure 1: Topology of a hybrid heavy-duty vehicle

2 Approach

In [1], a dual decomposition approach is proposed to solve the CVEM problem for a heavy-duty vehicle with an electric machine, a high-voltage battery and a refrigerated semi-trailer over a horizon of 800 time steps with exact knowledge of the driving conditions. This approach is interesting for obtaining the optimal solution of the problem, but cannot be used in real-time as it requires exact knowledge of future driving conditions and it is too slow for real-time implementation. To use this approach for real-time implementations, the dual decomposition approach of [1] is cast into a receding horizon framework and the CVEM problem is solved with a prediction of the future driving conditions [2].

Variable sample interval lengths are used to allow relatively long prediction horizons with a small amount of decision variables and constraints.

3 Implementation and Results

The algorithm is implemented in Simulink and simulated together with a high-fidelity model of the truck to evaluate the fuel consumption reduction and computation times. The results are shown in Fig. 2 for a drive cycle from Aachen to Cologne to Aachen. It shows that the fuel consumption can be reduced by 0.84 % if all auxiliaries are considered. The fuel reduction with only one of the auxiliaries is also given. The average computation time for solving the receding horizon problem is only 11.4 ms which demonstrates that the algorithm can indeed be executed in real-time.
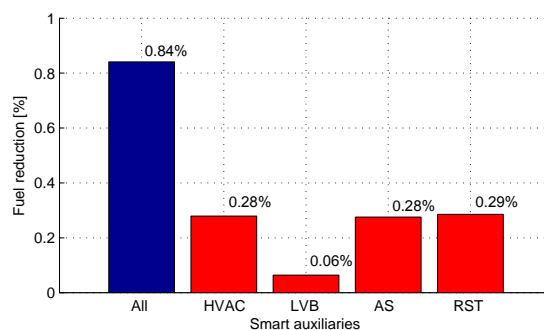
Figure 2: Fuel reduction with smart control of auxiliaries

4 Acknowledgements

References

[1] T.C.J. Romijn, M.C.F. Donkers, J.T.B.A. Kessels and S. Weiland, *A Dual Decomposition Approach to Complete Energy Management for a Heavy-Duty Vehicle,* Proc. 53rd Annu. Conf. on Decision and Control, 2014.

[2] T.C.J. Romijn, M.C.F. Donkers, J.T.B.A. Kessels and S. Weiland, *Receding Horizon Control for Distributed Energy Management of a Hybrid Heavy-Duty Vehicle with Auxiliaries,* Proc. 4th {IFAC} Workshop on Engine and Powertrain Control, Simulation and Modeling E-COSM, 2015.

Model Predictive Control and Wheel Slip Estimation for Autonomous Navigation of a Tractor

Andreas De Preter
PhD Baekeland in Octinion
Email: adepreter@octinion.com
Jan Anthonis
Industrial supervisor from Octinion
Email: janthonis@octinion.com
Romeinsestraat 18
3001 Leuven-Heverlee
Belgium

Goele Pipeleers
Scientific supervisor KU Leuven
Email: goele.pipeleers@kuleuven.be
Jan Swevers
Scientific supervisor KU Leuven
Email: jan.swevers@kuleuven.be
Celestijnenlaan 300 - bus 2420
3001 Leuven
Belgium

1 Introduction

The goal of this project is to design a controller for the autonomous navigation of a tractor. It has mainly two specifications: Firstly, the controller should be implementable on a range of tractors (e.g. different weight/dimensions) with limited changes in the algorithm. Secondly, the controller has to take variations of the soil conditions into account. The interaction between the soil and the tires determines the handling of the vehicle.

In order to realize autonomous navigation and satisfy the specifications above, a model-predictive control strategy combined with system parameter and state estimation is developed and experimentally validated.

2 MPC

The MPC is developed based on a dynamic bicycle model. The reference trajectory is projected into the system of axes that is fixed to the vehicle in order to linearise the model [1]. The MPC minimizes the quadratic deviation between the predicted and reference trajectory with constraints on the inputs and states[2].

The model misleads the controller while backwards driving due to a swing-movement of the reference-point that is located before the rear axle (e.g. reference-point moves to the right while turning left). Some modifications are proposed for this inconvenience.

3 State and Parameter estimation

The controller makes use of the information provided by both a state and parameter estimator in order to perform a stable control. The state are its plane coördinates, its heading angle and the respective velocities. The estimator is an extended kalman filter (EKF), which makes use of the following sensors: wheel encoders, steering wheel encoder and a GPS.

The parameters in the bicycle model that are responsible for describing the interaction between the wheels and the soil are the cornering stiffnesses of every tire. An on-line estimation of these parameters with a recursive least-squares estimator (RLS) increases the accuracy of the vehicle model and thereby also improves its control.

4 Implementation and improvements

The system is experimentally evaluated on a set-up. The validation trajectory that has to be tracked contains segments for both forward and backward driving.

During the first tests an oscillation is observed in the steering behaviour and the tractor maintains a constant deviation from the trajectory while turning. In order to eliminate these inconveniences the following modifications are added to the vehicle model: an integrator to eliminate the constant deviation and some dummy-states to simulate the delay in the steer actuator. Finally some extra experiments test explicitly the functionality of the parameter estimator.

References

[1]   S. De Bruyne, "Model-based control of mechatronic systems," PhD thesis, KU Leuven, 2013.

[2]   E.F. Camacho and C. Bordons, "Model Predictive Control," 2nd Edition. Springer, 2007.

[3]   A. Tsumasaka, H. Fujimoto, and T. Noguchi, "Running stabilization control of electric vehicle based on cornering stiffnes estimation," Wiley Interscience, 2008.

Thermal-aware workload scheduling in data centers

Tobias Van Damme
ENTEG - Smart Manufacturing Systems
University of Groningen
Nijenborgh 4, 9747AG Groningen
The Netherlands
Email: t.van.damme@rug.nl

Claudio De Persis
ENTEG - Smart Manufacturing Systems
University of Groningen
Nijenborgh 4, 9747AG Groningen
The Netherlands
Email: c.de.persis@rug.nl

Pietro Tesi
ENTEG - Smart Manufacturing Systems
University of Groningen
Nijenborgh 4, 9747AG Groningen
The Netherlands
Email: p.tesi@rug.nl

1 Abstract

Recent years have seen a huge increase in online data traffic. Nowadays everything is computed and stored in the cloud. Web giants as Google and Facebook process huge amounts of data on a daily basis. All this processing and storing is done in data centers, halls with thousands of servers. The size of these data centers have increased to the point where they consume megawatts of energy on a yearly basis. With this increase of energy consumption has come a corresponding drive to optimize the control and cooling of a data center such that the operational costs can be kept as low as possible.

Major challenges in controlling data centers lie in providing adequate cooling and preventing thermal hot spots from occurring, and optimizing the number of servers which are on at any given time[1, 2, 3]. In an attempt to reduce power consumption, thermal-aware control strategies have been studied and analyzed. The main control objective for a thermal-aware workload scheduler is to keep the temperature of all data processing units below a certain threshold while at the same time maximizing energy efficiency of the system.

2 Thermodynamical Model

To address this problem a thermodynamical model of the data center is derived, see Fig. 1. The change of temperature of a part of the data center can then be given by[1]:

$$mc_p \dot{T}(t) = Q_{\text{in}}(t) - Q_{\text{out}}(t) + P(t)$$

where m is the mass of the air, c_p is the heat capacity, $Q_{\text{in}}(t)$ is the heat entering the unit, $Q_{\text{out}}(t)$ is the heat exiting the unit and $P(t)$ is the power consumed by the unit. Next an optimization problem is set up which aims at minimizing the total power consumption of the data center. The thermal model links the thermal effects of consuming power to any decision in power distribution stemming from the optimization problem. With this optimization it is possible to find optimal power distributions even under varying total workloads.

References

[1]   N. Vasic, T. Scherer, and W. Schott, *Thermal-Aware Workload Scheduling for Energy Efficient Data Centers*, Proc. 7th int. conf. on Autonomic computing, 2010, pp.169-174.

[2]   Parolini, L. and Krogh, B., *A cyber-physical systems approach to data center modeling and control for energy efficiency*, Proceedings of the IEEE, 1(2012), 100, pp.254-268.

[3]   S. Li, H. Le, N. Pham, J. Heo and T. Abdelzaher, *Joint Optimization of Computing and Cooling Energy: Analytic Model and A Machine Room Case Study*, 32nd Int. Conf. on Distributed Computing Systems, 2012, pp. 396-405.
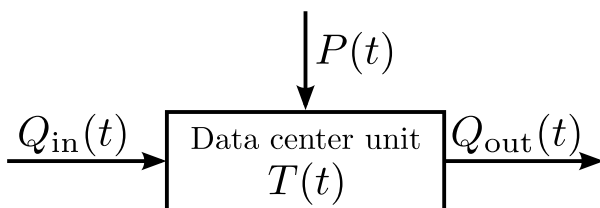
Figure 1: Heatmodel for a unit of the data center

Characterization of the tracking error for OBF based MPC

A. A. Bachnas, S.Weiland and R. Tóth
Dept. of Electical Engineering
Control System group, TU/e
a.a.bachnas@tue.nl, s.weiland@tue.nl, r.toth@tue.nl

1 Introduction

Model predictive control (MPC) is widely applied in the process control field. This control scheme allows safe operation of the controlled plant subject to boundary and operational conditions. However, due to wear in the process and possible changes in the operational conditions, the desired performance of the controller can only be sustained in a limited time period after its commissioning. Such problems are either solved by enforcing the MPC to be robust w.r.t. all possible changes of operational conditions and disturbances, or by equipping the MPC with adaptation capabilities. In our recent investigation, we found that the utilization of *orthonormal basis functions* (OBFs) based model structures in the MPC scheme, called as the MPC-OBF method, allows adaptation w.r.t. possible changes in the plant while stability of the closed-loop system in the allowed range of adaptation is guaranteed.

The aforementioned MPC-OBF scheme is formulated such that the stability and adaptability are detached from each other. The stability is ensured by a terminal controller, while the adaptability is governed by the iterative identification of the model coefficients. Due to attractive properties of the OBFs, the identification procedure results in consistent and unbiased model estimates. Under minor conditions, it is possible to show that the resulting adaptive scheme guarantee control performance in the sense of asymptotic set point tracking. However, the possible tracking error, before it disappears asymptotically, has not been characterized. With a characterization of the error, we can analyze the performance of the MPC-OBF scheme during the adaption. The goal of this work is to characterize or derive a possible bound on the aforementioned error either via numerical experiment or analytical expression.

2 Problem Setting

The cost function of the MPC-OBF is given as:

$$V_N(x(k), u(k-1)) = (x(i) - x_r(i))^\top P(x(i) - x_r(i)) +$$

$$\sum_{i=0}^{N-1} \| y(i|k) - r(k+i) \|_Q^2 + \| \Delta u(i|k) \|_R^2, \quad (1)$$

where $r(i)$ is the reference, $y(i|k)$ is the predicted output, $\Delta u(i|k)$ is the control action increment, $Q \succ 0$ and $R \succ 0$ are the weighting matrices expressing the control objective, and $P \succ 0$ is the solution of the control Lyapunov problem. The i-th step ahead predicted output is given by:

$$y(i|k) = \hat{\theta}_k x(i|k), \quad (2)$$

which depends on the collection of model coefficients $\hat{\theta}_k$ and the predicted state $x(i|k)$. For the particular (A,B)-form of the OBF model, the state equation depends on the selected basis functions which are determined by basis generating filters. Since the filters are stable, the effect of initial state gradually dies out. We can opt to avoid state estimation procedure and let the state evolution to depend only on the input (control action) of the system. Hence, the tracking error (in an appropriate signal norm) can be characterized by the mismatch between the estimated coefficient $\hat{\theta}_k$ and the true coefficient θ_k.

3 Problem Statement

Introduce the OBFs $\{\phi_i(z)\}_{i=1}^n$ that span the space $\Phi \subset \mathscr{RH}_2$ (*Hardy space* of all stable transfer functions, i.e. analytic functions at the exterior of the unit disc). The OBFs are chosen such that the true system

$$G_k(z) = \bar{G}_k(z) + G_k^\perp(z), G_k(z) \in \mathscr{RH}_2 \quad (3)$$

have negligible unmodeled dynamics $G_k^\perp \in \Phi^\perp$ (the orthogonal complement of Φ). Given a current estimate of the system $\hat{G}_k(z) \in \Phi$, the model mismatch can be characterized as:

$$\| \bar{G}_k(z) - \hat{G}_k(z) \|_{\mathscr{H}_2} = \| \theta_k - \hat{\theta}_k \|_2 \leq \gamma, \quad (4)$$

where $\gamma \in \mathbb{R}_+$ is the bound on the model error. Using this expression, we can analyze the relation between γ, the cost function (1), and the tracking error for a given reference value. A possible analysis can be conducted numerically using experiments with scenarios such as:

- Fixed $\hat{\theta}_k$.
- Slowly varying $\hat{\theta}_k$ with a fixed error bound γ.

Moreover, due to the terminal cost formulation of (1), the MPC controller is none other than an LQR controller if the operational constraints on the MPC controller are not active. Hence, an analytical expression can be derived in the similar manner as in robust performance analysis.

4 Acknowledgments

References

[1] Bachnas, A. A., S. Weiland, R. Tóth, *Data Driven Predictive Control Based on Orthonormal Basis Functions*. In Proc. of the 54th IEEE Conference on Decision and Control, 15-18 December 2015, Osaka, Japan, (pp 3026-3031).

Feedforward control for flexible motion systems with a time-varying state-to-output map

Yanin Kasemsinsup[1], Siep Weiland[1], Marcel Heertjes[1,2], Hans Butler[1,2]

[1]Eindhoven University of Technology, Eindhoven, The Netherlands

[2]ASML, Veldhoven, The Netherlands

y.kasemsinsup@tue.nl

1 Introduction

In many high-accuracy positioning systems, performance is defined at points that varies with time and position. A typical example is given by wafer stage positioning systems in the lithographic industry. The illumination process of such a system happens in a scanning fashion to varying target locations, the so-called Point of Interest (PoI). See Figure 1. The relation between the system states and PoI exhibits time-varying properties relating to a pre-defined scanning pattern, hence a *time-varying state-to-output map*.

To obtain position performance with nano-scale accuracy, *feedforward* controllers play a key role in compensating for structural dynamics. However, with conventional feedforward designs, a mismatch occurs between the calculated force and the ideal force. This mismatch is largely caused by position / time-varying behavior of the system. Therefore, we propose to explicitly take such time or position-varying characteristics into account in the feedforward compensator design to enhance the positioning performance.

2 Problem formulation and Discussion

Consider a flexible system in a linear modal state-space form with the modal state $x(t) := \begin{bmatrix} q^\top(t) & \dot{q}^\top(t) \end{bmatrix}^\top$. Here, the entries of the state vector $x(t)$ appear as the modal coefficients $q(t) \in \mathbb{R}^p$ and their time derivatives $\dot{q}(t)$, whereas p denotes the number of vibration modes used in the approximation. Thus, we obtain the system:

$$\begin{cases} \dot{x}(t) = Ax(t) + Bu(t) \\ y(t) = C(t)x(t). \end{cases} \tag{1}$$

Note that system (1) is time-varying in the state-to-output mapping $C(t)$ with $u(t) \in \mathbb{R}^b$ and $y(t) \in \mathbb{R}$ as the inputs and output, respectively. Specifically

$$A := \begin{bmatrix} 0_{(p \times p)} & I_{(p \times p)} \\ -\Omega^2_{(p \times p)} & -2\zeta\Omega^2_{(p \times p)} \end{bmatrix}, B := \begin{bmatrix} 0_{(p \times b)} \\ \Phi_{ac}^\top \end{bmatrix} \tag{2}$$

$$C(t) := \begin{bmatrix} \phi_{s_1}(t) & \phi_{s_2}(t) & \cdots & \phi_{s_p}(t) & 0_{(1 \times p)} \end{bmatrix}.$$

The modal frequencies are contained in the matrix $\Omega := diag(\omega_1, \omega_1, \cdots, \omega_p)$. The diagonal matrix $\zeta \in \mathbb{R}^{p \times p}$ and matrix $\Phi_{ac} \in \mathbb{R}^{b \times p}$ denote the modal relative damping and the mode shape gains at actuation nodes, respectively. The position dependency of the system output is modeled by making the state-to-output mapping $C(t)$ time-varying according to the pre-defined (and time-varying) reference PoI trajectories. More specifically, this mapping represents the time-varying mode shape gains of the flexible structure, $\phi_{s_i}(t) \in \mathbb{R}$ for $i = 1, 2, .., p$, along the time trajectories of the PoI.
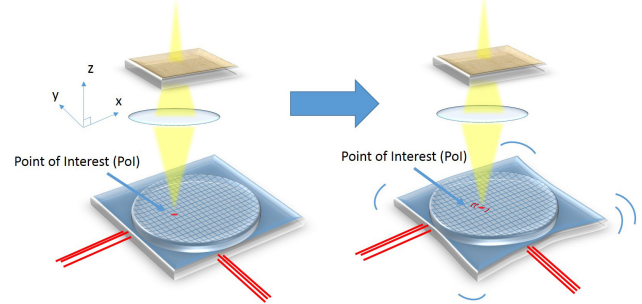
Figure 1: Point of Interest(PoI) and flexible behaviour of the stage

With the given knowledge about the plant parametric model and the desired output trajectory $y_{\text{desired}}(t)$, it is aimed to find a feedforward input $u_{\text{ff}}(t)$, that satisfies the following nominal system:

$$\begin{cases} \dot{x}_{\text{ref}}(t) & = Ax_{\text{ref}}(t) + Bu_{\text{ff}}(t) \\ y_{\text{desired}}(t) & = C(t)x_{\text{ref}}(t). \end{cases} \tag{3}$$

Here, $x_{\text{ref}}(t)$ denotes the reference state trajectory corresponding to $y_{\text{desired}}(t)$. In other words, for a given $y_{\text{desired}}(t)$, we aim to find a pair $[u_{\text{ff}}(t), x_{\text{ref}}(t)]$ such that the nominal system description (3) holds. Such an inversion-based problem formulation has been posed, for example, for LTI systems in [1] and for nonlinear systems in [2]. Clearly, the pair $[u_{\text{ff}}(t), x_{\text{ref}}(t)]$ does not need to exist for any given $y_{\text{desired}}(t)$ if not being compatible with (3). Solving this problem yields several benefits. Firstly, it gives insight in whether the desired trajectory $y_{\text{desired}}(t)$ is realizable in the considered system setting or not. Secondly, the obtained solution(s) exactly provide the required input $u_{\text{ff}}(t)$ that drives the system according to $y_{\text{desired}}(t)$ (when feasible); such input(s) can be utilized as feedforward signal(s) in the implementation. Thirdly, it enables us to determine, from a given $y_{\text{desired}}(t)$, the corresponding reference state trajectory $x_{\text{ref}}(t)$ that appropriately satisfies the system dynamics; this is essential when utilizing control techniques involving *state feedback* mechanisms.

References

[1]   Zou, Qingze, and Santosh Devasia. "Preview-based stable-inversion for output tracking." American Control Conference, 1999. Proceedings of the 1999. Vol. 5. IEEE, 1999.

[2]   Chen, Degang, and BRAD PADEN. "Stable inversion of nonlinear non-minimum phase systems." International Journal of Control 64.1 (1996): 81-97.

Multivariable Fuel Injection Control in Diesel Combustion

Xi Luo, Bram de Jager and Frank Willems

Control Systems Technology Group, Department of Mechanical Engineering

Eindhoven University of Technology

P.O. Box 513, 5600 MB EINDHOVEN, The Netherlands

Email: {X.Luo, A.G.de.Jager, F.P.T.Willems}@tue.nl

1 Introduction

With an increased number (up to nine) of fuel injections per combustion cycle, the diesel combustion can achieve better fuel economy and lower engine-out emissions. Meanwhile, the problem in controlling the fuel injection becomes challenging. The combustion process depends on all fuel injection pulses in a coupled way and the consequence of changing individual injections becomes correlated. Currently applied combustion control schemes manipulate injection pulses individually by using multiple single-input single-output (SISO) controllers. Without considering the coupling effect, they have limited dynamical performance and no stability guarantee. Therefore, it is desired to design a multivariable combustion controller for diesel combustion with multi-pulse fuel injection, which has better dynamical performance and stability guarantees. It is also of interest to achieve robust closed-loop performance against cylinder-to-cylinder variations.
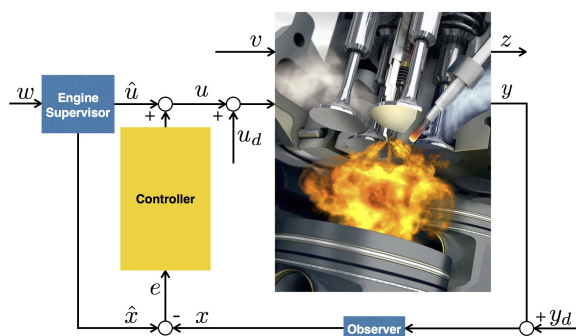
Figure 1: Block diagram of cylinder pressure-based combustion control scheme [1].

2 Approach

Several metrics are extracted from the crank angle and cylinder pressure signal y and used to describe a combustion process, e.g. the crank angle degree reaching 50% accumulated heat release (CA50) and the indicated mean effective pressure (IMEP). To achieve the desired engine performance in z, they are used as the feedback signal x and compared to the reference $\hat{x}$. Based on the error signal e, the combustion controller modifies the fueling profile u on a combustion cycle basis, which is known as the cycle-to-cycle control scheme. The block diagram of the control scheme is shown in Figure

1. By perturbing the fueling profile, the (coupled) sensitivity of the feedback signal is acquired for all cylinders at a certain working condition [1]. Based on this, the closed-loop performance of a combustion controller can be studied. By solving Linear Matrix Inequalities (LMI), a single multivariable combustion controller for multiple cylinders can be designed with guaranteed stability and performance.

3 Results

The closed-loop performance of the designed multivariable combustion controller was studied using a map-based cylinder-individual engine model, which is developed based on experimental data from a six-cylinder heavy-duty diesel engine. As shown in Figure 2, the different feedback signals from six cylinders denote the cylinder-to-cylinder variation before the controller was applied at combustion cycle 10. After that, this variation is quickly compensated by assigning different fueling profiles to different cylinders. The controller's satisfying and robust dynamical performance was demonstrated with fast reference tracking for all six differently behaving cylinders.
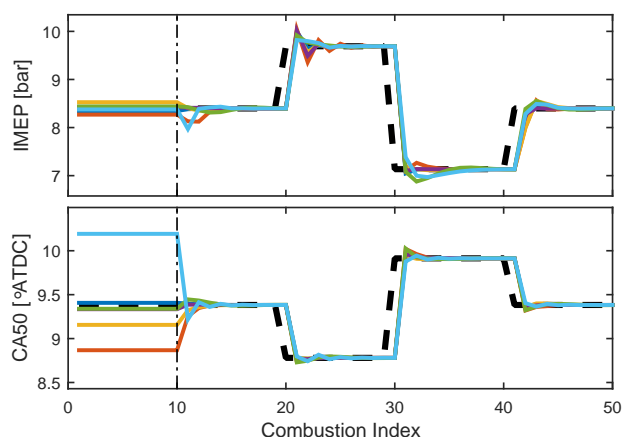
Figure 2: Closed-loop simulation with step reference (black) and the feedback signals of six cylinders (color).

References

[1] Xi Luo, Shuli Wang, Bram de Jager, and Frank Willems. Cylinder pressure-based combustion control with multi-pulse fuel injection. *IFAC Workshop on Engine and Powertrain Control, Simulation and Modeling (E-COSM)*, 2015.

Batch-to-Batch Rational Feedforward Tuning:
From Learning to Identification Approaches

Lennart Blanken[1], Frank Boeren[1], Dennis Bruijnen[2], Tom Oomen[1]

[1]Eindhoven University of Technology, Dept. of Mechanical Engineering, Control Systems Technology, The Netherlands

[2]Philips Innovation Services, Mechatronics Technologies, Eindhoven, The Netherlands

l.l.g.blanken@tue.nl

Introduction

Feedforward control enables high performance for industrial motion systems that perform non-repeating motion tasks. Recently, learning techniques have been proposed that improve both performance and flexibility to non-repeating tasks in a batch-to-batch fashion by using a rational parametrization in feedforward control. The aim here is to investigate the merits of these approaches. Experimental results on an industrial motion system confirm the theoretical findings and illustrate benefits of rational feedforward tuning in motion systems, including pre- and post-actuation.

Batch-to-Batch Feedforward from a System Identification Perspective

The goal in batch-to-batch feedforward control is to iteratively improve control performance by updating a feedforward controller C_{ff} from measured data in a batch-to-batch fashion, see Fig. 1. Here, the batch-to-batch feedforward techniques are interpreted in a system identification perspective [4], illustrated in Fig. 2. Essential for the achievable performance are i) the batches of measured data, ii) the feedforward controller parameterization, and iii) the optimization criterion.
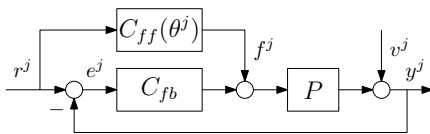
Figure 1: In batch-to-batch feedforward control with parameterized feedforward, parameters θ of $C_{ff}(\theta^j)$ are updated based on measured data after each task j.
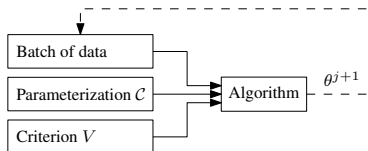
Figure 2: Batch-to-batch feedforward tuning from a system identification perspective. Based on a batch of data, parameterization $\mathcal{C}$ and criterion V, θ_{j+1} is determined and implemented to obtain a new batch of data.

Two techniques to batch-to-batch feedforward are investigated: an instrumental variable-based technique [1], and an Iterative Learning Control (ILC) based technique [2]. In the framework of Fig. 2, these approaches turn out to be very similar. Their algorithms to compute θ^{j+1} can be interpreted in terms of a standard ILC update law, given by

$$\theta^{j+1} = Q\theta^j + Le^j, \tag{1}$$

with corresponding robustness and learning matrices Q, L.

Implementation & Experimental Results

Interestingly, rational feedforward controllers can also be used to generate pre-actuation by means of stable inversion procedures, see, e.g., [5]. The proposed approaches are implemented on a wafer stage. The results in Fig. 3 demonstrate preactuation, used to prevent transient errors at the start of the motion task, and postactuation, used to reduce residual vibrations in the system. This feature is key for the potential performance improvement of rational feedforward.

(a) Pre-actuation.   (b) Post-actuation.
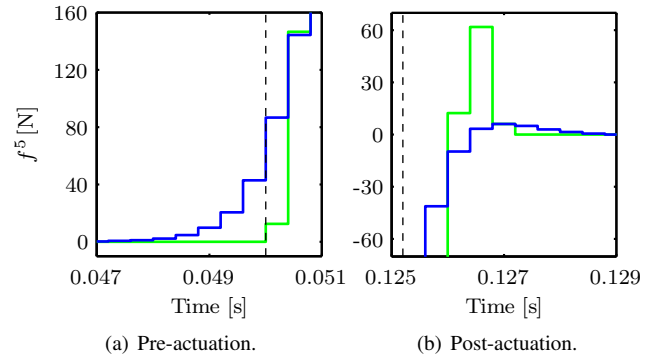
Figure 3: The rational parameterization (——) enables pre- and post-actuation of the system, in contrast to the polynomial parametrization (——). The start and end times of the motion task are indicated by black dashed lines.

References

[1]   F. Boeren, T. Oomen and M. Steinbuch, Iterative motion feedforward tuning: A data-driven approach based on instrumental variable identification, *Control Engineering Practice*, vol. 37, 11-19, 2015.

[2]   J. Bolder and T. Oomen, Rational basis functions in iterative learning control - With experimental verification on a motion system, *IEEE Transactions on Control Systems Technology*, 23(22):722-729, 2015.

[3]   D. Bristow, M. Tharayil, and A. Alleyne, A Survey of Iterative Learning Control, *IEEE Control Systems*, 26(3):96-114, 2006.

[4]   L. Ljung, *System identification - Theory for the User*, Upper Saddle River, New York, USA: Prentice Hall, 1999.

[5]   Q. Zou and S. Devasia, Preview-based stable-inversion for output tracking of linear systems, *ASME Journal of Dynamic Systems, Measurement and Control*, 121(1):625-630, 1999.

Enhancing Performance and Cost-Effectiveness in Motion Control Via Multi-Rate Sampling

Jurgen van Zundert[1], Tom Oomen[1], Wouter Aangenent[2], W.P.M.H. (Maurice) Heemels[1]

[1]Eindhoven University of Technology, Department of Mechanical Engineering, Control Systems Technology group, The Netherlands

[2]ASML Research Mechatronics, Veldhoven, The Netherlands

1 Motivation

In traditional feedback control, a single sampling frequency is used for all control loops and increasing performance requirements typically lead to an increase of the sampling frequency. This is often very costly in terms of required hardware and hence there exists a trade-off between performance and cost-effectiveness, see Figure 1. Usually, this high sampling frequency is only required for some of the control loops, and not necessary in the other loops. Therefore, the trade-off can be ameliorated by use of multi-rate control: using different sampling frequencies in the different control loops.
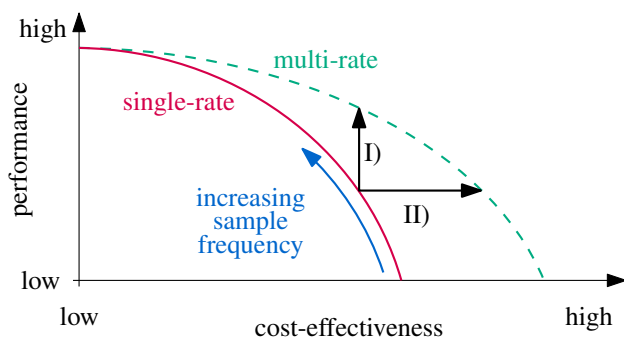
Figure 1: The performance/cost-effectiveness trade-off observed in classical control can be enhanced by use of multi-rate control: I) higher performance for equal cost; or II) same level of performance for lower cost.

Multi-rate control has a strong potential in many motion control problems, including dual stages, sampled-data control [1], master/slave configurations [2], thermo-mechanical applications, and non-equidistant sampling [3].

Although a large number of theoretical issues have been solved, the design of multi-rate controllers is by no means straightforward. Indeed, multi-rate systems are LPTV (linear, periodically time-varying), so common design techniques for LTI systems are not directly applicable. The aim of this research is to develop a systematic design framework for multi-rate control. The framework is demonstrated in the context of wafer scanner systems.

2 Case study: dual stage in wafer scanner systems

Wafer scanner systems perform a key role in the automated production of integrated circuits (ICs). An important aspect is the positioning of the wafer stage containing the wafer with ICs. The wafer stage covers a stroke of a meter, while at the same time it achieves a position accuracy in the order of nanometers. The large ratio between stroke and accuracy is often addressed using a dual stage approach: a coarse stage (long stroke) used for micrometer accuracy, with on top a fine stage (short stroke) used for nanometer position accuracy. Since the long stroke requires a much lower accuracy than the short stroke, its sampling frequency can be much smaller. This opens up the possibility of an improved accuracy-cost trade-off by using a multi-rate approach.

3 Approach

The research in this paper focuses at multi-rate feedforward controller design, since for motion applications feedforward constitutes the largest part of the system's control input. For multi-rate feedback controller design see, for example, [4]. In the developed framework, multi-rate systems are described using the finite-time/lifting framework [1]. The framework is used for norm-based feedforward controller optimization along the lines of [5]. Initial results, including simulations of the dual stage case study, are reported in [6].

Acknowledgements

References

[1] Tongwen Chen and Bruce A. Francis. "Optimal Sampled-Data Control Systems", *Springer*, London, Great Britain, 1995.

[2] Cees J.H. Lambregts, Marcel F. Heertjes, and Bartel J. van de Veek, "Multivariable Feedback Control in Stage Synchronization", *in 2015 American Control Conference*, pages 4149-4154, Chicago, Illinois, 2015.

[3] Jurgen van Zundert, Tom Oomen, Dip Goswami, and W.P.M.H. (Maurice) Heemels, "On the Potential of Lifted Domain Feedforward Controllers with a Periodic Sampling Sequence", [in preparation].

[4] Tom Oomen, Marc van de Wal, and Okko Bosgra, "Design framework for high-performance optimal sampled-data control with application to a wafer stage", *International Journal of Control*, 80(6):919-934, 2007.

[5] Stan H. van der Meulen, Rob L. Tousain, and Okko H. Bosgra, "Fixed Structure Feedforward Controller Design Exploiting Iterative Trials: Application to a Wafer Stage and a Desktop Printer", *Journal of Dynamic Systems, Measurement, and Control*, 130(5):051006:1-16, 2008.

[6] J.C.D. van Zundert, J.L.C. Verhaegh, W.H.T.M. Aangenent, T. Oomen, D. Antunes, and W.P.M.H. Heemels. "Feedforward for Multi-Rate Motion Control: Enhanced Performance and Cost-Effectiveness", *in 2015 American Control Conference*, pages 2831-2836, Chicago, Illinois, 2015.

Dynamic event-triggered control with time regularization for linear systems

D.P. Borgers, V.S. Dolk, and W.P.M.H. Heemels

Eindhoven University of Technology, P.O. Box 513, 5600 MB Eindhoven, The Netherlands

`{d.p.borgers,v.s.dolk,m.heemels}@tue.nl`

1 Introduction

In most digital control systems, the execution of the control tasks (sampling the plant's output and computing and updating the control input) occur periodically, regardless of the state the system is in. This possibly leads to a waste of (e.g., computation, communication, and energy) resources, as many of the control updates are not actually necessary to achieve the desired performance guarantees. In recent years, many *event-triggered* control (ETC) strategies have been proposed which generate the execution times based on the state of the system $\xi(t) \in \mathbb{R}^{n_\xi}$, thereby bringing feedback into the execution times and communication process, such that the control task is only executed when this is really necessary. Typical event-generators are of the form

$$t_{k+1} = \inf\{t \geqslant t_k \mid \phi(\xi(t)) \leqslant 0\}, \ k \in \mathbb{N}, \tag{1}$$

for a certain function $\phi : \mathbb{R}^{n_\xi} \to \mathbb{R}$. Thus, execution times are generated based on a *static* condition on the state ξ. However, static event-generators as in (1) can sometimes generate many executions when the system is close to its equilibrium, and can often lead to Zeno behavior. In [2], we proposed an event-triggered control strategy for nonlinear systems which does not have these issues. In this work the event-generator has the form

$$t_{k+1} = \inf\{t \geqslant t_k + h \mid \eta(t) \leqslant 0\}, \tag{2}$$

where $h \in \mathbb{R}_{>0}$ is a minimum inter-execution time, and $\eta \in \mathbb{R}_{\geqslant 0}$ is an additional dynamical variable which is included in the event-generator. This leads to a *dynamic* event-triggered control (DETC) system, with a guaranteed $\mathcal{L}_p$-gain and positive minimum inter-execution time.

In the case of linear systems with the event-generator (2), we obtain the hybrid closed-loop system

$$\frac{\mathrm{d}}{\mathrm{d}t}\begin{bmatrix} \xi \\ \tau \\ \eta \end{bmatrix} = \begin{bmatrix} A\xi + Bw \\ 1 \\ \Psi(o) \end{bmatrix}, \quad \begin{array}{l} \text{when } \tau \in [0,h] \\ \text{and } \eta \geqslant 0 \end{array} \tag{3a}$$

$$\begin{bmatrix} \xi^+ \\ \tau^+ \\ \eta^+ \end{bmatrix} = \begin{bmatrix} J\xi \\ 0 \\ \eta_0(o) \end{bmatrix}, \quad \begin{array}{l} \text{when } \tau \in [h,\infty) \\ \text{and } \eta \leqslant 0 \end{array} \tag{3b}$$

$$z = C\xi + Dw, \tag{3c}$$

where the functions Ψ and η_0 depend only on $o \in \mathbb{R}^{n_o}$ which contains all the signals that are available to the event-generator. When the functions Ψ, and η_0 are properly designed, the proposed dynamic ETC system (3) can be shown to outperform both periodically sampled systems and static ETC systems, see [2, 3].

2 Improved DETC design for *linear* systems

The dynamic event-generators proposed in [2, 3] are formulated for *nonlinear* systems. In this work, we further improve upon these results for the case of *linear* systems. By exploiting linearity and making use of techniques from [1] and [4], we can provide more tailored design techniques for Ψ and η_0, such that less conservative results are obtained than in [2, 3], with larger inter-execution times and tighter $\mathcal{L}_2$-gain estimates. These techniques are based on using Riccati differential equations for (3a) with appropriate jump conditions related to the jump dynamics (3b).

Just as in [2, 3], for the system (3) we are able to guarantee GES with a certain decay rate $\rho > 0$ and $\mathcal{L}_2$-stability from disturbance w to output z with a certain $\mathcal{L}_2$-gain $\gamma > 0$. Simulations show that for identical ρ and γ the event-generator (2) with Ψ and η_0 designed using the proposed tools for linear systems yields larger average inter-execution times than the event-generator proposed in [2].

3 Acknowledgements

References

[1] W.P.M.H. Heemels, M.C.F. Donkers, and A.R. Teel, "Periodic event-triggered control for linear systems," TAC, 58(4):847–861, 2013.

[2] V.S. Dolk, D.P. Borgers, and W.P.M.H. Heemels, "Event-triggered control: Tradeoffs between transmission intervals and performance," CDC, 2014, pp. 2764–2769.

[3] V.S. Dolk, D.P. Borgers, and W.P.M.H. Heemels, "Output-based and Decentralized Dynamic Event-triggered Control with Guaranteed $\mathcal{L}_p$-gain Performance and Zeno-freeness," submitted.

[4] S.J.L.M. van Loon, W.P.M.H. Heemels, and A.R. Teel, "Improved $\mathcal{L}_2$-gain analysis for a class of hybrid systems with applications to reset and event-triggered control," CDC, 2014, pp. 1221–1226.

Robust constrained control of nonlinear systems: the Explicit Reference Governor approach

Marco M. Nicotra, Emanuele Garone
Service d'Automatique et d'Analyse des Systèmes
Université Libre de Bruxelles
Av. Roosevelt 50, CP 165/55, 1050 Brussels, Belgium
Email: mnicotra@ulb.ac.be
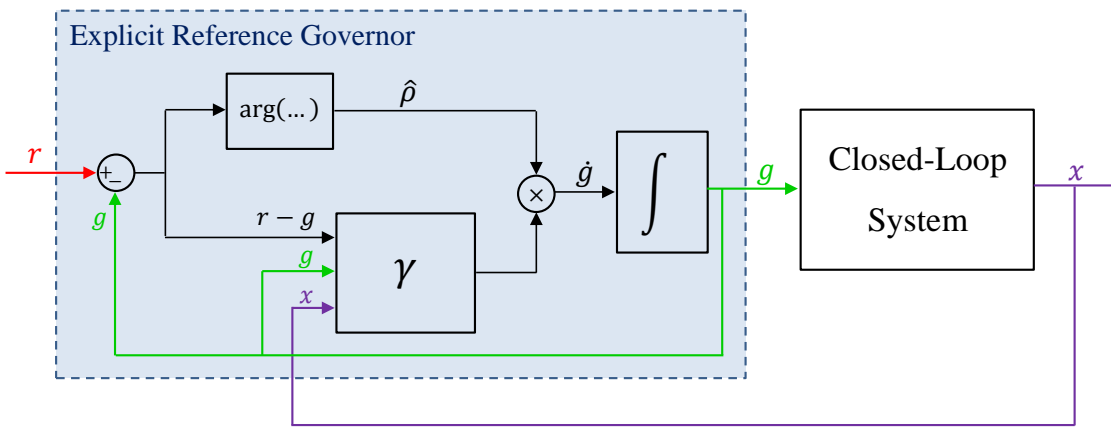
Figure 1: Proposed control architecture.

1 Introduction

The Explicit Reference Governor (ERG) is an auxiliary control law that dynamically modifies the reference of a pre-compensated nonlinear system to ensure the constraint satisfaction without resorting to online optimization [1]. The approach is based on the idea that any set of state-space constraints can be translated into a single constraint on the Lyapunov function. The constraint on the Lyapunov function can be enforced by modulating the derivative of the applied reference. The basic scheme is illustrated in Figure 1. The objective of this talk is to extend the ERG framework by detailing its robustness properties with respect to parametric uncertainties and external disturbances.

2 Problem Statement

Consider a pre-compensated nonlinear system subject to parametric uncertainties $\mu \in \mathcal{M}$, bounded external disturbances $\|\delta\|_\infty$, and a set of constraints $c(x, v) \geq 0$. Given a desired reference signal $r(t)$, not known in advance, the robust ERG problem is that of generating, at each time instant t, an auxiliary reference $g(t)$ such that:
1) if $g(t)$ is kept constant, constraints are not violated;
2) $g(t)$ approximates $r(t)$ as much as possible.

3 Basic Idea

Having translated the state-space constraints into a single constraint on the Lyapunov function, the robust ERG framework will focus on recovering the fundamental properties of the basic ERG approach.

In particular, the robustness with respect to parametric uncertainties will be addressed by considering the case of Lyapunov functions that can present a common upper and lower bound function $\mu \in \mathcal{M}$.

The robustness with respect to external disturbances will then be addressed by considering the case of ISS-Lyapunov functions [2] and determining a suitable safety margin such that the system constraints will be satisfied for any bounded disturbance.

References

[1]   Emanuele Garone and Marco M. Nicotra. Explicit reference governor for constrained nonlinear systems. *IEEE Transactions on Automatic Control; Avalable on Pre-Print.*

[2]   Eduardo D. Sontag and Y. Wang. On characterizations of the input-to-state stability property. *System and Control Letters*, 24:351–359, 1995.

Sub-Optimal Extremum Seeking

Christophe Labar and Emanuele Garone
Department of Control Engineering and System Analysis
Université Libre de Bruxelles (ULB)
50, av. F.D. Roosevelt, CP 165/55, 1050 Brussels, Belgium
Email: {Christophe.Labar,Emanuele.Garone}@ulb.ac.be

1 Introduction

In many practical applications, one aims at optimizing the performance of the system (e.g. the efficiency, power produced, etc.). However, in some applications, it may be required that a certain known margin with respect to the optimum exists, so that it can be used as a "reserve". A possible example concerns the wind energy sector where the capability of maintaining a known amount of reserve could be used as a knob to counteract imbalances on the networks due to load/production variations [1]. Due to the presence of uncertainties in the system, the optimal (and sub-optimal) point cannot be determined a priori (e.g. uncertainty on the wind field distribution at the wind turbine location). The aim of this work is to propose a non-model based approach for reaching a given percentage of the optimal point.

2 Problem Statement

Consider a single-input-single-output system whose dynamics is

$$\begin{cases} \dot{x}(t) &= f(x(t), u(t)) \\ y(t) &= g(x(t)) \end{cases} \tag{1}$$

with $x(t) \in \mathbb{R}^n$ the vector of system states, $u(t) \in \mathbb{R}$ the control input and $y(t) \in \mathbb{R}$ the measurable system output.

Furthermore, consider a cost function

$$z = C(y), \tag{2}$$

where $C : \mathbb{R} \to \mathbb{R}$, whose analytical expression in function of the system output is not available (or only poorly known) but whose output can be measured on line.

Assumption 2.1 *There exists an output $y^* \in \mathbb{R}$ and a corresponding state vector $x^* \in \mathbb{R}^n$ which is a maximum for $C(y)$, i.e. $\exists x^* : y^* = g(x^*)$ ensuring that*

$$C'(y^*) = 0 \text{ and } C''(y^*) \le 0 \tag{3}$$

The goal of our research is to develop a control strategy able to steer the system (1) to reach a given ratio $0 < \rho \le 1$ of the optimal cost C^* (with $C^* = C(y^*)$).

3 Proposed Approach

To address the stated problem, the proposed approach consists in 4 steps

1. The stated problem is reformulated as the minimization of an auxiliary cost function ϕ defined as

$$\phi(y) = (C(y) - \rho C^*)^2. \tag{4}$$

2. Having no a priori knowledge of C^*, it is estimated locally (i.e. at the current point y) by using the truncated second order Taylor expansion as follows

$$\hat{C}^*(y) = C(y) - \frac{C'^2(y)}{2C''(y)} \tag{5}$$

This results in the approximated cost function

$$\phi_a(y) = \left((1 - \rho)C(y) + 0.5\rho \frac{C'^2(y)}{C''(y)} \right)^2 \tag{6}$$

3. In most of the cases, $C'(y)$ and $C''(y)$ cannot be measured. Therefore, an estimation of those values is obtained from data-points $(y, C(y))$ recorded during the optimization process.

4. The minimization of the cost function obtained with the approximated values of $C'(y)$ and $C''(y)$ is performed by the Extremum Seeking Control [2]. This control strategy is able to move a system so as to optimize a given cost function, without requiring any knowledge of the latter. It is therefore suited to our application in which the relation between the system input and the cost function output is not known.

References

[1] Jacob Aho, Andrew Buckspan, Jason Laks, Yunho Jeong, Fiona Dunne, and Lucy Pao. A tutorial of wind turbine control for supporting grid frequency through active power control. In *American Control Conference (ACC) 2012*.

[2] Ying Tan, Drangan Nesic, and Iven Mareels. On non-local stability properties of extremum seeking control. *Automatica*, pages 889–903, 2006.

Second-order reset elements for improved stage control design

Leroy Hazeleger[*], Marcel Heertjes[**], and Henk Nijmeijer[*]

[*]Eindhoven University of Technology, P.O. Box 513, 5600 MB Eindhoven, The Netherlands
[**]ASML Netherlands B.V., P.O. Box 324, 5500 AH Veldhoven, The Netherlands
L.Hazeleger@tue.nl

1 Introduction

In this work, the focus is on coping with the unavoidable phase lag involved with linear control elements that limit the increase of closed-loop bandwidth, without compromising control system specifications. As such, reset control is of particular interest. Describing function (DF) analysis showed that reset elements, such as the Clegg integrator [1], possess similar magnitude characteristics as their equivalent linear elements, while their phase lag is drastically reduced. Exploiting this phase advantage, the possibilities of improved closed-loop performance of a stage control design by the aid of a new reset element are studied; namely, a second-order reset element (SORE) $\mathscr{R}_{sore}$. This results in the reset control scheme shown in Figure 1, in which a linear second-order element is replaced by $\mathscr{R}_{sore}$. The main motivation is the fact that second-order filters, e.g. notch filters or low-pass filters, form key elements of (industrial) motion control. As the second-order low-pass filter comes at the expense of significant phase lag, a reduction of phase lag by means of reset allows for higher achievable bandwidths. Hence improved motion control performance.

2 Second-order reset element

A minimal state-space realization of a second-order low-pass filter with reset functionality (triggered upon zero input $e(t) = 0$) is given by

$$\mathscr{R}_{sore} := \begin{cases} \dot{x}_r(t) = A_r x_r(t) + B_r e(t) & \forall e(t) \neq 0 \\ x_r(t^+) = A_\rho x_r(t) & \forall e(t) = 0 \\ u_r(t) = C_r x_r(t) + D_r e(t) \end{cases}, \quad (1)$$

with state $x_r \in \mathbb{R}^2$ and matrices

$$A_r = \begin{bmatrix} 0 & 1 \\ -\omega_p^2 & -2\beta_p \omega_p \end{bmatrix}, \quad B_r = \begin{bmatrix} 0 \\ \omega_p^2 \end{bmatrix},$$
$$C_r = \begin{bmatrix} 1 & 0 \end{bmatrix}, \qquad\qquad D_r = 0.$$

Moreover, the so-called reset matrix A_ρ is defined as

$$A_\rho = \begin{bmatrix} 0 & 0 \\ 0 & 0 \end{bmatrix}, \quad (2)$$

yielding a SORE with full reset. The Bode diagram of the DF of said reset element shows significantly less phase lag (up to 129 degrees less phase lag for high frequencies) than the linear second-order low-pass filter, while their magnitude characteristics are similar (depending upon the dimensionless damping coefficient β_p). Moreover, time-domain
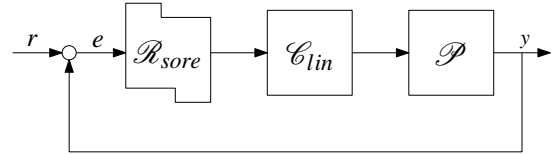
Figure 1: Reset control scheme

analysis shows that properties of a second-order low-pass filter are largely preserved.

3 Loopshaping with DF

Being part of a reset control design procedure, loopshaping of the linear feedback loop with a SORE, based on the DF description of said element, leads to higher achievable bandwidths from a linear point-of-view. The validity and predictive value of the control design procedure are based on a low-pass property of the linear control elements and the plant dynamics in the loop, attenuating significant higher-order harmonics induced by the reset. As such, the frequency-domain characteristics of the open-loop, involving the DF description of the SORE, are sufficient to approximate its input-output behavior. Figure 2 shows the sensitivity function $S(j\omega)$ and cumulative power spectral density (cPSD) of the tracking error for 3 cases, illustrating the improvement of performance tradeoff by means of reset. The results are confirmed on an industrial wafer stage system.
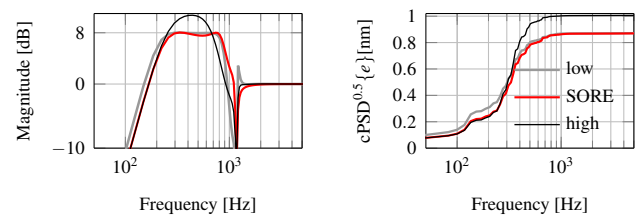
Figure 2: Sensitivity (left) and the cPSD of the tracking error (right). Linear case in gray has maximum bandwidth considering specs, linear case in black (does not meet specs) and reset case in red have same controller parameters, the latter based on the DF of the SORE.

References

[1]   J.C. Clegg, A nonlinear integrator for servomechanisms, Trans. AIEE. 77, pp 41-42, 1958.

Fraction-model-independent Stability Analysis for SMA-actuators

Rolf Gaasbeek, Bram de Jager

Eindhoven University of Technology, Department of Mechanical Engineering, P.O. Box 513, 5600 MB Eindhoven, The Netherlands.

Email: R.I.Gaasbeek@tue.nl *

1 Introduction

Shape Memory Alloy (SMA) is a lightweight material with considerable higher actuation strain and work output than other active materials such as (high strain) piezo-materials [1]. For this reason SMA-actuators have a great potential in micro-robotic systems. The actuating effect in SMA is caused by a changing crystallographic structure (increasing or decreasing the fraction of detwinned martensite). This transformation (and thus the actuation) is controlled by changing the temperature of the SMA material. The relation between temperature and fraction of detwinned martensite is highly non-linear and experts do not agree on the most suitable fraction-model. Typically, stability-analysis are model-based, thus stability analysis of a closed-loop SMA-actuated system should be treated with caution. The main contribution of this work is a stability analysis for SMA-actuators that is not based on a full fraction-model. The latter allows for a stronger and more general stability analysis.

2 SMA-actuators

SMA is able to recover from large deformation by changing crystallographic structure. In actuators, this principle can be used by applying a bias force to a SMA-wire. When enough force is applied, the SMA-wire is in the detwinned martensite phase (the crystallographic structure is completely dominated by detwinned martensite) at low temperatures and the wire is stretched. If the temperature is increased the crystallographic structure changes to the austenite phase, causing the wire to contract again. This process is assumed to be instantanious. Furthermore, it is assumed that no crystallographic changes occur when the temperature is constant. The latter is generally accepted and matches with experimental observations.

The above can be mathematically summarized as follows: $\text{sign}(\dot{T}) = \text{sign}(\dot{\xi})$ and if $\dot{T} = 0$, also $\dot{\xi} = 0$. Where T denotes the temperature and ξ denotes the fraction of austenite present in the material ($0 \leq \xi \leq 1$).

3 Experimental example

The methodology presented in this paper will be demonstrated using a 1D SMA-actuator. A bias force is applied by means of a spring. The actuator input (current through the wire) is chosen such that the actuator goes through a full cycle (a full transformation between austenite and detwinned martensite and visa versa), after which several

'inner cycles' (non full transformations) are followed at different actuation speed (thus the rate of temperature varies among cycles). The response of the actuator is provided in Figure 1 (black crosses), where the rate of temperature is plotted against the rate of fraction change. It can be seen that the second and last quadrant of the plot are empty, as follows from the insight provided in Section 2. Furthermore, the response is clearly bounded by the black lines, which are equal to $[0, \alpha]\dot{T} = [0, 0.1]\dot{T}$.
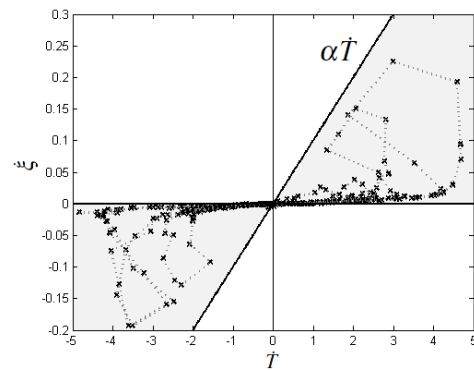
Figure 1: Actuator response

4 Stability Analysis

Several conditions should be valid to proof input-to-state stability. One can use the fact that the grey sector in Figure 1 is bounded by $[0, \alpha]$. In this case the circle criterion can be used to proof stability [2]. Note that the linear temperature dynamics and fraction to displacement relation can be determined seperately by system identification techniques. When an appropriate controller is designed, the cascade of the linear relations are globally asymptotically stable and strictly proper. Hence, input-to-state stability is achieved when:

$$\text{Re}\left(\frac{L(i\omega)}{1+L(i\omega)}\right) > -\frac{1}{\alpha}$$

Note that $L(i\omega)$ denotes the linear time invariant dynamics, which can be determined using an arbitrary linear system identification technique.

5 Overview

The presented work provides a stability analysis that is not dependent on a full fraction-model. Although the method is conservative it allows for a general stability criteria. In the future, the method should be extended to comprehend non-linear control design.

References

[1]   Stéphane Lederlé, "Issues in the design of shape memory alloy actuators," *Master Thesis, Massachusetts Institute of Technology*, 2002.

[2]   Hassan K. Khalil, "Nonlinear Systems", *Prentice Hall*, 2002.

Contraction-based Control of Physical Systems

Rodolfo Reyes-Báez, Arjan van der Schaft, Bayu Jayawardhana
Jan C. Willems Center for Systems and Control, University of Groningen
{r.reyes-baez, a.j.van.der.schaft, b.jayawardhana}@rug.nl

1 Introduction

In this work, we investigate constructive control methods for affine nonlinear systems based on recent results on contraction theory [1] and related notion of control metric function discussed in [2]. In particular, we study the problem of designing a control law such that the closed-loop system is contracting and able to track a desired time-varying state trajectory.

2 Contraction based control design

Given the prolonged system

$$\delta\Sigma : \begin{cases} \dot{x} = f(x) \\ \delta\dot{x} = \frac{\partial f}{\partial x}(x)\delta x \end{cases} \tag{1}$$

where $x \in \mathbb{R}^n$ is the state, f is a smooth vector field and $\delta x \in \mathbb{R}^n$ is the first variation of the state. If there exists a symmetric positive-definite metric function $\Pi(x) \in \mathbb{R}^{n \times n}$ such that

$$\frac{\partial\Pi(x)}{\partial x}f(x) + \frac{\partial f^\top}{\partial x}\Pi(x) + \Pi(x)\frac{\partial f}{\partial x} \leq 2\lambda\Pi(x) \tag{2}$$

then all the trajectories in the state space converge exponentially to each other with rate λ, and the $x-$system in (1) is said to be contractive.

In order to find a way to extend contraction theory to systems with inputs, consider the prolonged system

$$\delta\Sigma : \begin{cases} \dot{x} = f(x) + Bu \\ \delta\dot{x} = \frac{\partial f}{\partial x}(x)\delta x + B\delta u \end{cases} \tag{3}$$

with B a constant matrix. Using the idea of control contraction metrics as in [1], consider the distance given by the Finsler-Lyapunov function $V : \mathbb{R}^n \times \mathbb{R}^n \to \mathbb{R}_{\geq 0}$, with

$$V(x, \delta x) := \delta x^\top \Pi(x)\delta x \tag{4}$$

where $\Pi(x)$ is as in (2). By taking the time derivative of the system along the trajectories of (3) and defining the variational control as $\delta u := -\rho(x)B^\top\Pi(x)\delta x$ with $\rho(x)$ a positive definite function, we get the so called *generalized differential Riccati equation* [3]

$$\frac{\partial\Pi}{\partial x}f(x) + \frac{\partial f^\top}{\partial x}\Pi(x) + \Pi(x)\frac{\partial f}{\partial x} - \rho(x)\Pi(x)BB^\top\Pi(x) = -Q(x), \tag{5}$$

when $\frac{\partial\Pi}{\partial x}B = 0$ and $Q(x)$ is an uniformly positive-definite matrix. The solution $\Pi(x)$ to (5) is obtained by means of the nonlinear eigenvalue method proposed in [4].

The tracking control law can be computed by integration of the variational control. Let $\gamma : [0,1] \to \mathbb{R}^n$ be a path connecting the reference state x_r trajectory with the state x trajectory such that

$$u(t) = u_r(t) - \frac{1}{2}\int_0^1 \rho(\gamma(s))B^\top\Pi(\gamma(s))\frac{\partial\gamma(s)}{\partial s}ds \tag{6}$$

with $u_r(t)$ is the nominal control input for the state reference trajectory x_r.

Example 1 (Water tank system) *The dynamics of this system is given by*

$$\dot{x} = \frac{C}{A}\sqrt{x} + \frac{1}{A}u \tag{7}$$

with $A, C \in \mathbb{R}_+$. The associated variational dynamics is

$$\delta\dot{x} = \frac{C}{2A\sqrt{x}}\delta x + \frac{1}{A}\delta u \tag{8}$$

Solving the equation (5) for this system with $Q(x) = \frac{1}{k}\left(1 - \frac{C}{A\sqrt{x}}\right)$ we get $\Pi(x) = 1/k$, with k been a positive constant. In this case, by taking $\rho(x) = x^2$ and by using $\gamma(s) = x_r + s(x - x_r)$, the contraction-based controller is given by

$$u = u_r - \frac{1}{Ak}x_r^2[x - x_r] - \frac{1}{Ak}x_r[x - x_r]^2 - \frac{1}{3Ak}[x - x_r]^3. \tag{9}$$

References

[1] I. R. Manchester and J.J. Slotine, "Control Contraction Metrics: Convex and Intrinsic Criteria for Nonlinear Feedback Design", CoRR, 2015.

[2] V. Andrieu, B. Jayawardhana, and L. Praly, "Transverse exponential stability and applications", IEEE Transaction of Automatic Control, to appear.

[3] A.J. van der Schaft, "A geometric approach to differential Hamiltonian systems and differential Riccati equations", in Proc. 54th IEEE Conference on Decision and Control, December 2015.

[4] Y. Kawano and T Ohtsuka, "Nonlinear eigenvalue approach to analysis of generalised differential Riccati equations", submitted, 2014.

Testosterone regulation: A new mathematical model

Hadi Taghvafard, Anton V. Proskurnikov and Ming Cao
ENTEG, Faculty of Mathematics and Natural Sciences
University of Groningen
Groningen, The Netherlands
Email: {h.taghvafard, a.v.proskurnikov, m.cao}@rug.nl

1 Introduction

The study of hormonal regulatory processes and their mathematical modeling are important for systems and control scientists because they are complex dynamical biological systems interacting through feedback(inhibitory) and feedforward(stimulatory) controls. In this paper, we deal with a mathematical model for testosterone regulation. Testosterone regulation is important for the treatment of reproductive failure, prostate cancer and critical for understanding the aging process [1].

In the endocrine system of Testosterone (Te) regulation in males, the Gonadotropin-Releasing Hormone (GnRH) and the Luteinising Hormone (LH) play essential roles. GnRH is secreted by the hypothalamus and carried to the pituitary gland in the blood through the hypophyseal portal vessels. LH, which is secreted by the pituitary gland, in turn stimulates the gonadal secretion of testosterone while testosterone inhibits the secretion of GnRH. However, there is experimental evidence that Te inhibits the production of LH as well [1],[2]. In this paper, we extend the mathematical model presented in [3] with an additional nonlinear negative feedback from Te to LH and investigate the qualitative behaviors of the new system.

2 The mathematical model

The mathematical model for the GnRH-LH-Te regulation was originally proposed by Smith [3], which in essence is the Goodwin biochemical oscillator model. In Smith's model, there is only a *single* feedback that reflects the fact that testosterone inhibits the secretion of GnRH. However, as the full physiological process of testosterone regulation is being better understood, it is believed that Te inhibits LH as well [1], [2]. This motivates us to introduce an additional negative feedback from Te to LH into Smith's model and obtain a new mathematical model for Te regulation. Namely, we examine the system as follows:

$$\begin{cases} \dot{R} = -b_1 R + f_1(T), \\ \dot{L} = g_1 R - b_2 L + f_2(T), \\ \dot{T} = g_2 L - b_3 T, \end{cases} \quad (1)$$

where R, L and T are the serum concentrations of the hormones GnRH, LH and Te respectively, b_1, b_2, b_3 are positive

constants describing clearing rates of GnRH, LH and Te respectively, and g_1, g_2 are positive constants determining the rates of secretion for LH and Te. Moreover, $f_1(\cdot), f_2(\cdot)$ are positive and decreasing functions being negative feedback from Te to GnRH and LH, respectively. Here $f_1(\cdot)$ and $f_2(\cdot)$ are smooth functions. Removing $f_2(T)$ term in the second equation, system (1) becomes the conventional Goodwin-Smith model [3]. Models of biochemical oscillators usually express the negative feedbacks in the form of Hill-type nonlinearities, i.e. $f(x) = \frac{K}{1+\beta x^\rho}$ where K, β and ρ are positive constants.

3 Qualitative behaviors

We establish the following mathematical properties for system (1):

1. A unique steady state

2. Local stability and instability of the steady state

3. Switching from a stable to an unstable equilibrium point, the system undergoes the Hopf bifurcation

4. If the steady state is unstable, then for almost any initial condition, the solution converges to a non-trivial periodic orbit.

References

[1] J. Veldhuis, "Recent insights into neuroendocrine mechanisms of aging of the human male hypothalamic-pituitary-gonadal axis. Journal of Andrology," 20(1), 1–18, 1999.

[2] C.B. Scheckter, A.M. Matsumoto, W.J. Bremner, "Testosterone administration inhibits gonadotropin secretion by an effect directly on the human pituitary," Journal of Clinical Endocrinology and Metabolism, 68, 397–401, 1989.

[3] W.R. Smith, "Hypothalamic regulation of pituitary secretion of luteinizing hormone (II): feedback control of gonadotropin secretion," Bulletin of Mathematical Biology, 42(1), 57–78, 1980.

Identifying a C-arc Medical X-ray System: A 2D-LRM Approach

Annemiek van der Maas,   Rick van der Maas,   Robbert Voorhoeve,   Tom Oomen
Department of Mechanical Engineering, Eindhoven University of Technology
P.O. Box 513, 5300 MB Eindhoven, The Netherlands
Email: { A.v.d.Maas, R.J.R.v.d.Maas, R.J.Voorhoeve, T.A.E.Oomen}@tue.nl

1 Introduction

The calibration of a C-arc based medical X-ray systems, as depicted in Fig. 1, can either be approached from a motion control point of view or using model-based approaches, [1]. The dynamical behavior of the system is depending on the operating conditions; the system is linear parameter varying (LPV). This provides a systematic framework for controller design. The aim of this work is to develop a nonparametric identification approach to obtain accurate FRFs of the X-ray system for a set of "frozen" workpoints. These accurate FRFs can be the basis for both controller design and (local) LPV modeling, [2], [3], [4].
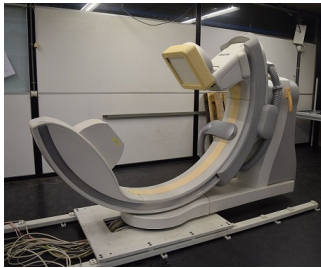
Figure 1: Philips Allura Centron interventional X-ray System.

2 Local Parametric Methods for LPV systems

State-of-the-art identification methods exploit the smoothness of a FRF over the frequencies, [2]. Here, we propose a nD-LRM to also exploit smoothness over the scheduling parameters, [5]. In particular, for traditional local parametric methods, a rational function is fitted on a local frequency window for each LTI experiment, as indicated in Fig. 2a. The proposed nD-LRM approach identifies the systems' dynamics on a local surface, as indicated in Fig. 2b.

(a) Local rational method   (b) 2D-local rational method
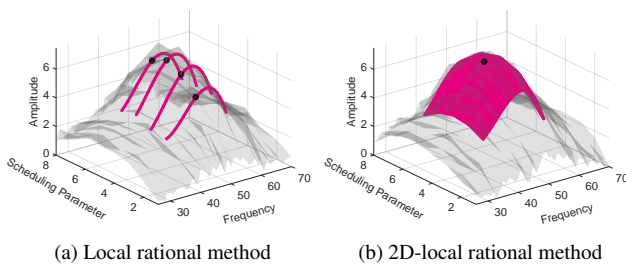
Figure 2: Proposed approach, compared to traditional LTI methods.

3 Measurement Results

The medical X-ray system in Fig. 1 has several degrees of freedom, which each cause varying dynamics. Here, a single degree of freedom has been identified at 13 individual poses of the system. The data obtained from the same identification experiments are processed using traditional local rational methods and using the proposed 2D-LRM approach, for which the resulting Bode diagrams are shown in Fig. 3.

(a) Traditional LRM   (b) Proposed 2D-LRM
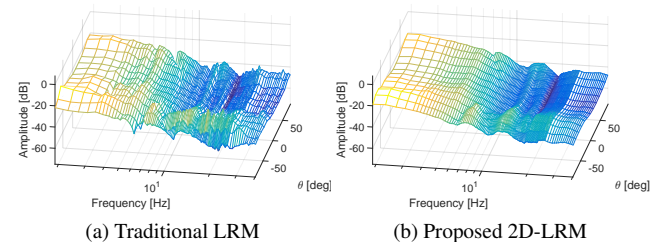
Figure 3: Comparison of traditional method with the proposed method based on measurements.

4 Conclusions

For the medical X-ray system, the proposed nD-LRM approach shows significant potential in terms of estimation quality and measurement times. With identical measurement times, smoother Bode diagrams with significantly reduced variances are obtained. These improved identified FRFs are directly usable for state estimations or controller design, [4].

References

[1]   R. van der Maas, B. de Jager, M. Steinbuch, and J. Dries, "Model-Based geometric calibration for medical X-ray systems", in *Medical Physics*, 42(11), pp. 6170-6181, 2015.

[2]   J. Schoukens, G. Vandersteen, K. Barbé, and R. Pintelon, "Nonparametric Preprocessing in System Identification: a Powerful Tool", *European Journal of Control*, 2009(3), pp. 260 - 274, 2009.

[3]   F. Felici, J. van Wingerden, and M. Verhaegen, "Subspace identification of MIMO LPV systems using a periodic scheduling sequence", *Automatica*, 43, pp. 1684 - 1697, 2007.

[4]   R. Tóth, "Modeling and Identification of Linear Parameter-Varying Systems", Springer-Verlag Berlin, 2010.

[5]   R. van der Maas, A. van der Maas, T. Oomen, "Accurate Frequency Response Function Identification of LPV Systems : A 2D Local Parametric Modeling Approach", in *Proc. of the Conf. on Decision and Ctrl.*, pp. 1465 - 1470, 2015

Improving the selection of differentially expressed genes by spatiotemporal ICA

E. Renard[1]   A. E. Teschendorff[2,3]   P.-A. Absil[1]

emilie.renard@uclouvain.be   a.teschendorff@ucl.ac.uk   pa.absil@uclouvain.be

[1] ICTEAM Institute, Université catholique de Louvain, Belgium
[2] Cancer Institute, University College London, United Kingdom
[3] PI Computational Systems Genomics, Shanghai, China

1 Introduction

We present recent work [2] where we address the problem of selecting genes differentially expressed with some phenotype of interest in large genomic datasets. We use matrix factorization to model biological and confounding sources of variation. Including those confounding factors (or CF) in the modeling is of critical importance, as not doing so may adversely affect the validity of biological conclusions drawn from the datasets. A popular approach to address batch effects is surrogate variable analysis (SVA) [3] which includes an SVD matrix factorisation step. It was subsequently shown that using an ICA can improve results. Applying ICA methods to the feature-by-sample matrix X yields a decomposition $X \approx AB^T = \sum_{k=1}^{K} A_{:,k} B_{:,k}^T$ where $A_{:,k}$ can be interpreted as the gene activation pattern of component k and $B_{:,k}$ as the weights of this pattern in the samples. In [1], a continuum between independence on columns of matrices A or B was investigated using a "spatiotemporal" ICA method. In this work, building on [1] and [3], we study how combining information from different values of the spatiotemporal parameter α may help to improve the list of selected genes.

2 Model

The model assumes that the expression level of a gene is the result of interactions between different phenomena, where one in particular is of interest (the phenotype of interest, or POI) and the others are not. Under the assumption that those interactions are linear, the model can be written as:

$$\underbrace{X_{g,:}}_{\substack{activation \\ levels \\ of\ gene\ g}} = \underbrace{f_g(\mathbf{y}^T)}_{\substack{phenotype \\ of\ interest}} + \sum_{k=1}^{K} \mathbf{A}_{gk} \underbrace{\mathbf{r}_k^T}_{\substack{confounding \\ factors}} + \underbrace{\varepsilon_g}_{noise}, \quad g = 1,...,p.$$

The CFs are represented by a basis of surrogate variables v_k that spans the same space: $\sum_k \mathbf{A}_{gk}\mathbf{r}_k^T = \sum_k \mathbf{A'}_{gk}\mathbf{v}_k^T$, where variables v_k are inferred from X and y using the spatiotemporal ICA developed in [1]. Finally, we keep as differentially expressed the genes whose activation can be better predicted including the POI in the model. To improve the stability of
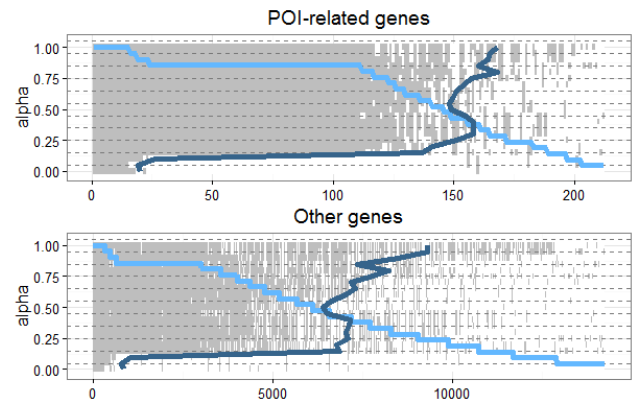
Figure 1: Grey tile: gene selected for the corresponding α value. Light blue curve: number of selections of each gene. Dark blue curve: number of genes selected for each α.

the set of selected genes, we compare all lists of selected genes obtained for different values of α. We retain as final selection the genes present in most of those lists.

3 Results

We tested our approach on breast cancer data. We compared the final list of selected genes with lists of genes known to be differentially activated with the POI. Figure 1 shows the list of selected genes for 21 equispaced values of the parameter α. The list of selected genes differs from one α value to another, but with significant overlaps. Moreover, this overlap is proportionally bigger for POI-related genes than for others genes. So returning genes selected in most of the 21 lists clearly improves the gene selection.

References

[1] E. Renard, A. E. Teschendorff, P.-A and Absil ,"Capturing confounding sources of variation in DNA methylation data by spatiotemporal independent component analysis", ESANN 2014.

[2] E. Renard, A. E. Teschendorff, P.-A and Absil ,"Spatiotemporal ICA improves the selection of differentially expressed genes", submitted to ESANN 2016.

[3] J.T. Leek, J.D. Storey, "Capturing Heterogeneity in Gene Expression Studies by Surrogate Variable Analysis", PLoS Genet 2007.

Differentiable 2D Bézier interpolation on manifolds

Pierre-Yves Gousenbourger, P.-A. Absil
ICTEAM Institute,
Université catholique de Louvain,
Avenue Georges Lemaître, 4,
B-1348 Louvain-la-Neuve, Belgium
pierre-yves.gousenbourger@uclouvain.be
absil@inma.ucl.ac.be

Paul Striewski, Benedikt Wirth
Institute for Numerical and Applied Mathematics,
University of Münster,
Einsteinstraße 62,
D-48149 Münster, Germany
paul.striewski@uni-muenster.de
benedikt.wirth@uni-muenster.de

1 Introduction

This abstract introduces bivariate interpolation of manifold-valued data points p_{ij}. The considered manifold is denoted by $\mathcal{M}$. The data points are associated with nodes $(i, j) \in \mathbb{Z}^2$ of a Cartesian grid in $\mathbb{R}^2$. In the present work, we seek a bivariate piecewise-cubic $\mathcal{C}^1$ Bézier function $\mathfrak{B} : \mathbb{R}^2 \to \mathcal{M}$ such that $\mathfrak{B}(i, j) = p_{ij}$.

Several applications motivate this problem, such as projection-based model order reduction of a dynamical system depending on a few parameters (where $\mathcal{M}$ is a Grassmann manifold) [3].

A detailed report about the work proposed here is available in [1].

2 Differentiable bivariate Bézier splines

In a Euclidean space $\mathbb{R}^r$, cubic Bézier surfaces are functions of the form

$$\beta_3(\cdot, \cdot; (b_{ij})_{i,j=0,\ldots,3}) : [0,1]^2 \to \mathbb{R}^r,$$
$$(t_1, t_2) \mapsto \sum_{i,j=0}^{K} b_{ij} B_{i3}(t_1) B_{j3}(t_2),$$

where $B_{j3}(t) = \binom{3}{j} t^j (1-t)^{3-j}$ are Bernstein polynomials. The Bézier surfaces are parameterized by *control points* $(b_{ij})_{i,j=0,\ldots,3} \subset \mathbb{R}^r$: they define how the surface spatially behaves and are interpolated when their indices i, j are both in $\{0, 3\}$.

A bivariate Bézier spline corresponds to several Bézier surfaces β_3^{mn} patched together respectively in the x and y direction. They are continuously patched if, at the shared border of the two surfaces, their control points are exactly the same. Furthermore, on the Euclidean space, a simple linear constraint on the control points suffices to achieve the differentiability of the spline.

It is quite simple to extend the definition of Bézier surfaces to manifolds (we propose different techniques leading to slightly different results), as well as the continuity condition. However, differentiability no longer holds by simply generalizing the simple Euclidean constraint. We hence introduce a modified definition of the Bézier surfaces such that we obtain $\mathcal{C}^1$ splines on any Riemannian manifold.

3 Optimal splines

We optimize the control points under the $\mathcal{C}^0$ and $\mathcal{C}^1$ constraints such that the mean square acceleration of the surface is minimized when the manifold is the Euclidean space $\mathbb{R}^r$. In other words, we minimize the objective function

$$f[b_{ij}^{mn}] = \sum_{m=0}^{M-1} \sum_{n=0}^{N-1} \hat{F}[\beta_3^{mn}]$$

where $\hat{F}[\beta_3^{mn}]$ is the energy of the Bézier function on the patch (m, n). In $\mathbb{R}^r$, in view of the translation invariance of the problem, the optimal control points can be expressed as affine combinations of the data points. We generalize this result to the manifold setting as a linear expression in a given tangent space, using a technique close to the one developed in [2].

We illustrate our method with surfaces computed on several manifolds such as the sphere or the special orthogonal group $SO(3)$ in order to interpolate rigid body positions.

References

[1] P.-A. Absil, P.-Y. Gousenbourger, P. Striewski, B. Wirth. *Differentiable piecewise-Bézier surfaces on Riemannian manifolds*, 2016. Technical report UCL-INMA-2015.10-v1, Université catholique de Louvain.

[2] A. Arnould, P.-Y. Gousenbourger, C. Samir, P.-A. Absil, M. Canis. *Fitting Smooth Paths on Riemannian Manifolds: Endometrial Surface Reconstruction and Preoperative MRI-Based Navigation*, 2015. In F. Nielsen and F. Barbaresco, editors, GSI2015, pages 491498. Springer International Publishing.

[3] L. Pyta, D. Abel. *Model based control of the incompressible Navier-Stokes-equations using interpolatory model reduction*, 2015. To appear in the proceedings of the 54th IEEE Conference on Decision and Control.

In-eye Optical-Coherence-Tomography-based proximity control

Y.G.M. Douven, M.J.G. van de Molengraft, M. Steinbuch
Control Systems Technology Group, Eindhoven University of Technology
P.O. Box 513, 5600MB Eindhoven, the Netherlands. E-mail: y.g.m.douven@tue.nl

1 Introduction

Vitreoretinal surgery addresses sight-threatening conditions on the back of the eye. Since structures on the back of the eye are often only a few micrometers, the technical demands placed on the surgeon by these procedures are very high. Robotic systems can provide a distinct and positive alteration in patient outcome when they can show to really enhance the surgeon's capability by providing both physical and mental assistance. The back of the eye is viewed through a stereo-microscope, which provides a three dimensional image to the physician. Still, determining distance between instrument-tip and retina proves to be very hard.

2 Control scheme for robot-assisted safety

Until now, the focus of surgical robotic systems has been on precision. To further improve patient safety and surgical performance, new concepts for (semi-)automated robot-assisted surgeries are being developed. These concepts incorporate sensor guarded and sensor guided motions. From a control point of view, this leads to a cascaded control loop that exists of three layers (see Figure 1). The innermost layer (denoted in blue) ensures closed-loop stability of a telemanipulator system. The complete loop is closed by the surgeon (denoted by the orange feedback line). The green loop is established by adding a local sensor to provide fast and reliable information about the distance between the instrument and the retina. This information is primarily used to prevent accidental penetration of the retinal surface. The third layer (denoted in red) combines all measurements of the environment into a world model of the inside of the eye.
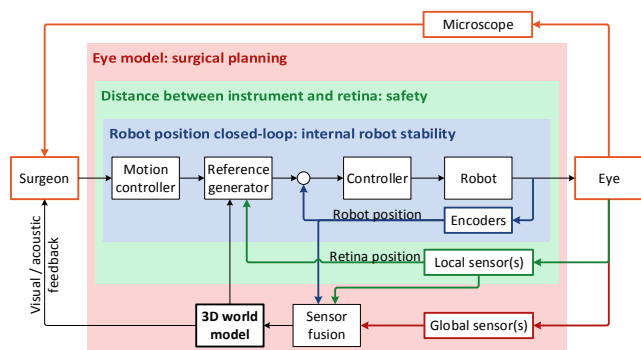
Figure 1: Sensor integration in the surgical system.

3 Optical Coherence Tomography probe

Optical Coherence Tomography (OCT) [1] is a sensor solution based on interference between two light paths, a reference path and a path that reflects on the to be measured sample. An interference spectrum is measured and processed to obtain a one-dimensional depth image (A-scan) of the sample. To remove optical disturbances, the measured spectrum is apodized [2] using a custom apodization spectrum. Generally, a spectrum measurement of air would include all optical disturbances inside the probe and reference stage. But these disturbances can change over time. Since the sensor is used in a closed-loop implementation, it is not preferred to interrupt surgery for a new apodization measurement. Therefore a low-pass filter with a time constant of 60s is applied to the measured spectra. It is assumed that the probe will move sufficiently, so that the sample is filtered out. Hence the apodization will not remove the sample.

To accurately measure the distance between the instrument tip and the retina, the position of the OCT measurement window should be known. The OCT probe is rigidly connected to the instrument, and hence the distance between probe tip and instrument tip is known. By changing the reference stage length by a known value, the measurement window can be shifted to include the probe tip. The offset between probe tip and the position of the OCT measurement window can then be calculated. This calibration step should be performed every few seconds. It only takes a few milliseconds, and hence the closed-loop safety control is not undermined.

4 Virtual bounds

As a proof of concept, a virtual bound is implemented on a paper phantom eye. The distance to the paper is calculated from the A-scan and sent to the robot. When the distance to the paper is closer than the bound, the reference to the slave robot is reset to the bound value, and the telemanipulation setup is essentially being decoupled in one direction.

References

[1]   Yaqoob, Z., Wu, J., & Yang, C. (2005). Spectral domain optical coherence tomography: a better OCT imaging strategy. BioTechniques, 39

[2]   Marks, D., Carney, P. S., & Boppart, S. a. (2004). Adaptive spectral apodization for sidelobe reduction in optical coherence tomography images. Journal of Biomedical Optics, 9

Optimization-based iterative learning control for robotic manipulators

Armin Steinhauser, Goele Pipeleers and Jan Swevers
Division PMA, Department of Mechanical Engineering
Katholieke Universiteit Leuven
Celestijnenlaan 300B, B-3001 Heverlee, Belgium
Email: armin.steinhauser@kuleuven.be

1 Introduction

Iterative learning control (ILC) has been intensely researched for over 30 years to improve the performance of repetitive processes [1]. Most ILC algorithms use a known, but potentially inaccurate model to compute the next iteration's control signal. The majority of publications on the topic of ILC considers linear-time-invariant or linear-parameter-varying systems, although many applications require nonlinear models to represent the system's dynamics sufficiently. An example for such an application is a robotic manipulator executing the same task repeatedly.

2 Approach

This paper adapts a general optimization-based ILC approach for arbitrary nonlinear systems [2] to be used for manipulators with n degrees-of-freedom in a closed-loop configuration. Having derived the nonlinear inverse dynamics $\mathbf{f}$, the closed loop can be written as

$$\mathbf{f}(\mathbf{y}_i(t), \mathbf{p}) = \mathbf{u}_i(t) = \mathbf{c}(\mathbf{r}_i(t), \mathbf{y}_i(t))$$

with iteration index i, the controller function $\mathbf{c}$, output $\mathbf{y} \in \mathbb{R}^{n \times 1}$, parameter vector $\mathbf{p}$, input $\mathbf{u} \in \mathbb{R}^{n \times 1}$ and reference $\mathbf{r} \in \mathbb{R}^{n \times 1}$. Existing ILC approaches for robot manipulators [3] use approximations of this nonlinear model, e.g. obtained by linearizing $\mathbf{f}$ along a desired trajectory $\mathbf{y}_d$. In this research we consider the full nonlinear system dynamics and two possible modelling errors: unmodelled dynamics and model parameter mismatch. The developed learning approach consists of two steps that are executed at each iteration, as shown in Fig. 1. First, a model correction is

computed by processing the torque and joint angular position measurements, $\mathbf{u}_{i,\mathrm{m}}(t)$ and $\mathbf{y}_{i,\mathrm{m}}(t)$, respectively. This correction can be parametric or nonparametric such that the above mentioned modelling errors can be compensated for, and is found by solving the optimization problem

$$\min_{\boldsymbol{\varepsilon}_{i+1}} \quad \|\mathbf{u}_{i,\mathrm{m}} - \mathbf{f}(\mathbf{y}_{i,\mathrm{m}}, \mathbf{p}, \boldsymbol{\varepsilon}_{i+1})\|$$
$$\text{s.t.} \quad \underline{\boldsymbol{\varepsilon}} \leq \boldsymbol{\varepsilon}_{i+1} \leq \overline{\boldsymbol{\varepsilon}}$$

with the correction term $\boldsymbol{\varepsilon}$. The resulting correction is then used in the second step, the model inversion, to compute a reference update $\Delta\mathbf{r}_i$ by solving another optimization problem

$$\min_{\Delta\mathbf{r}_{i+1}} \quad \|\mathbf{c}(\mathbf{y}_d + \Delta\mathbf{r}_{i+1}, \mathbf{y}_d) - \mathbf{f}(\mathbf{y}_d, \mathbf{p}, \boldsymbol{\varepsilon}_i)\|$$
$$\text{s.t.} \quad \underline{\mathbf{y}} \leq \mathbf{y}_d + \Delta\mathbf{r}_{i+1} \leq \overline{\mathbf{y}}$$

with $\mathbf{y}_d$ being the iteration independent desired output and the resulting reference $\mathbf{r}_{i+1} = \mathbf{y}_d + \Delta\mathbf{r}_{i+1}$, which is finally applied as the next iteration's input to the closed loop. This research focuses on the efficient solution of the optimization problems and the trade-off between convergence speed and robustness. The developed ILC approach is validated both in simulation and experimentally for a 6 degrees-of-freedom robotic manipulator.

3 Acknowledgements

References

[1]   D. A. Bristow, M. Tharayil, and A. G. Alleyne, "A Survey of Iterative Learning Control: a learning based method for high-performance tracking control," *IEEE Control Syst. Mag.*, vol. 26 (3), pp. 96–114, 2006.

[2]   M. Volckaert, M. Diehl, and J. Swevers, "Generalization of norm optimal ILC for nonlinear systems with constraints," *Mechanical Systems and Signal Processing*, 39 (1-2), pp. 280–296, 2013.

[3]   M. Norrlöf, "An Adaptive Iterative Learning Control Algorithm With Experiments on an Industrial Robot," *IEEE Trans. Robot. Autom.*, vol. 18 (2), pp. 245–251, 2002.
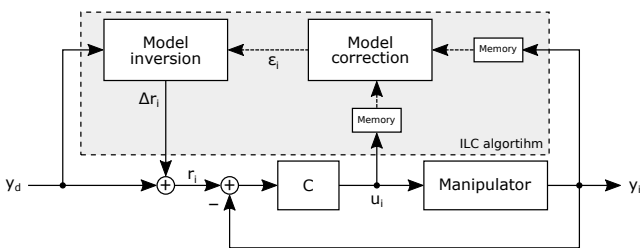
Figure 1: Closed-loop configuration and the ILC components

A direct force-reflecting two-layer approach for stable bilateral teleoperation with time delays

Dennis Heck[1], Alessandro Saccon[2], Ruud Beerens[3], Henk Nijmeijer[4]
Dynamics and Control
Eindhoven University of Technology
P.O. Box 513, 5600 MB Eindhoven
the Netherlands
{ [1]d.j.f.heck, [2]a.saccon, [3]r.beerens [4]h.nijmeijer } @tue.nl

1 Introduction

This work proposes a controller for direct force-reflection to guarantee passivity of a teleoperator in the presence of time delays. Numerous architectures have been proposed over the past thirty years to control bilateral teleoperators with communication delays (see e.g., [1]). These architectures can be classified in bilateral motion synchronization schemes (master and slave controllers implement an as-stiff-as-possible coupling between the two devices) and direct force-reflection schemes (the slave controller mimics the operator action, while the master controller reflects the slave-environment interaction). The focus is on the latter, since these architectures seem to have the most potential in terms of performance. Direct force-reflecting architectures, however, suffer from contact instabilities that manifest itself as a violent recoiling of the master device, such that the operator is not able to make stable contact of the slave with the remote environment. Communication delays play a significant role in this unstable behavior. We therefore propose a two-layer architecture designed according to the direct force-reflection philosophy, such that stable slave-environment interaction can be achieved.

2 The 2-layer architecture

The architecture is structured with an (inner) *performance layer* and an (outer) *passivity layer*. In the performance layer, any traditional controller for bilateral teleoperation can be implemented. Here, we use the Position/Force-Force controller. The passivity layer guarantees that, from the operator and environment perspective, the overall teleoperator is passive: the amount of energy that can be extracted from the teleoperator is bounded from below and the rate of increase of the stored energy in the teleoperator is bounded by (twice) the environment and operator supplied power. Passivity is ensured by modulating the performance layer outputs and by *injecting a variable amount of damping* via an energy-based logic that follows the innovative principle of energy duplication and takes into account the detrimental effects of time delays.

3 Experiments

The effectiveness of the proposed architecture is experimentally verified by implementing it on a physical setup. The round-trip communication delay is 100 ms, while the slave is in free motion first, and then makes and breaks contact with a hard environment. Without the passivity layer applied, stable slave-environment interaction could not be achieved due to recoiling of the master device. With the proposed 2-layer architecture applied, stable contact is achieved, see Figure 1. Moreover, the injected damping is low in free motion, such that the operator effort is low. When the slave makes contact with the environment, the architecture prevents active behavior by temporarily increasing the damping gains.
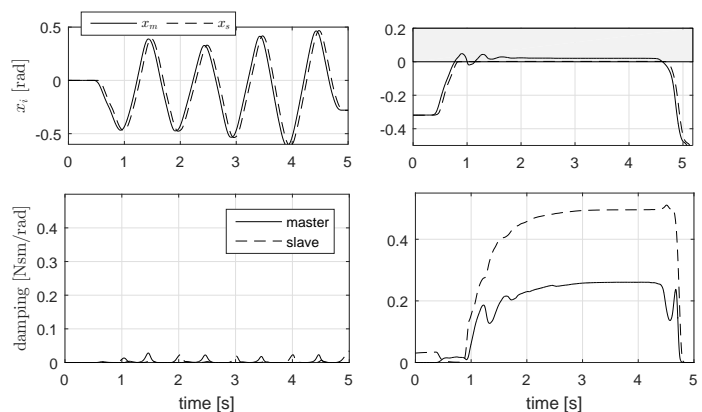
Figure 1: Master- and slave positions (x_m and x_s, resp.) in free motion (top left) and contact (top right). The damping gains are low in free motion (bottom left) and increase during impact and contact (bottom right), to prevent active behavior.

References

[1]   P. Hokayem and M. Spong, "Bilateral teleoperation: An historical survey", *Automatica*, vol. 42, pp. 2035-2057, 2006

Task assignment for robotic networks with limited communication range

Xiaoshan Bai
Faculty of Mathematics and Natural Sciences
University of Groningen
Groningen 9747 AG, The Netherlands
xiaoshan.bai@rug.nl

Ming Cao
Faculty of Mathematics and Natural Sciences
University of Groningen
Groningen 9747 AG, The Netherlands
m.cao@rug.nl

1 Abstract

The robotic task assignment problem is important in applications such as transport logistics and distribution systems [1]. We investigate this problem under the setting where $m > 1$ initially randomly distributed robots need to visit $n > 1$ dispersed target points as fast as possible. The robots know the position of every target and can communicate with other robots that are within their limited communication range.

Generally, the multi-robot task assignment problem can be solved by either centralized or distributed algorithms [2]. Centralized algorithms can obtain the optimal solution by choosing one robot as the leader to collect all necessary data and make decisions for the other robots [3], while distributed ones let each robot make its own plan based on the available local information [4]. In our setup, one robot does not know the positions of those robots that are out of this robot's communication range. As the robots move around, however, the robotic network may connect over time. To solve the task assignment problem, we propose two kinds of hybrid algorithms borrowing advantages from both centralized and distributed algorithms.

The first kind of task assignment algorithms is the single traveling salesman algorithm (STSA), which is inspired by [5]. STSA lets each robot precalculate an optimal closed tour connecting in order the n targets as the traveling salesman problem (TSP). Since every robot has the same information of the target positions, the obtained TSP tours for all the robots are the same if all of them utilize the same exact task assignment algorithm. Then, every robot moves towards the nearest target on the TSP tour. Based on different cooperative strategies for robots within communication range, we design the follower-based STSA (STSA-F), the jump-based STSA (STSA-J) and the division-based STSA (STSA-D). For robots that have not communicated with any other robots, they move along the TSP tour to find the next available target after reaching a target.

Extending the STSA, we get the multiple traveling salesman algorithm (MTSA). First, MTSA divides the n target points into m subsets and connects the targets within each subset in an optimal TSP tour. Then, each robot chooses the nearest TSP tour and visits the targets on the tour in the clockwise direction. If one TSP tour is chosen by two robots, they negotiate to resolve the conflict based on their distances to the nearest target on the TSP tour when they can communicate with each other.

The two kinds of algorithms assign tasks as described above when the whole communication network is initially unconnected. Once it is connected during the robots' movement, we choose that robot with the most 1-hop neighbours as the leader to assign the unvisited targets to all the robots in a centralized manner based on the position information of the robots and the unvisited targets. If two or more robots have the same number of the most 1-hop neighbours, we randomly choose one as the leader.

We compare the proposed algorithms with a greedy task assignment algorithm (GTAA), where robots always move to the nearest available target. Simulation results show that the STSA-D obtains satisfying solutions and longer communication range does not necessarily lead to better performance.

References

[1]   B. Chen and H. H. Cheng, "A review of the applications of agent technology in traffic and transportation systems," *Intelligent Transportation Systems, IEEE Transactions on*, vol. 11, no. 2, pp. 485–497, 2010.

[2]   B. P. Gerkey and M. J. Matarić, "A formal analysis and taxonomy of task allocation in multi-robot systems," *The International Journal of Robotics Research*, vol. 23, no. 9, pp. 939–954, 2004.

[3]   H.-L. Choi, L. Brunet, and J. P. How, "Consensus-based decentralized auctions for robust task allocation," *Robotics, IEEE Transactions on*, vol. 25, no. 4, pp. 912–926, 2009.

[4]   N. Michael, M. M. Zavlanos, V. Kumar, and G. J. Pappas, "Distributed multi-robot task assignment and formation control," in *Robotics and Automation, 2008. ICRA 2008. IEEE International Conference on*.   IEEE, 2008, pp. 128–133.

[5]   S. L. Smith and F. Bullo, "Monotonic target assignment for robotic networks," *Automatic Control, IEEE Transactions on*, vol. 54, no. 9, pp. 2042–2057, 2009.

Towards a navigation system for an autonomous UAV in indoor environment

Thoa Mac Thi[1,2], Cosmin Copot[1], Trung Tran Duc[2], and Robin De Keyser[1]

[1]Department of Dynamics Systems and Control (DySC), Ghent University, Belgium.
[2]School of Mechanical Engineering, Hanoi University of Science and Technology, Vietnam.
Thoa.MacThi@UGent.be

1 Introduction

In recent years, research interest in unmanned aerial vehicles (UAVs) has emerged due to their potential use for a wide range of applications such as: smart flying sensor, formation control of unmanned ground vehicles (UGVs) using an UAV and habitat mapping. In order to accomplish the above mentioned missions, a prerequisite requirement is that the UAV should be able to implement real-time autonomous navigation. Whereas most of the proposed approaches are suitable for outdoors, only few techniques have been developed for indoor environments. In this paper, a solution using only onboard visual and inertial sensing which enables an UAV to operate indoors is proposed. The approach comprises three key components: pattern-based localization, IMU data process, designed path planning and controller. This methodology opens new possibilities for the UAV to perform autonomous navigation.

2 System setup

The proposed approach consists of three major components running on a laptop connected to the UAV (Ar. Drone 2.0) via wireless communication as shown in Figure 1. The first component is the pattern based localization which allows Ar. Drone 2.0 to determine its location and orientation in a working space. The second component is IMU data process which transmits and receives signals between Ar. Drone 2.0 and the ground station. The last component is a cascade control which guides the drone to follow the desired trajectories.

3 Path planning and control design

The paths are obtained base on modified A*, D* and Potential Fields algorithms. To perform experiments, a cascade control is designed (Figure 2) such that the drone follows the generated trajectories. There are two parts of the cascade controller: inner-loop controller and outer-loop controller. The inner-loop controller is performed inside the drone as a black-box. The outer-loop controller is designed to implement position control. The localization process provides the current the drone pose in world coordinate based on the ground patterns. The obtained free-collision path is sent to the controller by a list of way-points [1].
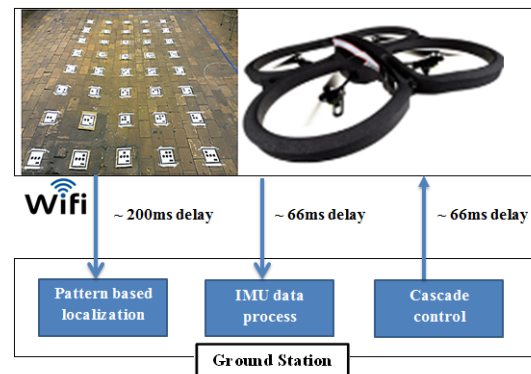
Figure 1: The proposed navigation approach of an AR.Drone 2.0
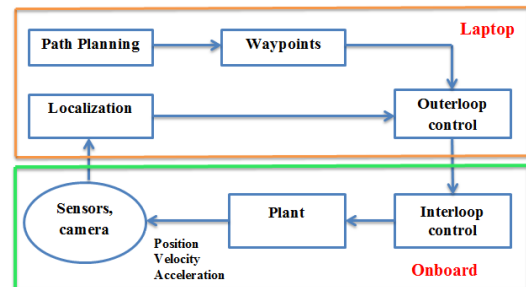
Figure 2: The proposed cascade controller of an AR.Drone 2.0

4 Conclusion

In this study, we have presented an indoor flight approach for a low-cost commercial AR. Drone 2.0 using only onboard visual and internal sensing. The real-time experiment demonstrates the feasibility of the proposed strategy which opens an autonomous navigation possibility for the drone in indoor environment.

References

[1] Mac. T.T, Copot. C, Hernandez. A, De Keyser R, Improved Potential Field Method for Unknown Obstacle Avoidance Using UAV in Indoor Environment, IEEE 14th International Symposium on Applied Machine Intelligence and Informatics, Herlany, Slovakia, pp. 345- 350, 2016.

Formation feasibility of networked heterogenous systems with drift terms

Zhiyong Sun and Brian D. O. Anderson

Research School of Engineering, The Australian National University, Canberra ACT 2601, Australia

{zhiyong.sun, brian.anderson}@anu.edu.au

1 Introduction

In this paper we consider the problem of determining formation feasibility for networked multiple agents when individual agents are modelled by affine nonlinear control systems with drift terms, and different agents may have *different* dynamics (i.e. heterogenous systems). By a formation graph is meant an undirected graph whose nodes represent individual agents with kinematics or dynamics constraints, and whose edges capture inter-agent constraints that should be satisfied to maintain a desired formation. We will give a feasibility condition as well as formation abstraction control to generate feasible motions for a group of heterogenous agents to achieve the desired formation maintenance task.

2 Formation feasibility and application

We assume that each individual agent's dynamics are described by the following affine nonlinear control system

$$\dot{p}_i = f_{i,0} + \sum_{j=1}^{l} f_{i,j} u_{i,j} \qquad (1)$$

where $p_i \in \mathbb{R}^{n_i}$ is the state of agent i, n_i is the number of the state, $f_{i,0}$ is a drift term, and $u_{i,j}$ is the control associated with the vector field $f_{i,j}$. Such affine control system (1) with the drift term is very general to describe many different types of control systems, including control systems with underactuation property or nonholonomic constraints. For the system with drifts (1), we could write a corresponding equation with equivalent constraints

$$\omega_{i,j}(p_i)\dot{p}_i = q_{i,j}, j = 1, \cdots, n_i - l$$

where $\omega_{i,j}$ is a *row* covector in the dual space $(\mathbb{R}^{n_i})^\star$ and the parameter $c_{i,j}$ can be obtained by the drift term $f_{i,0}$. We collect all the row vectors $\omega_{i,j}$ in a compact form by writing them as $\omega_{K_i}(p_i)\dot{p} = q_{K_i}$. By collecting all the kinematics constraints for all the agents, one can obtain $\omega_K = [\omega_{K_1}^T, \omega_{K_2}^T, \cdots, \omega_{K_n}^T]^T, q_K = [q_{K_1}^T, q_{K_2}^T, \cdots, q_{K_n}^T]^T$.

A family of formation constraints C is indexed by the edge set, as $C = \{c_{ij}\}_{(v_i, v_j)} \in E$. For each edge (v_j, v_j), c_{ij} is a vector function defining the formation constraints between agents i and j; the constraint is enforced if $c_{ij}(p_i, p_j) = 0$.

Formation feasibility means that the constraints are satisfied along the formation trajectories. We collect the formation constraints for all the edges and define an overall formation constraint denoted by $C_E = \mathbf{0}$, where $C_E = [\cdots, c_{ij}^T, \cdots]^T$. By doing this, one can derive $\frac{d}{dt}C_E = \mathscr{L}_P C_E + \frac{\partial C_E}{\partial t} = 0$, where $\mathscr{L}_P C_E$ denotes the Lie derivative of C_E along P (the column vector which collects all agents' vector states). By grouping all the constraints for all the edges and write down $T_F = -[(\frac{\partial C_1}{\partial t})^T, (\frac{\partial C_2}{\partial t})^T, \cdots, (\frac{\partial C_m}{\partial t})^T]^T$, we can reexpress the above equation for formation constraint as $w_F(P) = T_F$, where $w_F(P) := \mathscr{L}_P C_E$.

The motion feasibility problem can be described as the solution problem to the following equation

$$\Omega(P) = T \qquad (2)$$

where $\Omega = [\omega_F^T, \omega_K^T]^T$, and $T = [T_F^T, q_K^T]^T$.

Theorem 1 *The undirected formation has feasible motions if the above equation* (2) *has solutions, or equivalently if T belongs to the range of Ω.*

Remark 1 *For time-invariant formation we have $\frac{\partial C_E}{\partial t} = 0$ and thus $T_F = \mathbf{0}$; in the drift-free model case there holds $q_{i,j} = 0$ and thus $q_K = \mathbf{0}$. In such special cases one has $T = \mathbf{0}$, and Theorem 1 reduces to Theorem 4.1 of [1].*

Application to coordination control of constant-speed agents: Dynamics of constant-speed agent can be described by (1). Such control problem has been discussed in [2], [3] etc. The above obtained formation feasibility condition (as well as the abstraction control concept [4]) provides more insights to coordinate such networked heterogenous agents with constant-speed constraints. More results will come in a forthcoming paper.

References

[1]   P. Tabuada, G. J. Pappas, and P. Lima, "Motion feasibility of multi-agent formations," *Robotics, IEEE Transactions on*, vol. 21, no. 3, pp. 387–392, 2005.

[2]   R. Sepulchre, D. Paley, N. E. Leonard, *et al.*, "Stabilization of planar collective motion with limited communication," *Automatic Control, IEEE Transactions on*, vol. 53, no. 3, pp. 706–719, 2008.

[3]   Z. Sun, G. S. Seyboth, and B. D. O. Anderson, "Collective control of multiple unicycle agents with non-identical constant speeds: Tracking control and performance limitation," in *Proc. of 2015 IEEE Multi-Conference on Systems and Control (MSC)*, pp. 1361–1366, IEEE, 2015.

[4]   C. Belta and V. Kumar, "Abstraction and control for groups of robots," *Robotics, IEEE Transactions on*, vol. 20, no. 5, pp. 865–875, 2004.

Predictor-based Controller Design under Denial-of-Service

Shuai Feng, Pietro Tesi
ENTEG, Faculty of Mathematics and Natural Sciences, University of Groningen
Nijenborgh 4, 9747 AG Groningen , The Netherlands
Email: {s.feng, p.tesi}@rug.nl

1 Introduction

Owing to many advances in computing and communication technologies, recent years have witnessed a growing interest towards cyber-physical systems (CPSs), *i.e.*, systems where physical processes are monitored by embedded computers through networks[1]. The networked control architecture, on the other hand, exposes the system to malicious attacks.

Our research deals with Denial-of-Service (DoS) attacks. DoS attacks affect communication between process and controllers, *e.g.* it may disrupt sensor-controller channel, controller-actuator channel or both channels. In this work, we consider controller-actuator collocation scenario as shown in Figure 1, *i.e.* DoS attacks only presents in sensor-controller channel, under which our control objective is to maintain closed-loop stability.
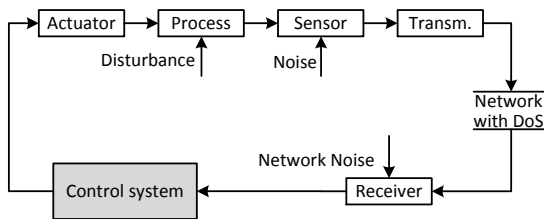
Figure 1: Controller-actuator collocation under DoS attack

2 Predictor-based controller design against DoS

We propose a predictor-based controller, as shown in Figure 2, consisting of a finite-time observer, a predictor and feedback gain. Both observer and predictor are equipped with state-resetting mechanism and the resettings are triggered when new measurements are available (in the absence of DoS attack). In the presence of DoS attack, the controller feeds the actuators with predicted control input.

Under such control scheme, we significantly improve system robustness against DoS. One point to mention is that robustness depends on observability of process [2].

3 Virtual one-step observability

In order to design a maximally robust controller, *i.e.* remove the impact of process observability on robustness,
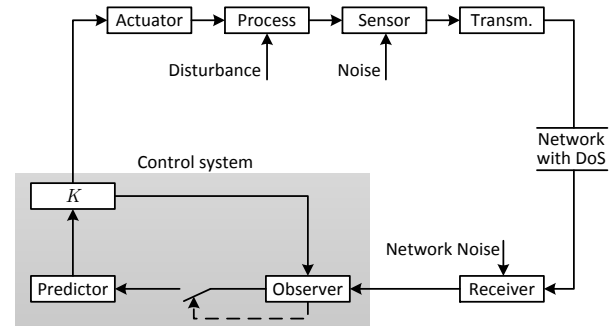
Figure 2: Control configuration with predictor-based controller

we propose virtual one-step observation system as shown in Figure 3. The network communication protocol is acknowledgment-based. A predictor-based controller with state resetting forms our control system.

With the control configuration in Figure 3, we maximize the amount of DoS that one system can tolerate for a general class of DoS signals [2].
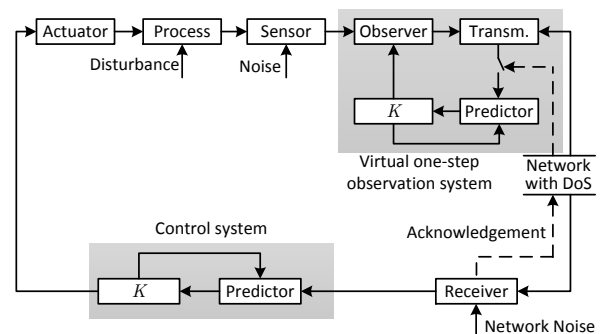
Figure 3: Virtual one-step observability control architecture

References

[1]   C. De. Persis and P. Tesi, "Input-to-stabilizing control under Denial-of-Service," *IEEE Transactions on Automatic Control*, 2015. DOI: 10.1109/TAC.2015.2416924.

[2]   S. Feng and P. Tesi, "Resilient control under Denial-of-Service: Robust Design" submitted to *Automatica*.

Issues of carrier aggregation intermodulation distortions in LTE-Advanced System

NIYONKURU Leonidas
Vrije Universiteit Brussel
Niyonkuru.Leonidas@vub.ac.be

Leo VAN BIESEN
Vrije Universiteit Brussel
lvbiesen@vub.ac.be

Gerd VANDERSTEEN
Vrije Universiteit Brussel
Gerd.Vandersteen@vub.ac.be

1 Background

Increasing transmission speed has always been the target for any telecommunication system. For that purpose, LTE-Advanced adopted components carrier aggregation. Up to 5 components carrier can be aggregated (in 3GPP Release 10), and with 20 Mhz bandwith for each component, a total bandwith of 100 Mhz can be reached. 3GPP Release 13 will allow up to 32 components carrier aggregation. On the other hand, power amplifier's high efficiency is only possible in the nonlinear operation mode. But carrier aggregated signal amplification in that mode leads to intermodulation products. This paper focuses on intermodulation of carrier aggregated components.

2 Introduction

As stated above, nonlinear amplification results in intermodulation of carrier aggregated signals. Based on 3GPP Release 12, we will list all the possible carrier aggregations and analyze all their intermodulations. We will answer to the following questions:

-What are the frequencies of intermodulation products?

-Can transmission intermodulation products fall in the reception frequencies of considered band? If they can, they will cause interference with the received signal. This can happen for the uplink transmission as well as for the downlink transmission.

-For a given eNodeB(Base Station for LTE-Advanced), can the downlink transmission intermodulation products fall in the reception frequency bands of other LTE/LTE-A bands?

3 Methodology

Intermodulation products are calculated from band aggregations listed by 3GPP Release 12 and for a given transmission direction and the direction in which influence of intermodulation products is analyzed. The number of aggregated bands is limited to three, and the order of intermodulation products is also limited to three. The following figure illustrates the interference of uplink transmission intermodulation products with the reception frequencies. The example is given for carrier aggregation of band 4 and band 17 in uplink transmission.
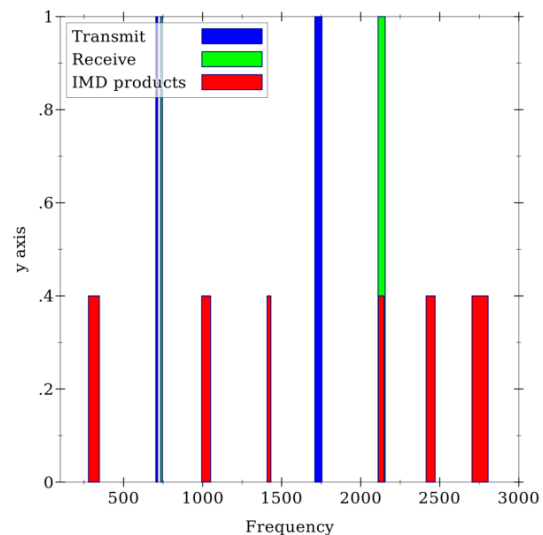
Figure 1: Bands 4 and 17 and their IMD products, transmission up

4 Results and Discussion

We were able to calculate the intermodulation products of aggregated bands in LTE-Advanced system. The calculation showed that the answer for both question in the introduction section is positive. There are intermodulation products which fall in reception frequencies of a given band. This will put more requirements on linearity of power amplifiers both in uplink and downlink transmission.

5 Conclusion

Carrier aggregation is an attractive technique but his practical implementation remains difficult due to, among other things, intermodulation distortions. The above example illustrated that phenomena with only 2 bands aggregation. 3GPP Release 13 will allow up to 32 carriers, and there will be more intermodulation products.

6 Aknowlegment

On stability and stabilization of nonlinear systems

Alina Doban
Eindhoven University of Technology
a.i.doban@tue.nl

Mircea Lazar
Eindhoven University of Technology
m.lazar@tue.nl

1 Abstract

We consider the stability analysis and feedback stabilization of nonlinear continuous time dynamical systems that arise in biomedical and biological applications. The stability analysis problem for the underlying classes of systems translates into computing domains of attraction of equilibria of interest. The feedback stabilization problem is aimed at either enlarging the domain of attraction(DOA) or at destabilizing one equilibrium and stabilizing another. The tool for answering the problems above consists of Lyapunov functions (LFs). It is well known that finding an explicit form of a LF for general nonlinear systems is a very difficult problem, still not systematically tackled for general system classes.

For evolutionary models, such as those describing tumor growth of HIV, one can construct, as stemming from Zubov's method, rational LFs. These functions can be used to estimate nonconservative DOAs. In [1], a recursive procedure which generates a rational control LF and a polynomial feedback stabilizer for nonlinear systems was proposed. For polynomial systems, it was shown that the existence of a polynomial feedback stabilizer is guaranteed by the existence of a rational control LF. The proposed procedure is illustrated in Figure 1 for a classical Lotka–Voltera tumor growth model [1]. For that system the problem of enlarging
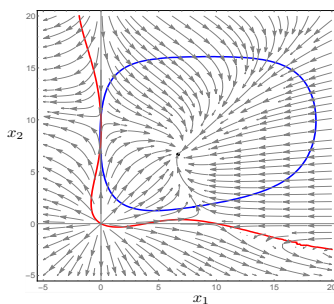
Figure 1: DOA estimate and vector fields of the closed loop tumor system.

the tumor dormancy equilibrium via feedback stabilization was considered.

For nonevolutionary models, derived via biochemical reactions which lead to rational (Hill terms) systems, the procedures based on the rational (control) LF are conservative, due to required polynomial approximations. An approach for computing Lyapunov functions for nonlinear continuous–time differential equations is developed via a

new, Massera–type construction [2],

$$W(x(t)) := \int_{t}^{t+d} V(x(\tau))\mathrm{d}\tau.$$

This construction is enabled by imposing a finite–time criterion on the integrated function V. By means of this approach, we relax the assumptions of exponential stability on the system dynamics, while still allowing integration over a finite time interval. The resulting Lyapunov function can be computed based on any $\mathcal{K}_\infty$–function of the norm of the solution of the system. In addition, we show how the developed converse theorem can be used to construct an estimate of the domain of attraction. We consider the Hypothalamus-Pituitary-Adrenal glands (HPA) axis system, defined by

$$
\begin{aligned}
\dot{x}_1 &= \left(1 + \xi \frac{x_3^\alpha}{1+x_3^\alpha} - \psi \frac{x_3^\gamma}{x_3^\gamma + \tilde{c}_3^\gamma}\right) - \tilde{w}_1 x_1 \\
\dot{x}_2 &= \left(1 - \rho \frac{x_3^\alpha}{1+x_3^\alpha}\right) x_1 - \tilde{w}_2 x_2 \\
\dot{x}_3 &= x_2 - \tilde{w}_3 x_3.
\end{aligned}
\tag{1}
$$

The HPA axis is a system which acts mainly at maintaining body homeostasis by regulating the level of cortisol. The three hormones involved in the HPA axis are the CRH (x_1), the ACTH (x_2) and the cortisol (x_3). Disorders of the HPA
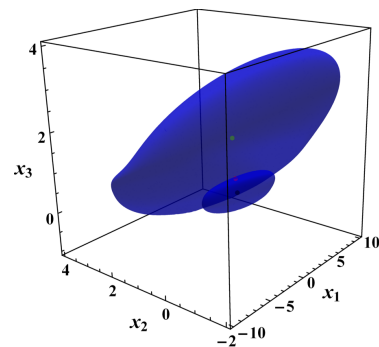
Figure 2: DOA estimates of the two stable equilibria of the HPA system.

axis lead to bistability, corresponding to stable hypocortisolic and hypercortisolic equilibria, with DOAs shown in Figure 2.

References

[1] A. I. Doban and M. Lazar, "Feedback stabilization via Rational Control Lyapunov Functions," in *54th IEEE Conference on Decision and Control (CDC)*, Osaka, Japan, 2015, pp. 1148–1153.

[2] ——, "Computation of Lyapunov functions for nonlinear differential equations via a Massera-type converse," submitted to the 15th annual European Control Conference (ECC), 2016.

Sampling–based stability verification

Ruxandra Bobiti and Mircea Lazar
Department of Electrical Engineering
Technische Universiteit Eindhoven
P.O. Box 513, 5600 MB Eindhoven
The Netherlands
Email: `r.v.bobiti@tue.nl, m.lazar@tue.nl`

1 Introduction

The problem of stability verification for discrete–time non-linear systems via Lyapunov functions is considered. Depending on the system dynamics, the candidate Lyapunov function and the set of initial states of interest, one generally needs to handle large, possibly non–feasible optimization problems. To avoid such problems, we put forward a constructive sampling–based approach to stability analysis.

The proposed approach verifies the decrease condition for a candidate Lyapunov function on a finite sampling of a bounded set of initial conditions and then it extends the validity of the Lyapunov function to an infinite set of initial conditions by exploiting continuity properties. This result involves no apriori analytic description of the continuity property and it is based on multi–resolution sampling, to perform efficient state–space exploration. Moreover, the stability verification is decentralized in the sampling points, which makes the method scalable to any degree.

2 Main result

Verification of an inequality of the type $F(x) \leq 0$ for all $x \in \mathcal{S}$, where $F : \mathbb{R}^n \to \mathbb{R}$ and $S \subset \mathbb{R}^n$ is a set, can be posed [1] as the verification of the inequality $F(x_\delta) \leq -\sigma(\delta)$ in all the sampling points x_δ generated using δ–sampling for the set $\mathcal{S}$, where σ is the continuity function of the nonlinear function F.

Here, the following improvements are proposed. Firstly, the σ function is computed automatically, and not analytically, for every sampling point as follows: linearize the system in every sampling point x_s and compute a σ in the form of a Lipschitz constant for every sampling box and account for the linearization error to maintain formal guarantees. Secondly, allow for multi–resolution state–space sampling to avoid unnecessary verification in regions where a very coarse sampling suffices, thus improving scalability.

Consider the discrete–time autonomous nonlinear system

$$x_{k+1} = G(x_k), \quad k \in \mathbb{Z}_+, \qquad (1)$$

where $x_k \in \mathcal{S}$ is the state, $\mathcal{S}$ is a compact set with $0 \in int(\mathcal{S})$, and $G : \mathbb{R}^n \to \mathbb{R}^n$ is a nonlinear function. The problem of verifying $\mathcal{KL}$–stability of system (1) on a compact set $\mathcal{S}$, can be posed via Finite–Step Lyapunov functions (FSLFs). For a fixed candidate FSLF V, which is continuous, two times differentiable (e.g., a quadratic function), the property function to be verified is:

$$F(x) = V(G^M(x)) - \rho\left(V(x)\right), \quad \forall x \in \mathcal{S}, \qquad (2)$$

with $\sigma \in \mathcal{K}$ and $\sigma < id$.

By applying this approach to compute the DOA of origin for the 2D example in [2], we obtain the result in Figure 1, which is larger than the one reported in [2].
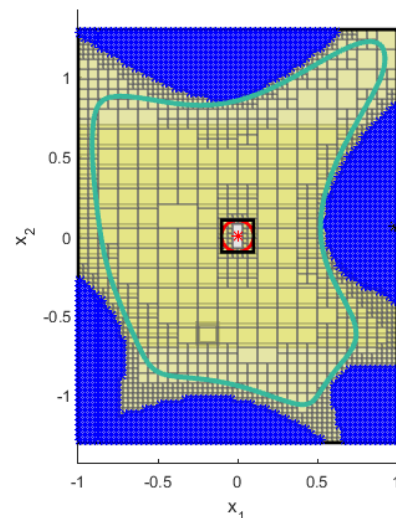
Figure 1: DOA for the origin of a 2D system (green).

References

[1]   R.V. Bobiti, and M. Lazar, "A delta–sampling verification theorem for discrete–time, possibly discontinuous systems." In Proceedings of the 18th International Conference on Hybrid Systems: Computation and Control, Seattle, Washington, USA, 2015

[2]   Giesl, Peter, "On the determination of the basin of attraction of discrete dynamical systems." Journal of Difference Equations and Applications, vol. 13, no. 6, pp. 523–546, 2007.

Characterizing the ℓ_2-gain of constrained switching systems using multiple storage functions.

M. Philippe & R. M. Jungers[1]

ICTEAM, Université catholique de Louvain. Louvain-la-Neuve, 1348, Belgium
{matthew.philippe, raphael.jungers}@uclouvain.be

R. Essick & G. E. Dullerud[2]

MecSE and CSL, University of Illinois at Urbana-Champaign. Urbana, IL 61801, USA
{ressick2, dullerud}@illinois.edu

1 Abstract

The object of our work is the ℓ_2-gain analysis of discrete-time linear switching systems. These systems can be found in many areas of applications, such as networked control systems, viral mitigation, congestion control, etc... The systems considered are of the form

$$
\begin{aligned}
x_{t+1} &= A_{\sigma(t)} x_t + B_{\sigma(t)} w_t, \\
z_t &= C_{\sigma(t)} x_t + D_{\sigma(t)} w_t,
\end{aligned}
\tag{1}
$$

where $x_t \in \mathbb{R}^n$, $z_t \in \mathbb{R}^m$ and $w_t \in \mathbb{R}^d$ are respectively the state of the system, its output and disturbance input at time t. The parameter $\sigma(t)$ is the *mode* of the system at time t, and takes value in a finite set $\{1, \cdots, N\}$.

The sequence of modes, $\sigma(0), \sigma(1), \ldots$, is called the *switching sequence* of the system. These sequences are often assumed to be non-deterministic. They may also be subjected to logical constraints. We encode these constraints through a graph Θ on N nodes. In this graph, a directed edge is present between node i and node j if $\sigma(t) = i$, $\sigma(t+1) = j$ is valid. Our interest lies in the computation of the *L2-gain* of such systems. This quantity is defined as

$$
\gamma = \sup_{x_0 = 0, \sum_{t=0}^{\infty} |w_t|_2^2 = 1, \sigma(\cdot) \text{ accepted.}} \left(\sum_{t=0}^{\infty} |z_t|_2^2 \right).
$$

The ℓ_2-gain can be interpreted as the maximum output energy produced by the system relative to the energy of the disturbance signal. When $\gamma < 1$, we say that the system (1) is *contractive*.

For LTI systems we can decide contractivity by using the well-known KYP Lemma. The LTI system is contractive if and only if there exists a quadratic norm $|x|_Q^2 = x^\top Q x$ acting as a *storage function*. The condition is easily cast under the form of a LMI. Since switching systems generalize LTI systems, it is natural to ask to which extend the KYP Lemma

can still be used for analyzing the ℓ_2-gain of switching systems. We give answers to the two following questions.

Question 1. *Is there an exact characterization of the gain in terms of storage functions?*
We show that for any constant $\bar{\gamma}$, the gain is $\gamma < \bar{\gamma}$ if and only if there exists a set of N norms of $\mathbb{R}^n$, $\{|\cdot|_\sigma\}_{\sigma \in \{1,\ldots,N\}}$, such that $\forall x \in \mathbb{R}^n, \forall w \in \mathbb{R}^d$, for all accepted transitions (σ^-, σ^+) in the graph Θ,

$$
|A_{\sigma_+} x + B_{\sigma_+} w|_{\sigma_+}^2 + |C_{\sigma_+} x + D_{\sigma_+} w|_2^2 \le |x|_{\sigma_-}^2 + \bar{\gamma}^2 |w|_2^2, \tag{2}
$$

In other words, the gain can be exactly characterized in terms of switching storage functions. The fact that the norms are not necessarily quadratic naturally leads us to a second question.

Question 2. *When is there a solution to (2) where all norms are quadratic?*
We will show that if the gain of the system on the switching system obtained by scaling the matrices of (1) as follows, $\{\sqrt{n}A_\sigma, \sqrt{n}B_\sigma, C_\sigma, D_\sigma\}_{\sigma \in \{1,\ldots,N\}}$, is lower than $\bar{\gamma}$, then there is a set of quadratic norms solving eq. (2). This can be turned into a sufficient condition for deciding whether a system is not contractive.

Our results take root in the frameworks developed in [1] for stability and performance analysis of switching systems and [2] for the exact characterization of stability of switching systems through the existence of *multinorms*. This research is part of an ongoing work whose goal is to establish arbitrarily precise estimations of the ℓ_2-gain of switching systems.

References

[1]   R. Essick, J.-W. Lee, and G. E. Dullerud, "Control of linear switched systems with receding horizon modal information," *IEEE Transactions on Automatic Control*, vol. 59, no. 9, pp. 2340–2352, 2014.

[2]   M. Philippe, R. Essick, G. Dullerud, and R. M. Jungers, "Stability of discrete-time switching systems with constrained switching sequences," *arXiv preprint arXiv:1503.06984*, 2015.

Stability of Matrix Sets with Common Invariant Polyhedra [1]

Pierre-Yves Chevalier, Julien M. Hendrickx, Raphaël M. Jungers[2]

ICTEAM, Université catholique de Louvain, Belgium

{pierre-yves.chevalier, julien.hendrickx,
raphael.jungers}@uclouvain.be

1 Introduction

We consider the problem of determining the stability of matrix sets, that is, determining whether all infinite products of matrices from a given set converge to zero, or more generally to a common invariant subspace. This problem appears in several situations in control engineering, computer science, and applied mathematics. For instance, the stability of matrix sets characterizes the stability of switching dynamical systems, which have numerous applications in control (see [2] and references therein).

Deciding the stability of a matrix set is notoriously difficult and its decidability is not known. The related problem of the existence of an infinite product whose norm diverges is undecidable [2]. However, it is possible to decide stability when the set has the *finiteness property*, that is, when there is a bound k such that the existence of an infinite nonconverging product implies the existence of an infinite nonconverging *periodic* product with period smaller than or equal to k. Indeed, when such a bound k exists, checking the stability of the set can be done by checking the stability of all products whose length is smaller than or equal to k. The finiteness property is known to hold if the matrix set has a common nonincreasing polyhedral norm and in this case, a bound k is known, which only depends on the nonincreasing norm [3].

In this work, we push further the analysis of sets with a common nonincreasing polyhedral norm and we look for the smallest valid bound k.

2 Application: Stochastic Matrices

Our work is motivated by problems in consensus systems, where the matrices are stochastic (nonnegative matrices with rows summing to one), and hence always share a same common nonincreasing polyhedral seminorm. The convergence to a rank one matrix of all products of matrices taken from a set of stochastic matrices is also of crucial importance in the context of nonhomogeneous Markov chains [4].

3 Main Results

We provide a stronger bound k such that the existence of an infinite nonconverging product implies the existence of an infinite nonconverging periodic product with period smaller than or equal to k. This bound holds for both polyhedral norms and polyhedral seminorms. In the latter case, the matrix products do not necessarily converge to 0, but to a common invariant space. We prove the tightness of our bound, in the sense that for any polyhedral seminorm, there is a set of matrices such that not all infinite products converge, but every periodic product with period smaller than our bound does converge. Our technique is based on the analysis of the structure of the face lattice of the unit ball of the nonincreasing seminorm (see [1] for proofs and further explanations).

4 Computing the Bound

Explicitly evaluating our bound requires evaluating the size of the largest antichain in the lattice of the unit ball of the nonincreasing seminorm. This may be challenging in some cases. We therefore link our problem with the *Sperner property*: the property that, for some graded posets, – in this case the face lattice of the unit ball of the norm – the size of the largest antichain is equal to the size of the largest rank level.

On the one hand, we show that this property holds for a polyhedron that is invariant for stochastic matrices. This allows us to evaluate our bound in that case. The value that we obtain for stochastic matrices is smaller by a factor of $\frac{3}{2\sqrt{\pi n}}$ than the best bound that was previously known for these matrices, n being the dimension of the matrices. One the other hand, we show that some other sets of matrices with invariant polyhedral seminorms lead to posets that do not have the Sperner property.

References

[1] P.-Y. Chevalier, J. M. Hendrickx and R. M. Jungers, *Tight Bounds for Consensus Systems Convergence*, Submitted, 2015.

[2] R. M. Jungers, *The Joint Spectral Radius: Theory and Applications*, Springer, 2009.

[3] J. C. Lagarias and Y. Wang, *The finiteness conjecture for the generalized spectral radius of a set of matrices*. Linear Algebra and its Applications, 1995.

[4] A. Paz, *Introduction to Probabilistic Automata*, Academic Press, New York, 1971.

Self-triggered Coordination over a Shared Network under Denial-of-Service

Danial Senejohnny   Pietro Tesi
d.senejohnny@rug.nl   p.tesi@rug.nl.

Claudio De Persis
Faculty of Mathematics and Natural Sciences, University of Groningen, The Netherlands
c.de.persis@rug.nl

1 Abstract

In recent years, the issue of security has become ever more prevalent in the analysis and design of cyber-physical systems (CPSs), namely systems that exhibit a tight conjoining of computational resources and physical resources. This research is concerned with a type of attacks to the communication links, such that timeliness of the information exchange is disrupted via packet loss, namely DoS attack [1]-[4].

We investigate the issue of DoS with respect to consensus networks [9]. Consensus is a prototypical problem in distributed settings with a huge range of applications, spanning from formation and cooperative robotics to surveillance and distributed computing; see for instance [5]-[7]. On the other hand, self-triggered coordination turns out to be of major interest when consensus has to be achieved in spite of possibly severe communication constraints [8]. In this respect, a remarkable feature of self-triggered coordination lies in the possibility of ensuring consensus properties in the absence of any global information on the graph topology and with no need to synchronize the agents local clocks [5].

Specifically, inspired by [5], we consider a self-triggered consensus network. At each sampling time, a certain subset of active agents poll their neighbors obtaining relative measurements of the consensus variable of interest: the available information is then used by the active agents to update their controls and compute their next update times. The attacker objective is to prevent consensus by denying communication among the agents. We assume that the network nodes make use of a shared communication medium. Under DoS, none of the network nodes can send or receive information. By introducing a notion of Persistency-of-Communication (PoC), we provide a characterization of DoS frequency and duration such that consensus is not destroyed. Consistent with the constraints imposed by the communication medium, PoC stipulates that disruptions of the graph connectivity cannot exceed a prescribed threshold.

These results land themselves to many possible extensions. First, it is interesting to quantify the effect of DoS on convergence time. Second, it is important to investigate the case of partial communication failure, i.e. the case where DoS can affect the various network links separately.

References

[1]   A.Teixeira, K. Sou, H. Sandberg, and K. Johansson. "Secure Control Systems: A Quantitative Risk Management Approach." IEEE Control Systems Magazine, vol.35, no. 1, pp. 24-45, 2015.

[2]   W. Xu, K. Ma, W. Trappe, and Y. Zhang, "Jamming sensor networks: Attack and defense strategies," IEEE Network, vol. 20, pp. 41-47, 2006.

[3]   D. Thuente and M. Acharya, "Intelligent jamming in wireless networks with applications to 802.11b and other networks," Proc. 25th IEEE Communications Society Military Communications Conference, Washington, DC, USA, 2006.

[4]   C. De Persis and P. Tesi. "Input-to-state stabilization under Denial of Service," IEEE Trans. on Automatic Control, vol. 60, pp. 2930 - 2944, 2015.

[5]   C. De Persis and P. Frasca, "Robust self-triggered coordination with ternary controllers," IEEE Trans. on Automatic Control, vol. 58, pp. 3024-3038, 2013.

[6]   R. Olfati-Saber, R M. Murray. "Consensus problems in networks of agents with switching topology and time-delays," IEEE Trans. on Automatic Control, vol.49, no.9, pp.1520-1533, 2004.

[7]   A. Jadbabaie, J. Lin, A. Morse. "Coordination of groups of mobile autonomous agents using nearest neighbor rules," IEEE Trans. on Automatic Control, vol.48, no.6, pp.988-1001, 2003.

[8]   Heemels, W. P. M. H., Karl H. Johansson, and Paulo Tabuada. "An introduction to event-triggered and self-triggered control." Decision and in Proc. of the IEEE Conference on Decision and Control, Maui, Hawaii, USA, 2012.

[9]   D. Senejohnny, P. Tesi, and C. De Persis, Self-triggered coordination over a shared network under denial-of-service, in Proc. of the IEEE Conference on Decision and Control, Osaka, Japan, 2015.

Aggregative game theoretic control for large populations of non-cooperative agents

Sergio Grammatico

Control Systems group, Eindhoven University of Technology, The Netherlands

s.grammatico@tue.nl

INTRODUCTION

Decentralized control and optimization in large populations of non-cooperative agents are of interest to various scientific disciplines, such as engineering, mathematics, social sciences, system biology and economics. Since for large populations the analytic solution of the game equations becomes computationally intractable, aggregative games [1]–[3] represent a viable solution method to address large population control objectives where the behavior of each agent is affected by some aggregate effect of all the agents, rather than by specific one-to-one effects. This feature appears in several applications, including demand side management (DSM) for smart grids [4]–[8], and congestion control for networks of shared resources [9].

Along these lines, Mean Field (MF) games have emerged as a methodology to study multi-agent coordination problems where each individual agent is influenced by the statistical distribution of the population, and its contribution to the population distribution vanishes as the number of agents grows [10], [11]. Unlike aggregative games, the distinctive feature of MF games is the emphasis on the limit of infinite population size, as this abstraction allows one to approximate the average population behavior based on its statistical properties only.

Here we consider aggregative games, as in [7], [8], where we assume that the agents do not have access to the statistical properties of the population but, on the contrary, react optimally to a common external signal, which is broadcast by a central coordinator. The *aggregative control* problem is then defined as the task of designing an incentive signal that the central coordinator should broadcast so that the decentralized optimal responses of the agents generate a MF Nash equilibrium. Unlike state-of-the-art approaches, our methods can handle agents subject to *heterogeneous, compact, convex constraints*, e.g. arising from different linear dynamics, convex state and input constraints. We build on mathematical definitions and tools from convex analysis and operator theory [12], [13], establishing useful regularity properties of the mapping describing the aggregate population behavior. In this way, we solve the aggregative control problem iteratively via specific feedback mappings and show global asymptotic convergence to a desired incentive signal generating a MF almost Nash equilibrium in a *decentralized* fashion, making our methods scalable with the population size.

DYNAMIC AGGREGATIVE CONTROL

Given the aggregative game formulation in [14], we assume that each agent i reacts to a broadcast incentive signal $z \in \mathbb{R}^n$

through the *optimal-response* mapping

$$x^{i\,\star}(z) := \arg \min_{y \in \mathcal{X}^i} y^\top Q y + 2(Cz + c)^\top y,$$

where $Q \succ 0$. Moreover, we formalize the average population behavior through the aggregation mapping $\mathcal{A}(z) := \frac{1}{N} \sum_{i=1}^{N} x^{i\,\star}(z)$.

Our main results provide mild conditions on the problem data Q, C under which a dynamic control of the kind

$$z_{(k+1)} = (1 - \alpha_k) z_{(k)} + \alpha_k \mathcal{A} \left(z_{(k)} \right),$$

where $\alpha_k \sim 1/k$, ensures global convergence to a fixed point $\bar{z}$ of $\mathcal{A}$, which generates the MF ε-Nash equilibrium $\left\{ x^{i\,\star}(\bar{z}) \right\}_{i=1}^{N}$, with $\varepsilon = \mathcal{O}(1/N)$.

REFERENCES

[1] N. S. Kukushkin, "Best response dynamics in finite games with additive aggregation," *Games and Economic Behavior*, vol. 48, no. 1, pp. 94–10, 2004.

[2] P. Dubey, O. Haimanko, and A. Zapechelnyuk, "Strategic complements and substitutes, and potential games," *Games and Economic Behavior*, vol. 54, pp. 77–94, 2006.

[3] M. Jensen, "Aggregative games and best-reply potentials," *Economic Theory, Springer*, vol. 43, pp. 45–66, 2010.

[4] A.-H. Mohsenian-Rad, V. Wong, J. Jatskevich, R. Schober, and A. Leon-Garcia, "Autonomous demand-side management based on game-theoretic energy consumption scheduling for the future smart grid," *IEEE Trans. on Smart Grid*, vol. 1, no. 3, pp. 320–331, 2010.

[5] H. Chen, Y. Li, R. Louie, and B. Vucetic, "Autonomous demand side management based on energy consumption scheduling and instantaneous load billing: An aggregative game approach," *IEEE Trans. on Smart Grid*, vol. 5, no. 4, pp. 1744–1754, 2014.

[6] K. Ma, G. Hu, and C. Spanos, "Distributed energy consumption control via real-time pricing feedback in smart grid," *IEEE Trans. on Control Systems Technology*, vol. 22, no. 5, pp. 1907–1914, 2014.

[7] Z. Ma, D. Callaway, and I. Hiskens, "Decentralized charging control of large populations of plug-in electric vehicles," *IEEE Trans. on Control Systems Technology*, vol. 21, no. 1, pp. 67–78, 2013.

[8] F. Parise, M. Colombino, S. Grammatico, and J. Lygeros, "Mean field constrained charging policy for large populations of plug-in electric vehicles," in *Proc. of the IEEE Conference on Decision and Control*, Los Angeles, California, USA, 2014, pp. 5101–5106.

[9] J. Barrera and A. Garcia, "Dynamic incentives for congestion control," *IEEE Trans. on Automatic Control*, vol. 60, no. 2, pp. 299–310, 2015.

[10] M. Huang, P. Caines, and R. Malhamé, "Large-population cost-coupled LQG problems with nonuniform agents: Individual-mass behavior and decentralized ε-Nash equilibria," *IEEE Trans. on Automatic Control*, vol. 52, no. 9, pp. 1560–1571, 2007.

[11] J.-M. Lasry and P.-L. Lions, "Mean field games," *Japanese Journal of Mathematics*, vol. 2, pp. 229–260, 2007.

[12] H. H. Bauschke and P. L. Combettes, *Convex analysis and monotone operator theory in Hilbert spaces*. Springer, 2010.

[13] V. Berinde, *Iterative Approximation of Fixed Points*. Springer, 2007.

[14] S. Grammatico, F. Parise, M. Colombino, and J. Lygeros, "Decentralized convergence to Nash equilibria in constrained deterministic mean field control," *IEEE Trans. on Automatic Control* (in press) [http://dx.doi.org/10.1109/TAC.2015.2513368], 2016.

bandicoot: an open-source Python toolbox to analyze mobile phone metadata

Yves-Alexandre de Montjoye
Media Lab
Massachusetts Institute of Technology (MIT)
`yvesalexandre@demontjoye.com`

Luc Rocher[1]
ICTEAM Institute
Université Catholique de Louvain, Belgium
`luc.rocher@uclouvain.be`

Alex 'Sandy' Pentland
Media Lab
Massachusetts Institute of Technology (MIT)
`pentland@media.mit.edu`

1 Motivation and Introduction

Every time we send or received a text or a phone call, our mobile phones generate metadata. Collected at large scale, they have been used to design transportation systems, planning disaster responses, and fight epidemics [1]. Whereas the field and the use of machine learning algorithms on mobile phone metadata has been evolving fast, it however currently lacks the standardization needed to thrive. Numerous crucial implementation choices are often lost from one research paper to another making it hard to replicate results, quantify the impact of new methods, and transfer learning.

2 Proposed approach

We have introduced *bandicoot*[2], an open-source Python toolbox, to solve these issues. It extracts more than 160 robust behavioral features from mobile phone metadata, and focuses on making it easy for researchers and practitioners to load metadata and compute robust features from them.

bandicoot indicators fall into three categories (see fig. 1):

- Individual indicators (e.g. percent of nocturnal interactions, time it takes someone to answer text messages) describe an individual's phone usage.

- Spatial indicators (e.g. entropy of visited antennas, radius of gyration) describe mobility patterns.

- Social network (e.g. clustering coefficient, assortativity) describe individuals' social network and compare their behaviors with those of their contacts.

Emphasis is put on correctness and consistency through numerous unit tests covering 91% of the source code, by the detection of incorrect entries, and reporting variables to assess data quality.

Figure 1: *bandicoot* indicators are computed from individual, spatial, and social network patterns

bandicoot is currently used with machine learning techniques to perform large scale experiments, by both carriers (e.g. Orange, Telenor), NGOs, and international organizations. Researches include gender or personality prediction [2], marketing experiments [3], and contributions from the Orange 'D4D' Challenge to address socio-economic development in Ivory Coast.

References

[1]   V. D. Blondel, A. Decuyper, and G. Krings. A survey of results on mobile phone datasets analysis. *arXiv preprint arXiv:1502.03406*, 2015.

[2]   Y.-A. de Montjoye, J. Quoidbach, F. Robic, and A. Pentland. Predicting personality using novel mobile phone-based metrics. In *Social Computing, Behavioral-Cultural Modeling and Prediction*, pages 48–55. Springer, 2013.

[3]   P. Sundsøy, J. Bjelland, A. Iqbal, Y.-A. de Montjoye, et al. Big data-driven marketing: How machine learning outperforms marketers' gut-feeling. In *Social Computing, Behavioral-Cultural Modeling and Prediction*, pages 367–374. Springer, 2014.

---

[2]The *bandicoot* website is accessible at `bandicoot.mit.edu`. The source code is distributed under the permissive MIT license, and hosted on GitHub.

148

Disturbance feedforward control for air mount systems with acoustic resonances

M.A. Beijen, M.F. Heertjes, and H. Butler

Eindhoven University of Technology, PO Box 513, 5600 MB Eindhoven (NL), E-mail: M.A.Beijen@tue.nl

1 Introduction

Disturbance feedforward control (DFC) can be used to improve disturbance suppression performance of air mount systems with air tanks. Those tanks often give rise to acoustic resonances that subsequently limit performance. This paper, which is in line with our work in [1], presents a self-tuning DFC strategy that improves performance and can deal with acoustic resonances.

A description of the uncontrolled air mount system consists of the transfer functions P_1 (from base frame acceleration r to payload accleration y), and P_2 (from control force u to y). Bode diagrams for P_1 and P_2 are given in Figure 1, which assumes a fourth-order model with one acoustic resonance.
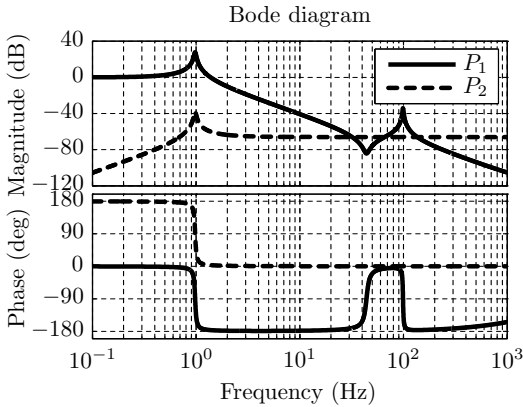
Figure 1: Bode diagrams for P_1 (solid) and P_2 (dashed).

2 Disturbance feedforward control

Figure 2 shows the self-tuning controller structure. Using the z-transformation, the control signal reads

$$U(z) = \sum_{i=1}^{4} w_i(z)\mathcal{B}_i(z)R(z), \qquad (1)$$

with $z \in \mathbb{C}$, basis functions $\mathcal{B}_i$ which are orthonormal [2] to optimize convergence speed, and self-tuning weights w_i. The goal is to find all w_i such that the filtered-error e is minimized. This is done with a self-tuning algorithm based on Filtered-error Least Mean Squares (FeLMS). The update block in Figure 2 performs the updates of w_i. Filter F removes sensor noise, and N is used for residual output shaping in the frequency domain. Two feedforward controllers C_{FF} are considered, i.e. a reduced-order (RO) controller and a full-order (FO) controller. The RO controller has two basis functions, while the FO controller has four basis functions. The latter can compensate for the acoustic resonance.
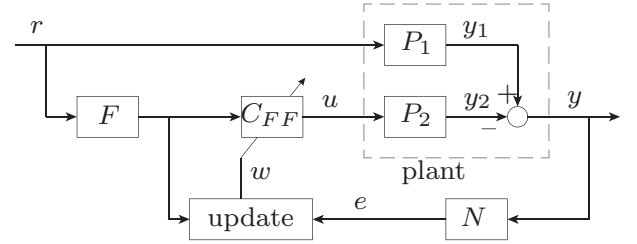
Figure 2: Implementation of the self-tuning controller.

3 Results

Figure 3 shows Bode plots of transmissibility functions,

$$T(s) = P_1(s) + P_2(s)C_{FF}(s)F(s), \qquad (2)$$

i.e. the transfer functions from r to y. It is observed that the RO controller only increases disturbance suppression up to the acoustic resonance frequency. The FO controller also increases performance at frequencies beyond the acoustic resonance. The controlled systems suffer from performance deterioration at very low and high frequencies due to causality aspects [3].
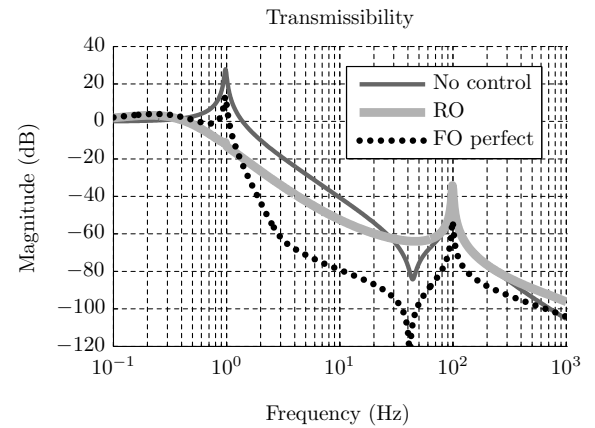
Figure 3: Transmissibility functions

References

[1]   M.A. Beijen et al., *Modeling and feedforward compensation of air mounts with internal Helmholtz resonances.* Accepted at *the American Control Conference (2016)*, Boston, MA, USA.

[2]   P.S.C. Heuberger et al., *Modelling and Identification with Rational Orthogonal Basis Functions.* Springer, 2005.

[3]   M.M. Seron et al., *Fundamental limitations in Filtering and Control.* Springer, 1997.

Huygens' Synchronization: Experiments, Modeling, and Local Stability Analysis

F.N. Hoogeboom, A.Y. Pogromsky, H. Nijmeijer

Dept. of Mechanical Engineering, Dynamics and Control Eindhoven University of Technology, The Netherlands

F.N.Hoogeboom@tue.nl, A.Pogromsky@tue.nl, H.Nijmijer@tue.nl

1 Introduction

The Dutch scientist Huygens was in 1665 probably the first scientist who observed synchronization among pendulum clocks, and although synchronization of coupled mechanical oscillators has a long history in science, some properties are still not fully understood. In this project we investigate local stability of the synchronized solutions of two coupled metronomes.

2 Experimental Results

Figure 1 depicts the experimental setup that was used in this study [1], consisting of a rectangular platform made of lightweight foam that is suspended at the corners by thin cables. Experimental results show that, depending on the platform parameters, it is possible to observe a regime with only in-phase synchronization or a regime with coexisting in- and anti-phase synchronization.
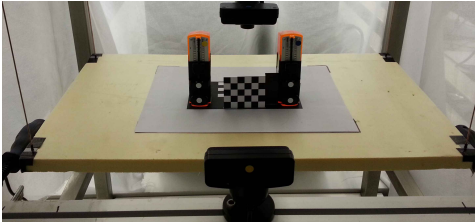
Figure 1: Experimental setup with metronomes placed side by side.

3 Modeling the Experimental Setup

Figure 2 shows a schematic representation of the experimental setup, which is modeled as a beam with one degree of freedom and its motion is constrained by an assumed constant linear spring and damper.
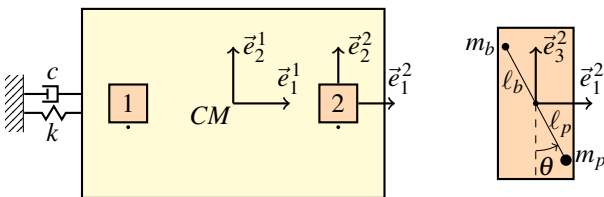
Figure 2: Schematic diagram of experimental setup. Top view of the setup (left) and front view of a metronome (right).

The equations of motion for this setup are given by

$$M_t \ddot{x} + c\dot{x} + kx = -\sum_{i=1}^{2} p(\ddot{\theta}_i \cos\theta_i - \dot{\theta}_i^2 \sin\theta_i), \quad (1)$$

$$I\ddot{\theta}_1 + d\dot{\theta}_1 + pg\sin\theta_1 = u(\theta_1, \dot{\theta}_1) - p\ddot{x}\cos\theta_1, \quad (2)$$

$$I\ddot{\theta}_2 + d\dot{\theta}_2 + pg\sin\theta_2 = u(\theta_2, \dot{\theta}_2) - p\ddot{x}\cos\theta_2. \quad (3)$$

where $M_t = M + 2m_p + 2m_b$, $p = m_p\ell_p - m_b\ell_b$, $I = m_p\ell_p^2 + m_b\ell_b^2$, and $u(\theta, \dot{\theta})$ is a pulsating escapement function which drives the pendulum. This model is verified by comparing experimental results with computer simulations.

4 Local Stability Analysis

To investigate synchronization regimes, a numerical continuation and bifurcation tool is used. With this tool, existence and local stability of the limit synchronized solutions is determined as the platform parameter values are varied.

Figure 3 presents the result when the platform mass M is subject to change. Note that the upper line represents the anti-phase solution branch and the lower line the in-phase solution branch. As can be seen, only the in-phase solution is stable for the estimated platform mass. By lowering the platform mass to, for example, $M = 0.1$ kg, a stable in- as well anti-phase solution is obtained.
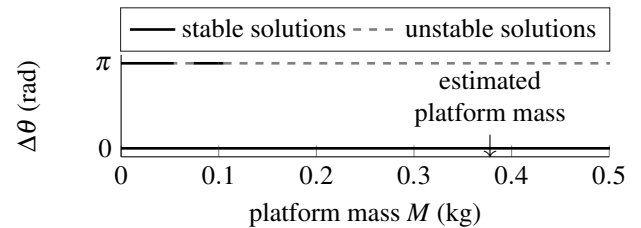
Figure 3: Bifurcation diagram for phase difference $\Delta\theta$ as function of the platform mass M. Upper/lower line denote anti/in-phase solution.

References

[1] FN Hoogeboom, AY Pogromsky, and H Nijmeijer. Huygens synchronization: Experiments, modeling, and local stability analysis. *IFAC-PapersOnLine*, 48(18):146–151, 2015.

Scheduled controller design for systems with varying sensor configurations: A frequency-domain approach

R. van der Weijst*, S.J.L.M. van Loon*, M.F. Heertjes*,**, and W.P.M.H. Heemels*

* Control Systems Technology Group, Eindhoven University of Technology
P.O. Box 513, 5600MB Eindhoven, the Netherlands. E-mail: r.v.d.weijst@tue.nl
** ASML the Netherlands B.V., Veldhoven, the Netherlands

1 Introduction

In this abstract, we propose a scheduled controller design for systems which, from an input/output point-of-view, exhibit switched dynamics as a result of varying sensor configurations available in the measurement system. Input-to-state stability (ISS) of the closed-loop system is guaranteed from data-based conditions using measured plant frequency response functions (FRFs), opposed to approaches known from literature that often require parametric plant models. Moreover, the scheduled controller is based on local linear time-invariant (LTI) controllers designed using classical frequency-domain loop-shaping techniques and plant FRFs. Therefore, for the considered class of systems, this work bridges the gap between switched systems theory (with formal stability guarantees) and industrial control practice, commonly exploiting frequency-domain design tools and non-parametric models, e.g., plant FRFs.

2 Class of Systems

The considered class of systems is given by the following switched single-input-multi-output (SIMO) model

$$P : \begin{cases} \dot{x}_P(t) &= A_P x_P(t) + B_P u_P(t) \\ y_{P_0}(t) &= C_{P_0} x_P(t) \\ y_{P_1}(t) &= \begin{cases} C_{P_1} x_P(t) & \text{if } \theta(t) \in \Lambda \\ \varnothing & \text{if } \theta(t) \notin \Lambda, \end{cases} \end{cases} \quad (1)$$

with $x_P \in \mathbb{R}^{n_P}$ the state vector, n_P the number of states, $A_P \in \mathbb{R}^{n_P \times n_P}$, $B_P \in \mathbb{R}^{n_P \times 1}$, input $u_P \in \mathbb{R}$, $C_{P_i} \in \mathbb{R}^{1 \times n_P}$, outputs $y_{P_i} \in \mathbb{R}$, $i = 0, 1$, where $\varnothing$ indicates that $y_{P_1}(t)$ is unavailable, $\theta(t) \in \Theta \subset \mathbb{R}^{n_\theta}$, a vector of n_θ time varying parameters, and $\Lambda \subset \Theta$. We associate the following single-input-single-output (SISO) transfer functions

$$P_i(s) = \frac{y_{P_i}(s)}{u_P(s)}, \ i = 0, 1, \quad (2)$$

to (1), with $s \in \mathbb{C}$ and $y_{P_i}(s)$, $u_P(s)$, the Laplace transforms of $y_{P_i}(t)$, $u_P(t)$, respectively.

3 Scheduled Control

A simplified version of the scheduled control system proposed in [1] is depicted in Figure 1, with disturbance $d(t) \in$
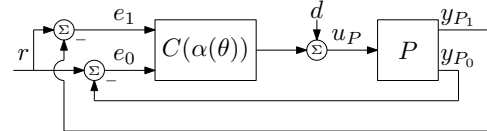
Figure 1: Simplified scheduled control system representation.

$\mathbb{R}$, reference signal $r(t) \in \mathbb{R}$, and tracking errors $e_i(t) = r(t) - y_{P_i}(t)$, $i = 0, 1$. The scheduled controller $C(\alpha(\theta))$ is based on local LTI controllers $C_0(s)$, $C_1(s)$, which are dedicated designs for $P_0(s)$, $P_1(s)$, respectively. For $\alpha(\theta) = 0$, the controller output resembles $C_0(s)e_0(s)$, for $\alpha(\theta) = 1$ it resembles $C_1(s)e_1(s)$. The dynamics of the closed-loop system are described by a non-minimal LTI system in negative feedback with a varying $\alpha(\theta(t)) \in [0, 1]$, i.e., a Lur'e-type system. As a result, stability can be studied using a generalized version of the circle criterion presented in [1], which only requires FRFs of $P_0(s)$ and $P_1(s)$ to establish ISS of the closed-loop system with respect to r and d .

4 Wafer Stage Measurements

Measurements with the scheduled controller are performed on the z-axis (vertical direction) of an industrial wafer stage system, which is well described by (1). A significant performance increase can be seen in Figure 2, where the measurement results in time-domain are depicted and compared to the case where $P_0(s)$ and $C_0(s)$ are used for all $\theta \in \Theta$. A detailed analysis can be found in [1].
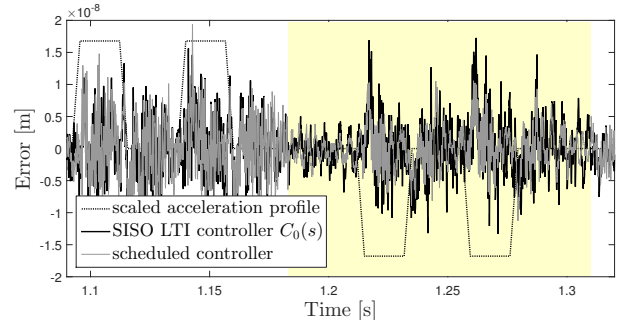
Figure 2: The z-axis error in time-domain. We have, $\alpha(\theta) = 1$ and $\theta(t) \in \Lambda$ in the yellow window, while $\alpha(\theta) = 0$ and $\theta(t) \notin \Lambda$ elsewhere, i.e. $\alpha(\theta)$ is switched.

References

[1]   R. van der Weijst, S.J.L.M van Loon, M.F. Heertjes, and W.P.M.H. Heemels, "Scheduled controller design for systems with varying sensor configurations: A frequency-domain approach", *IEEE Transactions on Control Systems Technology, under review*

SOC and SOH estimation for Li-ion battery, Part I: SOC estimation

Luis D. Couto, Julien Schorsch, Marco M. Nicotra and Michel Kinnaert
Department of Control Engineering and System Analysis
Université libre de Bruxelles (ULB)
lcoutome@ulb.ac.be, julien.schorsch@ulb.ac.be, mnicotra@ulb.ac.be,
michel.kinnaert@ulb.ac.be

Li-ion batteries are the most promising energy storage systems due to their high energy/power densities and high efficiency. Nevertheless, safety concerns force the utilization of battery-management systems (BMS). Among its tasks, a BMS must be able to monitor internal state evolution, such as state-of-charge (SOC) and state-of-health (SOH). To do so, a model of the system along with an estimator are required.

Many kinds of battery models have been proposed in the literature. Among them, the electrochemical model is the most suitable to control the electrochemical states in a wide operating range. Although more accurate and physically meaningful, this model comes associated with a computational burden due to its complexity. Therefore, reduced-order models must be considered for the BMS design. In this context, the equivalent-hydraulic model (EHM) [1] is a simple representation of the lithium diffusion process that takes place within the electrode solid particles. It is based on two relevant electrochemical states, namely bulk and surface concentration. On the one hand, the lithium at the bulk defines the SOC of the battery-cell. On the other hand, the lithium at the surface is related to the instantaneous available energy. Although the EHM is originally a linear model, it depends on the diffusion coefficient, which is unknown. To tackle this problem, an extra state was included to account for the uncertain parameter in state estimation. This EHM was used to design an extended Kalman filter (EKF) for state estimation from available measurements (current and voltage).

Regarding estimators, most of the estimators proposed in the literature rely on state observers. In this context, the EKF is able to properly handle measurement noise and modeling uncertainties. As stochastic stability of the EKF is not guaranteed, sufficient conditions for its stability were analysed. These conditions are based on the so-called observability rank condition, double differentiability of the model functions as well as state boundedness. While the first and second conditions were not difficult to prove, numerical simulations were performed to check the third one. The results show that, given a sufficiently small initial estimation error, the estimation error remains bounded, even for large measurement noise.

The designed state observer based on EHM was used as the first step out of a two steps procedure (see Figure 1). Step
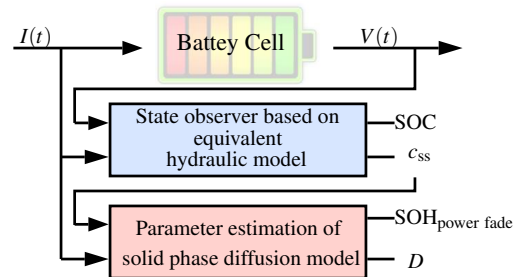
Figure 1: Block diagram of the estimation scheme.

1 consisted in the estimation of the SOC and the surface concentration (c_{ss}). The latter state estimate is then used in step 2 of the procedure to estimate the SOH power fade [2].

The proposed approach was compared with two other methods proposed in the literature. The first one consists of an adaptive output function inversion, while the second one uses a fourth-order EKF based on the so-called electrode average model. In order to perform this study, virtual data was generated using a battery-cell simulator fed with an UDDS (urban dynamometer driving schedule) current profile. The initial state estimates were set to incorrect values. Under these conditions, the EKF based on EHM provided an overall good estimation of the considered state trajectories for both SOC and surface concentration. Moreover, the proposed method outperforms the other two methods with respect to surface concentration estimation of the negative electrode. In contrast with the other two methods, the one proposed here is based on a simple third-order model that allows a straightforward and more accurate estimation of SOC and surface concentration. Other contributions of the proposed approach include the estimation of both state and model parameters (i.e. the imperfect knowledge of the model has been accounted for) and the analysis of the stability properties of the designed EKF.

Acknowledgement

References

[1] R. H. Milocco, J. E. Thomas, and B. E. Castro, Generic dynamic model of rechargeable batteries. Journal of Power Sources, 2014. 246: p. 609-620.

[2] J. Schorsch, L. D. Couto and M. Kinnaert, SOC and SOH estimation for Li-ion battery, Part II: SOH estimation. Benelux Meeting, 2016.

An LTI control toolbox – simplifying feedback controller design

Maarten Verbandt, Goele Pipeleers and Jan Swevers
KU Leuven, BE-3001 Heverlee, Belgium
Department of Mechanical Engineering, Division PMA
maarten.verbandt@kuleuven.be

1 Abstract

Throughout the years, the study of feedback control has yielded a variety of design techniques. Although control engineers stick to classical open loop shaping, modern techniques gain relevance as they provide the means to push performance to the limit while taking uncertainty into account. The $\mathscr{H}_\infty$ design framework [1] is a modern approach which takes objectives and constraints rigorously into account. However, practical difficulties are still overruling their benefits, sustaining the dominance of standard PID control.

In order to ease $\mathscr{H}_\infty$ controller design, we are developing a Matlab LTI Control Toolbox[1] that provides the means to do a state-of-the-art controller design. It provides an interface to specify the control configuration and a set of requirements. Unstable and improper weighting functions are allowed, reducing the amount of post-processing. The following paragraphs show how to use this LTI toolbox.

2 Control configuration

The control configuration incorporates the connections between all dynamic systems. As an example, the plant in Fig. 1 is described by Code example 1.

In order to make systems G and S available to the toolbox, they are declared as an *LTIsys*. Their inputs and outputs can then be assigned to a new convenience variable, e.g. '$u = G.in$', or connected to eachother, e.g. '$S.in == y$'.
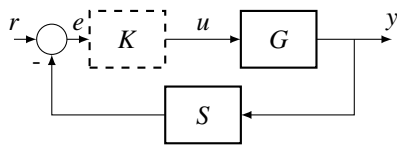
Figure 1: Representation of a control configuration. *G* and *S* are dynamic systems which make up the plant. *K* indicates the controller which eventually closes the loop.

```
1   G = LTIsys(G); %make G.in and G.out available
2   S = LTIsys(S);
3
4   lti_begin()
5       signal r            %declare the reference
6
7       u = G.in;           %define u as G's input
8       y = G.out;          %define y as G's output
9       e = r - S.out;      %define the error
```

```
10      S.in == y;          %connect S to G
11      K.in = e;           %set controller input
12      K.out = u;          %set controller output
13  lti_end
```

Code example 1: LTI control toolbox code to describe the control configuration depicted in Figure 1.

3 Control requirements

The control requirements are formulated as a set of objectives and constraints. These usually consist of some target closed-loop transfer function, multiplied by some frequency dependent weight.

As an example, consider the problem of a servo mechanism with a fixed required bandwidth. This translates to a constraint on the sensitivity, $r \to e$ (2). Also robustness can be maximized (1), leading to the next optimization problem:

$$\underset{K}{\text{minimize}} \; \left\| W_T \frac{y}{r} \right\|_\infty \tag{1}$$

$$\text{subject to} \; \left\| W_S \frac{e}{r} \right\|_\infty \leqslant 1 \tag{2}$$

```
1   WT = Weight.HF(10,2);
2   WS = Weight.LF(1,1);
3
4   lti_begin()
5       %% ... %% plant declaration
6
7       ctrl_begin('my_controller')
8           minimize(WT*(y/r))
9           subject to
10              WS*(e/r) <= 1
11      ctrl_end
12  lti_end
```

Code example 2: LTI control toolbox code to design the controller as described by problem (1)-(2).

References

[1]   C. Scherer, P. Gahinet and M. Chilali, "Multiobjective output-feedback control via LMI optimization," Automatic Control, IEEE Transactions on, Vol. 42, 7, 896–911, 1997.

Parasitic forces and torques compensation in ironless linear motors

Tuan T. Nguyen, Mircea Lazar, Hans Butler
Control Systems Group, Department of Electrical Engineering
Eindhoven University of Technology, 5600 MB Eindhoven, The Netherlands
{t.t.nguyen, m.lazar, h.butler}@tue.nl

1 Introduction

Ironless linear motors (ILMs), as shown in Figure 1, ideally have very high precision. The parasitic forces and torques are minimized by design thanks to the symmetrical stator topology and the lack of an iron core.
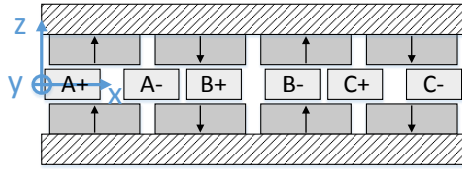
Figure 1: Cross-sectional view of an ironless linear motor.

However, in reality, there are deviations from the design parameters which result in various parasitic forces and torques [1]. Most of the research in the literature focused on compensation for parasitic force in the driving direction, while the parasitic forces and torques in non-driving directions are usually neglected. The aim of this paper is to develop a feedback linearization law, which is known as commutation in linear motors literature, to compensate for parasitic forces and torques in ILMs simultaneously.

2 Modeling

By using Fourier modeling, a modeling technique based on Fourier approximation, the propulsion force F_x, the normal force F_z and the torque T_y can be modeled as [2]:

$$F_x = K_x(q)i, \qquad (1)$$

$$F_z = K_z(q)i + i^T G_z(q)i, \qquad (2)$$

$$T_y = K_t(q)i + i^T G_t(q)i, \qquad (3)$$

where q is the position vector of the translator:

$$q = \begin{bmatrix} x & z \end{bmatrix}^T, \qquad (4)$$

i is the vector of the currents through the coils:

$$i = \begin{bmatrix} i_{A_1} & i_{B_1} & i_{C_1} & \dots & i_{A_{N_c}} & i_{B_{N_c}} & i_{C_{N_c}} \end{bmatrix}^T, \qquad (5)$$

N_c is the number of sets of three-phase coils, $K_x(q)$, $K_z(q)$, $K_t(q)$ are $[1 \times 3N_c]$ matrices, $G_z(q)$, $G_t(q)$ are $[3N_c \times 3N_c]$ matrices which are dependent on the position q of the translator.

3 Commutation

Commutation in linear motors is a mechanism that calculates the currents through the coils to achieve the desired forces and torque. Let us consider the case where the translator consists of two sets of three-phase coils, i.e. $N_c = 2$. Denoting the desired forces and torque as F_x^*, F_z^* and T_y^*. The commutation problem can be formulated as:

$$\min_i i^T i$$

subject to

$$\Phi(i) = \begin{bmatrix} K_x i - F_x^* \\ i^T G_z i + K_z i - F_z^* \\ i^T G_t i + K_t i - T_y^* \\ i_{A_1} + i_{B_1} + i_{C_1} \\ i_{A_2} + i_{B_2} + i_{C_2} \end{bmatrix} = 0. \qquad (6)$$

The optimization problem is then solved by the following proposed iteration:

$$i_{k+1} = \nabla\Phi(i_k)^{-R}\nabla\Phi(i_k)i_k - \nabla\Phi(i_k)^{-R}\Phi(i_k), \qquad (7)$$

where $\nabla\Phi(i_k)^{-R}$ is the minimum norm generalized inverse, or the right inverse, of $\nabla\Phi(i_k)$:

$$\nabla\Phi(i_k)^{-R} = \nabla\Phi(i_k)^T \left(\nabla\Phi(i_k)\nabla\Phi(i_k)^T\right)^{-1}. \qquad (8)$$

The proposed commutation algorithm is simulated with the finite element method model of an example motor. It is verified that with the proposed commutation, the desired propulsion force is achieved and the parasitic forces and torques in non-driving directions are eliminated. This is promising for real time application since the method does not require any embedded optimization solver.

References

[1] J. W. Jansen, E. A. Lomonova, and J. C. Compter, "Analysis of the parasitic forces and torques in coreless linear motors," in Electrical Machines and Systems (ICEMS), 2011 International Conference on, pp. 1-6, Aug 2011.

[2] T. T. Nguyen, M. Lazar, and H. Butler, "Cancellation of normal parasitic forces in coreless linear motors," in System Theory, Control and Computing (ICSTCC), 19th International Conference on, Oct 2015.

Study on an Extension of Generalized Repetitive Control to Variable Speed Region Based on Oppenheim's Frequency Transformation

Masato Kanematsu, Hiroshi Fujimoto

Department of Electrical Engineering, the University of Tokyo

5-1-5 Kashiwanoha, Kashiwa, Chiba, 277-8561, Japan

Email: kanematsu@hflab.k.u-tokyo.ac.jp, fujimoto@k.u-tokyo.ac.jp

1 Introduction

Generalized Repetitive Control(GRC) proposed in [1] has an excellent performance to reject periodic disturbances. This controller is designed by convex optimization, and it makes the difficulty to re-design GRC online. In motor drive applications, disturbance frequency changes according to the rotation speed. Therefore, it is needed to re-design the GRC controller online. In this paper, we propose a new algorithm which enables us to re-design GRC online. This method is based on FIR re-designing method proposed in [2].

2 FIR Redesigning Method

When GRC is added to the loop, the frequency characteristics of the modifying sensitivity function is expressed as

$$M_S(z) = 1 - X(z) \tag{1}$$

$$X(z) := \sum_{k=K_1}^{K_2} X_k z^{-k} \tag{2}$$

This research objective is to transform the frequency characteristics of the modifying sensitivity function by the transformation of the frequency characteristics of $X(z)$. $X(z)$ is designed as a linear phase FIR filter to which FIR re-designing method proposed in [2] is applied.

Firstly, $X(z)$ is expressed in the form

$$X_0(z) = z^{-N_d} \sum_{k=-N}^{N} a_k z^k$$

$$:= H_{0:\mathrm{p}}(z) H_{0:\mathrm{a}}(z) \tag{3}$$

$$H_{0:\mathrm{p}}(z) := z^{-N_d} \tag{4}$$

$$H_{0:\mathrm{a}}(z) := \sum_{n=0}^{N} A_n \left(\frac{z + z^{-1}}{2} \right)^n \tag{5}$$

The amplitude of $H_{0:p}(z)$ is 1 and there is no phase delay in $H_{0:a}$. The characteristics of $H_{0:p}(z)$ and $H_{0:a}(z)$ is designed separately to achieve desirable frequency characteristics. The phase characteristics are stretched by adding delay operators to $H_{0:p}(z)$. Noting that the amplitude characteristics of $H_{0:a}$ is a polynomial function of $\cos\Omega$, the amplitude characteristics is transformed by distorting the fre-
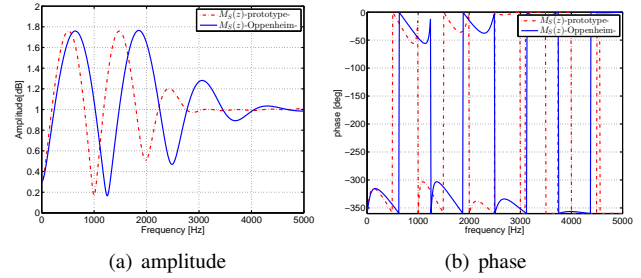
Figure 1: Simulation Result of FIR Redesigning Method

quency axis. Such a transformation is realized by the substitution of variables

$$\frac{z + z^{-1}}{2} = K_0 + K_1 \left(\frac{Z + Z^{-1}}{2} \right) \tag{6}$$

The property of this linear mapping is decided by the parameters K_0 and K_1. These parameters should be set according to the relationship between prototype frequency response $H_{0:a}(z)$ and the transformed frequency response $H_{1:a}(z)$. In this paper, the parameters which equalize the properties of $H_{1:a}(z)$ and $H_{0:a}(z)$ at zero and cutoff frequency are selected. Figure 1 demonstrates this re-designing method.

3 Conclusion

In this paper, a new algorithm which enables to re-design GRC online is proposed. It is our next step to update the filter coefficients dynamically to achieve dynamic loop shaping.

References

[1] G. Pipeleers, B. Demeulenaere, J. D. Schutter, and J. Swevers: "Generalized repetitive control: relaxing the period-delay-based structure", IET Control Theory and Applications, Vol. 3, No. 11, pp. 1528-1536, 2009

[2] A.V. Oppenheim, W.F.G. Mecklenbrauker, R.M. Mersereau: "Variable cutoff linear phase digital filters", IEEE Trans. Circuits and Systems, Vol.23, No.4, pp.199-203, 1976

Nanometer-accurate planar actuation system (NAPAS)

Ioannis Proimadis
Dept. of Electrical Engineering
Eindhoven University of Technology
The Netherlands
Email: i.proimadis@tue.nl

Roland Tóth
Dept. of Electrical Engineering
Eindhoven University of Technology
The Netherlands
Email: r.toth@tue.nl

1 Introduction

In our modern society there is an ever increasing need for higher computational power and storage capacities together with a reduction at the production costs. In the semiconductor industry, these demands are translated into an effort to achieve a larger wafer size and a smaller circuit detail, from the scale of 30nm down to 5nm, together with an increase in the positioning speed. The transition from dual-stage positioning systems [1] to a magnetically levitated planar actuator is necessary towards the successful implementation of the concept. However, the nonlinear position- and velocity-dependent electromagnetic interaction between the translator and the coils as well as deformation due to thermal effects and the high accelerations of the translator restrict the performance capabilities of this approach.

In this research we will introduce a Linear Parameter Varying (LPV) framework to model these effects and capture the unknown relations in terms of a low complexity model by using a data driven modelling approach. By making use of this model we will synthesize controllers that can attenuate these dynamical aspects and realize the intended high accuracy behaviour of the magnetically levitated positioning system under high throughput demands. The LPV framework is capable of capturing position dependent and nonlinear behaviour, nonstationary characteristics or dependence on external variables by employing a low complexity model, which is achieved by capturing these effects in terms of scheduling variables that are assumed to be measurable in the system.

2 Modelling and identification of planar motor system

Modelling the magnetically levitated planar motor requires the derivation of an analytic description of the underlying mathematical relations. For this reason a multi-physical model of the motor has been already established in previous research, which entails a magnetostatic, a mechanical and a thermal model. Nonetheless, this analytic model has its own limitations due to manufacturing imperfections or unforeseen dynamics. For this reason, it is our aim to complement it by employing an LPV identification approach, since it allows for the incorporation of the position and velocity dependence in the coil-magnet interaction.

To this end, the recent developments in the machine learning community and their close interaction with system identification have proven themselves a valuable tool towards the increase of the accuracy of the estimated model. This synergy offers an increased flexibility to system identification through the use of kernel functions and it has recently been formulated to achieve data-driven LPV modelling, both within the prediction error [2] and subspace [3] context.

3 Control of planar motor system

Following the development of a reliable and low complexity LPV model of the planar motor system, in this research we will focus on controlling the planar motor in 6 degrees of freedom using LPV control techniques. Two main targets will be pursued: the efficient cancellation of the deformations in the plate due to the thermal aberrations and the asymmetric spatial distribution of the forces during high accelerations, as well as the nanometer accurate reference tracking during a high speed scanning. Due to a possibly high-dimensional model, model reduction techniques can be of use prior to the implementation of the controller. Moreover, the highly coupled nature of the system dynamics will be tackled with the use of a multiple input multiple output (MIMO) controller based on the LPV concept. The design of an LPV feedforward controller will enable the significant reduction of the error within the required margins. Finally, the feedback controller will compensate for the remaining errors due to model uncertainty. The designed controller will be experimentally validated in the magnetic planar motor prototype, which was designed and contructed in the technological university of Eindhoven [4].

References

[1] H. Butler, "Position control in lithographic equipment," *IEEE Control Systems Magazine*, vol. 31, no. 5, pp. 28–47, 2011.

[2] M. Darwish, P. Cox, G. Pillonetto, and R. Tóth, "Bayesian identification of lpv box-jenkins models," in *Proceedings of the 54th IEEE Conference on Decision and Control (CDC), Osaka, Japan*, IEEE, 2015.

[3] I. Proimadis, H. Bijl, and J. W. van Wingerden, "A kernel based approach for lpv subspace identification," in *Proceedings of the 1st IFAC Workshop on Linear Parameter Varying Systems, Grenoble, France*, 2015.

[4] J. Jansen, J. P. Smeets, T. T. Overboom, J. Rovers, and E. Lomonova, "Overview of analytical models for the design of linear and planar motors," *Magnetics, IEEE Transactions on*, vol. 50, no. 11, pp. 1–7, 2014.

SOC and SOH estimation for Li-ion battery, Part II: SOH estimation

Julien Schorsch, Luis D. Couto and Michel Kinnaert

Université Libre de Bruxelles (ULB),

Department of Control Engineering and System Analysis

jschorsc@ulb.ac.be, lcoutome@ulb.ac.be, michel.kinnaert@ulb.ac.be

Abstract: *Based on the electrochemical processes within a lithium-ion battery, state of health indicators are deduced from the solid phase diffusion coefficients that describe the propagation of lithium in each electrode. The estimation of these coefficients, which is seen as a partial differential equation (PDE) identification problem, is here the focus.*

The reliability and the durability of lithium-ion batteries can be strongly affected by their operating conditions. Therefore, there is a need for an on-line monitoring system that constantly provides an estimate of their state-of-charge (SOC) and their state-of-health (SOH). This is one of the roles of a battery-management system. Contrary to the SOC, there is no fixed definition for the SOH. In general, the SOH is related to the physical quantities that control the electrochemical processes inside the battery. Therefore, any parameter that varies with the battery usage could be considered as an indication of the battery SOH. Here, the SOH power fade is computed from the solid phase diffusion coefficient, denoted as D, which describes the lithium propagation in each electrode. Considering the single-particle model in which each electrode is idealized as a single spherical particle, the lithium propagation is described by the following PDE [1]:

$$
\begin{cases}
\dfrac{\partial \bar{c}_{\mathrm{s}}}{\partial t}(t,r) = D \dfrac{\partial^2 \bar{c}_{\mathrm{s}}}{\partial r^2}(t,r) \text{ for } r \in [0,\ R],\, t > 0 \\[4pt]
\bar{c}_{\mathrm{s}}(t,r) = 0 \text{ for } r = 0,\, t > 0 \\[4pt]
R \dfrac{\partial \bar{c}_{\mathrm{s}}}{\partial r}(t,r) - \bar{c}_{\mathrm{s}}(r,t) = -\dfrac{R^2}{D} J(t) \text{ for } r = R,\, t > 0 \\[4pt]
\text{with } \bar{c}_{\mathrm{s}}(t,r) = r c_{\mathrm{s}}(t,r)
\end{cases}
\tag{1}
$$

where $c_{\mathrm{s}}(t,r)$ is the lithium concentration, within each particle which is dependent on both time t and polar coordinate r. The pore-wall molar flux $J(t)$ is related to the input current $I(t)$.

Although the parameter D is assumed to be constant in (1), it actually evolves with aging and operating conditions. This feature is used to define a SOH power fade indicator from the diffusion time constant defined as $\tau = \frac{R^2}{D}$ [2]. Letting τ_{init} denote the value of τ when the battery is operated for the first time, and τ_{pres} denote the present value of τ, this indicator can be written as

$$
\mathrm{SOH} = \frac{\tau_{\mathrm{pres}}}{\tau_{\mathrm{init}}}.
\tag{2}
$$

To determine (2), it is necessary to estimate D and R from
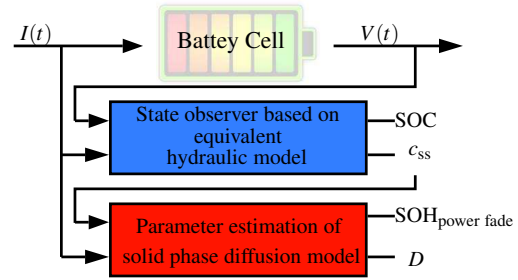
Figure 1: Organization chart for diffusion parameter estimation.

battery operating data. The SOH power fade estimation can then be seen as a PDE parameter estimation problem.

In Fig. 1, a two step procedure is proposed to estimate this diffusion coefficient. In step 1, the lithium concentration at the particle surfaces of each electrode, c_{ss}, is estimated from the current intensity and the voltage. This part is the focus of the companion paper [3]. From the latter estimate and the current intensity, the diffusion coefficient is then identified. This paper focusses on step 2 where the lithium concentration, c_{ss}, is supposed to be known.

The proposed method properly accounts for measurement noise and provides a confidence interval for the estimates. It relies on a three step procedure. A temporal transfer function (TF) is first highlighted from the PDE describing the evolution of the lithium concentration inside the particles. Because the obtained TF is unstable, a solution based on the pre-filtering of the data is then developed. Next a nonlinear parameter estimation problem for the TF identification is solved by resorting to the so-called simplified refined instrumental variable method. This method is known to deliver unbiased estimated parameters whatever the kind of noise is. From this first estimation, the diffusion coefficients are then computed by employing the weighted least-squares method. A resampling scheme is used to estimate a confidence interval for the estimated parameters.

References

[1]   J. Newman and K.E. Thomas-Alyea. Electrochemical Systems. 3rd Edition. John Wiley & Sons, Inc., Hoboken, New Jersey, 2004.

[2]   G.K. Prasad and C.D. Rahn. Model based identification of aging parameters in lithium ion batteries. Journal of Power Sources, 232 p: 79-85, 2013.

[3]   L. D. Couto, J. Schorsch, M. M. Nicotra and M. Kinnaert, SOC and SOH estimation for Li-ion battery, Part I: SOC estimation. Benelux Meeting, 2016.

Part 3

Plenary Lectures

Motivating example I: pollution propagation   (Fukushima)
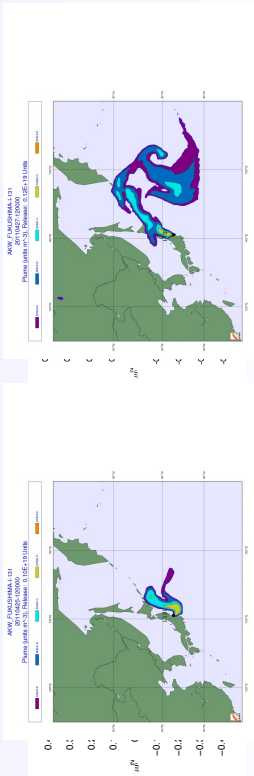
Stokes equation and advection diffusion equation

2 / 56

Data-driven model reduction for large-scale dynamical systems

PART I: General considerations

Thanos Antoulas

Rice University and Jacobs University

email: aca@rice.edu
URL: www.ece.rice.edu/~aca

35th BENELUX Meeting on Systems and Control
22-24 March 2016
Kontakt der Kontinenten, Soesterberg, The Netherlands

1 / 56

Motivating example III: Thermal treatment of railroad rails
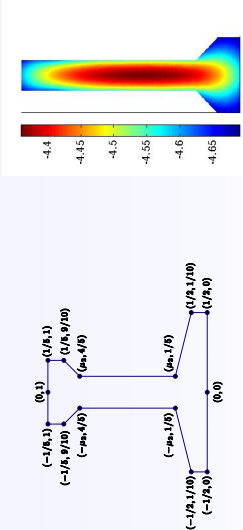
Convection diffusion PDE with inhomogeneous Robin boundary conditions.

4 / 56

Motivating example II: Viscous fingering in porous media (EOR)

Enhanced oil recovery from underground reservoirs

Darcy's law and advection diffusion equation (twice)

3 / 56

Motivating example IV: microstrip device

Microstrip: thin metallic conductors mounted on a flat dielectric substrate, itself mounted on a ground plane. Common applications are transmission lines, antennas and filters.
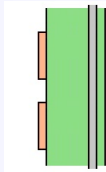
Microstrip transmission lines are a common way to connect two devices. They consist of two thin parallel (metal) strips, mounted on the same dielectric substrate.

Microstip devices are described by **S-parameters**.

5 / 56

Outline

1. **Reduction of systems governed by differential equations**
   - Introduction
   - Model reduction: SVD based methods
   - Model reduction: Moment matching or interpolatory methods

2. **Data-driven model reduction**
   - Model reduction from measurements
   - The Loewner framework

3. **Summary and challenges**

6 / 56

Outline

1. **Reduction of systems governed by differential equations**
   - Introduction
   - Model reduction: SVD based methods
   - Model reduction: Moment matching or interpolatory methods

2. **Data-driven model reduction**
   - Model reduction from measurements
   - The Loewner framework

3. **Summary and challenges**

7 / 56

The overall problem

Physical system

$\Rightarrow$

PDEs

$\Rightarrow$

ODEs

$\Rightarrow$

Model reduction
(Reduced number of ODEs) $\Longleftarrow$ **DATA**

$\Rightarrow$

Simulation, Design, Control

8 / 56

Dynamical systems

$$\mathbf{u}_1(\cdot) \longrightarrow \qquad \longrightarrow \mathbf{y}_1(\cdot)$$
$$\mathbf{u}_2(\cdot) \longrightarrow \qquad \boldsymbol{\Sigma} : \left\{ \begin{array}{l} \dot{\mathbf{x}}(t) = \mathbf{f}(\mathbf{x}(t), \mathbf{u}(t)) \\ \mathbf{y}(t) = \mathbf{h}(\mathbf{x}(t), \mathbf{u}(t)) \end{array} \right. \qquad \longrightarrow \mathbf{y}_2(\cdot)$$
$$\vdots \qquad \qquad \vdots$$
$$\mathbf{u}_m(\cdot) \longrightarrow \qquad \longrightarrow \mathbf{y}_p(\cdot)$$

We consider **explicit** state equations

$$\boldsymbol{\Sigma} : \quad \dot{\mathbf{x}}(t) = \mathbf{f}(\mathbf{x}(t), \mathbf{u}(t)), \quad \mathbf{y}(t) = \mathbf{h}(\mathbf{x}(t), \mathbf{u}(t))$$

with **state** $\mathbf{x}(\cdot)$ of dimension $n \gg m, p$.

9 / 56

Problem statement

Model order reduction (**MOR**) seeks to reduce the complexity of large-scale dynamical systems by approximations of much lower dimension that produce nearly the same input/output response characteristics.

Given: Dynamical system

$$\boldsymbol{\Sigma} = (\mathbf{f}, \mathbf{h}) : \quad \text{where} \quad \mathbf{u}(t) \in \mathbb{R}^m, \ \mathbf{x}(t) \in \mathbb{R}^n, \ \mathbf{y}(t) \in \mathbb{R}^p.$$

Problem: Approximate $\boldsymbol{\Sigma}$ with:

$$\boldsymbol{\Sigma}_k = (\mathbf{f}_k, \mathbf{h}_k), \quad \mathbf{u}(t) \in \mathbb{R}^m, \ \mathbf{x}_k(t) \in \mathbb{R}^k, \ \mathbf{y}_k(t) \in \mathbb{R}^p, \quad k \ll n :$$

> (1) Approximation error small.
> (2) Structure preservation: stability, passivity, · · · .
> (3) Procedure computationally efficient.

10 / 56

Petrov-Galerkin projection

Common framework for (most) MOR methods:

Petrov-Galerkin projection

Choose k-dimensional subspaces $\mathcal{V}_k = \text{span}(\mathbf{V}_k)$, $\mathcal{W}_k = \text{span}(\mathbf{W}_k) \subset \mathbb{C}^n$, such that $\boldsymbol{\Pi} = \mathbf{V}_k \mathbf{W}_k^*$ is a projection.

Find $\mathbf{v}(t) = \mathbf{V}_k \mathbf{x}_k(t) \in \mathcal{V}_k$, $\mathbf{x}_k \in \mathbb{C}^k$, such that

$$\dot{\mathbf{v}}(t) - \mathbf{f}(\mathbf{v}(t), \mathbf{u}(t)) \perp \mathcal{W}_k \quad \Rightarrow \quad \mathbf{W}_k^* (\dot{\mathbf{v}}(t) - \mathbf{f}(\mathbf{v}(t), \mathbf{u}(t))) = \mathbf{0},$$

Then the reduced system is:

$$\boldsymbol{\Sigma}_k : \quad \dot{\mathbf{x}}_k(t) = \mathbf{W}_k^* \mathbf{f}(\mathbf{V}_k \mathbf{x}_k(t), \mathbf{u}(t)), \quad \mathbf{y}_k(t) = \mathbf{h}(\mathbf{V}_k \mathbf{x}_k(t), \mathbf{u}(t)).$$

Criterion: $\boldsymbol{\Sigma}_k$ is a "good" approximation of $\boldsymbol{\Sigma}$, if $\mathbf{x} - \boldsymbol{\Pi}\mathbf{x}$ is "small".
The quality of the reduced system depends on the choice of $\mathcal{V}_k$ and $\mathcal{W}_k$.

11 / 56

Model reduction via projection

Given the linear system

$$\boldsymbol{\Sigma} : \quad \mathbf{E}\dot{\mathbf{x}}(t) = \mathbf{A}\mathbf{x}(t) + \mathbf{B}\mathbf{u}(t), \quad \mathbf{y}(t) = \mathbf{C}\mathbf{x}(t) + \mathbf{D}\mathbf{u}(t)$$

find $\mathbf{v}(t) = \mathbf{V}_k \mathbf{x}_k(t) \in \mathcal{V}_k$, $\mathbf{x}_k \in \mathbb{C}^k$, such that

$$\mathbf{E}\dot{\mathbf{v}}(t) - \mathbf{A}\mathbf{v}(t) - \mathbf{B}\mathbf{u}(t) \perp \mathcal{W}_k \quad \Rightarrow \quad \mathbf{W}_k^* (\mathbf{E}\mathbf{V}_k \dot{\mathbf{x}}_k(t) - \mathbf{A}\mathbf{V}_k \mathbf{x}_k(t) - \mathbf{B}\mathbf{u}(t)) = \mathbf{0},$$

$$\Rightarrow \quad \boldsymbol{\Sigma}_k : \quad \mathbf{E}_k \dot{\mathbf{x}}_k(t) = \mathbf{A}_k \mathbf{x}_k(t) + \mathbf{B}\mathbf{u}(t), \quad \mathbf{y}_k(t) = \mathbf{C}_k \mathbf{x}_k(t) + \mathbf{D}_k \mathbf{u}(t)$$

Reduced order system

$$\mathbf{E}_k = \mathbf{W}_k^* \mathbf{E} \mathbf{V}_k, \quad \mathbf{A}_k = \mathbf{W}_k^* \mathbf{A} \mathbf{V}_k, \quad \mathbf{B}_k = \mathbf{W}_k^* \mathbf{B}, \quad \mathbf{C}_k = \mathbf{C} \mathbf{V}_k \quad \text{and} \quad \mathbf{D}_k = \mathbf{D}.$$

12 / 56

Issues and requirements

Goal

- Fast simulation for design and control

Issues with large-scale systems

- Storage – Computational speed – Accuracy

Requirements for model reduction

- Approximation error small
- Structure preservation (e.g. stability/passivity)
- Procedure computationally efficient and automatic

Outline

1. **Reduction of systems governed by differential equations**
   - Introduction
   - Model reduction: SVD based methods
   - Model reduction: Moment matching or interpolatory methods

2. **Data-driven model reduction**
   - Model reduction from measurements
   - The Loewner framework

3. **Summary and challenges**

Approximation methods: Overview

SVD

Krylov
- Interpolation

Nonlinear systems	Linear systems
• POD methods	• Balanced truncation
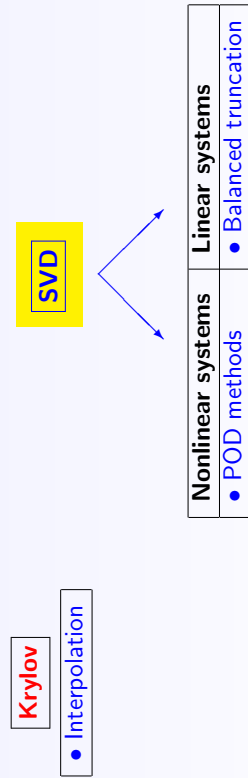
SVD (Singular Value Decomposition)

Prototype approximation problem SVD : $A = U \Sigma V^* \approx U_k \Sigma_k V_k^*$

Singular values Σ provide trade-off between accuracy and complexity.

original: 2048 × 4608
rank = 1681

rank = 20

rank = 50

POD (Proper Orthogonal Decomposition)

Consider: $\dot{\mathbf{x}}(t) = \mathbf{f}(\mathbf{x}(t))$.

Collect snapshots of the state: $\mathcal{X} = [\mathbf{x}(t_1)\ \mathbf{x}(t_2)\ \cdots\ \mathbf{x}(t_N)] \in \mathbb{R}^{n\times N}$.

SVD: $\mathcal{X} = \mathbf{U}\Sigma\mathbf{V}^* \approx \mathbf{U}_k\Sigma_k\mathbf{V}_k^*$, $k \ll n$. Approximation of the state:

$$\mathbf{x}_k(t) = \mathbf{U}_k^*\mathbf{x}(t) \ \Rightarrow\ \mathbf{x}(t) \approx \mathbf{U}_k\mathbf{x}_k(t), \quad \mathbf{x}_k(t) \in \mathbb{R}^k.$$

Project state equations $\Rightarrow$ reduced order system:

$$\boxed{\dot{\mathbf{x}}_k(t) = \mathbf{U}_k^*\mathbf{f}(\mathbf{U}_k\mathbf{x}_k(t))}$$

$\Rightarrow \mathbf{x}_k(t)$ evolves in a **low-dimensional** space.

Issues with POD: (a) Choice of snapshots, (b) singular values not I/O invariants, (c) computation of $\mathbf{f}(\mathbf{U}_k\cdot)$ costly. Remedy: **DEIM.**

Viscous fingering in porous media

$\nabla \cdot \mathbf{u} = 0$ (incompressibility)

$\nabla\pi = -\mu\,\mathbf{u}$ (Darcy's law)
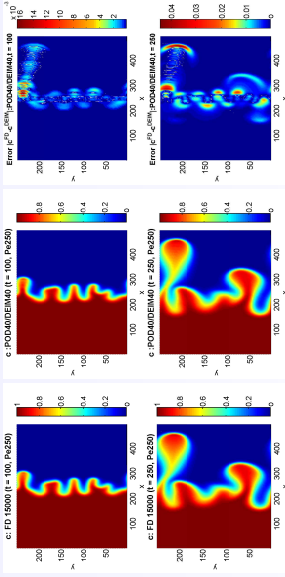
$\dfrac{\partial c}{\partial t} + \mathbf{u}\cdot\nabla c = \alpha\,\nabla^2 c + \beta f(c)$ (convection, diffusion for c)

$\dfrac{\partial\Theta}{\partial t} + \mathbf{u}\cdot\nabla\Theta = \gamma\,\nabla^2\Theta + \delta f(c)$ (convection, diffusion for Θ)

$\mathbf{u}$: velocity, π: pressure, c: concentration, Θ: temperature, $\alpha,\beta,\gamma,\delta$ constants, $\mu(c,\Theta)$: viscosity of injected fluid, $f(c)$ nonlinear function of c.

Some references:

- T. Bui-Thanh, M. Damodaran, and K. Willcox, *Aerodynamic data reconstruction and inverse design using proper orthogonal decomposition*, AIAA J., 42 (2004), pp. 1505-1516.
- K. Kunisch and S. Volkwein, *Control of the Burgers equation by a reduced-order approach using proper orthogonal decomposition*, J. Optim. Theory Appl., 102 (1999), pp. 345-371.
- K. Kunisch and S. Volkwein, *Galerkin proper orthogonal decomposition methods for a general equation in fluid dynamics*, SIAM J. Numer. Anal., 40 (2002), pp. 492-515.
- C. W. Rowley, T. Colonius, and R. M. Murray, *Model reduction for compressible flows using POD and Galerkin projection*, Phys. D, 189 (2004), pp. 115-129.
- S. Chaturantabut and D.C. Sorensen, *Nonlinear model reduction via discrete empirical interpolation*, SIAM J. Scientific Computing, Vol. 32, pp. 2737-2764 (2010).

SVD methods: Balanced Truncation

- SVD for linear systems $\Rightarrow$ Balanced truncation (BT)
- Trade-off between accuracy and complexity for linear systems is provided by the **Hankel Singular Values.**
- Define the **gramians**:

$$\mathcal{P} = \int_0^\infty e^{\mathbf{A}t}\mathbf{B}\mathbf{B}^* e^{\mathbf{A}^* t}\,dt, \quad \mathcal{Q} = \int_0^\infty e^{\mathbf{A}^* t}\mathbf{C}^*\mathbf{C} e^{\mathbf{A}t}\,dt$$

- To compute the gramians we need to solve **2 Lyapunov equations**:

$$\left.\begin{array}{l}\mathbf{A}\mathcal{P} + \mathcal{P}\mathbf{A}^* + \mathbf{B}\mathbf{B}^* = \mathbf{0}, \quad \mathcal{P} > \mathbf{0}\\[4pt] \mathbf{A}^*\mathcal{Q} + \mathcal{Q}\mathbf{A} + \mathbf{C}^*\mathbf{C} = \mathbf{0}, \quad \mathcal{Q} > \mathbf{0}\end{array}\right\} \Rightarrow \boxed{\sigma_i = \sqrt{\lambda_i(\mathcal{P}\mathcal{Q})}}$$

σ_i: **Hankel singular values** of system $\mathbf{\Sigma}$.

What should we be looking for?

Illustrative example: the eigenvalue problem.

Given $A \in C^{n \times n}$, the conventional solution consists of 2 steps: (a) compute the characteristic polynomial $\chi_A(s) = \det(sI - A)$, to obtain the eigenvalues $\lambda_i \in C$, (b) solve $\ker(\lambda_i I - A)$, to obtain the corresponding eigenvectors.

This may work for small matrices.

For larger matrices the characteristic polynomial is not computable:

```
poly(randn(5, 5));        [max(abs(ans))/min(abs(ans))] = 1.3199e + 001
poly(randn(10, 10));      [max(abs(ans))/min(abs(ans))] = 8.5068e + 002
poly(randn(20, 20));      [max(abs(ans))/min(abs(ans))] = 5.4973e + 008
poly(randn(30, 30));      [max(abs(ans))/min(abs(ans))] = 7.5186e + 015
poly(randn(50, 50));      [max(abs(ans))/min(abs(ans))] = 2.4463e + 032
poly(randn(100, 100));    [max(abs(ans))/min(abs(ans))] = 1.6750e + 078
poly(randn(200, 200));    [max(abs(ans))/min(abs(ans))] = 1.0637e + 188
```

Thus, for large matrices only a few eigenvalues and the corresponding eigenvectors can be computed.

Methods used: **iterative eigenvalue computations.**

Properties of balanced truncation

1. **Stability is preserved**.
2. **Global error bound**: $\sigma_{k+1} \leq \| \Sigma - \Sigma_k \|_\infty \leq 2(\sigma_{k+1} + \cdots + \sigma_n)$.

Drawbacks

1. **Dense** computations $\Rightarrow$ number of operations $\mathcal{O}(n^3)$.
2. **Bottleneck: solution of two Lyapunov equations**, hence use iterative methods to compute approximate low rank solutions (ADI, Smith).

References   • U. Baur, P. Benner, L. Feng, Model order reduction for linear and nonlinear systems: a system-theoretic perspective, Preprint, Max Planck Institute Magdeburg, February 2014.

• V. Mehrmann, T. Stykel, Balanced truncation model reduction for large-scale systems in descriptor form. In Dimension Reduction of Large-Scale Systems, P. Benner, V. Mehrmann and D. Sorensen, eds., Lec. Notes Comput. Sci. & Eng. 45, Springer, pp. 83-115 (2005).

Example

Semidiscretized advection diffusion equation (concentration of pollutant c):

$$\frac{\partial}{\partial t} c(\xi, t) - \nabla \cdot (\kappa \nabla c(\xi, t)) + \mathbf{v}(\xi) \cdot \nabla c(\xi, t) = u(\xi, t)$$

advection $\mathbf{v}$: solution of steady state Stokes equation; diffusivity $\kappa = 0.005$.

	Original	Reduced
	$m = 16$	$m = 16$
	$n = 2673$	$k = 10$
	$p = 283$	$p = 283$

Drawbacks of balanced truncation

1. Dense – as opposed to sparse – computations, matrix factorizations and inversions $\Rightarrow$ may be ill-conditioned; number of operations $\mathcal{O}(n^3)$
2. Bottleneck: solution of Lyapunov equations: $AP + PA^* + BB^* = \mathbf{0}$. For large A such equations cannot be solved exactly.

Instead, since $P > 0 \Rightarrow$ **square root L exists**: $P = LL^*$.
Hence compute **approximations V** to **L**: $\hat{P} = VV^*$: rank $V = k \ll n$:

$$P = L \, L^* \approx V \, V^* = \hat{P}$$

Iterative solution: ADI, modified Smith (guaranteed convergence).

Outline

1 Reduction of systems governed by differential equations
- Introduction
- Model reduction: SVD based methods
- Model reduction: Moment matching or interpolatory methods

2 Data-driven model reduction
- Model reduction from measurements
- The Loewner framework

3 Summary and challenges

Time	Original n=2673	Reduced k=10
t = 0.0		
t = 0.4		
t = 0.8		
t = 2.0		

Krylov methods: Approximation by moment matching

Given $\mathbf{E}\dot{\mathbf{x}}(t) = \mathbf{A}\mathbf{x}(t) + \mathbf{B}\mathbf{u}(t)$, $\mathbf{y}(t) = \mathbf{C}\mathbf{x}(t) + \mathbf{D}\mathbf{u}(t)$, the transfer function is :

$$\mathbf{H}(s) = \mathbf{C}(s\mathbf{E} - \mathbf{A})^{-1}\mathbf{B} + \mathbf{D}.$$

With $(\,\cdot\,)^{(j)}$ denoting the jth derivative of $(\,\cdot\,)$ wrt s, the **moments** of the system at a given $\sigma \in \mathbb{C}$ are: $\left.\right\}$ $\mathbf{H}^{(j)}(\sigma)$, $j = 0, 1, 2, \cdots$.

Find $\mathbf{E}_k\dot{\mathbf{x}}_k(t) = \mathbf{A}_k\mathbf{x}_k(t) + \mathbf{B}_k\mathbf{u}(t)$, $\mathbf{y}_k(t) = \mathbf{C}_k\mathbf{x}_k(t) + \mathbf{D}_k\mathbf{u}(t)$, such that

$$\mathbf{H}_k^{(j)}(\sigma) = \mathbf{H}^{(j)}(\sigma),$$

for given points σ, and a given number of derivatives at each point. Consequently:

Approximation by rational interpolation

Approximation methods: Overview

Krylov
- Interpolation

SVD

Nonlinear systems	Linear systems
• POD methods	• Balanced truncation

167

The general interpolation framework

- **Goal**: produce $\mathbf{H}_k(s)$, that approximates a large order $\mathbf{H}(s)$, by means of **interpolation** at a set of points σ_i: $\quad \mathbf{H}_k(\sigma_i) = \mathbf{H}(\sigma_i), \quad i = 1, \cdots, k$.

- For MIMO systems interpolation conditions are imposed in specified directions: **tangential interpolation**.

Problem: Find reduced model satisfying:

$$\boldsymbol{\ell}_j^* \mathbf{H}_k(\mu_i) = \boldsymbol{\ell}_j^* \mathbf{H}(\mu_i), \ \mathbf{H}_k(\lambda_j)\mathbf{r}_j = \mathbf{H}(\lambda_j)\mathbf{r}_j, \ i,j = 1, \cdots, k.$$

Interpolatory projections

$$\mathbf{V}_k = \left[(\lambda_1 \mathbf{E} - \mathbf{A})^{-1}\mathbf{B}\mathbf{r}_1, \cdots, (\lambda_k \mathbf{E} - \mathbf{A})^{-1}\mathbf{B}\mathbf{r}_k \right], \ \mathbf{W}_k^* = \begin{bmatrix} \boldsymbol{\ell}_1^* \mathbf{C}(\mu_1 \mathbf{E} - \mathbf{A})^{-1} \\ \vdots \\ \boldsymbol{\ell}_k^* \mathbf{C}(\mu_k \mathbf{E} - \mathbf{A})^{-1} \end{bmatrix}.$$

- **Consequence**: Krylov methods match moments **without** computing them.

Q: How to choose the interpolation points and tangential directions?

Choice of interpolation points: Optimal $\mathcal{H}_2$ model reduction

Recall: the $\mathcal{H}_2$ norm of a stable system $\boldsymbol{\Sigma}$ is:

$$\|\boldsymbol{\Sigma}\|_{\mathcal{H}_2} = \left(\frac{1}{2\pi} \int_{-\infty}^{+\infty} \text{trace}\,[\mathbf{H}(i\omega)\mathbf{H}^*(-i\omega)]\,d\omega \right)^{\frac{1}{2}}$$

where $\mathbf{H}(s) = \mathbf{C}(s\mathbf{E} - \mathbf{A})^{-1}\mathbf{B}$, is the system transfer function.

Goal: construct a *reduced system* such that $\boldsymbol{\Sigma}_k = \underset{\deg(\hat{\boldsymbol{\Sigma}})=k}{\arg\min} \ \left\| \boldsymbol{\Sigma} - \hat{\boldsymbol{\Sigma}} \right\|_{\mathcal{H}_2}$.

The optimization problem is **nonconvex**. We propose finding reduced order models that satisfy first-order necessary optimality conditions.

First-order necessary optimality conditions

Let $\mathbf{H}_k$ solve the optimal $\mathcal{H}_2$ problem and let $\hat{\lambda}_i$ denote its poles. Assuming for simplicity that $m = p = 1$, the following **interpolation conditions** hold:

$$\mathbf{H}(-\hat{\lambda}_i^*) = \mathbf{H}_k(-\hat{\lambda}_i^*) \text{ and } \ \frac{d}{ds}\mathbf{H}(s)\bigg|_{s=-\hat{\lambda}_i^*} = \frac{d}{ds}\mathbf{H}_k(s)\bigg|_{s=-\hat{\lambda}_i^*}$$

Thus the optimal reduced system $\mathbf{H}_k$ matches the first two moments of the original system at the **mirror image of its poles**.

IRKA (Iterative Rational Krylov Algorithm)

1. Make an initial selection of σ_i, for $i = 1, \cdots, k$

2. $\mathbf{W} = [(\sigma_1 \mathbf{E}^* - \mathbf{A}^*)^{-1}\mathbf{C}^*, \cdots, (\sigma_k \mathbf{E}^* - \mathbf{A}^*)^{-1}\mathbf{C}^*]$

3. $\mathbf{V} = [(\sigma_1 \mathbf{E} - \mathbf{A})^{-1}\mathbf{B}, \cdots, (\sigma_k \mathbf{E} - \mathbf{A})^{-1}\mathbf{B}]$

4. while (not converged)
   - $\mathbf{E}_k = \mathbf{W}^*\mathbf{E}\mathbf{V}, \ \mathbf{A}_k = \mathbf{W}^*\mathbf{A}\mathbf{V}$,
   - $\sigma_i \longleftarrow -\lambda_i(\mathbf{A}_k, \mathbf{E}_k) + \text{Newton correction}, \ i = 1, \cdots, k$,
   - $\mathbf{W} = [(\sigma_1 \mathbf{E}^* - \mathbf{A}^*)^{-1}\mathbf{C}^*, \cdots, (\sigma_k \mathbf{E}^* - \mathbf{A}^*)^{-1}\mathbf{C}^*]$,
   - $\mathbf{V} = [(\sigma_1 \mathbf{E} - \mathbf{A})^{-1}\mathbf{B}, \cdots, (\sigma_k \mathbf{E} - \mathbf{A})^{-1}\mathbf{B}]$.

5. $\mathbf{E}_k = \mathbf{W}^*\mathbf{E}\mathbf{V}, \ \mathbf{A}_k = \mathbf{W}^*\mathbf{A}\mathbf{V}, \ \mathbf{B}_k = \mathbf{W}^*\mathbf{B}, \ \mathbf{C}_k = \mathbf{C}\mathbf{V}$

- Example: Cooling process in a rolling mill. Boundary control of 2D heat equation: finite element discretization yields:

$$\mathbf{A}, \mathbf{E} \in \mathbb{R}^{79841 \times 79841}, \quad \mathbf{B} \in \mathbb{R}^{79841 \times 7}, \quad \mathbf{C} \in \mathbb{R}^{6 \times 79841}.$$

Numerical results

IRKA is compared with:

1. Modal Approximation H_{modal}: choose 20 dominant modes of $H(s)$.
2. $H_{j\omega}$: interpolation points $j\omega$ where $\|H(j\omega)\|$ is dominant.
3. H_{real}: 20 interpolation points in the mirror images of the poles of $H(s)$.

	H_{IRKA}	H_{modal}	$H_{j\omega}$	H_{real}
Relative $\mathcal{H}_\infty$ error	0.030	0.103	0.542	0.247
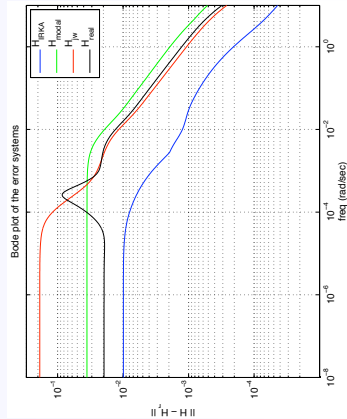
Bode plot of the error systems

Some references: Interpolatory model reduction

- A.C. Antoulas, C.A. Beattie, and S. Gugercin, *Interpolatory model reduction of large-scale systems*, in Efficient modeling and control of large-scale systems, K. Grigoriadis and J. Mohammadpour Eds, Springer Verlag, pages 3-58 (2010).
- A.R. Kellems, D. Roos, N. Xiao, S.J. Cox: Low-dimensional, morphologically accurate models of subthreshold membrane potential, J. Comput. Neuroscience, 27:161-176 (2009).
- C.A. Beattie and S. Gugercin, *Interpolatory projection methods for structure preserving model reduction*, Syst. Cont. Lett., 58 (2009).
- C.A. Beattie and S. Gugercin, *Model Reduction by Rational Interpolation*, in "Model Reduction and Approximation for Complex Systems", edited by Peter Benner, Albert Cohen, Mario Ohlberger, and Karen Willcox, Birkhäuser International Series of Numerical Mathematics, 2014.
- S. Gugercin, C.A. Beattie and A.C. Antoulas, *Data-driven and interpolatory model reduction*, book in preparation, SIAM (2016).

Outline

1. **Reduction of systems governed by differential equations**
   - Introduction
   - Model reduction: SVD based methods
   - Model reduction: Moment matching or interpolatory methods
2. **Data-driven model reduction**
   - Model reduction from measurements
   - The Loewner framework
3. **Summary and challenges**

Outline

1. Reduction of systems governed by differential equations
   - Introduction
   - Model reduction: SVD based methods
   - Model reduction: Moment matching or interpolatory methods
2. **Data-driven model reduction**
   - Model reduction from measurements
   - The Loewner framework
3. Summary and challenges

A motivation: electronic systems

In the elctronics industry the streamlining of the simulation of entire complex systems from chips to packages to boards, etc., is required. Semiconductor manufacturers do not provide to customers with models of heat dissipation.

Semiconductor package	Temperature distribution
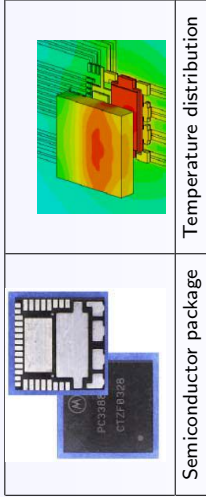
Procedure: from frequency response measurements, derive a reduced order model describing heat dissipation. **Tool**: **S (Scattering) – parameters**

37 / 56

Measurement of S-parameters
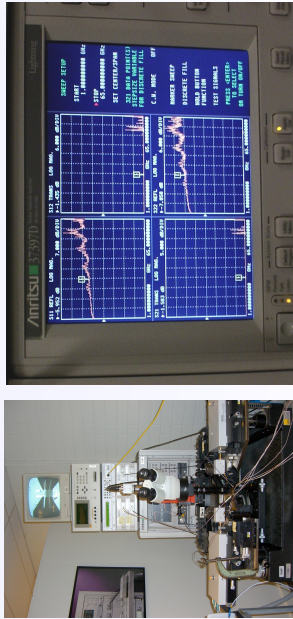
Figure: VNA (Vector Network Analyzer) and VNA screen showing the magnitude of the S-parameters for a 2 port device.

38 / 56

Outline

1. **Reduction of systems governed by differential equations**
   - Introduction
   - Model reduction: SVD based methods
   - Model reduction: Moment matching or interpolatory methods

2. **Data-driven model reduction**
   - Model reduction from measurements
   - The Loewner framework

3. **Summary and challenges**

39 / 56

The Loewner matrix

Given:
row array $(\mu_j, \mathbf{v}_j),\ j = 1, \cdots, k,$ and
column array $(\lambda_i, \mathbf{w}_i),\ i = 1, \cdots, q,$

the associated **Loewner matrix** is:

$$\mathbb{L} = \begin{bmatrix} \frac{\mathbf{v}_1 - \mathbf{w}_1}{\mu_1 - \lambda_1} & \cdots & \frac{\mathbf{v}_1 - \mathbf{w}_q}{\mu_1 - \lambda_q} \\ \vdots & \ddots & \vdots \\ \frac{\mathbf{v}_k - \mathbf{w}_1}{\mu_k - \lambda_1} & \cdots & \frac{\mathbf{v}_k - \mathbf{w}_q}{\mu_k - \lambda_q} \end{bmatrix} \in \mathbb{C}^{k \times q}$$

- If there is a known underlying function $\mathbf{g}$, then $\mathbf{w}_i = \mathbf{g}(\lambda_i)$, and $\mathbf{v}_j = \mathbf{g}(\mu_j)$.

- If $\mu_i = \lambda_i \Rightarrow (\mathbb{L})_{i,j} = \mathbf{w}_i^{(1)}$, which in case of a known underlying function $\mathbf{g}$ becomes: $\mathbf{w}_i^{(1)} = \frac{d\mathbf{g}}{ds}|_{s=\lambda_i}$.

40 / 56

Karel Löwner 1893 - 1968
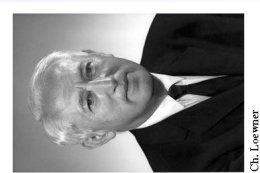
- Born in Bohemia
- Studied in Prague under Georg Pick
- Emigrated to the US in 1939
- adapted his name to Charles Loewner

Ch. Loewner

Seminal paper: Über monotone Matrixfunctionen, Math. Zeitschrift (1934).

Model construction from data: Interpolation

Assume for simplicity that the given data are scalar:

$$(s_i, \phi_i), \ i = 1, 2, \cdots, N, \quad s_i \neq s_j, \ i \neq j$$

Find $H(s) = \frac{n(s)}{d(s)}$, such that $H(s_i) = \phi_i$, $i = 1, 2, \cdots, N$, and n, d: coprime.

Main tool: Loewner matrix. Divide the data in disjoint sets:

(λ_i, w_i), $i = 1, 2, \cdots, k$, (μ_j, v_j), $j = 1, 2, \cdots, q$, $k + q = N$:

$$\mathbb{L} = \begin{bmatrix} \frac{v_1 - w_1}{\mu_1 - \lambda_1} & \cdots & \frac{v_1 - w_k}{\mu_1 - \lambda_k} \\ \vdots & \ddots & \vdots \\ \frac{v_q - w_1}{\mu_q - \lambda_1} & \cdots & \frac{v_q - w_k}{\mu_q - \lambda_k} \end{bmatrix} \quad \in \mathbb{C}^{q \times k}$$

Main property

Let $\mathbb{L}$ be a $p \times k$ Loewner matrix. Then $p, k \geq \deg \mathbf{g} \Rightarrow \operatorname{rank} \mathbb{L} = \deg \mathbf{g}$.

$\Rightarrow$ for approximation, the SVD of $\mathbb{L}$ provides a trade-off between accuracy and complexity

General framework – tangential interpolation

Given: • right data: $(\lambda_i; r_i, w_i)$, $i = 1, \cdots, k$;

• left data: $(\mu_j; \ell_j^*, v_j^*)$, $j = 1, \cdots, q$; (all points are assumed distinct).

Problem: Find rational $p \times m$ matrices $H(s)$, such that

$$H(\lambda_i) r_i = w_i \quad \text{and} \quad \ell_j^* H(\mu_j) = v_j^*$$

Define the **right data**:

$$\Lambda = \begin{bmatrix} \lambda_1 & & \\ & \ddots & \\ & & \lambda_k \end{bmatrix} \in \mathbb{C}^{k \times k}, \quad R = [r_1 \ r_2, \ \cdots \ r_k] \in \mathbb{C}^{m \times k}, \quad W = [w_1 \ w_2 \ \cdots \ w_k] \in \mathbb{C}^{p \times k},$$

and the **left data**:

$$M = \begin{bmatrix} \mu_1 & & \\ & \ddots & \\ & & \mu_q \end{bmatrix} \in \mathbb{C}^{q \times q}, \quad L = \begin{bmatrix} \ell_1^* \\ \vdots \\ \ell_q^* \end{bmatrix} \in \mathbb{C}^{q \times p}, \quad V = \begin{bmatrix} v_1^* \\ \vdots \\ v_q^* \end{bmatrix} \in \mathbb{C}^{q \times m}.$$

Tangential interpolation: the Loewner pencil

Recall data: $H(\lambda_i) r_i = w_i$, $\ell_j^* H(\mu_j) = v_j^*$.

The **Loewner matrix** $\mathbb{L} \in \mathbb{C}^{q \times k}$ is:

$$\mathbb{L} = \begin{bmatrix} \frac{v_1^* r_1 - \ell_1^* w_1}{\mu_1 - \lambda_1} & \cdots & \frac{v_1^* r_k - \ell_1^* w_k}{\mu_1 - \lambda_k} \\ \vdots & \ddots & \vdots \\ \frac{v_q^* r_1 - \ell_q^* w_1}{\mu_q - \lambda_1} & \cdots & \frac{v_q^* r_k - \ell_q^* w_k}{\mu_q - \lambda_k} \end{bmatrix}$$

The **shifted Loewner matrix** $\mathbb{L}_s \in \mathbb{C}^{q \times k}$ is:

$$\mathbb{L}_s = \begin{bmatrix} \frac{\mu_1 v_1^* r_1 - \ell_1^* w_1 \lambda_1}{\mu_1 - \lambda_1} & \cdots & \frac{\mu_1 v_1^* r_k - \ell_1^* w_k \lambda_k}{\mu_1 - \lambda_k} \\ \vdots & \ddots & \vdots \\ \frac{\mu_q v_q^* r_1 - \ell_q^* w_1 \lambda_1}{\mu_q - \lambda_1} & \cdots & \frac{\mu_q v_q^* r_k - \ell_q^* w_k \lambda_k}{\mu_q - \lambda_k} \end{bmatrix}$$

if we are given $H(s) = C(sE - A)^{-1}B$:

$x_i = (\lambda_i E - A)^{-1} B r_i \Rightarrow$

X: generalized reachability matrix

$y_j^* = \ell_j^* C(\mu_j E - A)^{-1} \Rightarrow$

Y*: generalized observability matrix.

L can be factored as

$\Rightarrow \boxed{L = -Y^* E X}$

$\mathbb{L}_s$ can be factored as

$\Rightarrow \boxed{\mathbb{L}_s = -Y^* A X}$

Construction of Interpolants

- If the pencil $(\mathbb{L}_s, \mathbb{L})$ is regular, i.e.
  $\Phi(s) = \mathbb{L}_s - s\,\mathbb{L}$, is invertible, then

  $$\mathbf{E} = -\mathbb{L}, \quad \mathbf{A} = -\mathbb{L}_s, \quad \mathbf{B} = \mathbf{V}, \quad \mathbf{C} = \mathbf{W}$$
  is a minimal interpolant of the data

  $\Rightarrow \quad \boxed{\mathbf{H}(s) = \mathbf{W}\,\Phi(s)^{-1}\,\mathbf{V}}$

- If $\Phi(s) = \mathbb{L}_s - s\,\mathbb{L}$, is singular, let
  $\Phi(s)^{\#}$ be a generalized inverse of $\Phi(s)$
  (Drazin or Moore-Penrose).

  $\Rightarrow \quad \boxed{\mathbf{H}(s) = \mathbf{W}\,\Phi(s)^{\#}\,\mathbf{V}}$

- In this case, if the **numerical** $\mathrm{rank}\,\mathbb{L} = k$, compute the rank revealing *SVD*:

  $$\mathbb{L} = \mathbf{Y}\Sigma\mathbf{X}^* \approx \mathbf{Y}_k \Sigma_k \mathbf{X}_k^*$$

Theorem. A realization $[\mathbf{C}, \mathbf{E}, \mathbf{A}, \mathbf{B}]$, of an approximate interpolant is given as:

$$\mathbf{E} = -\mathbf{Y}_k^*\mathbb{L}\mathbf{X}_k, \quad \mathbf{A} = -\mathbf{Y}_k^*\mathbb{L}_s\mathbf{X}_k, \quad \mathbf{B} = \mathbf{Y}_k^*\mathbf{V}, \quad \mathbf{C} = \mathbf{W}\mathbf{X}_k.$$

Microstrip - data: *1001 S-parameter measurements between 10-18 GHz (CST)*

Data frequency response $\|\mathbf{S}_{i,j}\|$, $i,j=1,2$.	Data two singular values.
Singular values of 1001×1001 Loewner matrix	Singular-value fit of model $k=72$
S-parameter-error: $\in [10^{-6}, 10^{-4}]$	Two singular values of model: $\omega \in [0, 10\,\mathrm{THz}]$

Generalizations of the Loewner framework to:

1. Linear parameter-dependent systems
2. Linear port-Hamiltonian systems
3. Linear infinite-dimensional systems described by transfer functions
4. Linear switched systems
5. Bilinear systems
6. Nonlinear systems with analytic nonlinearities

Summary

Data-driven MOR (e.g. from S-parameters or DNS)

Key tool: **Loewner pencil** and tangential interpolation

Given input/output data, we can construct with **no computation**, a singular high order model in descriptor form $\Rightarrow$ natural way to construct reduced models

$\Rightarrow$ **SVD of $\mathbb{L}$ provides trade-off between accuracy and complexity**

$\Rightarrow$ does not force inversion of $\mathbf{E}$ or require persistence of excitation

$\Rightarrow$ can deal with many input/output ports

Philosophy: $\boxed{\text{Collect data and extract desired information}}$

Some references on data-driven model reduction, parametrized systems, nonlinear systems

- S. Lefteriu and A.C. Antoulas: A New Approach to Modeling Multiport Systems from Frequency-Domain Data, IEEE Trans. CAD, 29: 14-27 (2010).

- A.C. Antoulas, A.C. Ionita, and S. Lefteriu, *On two-variable rational interpolation*, Linear Algebra and Its Applications, **436**: 2889-2915 (2012).

- A.C. Ionita and A.C. Antoulas, Parametrized model order reduction from transfer function measurements, in Reduced Order Methods for modeling and computational reduction, Book Series: Modeling, Comutations and Applications, A. Quarteroni, G. Rozza (Editors), Springer Verlag (2013).

- A.C. Ionita and A.C. Antoulas, Data-driven parametrized model reduction in the Loewner framework, SIAM J. Scientific Computing, 2014.

- A.C. Antoulas, S. Lefteriu and A.C. Ionita, A tutorial introduction of the Loewner framework in model reduction, in Model Reduction and Approximation for Complex Systems, edited by P. Benner, A. Cohen, M. Ohlberger, and K. Willcox, Birkhäuser Intl Series of Numerical Mathematics, 2014.

- T. Breiten, T. Damm, Krylov subspace methods for model reduction of bilinear systems, Systems and Control Letters, **59**: 443-450 (2010).

- T. Breiten, Interpolatory methods for model reduction of large-scale dynamical systems, PhD Dissertation, Magdeburg, March 2013.

- P. Benner and T. Breiten, *Two-sided moment matching methods for nonlinear model reduction*, Preprint No. MPIMD/12-12, MPI Magdeburg, 2012.

- P. Benner, S. Gugercin, K. Willcox, A Survey of Model Reduction Methods for Parametric Systems, SIAM Review, vol 54, pp. 483-531, 2015.

Outline

1. **Reduction of systems governed by differential equations**
   - Introduction
   - Model reduction: SVD based methods
   - Model reduction: Moment matching or interpolatory methods

2. **Data-driven model reduction**
   - Model reduction from measurements
   - The Loewner framework

3. **Summary and challenges**

Summary
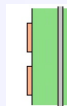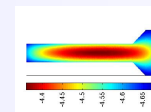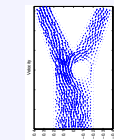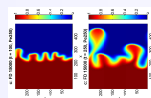
Equations
- Darcy's
- Stokes
- Advection diffusion
- Maxwell's
- Wave

Data
- From measurements
- From equations (DNS)

Methods
1. POD (SVD)
2. Approximate balanced truncation (SVD)
3. Optimal $\mathcal{H}_2$ (interpolatory)
4. Loewner framework (interpolatory)

Methods ② & ④ provide a trade-off between accuracy of fit and complexity of the model.

Challenge: *Microfluidic Biochip*

Lab-on-a-Chip

- Microfluidic systems represent a promising approach towards a realization of a so called 'lab-on-a-chip'.

- A 'lab-on-a-chip' is a device made by integration of several lab functions on a chip. Such a device dealing with microfluids is called microfluidic biochip.

- Such biochips are used in pharmaceutical, medical, and forensic applications for genotyping, and sequencing in genomics, protein profiling in proteomics, and cytometry in cell analysis.
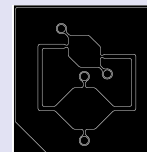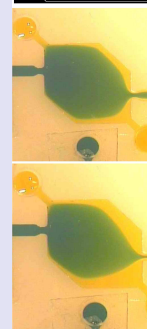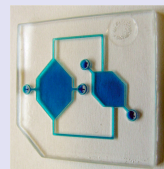
Reference: Antil, Heinkenschloss, Hoppe, Linsenmann, Wixforth.

Challenge: Neural models
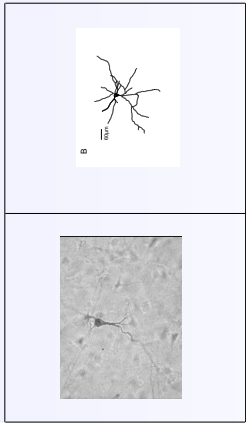
Image from Neuromart (Rice-Baylor archive of neural morphology)

Goal: • How a cell distinguishes between inputs.
Goal: • Propagation of action potentials by simulation of systems containing several million neurons.

• simulations currently limited to systems with $\approx$10K neurons.

• **Hodgkin-Huxley model.**

Reference: A.J. Kellems, S.J. Cox, D.C. Sorensen, S. Chaturantabut.

Challenge: Damping of lightweight bridges

| Lamot footbridge | One damper | Frequency response 3-5Hz |

• Lamot lightweight bridge in Mechelen: finite element model $n = 25,962$.

• The goal: determine optimal stiffness and damping coefficients of the four bridge dampers (8 parameters).

• Example due to Karl Meerbergen (KU Leuven).

Collaborators

- Branimir Anic
- Chris Beattie
- Peter Benner
- Lihong Feng
- Victor Gosea
- Serkan Gugercin
- Matthias Heinkenschloß
- Cosmin Ionita
- Roxana Ionutiu
- Sanda Lefteriu
- Andrew Mayo
- Timo Reis
- Joost Rommes
- Dan Sorensen

General reference: Antoulas SIAM 2005
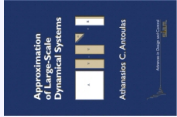
The sequel

- **Part II:** Interpolatory methods in model reduction
- **Part III:** The Loewner framework for model reduction I
- **Part IV:** The Loewner framework for model reduction II

Slide 1/26

Data-driven and interpolatory model reduction: PART II

Thanos Antoulas

Rice University and Jacobs University

email: aca@rice.edu
URL: www.ece.rice.edu/~aca

35th BENELUX Meeting on Systems and Control
22-24 March 2016
Kontakt der Kontinenten, Soesterberg, The Netherlands

Slide 2/26

Outline

Model Reduction via Projection

Model Reduction by Interpolation

Interpolatory Projections for $\mathcal{H}_2$ Optimal Approximation

IRKA

Descent algorithms

Slide 3/26

Outline

Model Reduction via Projection

Model Reduction by Interpolation

Interpolatory Projections for $\mathcal{H}_2$ Optimal Approximation

IRKA

Descent algorithms

Slide 4/26

The Model Reduction Problem

Consider:

$$\Sigma : \quad \mathbf{E}\dot{\mathbf{x}}(t) = \mathbf{A}\mathbf{x}(t) + \mathbf{B}\mathbf{u}(t), \quad \mathbf{y}(t) = \mathbf{C}\mathbf{x}(t) + \mathbf{D}\mathbf{u}(t)$$

where $\mathbf{A}, \mathbf{E} \in \mathbb{R}^{n \times n}$, $\mathbf{B} \in \mathbb{R}^{n \times m}$, $\mathbf{C} \in \mathbb{R}^{q \times n}$, and $\mathbf{D} \in \mathbb{R}^{q \times m}$.

Goal: replace Σ with a simpler reduced model:

$$\widehat{\Sigma} : \quad \widehat{\mathbf{E}}\dot{\widehat{\mathbf{x}}}(t) = \widehat{\mathbf{A}}\widehat{\mathbf{x}}(t) + \widehat{\mathbf{B}}\mathbf{u}(t), \quad \widehat{\mathbf{y}}(t) = \widehat{\mathbf{C}}\widehat{\mathbf{x}}(t) + \widehat{\mathbf{D}}\mathbf{u}(t),$$

where $\widehat{\mathbf{A}}, \widehat{\mathbf{E}} \in \mathbb{R}^{r \times r}$, $\widehat{\mathbf{B}} \in \mathbb{R}^{r \times m}$, $\widehat{\mathbf{C}} \in \mathbb{R}^{q \times r}$, $\widehat{\mathbf{D}} \in \mathbb{R}^{q \times m}$ with $r \ll n$.

The transfer functions and the error are:

$$\mathbf{H}(s) = \mathbf{C}\left(s\mathbf{E} - \mathbf{A}\right)^{-1}\mathbf{B} + \mathbf{D}, \quad \widehat{\mathbf{H}}(s) = \widehat{\mathbf{C}}\left(s\widehat{\mathbf{E}} - \widehat{\mathbf{A}}\right)^{-1}\widehat{\mathbf{B}} + \widehat{\mathbf{D}}.$$

$$\Rightarrow \mathbf{Y}(s) - \widehat{\mathbf{Y}}(s) = \left[\mathbf{H}(s) - \widehat{\mathbf{H}}(s)\right]\mathbf{U}(s).$$

Error Measures

- The $\mathcal{H}_\infty$ norm is
$$\|\mathbf{H}\|_{\mathcal{H}_\infty} = \sup_{\omega \in \mathbb{R}} \|\mathbf{H}(\imath\omega)\|_2,$$
where $\|\mathbf{M}\|_2$ denotes the spectral norm of $\mathbf{M}$. When $\mathbf{E}$ is nonsingular, all eigenvalues of the matrix pencil $\lambda\mathbf{E} - \mathbf{A}$ must lie in the left-half plane. When $\mathbf{E}$ is singular, we assume additionally that 0 is not a defective eigenvalue of $\mathbf{E}$. This guarantees that $\mathbf{H}(s)$ remains bounded as $s \to \infty$. With $\|\mathbf{z}\|_{L_2} = \sqrt{\int_0^\infty \|\mathbf{z}(t)\|_2^2\, dt}$, there holds

$$\boxed{\|\mathbf{y} - \hat{\mathbf{y}}\|_{L_2} \le \left\|\mathbf{H} - \hat{\mathbf{H}}\right\|_{\mathcal{H}_\infty} \|\mathbf{u}\|_{L_2}}$$

- The $\mathcal{H}_2$ norm is
$$\|\mathbf{H}\|_{\mathcal{H}_2} = \left(\frac{1}{2\pi}\int_{-\infty}^\infty \|\mathbf{H}(\imath\omega)\|_F^2\right)^{1/2},$$
where $\|\mathbf{M}\|_F$ denotes the Frobenius norm of $\mathbf{M}$.
The $\mathcal{H}_2$ norm bears a direct relationship to the time domain norm of $\mathbf{y}(t)$:
$$\|\mathbf{y}\|_{L_\infty} = \sup_{t>0}\|\mathbf{y}(t)\|_\infty \le \|\mathbf{H}\|_{\mathcal{H}_2}\|\mathbf{u}\|_{L_2},$$

For model reduction, there holds
$$\boxed{\|\mathbf{y} - \hat{\mathbf{y}}\|_{L_\infty} \le \left\|\mathbf{H} - \hat{\mathbf{H}}\right\|_{\mathcal{H}_2}\|\mathbf{u}\|_{L_2}}$$

Petrov-Galerkin Projections

Let $\mathbf{V} \in \mathbb{R}^{n\times r}$ and assume that $\mathbf{x}(t) \approx \mathbf{V}\hat{\mathbf{x}}(t)$ for some $\hat{\mathbf{x}}(t) \in \mathbb{R}^r$. It follows that
$$\text{Residue}(\hat{\mathbf{x}}(t)) = \mathbf{E}\mathbf{V}\dot{\hat{\mathbf{x}}}(t) - \mathbf{A}\mathbf{V}\hat{\mathbf{x}}(t) - \mathbf{B}\,\mathbf{u}(t)$$
and the approximate output is
$$\hat{\mathbf{y}}(t) = \mathbf{C}\mathbf{V}\hat{\mathbf{x}}(t) + \mathbf{D}\mathbf{u}(t).$$
The reduced state trajectory, $\hat{\mathbf{x}}(t)$, is determined by picking a second r dimensional subspace with a basis $\mathbf{W} \in \mathbb{R}^{n\times r}$ and imposing the Petrov-Galerkin condition:
$$\mathbf{W}^T\text{Residue}(\hat{\mathbf{x}}(t)) = \mathbf{W}^T\left(\mathbf{E}\mathbf{V}\dot{\hat{\mathbf{x}}}(t) - \mathbf{A}\mathbf{V}\hat{\mathbf{x}}(t) - \mathbf{B}\mathbf{u}(t)\right) = \mathbf{0}.$$
This leads to a reduced model
$$\hat{\mathbf{E}}\dot{\hat{\mathbf{x}}}(t) = \hat{\mathbf{A}}\hat{\mathbf{x}}(t) + \hat{\mathbf{B}}\mathbf{u}(t), \quad \hat{\mathbf{y}}(t) = \hat{\mathbf{C}}\hat{\mathbf{x}}(t) + \hat{\mathbf{D}}\mathbf{u}(t)$$
with:
$$\hat{\mathbf{E}} = \mathbf{W}^T\mathbf{E}\mathbf{V}, \quad \hat{\mathbf{A}} = \mathbf{W}^T\mathbf{A}\mathbf{V}, \quad \hat{\mathbf{B}} = \mathbf{W}^T\mathbf{B}, \quad \hat{\mathbf{C}} = \mathbf{C}\mathbf{V}, \quad \hat{\mathbf{D}} = \mathbf{D}.$$

Outline

Model Reduction via Projection

Model Reduction by Interpolation

Interpolatory Projections for $\mathcal{H}_2$ Optimal Approximation

IRKA

Descent algorithms

Tangential interpolation

$\hat{\mathbf{H}}(s)$ is a right-tangential interpolant to $\mathbf{H}(s)$ at $s = \sigma_i$ along the right tangent direction $\mathbf{r}_i \in \mathbb{C}^m$, if
$$\mathbf{H}(\sigma_i)\mathbf{r}_i = \hat{\mathbf{H}}(\sigma_i)\mathbf{r}_i.$$

Similarly, $\hat{\mathbf{H}}(s)$ is a left-tangential interpolant to $\mathbf{H}(s)$ at $s = \mu_i$ along the left tangent direction $\boldsymbol{\ell}_i \in \mathbb{C}^q$, if
$$\boldsymbol{\ell}_i^T\mathbf{H}(\mu_i) = \boldsymbol{\ell}_i^T\hat{\mathbf{H}}(\mu_i).$$

We say that $\hat{\mathbf{H}}(s)$ is a bitangential Hermite interpolant to $\mathbf{H}(s)$ at $s = \sigma_i$ along the right tangent direction $\mathbf{r}_i \in \mathbb{C}^m$ and the left tangent direction $\boldsymbol{\ell}_i \in \mathbb{C}^q$, if
$$\boldsymbol{\ell}_i^T\mathbf{H}'(\sigma_i)\mathbf{r}_i = \boldsymbol{\ell}_i^T\hat{\mathbf{H}}'(\sigma_i)\mathbf{r}_i.$$

where $'$ denotes differentiation with respect to s.

Petrov-Galerkin Projections for Tangential Interpolation

Theorem. Given $H(s)$, let $\widehat{H}(s)$ denote a reduced transfer function obtained by projection using the bases V and W.

Given are $\sigma, \mu \in \mathbb{C}$, $r \in \mathbb{C}^m$ and $\ell \in \mathbb{C}^q$.

(a) If
$$(\sigma E - A)^{-1} Br \in \text{Range}(V),$$
then
$$H(\sigma)r = \widehat{H}(\sigma)r;$$

(b) If
$$\left(\ell^T C(\mu E - A)^{-1}\right)^T \in \text{Range}(W),$$
then
$$\ell^T H(\mu) = \ell^T \widehat{H}(\mu);$$

(c) If both (a) and (b) hold, and $\sigma = \mu$, then
$$\ell^T H'(\sigma)r = \ell^T \widehat{H}'(\sigma)r.$$

Remark. Notice that the values that are interpolated are **never explicitly computed**; this is a significant **advantage** of the Petrov-Galerkin projection framework.

A simple example (Beattie - Gugercin)

Consider the system

$$A = \begin{bmatrix} -6 & -11 & -6 \\ 1 & 0 & 0 \\ 0 & 1 & 0 \end{bmatrix}, \quad B = \begin{bmatrix} -1 & 1 \\ 0 & 1 \\ 1 & 0 \end{bmatrix}, \quad C = \begin{bmatrix} 1 & 0 & 1 \\ 1 & -1 & 0 \end{bmatrix}, \quad E = I_3, \quad D = 0.$$

$$\Rightarrow H(s) = \frac{1}{s^3 + 6s^2 + 11s + 6} \begin{bmatrix} 10 & s^2 - 10s + 1 \\ -s^2 - 5s + 6 & -18s - 6 \end{bmatrix}.$$

We choose $\sigma_1 = \mu_1 = 0$, and tangent directions

$$r_1 = \begin{bmatrix} 1 \\ 2 \end{bmatrix} \quad \text{and} \quad \ell_1 = \begin{bmatrix} 3 \\ 1 \end{bmatrix}.$$

The corresponding Petrov-Galerkin projection is given by:

$$V = (\sigma_1 E - A)^{-1} Br_1 = \begin{bmatrix} -2 \\ -1 \\ 4 \end{bmatrix}, \quad W = (\sigma_1 E - A)^{-T} C^T \ell_1 = \begin{bmatrix} 0.5 \\ -1 \\ 6.5 \end{bmatrix}.$$

This projection yields the reduced model

$$\hat{E} = 26, \hat{A} = -5, \hat{B} = \begin{bmatrix} 6 & -0.5 \end{bmatrix}, \hat{C} = \begin{bmatrix} 2 \\ -1 \end{bmatrix} \Rightarrow \hat{H}(s) = \frac{1}{26s + 5} \begin{bmatrix} 12 & -1 \\ -6 & 0.5 \end{bmatrix}.$$

Checking the interpolation conditions:

$$H(\sigma_1)r_1 = \widehat{H}(\sigma_1)r_1 = \begin{bmatrix} 2 \\ -1 \end{bmatrix}, \quad \checkmark$$

$$\ell_1^T H(\sigma_1) = \ell_1^T \widehat{H}(\sigma_1) = \begin{bmatrix} 6 & -0.5 \end{bmatrix}, \quad \checkmark$$

$$\ell_1^T H'(\sigma_1)r_1 = \ell_1^T \widehat{H}'(\sigma_1)r_1 = -26. \quad \checkmark$$

Notice that $\widehat{H}(s)$ does not fully interpolate $H(s)$ at $s = \sigma_1 = 0$:

$$H(\sigma_1) = \begin{bmatrix} 5/3 & 1/6 \\ 1 & -1 \end{bmatrix} \neq \begin{bmatrix} 2.4 & -0.2 \\ -1.2 & 0.1 \end{bmatrix} = \widehat{H}(\sigma_1).$$

To enforce full matrix interpolation, we need

$$V_m = (\sigma_1 E - A)^{-1} B = \begin{bmatrix} 0 & -1 \\ -1 & 0 \\ 5/3 & 7/6 \end{bmatrix}, \quad W_m = (\sigma_1 E - A)^{-T} C^T = \begin{bmatrix} 1/6 & 0 \\ 0 & -1 \\ 11/6 & 1 \end{bmatrix}.$$

This leads to a reduced system of order 2:

$$\widehat{H}_m(s) = \begin{bmatrix} 10 & 1 \\ 6 & -6 \end{bmatrix} \left(s \begin{bmatrix} 110 & 71 \\ 96 & 42 \end{bmatrix} - \begin{bmatrix} -60 & -6 \\ -36 & 36 \end{bmatrix} \right)^{-1} \begin{bmatrix} 10 & 1 \\ 6 & -6 \end{bmatrix}$$

$\widehat{H}_m(s)$ interpolates $H(s)$ and $H'(s)$ at $s = \sigma_1 = 0$:

$$H(\sigma_1) = \widehat{H}_m(\sigma_1) = \begin{bmatrix} 5/3 & 1/6 \\ 1 & -1 \end{bmatrix}, \quad H'(\sigma_1) = \widehat{H}_m(\sigma_1) = \begin{bmatrix} -55/18 & -71/36 \\ -8/3 & -7/6 \end{bmatrix}.$$

Conclusion. The fundamental difference between tangential and full interpolation is that in the former case, each interpolation condition contributes **one** additional order to the reduced dimension. In the latter case **generically** m or p dimensions are added.

The general case

Given
$$\mathbf{H}(s) = \mathbf{C}(s\mathbf{E} - \mathbf{A})^{-1}\mathbf{B} + \mathbf{D},$$

r right interpolation points $\{\sigma_i\}_{i=1}^r$ and right directions $\{\mathbf{r}_k\}_{k=1}^r \in \mathbb{C}^m$,
r left interpolation points $\{\mu_j\}_{j=1}^r$ and left directions $\{\ell_k\}_{k=1}^r \in \mathbb{C}^q$, construct

$$\mathbf{V} = \left[(\sigma_1\mathbf{E} - \mathbf{A})^{-1}\mathbf{Br}_1, \cdots, (\sigma_r\mathbf{E} - \mathbf{A})^{-1}\mathbf{Br}_r\right] \text{ and}$$

$$\mathbf{W} = \left[(\mu_1\mathbf{E} - \mathbf{A})^{-T}\mathbf{C}^T\ell_1, \cdots, (\mu_r\mathbf{E} - \mathbf{A})^{-T}\mathbf{C}^T\ell_r\right].$$

Then,
$$\widehat{\mathbf{H}}(s) = \widehat{\mathbf{C}}(s\widehat{\mathbf{E}} - \widehat{\mathbf{A}})^{-1}\widehat{\mathbf{B}}$$

constructed by a Petrov-Galerkin projection satisfies the interpolation conditions:

$$\mathbf{H}(\sigma_i)\mathbf{r}_i = \widehat{\mathbf{H}}(\sigma_i)\mathbf{r}_i,$$
$$\ell_i^T\mathbf{H}(\mu_i) = \ell_i^T\widehat{\mathbf{H}}(\mu_i);$$

additionally if $\quad \mu_i = \sigma_i \Rightarrow \ell_i^T\mathbf{H}'(\sigma_i)\mathbf{r}_i = \ell_i^T\widehat{\mathbf{H}}'(\sigma_i)\mathbf{r}_i$.

Remark. The main cost in interpolatory model reduction results from solving large-scale (typically sparse) systems. There is no need to solve large-scale Lyapunov or Riccati equations, giving interpolatory methods a **computational advantage**.

Outline

Model Reduction via Projection

Model Reduction by Interpolation

Interpolatory Projections for $\mathcal{H}_2$ Optimal Approximation

IRKA

Descent algorithms

Optimization problem: given $\mathbf{H}(s)$, find a reduced model $\widehat{\mathbf{H}}(s)$, that minimizes the $\mathcal{H}_2$ error:

$$\left\|\mathbf{H} - \widehat{\mathbf{H}}\right\|_{\mathcal{H}_2} = \min_{\dim(\widetilde{\mathbf{H}})=r}\left\|\mathbf{H} - \widetilde{\mathbf{H}}\right\|_{\mathcal{H}_2}.$$

Recall: small $\mathcal{H}_2$ error induces small time domain error $\|\mathbf{y} - \widehat{\mathbf{y}}\|_{L_\infty}$.

The $\mathcal{H}_2$ optimization problem is nonconvex; finding a global minimizer is typically infeasible. Instead a common approach involves finding locally optimal reduced models that satisfy first-order necessary conditions for optimality.

For MIMO systems, let

$$\widehat{\mathbf{H}}(s) = \widehat{\mathbf{C}}(s\widehat{\mathbf{E}} - \widehat{\mathbf{A}})^{-1}\widehat{\mathbf{B}} = \sum_{i=1}^r \frac{\ell_i\mathbf{r}_i^T}{s - \lambda_i};$$

$\ell_i \in \mathbb{C}^q$ and $\mathbf{r}_i \in \mathbb{C}^m$ are left/right residue directions associated with the pole λ_i;
$\ell_i\mathbf{r}_i^T$ is the matrix residue.

Historical remarks

The $\mathcal{H}_2$ norm: $\quad \mathbf{H}(s) = \sum_{k=1}^n \frac{\phi_k}{s-\lambda_k} \quad \Rightarrow \quad \boxed{\|\mathbf{H}\|_{\mathcal{H}_2}^2 = \sum_{k=1}^n \phi_k\,\mathbf{H}(-\lambda_k)}$

S. Gugercin and A.C. Antoulas, An H2 error expression for the Lanczos procedure, IEEE CDC, 2003.

Corollary. With $\widehat{\mathbf{H}}(s) = \sum_{k=1}^r \frac{\widehat{\phi}_k}{s - \widehat{\lambda}_k}$, the $\mathcal{H}_2$ norm of the error is

$$\mathcal{J} = \left\|\mathbf{H} - \widehat{\mathbf{H}}\right\|_{\mathcal{H}_2}^2 = \sum_{i=1}^n \phi_i\left[\mathbf{H}(-\lambda_i) - \widehat{\mathbf{H}}(-\lambda_i)\right] + \sum_{j=1}^r \widehat{\phi}_j\left[\widehat{\mathbf{H}}(-\widehat{\lambda}_j) - \mathbf{H}(-\widehat{\lambda}_j)\right].$$

Thus
$$\frac{\partial\mathcal{J}}{\partial\phi_i} = 0 \Rightarrow \mathbf{H}(-\widehat{\lambda}_i) = \widehat{\mathbf{H}}(-\widehat{\lambda}_i) \quad \text{and} \quad \frac{\partial\mathcal{J}}{\partial\widehat{\lambda}_i} = 0 \Rightarrow \mathbf{H}'(-\widehat{\lambda}_i) = \widehat{\mathbf{H}}'(-\widehat{\lambda}_i).$$

Conclusion. The $\mathcal{H}_2$ error is due to the mismatch of the transfer functions $\mathbf{H} - \widehat{\mathbf{H}}$ at the mirror images of the full-order and reduced system poles λ_i, $\widehat{\lambda}_i$.

The general case

Theorem. Let $\widehat{H}(s)$ be the best rth order rational approximation of $H(s)$ with respect to the $\mathcal{H}_2$ norm. Then,

$$H(-\lambda_k)r_k = \widehat{H}(-\lambda_k)r_k,$$
$$\ell_k^T H(-\lambda_k) = \ell_k^T \widehat{H}(-\lambda_k),$$
$$\ell_k^T H'(-\lambda_k)r_k = \ell_k^T \widehat{H}'(-\lambda_k)r_k,$$

for $k = 1, 2, \cdots, r$.

Remarks. (a) Any optimal $\mathcal{H}_2$ approximation $\widehat{H}(s)$ must be a bitangential interpolant to $H(s)$.

(b) Interpolatory conditions for SISO systems were initially introduced by Meier and Luenberger.

(c) Until recently effective numerical algorithms to find reduced systems that satisfy these conditions were lacking. Gugercin-Beattie-A. introduced such an algorithm, called the **Iterative Rational Krylov Algorithm (IRKA)**.

(d) In practice, **IRKA** has significantly expanded the utility of optimal $\mathcal{H}_2$ model reduction.

Outline

Model Reduction via Projection

Model Reduction by Interpolation

Interpolatory Projections for $\mathcal{H}_2$ Optimal Approximation

IRKA

Descent algorithms

IRKA for optimal $\mathcal{H}_2$ approximation

Given initial interpolation points $\{\sigma_i\}_{i=1}^r$ and directions $\{r_i\}_{i=1}^r$ and $\{\ell_i\}_{i=1}^r$, construct a reduced model $\widehat{H}(s)$. Then, compute the pole-residue decomposition of $\widehat{H}(s)$. Then set

$$\sigma_i \longleftarrow -\lambda_i, \quad r_i \longleftarrow \widehat{r}_i, \quad \text{and} \quad \ell_i \longleftarrow \widehat{\ell}_i, \quad \text{for} \quad i = 1, \ldots, r$$

as the next interpolation data and iterate until convergence is reached.

> **Algorithm: MIMO $\mathcal{H}_2$-Optimal Tangential Interpolation (IRKA)**
>
> 1. Make an initial shift selection: $\{\sigma_1,\ldots,\sigma_r\}$ and initial tangent directions selection: $r_1,\ldots,r_r$ and $\ell_1,\ldots,\ell_r$.
>
> 2. $V = \left[(\sigma_1 E - A)^{-1}B r_1 \ \cdots \ (\sigma_r E - A)^{-1}B r_r\right]$
>
> 3. $W = \left[(\sigma_1 E^T - A^T)^{-1}C^T \ell_1 \ \cdots \ (\sigma_r E^T - A^T)^{-1}C^T \ell_1\right]$
>
> 4. while (not converged)
>
>   4.1 $\widehat{A} = W^T AV, \ \widehat{E} = W^T EV, \ \widehat{B} = W^T B$, and $\widehat{C} = CV$
>
>   4.2 Compute a pole-residue expansion of
> $$\widehat{H}(s) = \widehat{H}(s) = \widehat{C}(s\widehat{E} - \widehat{A})^{-1}\widehat{B} = \sum_{i=1}^{r} \frac{\widehat{\ell}_i \widehat{r}_i^T}{s - \lambda_i}.$$
>
>   4.3 $\sigma_i \longleftarrow -\lambda_i, \quad r_i \longleftarrow \widehat{r}_i, \quad \text{and} \quad \ell_i \longleftarrow \widehat{\ell}_i, \quad \text{for} \quad i = 1,\ldots,r$
>
>   4.4 $V = \left[(\sigma_1 E - A)^{-1}B r_1 \ \cdots \ (\sigma_r E - A)^{-1}B r_r\right]$
>
>   4.5 $W = \left[(\sigma_1 E^T - A^T)^{-1}C^T \ell_1 \ \cdots \ (\sigma_r E^T - A^T)^{-1}C^T \ell_1\right]$
>
> 5. $\widehat{A} = W^T AV, \ \widehat{E} = W^T EV, \ \widehat{B} = W^T B, \ \widehat{C} = CV$

Remarks on IRKA

▲ Upon convergence, the reduced model, $\widehat{H}(s)$, satisfies the interpolatory first-order necessary conditions for $\mathcal{H}_2$ optimality by construction.

▲ Convergence is generally observed to be rapid; though it slows as input/output orders grow. Convergence may be guaranteed a priori in some circumstances; yet there are known cases where convergence may fail.

▲ When convergence occurs, the resulting reduced model is guaranteed to be a local $\mathcal{H}_2$-minimizer since the local maxima of the $\mathcal{H}_2$ minimization problem are known to be repellent.

▲ Overall in practice, IRKA has seen significant success in computing high fidelity (locally) optimal reduced models and has been successfully applied in large-scale settings to find $\mathcal{H}_2$-optimal reduced models for systems with hundreds of thousands of state variables;

▲ Examples: application in cellular neurophysiology, energy efficient building design in order to produce accurate compact models for the indoor-air environment, optimal cooling for steel profiles.

▲ IRKA has been extended to the reduction of bilinear dynamical systems.

Outline

21 / 26

Descent Algorithms for $\mathcal{H}_2$ Model Reduction

- IRKA is a fixed point iteration. Only for symmetric state-space systems, is convergence guaranteed.
- IRKA is not a descent algorithm; that is, the $\mathcal{H}_2$ error might fluctuate during intermediate steps.
- To address these issues, Beattie and Gugercin developed an $\mathcal{H}_2$ descent algorithm that reduces the $\mathcal{H}_2$ error at each step and assures global convergence to a local minimum.

Theorem. Given a full-order model $\mathbf{H}(s)$, let $\widehat{\mathbf{H}}(s)$ have the form

$$\widehat{\mathbf{H}}(s) = \sum_{i=1}^{r} \frac{\boldsymbol{\ell}_i \mathbf{r}_i^T}{s - \lambda_i}.$$

Then, the $\mathcal{H}_2$ norm of the error system is given by

$$\left\| \mathbf{H} - \widehat{\mathbf{H}} \right\|_{\mathcal{H}_2}^2 = \|\mathbf{H}\|_{\mathcal{H}_2}^2 - 2\sum_{k=1}^{r} \boldsymbol{\ell}_k^T \mathbf{H}(-\lambda_k)\mathbf{r}_k + \sum_{k,j=1}^{r} \frac{\boldsymbol{\ell}_k^T \boldsymbol{\ell}_j \mathbf{r}_j^T \mathbf{r}_k}{-\lambda_k - \lambda_j}.$$

This expression leads to the computation of the gradient and Hessian of the error with respect to unknowns and construct globally convergent descent (optimization) algorithms.

22 / 26

Theorem. (For brevity only the gradient is given.) Consider the full-order model $\mathbf{H}(s)$ and the reduced model $\widehat{\mathbf{H}}(s)$, and define

$$\mathcal{J} \stackrel{\text{def}}{=} \left\| \mathbf{H} - \widehat{\mathbf{H}} \right\|_{\mathcal{H}_2}^2 \Rightarrow \frac{\partial \mathcal{J}}{\partial \lambda_i} = -2\,\boldsymbol{\ell}_i^T \left(\widehat{\mathbf{H}}'(-\lambda_i) - \mathbf{H}'(-\lambda_i) \right) \mathbf{r}_i, \; i = 1, \ldots, r.$$

Moreover, the gradient of $\mathcal{J}$ with respect to residue directions listed as

$$\{\mathbf{r}, \boldsymbol{\ell}\} = [\mathbf{r}_1^T, \boldsymbol{\ell}_1^T, \mathbf{r}_2^T, \boldsymbol{\ell}_2^T, \ldots, \mathbf{r}_r^T, \boldsymbol{\ell}_r^T]^T,$$

is given by

$$(\nabla_{\{\mathbf{r},\boldsymbol{\ell}\}}\mathcal{J})_k = \begin{bmatrix} 2\left(\boldsymbol{\ell}_k^T \widehat{\mathbf{H}}(-\lambda_k) - \boldsymbol{\ell}_k^T \mathbf{H}(-\lambda_k)\right)^T \\ 2\left(\widehat{\mathbf{H}}(-\lambda_k)\mathbf{r}_k - \mathbf{H}(-\lambda_k)\mathbf{r}_k\right) \end{bmatrix}, \; k = 1, 2, \ldots, r.$$

This is a vector of length $r(m + q)$, partitioned into r vectors of length $m + q$.

Unlike in IRKA, the intermediate reduced models are not interpolatory. However, upon convergence, they satisfy the interpolatory optimality conditions.

23 / 26

ISS 12a Module

▲ $n = 1412$. Reduce to $r = 2 : 2 : 60$
▲ Compare with balanced truncation
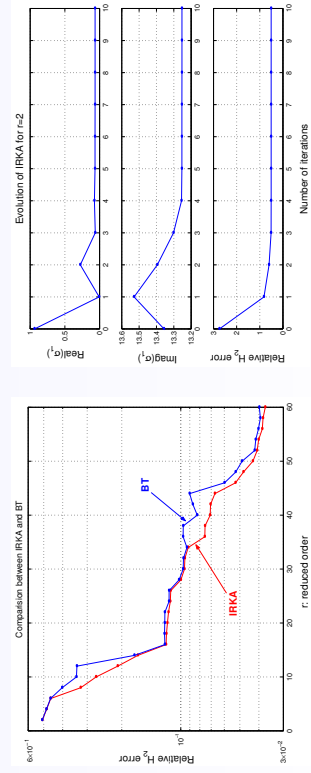
24 / 26

A Transmission Line Model

▲ Modeling the impedance of interconnect structures

▲ $n = 256$. Reduce it to order $r = 26$ using **IRKA.**

▲ Convergence after 6 steps.
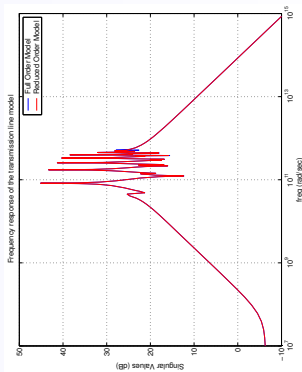
Frequency response of the transmission line model

25/26

Some References

C.A. Beattie, and S. Gugercin, Model reduction by rational interpolation, in *Model Reduction and Approximation for Complex Systems*, Edited by P. Benner, A. Cohen, M. Ohlberger, and K. Willcox, SIAM, (2016).

S. Gugercin and A. Antoulas, An H2 error expression for the Lanczos procedure, in Proceedings of the 42nd IEEE Conference on Decision and Control, 2003. (Cited on p. 17)

C.A. Beattie, and S. Gugercin, Realization–independent $\mathcal{H}_2$ approximation, Proceedings of the 51st IEEE Conference on Decision and Control, pages 4953–4958, 2012.

G. Flagg, C.A. Beattie, and S. Gugercin, Convergence of the Iterative Rational Krylov Algorithm, Systems & Control Letters, vol 61, pages 688–691, 2012.

B. Anić, C.A. Beattie, S. Gugercin, and A.C. Antoulas, Interpolatory weighted-$\mathcal{H}_2$ model reduction, Automatica, 2013.

A.C. Antoulas, C.A. Beattie, and S. Gugercin, Interpolatory model reduction of large-scale dynamical systems, in Efficient Modeling and Control of Large-Scale Systems, J. Mohammadpour and K. Grigoriadis, Eds, Springer-Verlag, pages 2–58, 2010.

L. Baratchart, M. Cardelli, and M. Olivi, Identification and rational L_2 approximation: a gradient algorithm, Automatica, vol 27, pages 413–418, 1991.

C. De Villemagne and R. Skelton, Model reductions using a projection formulation, International Journal of Control, vol 46, pages 2141–2169, 1987.

S. Gugercin, A.C. Antoulas and C.A. Beattie, $\mathcal{H}_2$ Model Reduction for Large-Scale Linear Dynamical Systems, SIAM Journal on Matrix Analysis and Applications, vol 30, pages 609–638, 2008.

L. Meier III and D. Luenberger, Approximation of linear constant systems, IEEE Transactions on AC, vol 12, pages 585–588, 1967.

P. van Dooren, K.A. Gallivan and P.A. Absil, $\mathcal{H}_2$-optimal model reduction of MIMO systems, Applied Mathematics Letters, vol 21, pages 1267–1273, 2008.

C.A. Beattie and S. Gugercin, A trust region method for optimal $\mathcal{H}_2$ model reduction, 48th IEEE Conference on Decision and Control, 2009.

26/26

Outline

Introduction

The Loewner framework

The Loewner pencil

Construction of interpolants - models

Generalized inverses and rectangular systems

The Loewner algorithm

ROM from data

Conclusion

2/42

Data-driven and interpolatory model reduction: PART III

Thanos Antoulas

Rice University and Jacobs University

email : aca@rice.edu
URL : www.ece.rice.edu/~aca

35th BENELUX Meeting on Systems and Control 2016
22-24 March 2016
Kontakt der Kontinenten, Soesterberg, The Netherlands

1/42

Outline

Introduction

The Loewner framework

The Loewner pencil

Construction of interpolants - models

Generalized inverses and rectangular systems

The Loewner algorithm

ROM from data

Conclusion

3/42

Model reduction of descriptor systems

A *descriptor-form representation* is a set of differential and algebraic equations (DAEs):

$$\Sigma:\ \mathbf{E}\frac{d}{dt}\mathbf{x}(t) = \mathbf{A}\mathbf{x}(t) + \mathbf{B}\mathbf{u}(t),\quad \mathbf{y}(t) = \mathbf{C}\mathbf{x}(t) + \mathbf{D}\mathbf{u}(t),$$

where $\mathbf{E}, \mathbf{A} \in \mathbb{R}^{n\times n}$, $\mathbf{B} \in \mathbb{R}^{n\times m}$, $\mathbf{C} \in \mathbb{R}^{p\times n}$, $\mathbf{D} \in \mathbb{R}^{p\times m}$.

Remark. The D-term. Consider a rank-revealing factorization

$$\mathbf{D} = \mathbf{D}_1 \mathbf{D}_2 \quad\text{where}\quad \mathbf{D}_1 \in \mathbb{R}^{p\times\rho},\ \mathbf{D}_2 \in \mathbb{R}^{\rho\times m},$$

and $\rho = \text{rank } \mathbf{D}$. It readily follows that:

$$\mathbf{E}_\delta = \begin{bmatrix} \mathbf{E} \\ & \mathbf{0}_{\rho\times\rho} \end{bmatrix},\ \mathbf{A}_\delta = \begin{bmatrix} \mathbf{A} \\ & -\mathbf{I}_\rho \end{bmatrix},\ \mathbf{B}_\delta = \begin{bmatrix} \mathbf{B} \\ \mathbf{D}_2 \end{bmatrix},\ \mathbf{C}_\delta = \begin{bmatrix} \mathbf{C} & \mathbf{D}_1 \end{bmatrix},$$

is a descriptor realization of the same system with no **D**-term (i.e. $\mathbf{D}_\delta = \mathbf{0}$).
Reason: the Loewner framework yields precisely such descriptor realizations.

Model reduction: construct reduced-order DAE systems of the form:

$$\hat{\Sigma}:\ \hat{\mathbf{E}}\frac{d}{dt}\hat{\mathbf{x}}(t) = \hat{\mathbf{A}}\hat{\mathbf{x}}(t) + \hat{\mathbf{B}}\mathbf{u}(t),\quad \hat{\mathbf{y}}(t) = \hat{\mathbf{C}}\hat{\mathbf{x}}(t) + \hat{\mathbf{D}}\mathbf{u}(t),$$

where $\hat{\mathbf{E}}, \hat{\mathbf{A}} \in \mathbb{R}^{r\times r}$, $\hat{\mathbf{B}} \in \mathbb{R}^{r\times m}$, $\hat{\mathbf{C}} \in \mathbb{R}^{p\times r}$, $\hat{\mathbf{D}} \in \mathbb{R}^{p\times m}$.

4/42

Interpolatory reduction for linear systems

Given *left interpolation points*: $\{\mu_j\}_{j=1}^q \subset \mathbb{C}$, *left tangential directions*: $\{\ell_j\}_{j=1}^q \subset \mathbb{C}^p$, and *right interpolation points*: $\{\lambda_i\}_{i=1}^k \subset \mathbb{C}$, with *right tangential directions*: $\{\mathbf{r}_i\}_{i=1}^k \subset \mathbb{C}^m$, find $\hat{\Sigma}$, such that the associated transfer function $\hat{\mathbf{H}}(s)$ is a *tangential interpolant* to $\mathbf{H}(s)$:

$$\ell_j^T \hat{\mathbf{H}}(\mu_j) = \ell_j^T \mathbf{H}(\mu_j),\ \text{for } j = 1,\cdots,q \quad\text{and}\quad \hat{\mathbf{H}}(\lambda_i)\mathbf{r}_i = \mathbf{H}(\lambda_i)\mathbf{r}_i,\ \text{for } i = 1,\cdots,k.$$

If instead of Σ we are given *left responses*: $\{\mathbf{v}_j\}_{j=1}^q \subset \mathbb{C}^m$, *right responses*: $\{\mathbf{w}_i\}_{i=1}^k \subset \mathbb{C}^p$, find a (low order) system $\hat{\Sigma}$, such that $\hat{\mathbf{H}}(s)$, is an (*approximate*) *tangential interpolant*:

$$\ell_j^T \hat{\mathbf{H}}(\mu_j) = \mathbf{v}_j^T,\ \text{for } j = 1,\cdots,q \quad\text{and}\quad \hat{\mathbf{H}}(\lambda_i)\mathbf{r}_i = \mathbf{w}_i,\ \text{for } i = 1,\cdots,k.$$

For SISO systems, left and right directions can be taken equal to one and hence

$$\hat{\mathbf{H}}(\mu_j) = \mathbf{H}(\mu_j),\ j = 1,\cdots,q,\quad \hat{\mathbf{H}}(\lambda_i) = \mathbf{H}(\lambda_i),\ i = 1,\cdots,k,$$

$$\hat{\mathbf{H}}(\mu_j) = \mathbf{v}_j,\ j = 1,\cdots,q,\quad \hat{\mathbf{H}}(\lambda_i) = \mathbf{w}_i,\ i = 1,\cdots,k.$$

5/42

Recall: Frequency responses can be measured using *Vector Network Analyzers* (VNA):
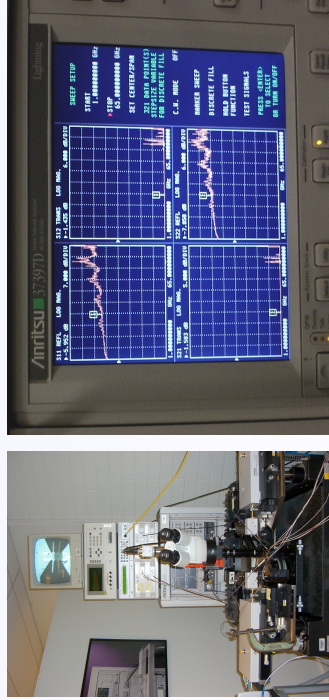
Left pane: VNA (Vector Network Analyzer).

Right pane: screen showing the magnitude of the *S*-parameters for a 2-port device.

6/42

Outline

The Loewner matrix

Given a *row array* of pairs $(\mu_j, \mathbf{v}_j), j = 1, \cdots, q,$

and a *column array* of pairs $(\lambda_i, \mathbf{w}_i), i = 1, \cdots, k, \lambda_i \neq \mu_j,$

the associated **Loewner** or **divided-differences matrix** is:

$$\mathbb{L} = \begin{bmatrix} \dfrac{\mathbf{v}_1 - \mathbf{w}_1}{\mu_1 - \lambda_1} & \cdots & \dfrac{\mathbf{v}_1 - \mathbf{w}_k}{\mu_1 - \lambda_k} \\ \vdots & \ddots & \vdots \\ \dfrac{\mathbf{v}_q - \mathbf{w}_1}{\mu_q - \lambda_1} & \cdots & \dfrac{\mathbf{v}_q - \mathbf{w}_k}{\mu_q - \lambda_k} \end{bmatrix} \in \mathbb{C}^{q \times k}.$$

This matrix was introduced by Karel Löwner (later Charles Loewner) in 1934.

The data

We are given respectively, the *right* or *column data* and the *left* or *row data*:

$$(\lambda_i; \mathbf{r}_i, \mathbf{w}_i), i = 1, \cdots, k, \quad (\mu_j; \boldsymbol{\ell}_j^T, \mathbf{v}_j^T), j = 1, \cdots, q.$$

The *right data* is organized as:

$$\left. \begin{array}{l} \boldsymbol{\Lambda} = \text{diag}\,[\lambda_1, \cdots, \lambda_k] \in \mathbb{C}^{k \times k}, \\ \mathbf{R} = [\mathbf{r}_1 \ \mathbf{r}_2 \ \cdots \ \mathbf{r}_k] \in \mathbb{C}^{m \times k}, \\ \mathbf{W} = [\mathbf{w}_1 \ \mathbf{w}_2 \ \cdots \ \mathbf{w}_k] \in \mathbb{C}^{p \times k} \end{array} \right\}$$

and the *left data* is organized as:

$$\left. \begin{array}{l} \mathbf{M} = \text{diag}\,[\mu_1, \cdots, \mu_q] \in \mathbb{C}^{q \times q}, \\ \mathbf{L}^T = [\ \boldsymbol{\ell}_1 \ \cdots \ \boldsymbol{\ell}_q \ ] \in \mathbb{C}^{p \times q}, \\ \mathbf{V}^T = [\ \mathbf{v}_1 \ \cdots \ \mathbf{v}_q \ ] \in \mathbb{C}^{m \times q}. \end{array} \right\}$$

Outline

The Loewner pencil

The *Loewner* and *shifted Loewner* matrices, referred to as the *Loewner pencil*, are:

$$\mathbb{L} = \begin{bmatrix} \frac{v_1^T r_1 - \ell_1^T w_1}{\mu_1 - \lambda_1} & \cdots & \frac{v_1^T r_k - \ell_1^T w_k}{\mu_1 - \lambda_k} \\ \vdots & \cdots & \vdots \\ \frac{v_q^T r_1 - \ell_q^T w_1}{\mu_q - \lambda_1} & \cdots & \frac{v_q^T r_k - \ell_q^T w_k}{\mu_q - \lambda_k} \end{bmatrix} \in \mathbb{C}^{q \times k}.$$

$\mathbb{L}$ satisfies the Sylvester equation

$$\mathbb{M}\mathbb{L} - \mathbb{L}\Lambda = \mathbf{VR} - \mathbf{LW}.$$

The *shifted Loewner matrix* is:

$$\mathbb{L}_s = \begin{bmatrix} \frac{\mu_1 v_1^T r_1 - \ell_1^T w_1 \lambda_1}{\mu_1 - \lambda_1} & \cdots & \frac{\mu_1 v_1^T r_k - \ell_1^T w_k \lambda_k}{\mu_1 - \lambda_k} \\ \vdots & \cdots & \vdots \\ \frac{\mu_q v_q^T r_1 - \ell_q^T w_1 \lambda_1}{\mu_q - \lambda_1} & \cdots & \frac{\mu_q v_q^T r_k - \ell_q^T w_k \lambda_k}{\mu_q - \lambda_k} \end{bmatrix} \in \mathbb{C}^{q \times k},$$

and satisfies the Sylvester equation

$$\mathbb{M}\mathbb{L}_s - \mathbb{L}_s\Lambda = \mathbf{MVR} - \mathbf{LW}\Lambda.$$

If the data is sampled from $\mathbf{H}(s) = \mathbf{C}_\delta(s\mathbf{E}_\delta - \mathbf{A}_\delta)^{-1}\mathbf{B}_\delta$, we define:

$$\mathcal{O}_q = \begin{bmatrix} \ell_1^T \mathbf{C}_\delta(\mu_1\mathbf{E}_\delta - \mathbf{A}_\delta)^{-1} \\ \vdots \\ \ell_q^T \mathbf{C}_\delta(\mu_q\mathbf{E}_\delta - \mathbf{A}_\delta)^{-1} \end{bmatrix},$$

$$\mathcal{R}_k = [(\lambda_1\mathbf{E}_\delta - \mathbf{A}_\delta)^{-1}\mathbf{B}_\delta r_1, \cdots, (\lambda_k\mathbf{E}_\delta - \mathbf{A}_\delta)^{-1}\mathbf{B}_\delta r_k]$$

of size $q \times n$, $n \times k$, respectively. These are the *generalized tangential observability* and *generalized tangential controllability* matrices. It follows that

$$(\mathbb{L})_{j,i} = \frac{v_j^T r_i - \ell_j^T w_i}{\mu_j - \lambda_i} = -\ell_j^T \mathbf{C}_\delta(\mu_j\mathbf{E}_\delta - \mathbf{A}_\delta)^{-1}\mathbf{E}_\delta(\lambda_i\mathbf{E}_\delta - \mathbf{A}_\delta)^{-1}\mathbf{B}_\delta r_i,$$

$$(\mathbb{L}_s)_{j,i} = \frac{\mu_j v_j^T r_i - \lambda_i \ell_j^T w_i}{\mu_j - \lambda_i} = -\ell_j^T \mathbf{C}_\delta(\mu_j\mathbf{E}_\delta - \mathbf{A}_\delta)^{-1}\mathbf{A}_\delta(\lambda_i\mathbf{E}_\delta - \mathbf{A}_\delta)^{-1}\mathbf{B}_\delta r_i.$$

$$\Rightarrow \boxed{\mathbb{L} = -\mathcal{O}_q \mathbf{E}_\delta \mathcal{R}_k \quad \text{and} \quad \mathbb{L}_s = -\mathcal{O}_q \mathbf{A}_\delta \mathcal{R}_k}$$

The following hold:
(a) rank $\mathbb{L}$ = rank $\mathbf{E}_\delta$ = rank $\mathbf{E}$ = McMillan degree of the underlying rational fuction
(b) rank $\mathbb{L}_s$ = rank $\mathbf{A}_\delta$ = rank $\mathbf{A}$ + rank $\mathbf{D}$.

Outline

Mimimal amount of data

Theorem.

Assume that $k = q$ and let $(\mathbb{L}_s, \mathbb{L})$ be a regular pencil.

(a) The quadruple

$$\mathbf{E}_\delta = -\mathbb{L}, \quad \mathbf{A}_\delta = -\mathbb{L}_s, \quad \mathbf{B}_\delta = \mathbf{V}, \quad \mathbf{C}_\delta = \mathbf{W},$$

is a minimal descriptor realization of an interpolant of the data, i.e.,

$$\mathbf{H}(s) = \mathbf{W}(\mathbb{L}_s - s\mathbb{L})^{-1}\mathbf{V},$$

is a rational interpolant of the data.

(b) All solutions of the same McMillan degree are parametrized as

$$\mathbf{E} = -\mathbb{L}, \quad \mathbf{A} = -(\mathbb{L}_s + \mathbf{LKR}), \quad \mathbf{B} = \mathbf{V} - \mathbf{LK}, \quad \mathbf{C} = \mathbf{W} - \mathbf{KR}, \quad \mathbf{D} = \mathbf{K},$$

where the parameter $\mathbf{K} \in \mathbb{C}^{p \times m}$.

Construction of interpolants: The case of redundant data

As shown in Mayo and A. (2007), the problem has a solution provided that

$$\text{rank } \{\xi \mathbb{L} - \mathbb{L}_s\} = \text{rank } [\mathbb{L}, \ \mathbb{L}_s] = \text{rank} \begin{bmatrix} \mathbb{L} \\ \mathbb{L}_s \end{bmatrix} = r,$$

for all $\xi \in \{\lambda_j\} \cup \{\mu_j\}$.

Consider then, the short SVDs:

$$[\mathbb{L}, \ \mathbb{L}_s] = \mathbf{Y}\hat{\Sigma}_r\hat{\mathbf{X}}^*, \quad \begin{bmatrix} \mathbb{L} \\ \mathbb{L}_s \end{bmatrix} = \check{\mathbf{Y}}\check{\Sigma}_r\mathbf{X}^*,$$

where $\hat{\Sigma}_r, \Sigma_r \in \mathbb{R}^{r \times r}$, $\mathbf{Y} \in \mathbb{C}^{q \times r}$, $\mathbf{X} \in \mathbb{C}^{k \times r}$.

Remark. r can be taken as the **numerical rank** of the corresponding quantities.

Outline

Introduction

The Loewner framework

The Loewner pencil

Construction of interpolants - models

Generalized inverses and rectangular systems

The Loewner algorithm

ROM from data

Conclusion

Proof. (a) Multiplying equation the first Sylvester equation by s and subtracting it from equation the second one, we get

$$\mathbf{M}(\mathbb{L}_s - s\mathbb{L}) - (\mathbb{L}_s - s\mathbb{L})\Lambda = (\mathbf{M} - s\mathbf{I})\mathbf{VR} - \mathbf{LW}(\Lambda - s\mathbf{I}).$$

Multiplying this equation by $\mathbf{e}_i$ on the right and setting $s = \lambda_i$, we obtain

$$(\mathbf{M} - \lambda_i \mathbf{I})(\mathbb{L}_s - \lambda_i \mathbb{L})\mathbf{e}_i = (\mathbf{M} - \lambda_i \mathbf{I})\mathbf{Vr}_i \Rightarrow$$

$$(\mathbb{L}_s - \lambda_i \mathbb{L})\mathbf{e}_i = \mathbf{Vr}_i \Rightarrow \mathbf{We}_i = \mathbf{W}(\mathbb{L}_s - \lambda_i \mathbb{L})^{-1}\mathbf{Vr}_i.$$

Thus $\mathbf{w}_i = \mathbf{H}(\lambda_i)\mathbf{r}_i$.

Next, we multiply the above equation by $\mathbf{e}_j^T$ on the left and set $s = \mu_j$:

$$\mathbf{e}_j^T(\mathbb{L}_s - \mu_j \mathbb{L})(\Lambda - \mu_j \mathbf{I}) = \mathbf{e}_j^T \mathbf{LW}(\Lambda - \mu_j \mathbf{I}) \Rightarrow$$

$$\mathbf{e}_j^T(\mathbb{L}_s - \mu_j \mathbb{L}) = \ell_j^T \mathbf{W} \Rightarrow \mathbf{e}_j^T \mathbf{V} = \ell_j^T \mathbf{W}(\mathbb{L}_s - \mu_j \mathbb{L})^{-1}\mathbf{V}.$$

Thus $\mathbf{v}_j^T = \ell_j^T \mathbf{H}(\mu_j)$.

(b) With $\mathbf{K} \in \mathbb{C}^{p \times m}$, the Sylvester equations can be rewritten as

$$\mathbf{ML} - \mathbb{L}\Lambda = (\mathbf{V} - \mathbf{LK})\mathbf{R} - \mathbf{L}(\mathbf{W} - \mathbf{KR}),$$

$$\mathbf{M}(\mathbb{L}_s + \mathbf{LKR}) - (\mathbb{L}_s + \mathbf{LKR})\Lambda = \mathbf{M}(\mathbf{V} - \mathbf{LK})\mathbf{R} - \mathbf{L}(\mathbf{W} - \mathbf{KR})\Lambda.$$

Repeating the procedure with the new quantities the desired result follows:

$$\bar{\mathbb{L}}_s = \mathbb{L}_s + \mathbf{LKR}, \quad \bar{\mathbf{V}} = \mathbf{V} - \mathbf{LK}, \quad \bar{\mathbf{W}} = \mathbf{W} - \mathbf{KR}.$$

Theorem. The quadruple $(\mathbf{E}_\delta, \mathbf{A}_\delta, \mathbf{B}_\delta, \mathbf{C}_\delta)$ of size $r \times r$, $r \times r$, $r \times m$, $p \times r$, given by:

$$\mathbf{E}_\delta = -\mathbf{Y}^*\mathbb{L}\mathbf{X}, \quad \mathbf{A}_\delta = -\mathbf{Y}^*\mathbb{L}_s\mathbf{X}, \quad \mathbf{B}_\delta = \mathbf{Y}^*\mathbf{V}, \quad \mathbf{C}_\delta = \mathbf{WX},$$

is a descriptor realization of an (approximate) interpolant of the data with McMillan degree $r = \text{rank}\,\mathbb{L}$.

Remarks. (a) The Loewner approach constructs a descriptor representation

$$(\mathbb{L}, \mathbb{L}_s, \mathbf{V}, \mathbf{W}),$$

of an underlying dynamical system exclusively from the data, with no further manipulations involved (i.e. matrix factorizations or inversions). In general, the pencil $(\mathbb{L}_s, \mathbb{L})$ is singular and needs to be projected to a regular pencil $(\mathbf{A}_\delta, \mathbf{E}_\delta)$.

(b) In the Loewner framework, by construction, **D** terms are absorbed in the other matrices of the realization. Extracting the **D** term involves an eigenvalue decomposition of $(\mathbb{L}_s, \mathbb{L})$.

Construction of Interpolants (Models)

- If the pencil $(\mathbb{L}_s, \mathbb{L})$ is regular, i.e. $\Phi(s) = \mathbb{L}_s - s\mathbb{L}$, is invertible, then

$E = -\mathbb{L}, \quad A = -\mathbb{L}_s, \quad B = V, \quad C = W$

is a minimal interpolant of the data

$\Rightarrow \qquad \boxed{H(s) = W\,\Phi(s)^{-1}V}$

- If $\Phi(s) = \mathbb{L}_s - s\mathbb{L}$, is singular, let $\Phi(s)^\#$ be a generalized inverse of $\Phi(s)$ (Drazin or Moore-Penrose).

$\Rightarrow \qquad \boxed{H(s) = W\,\Phi(s)^\# V}$

- In the latter case, if the numerical $\operatorname{rank}\mathbb{L} = k$, compute the rank revealing *SVD*:

$$\mathbb{L} = Y\Sigma X^* \approx Y_k \Sigma_k X_k^*$$

Theorem. A realization $[C, E, A, B]$, of an approximate interpolant is given as follows:

$$E = -Y_k^*\mathbb{L}X_k, \quad A = -Y_k^*\mathbb{L}_s X_k, \quad B = Y_k^* V, \quad C = W X_k.$$

A simple example   Consider the system

$$\dot{x}_1(t) = x_2(t),$$
$$\dot{x}_2(t) = -x_1(t) - x_2(t) + u(t), \quad y(t) = x_2(t) \quad \Rightarrow \quad H(s) = \frac{s}{s^2+s+1}.$$

We now wish to recover state equations equivalent to the ones above from measurements of the transfer function.

Data: obtained by evaluating the transfer function at $\lambda_1 = \frac{1}{2}, \lambda_2 = 1$, as well as $\mu_1 = -\frac{1}{2}$, $\mu_2 = -1$. The corresponding values of H are collected in the matrices

$$W = \left(\tfrac{2}{7} \quad \tfrac{1}{3} \right), \quad V = \left(-\tfrac{2}{3} \quad -1 \right)^T.$$

Furthermore with $R = [1\ 1], L = R^T$, we construct the *Loewner pencil*:

$$\mathbb{L} = \begin{bmatrix} \tfrac{20}{21} & \tfrac{2}{3} \\ \tfrac{6}{7} & \tfrac{2}{3} \end{bmatrix}, \quad \mathbb{L}_s = \begin{bmatrix} -\tfrac{4}{21} & 0 \\ -\tfrac{4}{7} & -\tfrac{1}{3} \end{bmatrix}.$$

Since the pencil $(\mathbb{L}_s, \mathbb{L})$ is regular, and the rank of both matrices is two:

$$H(s) = W\,\Phi(s)^{-1}V = \frac{s}{s^2+s+1}, \quad \text{where} \quad \Phi(s) = \mathbb{L}_s - s\mathbb{L}.$$

Hence, the measurements above yield a minimal (descriptor) realization of the system in terms of the (state) variables ξ_1, ξ_2:

$$\tfrac{20}{21}\dot{\xi}_1(t) + \tfrac{2}{3}\dot{\xi}_1(t) = -\tfrac{4}{21}\xi_1(t) + \tfrac{2}{3}u(t),$$
$$\tfrac{6}{7}\dot{\xi}_1(t) + \tfrac{2}{3}\dot{\xi}_2(t) = -\tfrac{4}{7}\xi_1(t) - \tfrac{1}{3}\xi_2(t) + u(t),$$
$$y(t) = \tfrac{2}{7}\xi_1(t) + \tfrac{1}{3}\xi_2(t).$$

Question: what happens if we collect more data that necessary:

$$\Lambda = \operatorname{diag}\left(\tfrac{1}{2} \quad 1 \quad \tfrac{3}{2} \quad 2 \right), \quad M = \operatorname{diag}\left(-\tfrac{1}{2} \quad -1 \quad -\tfrac{3}{2} \quad -2 \right).$$

In this case, the associated measurements are

$$W = \left(\tfrac{2}{7} \quad \tfrac{1}{3} \quad \tfrac{6}{19} \quad \tfrac{2}{7} \right), \quad V = \left(-\tfrac{2}{3} \quad -1 \quad -\tfrac{6}{7} \quad -\tfrac{2}{3} \right)^T,$$

and with $R = [1\ 1\ 1\ 1], L = R^T$, the Loewner pencil is:

$$\mathbb{L} = \begin{bmatrix} \tfrac{20}{21} & \tfrac{2}{3} & \tfrac{2}{3} & \tfrac{28}{57} \\ \tfrac{6}{7} & \tfrac{2}{3} & \tfrac{10}{19} & \tfrac{8}{21} \\ \tfrac{4}{7} & \tfrac{10}{21} & \tfrac{52}{133} & \tfrac{3}{7} \\ \tfrac{8}{21} & \tfrac{1}{3} & \tfrac{16}{57} & \tfrac{16}{49} \end{bmatrix}, \quad \mathbb{L}_s = \begin{bmatrix} -\tfrac{4}{21} & 0 & -\tfrac{1}{3} & \tfrac{4}{57} \\ -\tfrac{4}{7} & -\tfrac{1}{3} & -\tfrac{4}{19} & -\tfrac{1}{7} \\ -\tfrac{4}{7} & -\tfrac{8}{21} & -\tfrac{36}{133} & -\tfrac{10}{49} \\ -\tfrac{10}{21} & -\tfrac{1}{3} & -\tfrac{14}{57} & -\tfrac{4}{21} \end{bmatrix}.$$

It turns out that we can choose **arbitrary** $X, Y \in \mathbb{R}^{4\times 2}$, such that $Y^T X$ is nonsingular, e.g.

$$X = \begin{bmatrix} -1 & 0 \\ 0 & -1 \\ 0 & 0 \\ -2 & 1 \end{bmatrix}, \quad Y^T = \begin{bmatrix} 0 & 1 & 0 & -1 \\ 1 & -1 & -1 & 1 \end{bmatrix},$$

so that the projected quantities

$$\hat{W} = WX = \begin{bmatrix} -\tfrac{6}{7} & -\tfrac{1}{21} \end{bmatrix}, \quad \hat{\mathbb{L}} = Y^T\mathbb{L}X = \begin{bmatrix} -\tfrac{6}{7} & -\tfrac{1}{7} \\ \tfrac{18}{49} & \tfrac{1}{147} \end{bmatrix},$$

$$\hat{\mathbb{L}}_s = Y^T\mathbb{L}_s X = \begin{bmatrix} 0 & \tfrac{1}{21} \\ -\tfrac{48}{49} & -\tfrac{19}{147} \end{bmatrix}, \quad \hat{V} = Y^T V = \begin{bmatrix} -\tfrac{1}{3} \\ \tfrac{11}{21} \end{bmatrix},$$

constitute a minimal realization of $H(s)$:

$$\boxed{H(s) = \hat{W}\left(\hat{\mathbb{L}}_s - s\hat{\mathbb{L}}\right)^{-1}\hat{V} = \frac{s}{s^2+s+1}.}$$

Example (continued). The quantities needed are the generalized inverses of

$$\Phi(s) = \mathbb{L}_s - s\mathbb{L} = \begin{bmatrix} -\frac{20s}{21} - \frac{4}{21} & -\frac{2s}{3} & \frac{4}{57} - \frac{28s}{57} & \frac{2}{21} - \frac{8s}{21} \\ -\frac{6s}{7} - \frac{4}{7} & -\frac{2s}{3} - \frac{1}{3} & -\frac{10s}{19} - \frac{4}{19} & \frac{3s}{7} - \frac{1}{7} \\ -\frac{4s}{7} - \frac{4}{7} & -\frac{10s}{21} - \frac{8}{21} & -\frac{52s}{133} - \frac{36}{133} & -\frac{16s}{49} - \frac{10}{49} \\ -\frac{8s}{21} - \frac{10}{21} & -\frac{s}{3} - \frac{1}{3} & -\frac{16s}{57} - \frac{14}{57} & -\frac{5s}{21} - \frac{4}{21} \end{bmatrix} = \mathbf{X}\Delta(s)\mathbf{Y}^T.$$

Let the common range of the columns of $\mathbb{L}$, $\mathbb{L}_s$ be spanned by the columns of $\mathbf{X}$ and the common range of the rows of the same matrices by the rows of $\mathbf{Y}$; it follows that

$$\mathbf{X} = \begin{bmatrix} 1 & 0 \\ 0 & 1 \\ -\frac{3}{7} & \frac{8}{7} \\ -\frac{1}{2} & 1 \end{bmatrix}, \quad \mathbf{Y} = \begin{bmatrix} 1 & 0 & -\frac{7}{19} & -\frac{1}{2} \\ 0 & 1 & \frac{24}{19} & \frac{9}{7} \end{bmatrix} \quad \Rightarrow \quad \det(\mathbf{YX}) \neq 0.$$

Thus with $\Delta(s) = \Phi(1:2, 1:2)(s)$ there holds $\Phi(s)^{MP} = \frac{1}{80989667} \frac{1}{s^2 - s + 1}$.

$$\begin{bmatrix} -28\,(11610185s + 7274073) & 6076\,(32301s - 391) & 14\,(1516851s + 1670036) \\ 294\,(22518\,2s + 281171) & -2058\,(294944s + 15609) & -147\,(417597s + 261503) \\ 3724\,(54617s + 48189) & -26068\,(5715s + 1523) & -1862\,(833663s + 30704) \\ 98\,(2527157s + 2123670) & -98\,(1797669s + 409322) & -49\,(3777710s + 1247231) \end{bmatrix}.$$

Revisit: Construction of Interpolants

- If the pencil $(\mathbb{L}_s, \mathbb{L})$ is regular, i.e. $\Phi(s) = \mathbb{L}_s - s\mathbb{L}$, is invertible, then

$$\mathbf{E} = -\mathbb{L}, \quad \mathbf{A} = -\mathbb{L}_s, \quad \mathbf{B} = \mathbf{V}, \quad \mathbf{C} = \mathbf{W}$$

is a minimal interpolant of the data $\Rightarrow \boxed{\mathbf{H}(s) = \mathbf{W}\,\Phi(s)^{-1}\,\mathbf{V}}$

- If $\Phi(s) = \mathbb{L}_s - s\mathbb{L}$, is singular, let $\Phi(s)^\#$ be a generalized inverse of $\Phi(s)$ (Drazin or Moore-Penrose). $\Rightarrow \boxed{\mathbf{H}(s) = \mathbf{W}\,\Phi(s)^\#\,\mathbf{V}}$

- In the latter case, if the **numerical** rank $\mathbb{L} = k$, compute the rank revealing *SVD*:

$$\mathbb{L} = \mathbf{Y}\Sigma\mathbf{X}^* \approx \mathbf{Y}_k\Sigma_k\mathbf{X}_k^*$$

Theorem. A realization $[\mathbf{C}, \mathbf{E}, \mathbf{A}, \mathbf{B}]$, of an approximate interpolant is given as follows:

$$\mathbf{E} = -\mathbf{Y}_k^*\mathbb{L}\mathbf{X}_k, \quad \mathbf{A} = -\mathbf{Y}_k^*\mathbb{L}_s\mathbf{X}_k, \quad \mathbf{B} = \mathbf{Y}_k^*\mathbf{V}, \quad \mathbf{C} = \mathbf{W}\mathbf{X}_k.$$

There is another way to express the above relationship avoiding arbitrary projectors. Basic ingredients: the **Moore-Penrose generalized inverse** and the **Drazin generalized inverse.**

The Moore-Penrose inverse of the (rectangular) matrix $\mathbf{M} \in \mathbb{R}^{q \times q}$, is denoted by $\mathbf{M}^{MP} \in \mathbb{R}^{k \times q}$, and satisfies:
(a) $\mathbf{MM}^{MP}\mathbf{M} = \mathbf{M}$, (b) $\mathbf{M}^{MP}\mathbf{MM}^{MP} = \mathbf{M}^{MP}$
(c) $\left[\mathbf{MM}^{MP}\right]^T = \mathbf{MM}^{MP}$, (d) $\left[\mathbf{M}^{MP}\mathbf{M}\right]^T = \mathbf{M}^{MP}\mathbf{M}$.
This generalized inverse always exists and is unique.

Given a square matrix $\mathbf{M} \in \mathbb{R}^{q \times q}$, its *index* κ is the least nonnegative integer κ such that rank $\mathbf{M}^{\kappa+1} =$ rank $\mathbf{M}^\kappa$.
The Drazin inverse of $\mathbf{M}$ is the unique matrix $\mathbf{M}^D$ satisfying:
(a) $\mathbf{M}^{\kappa+1}\mathbf{M}^D = \mathbf{M}^\kappa$, (b) $\mathbf{M}^D\mathbf{MM}^D = \mathbf{M}^D$,
(c) $\mathbf{MM}^D = \mathbf{M}^D\mathbf{M}$.

In the sequel we will be concerned with rectangular $n \times m$ polynomial matrices which have an explicit (rank revealing) factorization as follows:

$$\mathbf{M} = \mathbf{X}\Delta\mathbf{Y}^T,$$

where $\mathbf{X}$, Δ, $\mathbf{Y}$ have dimension $q \times n$, $n \times n$, $n \times k$, $n \leq q, k$, and all have full rank k.

The **Moore-Penrose** generalized inverse is:
$$\mathbf{M}^{MP} = \mathbf{Y}(\mathbf{Y}^T\mathbf{Y})^{-1}\Delta^{-1}(\mathbf{X}^T\mathbf{X})^{-1}\mathbf{X}^T.$$

If $q = k$ and $\mathbf{Y}^T\mathbf{X}$ is invertible, the **Drazin generalized inverse** is:
$$\mathbf{M}^D = \mathbf{X}(\mathbf{Y}^T\mathbf{X})^{-1}\Delta^{-1}(\mathbf{Y}^T\mathbf{X})^{-1}\mathbf{Y}^T.$$

and $\Phi(s)^D = \frac{1}{4897369} \frac{1}{s^2 + s + 1}$.

$$\begin{bmatrix} -84\,(234677s + 152881) & 294\,(10652s - 13755) & 588\,(19079s - 641) & 42\,(330545s + 29086) \\ 126\,(31956s + 42829) & -147\,(11885s + 4) & -882\,(4184s + 2255) & -63\,(67611s + 42841) \\ 684\,(19079s + 17063) & -798\,(4184s - 2171) & -4788\,(1885s + 441) & -342\,(31631s + 10550) \\ 42\,(330545s + 281368) & -147\,(22537s - 13751) & -294\,(31631s + 6124) & -21\,(533378s + 157609) \end{bmatrix}.$$

In the **rectangular case**, where there are two less right measurements, i.e we only have $\widetilde{\mathbf{Y}} = \mathbf{Y}(1:2, 1:2)$. In this case the Moore-Penrose inverse is

$$\widetilde{\Phi}(s)^{MP} = \frac{1}{737\,(s^2 + s + 1)} \begin{bmatrix} -4767s - 3402 & \frac{1827}{2}s - \frac{2037}{2} & 3087s + 294 & 3297s + \frac{1365}{2} \\ 5838s + 5250 & -1596s + 903 & -4326s - 1218 & -4515s - 1722 \end{bmatrix}.$$

In the **rectangular case**, where there are two less right measurements, i.e we only have $\widetilde{\mathbf{W}} = \mathbf{W}(:, 1:2)$; hence $\widetilde{\Lambda} = \text{diag}\left[\frac{1}{2}, 1\right]$, while $\mathbf{M}$ remains the same, the right values are $\widetilde{\mathbf{W}} = \mathbf{W}(:, 1:2)$; hence

$$\widetilde{\Phi}(s) = \widetilde{\mathbb{L}}_s - s\widetilde{\mathbb{L}} = \begin{bmatrix} -\frac{20s}{21} - \frac{4}{21} & -\frac{2s}{3} \\ -\frac{6s}{7} - \frac{4}{7} & -\frac{2s}{3} - \frac{1}{3} \\ -\frac{4s}{7} - \frac{4}{7} & -\frac{10s}{21} - \frac{8}{21} \\ -\frac{8s}{21} - \frac{10}{21} & -\frac{s}{3} - \frac{1}{3} \end{bmatrix} = \mathbf{X}\Delta(s)\widetilde{\mathbf{Y}}^T,$$

has dimension 4×2, where $\widetilde{\mathbf{Y}} = \mathbf{Y}(1:2, 1:2)$. In this case the Moore-Penrose inverse is

$$\Rightarrow \quad \boxed{\mathbf{W}\Phi(s)^{MP}\mathbf{V} = \widetilde{\mathbf{W}}\,\widetilde{\Phi}(s)^{MP}\mathbf{V} = \mathbf{W}\Phi(s)^D\mathbf{V} = \mathbf{H}(s)}$$

Thus, the Loewner framework allows the definition of **rectangular and/or singular** systems.

Outline

27 / 42

The Loewner algorithm. Data: $(\mu_i, \ell_i, \mathbf{v}_i)$, $i = 1, \cdots, q$, $(\lambda_j, \mathbf{r}_j, \mathbf{w}_j)$, $j = 1, \cdots, k$.

1. Build the Loewner matrix pencil $(\mathbb{L}_s, \mathbb{L})$ of size $q \times k$.
2. There are two important positive integers to compute, namely the dimension of minimal (approximate) descriptor realizations and their McMillan degree.
   2.1 If condition (16) is satisfied, r is the dimension of the resulting minimal descriptor realizations;
   2.2 In this case $\nu = \text{rank}\,\mathbb{L}$ is the McMillan degree of the corresponding realization.
3. Construct matrices $\mathbf{X} \in \mathbb{C}^{k \times r}$, $\mathbf{Y} \in \mathbb{C}^{q \times r}$ as above. A descriptor realization given by:

$$(\mathbf{E}_\delta, \mathbf{A}_\delta, \mathbf{B}_\delta, \mathbf{C}_\delta) \in \mathbb{C}^{r \times r} \times \mathbb{C}^{r \times r} \times \mathbb{C}^{r \times m} \times \mathbb{C}^{p \times r}.$$

4. If $r = \nu$, the transfer function of the ensuing system is strictly proper rational.
5. If $r > \nu$, we need to decide whether there is a **D**-term or a polynomial term. Towards this goal we compute the generalized eigenvalues of the pencil $(\mathbf{A}_\delta, \mathbf{E}_\delta)$.
   5.1 If there is a multiple eigenvalue at infinity and the corresponding eigenspace has the same dimension, the system has a **D**-term.
   5.2 If there are Jordan blocks at infinity, the transfer function has a polynomial term.

28 / 42

An illustrative example

Illustration of the *relationship between the McMillan degree, the degree of minimal realizations, and the D-term.*

$$\mathbf{A} = \begin{bmatrix} 0 & 1 & 0 \\ 0 & 0 & 1 \\ 0 & 0 & 0 \end{bmatrix},\ \mathbf{C} = \begin{bmatrix} 1 & 0 & 0 \\ 0 & 1 & 0 \end{bmatrix},\ \mathbf{B} = \mathbf{I}_3,\ \mathbf{D} = \begin{bmatrix} 1 & 1 & 1 \\ 1 & 1 & 1 \end{bmatrix} \Rightarrow$$

$$\mathbf{H}(s) = \mathbf{C}(s\mathbf{I} - \mathbf{A})^{-1}\mathbf{B} + \mathbf{D} = \begin{bmatrix} \frac{1}{s}+1 & \frac{1}{s^2}+1 & \frac{1}{s^3}+1 \\ 1 & \frac{1}{s}+1 & \frac{1}{s^2}+1 \end{bmatrix}.$$

Let the interpolation points be:

$$\mathbf{M} = \text{diag}\,[1,\ 1,\ -\tfrac{1}{2},\ -\tfrac{1}{2},\ -\tfrac{1}{4},\ -\tfrac{1}{4}],$$
$$\mathbf{\Lambda} = \text{diag}\,[\tfrac{1}{2},\ \tfrac{1}{2},\ -1,\ -1,\ 2,\ 2].$$

The interpolation values $\mathbf{w}_i = \mathbf{H}(\lambda_i)$, $\mathbf{v}_i = \mathbf{H}(\mu_i)$, $i = 1, 2, 3$, are:

$$\mathbf{w}_1 = \begin{bmatrix} 3 & 5 & 9 \\ 1 & 3 & 5 \end{bmatrix},\ \mathbf{w}_2 = \begin{bmatrix} 0 & 2 & 0 \\ 1 & 0 & 2 \end{bmatrix},\ \mathbf{w}_3 = \begin{bmatrix} 3/2 & 5/4 & 9/8 \\ 1 & 3/2 & 5/4 \end{bmatrix},$$

$$\mathbf{v}_1 = \begin{bmatrix} 2 & 2 & 2 \\ 1 & 2 & 2 \end{bmatrix},\ \mathbf{v}_2 = \begin{bmatrix} -1 & 5 & -7 \\ 1 & -1 & 5 \end{bmatrix},\ \mathbf{v}_3 = \begin{bmatrix} -3 & 17 & -63 \\ 1 & -3 & 17 \end{bmatrix}.$$

29 / 42

This corresponds to *matrix interpolation* (the values considered are matrices) as opposed to tangential interpolation (which will follow next)

$$\mathbf{V} = \begin{bmatrix} 2 & 2 & 2 \\ 1 & 2 & 2 \\ -1 & 5 & -7 \\ 1 & -1 & 5 \\ -3 & 17 & -63 \\ 1 & -3 & 17 \end{bmatrix},\qquad \mathbf{W} = \begin{bmatrix} 3 & 5 & 9 & 0 & 2 & 0 & \tfrac{3}{2} & \tfrac{5}{4} & \tfrac{9}{8} \\ 1 & 3 & 5 & 1 & 0 & 2 & 1 & \tfrac{3}{2} & \tfrac{5}{4} \end{bmatrix},$$

$$\mathbf{R} = [\mathbf{I}_3\ \mathbf{I}_3\ \mathbf{I}_3],\qquad \mathbf{L} = \begin{bmatrix} \mathbf{I}_2 \\ \mathbf{I}_2 \\ \mathbf{I}_2 \end{bmatrix}.$$

$$\Rightarrow\quad \mathbb{L} = \begin{bmatrix} -2 & -6 & -14 & 1 & 0 & 1 & -\tfrac{1}{2} & -3 & -7 \\ 0 & -2 & -6 & 0 & 1 & 0 & -\tfrac{1}{2} & -1 & -\tfrac{8}{3} \\ 4 & 0 & 16 & -2 & 6 & -14 & 1 & -\tfrac{3}{2} & \tfrac{13}{4} \\ 0 & 4 & 0 & 0 & -2 & 6 & 1 & -\tfrac{3}{2} & -\tfrac{3}{2} \\ 8 & -16 & 96 & -4 & 20 & -84 & 2 & -7 & \tfrac{57}{2} \\ 0 & 8 & -16 & 0 & -4 & 20 & 0 & 2 & -7 \end{bmatrix} \in \mathbb{R}^{6 \times 9},$$

and

$$\mathbb{L}_s = \begin{bmatrix} 1 & -1 & 2 & 1 & 1 & 2 & 1 & \tfrac{1}{2} & 1 \\ 1 & 1 & -1 & 1 & 2 & 1 & -1 & 1 & \tfrac{1}{2} \\ 1 & 5 & 1 & -1 & 7 & 1 & 2 & 1 & 1 \\ 1 & 1 & 5 & 1 & 1 & -1 & 1 & 1 & 1 \\ 1 & 9 & -15 & 1 & -3 & 21 & 3 & -6 \\ 1 & 1 & 9 & 1 & 1 & -3 & 1 & 3 \end{bmatrix} \in \mathbb{R}^{6 \times 9}.$$

It readily follows that, while $\text{rank}\,\mathbb{L} = \text{rank}\,\mathbb{L}_s = 3$, the rank of $[\mathbb{L}, \mathbb{L}_s]$ is equal to the rank of $[\mathbb{L}, \mathbb{L}_s]$, which is equal to 4. Furthermore the rank of $\xi\mathbb{L} - \mathbb{L}_s$ is also 4, for all $\xi \in \{\mu_i\} \cup \{\lambda_j\}$. Consequently the dimension of the minimal realization is $r = 4$.

30 / 42

Tangential interpolation. If we define the index set $I = [1\ 2\ 3\ 4]$, we get:

$$\Lambda(I,I) = \text{diag}\begin{bmatrix} \tfrac{1}{2} & \tfrac{1}{2} & 1 & -1 \end{bmatrix}, \quad M(I,I) = \text{diag}\begin{bmatrix} 1 & 1 & -\tfrac{1}{2} & -\tfrac{1}{2} \end{bmatrix},$$

$$W(:,I) = \begin{bmatrix} 3 & 5 & 9 & 0 \\ 1 & 3 & 5 & 1 \end{bmatrix}, \quad V(I,:) = \begin{bmatrix} 2 & 2 \\ 1 & 2 \\ -1 & 5 \\ 1 & -7 \\ 1 & 5 \end{bmatrix},$$

$$\mathbb{L}(I,I) = \begin{bmatrix} -2 & -6 & -14 & 1 \\ 0 & -2 & -6 & 0 \\ 4 & 0 & 16 & -2 \\ 0 & 4 & 0 & 0 \end{bmatrix}, \quad \mathbb{L}_s(I,I) = \begin{bmatrix} 1 & -1 & -5 & 1 \\ 1 & 1 & -1 & 1 \\ 1 & 1 & 5 & 1 \\ 1 & 1 & 5 & 1 \end{bmatrix}.$$

Since condition (16) is satisfied with $r=4$ and the rank of the Loewner matrix is 3, we recover a minimal descriptor realization with incorporated **D** term:

$$W(:,I)(\mathbb{L}_s(I,I) - s\mathbb{L}(I,I))^{-1}V(I,:) = H(s).$$

An alternative way to obtain the interpolant is to project the original matrices by randomly generated projectors:

$$Y^T = \begin{bmatrix} 0 & 0 & 0 & 1 & -1 & 1 \\ 0 & 1 & 1 & 0 & 0 & -1 \\ 1 & 1 & 1 & 1 & 0 & 0 \\ 0 & 1 & 0 & -1 & -1 & 0 \end{bmatrix}, \quad X = \begin{bmatrix} 0 & 1 & -1 & 1 \\ 0 & 0 & 1 & -1 \\ 1 & 1 & 1 & 1 \\ -1 & 0 & 0 & 1 \\ 0 & 1 & 1 & 1 \\ 1 & 0 & 1 & 0 \\ 1 & 0 & 1 & -1 \end{bmatrix}, \quad \Rightarrow$$

$$E_\delta = \begin{bmatrix} -19 & 10 & 21 & 19 \\ -\tfrac{31}{2} & 3 & \tfrac{9}{2} & \tfrac{15}{2} \\ \tfrac{565}{8} & -\tfrac{103}{4} & -\tfrac{687}{8} & -\tfrac{641}{8} \\ \tfrac{45}{4} & -\tfrac{35}{2} & -\tfrac{95}{4} & -\tfrac{65}{4} \end{bmatrix}, \quad A_\delta = \begin{bmatrix} 12 & 6 & 1 & -4 \\ 14 & 18 & 16 & 5 \\ -\tfrac{63}{4} & \tfrac{41}{2} & \tfrac{153}{4} & \tfrac{127}{4} \\ -\tfrac{25}{2} & -5 & \tfrac{5}{2} & \tfrac{15}{2} \end{bmatrix},$$

$$B_\delta = \begin{bmatrix} 1 & -3 & 17 \\ 1 & 4 & 12 \\ -1 & 24 & -54 \\ 0 & 5 & -15 \end{bmatrix}, \quad C_\delta = \begin{bmatrix} \tfrac{65}{8} & \tfrac{45}{4} & \tfrac{37}{8} & -\tfrac{13}{8} \\ \tfrac{29}{4} & \tfrac{17}{2} & \tfrac{25}{2} & \tfrac{3}{4} \end{bmatrix} \Rightarrow C_\delta(A_\delta - sE_\delta)^{-1}B_\delta = H(s).$$

We thus obtain a different (equivalent) descriptor realization with incorporated **D** term. ■

Outline

Reduced order modeling from data

Data sets contain samples of the frequency response of an underlying system:

$$(\imath\omega_j, S^{(j)}), \quad \omega_j \in \mathbb{R}, \quad S^{(j)} \in \mathbb{C}^{p\times m}, \quad j=1,\cdots,N.$$

These measurements are arranged in two arrays, a *column* and a *row* array:

$$P_c = \{(\lambda_j, W_j) : j=1,\cdots,k\}, \quad P_r = \{(\mu_i, V_i) : i=1,\cdots,q\}, \quad \text{where}$$

$$\left.\begin{array}{ll} \lambda_j = \imath\omega_j, & W_j = S^{(j)}, \quad j=1,\cdots,k, \\ \mu_i = \imath\omega_{k+i}, & V_i = S^{(k+i)}, \quad i=1,\cdots,q \end{array}\right\} \quad \text{and} \quad q+k=N.$$

To obtain a real system, the given set must be closed under conjugation, i.e. in addition to the above, the pairs $(-\imath\omega_j, \overline{S^{(j)}}), j=1,\cdots,N$, must also belong to the set of measurements.

To generate *right and left tangential data sets* we need the right and left directions $r_i \in \mathbb{R}^m$, $\ell_j \in \mathbb{R}^p$ which can be chosen either as columns of the identity matrix or as random vectors. Thus the right data set is

$$\left\{\lambda_j, \overline{\lambda}_j; r_j, \overline{r}_j; w_j = W_j r_j, \overline{w}_j = \overline{W}_j \overline{r}_j\right\}, \quad j=1,\cdots,k,$$

while the left data set is

$$\left\{\mu_i, \overline{\mu}_i; \ell_i, \overline{\ell}_i; v_i^T = \ell_i^T V_i, \overline{v}_i^T = \ell_i^T \overline{V}_i\right\}, \quad i=1,\cdots,q.$$

Numerical results

The accuracy is assessed by means of:

▲ the normalized H_∞-norm of the error system, defined as:

$$H_\infty \text{ error} = \frac{\max_{l=1,\cdots,N} \sigma_1\left(\mathbf{H}(i\omega_l) - \mathbf{S}^{(l)}\right)}{\max_{l=1,\cdots,N} \sigma_1\left(\mathbf{S}^{(l)}\right)},$$

where $\sigma_1(\cdot)$ denotes the largest singular value of $(\cdot)$.

▲ the normalized H_2-norm of the error system:

$$(H_2 \text{ error})^2 = \frac{\sum_{i=1}^N \|\mathbf{H}(i\omega_l) - \mathbf{S}^{(l)}\|_F^2}{\sum_{i=1}^N \|\mathbf{S}^{(l)}\|_F^2},$$

where $\|\cdot\|_F^2$ stands for the (square of the) Frobenius-norm (namely the sum of the magnitude squared of all entries).

The associated Loewner and shifted Loewner matrices have dimension $2q \times 2k$. To ensure real matrix entries, we define

$$\mathbf{J}_r = \text{blkdiag}\left[\hat{\mathbf{J}}, \cdots, \hat{\mathbf{J}}\right] \in \mathbb{C}^{2r \times 2r}, \quad \hat{\mathbf{J}} = \frac{1}{\sqrt{2}}\begin{bmatrix} 1 & -i \\ 1 & i \end{bmatrix},$$

and transform the quantities of the Loewner framework as follows:

$$\begin{aligned}
\Lambda^R &= \mathbf{J}_k^* \Lambda \mathbf{J}_k, & \mathbf{R}^R &= \mathbf{R}\mathbf{J}_k, & \mathbf{W}^R &= \mathbf{W}\mathbf{J}_k,\\
\mathbf{M}^R &= \mathbf{J}_q^* \mathbf{M}\mathbf{J}_q, & \mathbf{L}^R &= \mathbf{J}_q^* \mathbf{L}, & \mathbf{V}^R &= \mathbf{J}_q^* \mathbf{V},\\
\mathbb{L}^R &= \mathbf{J}_q^* \mathbb{L}\mathbf{J}_k, & \mathbb{L}_s^R &= \mathbf{J}_q^* \mathbb{L}_s \mathbf{J}_k.
\end{aligned}$$

Computing the two SVDs of the Loewner pencil we obtain the projection defined by

$$\mathbf{X} \in \mathbb{R}^{2k \times r}, \quad \mathbf{Y} \in \mathbb{R}^{2q \times r}.$$

The quantity r is the numerical rank of the corresponding matrices. Thus

$$\mathbf{E}_\delta = -\mathbf{Y}^T \mathbb{L}^R \mathbf{X}, \quad \mathbf{A}_\delta = -\mathbf{Y}^T \mathbb{L}_s^R \mathbf{X}, \quad \mathbf{B}_\delta = \mathbf{Y}^T \mathbf{V}^R, \quad \mathbf{C}_\delta = \mathbf{W}^R \mathbf{X},$$

with **D** incorporated in the other matrices.

Singular value drop of the Loewner and shifted Loewner matrices

Algorithm	CPU time (sec)	H_∞ error	H_2 error
Loewner ($n = 59$ with $\mathbf{D} = \mathbf{0}$)	0.05	5.3266e-3	4.5556e-4
Loewner ($n = 9$ with $\mathbf{D} \neq \mathbf{0}$)	0.15	6.1575e-3	5.9957e-4

Results for a device with $p = 50$ ports (50 inputs, 50 outputs)

Example. *Model reduction from measured data.* Data: $k = 100$ S- (scattering-) parameter measurements of an electronic device with $p = 50$ ports (50 inputs and 50 outputs). Measurements were performed using a vector network analyzer (VNA) (CST AG).

The frequency of the 100 measurements (100 matrices of size 50×50) ranges between 10MHz and 1GHz.

MIMO case. The figure below shows the normalized singular values of the Loewner and shifted Loewner matrices constructed using all measurements in the MIMO case. The tangential directions have been chosen as columns of the identity matrix. According to the algorithm, the drop in the singular values suggests that there is an underlying **D**-term.

The singular values of the Loewner matrix decay about three orders of magnitude between the 9th and 10th, while the singular values of the shifted Loewner matrix decay several orders of magnitude between the 59th and 60th. The system can be decomposed into a strictly proper part of order 9 plus a direct feed-through term **D** of size 50×50 and full rank.

SISO case. We focus on the $(1, 31)$ entry of the S-parameter data. As in the MIMO case, the drop of the singular values of the Loewner pencil (see fig. 40) shows that the data suggests a model of order 4, together with a **D**-term. Knowing the order of the system, we construct models of order 5 with $\mathbf{D} = 0$, as well as of order 4 with $\mathbf{D} \neq 0$.
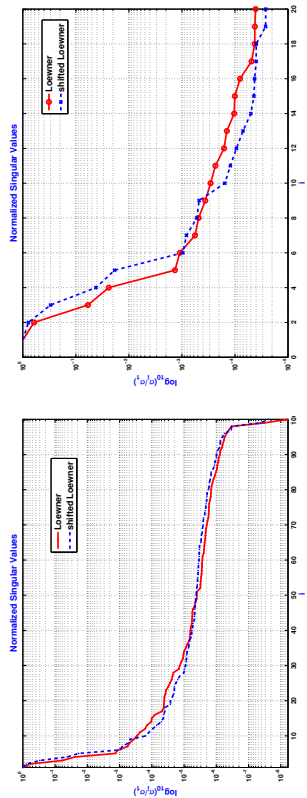
Left pane: the singular value drop of the Loewner matrix pencil for the $(1, 31)$ entry. Right pane: detail of left pane plot.

40 / 42

Left pane: Fit between the data and the 50 singular values (the device has 50 ports) of the transfer function of the model constructed from $k = 100$ samples. Right pane: Data versus model for the $(1, 31)$ entry

39 / 42

Outline

41 / 42

Summary

- Given input/output data, we can construct with *no computation*, a singular high order model in generalized state-space or descriptor form.
- In applications the singular pencil $(\mathbb{L}_s, \mathbb{L})$ must be reduced in order to obtain a minimal or low order model.
- It is a *natural way* to construct full and reduced models because it:
  - does not *force* the inversion of **E**,
  - can deal with many inputs and outputs.
- In this framework the *singular values* of $\mathbb{L}$, $\mathbb{L}_s$ offer a *trade-off between accuracy of fit and complexity of the reduced system*. The resulting (aposteriori computable) error is proportional to the first neglected singular value of $\mathbb{L}$.
- The Loewner framework has been extended to:
  - *multiple-point (Hermite) interpolation.*
  - *recursive modeling* (i.e. data become available successively).
  - *linear parametrized systems.*
  - *bilinear systems* by means of *generalized Loewner pencils.*
  - LSS (Linear Switched Systems).
- The underlying philosophy is: *Collect data and extract the desired information.*
- Overview paper:

  A.C. Antoulas, S. Lefteriu and A.C. Ionita, A tutorial introduction to the Loewner framework for model reduction, in *Model Reduction and Approximation for Complex Systems*, Edited by P. Benner, A. Cohen, M. Ohlberger, and K. Willcox, SIAM, (2016).

42 / 42

Data-driven and interpolatory model reduction: PART IV

Thanos Antoulas

Rice University and Jacobs University

email: aca@rice.edu
URL: www.ece.rice.edu/~aca

35th BENELUX Meeting on Systems and Control 2016
22-24 March 2016
Kontakt der Kontinenten, Soesterberg, The Netherlands

1/35

Outline

Quick overview of the Loewner framework

• PR interpolation and Port-Hamiltonian systems

• Model reduction of linear parametric systems

• Model reduction of bilinear systems

Summary and References

2/35

Outline

Quick overview of the Loewner framework

• PR interpolation and Port-Hamiltonian systems

• Model reduction of linear parametric systems

• Model reduction of bilinear systems

Summary and References

3/35

Interpolatory reduction for linear systems

We are given *left interpolation points, left tangential directions, left responses, and right interpolation points, right tangential directions, right responses:*

$$(\lambda_i; \mathbf{r}_i, \mathbf{w}_i),\ i = 1, \cdots, k,\quad (\mu_j; \ell_j^T, \mathbf{v}_j^T),\ j = 1, \cdots, q.$$

The *right data* is organized as:

$$\Lambda = \mathrm{diag}\,[\lambda_1, \cdots, \lambda_k] \in \mathbb{C}^{k \times k},$$
$$\mathbf{R} = [\mathbf{r}_1\ \mathbf{r}_2\ \cdots\ \mathbf{r}_k] \in \mathbb{C}^{m \times k},$$
$$\mathbf{W} = [\mathbf{w}_1\ \mathbf{w}_2\ \cdots\ \mathbf{w}_k] \in \mathbb{C}^{p \times k}$$

and the *left data* is organized as:

$$\mathbf{M} = \mathrm{diag}\,[\mu_1, \cdots, \mu_q] \in \mathbb{C}^{q \times q},$$
$$\mathbf{L}^T = [\ \ell_1\ \ \cdots\ \ \ell_q\ ] \in \mathbb{C}^{p \times q},$$
$$\mathbf{V}^T = [\ \mathbf{v}_1\ \ \cdots\ \ \mathbf{v}_q\ ] \in \mathbb{C}^{m \times q}.$$

Find a (low order) system $\hat{\boldsymbol{\Sigma}}$, such that $\hat{\mathbf{H}}(s)$, is an *(approximate) tangential interpolant:*

$$\boxed{\ell_j^T \hat{\mathbf{H}}(\mu_j) = \mathbf{v}_j^T,\ j = 1, \cdots, q} \quad \text{and} \quad \boxed{\hat{\mathbf{H}}(\lambda_i)\mathbf{r}_i = \mathbf{w}_i,\ i = 1, \cdots, k}$$

4/35

The Loewner pencil

The *Loewner* and *shifted Loewner* matrices, referred to as the *Loewner pencil*, are:

$$\mathbb{L} = \begin{bmatrix} \frac{v_1^T r_1 - \ell_1^T w_1}{\mu_1 - \lambda_1} & \cdots & \frac{v_1^T r_k - \ell_1^T w_k}{\mu_1 - \lambda_k} \\ \vdots & \cdots & \vdots \\ \frac{v_q^T r_1 - \ell_q^T w_1}{\mu_q - \lambda_1} & \cdots & \frac{v_q^T r_k - \ell_q^T w_k}{\mu_q - \lambda_k} \end{bmatrix} \in \mathbb{C}^{q \times k}.$$

$\mathbb{L}$ satisfies the Sylvester equation

$$M\mathbb{L} - \mathbb{L}\Lambda = VR - LW.$$

The *shifted Loewner matrix* is:

$$\mathbb{L}_s = \begin{bmatrix} \frac{\mu_1 v_1^T r_1 - \ell_1^T w_1 \lambda_1}{\mu_1 - \lambda_1} & \cdots & \frac{\mu_1 v_1^T r_k - \ell_1^T w_k \lambda_k}{\mu_1 - \lambda_k} \\ \vdots & \cdots & \vdots \\ \frac{\mu_q v_q^T r_1 - \ell_q^T w_1 \lambda_1}{\mu_q - \lambda_1} & \cdots & \frac{\mu_q v_q^T r_k - \ell_q^T w_k \lambda_k}{\mu_q - \lambda_k} \end{bmatrix} \in \mathbb{C}^{q \times k},$$

and satisfies the Sylvester equation

$$M\mathbb{L}_s - \mathbb{L}_s\Lambda = MVR - LW\Lambda.$$

5/35

If the data is sampled from $H(s) = C_\delta(sE_\delta - A_\delta)^{-1}B_\delta$, we define:

$$\mathcal{O}_q = \begin{bmatrix} \ell_1^T C_\delta(\mu_1 E_\delta - A_\delta)^{-1} \\ \vdots \\ \ell_q^T C_\delta(\mu_q E_\delta - A_\delta)^{-1} \end{bmatrix},$$

$$\mathcal{R}_k = [(\lambda_1 E_\delta - A_\delta)^{-1}B_\delta r_1, \cdots, (\lambda_k E_\delta - A_\delta)^{-1}B_\delta r_k]$$

of size $q \times n$, $n \times k$, respectively. These are the *generalized tangential observability* and *generalized tangential controllability* matrices. It follows that

$$(\mathbb{L})_{j,i} = \frac{v_j^T r_i - \ell_j^T w_i}{\mu_j - \lambda_i} = -\ell_j^T C_\delta(\mu_j E_\delta - A_\delta)^{-1} E_\delta(\lambda_i E_\delta - A_\delta)^{-1}B_\delta r_i,$$

$$(\mathbb{L}_s)_{j,i} = \frac{\mu_j v_j^T r_i - \lambda_i \ell_j^T w_i}{\mu_j - \lambda_i} = -\ell_j^T C_\delta(\mu_j E_\delta - A_\delta)^{-1} A_\delta(\lambda_i E_\delta - A_\delta)^{-1}B_\delta r_i.$$

$$\Rightarrow \boxed{\mathbb{L} = -\mathcal{O}_q E_\delta \mathcal{R}_k \quad \text{and} \quad \mathbb{L}_s = -\mathcal{O}_q A_\delta \mathcal{R}_k}$$

The following hold true:

(a) $\text{rank}\,\mathbb{L} = \text{rank}\,E_\delta = \text{rank}\,E = $ McMillan degree of the underlying rational fuction

(b) $\text{rank}\,\mathbb{L}_s = \text{rank}\,A_\delta = \text{rank}\,A + \text{rank}\,D$.

6/35

Construction of Interpolants (Models)

- If the pencil $(\mathbb{L}_s, \mathbb{L})$ is regular, i.e. $\Phi(s) = \mathbb{L}_s - s\mathbb{L}$, is invertible, then

$$E = -\mathbb{L}, \quad A = -\mathbb{L}_s, \quad B = V, \quad C = W$$

is a minimal interpolant of the data $\Rightarrow$ $\boxed{H(s) = W\Phi(s)^{-1}V}$

- If $\Phi(s) = \mathbb{L}_s - s\mathbb{L}$, is singular, let $\Phi(s)^\#$ be a generalized inverse of $\Phi(s)$ (Drazin or Moore-Penrose). $\Rightarrow$ $\boxed{H(s) = W\Phi(s)^\# V}$

- In the latter case, if the **numerical** $\text{rank}\,\mathbb{L} = k$, compute the rank revealing *SVD*:

$$\boxed{\mathbb{L} = Y\Sigma X^* \approx Y_k\Sigma_k X_k^*}$$

Theorem. A realization $[C, E, A, B]$, of an approximate interpolant is given as follows:

$$\boxed{E = -Y_k^*\mathbb{L}X_k, \quad A = -Y_k^*\mathbb{L}_s X_k, \quad B = Y_k^* V, \quad C = WX_k.}$$

7/35

Outline

- Quick overview of the Loewner framework
- **PR interpolation and Port-Hamiltonian systems**
- Model reduction of linear parametric systems
- Model reduction of bilinear systems
- Summary and References

8/35

Positive real (PR) interpolation in the Loewner framework

The classical PR problem is: given (λ_i, ϕ_i), $i = 1, \cdots, N$, find *positive real* functions $\phi(s)$ such that

$$\phi(\lambda_i) = \phi_i, \quad i = 1, \cdots, N.$$

If $\mathcal{Re}(\lambda_i) > 0$, the classical condition is that the *Pick matrix*

$$\Pi = \left[\frac{\phi_i^* + \phi_j}{\lambda_i^* + \lambda_j} \right]_{i,j=1,\cdots,N} = \Pi^* \geq 0.$$

Observation: Π is a *Loewner matrix* with column array (λ_i, ϕ_i), and row array the mirror-image set $(-\lambda_j^*, -\phi_j^*)$. Thus the interpolation data in the Loewner framework are

$$W = [\phi_1 \cdots \phi_N], \quad V = -W^*, \quad \Lambda = \text{diag}[\lambda_1, \cdots, \lambda_N], \quad M = -\Lambda^*,$$

and $R = [1, \cdots, 1] = L^*$ (the latter quantities do not appear in the classical framework). Consequently, the associated Loewner matrix pencil satisfies the Sylvester (Lyapunov) equations

$$\mathbb{L}\Lambda + \Lambda^*\mathbb{L} = W^*R + R^*W \quad \text{and} \quad \mathbb{L}_s\Lambda + \Lambda^*\mathbb{L}_s = R^*W\Lambda - \Lambda^*W^*R.$$

Lemma. Realization of PR interpolants. Assuming that $\Pi = \mathbb{L} \geq 0$, a minimal PR interpolant is:

$$H(s) = W(s\mathbb{L} - \mathbb{L}_s)^{-1}W^*.$$

Proof. Making use of the fact that $\mathbb{L} = \mathbb{L}^* > 0$ (Hermitian positive definite), and that $\mathbb{L}_s^* = -\mathbb{L}_s$ (skew Hermitian), we obtain

$$
\begin{aligned}
H(s) + H^*(-s) &= W(s\mathbb{L} - \mathbb{L}_s)^{-1}W^* + W(s^*\mathbb{L} - \mathbb{L}_s)^{-1}W^* \\
&= W(s\mathbb{L} - \mathbb{L}_s)^{-1}[(s + s^*)\mathbb{L} - \mathbb{L}_s - \mathbb{L}_s^*](s^*\mathbb{L} - \mathbb{L}_s)^{-1}W^* \\
&= \underbrace{W(s\mathbb{L} - \mathbb{L}_s)^{-1}}_{K(s)}[(s + s^*)\mathbb{L}]\underbrace{(s^*\mathbb{L} - \mathbb{L}_s)^{-1}W^*}_{K^*(s^*)} \\
&= (s + s^*)K(s)\mathbb{L}K^*(s^*) \geq 0 \quad \text{for} \quad s + s^* \geq 0.
\end{aligned}
$$

Corollary
The above is a realization in Port-Hamiltonian form.

Parametrization of minimal solutions

From

$$\mathbb{L}_s\Lambda + \Lambda^*\mathbb{L}_s = R^*W\Lambda - \Lambda^*W^*R,$$

follows

$$[\mathbb{L}_s - R^*\delta R]\Lambda + \Lambda^*[\mathbb{L}_s - R^*\delta R] = R^*[W - \delta R]\Lambda - \Lambda^*[W^* + R^*\delta]R.$$

Hence a parametrization of all solutions of degree N is given in terms of the (scalar) parameter δ. Hence the associated realization of these interpolants is:

$$\boxed{H(s) = \delta + [W - \delta R][s\mathbb{L} - (\mathbb{L}_s - R^*\delta R)]^{-1}[W^* + R^*\delta], \quad \delta \geq 0}$$

which is again a representation in Port-Hamiltonian form.

Port-Hamiltonian systems with feed-through terms

Port-Hamiltonian (PH) systems with feed-through terms, are described as follows:

$$
\begin{aligned}
\tfrac{d}{dt}\tilde{x}(t) &= [J - \hat{R}]Q\tilde{x}(t) + [G - P]u(t), \\
y(t) &= [G^* + P^*]Q\tilde{x} + [M + S]u(t),
\end{aligned}
$$

where

$$z = \begin{bmatrix} \hat{R} & P \\ P^* & S \end{bmatrix} \geq 0, \quad J = -J^*, \quad M = -M^*.$$

This can be rewritten with $x = Q\tilde{x}$, as

$$\left. \begin{array}{l} E\tfrac{d}{dt}x(t) = Ax(t) + Bu(t) \\ y(t) = Cx(t) + Du(t) \end{array} \right\} \text{ where } \left\{ \begin{array}{l|l} E = Q^{-1}, \ A = J - \hat{R}, & B = G - P \\ C = G^* + P^*, & D = M + S \end{array} \right..$$

Corollary. It readily follows that the realizations above are in Port-Hamiltonian form as
$E = \mathbb{L}$, $J = \mathbb{L}_s$, $\hat{R} = R^*\delta R$, $G = W^*$, $P = \delta R^*$, $M = 0$, $S = \delta$.

Reference: A.J. van der Schaft, *Port-Hamiltonian Differential-Algebraic systems*, Surveys in Differential-Algebraic Equations (2013).

Outline

- Quick overview of the Loewner framework
  - PR interpolation and Port-Hamiltonian systems
- Model reduction of linear parametric systems
  - Model reduction of bilinear systems
- Summary and References

The parametric model reduction problem

Parameter-dependent systems

$$E(p)\dot{x}(t;p) = A(p)x(t;p) + B(p)u(t)$$
$$y(t;p) = C(p)x(t;p) + D(p)u(t)$$

where $p \in \mathbb{R}^d$.

Then $y(s;p) = H(s;p)u(s)$, with $H(p;s) = C(p)(sE(p) - A(p))^{-1}B(p) + D(p)$, is the parameter-dependent transfer function of the system. H is a rational function in several variables: frequency s and parameters $p_1, \cdots, p_d$.

Model reduction: Approximation of multivariate function

$$H(s; p_1, \cdots, p_d)$$

Procedure
- Petrov-Galerkin projection
- Collect measurements of H for various frequencies s and parameter values $p_1, \cdots, p_d$.
- Collect measurements of H for various frequencies s and parameter values $p_1, \cdots, p_d$.

Reference: P. Benner, S. Gugercin, K. Willcox, A Survey of Model Reduction Methods for Parametric Systems, SIAM Review (2015).

Generalization: the Loewner matrix for parameter-dependent systems

- The generalized Loewner matrix has the form:

$$\ell_{i,j}^{k,l} := \frac{v_{k,l} - w_{i,j}}{(\mu_k - \lambda_i)(\nu_l - \pi_j)}.$$

Given $g(s,t)$ of complexity (n,m), construct $\mathbb{L}$, by means of its samples. Assume also that $n' \geq n+1$ and $m' \geq m+1$. The rank of the 2D Loewner matrix is:

$$\text{rank}\,\mathbb{L} = n'm' - (n'-n)(m'-m)$$

Property generalized: barycentric formula

Example: parameter-dependent microstrip

Parameter: width of microstrip (15 values between $60\mu m$ and $130\mu m$ in steps of $5\mu m$). For each parameter value, the 2 port scattering matrix was computed for 100 frequencies between 10MHz and 10GHz.
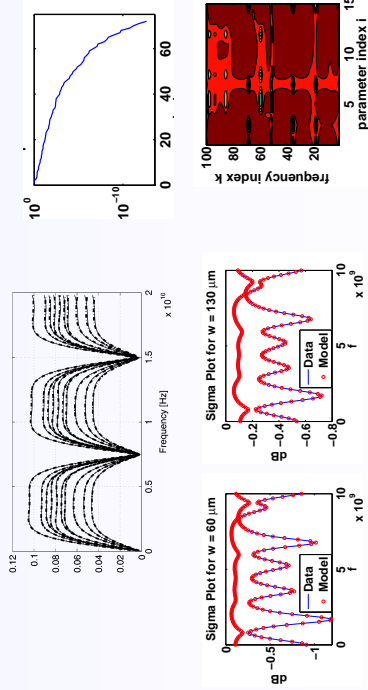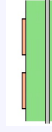
Upper left: S_{11} for different parameter values
Upper right: Singular values of 2D-Loewner matrix $\Rightarrow n = 17, m = 3$.
Lower left: σ-plots for $w = 60\mu m$ and $w = 130\mu m$
Lower right: Error as a function of ω and w

Thermal treatment of railroad rails

$$\frac{\partial \mathbf{u}(\mu_1, \mu_2, t)}{\partial t} - \Delta \mathbf{u}(\mu_1 \mu_2, t) = 0 \quad \text{in } \Omega_0(\mu_1, \mu_2)$$

$$\mathbf{u}(\mu_1, \mu_2, t = 0) = 0 \quad \text{in } \Omega_0(\mu_1, \mu_2)$$

$$\frac{\partial \mathbf{u}(\mu_1, \mu_2, t)}{\partial \mathbf{n}} + \mu_1 \mathbf{u}(\mu_1, \mu_2, t) = \mu_1 \mathbf{g}(t) \quad \text{on } \partial \Omega_0(\mu_1, \mu_2)$$

Parameters: μ_1: Biot number (convective transfer), μ_2: thickness of connecting part of rail.

Boundary conditions: heat exchange between fluid of thermal treatment and rail. Spatial discretization results in $N = 16737$ degrees of freedom.
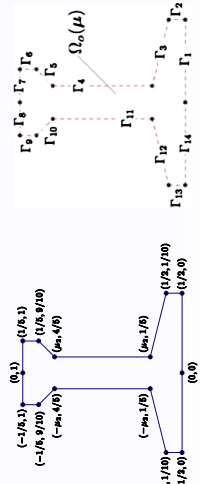
Reference: A. Quarteroni, G. Rozza, and A. Manzoni, Certified reduced basis approximation for parametrized partial differential equations and applications, Journal of Mathematics in Industry 1(1), 3 (2011).

$$\mathbf{A} = \left\{ \begin{array}{l} \frac{-400\mu_2^2 + 80\mu_2 - 13}{30\mu_2 - 12} \mathbf{A}_1 - \frac{4}{10\mu_2 - 5} \mathbf{A}_2 + \frac{1}{10\mu_2} \mathbf{A}_3 + \\[6pt] \frac{\mu_1\sqrt{5}}{15}\sqrt{\frac{10000\mu_2^4 - 16000\mu_2^3 + 8400\mu_2^2 - 1600\mu_2 + 109}{20\mu_2^2 - 8\mu_2 + 1}} \mathbf{A}_4 + \\[6pt] \frac{\mu_1\sqrt{2}}{8}\sqrt{\frac{641 - 5000\mu_2 + 15000\mu_2^2 - 20000\mu_2^3 + 10000\mu_2^4}{50\mu_2^2 - 50\mu_2 + 13}} \mathbf{A}_5 + \mathbf{A}_6 + \mu_1 \mathbf{A}_7 + \mu_2 \mathbf{A}_8 + \mu_2^2 \mathbf{A}_9 \end{array} \right.$$

$$\mathbf{B} = \left\{ \begin{array}{l} \frac{\mu_1\sqrt{5}}{15}\sqrt{\frac{10000\mu_2^4 - 16000\mu_2^3 + 8400\mu_2^2 - 1600\mu_2 + 109}{20\mu_2^2 - 8\mu_2 + 1}} \mathbf{B}_1 + \\[6pt] \frac{\mu_1\sqrt{2}}{8}\sqrt{\frac{641 - 5000\mu_2 + 15000\mu_2^2 - 20000\mu_2^3 + 10000\mu_2^4}{50\mu_2^2 - 50\mu_2 + 13}} \mathbf{B}_2 + \mu_1 \mathbf{B}_3 \end{array} \right.$$

$$\mathbf{C} = \frac{1}{N}[1 \; 1 \; \cdots \; 1], \quad \mathbf{E} = \mathbf{E}_1 + \mu_2 \mathbf{E}_2.$$

$$\mathbf{H}(s; \mu_1, \mu_2) = \mathbf{C}\left[s\mathbf{E}(\mu_1, \mu_2) - \mathbf{A}(\mu_1, \mu_2)\right]^{-1}\mathbf{B}(\mu_1, \mu_2).$$

Resulting system: $\mathbf{E}(\mu_1, \mu_2)\dot{\mathbf{x}}(t) = \mathbf{A}(\mu_1, \mu_2)\mathbf{x}(t) + \mathbf{B}(\mu_1, \mu_2)\mathbf{u}(t)$, $\mathbf{y}(t) = \mathbf{C}\mathbf{x}(t)$. where the state dimension is $n = 16,737$ and and the number of observations is 1.

For $\mu_1 = 10$, we take 50 measurements of $\mathbf{H}(s, \mu_1, \mu_2)$ with respect to s and 50 with respect to μ_2.

Singular values of $\mathbb{L}$ for constant μ_2

Singular values of $\mathbb{L}$ for constant s

Parameter values = (10, 0.02)

Parameter values = (10, 0.20)
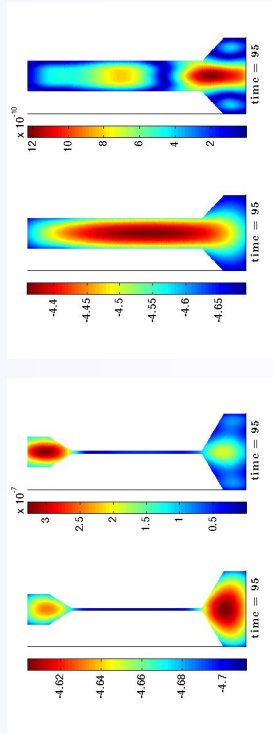
Using the 2D Loewner matrix framework, reduced systems with complexity **5 in the frequency and 10 in the parameter μ_2** were computed.

Value of parameters above, is outside the measurement range.

Outline

Bilinear systems:

$$\Sigma : \quad \mathbf{E}\dot{\mathbf{x}}(t) = \mathbf{A}\mathbf{x}(t) + \mathbf{N}\mathbf{x}(t)\mathbf{u}(t) + \mathbf{B}\mathbf{u}(t), \quad \mathbf{y}(t) = \mathbf{C}\mathbf{x}(t),$$

where $\mathbf{x} \in \mathbb{R}^n$, $\mathbf{u}, \mathbf{y} \in \mathbb{R}$. Such systems are equivalent to the infinite set of systems:

$$\mathbf{E}\dot{\mathbf{x}}_1(t) = \mathbf{A}\mathbf{x}_1(t) + \mathbf{B}\mathbf{u}(t),$$
$$\mathbf{E}\dot{\mathbf{x}}_2(t) = \mathbf{A}\mathbf{x}_2(t) + \mathbf{N}\mathbf{x}_1(t)\mathbf{u}(t),$$
$$\mathbf{E}\dot{\mathbf{x}}_3(t) = \mathbf{A}\mathbf{x}_3(t) + \mathbf{N}\mathbf{x}_2(t)\mathbf{u}(t),$$
$$\cdots$$

The solution is given as $\mathbf{x}(t) = \sum_{i=0}^{\infty} \mathbf{x}_i(t)$. Moreover, the frequency-domain behavior is characterized by a series of generalized (multi-variate) transfer functions:

$$\mathbf{H}_1(s_1) = \mathbf{C}\Phi(s_1)\mathbf{B}, \quad \mathbf{H}_2(s_1, s_2) = \mathbf{C}\Phi(s_1)\mathbf{N}\Phi(s_2)\mathbf{B}, \quad \cdots$$

where $\Phi(x) = (x\mathbf{E} - \mathbf{A})^{-1}$. Thus in general the mth transfer function is a multivariate rational function in the variables s_i, $i = 1, \cdots, m$:

$$\mathbf{H}_m(s_1, s_2, \cdots, s_m) = \mathbf{C}\Phi(s_1)\mathbf{N}\Phi(s_2)\mathbf{N}\cdots\mathbf{N}\Phi(s_m)\mathbf{B}, \quad m = 1, 2, \cdots.$$

Consequence. Use interpolatory methods.

Recall: linear systems

Assuming that the underlying transfer function is $\mathbf{H}(s) = \mathbf{C}(s\mathbf{E} - \mathbf{A})^{-1}\mathbf{B}$, recall that the Loewner quantities for linear systems can be factorized as

$$\boxed{\mathbb{L} = -\mathcal{O}\mathcal{E}\mathcal{R}, \quad \mathbb{L}_s = -\mathcal{O}\mathcal{A}\mathcal{R}, \quad \mathbf{V} = \mathcal{C}\mathcal{R}, \quad \mathbf{W} = \mathcal{O}\mathbf{B}}$$

where $\mathcal{O}$, $\mathcal{R}$ are the generalized reachability matrix and the generalized observability matrix.

Facts

- **Property generalized** to bilinear systems: **factorization** of $\mathbb{L}$, $\mathbb{L}_s$, $\mathbf{V}$, $\mathbf{W}$.

- Still valid: the singular values of the (generalized) Loewner matrix $\mathbb{L}$ provide a trade-off between accuracy of fit and complexity of the reduced model.

Example. Given the SISO bilinear system $(\mathbf{C}, \mathbf{E}, \mathbf{A}, \mathbf{N}, \mathbf{B})$, where $\mathbf{A}$ is $n \times n$, consider the ordered tuples of left and right interpolation points: $\left[\begin{array}{c} \{\mu_1\} \\ \{\mu_1, \mu_2\} \end{array} \right]$, $\left[\{\lambda_1\}, \{\lambda_2, \lambda_1\} \right]$.

The *generalized observability and controllability* matrices are

$$\mathcal{O} = \left[\begin{array}{c} \mathbf{C}(\mu_1\mathbf{E} - \mathbf{A})^{-1} \\ \mathbf{C}(\mu_1\mathbf{E} - \mathbf{A})^{-1}\mathbf{N}(\mu_2\mathbf{E} - \mathbf{A})^{-1} \end{array} \right],$$

$$\mathcal{R} = \left[(\lambda_1\mathbf{E} - \mathbf{A})^{-1}\mathbf{B}, \quad (\lambda_2\mathbf{E} - \mathbf{A})^{-1}\mathbf{N}(\lambda_1\mathbf{E} - \mathbf{A})^{-1}\mathbf{B} \right].$$

The projected matrices can be written in terms of the samples in the following way:

$$\mathbb{L} = \left[\begin{array}{cc} \dfrac{\mathbf{H}_1(\mu_1) - \mathbf{H}_1(\lambda_1)}{\mu_1 - \lambda_1} & \dfrac{\mathbf{H}_2(\mu_1, \lambda_1) - \mathbf{H}_2(\lambda_2, \lambda_1)}{\mu_1 - \lambda_2} \\ \dfrac{\mathbf{H}_2(\mu_1, \mu_2) - \mathbf{H}_2(\mu_1, \lambda_1)}{\mu_2 - \lambda_1} & \dfrac{\mathbf{H}_3(\mu_1, \mu_2, \lambda_1) - \mathbf{H}_3(\mu_1, \lambda_2, \lambda_1)}{\mu_2 - \lambda_2} \end{array} \right] = -\mathcal{O}\mathcal{E}\mathcal{R},$$

$$\mathbb{L}_s = \left[\begin{array}{cc} \dfrac{\mu_1\mathbf{H}_1(\mu_1) - \lambda_1\mathbf{H}_1(\lambda_1)}{\mu_1 - \lambda_1} & \dfrac{\mu_1\mathbf{H}_2(\mu_1, \lambda_1) - \lambda_2\mathbf{H}_2(\lambda_2, \lambda_1)}{\mu_1 - \lambda_2} \\ \dfrac{\mu_2\mathbf{H}_2(\mu_1, \mu_2) - \lambda_1\mathbf{H}_2(\mu_1, \lambda_1)}{\mu_2 - \lambda_1} & \dfrac{\mu_2\mathbf{H}_3(\mu_1, \mu_2, \lambda_1) - \lambda_2\mathbf{H}_3(\mu_1, \lambda_2, \lambda_1)}{\mu_2 - \lambda_2} \end{array} \right] = -\mathcal{O}\mathcal{A}\mathcal{R},$$

$$\psi = \left[\begin{array}{cc} \mathbf{H}_2(\mu_1, \mu_2) & \mathbf{H}_3(\mu_1, \lambda_2, \lambda_1) \\ \mathbf{H}_3(\mu_1, \mu_2, \lambda_1) & \mathbf{H}_4(\mu_1, \mu_2, \lambda_2, \lambda_1) \end{array} \right] = \mathcal{O}\mathcal{N}\mathcal{R},$$

$$\mathbf{V} = \left[\begin{array}{c} \mathbf{H}_1(\mu_1) \\ \mathbf{H}_2(\mu_1, \mu_2) \end{array} \right] = \mathcal{O}\mathbf{B},$$

$$\mathbf{W} = \left[\mathbf{H}_1(\lambda_1) \quad \mathbf{H}_2(\lambda_2, \lambda_1) \right] = \mathbf{C}\mathcal{R}.$$

It readily follows that given the bilinear system $(\mathbf{C}, \mathbf{E}, \mathbf{A}, \mathbf{N}, \mathbf{B})$, a reduced bilinear system of order two, can be obtained without computation (matrix factorizations or solves) as:

$$\hat{\mathbf{E}} = \mathcal{O}\mathbf{E}\mathcal{R}, \quad \hat{\mathbf{A}} = \mathcal{O}\mathbf{A}\mathcal{R}, \quad \hat{\mathbf{N}} = \mathcal{O}\mathbf{N}\mathcal{R}, \quad \hat{\mathbf{B}} = \mathcal{O}\mathbf{B}, \quad \hat{\mathbf{C}} = \mathbf{C}\mathcal{R}.$$

This reduced system matches eight moments of the original system, namely:

two of $\mathbf{H}_1$: $\mathbf{H}_1(\mu_1), \mathbf{H}_1(\lambda_1),$
three of $\mathbf{H}_2$: $\mathbf{H}_2(\mu_1, \mu_2), \mathbf{H}_2(\mu_1, \lambda_1), \mathbf{H}_2(\lambda_2, \lambda_1),$
two of $\mathbf{H}_3$: $\mathbf{H}_3(\mu_1, \mu_2, \lambda_1), \mathbf{H}_3(\mu_1, \lambda_2, \lambda_1),$ and
one of $\mathbf{H}_4$: $\mathbf{H}_4(\mu_1, \mu_2, \lambda_2, \lambda_1)$

i.e. in total $2k + k^2 = 8$ moments are matched using this procedure.

Alternatively, the tuples can be chosen as $\begin{bmatrix} \{\mu_1\} \\ \{\mu_2\} \end{bmatrix}$, $\begin{bmatrix} \{\lambda_2\}, & \{\lambda_1\} \end{bmatrix}$, and the generalized observability and controllability matrices are

$$\mathcal{O} = \begin{bmatrix} \mathbf{C}(\mu_1\mathbf{E} - \mathbf{A})^{-1} \\ \mathbf{C}(\mu_2\mathbf{E} - \mathbf{A})^{-1} \end{bmatrix}, \quad \mathcal{R} = \begin{bmatrix} (\lambda_1\mathbf{E} - \mathbf{A})^{-1}\mathbf{B}, & (\lambda_2\mathbf{E} - \mathbf{A})^{-1}\mathbf{B} \end{bmatrix}.$$

Here the associated $(\mathbf{V}, \mathbb{L}, \mathbb{L}_s, \mathbf{W})$ are as in the linear case while

$$\psi = \begin{bmatrix} \mathbf{H}_2(\mu_1, \lambda_1) & \mathbf{H}_2(\mu_1, \lambda_2) \\ \mathbf{H}_2(\mu_2, \lambda_1) & \mathbf{H}_2(\mu_2, \lambda_2) \end{bmatrix} = \mathcal{O}\mathbf{N}\mathcal{R},$$

and the 8 moments matched are: $\mathbf{H}_1(\mu_i), \mathbf{H}_1(\lambda_j), \mathbf{H}_2(\lambda_j), \mathbf{H}_2(\mu_i, \lambda_j), i, j = 1, 2.$

25 / 35

Recall that a bilinear system is completely described by means of the rational functions:

$$\mathbf{H}_m(\nu_1, \nu_2, \cdots, \nu_m) = \mathbf{C}(\nu_1\mathbf{E} - \mathbf{A})^{-1}\mathbf{N}(\nu_2\mathbf{E} - \mathbf{A})^{-1}\mathbf{N} \cdots \mathbf{N}(\nu_m\mathbf{E} - \mathbf{A})^{-1}\mathbf{B}, \quad m = 1, 2, \cdots.$$

(a) Selecting the data.
Given the kth ordered row and the ℓth ordered column tuples

$$(\mu_1, \cdots, \mu_{k-1}, \mu_k) \quad \text{and} \quad (\lambda_\ell, \lambda_{\ell-1}, \cdots, \lambda_1),$$

we need the following data:

$\mathbf{H}_k(\mu_1, \cdots, \mu_{k-1}, \mu_k), \mathbf{H}_\ell(\lambda_\ell, \lambda_{\ell-1}, \cdots, \lambda_1), \mathbf{H}_{k-\ell}(\mu_1, \cdots, \mu_{k-1}, \mu_k, \lambda_\ell, \lambda_{\ell-1}, \cdots, \lambda_1)$ and
$\mathbf{H}_{k+\ell-1}(\mu_1, \cdots, \mu_{k-1}, \lambda_\ell, \lambda_{\ell-1}, \cdots, \lambda_1), \mathbf{H}_{k+\ell-1}(\mu_1, \cdots, \mu_{k-1}, \mu_k, \lambda_{\ell-1}, \cdots, \lambda_1),$

(b) The generalized Loewner matrices.
The first element above is $\mathbf{V}(k, 1)$, the second is $\mathbf{W}(1, \ell)$, the third is $\psi(k, \ell)$, while

$$\mathbb{L}(j, i) = \frac{\mathbf{H}_{j+\ell-i}(\mu_1, \cdots, \mu_j, \lambda_{i-1}, \cdots, \lambda_1) - \mathbf{H}_{j+\ell-i}(\mu_1, \cdots, \mu_{j-1}, \lambda_i, \cdots, \lambda_1)}{\mu_j - \lambda_i},$$

$$\mathbb{L}_s(j, i) = \frac{\mu_j\mathbf{H}_{j+\ell-i}(\mu_1, \cdots, \mu_j, \lambda_{i-1}, \cdots, \lambda_1) - \lambda_i\mathbf{H}_{j+\ell-i}(\mu_1, \cdots, \mu_{j-1}, \lambda_i, \cdots, \lambda_1)}{\mu_j - \lambda_i},$$

(c) The reduced system of order N matches $N^2 + 2N$ moments of the original system.

26 / 35

Construction of interpolants.

Once the transfer function values have been chosen, the rest of the procedure is unchanged:

Lemma. Assume that $k = \ell$, and let $(\mathbb{L}_s, \mathbb{L})$, be a regular pencil. Then

$$\mathbf{E} = -\mathbb{L}, \quad \mathbf{A} = -\mathbb{L}_s, \quad \mathbf{N} = \psi, \quad \mathbf{B} = \mathbf{V}, \quad \mathbf{C} = \mathbf{W},$$

is a minimal realization of an interpolant of the data, i.e., the rational functions:

$$\mathbf{H}_k(s_1, \cdots, s_k) = \mathbf{W}(\mathbb{L}_s - s_1\mathbb{L})^{-1}\psi \cdots \psi(\mathbb{L}_s - s_k\mathbb{L})^{-1}\mathbf{V},$$

for $k \geq 1$, interpolate the data.

In the case of redundant data (pencil $(\mathbb{L}_s, \mathbb{L})$ singular) we construct $\mathbf{X}, \mathbf{Y} \in \mathbb{R}^{\rho \times k}$ as before.

Theorem. The quintuple $(\mathbf{C}, \mathbf{E}, \mathbf{A}, \mathbf{N}, \mathbf{B})$ given by:

$$\mathbf{E} = -\mathbf{Y}^*\mathbb{L}\mathbf{X}, \quad \mathbf{A} = -\mathbf{Y}^*\mathbb{L}_s\mathbf{X}, \quad \mathbf{N} = \mathbf{Y}^*\psi\mathbf{X}, \quad \mathbf{B} = \mathbf{Y}^*\mathbf{V}, \quad \mathbf{C} = \mathbf{W}\mathbf{X},$$

is the realization of an (approximate) interpolant of the data.

Remark. Thus, as in the linear case, if we have more data than necessary, we can either consider $(\mathbf{W}, -\mathbb{L}, -\mathbb{L}_s, \psi, \mathbf{V})$ as an exact but singular model of the data or

$$(\mathbf{W}\mathbf{X}, -\mathbf{Y}^*\mathbb{L}\mathbf{X}, -\mathbf{Y}^*\mathbb{L}_s\mathbf{X}, \mathbf{Y}^*\psi\mathbf{X}, \mathbf{Y}^*\mathbf{V}),$$

as an approximate (nonsingular) model of the data.

27 / 35

Numerical experiments: (a) Bilinear controlled heat transfer system.

On the unit square we consider the heat equation

$$\frac{\partial x}{\partial t} = \Delta x,$$

with the mixed Dirichlet and Robin boundary conditions:

$$n \cdot \nabla x = u_1(x - 1), \quad \text{on} \quad \Gamma_1 = \{0\} \times]0,1[,$$
$$n \cdot \nabla x = u_2(x - 1), \quad \text{on} \quad \Gamma_2 =]0,1[\times \{0\},$$
$$x = 0, \quad \text{on} \quad \Gamma_3 = \{1\} \times [0,1] \text{ and } \Gamma_4 = [0,1] \times \{1\}.$$

The heat transfer coefficients u_1 and u_2 and the lower boundaries Γ_1 and Γ_2 are the input variables. They can be interpreted as spraying-intensities of a cooling fluid acting on these boundaries.

The dynamics of the heat flow yield a bilinear system described by

$$\dot{\mathbf{x}} = \mathbf{A}\mathbf{x} + u_1\mathbf{N}_1\mathbf{x} + u_2\mathbf{N}_2\mathbf{x} + \mathbf{B}\mathbf{u},$$

where the system matrices are determined as follows:

$$\mathbf{A} = \frac{1}{h^2}(\mathbf{I} \otimes \mathbf{T}_k + \mathbf{T}_k \otimes \mathbf{I} + \mathbf{E}_1 \otimes \mathbf{I} + \mathbf{I} \otimes \mathbf{E}_k), \quad \mathbf{E}_j = \mathbf{e}_j\mathbf{e}_j^T,$$
$$\mathbf{N}_1 = \frac{1}{h}\mathbf{E}_1 \otimes \mathbf{I}, \quad \mathbf{N}_2 = -\frac{1}{h}\mathbf{I} \otimes \mathbf{E}_k, \quad \mathbf{b}_1 = -\frac{1}{h}\mathbf{E}_1 \otimes \mathbf{e}, \quad \mathbf{b}_2 = \frac{1}{h}\mathbf{e} \otimes \mathbf{E}_k, \quad \mathbf{e} = [1, 1, \cdots, 1]^T,$$
$$\mathbf{C} = \frac{1}{k^2}(\mathbf{e} \otimes \mathbf{e})^T.$$

28 / 35

We denote by Σ_B the 2500th order system obtained by discretizing the heat equation. This bilinear system will be reduced by means of the following methods:

1. Σ_B is reduced using Loewner to obtain Σ_1 of order 28.
2. Σ_B is reduced using BIRKA to obtain Σ_2 of order 28.

The first step is to collect samples from generalized bilinear transfer functions, and plot the singular values of the ensuing Loewner pencil. Since $\sigma_{28} \approx 10^{-15}$, we choose $k = 28$ for all reduced systems.

We compute the time-domain output of the original and of the reduced systems for

$$u(t) = 0.2\sin(40t)e^{-t/2} + e^{-t/2}.$$

Time domain simulation - Output signals

Singular values of the Loewner pencil
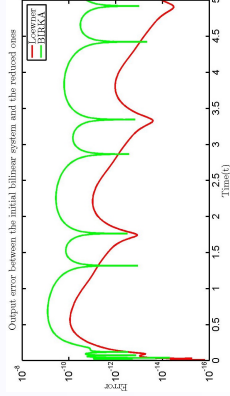
Time domain simulation - Approximation errors

Numerical experiments: (b) Viscous Burgers Equation:

$$\frac{\partial v(x,t)}{\partial t} + v(x,t)\frac{\partial v(x,t)}{\partial x} = \frac{\partial}{\partial x}\left(\nu\left(\frac{\partial v(x,t)}{\partial x}\right)\right), \quad (x,t) \in (0,1) \times (0,T),$$

subject to the initial and boundary conditions given by:

$$v(x,0) = f(x),\ x \in [0,1],\ v(0,t) = u(t),\ v(1,t) = 0,\ t \geqslant 0.$$

$v(x,t)$ is the velocity at (x,t). The viscosity coefficient $\nu(x,t)$ may depend on space and time. Spacial discretization yields:

$$\dot{v}_k = \begin{cases} -\frac{v\,v_2}{2h} + \frac{\nu}{h^2}(v_2 - 2v_1) + \left(\frac{v_1}{2h} + \frac{\nu}{h^2}\right)u, & k = 1, \\[4pt] -\frac{v_k}{2h}(v_{k+1} - v_{k-1}) + \frac{\nu}{h^2}(v_{k+1} - 2v_k + v_{k-1}), & 2 \leqslant k \leqslant N-1, \\[4pt] -\frac{v_N v_{N-1}}{2h} + \frac{\nu}{h^2}(-2v_N + 2v_{N-1}), & k = N. \end{cases}$$

We use the Carleman bilinearization to approximate the above Nth order nonlinear systems with a bilinear system Σ_B of order $N^2 + N$.

Σ_B is reduced using Loewner to Σ_1 and BIRKA to Σ_2.
Since $\sigma_{30} \approx 10^{-15}$, we choose the reduced order $k = 30$.
Time-domain simulation using $u(t) = 0.2\sin(40t)e^{-t/2} + e^{-t/2}$.

Model reduction from data, measured or computed: Summary

- Given input/output data, we can construct with no computation, a singular high order model in generalized state space form.

- Key tool: Loewner pencil.

- In applications the singular pencil must be reduced at some stage.

- Natural way to construct full and reduced models:
  - ⇒ does not **force** inversion of **E**,
  - ⇒ can deal with many input/output ports.

- In this framework the singular values of $\mathbb{L}$, $\mathbb{L}_s$ offer a trade-off between accuracy of fit and complexity of the reduced system.

- Extension to parametrized systems.

- Extension to nonlinear systems by means of generalized Loewner and shifted Loewner matrices.

- Philosophy: Collect data and extract desired information

Outline

- Quick overview of the Loewner framework

- PR interpolation and Port-Hamiltonian systems

- Model reduction of linear parametric systems

- Model reduction of bilinear systems

- Summary and References

Some recent references

- T. Breiten, T. Damm, Krylov subspace methods for model reduction of bilinear systems, Systems and Control Letters, **59**: 443-450 (2010).
- P. Benner, T. Breiten: Interpolation-Based ??-Model Reduction of Bilinear Control Systems, SIAM Journal on Matrix Analysis and Applications, vol. 33, 2012.
- T. Breiten, Interpolatory methods for model reduction of large-scale dynamical systems, PhD Dissertation, Magdeburg, March 2013.
- G. Flagg, Interpolatory methods for model reduction of bilinear systems, PhD Dissertation, Virginia Tech, May 2012.
- G. Flagg and S. Gugercin, Multipoint Volterra Series Interpolation and H_2 optimsl model reduction of bilinear systems, Technical Report, Virginia Tech, December 2013.
- C. Gu, QLMOR: A Projection-Based Nonlinear Model Order Reduction Approach Using Quadratic-Linear Representation of Nonlinear Systems, IEEE-CAD, vol 30, Sept 2011.
- Model reduction from data
  - A.J Mayo and A.C. Antoulas, *A framework for the solution of the generalized realization problem*, Linear Algebra and Its Applications, vol. 425, pages 634-662 (2007).
  - Lefteriu, Antoulas: A New Approach to Modeling Multiport Systems from Frequency-Domain Data, IEEE Trans. CAD, vol. 29, pages 14-27 (2010).
- Interpolatory model reduction
  - A.C. Antoulas, C.A. Beattie, and S. Gugercin, *Interpolatory model reduction of large-scale systems*, in Efficient modeling and control of large-scale systems, K. Grigoriadis and J. Mohammadpour Eds, Springer Verlag, pages 3-58 (2010).
  - S. Gugercin, C.A. Beattie and A.C. Antoulas, *Data-driven and interpolatory model reduction*, book in preparation, SIAM (2014).
- Parametric interpolatory model reduction
  - A.C. Antoulas, A.C. Ionita, and S. Lefteriu, *On two-variable rational interpolation*, Linear Algebra and Its Applications, **436**: 2889-2915 (2012).
  - A.C. Ionita and A.C. Antoulas, Parametrized model order reduction from transfer function measurements, in Reduced Order Methods for modeling and computational reduction, Book Series: Modeling, Comutations and Applications, A. Quarteroni, G. Rozza (Editors), Springer Verlag (2013).
  - A.C. Ionita and A.C. Antoulas, Data-driven parametrized model reduction in the Loewner framework, Technical Report, Rice University, March 2013.

A control theoretic framework for power grids

Claudio De Persis

Engineering and Technology Institute (ENTEG)
Jan C. Willems Center for Systems and Control
University of Groningen

/ university of groningen

Benelux meeting on Systems and Control
Soesterberg, the Netherlands
March 22 - 24, 2016

Power grids

Risk of failures

India, July 2012
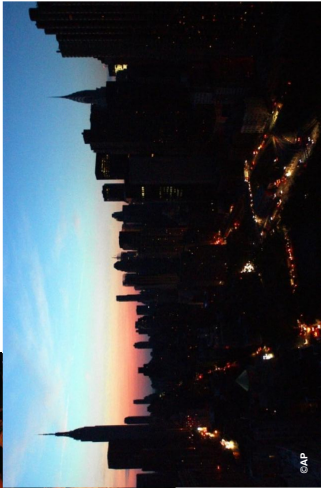
©AP

US, Aug 2003

©AP

Power grids

Increased uncertainty in power generation consumption

Shift towards distributed generation

- Environmental concerns
- Economical benefits
- Reduction of power losses
- Containment of fault propagation

Power grids

Power interface

AC(≠60Hz) ——— DC

?

DC

AC(60Hz)

Power grids

Power interface

AC(≠60Hz) — — **DC** — INVERTER — **DC**

AC(60Hz)

Microgrids

Schiffer et al. *Modeling of microgrids – from fundamental physics to phasors and voltage sources.* arXiv 1505.00136
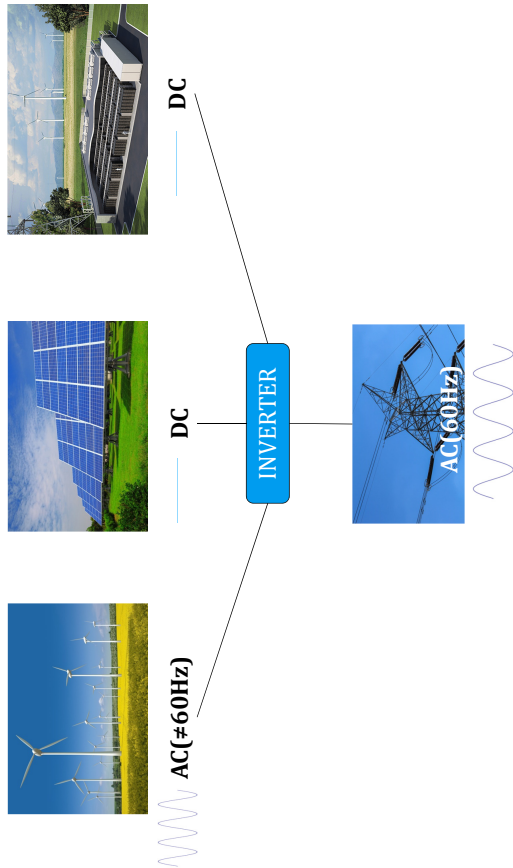
Models

Outline

Aims

- Microgrid models (5 slides)
- Frequency regulation and voltage stability (5 slides)
- Passivity (6 slides)
- Controller (7 slides)

Caveats

- No model derivation
- Technological aspects neglected
- Lossless transmission lines
- No constraints
- Network reduced models

Inverters

Power electronics devices with fast dynamics that perform DC-to-AC conversion
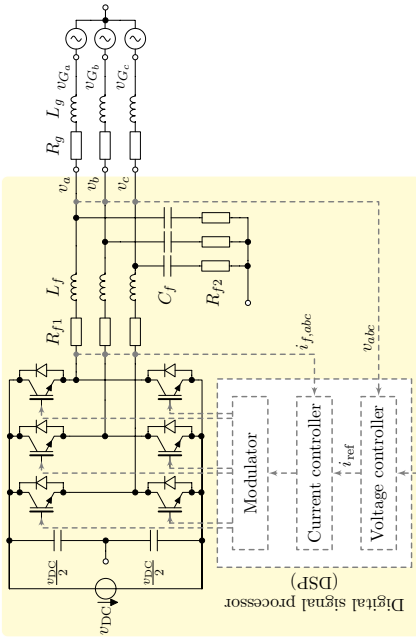
Schiffer et al. *Modeling of microgrids – from fundamental physics to phasors and voltage sources* arXiv 1505.00136.

$P_i = V_i I_{qi}$ active power at inverter i
$Q_i = V_i I_{di}$ reactive power at inverter i

Closed-loop

Inverters

Schiffer et al. *Modeling of microgrids – from fundamental physics to phasors and voltage sources.* arXiv 1505.00136

Inverters: AC (sinusoidal) voltage sources with controllable amplitude V_i and frequency $\dot\delta_i = \omega_i$
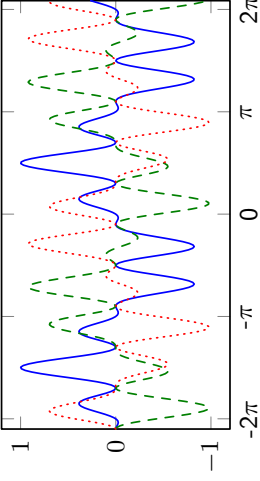
$$\dot\omega_i = u_i^\omega$$
$$\dot V_i = u_i^V$$

Inverter controllers

Frequency and voltage droop controllers

$$u_i^\omega = -(\omega_i - \omega^*) - K_{Pi}(P_i - P_i^*)$$
$$u_i^V = -(V_i - V^*) - K_{Qi}(Q_i - Q_i^*)$$

Closed-loop

$$\dot\delta_i = \omega_i$$
$$\dot\omega_i = -(\omega_i - \omega^*) - K_{Pi}(P_i - P_i^*)$$
$$\dot V_i = -(V_i - V^*) - K_{Qi}(Q_i - Q_i^*)$$

Network

Lossless case lines are purely inductive

$$P_i = \sum_{j\in N_i} V_i V_j |B_{ij}| \sin(\delta_{ij})$$
$$Q_i = |B_{ii}| V_i^2 - \sum_{j\in N_i} V_i V_j |B_{ij}| \cos(\delta_{ij})$$

where
$B_{ij} = -\frac{1}{\omega^* L_{ij}}$ susceptance of line $\{i,j\}$
$B_{ii} = \hat B_{ii} + \sum_{j\in N_i} B_{ij}$
$\hat B_{ii}$ shunt-susceptance

Active and reactive power

1 physical interconnection among the nodes
2 feedback information for inverter controllers

Frequency regulation

Control goals

$$\dot{\delta}_i = \omega_i$$
$$\dot{\omega}_i = -(\omega_i - \omega^*) - K_{Pi}(P_i - P_i^*)$$
$$\dot{V}_i = -(V_i - V^*) - K_{Qi}(Q_i - Q_i^*)$$

Ideal scenario

Frequency regulation $\omega_i \approx \omega^*$

Voltage regulation $V_i \approx V^*$

Active power sharing $\dfrac{P_i}{P_j} \approx \dfrac{K_{Pj}}{K_{Pi}}$

Reactive power sharing $\dfrac{Q_i}{Q_j} \approx \dfrac{K_{Qj}}{K_{Qi}}$

Frequency regulation

Steady state $\omega_i = \overline{\omega}$

$$0 = -(\overline{\omega} - \omega^*) - K_{Pi}(P_i - P_i^*)$$

Summing all the contributions and solving for $\overline{\omega}$

$$\overline{\omega} = \omega^* + \frac{\sum_i P_i^*}{\sum_i K_{Pi}^{-1}}$$

Additional control

$$0 = -(\overline{\omega} - \omega^*) - K_{Pi}(P_i - P_i^*) + u_{Pi}$$

resulting in

$$\overline{\omega} = \omega^* + \frac{\sum_i(P_i^* + u_{Pi})}{\sum_i K_{Pi}^{-1}}$$

Frequency regulation

Optimal resource allocation

$$\min_{u_P} \frac{1}{2}\sum_i K_{Pi}^{-1} u_{Pi}^2$$
$$\text{s.t.} \quad 0 = \sum_i(P_i^* + u_{Pi})$$

which returns

$$\overline{u}_P = -\mathbb{1}\frac{\mathbb{1}^T P^*}{\mathbb{1}^T K_P^{-1}\mathbb{1}}$$

Replacing in $0 = -(\overline{\omega} - \omega^*) - K_{Pi}(P_i - P_i^*) + \overline{u}_{Pi}$ and solving for P_i

Active power sharing

$$\frac{P_i}{P_j} = \frac{K_{Pj}}{K_{Pi}}$$

Synchronous solution

$$\dot{\delta}_i = \omega_i$$
$$\dot{\omega}_i = -(\omega_i - \omega^*) - (P_i - P_i^*) + u_{Pi}$$
$$\dot{V}_i = -V_i - Q_i + u_{Qi}$$

Synchronous solution

$$(\bar{\delta}, \bar{\omega}, \overline{V}) = (\bar{\delta}_0 + \mathbb{1}\omega^* t, \mathbb{1}\omega^*, \overline{V})$$

corresponding to $(\bar{u}_P, \bar{u}_Q)$.

Inverter controllers

Quadratic droop controllers

$$\dot{\delta}_i = \omega_i$$
$$\dot{\omega}_i = -(\omega_i - \omega^*) - (P_i - P_i^*) + u_{Pi}$$
$$\dot{V}_i = -V_i V_i - Q_i + V_i u_{Qi}$$

Averaging reactive power controllers

$$\dot{\delta}_i = \omega_i$$
$$\dot{\omega}_i = -(\omega_i - \omega^*) - (P_i - P_i^*) + u_{Pi}$$
$$\dot{V}_i = -V_i \sum_{j\in\mathcal{N}_i}(Q_j - Q_i) + V_i u_{Qi}$$

Reactive current controller

$$\dot{\delta}_i = \cdots \quad \cdots$$
$$\dot{V}_i = -V_i^{-1}Q_i + u_{Qi}$$

Passivity

Frequency and voltage dynamics

$$\dot{\delta} = \omega$$
$$\dot{\omega} = -(\omega - \mathbb{1}\omega^*) - (P - P^*) + u_P$$
$$\dot{V} = f(V, Q, u_Q)$$

$f(V, Q, u_Q)$ represents various voltage dynamics/controllers

	$f(V, Q, u_Q)$	u_Q
Droop	$-V - Q + u_Q$	$-V^* - Q^*$
Quadratic droop	$-[V]V - Q + [V]u_Q$	V^*
Reactive current	$-[V]^{-1}Q + u_Q$	$[V^*]^{-1}Q^*$
Reactive consensus	$-[V]L_Q Q + [V]u_Q$	0

Droop Zhong-Hornik '12, Schiffer *et al* '14
Quadratic droop Simpson-Porco *et al* '15
Reactive current Machowski *et al* '08, DP-Monshizadeh '15
Reactive consensus Schiffer *et al* '15, DP-Monshizadeh '15

Energy function

"Energy" inspired storage function

$$U(\delta, \omega, V) = \overbrace{\frac{1}{2}\omega^T \omega}^{\text{kinetic}} + \overbrace{\frac{1}{2}\mathbb{1}^T Q}^{\text{reactive power}}$$
$$= \sum_i \frac{\omega_i^2}{2} + \sum_i \frac{Q_i}{2}$$

Tsolas-Arapostathis-Varaiya. *A structure preserving energy function for power system transient stability analysis.* TCS 1985.
Chiang. *Direct Methods for Stability Analysis of Electric Power Systems.* Wiley 2011.

Bregman storage functions

Incremental storage function

$$\mathcal{U}(\delta, \omega, V) = U(\delta, \omega, V) - U(\bar\delta, \bar\omega, \bar V) - \frac{\partial U}{\partial \delta}\Big|_{-}^T (\delta - \bar\delta)$$
$$- \frac{\partial U}{\partial \omega}\Big|_{-}^T (\omega - \bar\omega) - \frac{\partial U}{\partial V}\Big|_{-}^T (V - \bar V)$$

Bregman (1967), Jayawardhana et al (2007)

1. $\mathcal{U}(\bar\delta, \bar\omega, \bar V) = 0$
2. $U(\delta, \omega, V)$ strictly convex $\Rightarrow \mathcal{U}(\delta, \omega, V) > 0$, $(\delta, \omega, V) \neq (\bar\delta, \bar\omega, \bar V)$

Bregman storage functions

Strict convexity

$$\nabla^2 U(\bar\delta, \bar\omega, \bar V) > 0 \qquad \text{modulo rotational invariance}$$

Satisfied for $\bar V_i \approx \bar V_j$ and $\bar\delta_i \approx \bar\delta_j$

DP-Monshizadeh. *A modular design of incremental Lyapunov functions for microgrid control with power sharing.* ECC'16
Dvijotham-Low-Chertkov. *Convexity of energy-like functions.* ArXiv, 2015.

A passive representation

Reactive current controller

$$\begin{bmatrix} \dot\varphi \\ \dot\omega \\ \dot V \end{bmatrix} = \overbrace{\begin{bmatrix} 0 & I & 0 \\ -I & -I & 0 \\ 0 & 0 & -I \end{bmatrix}}^{\mathcal{J}-\mathcal{R}} \overbrace{\begin{bmatrix} \frac{\partial \mathcal{U}}{\partial \varphi} \\ \frac{\partial \mathcal{U}}{\partial \omega} \\ \frac{\partial \mathcal{U}}{\partial V} \end{bmatrix}}^{\nabla \mathcal{U}} + \begin{bmatrix} 0 & 0 \\ I & 0 \\ 0 & I \end{bmatrix}\begin{bmatrix} u_P - \bar u_P \\ u_Q - \bar u_Q \end{bmatrix}$$

$$y - \bar y = \begin{bmatrix} y_P - \bar y_P \\ y_Q - \bar y_Q \end{bmatrix} = \begin{bmatrix} 0 & I & 0 \\ 0 & 0 & I \end{bmatrix}\nabla \mathcal{U} = \begin{bmatrix} \omega - \bar\omega \\ I_d - \bar I_d \end{bmatrix}$$

Incremental passivity

$$\dot{\mathcal{U}} = -\nabla \mathcal{U}^T R \nabla \mathcal{U} + (y - \bar y)^T (u - \bar u)$$

A *dissipative* representation

$$\mathcal{S} = \mathcal{U} + \mathcal{H}, \quad \mathcal{H}(V) = H(V) - H(\overline{V}) - \left.\frac{\partial H}{\partial V}\right|_{-}^{T}(V - \overline{V})$$

	$H(V)$	$x(V)$	$Y(V)$
Droop	$\mathbb{1}^T V - c^T \ln(V)$	$[V]$	I
Quadratic droop	$\frac{1}{2}V^T V$	$[V]$	$[V]$
Reactive current	0	I	I
Reactive consensus	$-c^T \ln V$	$[V]L_Q[V]$	$[V]$

$$\begin{bmatrix} \dot{\varphi} \\ \dot{\omega} \\ \dot{V} \end{bmatrix} = \begin{bmatrix} 0 & I & 0 \\ -I & -I & 0 \\ 0 & 0 & -x(V) \end{bmatrix}\nabla\mathcal{S} + \begin{bmatrix} 0 & 0 \\ I & 0 \\ 0 & Y(V) \end{bmatrix}\begin{bmatrix} u_P - \overline{u}_P \\ u_Q - \overline{u}_Q \end{bmatrix}$$

$$\begin{bmatrix} y_P - \overline{y}_P \\ y_Q - \overline{y}_Q \end{bmatrix} = \begin{bmatrix} 0 & I & 0 \\ 0 & 0 & I \end{bmatrix}\nabla\mathcal{S}$$

A *dissipative* representation

$$\mathcal{S} = \mathcal{U} + \mathcal{H}, \quad \mathcal{H}(V) = H(V) - H(\overline{V}) - \left.\frac{\partial H}{\partial V}\right|_{-}^{T}(V - \overline{V})$$

	$H(V)$	$x(V)$	$Y(V)$
Droop	$\mathbb{1}^T V - c^T \ln(V)$	$[V]$	I
Quadratic droop	$\frac{1}{2}V^T V$	$[V]$	$[V]$
Reactive current	0	I	I
Reactive consensus	$-c^T \ln V$	$[V]L_Q[V]$	$[V]$

Incremental dissipativity

$$\dot{\mathcal{S}} = -\nabla \mathcal{S}^T \mathcal{R}(V)\nabla \mathcal{S} + (y-\overline{y})^T \begin{bmatrix} I & 0 \\ 0 & Y(V) \end{bmatrix}(u-\overline{u})^T$$

Controllers

Output regulation

$$\begin{aligned}\dot{\delta} &= \omega \\ \dot{\omega} &= -(\omega - \omega^*) - (P - P^*) + u_P \\ \dot{V} &= f(V, Q, u_Q)\end{aligned}$$

$$\Updownarrow$$

$$\begin{aligned}\dot{x} &= F(x, u, w) \\ e &= K(x, u, w)\end{aligned}$$

where

$$K(x, u, w) = \begin{bmatrix} x - \overline{x} \\ u - \overline{u} \end{bmatrix}, \quad w = P^*$$

Find a feedback

$$\begin{aligned}\dot{\xi} &= \phi(\xi, e) \\ u &= \psi(\xi)\end{aligned}$$

such that

$$e \to \mathbf{0}$$

Output regulation

Solution consists of 3 steps

1. **Regulator equations** For any w, there exists $\bar{x}, \bar{u}$ such that

$$\dot{\bar{x}} = F(\bar{x}, \bar{u}, w)$$
$$0 = K(\bar{x}, \bar{u}, w)$$

[Existence of a synchronous solution]

2. **Internal model** For any w, there exists $\bar{\xi}$ such that

$$\dot{\bar{\xi}} = \phi(\bar{\xi}, e=0)$$
$$\bar{u} = \psi(\bar{\xi})$$

3. **Stabilizing feedback**

Internal model controller

Internal model A controller to generate $\bar{u}_P = -\mathbb{1}\dfrac{\mathbb{1}^T P^*}{\mathbb{1}^T K_P^{-1}\mathbb{1}}$

$$\dot{\xi} = -L_C\nabla C(\xi) + u_C$$
$$y_C = \nabla C(\xi)$$

where $C(\xi) = \frac{1}{2}\xi^T\xi$

For $u_C = \bar{u}_C = 0$, the trajectory

$$\bar{\xi} = -\mathbb{1}\frac{\mathbb{1}^T P^*}{\mathbb{1}^T K_P^{-1}\mathbb{1}}$$

is a solution of the controller providing the optimal control $\bar{u}_P$

$$\dot{\bar{\xi}} = -L_C\nabla C(\bar{\xi}) + \bar{u}_C$$
$$\bar{u}_P = \bar{y}_C = \nabla C(\bar{\xi})$$

Internal model controller

Incremental model w.r.t. input-state-output triple $(\bar{u}_C, \bar{\xi}, \bar{y}_C)$

$$\dot{\xi} = -L_C\nabla C(\xi - \bar{\xi}) + (u_C - \bar{u}_C)$$
$$y_C - \bar{y}_C = C(\xi - \bar{\xi})$$

where $C(\xi) = C(\xi) - C(\bar{\xi}) - \nabla C(\bar{\xi})^T(\xi - \bar{\xi}) = \frac{1}{2}(\xi - \bar{\xi})^T(\xi - \bar{\xi})$

Incremental passivity w.r.t. input-state-output triple $(\bar{u}_C, \bar{\xi}, \bar{y}_C)$

$$\frac{d}{dt}C = -\nabla C^\top L_C \nabla C + (y_C - \bar{y}_C)^T(u_C - \bar{u}_C)$$

Closed-loop system
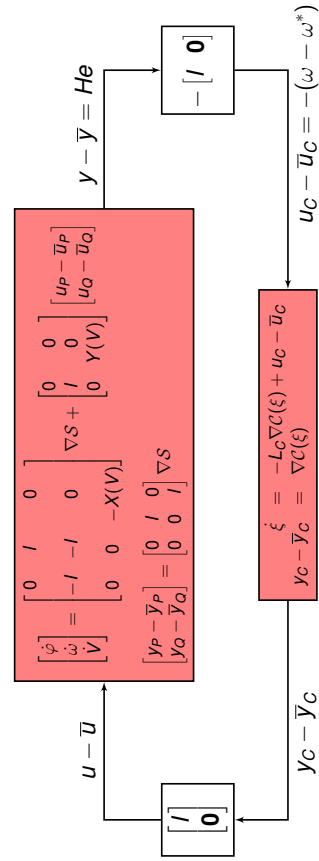
Convergence

Then

$$\begin{bmatrix} \dot\varphi \\ \dot\omega \\ \dot V \\ \dot\xi \end{bmatrix} = \begin{bmatrix} 0 & I & 0 & 0 \\ -I & -I & 0 & I \\ 0 & 0 & -X(V) & 0 \\ 0 & -I & 0 & -L_C \end{bmatrix} \nabla \mathcal{V}$$

where

$$\mathcal{V} = \mathcal{S} + \mathcal{C}$$

Hence

$$\dot{\mathcal{V}} = -\frac{\partial \mathcal{V}^\top}{\partial \omega}\frac{\partial \mathcal{V}}{\partial \omega} - \frac{\partial \mathcal{V}^\top}{\partial V} X(V)\frac{\partial \mathcal{V}}{\partial V} - \frac{\partial \mathcal{V}^\top}{\partial \xi} L_C \frac{\partial \mathcal{V}}{\partial \xi}$$

yielding convergence

$$\varphi \to \overline\varphi, \quad \omega \to \overline\omega = \mathbb{1}\omega^*, \quad V \to \overline V, \quad \xi \to \overline\xi$$

Reactive power sharing

	$f(\overline V, \overline Q, \overline u_Q)$	Reactive power sharing
Droop	$\overline V + \overline Q = \overline u_Q$	$\dfrac{\overline Q_i + \overline V_i}{\overline Q_j + \overline V_j} = \dfrac{\overline u_{Qi}}{\overline u_{Qj}}$
Quadratic droop	$\overline V - [\overline V]^{-1}\overline Q = \overline u_Q$	$\dfrac{\overline Q_i + \overline V_i^2}{\overline Q_j + \overline V_j^2} = \dfrac{\overline u_{Qi}}{\overline u_{Qj}}$
Reactive current	$[\overline V]^{-1}\overline Q = \overline u_Q$	$\dfrac{\overline u_{Qi}}{\overline u_{Qj}} = \dfrac{\overline V_j}{\overline V_i}\dfrac{\overline Q_i}{\overline Q_j}$
Reactive consensus	$0 = \overline u_Q$	$\overline Q_i = \overline Q_j$
		$\mathbb{1}^\top \textit{ln} \overline V = \mathbb{1}^\top \textit{ln} V(0)$

DP–Monshizadeh. *A modular design of incremental Lyapunov functions for microgrid control with power sharing.* arXiv 1510.05811v3, ECC16.

Outlook & Conclusions

Outlook

- Network preserved models

$$\dot\delta_I = \omega_I - \mathbb{1}\omega^*$$
$$T_P\dot\omega_I = -(\omega_I - \mathbb{1}\omega^*) - K_P(P_I - P_I^*) + u_P$$
$$T_Q\dot V_I = f(V_I, Q_I, u_Q)$$
$$0 = P_L - P_L^*$$
$$0 = Q_L - Q_L^*$$

Controllers for voltage regulation and reactive power sharing

$$V_L \simeq V_L^*, \quad Q_I \simeq \text{power sharing}$$

DP–Monshizadeh–Schiffer–Dörfler. *A Lyapunov approach to control of microgrids with a network-preserved differential-algebraic model.* Submitted.

- Voltage control
- Lossy networks

Outlook

Kuramoto oscillators with inertia

$$\dot{\delta}_i = \omega_i - \omega^*$$
$$\dot{\omega}_i = -\omega_i - \sum_{k \in \mathcal{N}_i} V_i V_k |B_{ik}| \sin(\delta_{ik}) + (\omega^* + P_i^*)$$
$$\dot{V}_i = -V_i - |B_{ii}| V_i^2 + \sum_{j \in \mathcal{N}_i} V_i V_j |B_{ij}| \cos(\delta_{ij}) + (V_i^* + Q_i^*)$$

Seliger et al. *Plasticity and learning in a network of coupled phase oscillators* Physical Review E, 2002.
Scardovi et al. *Clustering and synchronization in phase models with state dependent coupling.* CDC 2010.
Sepulchre et al. *Stabilization of planar collective motion: All-to-all communication.* TAC 2007.

Stegink-DP-van der Schaft. *Optimal power dispatch in networks of high-dimensional models of synchronous machines.* arXiv.
Pooya Monshizadeh et al. *Nonlinear analysis of an improved swing equation.* CDC2016.

Outlook

- Power networks and cyber-physical systems

Combined physical and cyber Lyapunov functions

DP-Postoyan. *A Lyapunov redesign of coordination algorithms for cyberphysical systems.* IEEE Transactions on Automatic Control arXiv 1404.0576
Trip-DP. *Communication requirements for optimal frequency regulation in power networks.* CDC 2016.

Outlook

- Power networks and cyber-physical systems

Robustness

DP-Tesi *Input-to-state stabilizing control under Denial-of-Service.* IEEE Transactions on Automatic Control, 60(11), 2930–2944, 2015.
Senejohnny et al. *A jamming-resilient algorithm for self-triggered network coordination.* arXiv 1603.02563.
Weitenberg et al. *Quantifying the performance of optimal frequency regulators in the presence of intermittent communication.* CDC 2016

Conclusion

Classical control theoretic tools such as incremental passivity, internal model principle, and Lyapunov analysis coupled with algebraic graph and dynamical network theory provide a powerful framework to deal with power network stability and control

On conditions under which receding horizon control delivers approximately optimal solutions

Lars Grüne

Mathematisches Institut, Universität Bayreuth, Germany

35th Benelux Meeting on Systems and Control
Soesterberg, The Netherlands, 22–24 March 2016

Setup

We consider nonlinear discrete time control systems

$$x_{\mathbf{u}}(n+1) = f(x_{\mathbf{u}}(n), \mathbf{u}(n)), \quad x_{\mathbf{u}}(0) = x$$

with $x_{\mathbf{u}}(n) \in X$, $\mathbf{u}(n) \in U$, X, U normed spaces

Usual interpretation:

$x_{\mathbf{u}}(n)$ = state of the system at time t_n

Setup

We consider nonlinear discrete time control systems

$$x_{\mathbf{u}}(n+1) = f(x_{\mathbf{u}}(n), \mathbf{u}(n)), \quad x_{\mathbf{u}}(0) = x$$

with $x_{\mathbf{u}}(n) \in X$, $\mathbf{u}(n) \in U$, X, U normed spaces

---

Setup

We consider nonlinear discrete time control systems

$$x_{\mathbf{u}}(n+1) = f(x_{\mathbf{u}}(n), \mathbf{u}(n)), \quad x_{\mathbf{u}}(0) = x$$

with $x_{\mathbf{u}}(n) \in X$, $\mathbf{u}(n) \in U$, X, U normed spaces

Usual interpretation:

$x_{\mathbf{u}}(n)$ = state of the system at time t_n

$\mathbf{u}(n)$ = control acting from time t_n to t_{n+1}

Setup

We consider nonlinear discrete time control systems

$$x_{\mathbf{u}}(n+1) = f(x_{\mathbf{u}}(n), \mathbf{u}(n)), \quad x_{\mathbf{u}}(0) = x$$

with $x_{\mathbf{u}}(n) \in X$, $\mathbf{u}(n) \in U$, $\quad X$, U normed spaces

Usual interpretation:

$x_{\mathbf{u}}(n)$	=	state of the system at time t_n
$\mathbf{u}(n)$	=	control acting from time t_n to t_{n+1}
f	=	solution operator of a controlled ODE/PDE or of a discrete time model (or a numerical approximation of one of these)

Setup

We consider nonlinear discrete time control systems

$$x_{\mathbf{u}}(n+1) = f(x_{\mathbf{u}}(n), \mathbf{u}(n)), \quad x_{\mathbf{u}}(0) = x$$

with $x_{\mathbf{u}}(n) \in X$, $\mathbf{u}(n) \in U$, $\quad X$, U normed spaces

Problem: infinite horizon optimal control

Setup

We consider nonlinear discrete time control systems

$$x_{\mathbf{u}}(n+1) = f(x_{\mathbf{u}}(n), \mathbf{u}(n)), \quad x_{\mathbf{u}}(0) = x$$

with $x_{\mathbf{u}}(n) \in X$, $\mathbf{u}(n) \in U$, X, U normed spaces

Problem: infinite horizon optimal control

Prototype problem: For a stage cost $\ell : X \times U \to \mathbb{R}$ solve

$$\operatorname*{minimize}_{\mathbf{u}} J_\infty(x, \mathbf{u}) = \sum_{n=0}^{\infty} \ell(x_{\mathbf{u}}(n), \mathbf{u}(n))$$

subject to state/control constraints $\quad x_{\mathbf{u}}(n) \in \mathbb{X}$, $\mathbf{u}(n) \in \mathbb{U}$

UNIVERSITÄT BAYREUTH   Lars Grüne, On conditions under which receding horizon control delivers approximately optimal solutions, p. 3

Receding horizon control

Direct solution of the problem is numerically hard

Alternative method: receding horizon or model predictive control (MPC)

UNIVERSITÄT BAYREUTH   Lars Grüne, On conditions under which receding horizon control delivers approximately optimal solutions, p. 4

Setup

We consider nonlinear discrete time control systems

$$x_{\mathbf{u}}(n+1) = f(x_{\mathbf{u}}(n), \mathbf{u}(n)), \quad x_{\mathbf{u}}(0) = x$$

with $x_{\mathbf{u}}(n) \in X$, $\mathbf{u}(n) \in U$, X, U normed spaces

Problem: infinite horizon optimal control

Prototype problem: For a stage cost $\ell : X \times U \to \mathbb{R}$ solve

$$\operatorname*{minimize}_{\mathbf{u}} J_\infty(x, \mathbf{u}) = \sum_{n=0}^{\infty} \ell(x_{\mathbf{u}}(n), \mathbf{u}(n))$$

UNIVERSITÄT BAYREUTH   Lars Grüne, On conditions under which receding horizon control delivers approximately optimal solutions, p. 3
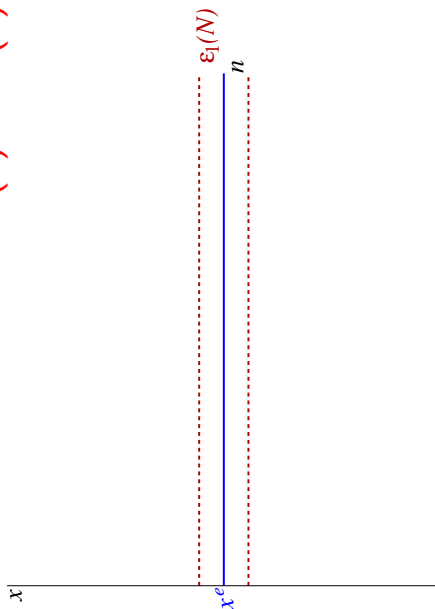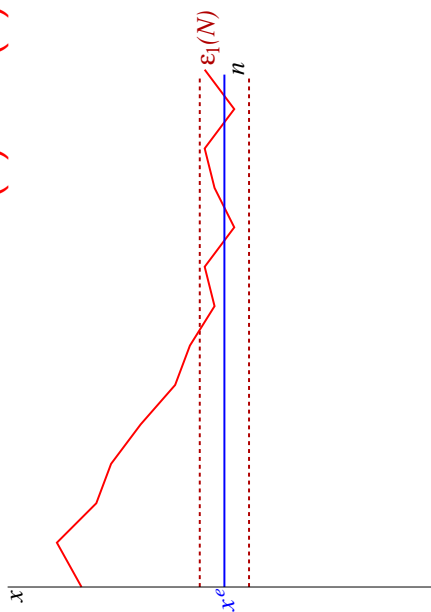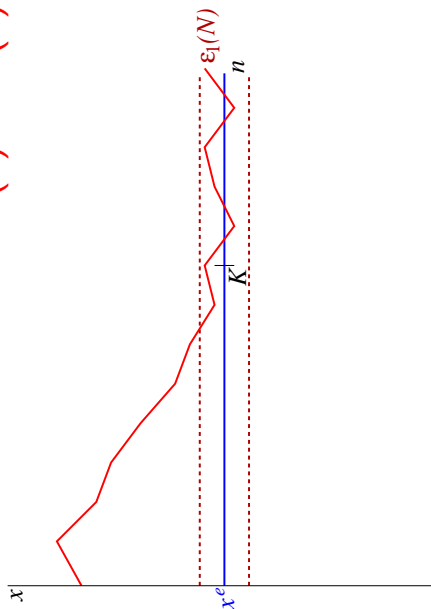
Setup

We consider nonlinear discrete time control systems

$$x_{\mathbf{u}}(n+1) = f(x_{\mathbf{u}}(n), \mathbf{u}(n)), \quad x_{\mathbf{u}}(0) = x$$

with $x_{\mathbf{u}}(n) \in X$, $\mathbf{u}(n) \in U$, X, U normed spaces

Problem: infinite horizon optimal control

Prototype problem: For a stage cost $\ell : X \times U \to \mathbb{R}$ solve

$$\operatorname*{minimize}_{\mathbf{u}} J_\infty(x, \mathbf{u}) = \sum_{n=0}^{\infty} \ell(x_{\mathbf{u}}(n), \mathbf{u}(n))$$

subject to state/control constraints $\quad x_{\mathbf{u}}(n) \in \mathbb{X}$, $\mathbf{u}(n) \in \mathbb{U}$

with optimal control in feedback form $\quad \mathbf{u}(n) = \mu(x_{\mathbf{u}}(n))$

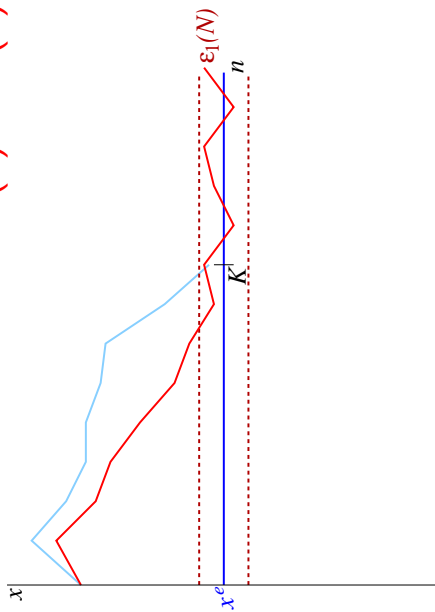UNIVERSITÄT BAYREUTH   Lars Grüne, On conditions under which receding horizon control delivers approximately optimal solutions, p. 3
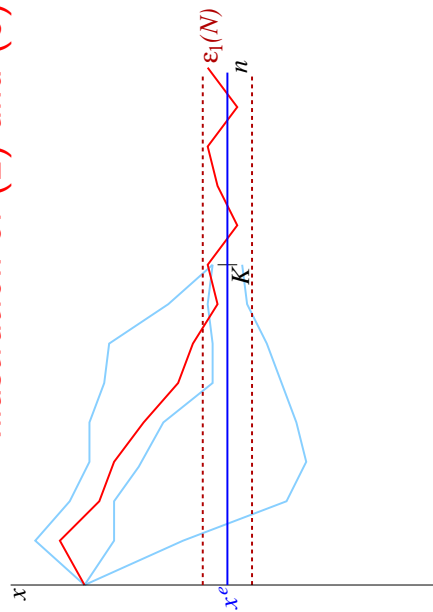
Receding horizon control

Direct solution of the problem is numerically hard

Alternative method: receding horizon or model predictive control (MPC)

Idea: replace the infinite horizon problem

$$\underset{\mathbf{u}}{\text{minimize}} \quad J_\infty(x, \mathbf{u}) = \sum_{n=0}^{\infty} \ell(x_\mathbf{u}(n), \mathbf{u}(n))$$

by the iterative solution of finite horizon problems

$$\underset{\mathbf{u}}{\text{minimize}} \quad J_N(x, \mathbf{u}) = \sum_{n=0}^{N-1} \ell(x_\mathbf{u}(k), \mathbf{u}(k))$$

with fixed $N \in \mathbb{N}$ and $x_\mathbf{u}(k) \in \mathbb{X}$, $\mathbf{u}(k) \in \mathbb{U}$

We obtain a feedback law μ_N by a receding horizon technique

UNIVERSITÄT BAYREUTH   Lars Grüne, On conditions under which receding horizon control delivers approximately optimal solutions, p. 4

MPC from the trajectory point of view

UNIVERSITÄT BAYREUTH   Lars Grüne, On conditions under which receding horizon control delivers approximately optimal solutions, p. 5

black = predictions (open loop optimization)

MPC from the trajectory point of view

black = predictions (open loop optimization)

red = MPC closed loop

Lars Grüne, On conditions under which receding horizon control delivers approximately optimal solutions, p. 5

UNIVERSITÄT BAYREUTH

MPC from the trajectory point of view

black = predictions (open loop optimization)

red = MPC closed loop

Lars Grüne, On conditions under which receding horizon control delivers approximately optimal solutions, p. 5

UNIVERSITÄT BAYREUTH

MPC from the trajectory point of view

black = predictions (open loop optimization)

red = MPC closed loop

Lars Grüne, On conditions under which receding horizon control delivers approximately optimal solutions, p. 5

UNIVERSITÄT BAYREUTH

MPC from the trajectory point of view
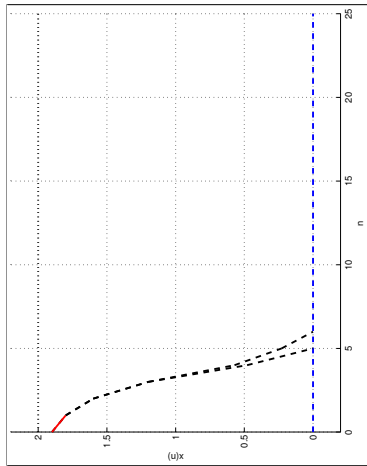

black = predictions (open loop optimization)

red = MPC closed loop

Lars Grüne, On conditions under which receding horizon control delivers approximately optimal solutions, p. 5

UNIVERSITÄT BAYREUTH

MPC from the trajectory point of view

black = predictions (open loop optimization)

red   = MPC closed loop

UNIVERSITÄT BAYREUTH   Lars Grüne, On conditions under which receding horizon control delivers approximately optimal solutions, p. 5

MPC from the trajectory point of view

black = predictions (open loop optimization)
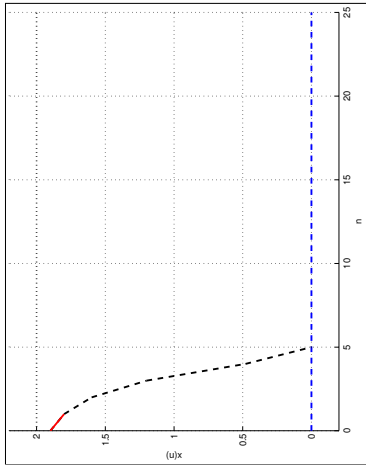
red   = MPC closed loop

UNIVERSITÄT BAYREUTH   Lars Grüne, On conditions under which receding horizon control delivers approximately optimal solutions, p. 5

MPC from the trajectory point of view

black = predictions (open loop optimization)
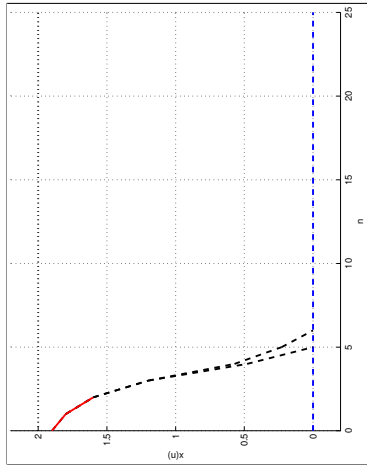
red   = MPC closed loop

UNIVERSITÄT BAYREUTH   Lars Grüne, On conditions under which receding horizon control delivers approximately optimal solutions, p. 5

MPC from the trajectory point of view

black = predictions (open loop optimization)

red   = MPC closed loop

UNIVERSITÄT BAYREUTH   Lars Grüne, On conditions under which receding horizon control delivers approximately optimal solutions, p. 5

MPC from the trajectory point of view

black = predictions (open loop optimization)

red = MPC closed loop
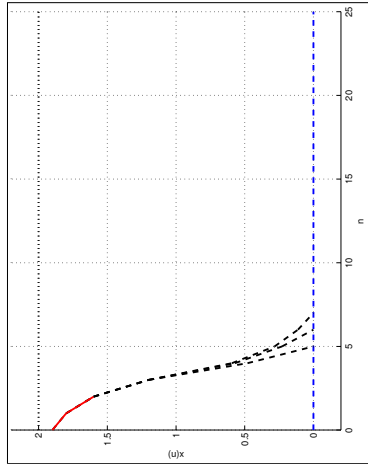
Lars Grüne, On conditions under which receding horizon control delivers approximately optimal solutions, p. 5

UNIVERSITÄT BAYREUTH

MPC from the trajectory point of view

black = predictions (open loop optimization)

red = MPC closed loop

Lars Grüne, On conditions under which receding horizon control delivers approximately optimal solutions, p. 5

UNIVERSITÄT BAYREUTH

MPC from the trajectory point of view

black = predictions (open loop optimization)

red = MPC closed loop

Lars Grüne, On conditions under which receding horizon control delivers approximately optimal solutions, p. 5

UNIVERSITÄT BAYREUTH

MPC from the trajectory point of view

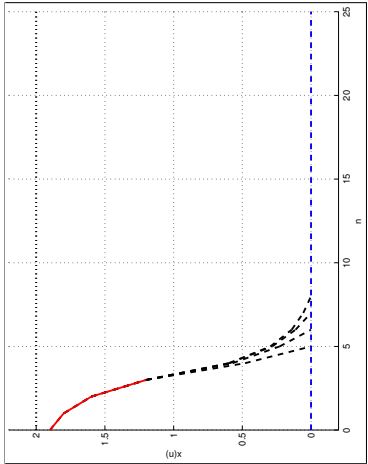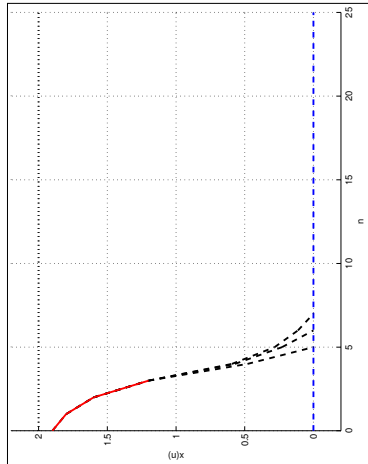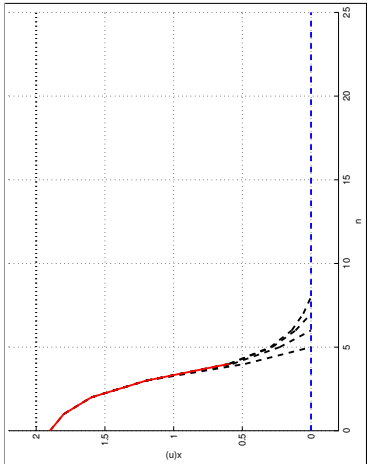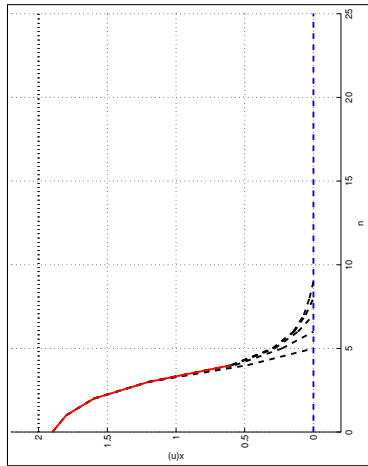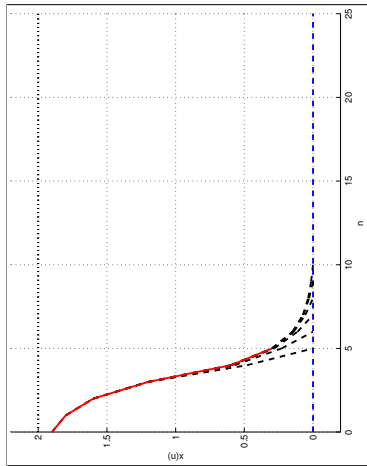
black = predictions (open loop optimization)

red = MPC closed loop $x_{\mu_N}(n, x_0)$

Lars Grüne, On conditions under which receding horizon control delivers approximately optimal solutions, p. 5

UNIVERSITÄT BAYREUTH

Model predictive control

Basic receding horizon MPC concept:

At each time instant n solve for the current state $x_{\mu_N}(n)$:

$$\underset{\mathbf{u}}{\text{minimize}}\ \ J_N(x_{\mu_N}(n),\mathbf{u}) = \sum_{k=0}^{N-1} \ell(x_u(k),\mathbf{u}(k)), \quad x_u(0)=x_{\mu_N}(n)$$

subject to the constraints $x_u(k)\in\mathbb{X}$, $\mathbf{u}(k)\in\mathbb{U}$

Model predictive control

Basic receding horizon MPC concept:

At each time instant n solve for the current state $x_{\mu_N}(n)$:

$$\underset{\mathbf{u}}{\text{minimize}}\ \ J_N(x_{\mu_N}(n),\mathbf{u}) = \sum_{k=0}^{N-1} \ell(x_u(k),\mathbf{u}(k)), \quad x_u(0)=x_{\mu_N}(n)$$

subject to the constraints $x_u(k)\in\mathbb{X}$, $\mathbf{u}(k)\in\mathbb{U}$

$\rightsquigarrow$ optimal trajectory $x^\star(0),\ldots,x^\star(N-1)$

Model predictive control

Basic receding horizon MPC concept:

At each time instant n solve for the current state $x_{\mu_N}(n)$:

$$\underset{\mathbf{u}}{\text{minimize}}\ \ J_N(x_{\mu_N}(n),\mathbf{u}) = \sum_{k=0}^{N-1} \ell(x_u(k),\mathbf{u}(k)), \quad x_u(0)=x_{\mu_N}(n)$$

subject to the constraints $x_u(k)\in\mathbb{X}$, $\mathbf{u}(k)\in\mathbb{U}$

Model predictive control

Basic receding horizon MPC concept:

At each time instant n solve for the current state $x_{\mu_N}(n)$:

$$\underset{\mathbf{u}}{\text{minimize}}\ \ J_N(x_{\mu_N}(n),\mathbf{u}) = \sum_{k=0}^{N-1} \ell(x_u(k),\mathbf{u}(k)), \quad x_u(0)=x_{\mu_N}(n)$$

subject to the constraints $x_u(k)\in\mathbb{X}$, $\mathbf{u}(k)\in\mathbb{U}$

$\rightsquigarrow$ optimal trajectory $x^\star(0),\ldots,x^\star(N-1)$

with optimal control $\mathbf{u}^\star(0),\ldots,\mathbf{u}^\star(N-1)$

Model predictive control

Basic receding horizon MPC concept:

At each time instant n solve for the current state $x_{\mu_N}(n)$:

$$\underset{\mathbf{u}}{\text{minimize}}\ \ J_N(x_{\mu_N}(n), \mathbf{u}) = \sum_{k=0}^{N-1} \ell(x_u(k), \mathbf{u}(k)), \quad x_u(0) = x_{\mu_N}(n)$$

subject to the constraints $x_u(k) \in \mathbb{X}$, $\mathbf{u}(k) \in \mathbb{U}$

$\rightsquigarrow$ optimal trajectory $\quad x^\star(0), \ldots, x^\star(N-1)$

with optimal control $\mathbf{u}^\star(0), \ldots, \mathbf{u}^\star(N-1)$

$\rightsquigarrow$ MPC feedback law $\quad \mu_N(x_{\mu_N}(n)) := \mathbf{u}^\star(0)$

$\rightsquigarrow$ closed loop system

$$x_{\mu_N}(n+1) = f(x_{\mu_N}(n), \mu_N(x_{\mu_N}(n))) = f(x_{\mathbf{u}^\star}(0), \mathbf{u}^\star(0)) = x_{\mathbf{u}^\star}(1)$$

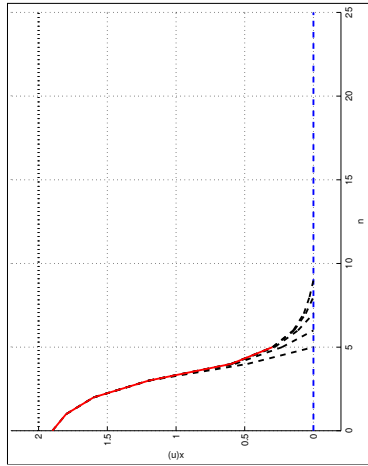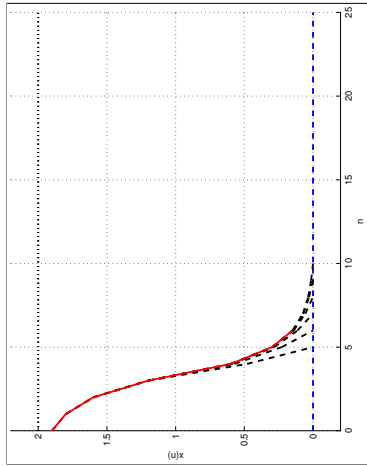UNIVERSITÄT BAYREUTH　　Lars Grüne, On conditions under which receding horizon control delivers approximately optimal solutions, p. 6

Why use MPC?

What is the advantage of MPC over other methods of solving optimal control problems?
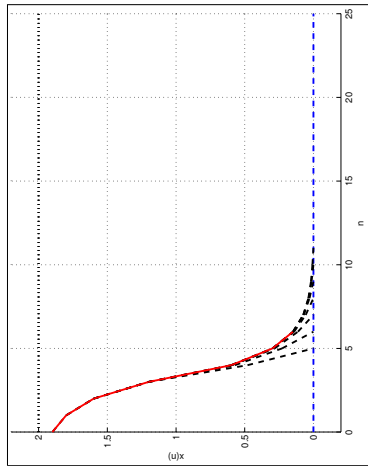
● significantly reduced computational complexity

UNIVERSITÄT BAYREUTH　　Lars Grüne, On conditions under which receding horizon control delivers approximately optimal solutions, p. 7

Why use MPC?

What is the advantage of MPC over other methods of solving optimal control problems?

- significantly reduced computational complexity
  ⤳ real time capability

UNIVERSITÄT BAYREUTH   Lars Grüne, On conditions under which receding horizon control delivers approximately optimal solutions, p. 7

Why use MPC?

What is the advantage of MPC over other methods of solving optimal control problems?

- significantly reduced computational complexity
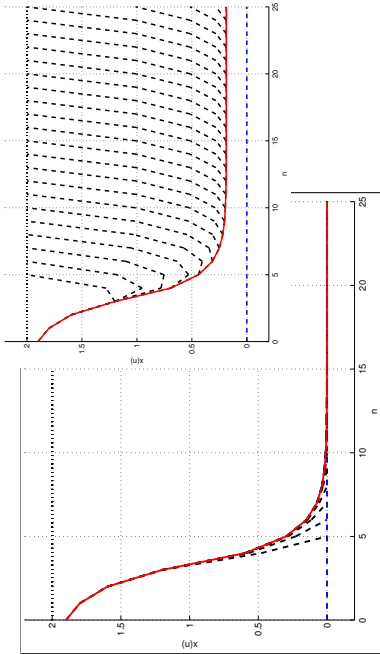 ⤳ real time capability
- ability to react to perturbations

UNIVERSITÄT BAYREUTH   Lars Grüne, On conditions under which receding horizon control delivers approximately optimal solutions, p. 7

Why use MPC?

What is the advantage of MPC over other methods of solving optimal control problems?

- significantly reduced computational complexity
  ⤳ real time capability
- ability to react to perturbations
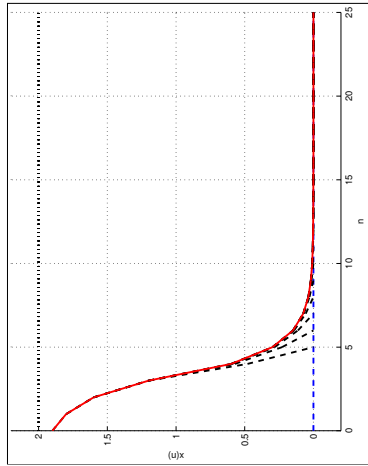- applicability to problems in which data becomes available online

UNIVERSITÄT BAYREUTH   Lars Grüne, On conditions under which receding horizon control delivers approximately optimal solutions, p. 7

Why use MPC?

What is the advantage of MPC over other methods of solving optimal control problems?

- significantly reduced computational complexity
  ⤳ real time capability
- ability to react to perturbations
- applicability to problems in which data becomes available online

But: The trajectory delivered by MPC can be far from optimal!

UNIVERSITÄT BAYREUTH   Lars Grüne, On conditions under which receding horizon control delivers approximately optimal solutions, p. 7

Why use MPC?

What is the advantage of MPC over other methods of solving optimal control problems?

- significantly reduced computational complexity
  - ⇝ real time capability
- ability to react to perturbations
- applicability to problems in which data becomes available online

But: The trajectory delivered by MPC can be far from optimal!

⇝ Key question in this talk: When does MPC yield closed loop trajectories with approximately optimal performance?

First question: How to define performance?

UNIVERSITÄT BAYREUTH   Lars Grüne, On conditions under which receding horizon control delivers approximately optimal solutions, p. 7

Performance

In this talk we do not want to limit ourselves to tracking type functionals, i.e., $\ell(x, u) = \|x - x_*\|^2 + \lambda \|u - u_*\|^2$

MPC with more general ℓ is often termed economic MPC. In this setting, performance of μ_N can be measured in two ways

UNIVERSITÄT BAYREUTH   Lars Grüne, On conditions under which receding horizon control delivers approximately optimal solutions, p. 8

Performance

In this talk we do not want to limit ourselves to tracking type functionals, i.e., $\ell(x,u) = \|x - x_*\|^2 + \lambda\|u - u_*\|^2$

MPC with more general ℓ is often termed economic MPC. In this setting, performance of μ_N can be measured in two ways

Infinite horizon averaged performance:

$$\overline{J}^{cl}_\infty(x,\mu_N) = \limsup_{K\to\infty} \frac{1}{K}\sum_{n=0}^{K-1} \ell(x_{\mu_N}(n,x),\mu_N(x_{\mu_N}(n,x)))$$

Finite horizon (or transient) performance:

$$J^{cl}_K(x,\mu_N) = \sum_{n=0}^{K-1} \ell(x_{\mu_N}(n,x),\mu_N(x_{\mu_N}(n,x)))$$

Performance

Example: minimum energy control

Example: Keep the state of the system inside the admissible set $\mathbb{X}$ minimizing the quadratic control effort

$$\ell(x,u) = u^2$$

with dynamics

$$x(n+1) = 2x(n) + \mathbf{u}(n)$$

and constraints $\mathbb{X} = [-2,2]$, $\mathbb{U} = [-3,3]$

Example: minimum energy control

Example: Keep the state of the system inside the admissible set $\mathbb{X}$ minimizing the quadratic control effort

$$\ell(x,u) = u^2$$

with dynamics

$$x(n+1) = 2x(n) + \mathbf{u}(n)$$

and constraints $\mathbb{X} = [-2,2]$, $\mathbb{U} = [-3,3]$

For this example, a good strategy is to control the system to $x^e = 0$ and keep it there with $u^e = 0$

$\rightsquigarrow$ (x^e, u^e) is an optimal equilibrium with $\ell(x^e, u^e) = 0$

UNIVERSITÄT BAYREUTH　　Lars Grüne, On conditions under which receding horizon control delivers approximately optimal solutions, p. 9

Example: minimum energy control

Example: Keep the state of the system inside the admissible set $\mathbb{X}$ minimizing the quadratic control effort

$$\ell(x,u) = u^2$$

with dynamics

$$x(n+1) = 2x(n) + \mathbf{u}(n)$$

and constraints $\mathbb{X} = [-2,2]$, $\mathbb{U} = [-3,3]$

For this example, a good strategy is to control the system to $x^e = 0$ and keep it there with $u^e = 0$

$\rightsquigarrow$ (x^e, u^e) is an optimal equilibrium with $\ell(x^e, u^e) = 0$

(recall: (x^e, u^e) equilibrium $\Leftrightarrow$ $f(x^e, u^e) = x^e$)

UNIVERSITÄT BAYREUTH　　Lars Grüne, On conditions under which receding horizon control delivers approximately optimal solutions, p. 9

Example: trajectories

$N = 5$

UNIVERSITÄT BAYREUTH　　Lars Grüne, On conditions under which receding horizon control delivers approximately optimal solutions, p. 10

Example: trajectories

$N = 5$

Lars Grüne, On conditions under which receding horizon control delivers approximately optimal solutions, p. 10

UNIVERSITÄT
BAYREUTH

Example: trajectories

$N = 5$

Lars Grüne, On conditions under which receding horizon control delivers approximately optimal solutions, p. 10

UNIVERSITÄT
BAYREUTH

Example: trajectories

$N = 5$

Lars Grüne, On conditions under which receding horizon control delivers approximately optimal solutions, p. 10

UNIVERSITÄT
BAYREUTH

Example: trajectories

$N = 5$

Lars Grüne, On conditions under which receding horizon control delivers approximately optimal solutions, p. 10

UNIVERSITÄT
BAYREUTH

Example: trajectories

$N = 5$

Lars Grüne, On conditions under which receding horizon control delivers approximately optimal solutions, p. 10

UNIVERSITÄT
BAYREUTH

Example: trajectories

$N = 5$

Lars Grüne, On conditions under which receding horizon control delivers approximately optimal solutions, p. 10

UNIVERSITÄT
BAYREUTH

Example: trajectories

$N = 5$

Lars Grüne, On conditions under which receding horizon control delivers approximately optimal solutions, p. 10

UNIVERSITÄT
BAYREUTH

Example: trajectories

$N = 5$

Lars Grüne, On conditions under which receding horizon control delivers approximately optimal solutions, p. 10
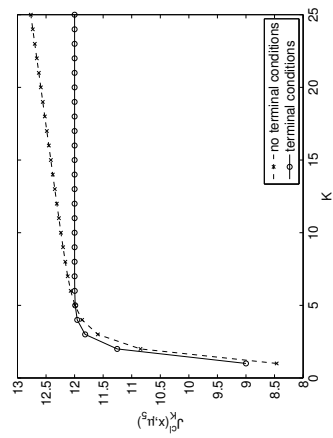
UNIVERSITÄT
BAYREUTH

Example: trajectories

$N = 5$

Lars Grüne, On conditions under which receding horizon control delivers approximately optimal solutions, p. 10

Example: trajectories

$N = 5$

Lars Grüne, On conditions under which receding horizon control delivers approximately optimal solutions, p. 10

Example: trajectories

$N = 5$

Lars Grüne, On conditions under which receding horizon control delivers approximately optimal solutions, p. 10

Example: trajectories

$N = 5$

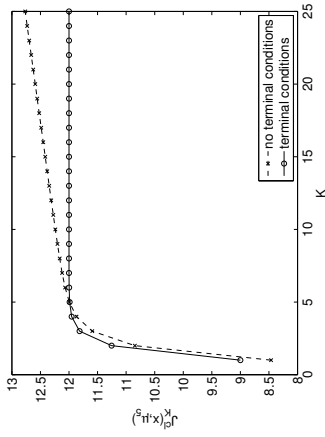Lars Grüne, On conditions under which receding horizon control delivers approximately optimal solutions, p. 10

Example: trajectories

Lars Grüne, On conditions under which receding horizon control delivers approximately optimal solutions, p. 10

UNIVERSITÄT
BAYREUTH

Example: trajectories

Lars Grüne, On conditions under which receding horizon control delivers approximately optimal solutions, p. 10

Example: trajectories

$N = 10$

$N = 5$

Lars Grüne, On conditions under which receding horizon control delivers approximately optimal solutions, p. 10

UNIVERSITÄT
BAYREUTH

Example: trajectories

$N = 10$

$N = 5$

Lars Grüne, On conditions under which receding horizon control delivers approximately optimal solutions, p. 10

UNIVERSITÄT
BAYREUTH

Example: trajectories

$N = 10$

$N = 5$

Lars Grüne, On conditions under which receding horizon control delivers approximately optimal solutions, p. 10

UNIVERSITÄT
BAYREUTH

Example: trajectories

$N = 10$

$N = 5$

Lars Grüne, On conditions under which receding horizon control delivers approximately optimal solutions, p. 10

UNIVERSITÄT
BAYREUTH

Example: trajectories

Example: trajectories

Example: averaged closed loop performance
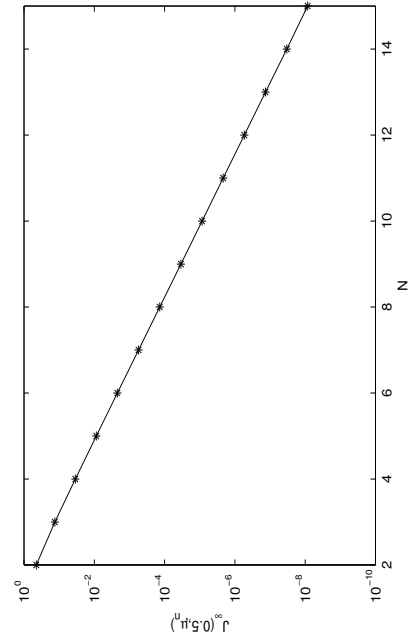
$$\overline{J}^{cl}_\infty(0.5, \mu_N) - \ell(x^e, u^e) \text{ depending on } N, \text{ logarithmic scale}$$

Example: trajectories

Observations

- optimal open loop trajectories approach the optimal equilibrium, stay near it for a while, and turn away
  − "turnpike property"

UNIVERSITÄT
BAYREUTH

Observations

- optimal open loop trajectories approach the optimal equilibrium, stay near it for a while, and turn away
  − "turnpike property"
- closed loop trajectories converge to a neighborhood of the optimal equilibrium whose size tends to 0 as $N \to \infty$
- the averaged closed loop performance satisfies
  $\overline{J}^{cl}_{\infty}(x, \mu_N) \to \ell(x^e, u^e)$ as $N \to \infty$ (exponentially fast)

UNIVERSITÄT
BAYREUTH

Observations

- optimal open loop trajectories approach the optimal equilibrium, stay near it for a while, and turn away
  − "turnpike property"
- closed loop trajectories converge to a neighborhood of the optimal equilibrium whose size tends to 0 as $N \to \infty$

UNIVERSITÄT
BAYREUTH

Observations

- optimal open loop trajectories approach the optimal equilibrium, stay near it for a while, and turn away
  − "turnpike property"

UNIVERSITÄT
BAYREUTH

Observations

- optimal open loop trajectories approach the optimal equilibrium, stay near it for a while, and turn away
  – "turnpike property"
- closed loop trajectories converge to a neighborhood of the optimal equilibrium whose size tends to 0 as $N \to \infty$
- the averaged closed loop performance satisfies
  $\overline{J}^{cl}_\infty(x,\mu_N) \to \ell(x^e,u^e)$ as $N \to \infty$ (exponentially fast)

Can we prove this behavior?

The first property will turn out to be the crucial one

Towards a performance estimate

Defining the optimal value function $V_N(x) := \inf_{\mathbf{u}} J_N(x,\mathbf{u})$, the "trick" in all MPC proofs lies in relating V_N and V_{N-1}

In economic MPC, the desired inequality is

$$V_N(x) \le V_{N-1}(x) + \ell(x^e,u^e) + \varepsilon$$

for a small error term $\varepsilon > 0$

Towards a performance estimate

Defining the optimal value function $V_N(x) := \inf_{\mathbf{u}} J_N(x, \mathbf{u})$, the "trick" in all MPC proofs lies in relating V_N and V_{N-1}

In economic MPC, the desired inequality is

$$\underbrace{V_N(x) \leq V_{N-1}(x) + \ell(x^e, u^e) + \varepsilon}$$

$$\ell(x, \mu_N(x)) + V_{N-1}(f(x, \mu_N(x)))$$

Towards a performance estimate

Defining the optimal value function $V_N(x) := \inf_{\mathbf{u}} J_N(x, \mathbf{u})$, the "trick" in all MPC proofs lies in relating V_N and V_{N-1}

In economic MPC, the desired inequality is

$$V_N(x) \leq V_{N-1}(x) + \ell(x^e, u^e) + \varepsilon$$

$$\Rightarrow \ell(x, \mu_N(x)) + V_{N-1}(f(x, \mu_N(x))) \leq V_{N-1}(x) + \ell(x^e, u^e) + \varepsilon$$

Using this inequality for $x = x_{\mu_N}(0), \ldots, x_{\mu_N}(K-1)$ yields

$$\overline{J}_K^{cl}(x, \mu_N) = \frac{1}{K}\sum_{n=0}^{K-1} \ell(x_{\mu_N}(n), \mu_N(x_{\mu_N}(n)))$$

Towards a performance estimate

Defining the optimal value function $V_N(x) := \inf_{\mathbf{u}} J_N(x, \mathbf{u})$, the "trick" in all MPC proofs lies in relating V_N and V_{N-1}

In economic MPC, the desired inequality is

$$V_N(x) \leq V_{N-1}(x) + \ell(x^e, u^e) + \varepsilon$$

$$\Rightarrow \ell(x, \mu_N(x)) + V_{N-1}(f(x, \mu_N(x))) \leq V_{N-1}(x) + \ell(x^e, u^e) + \varepsilon$$

Towards a performance estimate

Defining the optimal value function $V_N(x) := \inf_{\mathbf{u}} J_N(x, \mathbf{u})$, the "trick" in all MPC proofs lies in relating V_N and V_{N-1}

In economic MPC, the desired inequality is

$$V_N(x) \leq V_{N-1}(x) + \ell(x^e, u^e) + \varepsilon$$

$$\Rightarrow \ell(x, \mu_N(x)) + V_{N-1}(f(x, \mu_N(x))) \leq V_{N-1}(x) + \ell(x^e, u^e) + \varepsilon$$

Using this inequality for $x = x_{\mu_N}(0), \ldots, x_{\mu_N}(K-1)$ yields

$$\overline{J}_K^{cl}(x, \mu_N) = \frac{1}{K}\sum_{n=0}^{K-1} \ell(x_{\mu_N}(n), \mu_N(x_{\mu_N}(n)))$$

$$\leq \frac{1}{K}(V_{N-1}(x_{\mu_N}(0)) - V_{N-1}(x_{\mu_N}(K))) + \ell(x^e, u^e) + \varepsilon$$

Towards a performance estimate

Defining the optimal value function $V_N(x) := \inf_{\mathbf{u}} J_N(x, \mathbf{u})$, the "trick" in all MPC proofs lies in relating V_N and V_{N-1}

In economic MPC, the desired inequality is

$$V_N(x) \le V_{N-1}(x) + \ell(x^e, u^e) + \varepsilon$$

$\Rightarrow \ell(x, \mu_N(x)) + V_{N-1}(f(x, \mu_N(x))) \le V_{N-1}(x) + \ell(x^e, u^e) + \varepsilon$

Using this inequality for $x = x_{\mu_N}(0), \ldots, x_{\mu_N}(K-1)$ yields

$$\overline{J}_K^{cl}(x, \mu_N) = \frac{1}{K} \sum_{n=0}^{K-1} \ell(x_{\mu_N}(n), \mu_N(x_{\mu_N}(n)))$$
$$\le \frac{1}{K}(V_{N-1}(x_{\mu_N}(0)) - V_{N-1}(x_{\mu_N}(K))) + \ell(x^e, u^e) + \varepsilon$$

$\Rightarrow \overline{J}_K^{cl}(x, \mu_N) = \limsup_{K \to \infty} \overline{J}_K^{cl}(x, \mu_N) \le \ell(x^e, u^e) + \varepsilon$

Towards a performance estimate

Similarly, estimates for the non averaged J_K^{cl} can be obtained

Hence, the desired inequality is

$$V_N(x) \le V_{N-1}(x) + \ell(x^e, u^e) + \varepsilon$$

for a small $\varepsilon > 0$

Towards a performance estimate

Similarly, estimates for the non averaged J_K^{cl} can be obtained

Towards a performance estimate

Similarly, estimates for the non averaged J_K^{cl} can be obtained

Hence, the desired inequality is

$$V_N(x) \le V_{N-1}(x) + \ell(x^e, u^e) + \varepsilon$$

for a small $\varepsilon > 0$

In order to obtain this inequality, one

- takes an optimal trajectory corresponding to $V_{N-1}(x)$

Towards a performance estimate

Similarly, estimates for the non averaged J_K^{cl} can be obtained

Hence, the desired inequality is

$$V_N(x) \leq V_{N-1}(x) + \ell(x^e, u^e) + \varepsilon$$

for a small $\varepsilon > 0$

In order to obtain this inequality, one
- takes an optimal trajectory corresponding to $V_{N-1}(x)$
- prolongs this trajectory such that its value increases by no more than $\ell(x^e, u^e) + \varepsilon$
- uses the resulting $J_N(x, u)$ as an upper bound for $V_N(x)$

Towards a performance estimate

Similarly, estimates for the non averaged J_K^{cl} can be obtained

Hence, the desired inequality is

$$V_N(x) \leq V_{N-1}(x) + \ell(x^e, u^e) + \varepsilon$$

for a small $\varepsilon > 0$

In order to obtain this inequality, one
- takes an optimal trajectory corresponding to $V_{N-1}(x)$
- prolongs this trajectory such that its value increases by no more than $\ell(x^e, u^e) + \varepsilon$
- uses the resulting $J_N(x, u)$ as an upper bound for $V_N(x)$

This can be achieved by prolonging the trajectory close to x^e

Prolonging near x^e

Sketch of the idea:

$x^\star(\cdot)$

x^e

238

Prolonging near x^e

Sketch of the idea:

$x^\star(\cdot)$

x^e

Prolonging near x^e

Sketch of the idea:

$x^\star(\cdot)$

x^e

Assumptions needed for this construction

What do we need to make this construction work? [Gr. '13]

Prolonging near x^e

Sketch of the idea:

$x^\star(\cdot)$

x^e

Assumptions needed for this construction

What do we need to make this construction work? [Gr. '13]

(1) Continuity of V_N near x^e (uniform in x and N)
 ▸ ensures that we can prolong the trajectory in the middle without changing the value of the tail too much

(2) Turnpike property
 ▸ ensures that the finite horizon optimal trajectories stay for a certain time near the optimal equilibrium x^e

UNIVERSITÄT BAYREUTH   Lars Grüne, On conditions under which receding horizon control delivers approximately optimal solutions, p. 16

Assumptions needed for this construction

What do we need to make this construction work? [Gr. '13]

(1) Continuity of V_N near x^e (uniform in x and N)
 ▸ ensures that we can prolong the trajectory in the middle without changing the value of the tail too much

(2) Turnpike property
 ▸ ensures that the finite horizon optimal trajectories stay for a certain time near the optimal equilibrium x^e
 ▸ note: in numerical examples we often observe exponential turnpike, i.e., the minimum distance to x^e shrinks exponentially fast as N increases

Instead of the turnpike property, in the MPC literature another property is usually imposed: strict dissipativity

UNIVERSITÄT BAYREUTH   Lars Grüne, On conditions under which receding horizon control delivers approximately optimal solutions, p. 16

Assumptions needed for this construction

What do we need to make this construction work? [Gr. '13]

(1) Continuity of V_N near x^e (uniform in x and N)
 ▸ ensures that we can prolong the trajectory in the middle without changing the value of the tail too much

UNIVERSITÄT BAYREUTH   Lars Grüne, On conditions under which receding horizon control delivers approximately optimal solutions, p. 16

Assumptions needed for this construction

What do we need to make this construction work? [Gr. '13]

(1) Continuity of V_N near x^e (uniform in x and N)
 ▸ ensures that we can prolong the trajectory in the middle without changing the value of the tail too much

(2) Turnpike property
 ▸ ensures that the finite horizon optimal trajectories stay for a certain time near the optimal equilibrium x^e
 ▸ note: in numerical examples we often observe exponential turnpike, i.e., the minimum distance to x^e shrinks exponentially fast as N increases
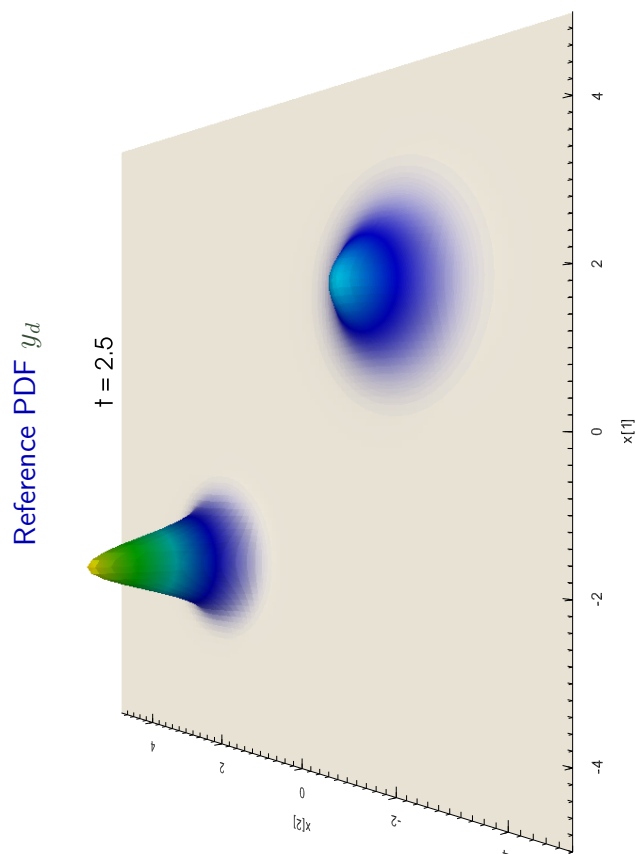
UNIVERSITÄT BAYREUTH   Lars Grüne, On conditions under which receding horizon control delivers approximately optimal solutions, p. 16

Strict dissipativity [Willems '72]

The optimal control problem is called strictly dissipative if there exists $\lambda : \mathbb{X} \to \mathbb{R}$ bounded from below and $\alpha \in \mathcal{K}_\infty$ with

$$\tilde{\ell}(x,u) := \ell(x,u) - \ell(x^e, u^e) + \lambda(x) - \lambda(f(x,u)) \geq \alpha(\|x - x^e\|)$$

for all $x \in \mathbb{X}, u \in \mathbb{U}$

UNIVERSITÄT BAYREUTH · Lars Grüne, On conditions under which receding horizon control delivers approximately optimal solutions, p. 17

Strict dissipativity [Willems '72]

The optimal control problem is called strictly dissipative if there exists $\lambda : \mathbb{X} \to \mathbb{R}$ bounded from below and $\alpha \in \mathcal{K}_\infty$ with

$$\tilde{\ell}(x,u) := \ell(x,u) - \ell(x^e, u^e) + \lambda(x) - \lambda(f(x,u)) \geq \alpha(\|x - x^e\|)$$

for all $x \in \mathbb{X}, u \in \mathbb{U}$

While originally introduced as a sufficient condition guaranteeing the turnpike property, a recent result shows:

Theorem [Gr./Müller '16]: Under suitable controllability conditions, strict dissipativity is equivalent to a robust turnpike property plus optimality of the equilibrium (x^e, u^e)

(details in the second part of this plenary)

UNIVERSITÄT BAYREUTH · Lars Grüne, On conditions under which receding horizon control delivers approximately optimal solutions, p. 17

Strict dissipativity [Willems '72]

The optimal control problem is called strictly dissipative if there exists $\lambda : \mathbb{X} \to \mathbb{R}$ bounded from below and $\alpha \in \mathcal{K}_\infty$ with

$$\tilde{\ell}(x,u) := \ell(x,u) - \ell(x^e,u^e) + \lambda(x) - \lambda(f(x,u)) \geq \alpha(\|x-x^e\|)$$

for all $x \in \mathbb{X}$, $u \in \mathbb{U}$

While originally introduced as a sufficient condition guaranteeing the turnpike property, a recent result shows:

Theorem [Gr./Müller '16]: Under suitable controllability conditions, strict dissipativity is equivalent to a robust turnpike property plus optimality of the equilibrium (x^e, u^e)

(details in the second part of this plenary)

The previous example is strictly dissipative with $\lambda(x) = -x^2/2$

Tracking type functionals are strictly dissipative with $\lambda \equiv 0$

Economic MPC theorem

Theorem: [Gr./Stieler '14]

Let f and ℓ be Lipschitz, $\mathbb{X}$ and $\mathbb{U}$ be compact and assume

(i) local controllability near x^e

(ii) strict dissipativity

(iii) reachability of x^e from all $x \in \mathbb{X}$

(iv) polynomial growth conditions for $\tilde{\ell}$

Economic MPC theorem

Theorem: [Gr./Stieler '14]

Let f and ℓ be Lipschitz, $\mathbb{X}$ and $\mathbb{U}$ be compact and assume

(i) local controllability near x^e $\left.\vphantom{\begin{array}{c}a\\b\end{array}}\right\}$ $\Rightarrow$ uniform continuity of V_N

(ii) strict dissipativity $\left.\vphantom{\begin{array}{c}a\\b\end{array}}\right\}$ $\Rightarrow$ turnpike property

(iii) reachability of x^e from all $x \in \mathbb{X}$

(iv) polynomial growth conditions for $\tilde{\ell}$

Lars Grüne, On conditions under which receding horizon control delivers approximately optimal solutions, p. 18

UNIVERSITÄT
BAYREUTH

Economic MPC theorem

Theorem: [Gr./Stieler '14]

Let f and ℓ be Lipschitz, $\mathbb{X}$ and $\mathbb{U}$ be compact and assume

(i) local controllability near x^e $\left.\vphantom{\begin{array}{c}a\\b\end{array}}\right\}$ $\Rightarrow$ uniform continuity of V_N

(ii) strict dissipativity $\left.\vphantom{\begin{array}{c}a\\b\end{array}}\right\}$ $\Rightarrow$ turnpike property

(iii) reachability of x^e from all $x \in \mathbb{X}$

(iv) polynomial growth conditions for $\tilde{\ell}$

(i)–(iv) $\Rightarrow$ exponential turnpike
[Damm/Gr./Stieler/Worthmann '14]

(for alternative conditions see also [Porretta/Zuazua '13]
[Trelat/Zuazua '14])

Lars Grüne, On conditions under which receding horizon control delivers approximately optimal solutions, p. 18

UNIVERSITÄT
BAYREUTH

Economic MPC theorem

Theorem: [Gr./Stieler '14]

Let f and ℓ be Lipschitz, $\mathbb{X}$ and $\mathbb{U}$ be compact and assume

(i) local controllability near x^e $\left.\vphantom{\begin{array}{c}a\\b\end{array}}\right\}$ $\Rightarrow$ uniform continuity of V_N

(ii) strict dissipativity $\left.\vphantom{\begin{array}{c}a\\b\end{array}}\right\}$ $\Rightarrow$ turnpike property

(iii) reachability of x^e from all $x \in \mathbb{X}$

(iv) polynomial growth conditions for $\tilde{\ell}$

(i)–(iv) $\Rightarrow$ exponential turnpike
[Damm/Gr./Stieler/Worthmann '14]

Lars Grüne, On conditions under which receding horizon control delivers approximately optimal solutions, p. 18

UNIVERSITÄT
BAYREUTH

Economic MPC theorem

Theorem: [Gr./Stieler '14]

Let f and ℓ be Lipschitz, $\mathbb{X}$ and $\mathbb{U}$ be compact and assume

(i) local controllability near x^e $\left.\vphantom{\begin{array}{c}a\\b\end{array}}\right\}$ $\Rightarrow$ uniform continuity of V_N

(ii) strict dissipativity $\left.\vphantom{\begin{array}{c}a\\b\end{array}}\right\}$ $\Rightarrow$ turnpike property

(iii) reachability of x^e from all $x \in \mathbb{X}$

(iv) polynomial growth conditions for $\tilde{\ell}$

Lars Grüne, On conditions under which receding horizon control delivers approximately optimal solutions, p. 18

UNIVERSITÄT
BAYREUTH

Economic MPC theorem

Under assumptions (i)–(iii), there exist $\varepsilon_1(N), \varepsilon_2(K) \to 0$ as $N \to \infty$ and $K \to \infty$, exponentially fast if additionally (iv) holds, such that the following properties hold

(1) Approximate average optimality:

$$\overline{J}^{cl}_\infty(x,\mu_N) \le \ell(x^e,u^e) + \varepsilon_1(N)$$

Illustration of (2) and (3)

x

x^e

n

Illustration of (2) and (3)

x

x^e

n

$\varepsilon_1(N)$

(2): $x_{\mu_N}(n)$ converges to the $\varepsilon_1(N)$-ball around x^e

Illustration of (2) and (3)

x

x^e

n

$\varepsilon_1(N)$

Illustration of (2) and (3)

x

x^e

n

K

$\varepsilon_1(N)$

(2): $x_{\mu_N}(n)$ converges to the $\varepsilon_1(N)$-ball around x^e

Illustration of (2) and (3)

(2): $x_{\mu_N}(n)$ converges to the $\varepsilon_1(N)$-ball around x^e

Lars Grüne, On conditions under which receding horizon control delivers approximately optimal solutions, p. 20

Illustration of (2) and (3)

(2): $x_{\mu_N}(n)$ converges to the $\varepsilon_1(N)$-ball around x^e

Lars Grüne, On conditions under which receding horizon control delivers approximately optimal solutions, p. 20

Illustration of (2) and (3)

(2): $x_{\mu_N}(n)$ converges to the $\varepsilon_1(N)$-ball around x^e

Lars Grüne, On conditions under which receding horizon control delivers approximately optimal solutions, p. 20

Illustration of (2) and (3)

(2): $x_{\mu_N}(n)$ converges to the $\varepsilon_1(N)$-ball around x^e

(3): cost of all other trajectories reaching the ball at time K is higher than that of $x_{\mu_N}(n)$ up to the error $K\varepsilon_1(N) + \varepsilon_2(K)$

Lars Grüne, On conditions under which receding horizon control delivers approximately optimal solutions, p. 20

Schemes with terminal constraints

If we know the equilibrium x^e, we may use it as a terminal constraint, i.e., in each step of the MPC scheme we optimize only over those trajectories satisfying $\quad x_{\mathbf{u}}(N) = x^e$

Example:
$N = 5$

Schemes with terminal constraints

If we know the equilibrium x^e, we may use it as a terminal constraint, i.e., in each step of the MPC scheme we optimize only over those trajectories satisfying $\quad x_{\mathbf{u}}(N) = x^e$

Example:
$N = 5$

Schemes with terminal constraints

If we know the equilibrium x^e, we may use it as a terminal constraint, i.e., in each step of the MPC scheme we optimize only over those trajectories satisfying $\quad x_{\mathbf{u}}(N) = x^e$

Example:
$N = 5$

Schemes with terminal constraints

If we know the equilibrium x^e, we may use it as a terminal constraint, i.e., in each step of the MPC scheme we optimize only over those trajectories satisfying $\quad x_{\mathbf{u}}(N) = x^e$

Example:
$N = 5$

Schemes with terminal constraints

If we know the equilibrium x^e, we may use it as a terminal constraint, i.e., in each step of the MPC scheme we optimize only over those trajectories satisfying $x_{\mathbf{u}}(N) = x^e$

Example:
$N = 5$

Schemes with terminal constraints

If we know the equilibrium x^e, we may use it as a terminal constraint, i.e., in each step of the MPC scheme we optimize only over those trajectories satisfying $\quad x_{\mathbf{u}}(N) = x^e$

Example:
$N = 5$

Schemes with terminal constraints

If we know the equilibrium x^e, we may use it as a terminal constraint, i.e., in each step of the MPC scheme we optimize only over those trajectories satisfying $x_{\mathbf{u}}(N) = x^e$

Example:
$N = 5$

UNIVERSITÄT
BAYREUTH   Lars Grüne, On conditions under which receding horizon control delivers approximately optimal solutions, p. 21

Schemes with terminal constraints

If we know the equilibrium x^e, we may use it as a terminal constraint, i.e., in each step of the MPC scheme we optimize only over those trajectories satisfying $x_{\mathbf{u}}(N) = x^e$

Example:
$N = 5$

UNIVERSITÄT
BAYREUTH   Lars Grüne, On conditions under which receding horizon control delivers approximately optimal solutions, p. 21

Schemes with terminal constraints

If we know the equilibrium x^e, we may use it as a terminal constraint, i.e., in each step of the MPC scheme we optimize only over those trajectories satisfying $x_{\mathbf{u}}(N) = x^e$

Example:
$N = 5$

UNIVERSITÄT
BAYREUTH   Lars Grüne, On conditions under which receding horizon control delivers approximately optimal solutions, p. 21

Schemes with terminal constraints

Imposing $x_{\mathbf{u}}(N) = x^e$ improves the previous results

UNIVERSITÄT
BAYREUTH   Lars Grüne, On conditions under which receding horizon control delivers approximately optimal solutions, p. 22

Schemes with terminal constraints

Imposing $x_{\mathbf{u}}(N) = x^e$ improves the previous results

Theorem: [Angeli/Amrit/Rawlings '12; Diehl/Rawlings '11]
Under strict dissipativity and controllability, the resulting MPC scheme yields averaged optimal trajectories, i.e,

$$\overline{J}_{\infty}^{cl}(x, \mu_N) \leq \ell(x^e, u^e) + \varepsilon_1(N)$$

Schemes with terminal constraints

Imposing $x_{\mathbf{u}}(N) = x^e$ improves the previous results

Theorem: [Angeli/Amrit/Rawlings '12; Diehl/Rawlings '11]
Under strict dissipativity and controllability, the resulting MPC scheme yields averaged optimal trajectories, i.e,

$$\overline{J}_{\infty}^{cl}(x, \mu_N) \leq \ell(x^e, u^e) + \varepsilon_1(N)$$

for which x^e is asymptotically stable

Schemes with terminal constraints

Imposing $x_{\mathbf{u}}(N) = x^e$ improves the previous results

Theorem: [Angeli/Amrit/Rawlings '12; Diehl/Rawlings '11]
Under strict dissipativity and controllability, the resulting MPC scheme yields averaged optimal trajectories, i.e,

$$\overline{J}^{cl}_{\infty}(x, \mu_N) \leq \ell(x^e, u^e) + \cancel{\varepsilon_1(N)}$$

for which x^e is asymptotically stable, i.e.,

$$\|x_{\mu_N}(k, x) - x^e\| \leq \beta(\|x - x^e\|, k) + \cancel{\varepsilon_1(N)}.$$

Schemes with terminal constraints

Imposing $x_{\mathbf{u}}(N) = x^e$ improves the previous results

Theorem: [Angeli/Amrit/Rawlings '12; Diehl/Rawlings '11]
Under strict dissipativity and controllability, the resulting MPC scheme yields averaged optimal trajectories, i.e,

$$\overline{J}^{cl}_{\infty}(x, \mu_N) \leq \ell(x^e, u^e) + \cancel{\varepsilon_1(N)}$$

for which x^e is asymptotically stable, i.e.,

$$\|x_{\mu_N}(k, x) - x^e\| \leq \beta(\|x - x^e\|, k) + \cancel{\varepsilon_1(N)}.$$

In addition [Gr./Panin '15] we get approx. transient optimality

$$J^{cl}_K(x, \mu_N(x)) \leq J_K(x, \mathbf{u}) + \cancel{K}\,\tilde{\varepsilon}_1(N) + \varepsilon_2(K)$$

Schemes with terminal constraints

Imposing $x_{\mathbf{u}}(N) = x^e$ improves the previous results

Theorem: [Angeli/Amrit/Rawlings '12; Diehl/Rawlings '11]
Under strict dissipativity and controllability, the resulting MPC scheme yields averaged optimal trajectories, i.e,

$$\overline{J}^{cl}_{\infty}(x, \mu_N) \leq \ell(x^e, u^e) + \cancel{\varepsilon_1(N)}$$

for which x^e is asymptotically stable, i.e.,

$$\|x_{\mu_N}(k, x) - x^e\| \leq \beta(\|x - x^e\|, k) + \cancel{\varepsilon_1(N)}.$$

Schemes with terminal constraints

Imposing $x_{\mathbf{u}}(N) = x^e$ improves the previous results

Theorem: [Angeli/Amrit/Rawlings '12; Diehl/Rawlings '11]
Under strict dissipativity and controllability, the resulting MPC scheme yields averaged optimal trajectories, i.e,

$$\overline{J}^{cl}_{\infty}(x, \mu_N) \leq \ell(x^e, u^e) + \cancel{\varepsilon_1(N)}$$

for which x^e is asymptotically stable, i.e.,

$$\|x_{\mu_N}(k, x) - x^e\| \leq \beta(\|x - x^e\|, k) + \cancel{\varepsilon_1(N)}.$$

In addition [Gr./Panin '15] we get approx. transient optimality

$$J^{cl}_K(x, \mu_N(x)) \leq J_K(x, \mathbf{u}) + K\,\varepsilon_1(N) + \varepsilon_2(K)$$

Example: closed loop cost

$$J_K^{cl}(x, \mu_N(x)) \leq J_K(x, \mathbf{u}) + K\varepsilon_1(N) + \varepsilon_2(K)$$

vs.

$$J_K^{cl}(x, \mu_N(x)) \leq J_K(x, \mathbf{u}) + \tilde{\varepsilon}_1(N) + \varepsilon_2(K)$$

UNIVERSITÄT BAYREUTH — Lars Grüne, On conditions under which receding horizon control delivers approximately optimal solutions, p. 23

Example: closed loop cost

$$J_K^{cl}(x, \mu_N(x)) \leq J_K(x, \mathbf{u}) + K\varepsilon_1(N) + \varepsilon_2(K)$$

vs.

$$J_K^{cl}(x, \mu_N(x)) \leq J_K(x, \mathbf{u}) + \tilde{\varepsilon}_1(N) + \varepsilon_2(K)$$

But: terminal constraints can cause infeasibility and severe numerical problems

UNIVERSITÄT BAYREUTH — Lars Grüne, On conditions under which receding horizon control delivers approximately optimal solutions, p. 23

Extensions, further results

- In the affine linear quadratic case our conditions are equivalent to the system being stabilizable [Gr./Stieler '14]

UNIVERSITÄT BAYREUTH — Lars Grüne, On conditions under which receding horizon control delivers approximately optimal solutions, p. 24

Extensions, further results

- In the affine linear quadratic case our conditions are equivalent to the system being stabilizable [Gr./Stieler '14]

- The optimal equilibrium can be replaced by an optimal periodic orbit   [Zanon/Gr. '16, Müller/Gr. '16]

- The terminal constraint $x_{\mathbf{u}}(N) = x^e$ can be relaxed to $x_{\mathbf{u}}(N) \in \mathbb{X}_0$ for a neighborhood $\mathbb{X}_0$ of x^e if the functional J_N is appropriately modified   [Amrit/Rawlings/Angeli '12, Gr./Panin '15]

Extensions, further results

- In the affine linear quadratic case our conditions are equivalent to the system being stabilizable [Gr./Stieler '14]

- The optimal equilibrium can be replaced by an optimal periodic orbit   [Zanon/Gr. '16, Müller/Gr. '16]

- The terminal constraint $x_{\mathbf{u}}(N) = x^e$ can be relaxed to $x_{\mathbf{u}}(N) \in \mathbb{X}_0$ for a neighborhood $\mathbb{X}_0$ of x^e if the functional J_N is appropriately modified   [Amrit/Rawlings/Angeli '12, Gr./Panin '15]

- The results can be formulated directly in continuous time [Faulwasser/Bonvin '15, Alessandretti/Aguiar/Jones '15]

- First results for time varying systems are available [Zanon/Gros/Diehl '13, Alessandretti/Aguiar/Jones '15]

Extensions, further results

- In the affine linear quadratic case our conditions are equivalent to the system being stabilizable [Gr./Stieler '14]

- The optimal equilibrium can be replaced by an optimal periodic orbit   [Zanon/Gr. '16, Müller/Gr. '16]

- The terminal constraint $x_{\mathbf{u}}(N) = x^e$ can be relaxed to $x_{\mathbf{u}}(N) \in \mathbb{X}_0$ for a neighborhood $\mathbb{X}_0$ of x^e if the functional J_N is appropriately modified   [Amrit/Rawlings/Angeli '12, Gr./Panin '15]

- The results can be formulated directly in continuous time [Faulwasser/Bonvin '15, Alessandretti/Aguiar/Jones '15]

Extensions, further results

- In the affine linear quadratic case our conditions are equivalent to the system being stabilizable [Gr./Stieler '14]

- The optimal equilibrium can be replaced by an optimal periodic orbit   [Zanon/Gr. '16, Müller/Gr. '16]

Extensions, further results

- In the affine linear quadratic case our conditions are equivalent to the system being stabilizable [Gr./Stieler '14]
- The optimal equilibrium can be replaced by an optimal periodic orbit [Zanon/Gr. '16, Müller/Gr. '16]
- The terminal constraint $x_{\mathbf{u}}(N) = x^e$ can be relaxed to $x_{\mathbf{u}}(N) \in \mathbb{X}_0$ for a neighborhood $\mathbb{X}_0$ of x^e if the functional J_N is appropriately modified [Amrit/Rawlings/Angeli '12, Gr./Panin '15]
- The results can be formulated directly in continuous time [Faulwasser/Bonvin '15, Alessandretti/Aguiar/Jones '15]
- First results for time varying systems are available [Zanon/Gros/Diehl '13, Alessandretti/Aguiar/Jones '15]
- First results for discounted optimal control problems [Gr./Semmler/Stieler '15, Gr./Kellett/Weller '16]

UNIVERSITÄT BAYREUTH · · · Lars Grüne, On conditions under which receding horizon control delivers approximately optimal solutions, p. 24

Example: Fokker-Planck Equation

Consider a stochastic process governed by a controlled Itô stochastic differential equation (SDE)

$$dX_t = b(X_t, t; u)dt + \sigma(X_t, t)dW_t, \qquad X_{t_0} = x_0$$

where the random variable $X_t \in \mathbb{R}^d$ represents the state

UNIVERSITÄT BAYREUTH · · · Lars Grüne, On conditions under which receding horizon control delivers approximately optimal solutions, p. 25

Example: Fokker-Planck Equation

Consider a stochastic process governed by a controlled Itô stochastic differential equation (SDE)

$$dX_t = b(X_t, t; u)dt + \sigma(X_t, t)dW_t, \qquad X_{t_0} = x_0$$

UNIVERSITÄT BAYREUTH · · · Lars Grüne, On conditions under which receding horizon control delivers approximately optimal solutions, p. 25

Example: Fokker-Planck Equation

Consider a stochastic process governed by a controlled Itô stochastic differential equation (SDE)

$$dX_t = b(X_t, t; u)dt + \sigma(X_t, t)dW_t, \qquad X_{t_0} = x_0$$

where the random variable $X_t \in \mathbb{R}^d$ represents the state

Idea: control the statistical properties of X_t by controlling its probability density function $y(x, t)$

UNIVERSITÄT BAYREUTH · · · Lars Grüne, On conditions under which receding horizon control delivers approximately optimal solutions, p. 25

The Fokker-Planck Equation

The probability density function (PDF) $y(x,t)$ of X_t solves the Fokker-Planck Equation

$$\partial_t y(x,t) - \sum_{i,j=1}^{d} \partial^2_{x_i x_j}\big(a_{ij}(x,t)y(x,t)\big) + \sum_{i=1}^{d} \partial_{x_i}\big(b_i(x,t;u)y(x,t)\big) = 0$$

$$y(\cdot,0) = y_0$$

where $y: \mathbb{R}^d \times [0,\infty[\to \mathbb{R}_{\geq 0}$ is the PDF

$y_0: \mathbb{R}^d \to \mathbb{R}_{\geq 0}$ is the initial PDF

$a = \sigma\sigma^T/2$ is a positive definite symmetric matrix

$b_i: \mathbb{R}^d \times [0,\infty[\times U \to \mathbb{R}, \ i=1,\ldots,d.$

UNIVERSITÄT BAYREUTH   Lars Grüne, On conditions under which receding horizon control delivers approximately optimal solutions, p. 26

MPC for the Fokker-Planck equation

$$\partial_t y(x,t) - \sum_{i,j=1}^{d} \partial^2_{x_i x_j}\big(a_{ij}(x,t)y(x,t)\big) + \sum_{i=1}^{d} \partial_{x_i}\big(b_i(x,t;u)y(x,t)\big) = 0$$

Idea: [Annunziato/Borzì '10ff.] Prescribe a desired PDF $y_d(x,t)$ and use MPC for the FP equation in order to track this PDF

$$\rightsquigarrow J_N(y,u) = \frac{1}{2}\sum_{n=0}^{N-1}\Big(\|y(t_{n+1}) - y_d(t_{n+1})\|^2_{L^2(\Omega)} + \lambda\|u(t_n)\|^2\Big)$$

$$t_n = nT$$

[Annunziato/Borzì '10ff.] used this idea with $N=2$ and u independent of the space variable x

UNIVERSITÄT BAYREUTH   Lars Grüne, On conditions under which receding horizon control delivers approximately optimal solutions, p. 27

MPC for the Fokker-Planck equation

$$\partial_t y(x,t) - \sum_{i,j=1}^d \partial^2_{x_i x_j}\left(a_{ij}(x,t)y(x,t)\right) + \sum_{i=1}^d \partial_{x_i}\left(b_i(x,t;u))y(x,t)\right) = 0$$

Idea: [Annunziato/Borzì '10ff.] Prescribe a desired PDF $y_d(x,t)$ and use MPC for the FP equation in order to track this PDF

$$\rightsquigarrow J_N(y,u) = \frac{1}{2}\sum_{n=0}^{N-1}\left(\|y(t_{n+1}) - y_d(t_{n+1})\|^2_{L^2(\Omega)} + \lambda\|u(t_n)\|^2\right)$$

$$t_n = nT$$

[Annunziato/Borzì '10ff.] used this idea with $N = 2$ and u independent of the space variable x

We extended this to arbitrary N and u depending on t and x

Numerical Example in 2D

2d Ornstein-Uhlenbeck type process on $\Omega = (-5,5)^2$

$$dX_t = b(X_t,t;u)dt + \sigma(X_t,t)dW_t, \qquad X_{t_0} = x_0$$

with

$$\sigma(x,t) = \begin{pmatrix} 0.8 & 0 \\ 0 & 0.8 \end{pmatrix}, \quad b(x,t;u) = \begin{pmatrix} -\mu_1 x_1 + u_1 \\ -\mu_2 x_2 + u_2 \end{pmatrix}$$

↝ Fokker-Planck equation

$$\partial_t y(x,t) - \sum_{i,j=1}^d \partial^2_{x_i x_j}\left(a_{ij}(x,t)y(x,t)\right) + \sum_{i=1}^d \partial_{x_i}\left(b_i(x,t;u))y(x,t)\right) = 0$$

with

$$a(x,t) = \begin{pmatrix} 0.32 & 0 \\ 0 & 0.32 \end{pmatrix}, \quad b(x,t;u) = \begin{pmatrix} -\mu_1 x_1 + u_1 \\ -\mu_2 x_2 + u_2 \end{pmatrix}$$

Reference PDF y_d

t = 0.0

Numerical Example in 2D

Reference PDF is a bi-modal Gaussian given by

$$y_d(x,t) = \frac{1}{2}\frac{\exp\left(-\frac{(x_1+\mu(t))^2}{2\sigma_{11}^2} - \frac{(x_2-\mu(t))^2}{2\sigma_{21}^2}\right)}{2\pi\sigma_{11}\sigma_{21}} + \frac{1}{2}\frac{\exp\left(-\frac{(x_1-\mu(t))^2}{2\sigma_{12}^2} - \frac{(x_2+\mu(t))^2}{2\sigma_{22}^2}\right)}{2\pi\sigma_{12}\sigma_{22}}$$

with $\mu(t) = 2\sin(\frac{\pi t}{5})$, $\sigma_{11} = \sigma_{21} = 0.4, \sigma_{12} = \sigma_{22} = 0.6$.

Reference PDF y_d

t = 4.5

Numerical Example in 2D

Cost functional

$$J(y, u) := \frac{1}{2} \|y(t+T) - y_d(t+T)\|_{L^2(\Omega)}^2 + \frac{\lambda}{2} \|u(t)\|_{L^2(\Omega)}^2$$

Reference PDF y_d

t = 5.0
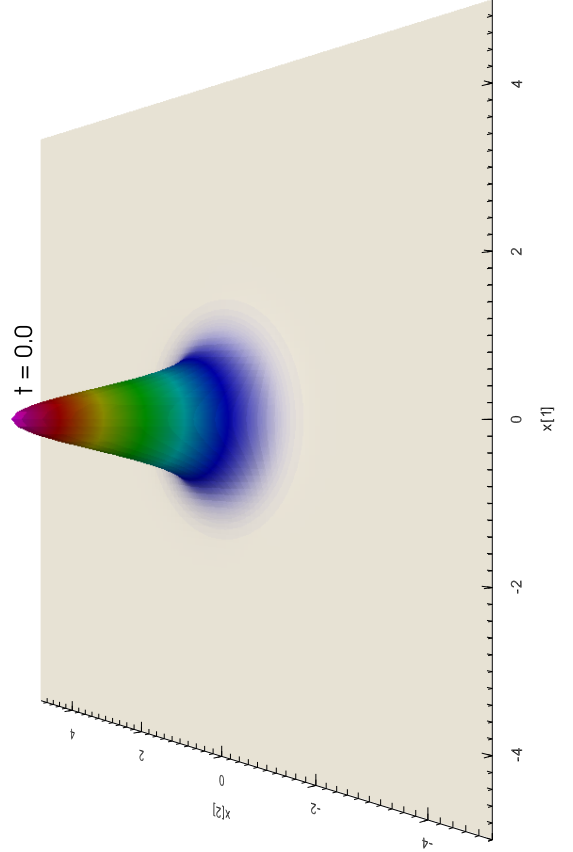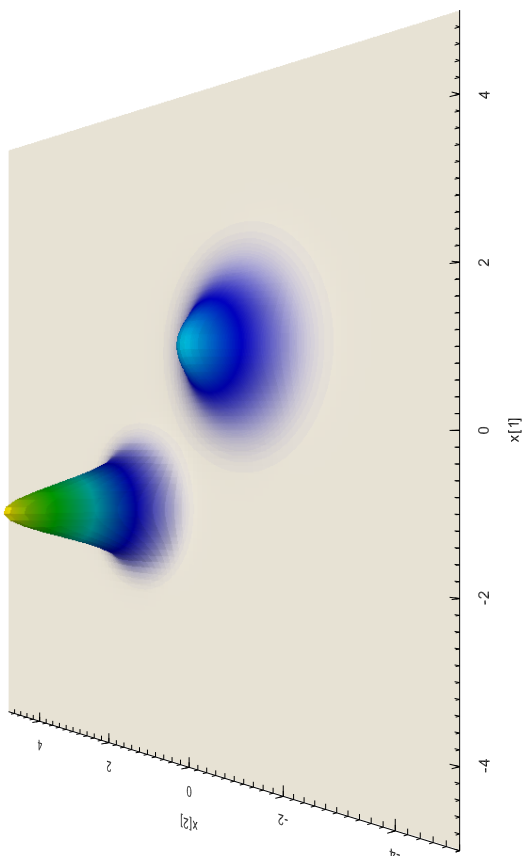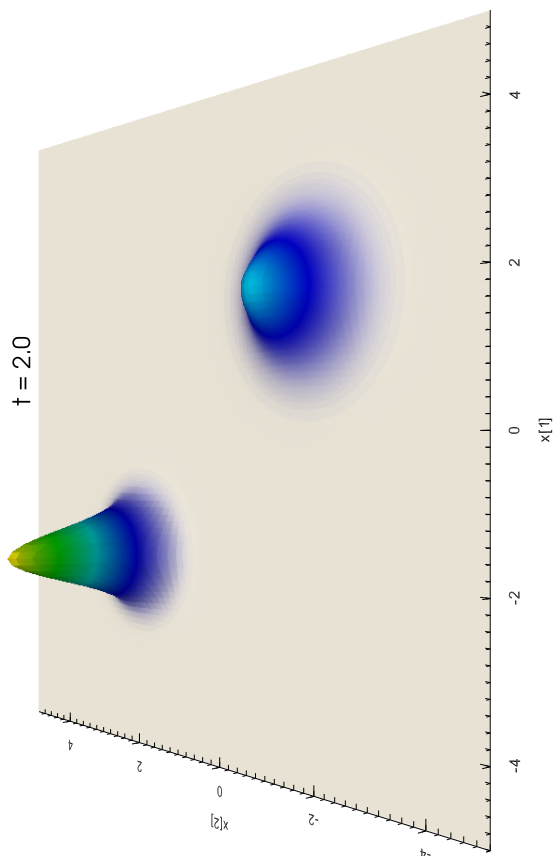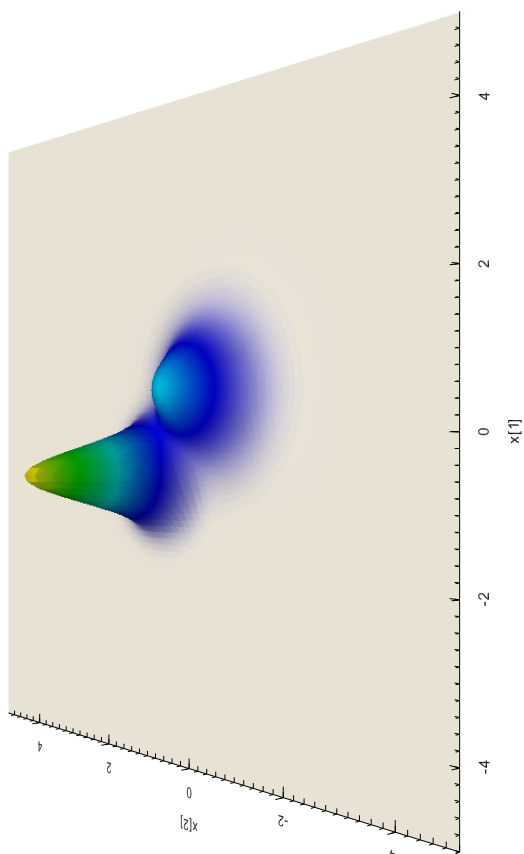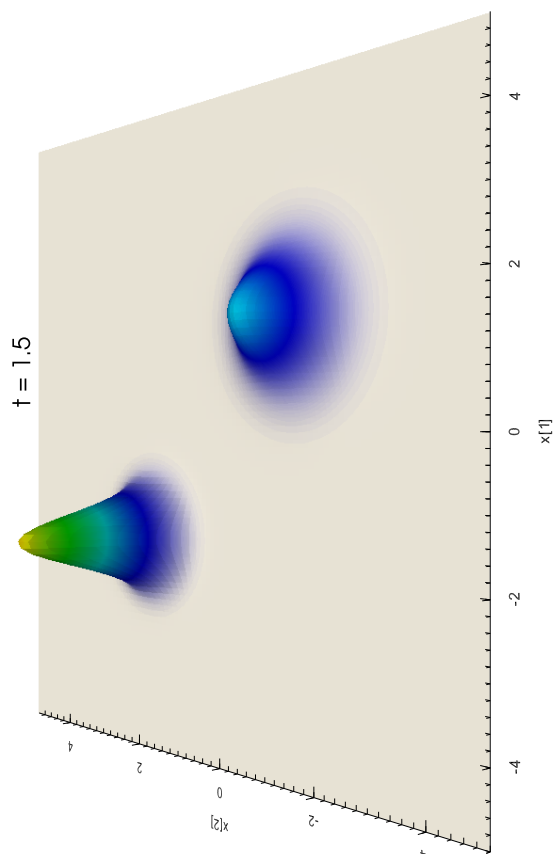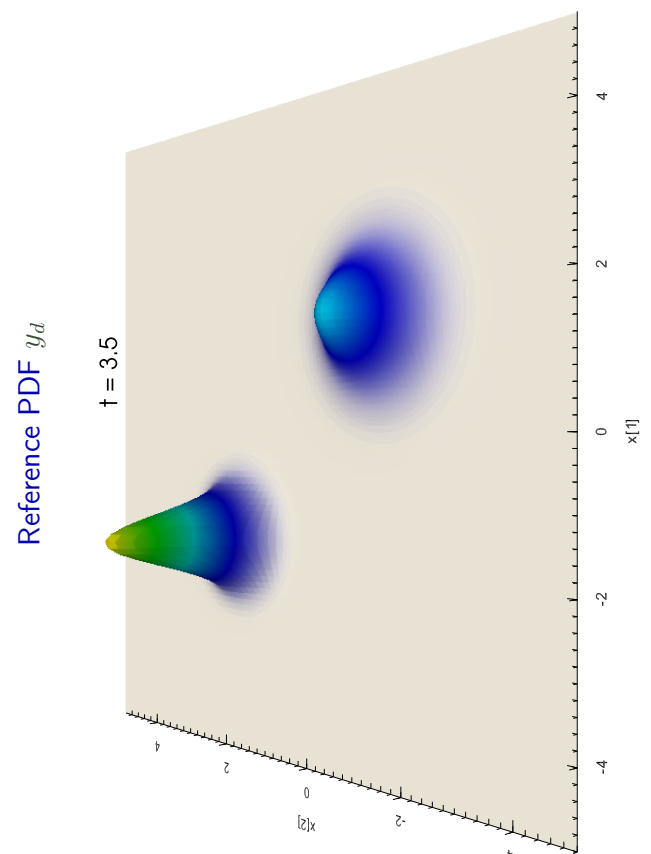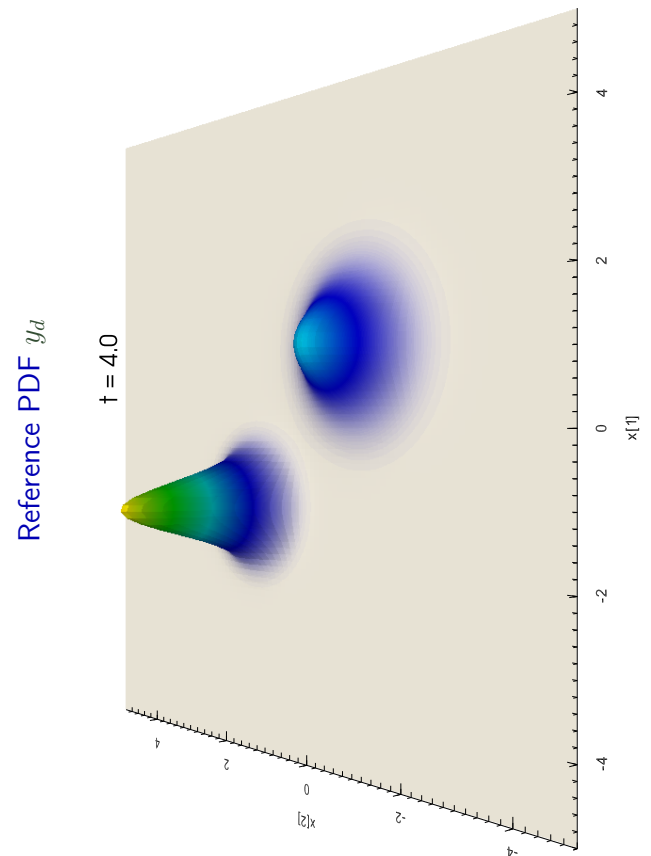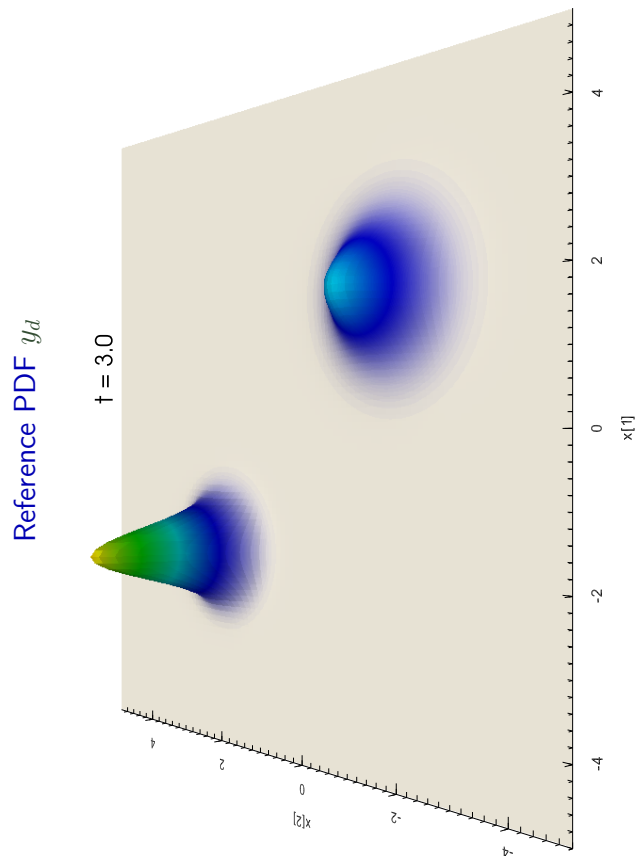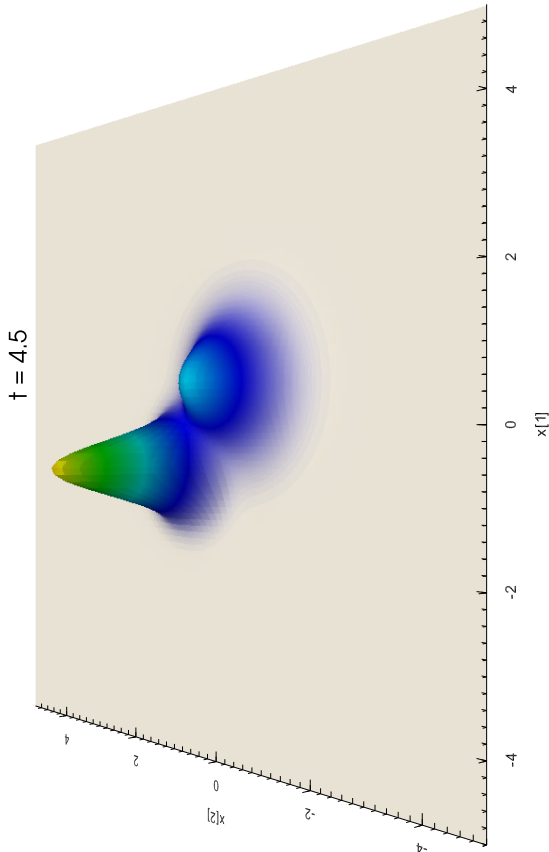
Numerical Example in 2D

Cost functional

$$J(y, u) := \frac{1}{2} \|y(t+T) - y_d(t+T)\|_{L^2(\Omega)}^2 + \frac{\lambda}{2} \|u(t)\|_{L^2(\Omega)}^2$$

Simulation parameters

- initial distribution $y_0(x) = y_d(x, 0)$
- optimization horizon $N = 2$
- sampling time $T = 0.5$
- control penalization $\lambda = 0.001$
- control range $u_{1/2} \in [-10, 10]$

Lars Grüne, On conditions under which receding horizon control delivers approximately optimal solutions, p. 31

Lars Grüne, On conditions under which receding horizon control delivers approximately optimal solutions, p. 31

UNIVERSITÄT
BAYREUTH

UNIVERSITÄT
BAYREUTH

MPC for the Fokker-Planck equation — theory

In the generality of this simulation there is no proof so far that MPC works

Lars Grüne, On conditions under which receding horizon control delivers approximately optimal solutions, p. 33

UNIVERSITÄT
BAYREUTH

MPC for the Fokker-Planck equation — theory

In the generality of this simulation there is no proof so far that MPC works

However, [Fleig/Gr. 16] contains first results for the case where

- the stage cost penalizes the L^2-distance to a desired reference PDF
- the control is independent of x

UNIVERSITÄT BAYREUTH

MPC for the Fokker-Planck equation — theory

In the generality of this simulation there is no proof so far that MPC works

However, [Fleig/Gr. 16] contains first results for the case where

- the stage cost penalizes the L^2-distance to a desired reference PDF
- the control is independent of x
- both the initial condition and the reference PDF are (higher dimensional) Gaussian PDFs

In this case, it can be shown that MPC stabilizes the reference PDF for the shortest possible horizon $N = 2$

UNIVERSITÄT BAYREUTH

Summary and conclusion

- Receding Horizon Control can be seen as a method for splitting up an infinite horizon optimal control problem into the iterative solution of finite horizon problems

- The existence of the turnpike property at an optimal equilibrium is the key ingredient to make this approach work

UNIVERSITÄT BAYREUTH

Summary and conclusion

- Receding Horizon Control can be seen as a method for splitting up an infinite horizon optimal control problem into the iterative solution of finite horizon problems

- The existence of the turnpike property at an optimal equilibrium is the key ingredient to make this approach work

- Strict dissipativity is essentially equivalent to this property and may be used as a checkable condition

- Good news: if MPC works, then it works regardless of whether we checked the conditions

UNIVERSITÄT BAYREUTH

Summary and conclusion

- Receding Horizon Control can be seen as a method for splitting up an infinite horizon optimal control problem into the iterative solution of finite horizon problems

UNIVERSITÄT BAYREUTH

Summary and conclusion

- Receding Horizon Control can be seen as a method for splitting up an infinite horizon optimal control problem into the iterative solution of finite horizon problems

- The existence of the turnpike property at an optimal equilibrium is the key ingredient to make this approach work

- Strict dissipativity is essentially equivalent to this property and may be used as a checkable condition

UNIVERSITÄT BAYREUTH

Summary and conclusion

- Receding Horizon Control can be seen as a method for splitting up an infinite horizon optimal control problem into the iterative solution of finite horizon problems

- The existence of the turnpike property at an optimal equilibrium is the key ingredient to make this approach work

- Strict dissipativity is essentially equivalent to this property and may be used as a checkable condition

- Good news: if MPC works, then it works regardless of whether we checked the conditions — but if we want to be sure we need to check

UNIVERSITÄT BAYREUTH   Lars Grüne, On conditions under which receding horizon control delivers approximately optimal solutions, p. 34

References

L. Grüne, *Approximation properties of receding horizon optimal control*, DMV Jahresbericht, 2016, to appear

L. Grüne, *Economic receding horizon control without terminal constraints*, Automatica, 49, 725–734, 2013

T. Damm, L. Grüne, M. Stieler, K. Worthmann, *An exponential turnpike theorem for dissipative discrete time optimal control problems*, SIAM J. Control Optim., 52, 1935–1957, 2014

L. Grüne, M. Stieler, *Asymptotic stability and transient optimality of economic MPC without terminal conditions*, Journal of Process Control, 24 (Special Issue on Economic MPC), 1187–1196, 2014

A. Fleig, L. Grüne, *Estimates on the minimal stabilizing horizon length in model predictive control for the Fokker-Planck equation*, submitted, 2016

L. Grüne, M.A. Müller, *On the relation between strict dissipativity and turnpike properties*, Syst. Control Lett., 90, 45–53, 2016

UNIVERSITÄT BAYREUTH   Lars Grüne, On conditions under which receding horizon control delivers approximately optimal solutions, p. 35

On the relation between dissipativity and the turnpike property

Lars Grüne

Mathematisches Institut, Universität Bayreuth

joint work with Matthias A. Müller (Universität Stuttgart)

35th Benelux Meeting on Systems and Control
Soesterberg, The Netherlands, 22–24 March 2016

Outline

- Dissipativity and strict dissipativity
- The turnpike property and its variants
- Known results
- New results and proof ideas

System class

We consider nonlinear discrete time control systems

$$x_{\mathbf{u}}(n+1) = f(x_{\mathbf{u}}(n), \mathbf{u}(n)), \quad x_{\mathbf{u}}(0) = x$$

with $x_{\mathbf{u}}(n) \in X$, $\mathbf{u}(n) \in U$, X, U normed spaces

System class

We consider nonlinear discrete time control systems

$$x_{\mathbf{u}}(n+1) = f(x_{\mathbf{u}}(n), \mathbf{u}(n)), \quad x_{\mathbf{u}}(0) = x$$

with $x_{\mathbf{u}}(n) \in X$, $\mathbf{u}(n) \in U$, X, U normed spaces

Brief notation $\qquad x^+ = f(x, u)$

System class

We consider nonlinear discrete time control systems

$$x_{\mathbf{u}}(n+1) = f(x_{\mathbf{u}}(n), \mathbf{u}(n)), \quad x_{\mathbf{u}}(0) = x$$

with $x_{\mathbf{u}}(n) \in X$, $\mathbf{u}(n) \in U$, X, U normed spaces

Brief notation $x^+ = f(x,u)$

Interpretation:

$x_{\mathbf{u}}(n) \;=\;$ state of the system at time t_n

System class

We consider nonlinear discrete time control systems

$$x_{\mathbf{u}}(n+1) = f(x_{\mathbf{u}}(n), \mathbf{u}(n)), \quad x_{\mathbf{u}}(0) = x$$

with $x_{\mathbf{u}}(n) \in X$, $\mathbf{u}(n) \in U$, X, U normed spaces

Brief notation $x^+ = f(x,u)$

Interpretation:

$x_{\mathbf{u}}(n) \;=\;$ state of the system at time t_n

$\mathbf{u}(n) \;=\;$ control acting from time t_n to t_{n+1}

$f \;=\;$ solution operator of a controlled ODE/PDE or of a discrete time model

System class

We consider nonlinear discrete time control systems

$$x_{\mathbf{u}}(n+1) = f(x_{\mathbf{u}}(n), \mathbf{u}(n)), \quad x_{\mathbf{u}}(0) = x$$

with $x_{\mathbf{u}}(n) \in X$, $\mathbf{u}(n) \in U$, X, U normed spaces

Brief notation $x^+ = f(x,u)$

Interpretation:

$x_{\mathbf{u}}(n) \;=\;$ state of the system at time t_n

$\mathbf{u}(n) \;=\;$ control acting from time t_n to t_{n+1}

System class

We consider nonlinear discrete time control systems

$$x_{\mathbf{u}}(n+1) = f(x_{\mathbf{u}}(n), \mathbf{u}(n)), \quad x_{\mathbf{u}}(0) = x$$

with $x_{\mathbf{u}}(n) \in X$, $\mathbf{u}(n) \in U$, X, U normed spaces

Brief notation $x^+ = f(x,u)$

Interpretation:

$x_{\mathbf{u}}(n) \;=\;$ state of the system at time t_n

$\mathbf{u}(n) \;=\;$ control acting from time t_n to t_{n+1}

$f \;=\;$ solution operator of a controlled ODE/PDE or of a discrete time model (or a numerical approximation of one of these)

Dissipativity and strict dissipativity

Dissipativity

$$x^+ = f(x,u)$$

Introduce functions $s : X \times U \to \mathbb{R}$ and $\lambda : X \to \mathbb{R}_0^+$

$s(x,u) \in \mathbb{R}$ supply rate, measuring the (possibly negative) amount of energy supplied to the system via the input u in the next time step

$\lambda(x) \geq 0$ storage function, measuring the amount of energy stored inside the system when the system is in state x

UNIVERSITÄT BAYREUTH

Dissipativity

Definition [Willems '72] The system is called dissipative if for all $x \in X$, $u \in U$ the inequality

$$\lambda(x^+) \leq \lambda(x) + s(x,u)$$

holds

UNIVERSITÄT BAYREUTH

Dissipativity

Definition [Willems '72] The system is called dissipative if for all $x \in X$, $u \in U$ the inequality

$$\lambda(x^+) \leq \lambda(x) + s(x,u)$$

holds

The system is called strictly dissipative if there are $x^e \in X$, $\alpha \in \mathcal{K}$ such that for all $x \in X$, $u \in U$ the inequality

$$\lambda(x^+) \leq \lambda(x) + s(x,u) - \alpha(\|x - x^e\|)$$

holds

UNIVERSITÄT BAYREUTH

269

Dissipativity

Definition [Willems '72] The system is called dissipative if for all $x \in X$, $u \in U$ the inequality

$$\lambda(x^+) \leq \lambda(x) + s(x,u)$$

holds

The system is called strictly dissipative if there are $x^e \in X$, $\alpha \in \mathcal{K}$ such that for all $x \in X$, $u \in U$ the inequality

$$\lambda(x^+) \leq \lambda(x) + s(x,u) - \alpha(\|x - x^e\|)$$

holds

$\alpha \in \mathcal{K}$: $\alpha : \mathbb{R}_0^+ \to \mathbb{R}_0^+$, continuous, strictly increasing, $\alpha(0) = 0$
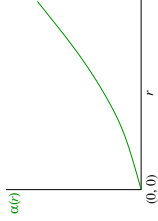
Lars Grüne, On the relation between dissipativity and the turnpike property, p. 6

Physical interpretation of dissipativity

$$\lambda(x^+) \leq \lambda(x) + s(x,u) \quad [\,-\alpha(\|x - x^e\|)\,]$$

physical interpretation of [strict] dissipativity

Lars Grüne, On the relation between dissipativity and the turnpike property, p. 7

Physical interpretation of dissipativity

$$\lambda(x^+) \leq \lambda(x) + s(x,u) \quad [\,-\alpha(\|x - x^e\|)\,]$$

physical interpretation of [strict] dissipativity:

$\lambda(x)$ = energy stored in the system
$s(x,u)$ = energy supplied to the system

Lars Grüne, On the relation between dissipativity and the turnpike property, p. 7

Physical interpretation of dissipativity

$$\lambda(x^+) \leq \lambda(x) + s(x,u) \quad [\,-\alpha(\|x - x^e\|)\,]$$

physical interpretation of [strict] dissipativity:

$\lambda(x)$ = energy stored in the system
$s(x,u)$ = energy supplied to the system

dissipativity: energy can only be dissipated (=lost) but not be generated inside the system

Lars Grüne, On the relation between dissipativity and the turnpike property, p. 7

Physical interpretation of dissipativity

$$\lambda(x^+) \leq \lambda(x) + s(x,u) \; \left[\, -\alpha(\|x - x^e\|)\,\right]$$

physical interpretation of [strict] dissipativity:

$\lambda(x)$ = energy stored in the system
$s(x,u)$ = energy supplied to the system

dissipativity: energy can only be dissipated (=lost) but not be generated inside the system

strict dissipativity: a certain amount of energy, depending on $\|x - x^e\|$ must be dissipated

Lars Grüne, On the relation between dissipativity and the turnpike property, p. 7

UNIVERSITÄT
BAYREUTH

History

Dissipativity was defined for continuous time systems in
[Jan C. Willems, Dissipative Dynamical Systems, Part I & II, 1972]

(this is one of the rare occasions in which the original paper can still be recommended as one of the best readings on the topic)

Lars Grüne, On the relation between dissipativity and the turnpike property, p. 8

UNIVERSITÄT
BAYREUTH

History

Dissipativity was defined for continuous time systems in
[Jan C. Willems, Dissipative Dynamical Systems, Part I & II, 1972]

(this is one of the rare occasions in which the original paper can still be recommended as one of the best readings on the topic)

Lars Grüne, On the relation between dissipativity and the turnpike property, p. 8

UNIVERSITÄT
BAYREUTH

History

Dissipativity was defined for continuous time systems in
[Jan C. Willems, Dissipative Dynamical Systems, Part I & II, 1972]

(this is one of the rare occasions in which the original paper can still be recommended as one of the best readings on the topic)

It was the result of the endeavour to generalise passivity

Lars Grüne, On the relation between dissipativity and the turnpike property, p. 8

UNIVERSITÄT
BAYREUTH

History

Dissipativity was defined for continuous time systems in [Jan C. Willems, Dissipative Dynamical Systems, Part I & II, 1972]

(this is one of the rare occasions in which the original paper can still be recommended as one of the best readings on the topic)

It was the result of the endeavour to generalise passivity

(passivity = dissipativity with $s(x, u) = \langle y, u \rangle$, where $y = h(x)$ is the output of the system)

Passivity, in turn, is a classical property of electrical circuits which do not contain active elements

Lars Grüne, On the relation between dissipativity and the turnpike property, p. 8

UNIVERSITÄT BAYREUTH

History

Dissipativity was defined for continuous time systems in [Jan C. Willems, Dissipative Dynamical Systems, Part I & II, 1972]

(this is one of the rare occasions in which the original paper can still be recommended as one of the best readings on the topic)

It was the result of the endeavour to generalise passivity

(passivity = dissipativity with $s(x, u) = \langle y, u \rangle$, where $y = h(x)$ is the output of the system)

Passivity, in turn, is a classical property of electrical circuits which do not contain active elements

Strict (or strong) dissipativity is mentioned in [Willems '72] but is not so often used; strict passivity is more commonly found

Translation to discrete time systems is quite straightforward
[Byrnes/Lin '94]

Lars Grüne, On the relation between dissipativity and the turnpike property, p. 8

UNIVERSITÄT BAYREUTH

Applications

Dissipativity can be used for designing asymptotically stabilising feedback controllers, i.e., for finding a map $u = F(x)$ such that $x^+ = f(x, F(x))$ has an asymptotically stable equilibrium x^*:

Applications

Dissipativity can be used for designing asymptotically stabilising feedback controllers, i.e., for finding a map $u = F(x)$ such that $x^+ = f(x, F(x))$ has an asymptotically stable equilibrium x^*:

If we can construct F with $s(x, F(x)) < 0$ for $x \neq x^*$, then

$$\lambda(x^+) \leq \lambda(x) + s(x, F(x)) < \lambda(x), \quad x \neq x^*$$

implies that λ becomes a Lyapunov function for the system

Applications

Dissipativity can be used for designing asymptotically stabilising feedback controllers, i.e., for finding a map $u = F(x)$ such that $x^+ = f(x, F(x))$ has an asymptotically stable equilibrium x^*:

If we can construct F with $s(x, F(x)) < 0$ for $x \neq x^*$, then

$$\lambda(x^+) \leq \lambda(x) + s(x, F(x)) < \lambda(x), \quad x \neq x^*$$

implies that λ becomes a Lyapunov function for the system

(in case of strict dissipativity with $x^* = x^e$, the non-strict inequality $s(x, F(x)) \leq 0$ is sufficient)

Applications

Dissipativity can be used for designing asymptotically stabilising feedback controllers, i.e., for finding a map $u = F(x)$ such that $x^+ = f(x, F(x))$ has an asymptotically stable equilibrium x^*:

If we can construct F with $s(x, F(x)) < 0$ for $x \neq x^*$, then

$$\lambda(x^+) \leq \lambda(x) + s(x, F(x)) < \lambda(x), \quad x \neq x^*$$

implies that λ becomes a Lyapunov function for the system

(in case of strict dissipativity with $x^* = x^e$, the non-strict inequality $s(x, F(x)) \leq 0$ is sufficient)

Constructing F is particularly easy in case of passivity, because for $s(x, u) = \langle y, u \rangle$ it suffices to define the output feedback $F(y) := -y$

UNIVERSITÄT BAYREUTH   Lars Grüne, On the relation between dissipativity and the turnpike property, p. 9

Applications

Various stability properties can be formulated via dissipativity:

- (asymptotic) stability of the equilibrium x^e can be concluded for all solutions if the system is (strictly) dissipative, $s(x, u) \leq 0$ and the storage function λ is bounded from below and above by $\mathcal{K}_\infty$-functions in $\|x - x^e\|$

UNIVERSITÄT BAYREUTH   Lars Grüne, On the relation between dissipativity and the turnpike property, p. 10

Applications

Various stability properties can be formulated via dissipativity:

- (asymptotic) stability of the equilibrium x^e can be concluded for all solutions if the system is (strictly) dissipative, $s(x, u) \leq 0$ and the storage function λ is bounded from below and above by $\mathcal{K}_\infty$-functions in $\|x - x^e\|$ ($\mathcal{K}_\infty$-functions = unbounded $\mathcal{K}$-functions)

UNIVERSITÄT BAYREUTH   Lars Grüne, On the relation between dissipativity and the turnpike property, p. 10

Applications

Various stability properties can be formulated via dissipativity:

- (asymptotic) stability of the equilibrium x^e can be concluded for all solutions if the system is (strictly) dissipative, $s(x,u) \leq 0$ and the storage function λ is bounded from below and above by $\mathcal{K}_\infty$-functions in $\|x - x^e\|$
  $(\mathcal{K}_\infty\text{-functions} = \text{unbounded } \mathcal{K}\text{-functions})$

- input-to-state stability of the equilibrium x^e can be concluded if the system is strictly dissipative, $s(x,u)$ is continuous and bounded from above by a $\mathcal{K}$-function in $\|u\|$ and the storage function λ is bounded from below and above by $\mathcal{K}_\infty$-functions in $\|x - x^e\|$

In both cases, λ is a Lyapunov function

Lars Grüne, On the relation between dissipativity and the turnpike property, p. 10

UNIVERSITÄT BAYREUTH

Applications

Dissipativity is also a very useful tool for analysing networks of systems:

under suitable conditions, a network of (strictly) dissipative systems is (strictly) dissipative, itself

Lars Grüne, On the relation between dissipativity and the turnpike property, p. 11

UNIVERSITÄT BAYREUTH

Applications

Dissipativity is also a very useful tool for analysing networks of systems:

under suitable conditions, a network of (strictly) dissipative systems is (strictly) dissipative, itself

Finally, strict dissipativity plays a major role in the analysis of so called economic model predictive control schemes (details later)

Lars Grüne, On the relation between dissipativity and the turnpike property, p. 11

UNIVERSITÄT BAYREUTH

Available storage

Theorem [Willems '72, Byrnes/Lin '94] A system is [strictly] dissipative with supply rate s [and $\alpha \in \mathcal{K}$] if and only if

$$\lambda(x) := \sup_{K,\mathbf{u}} \sum_{k=0}^{K-1} -s(x_\mathbf{u}(k),\mathbf{u}(k)) \left[+\alpha(\|x_\mathbf{u}(k) - x^e\|) \right] < \infty$$

for all $x = x_\mathbf{u}(0) \in X$.

Lars Grüne, On the relation between dissipativity and the turnpike property, p. 12

UNIVERSITÄT BAYREUTH

Available storage

Theorem [Willems '72, Byrnes/Lin '94] A system is [strictly] dissipative with supply rate s [and $\alpha \in \mathcal{K}$] if and only if

$$\sup_{K,\mathbf{u}} \sum_{k=0}^{K-1} -s(x_\mathbf{u}(k),\mathbf{u}(k)) \left[+\alpha(\|x_\mathbf{u}(k) - x^e\|) \right] < \infty$$

for all $x = x_\mathbf{u}(0) \in X$.

Lars Grüne, On the relation between dissipativity and the turnpike property, p. 12

UNIVERSITÄT BAYREUTH

Available storage

Theorem [Willems '72, Byrnes/Lin '94] A system is [strictly] dissipative with supply rate s [and $\alpha \in \mathcal{K}$] if and only if

$$\lambda(x) := \sup_{K,\mathbf{u}} \sum_{k=0}^{K-1} -s(x_\mathbf{u}(k),\mathbf{u}(k)) \left[+\alpha(\|x_\mathbf{u}(k) - x^e\|) \right] < \infty$$

for all $x = x_\mathbf{u}(0) \in X$. In this case, λ is a storage function

Lars Grüne, On the relation between dissipativity and the turnpike property, p. 12

UNIVERSITÄT BAYREUTH

Available storage

Theorem [Willems '72, Byrnes/Lin '94] A system is [strictly] dissipative with supply rate s [and $\alpha \in \mathcal{K}$] if and only if

$$\lambda(x) := \sup_{K,\mathbf{u}} \sum_{k=0}^{K-1} -s(x_\mathbf{u}(k),\mathbf{u}(k)) \left[+\alpha(\|x_\mathbf{u}(k)-x^e\|) \right] < \infty$$

for all $x = x_\mathbf{u}(0) \in X$. In this case, λ is a storage function

The proof of this theorem essentially relies on the dynamic programming principle

The particular storage function defined above is called

"available storage"

The turnpike property

The turnpike property describes a behaviour of (approximately) optimal trajectories for a finite horizon optimal control problem

$$\text{minimise} \quad J_N(x,\mathbf{u}) = \sum_{n=0}^{N-1} \ell(x_\mathbf{u}(n),\mathbf{u}(n))$$

The turnpike property

The turnpike property describes a behaviour of (approximately) optimal trajectories for a finite horizon optimal control problem

$$\underset{\mathbf{u}}{\text{minimise}} \;\; J_N(x, \mathbf{u}) = \sum_{n=0}^{N-1} \ell(x_{\mathbf{u}}(n), \mathbf{u}(n))$$

Informal description: an (approximately) optimal trajectory stays near an equilibrium x^e most of the time

We illustrate the property by two simple examples

UNIVERSITÄT
BAYREUTH

Lars Grüne, On the relation between dissipativity and the turnpike property, p. 14

Example 1: minimum energy control

Example: Keep the state of the system inside a given interval X minimising the quadratic control effort

$$\ell(x, u) = u^2$$

with dynamics

$$x^+ = 2x + u$$

and spaces $X = [-2, 2]$, $U = [-3, 3]$

For this example, the closer the state is to $x^e = 0$, the cheaper it is to keep the system inside X

UNIVERSITÄT
BAYREUTH

Lars Grüne, On the relation between dissipativity and the turnpike property, p. 15

Example 1: minimum energy control

Example: Keep the state of the system inside a given interval X minimising the quadratic control effort

$$\ell(x,u) = u^2$$

with dynamics

$$x^+ = 2x + u$$

and spaces $X = [-2,2]$, $U = [-3,3]$

For this example, the closer the state is to $x^e = 0$, the cheaper it is to keep the system inside X

⇝ optimal trajectory should stay near $x^e = 0$

Lars Grüne, On the relation between dissipativity and the turnpike property, p. 15

UNIVERSITÄT
BAYREUTH

Example 1: optimal trajectories

Optimal trajectory for $N = 5$

Lars Grüne, On the relation between dissipativity and the turnpike property, p. 16

UNIVERSITÄT
BAYREUTH

Example 1: optimal trajectories

Optimal trajectories for $N = 5, \ldots, 7$

Lars Grüne, On the relation between dissipativity and the turnpike property, p. 16

UNIVERSITÄT
BAYREUTH

Example 1: optimal trajectories

Optimal trajectories for $N = 5, \ldots, 9$

Lars Grüne, On the relation between dissipativity and the turnpike property, p. 16

UNIVERSITÄT
BAYREUTH

Example 1: optimal trajectories

Optimal trajectories for $N = 5, \ldots, 11$

Lars Grüne, On the relation between dissipativity and the turnpike property, p. 16

Example 1: optimal trajectories

Optimal trajectories for $N = 5, \ldots, 13$

Lars Grüne, On the relation between dissipativity and the turnpike property, p. 16

Example 1: optimal trajectories

Optimal trajectories for $N = 5, \ldots, 15$

Lars Grüne, On the relation between dissipativity and the turnpike property, p. 16

Example 1: optimal trajectories

Optimal trajectories for $N = 5, \ldots, 17$

Lars Grüne, On the relation between dissipativity and the turnpike property, p. 16

Example 1: optimal trajectories

Optimal trajectories for $N = 5, \ldots, 19$

Lars Grüne, On the relation between dissipativity and the turnpike property, p. 16

Example 1: optimal trajectories

Optimal trajectories for $N = 5, \ldots, 21$

Lars Grüne, On the relation between dissipativity and the turnpike property, p. 16

Example 1: optimal trajectories

Optimal trajectories for $N = 5, \ldots, 23$

Lars Grüne, On the relation between dissipativity and the turnpike property, p. 16

Example 1: optimal trajectories

Optimal trajectories for $N = 5, \ldots, 25$

Lars Grüne, On the relation between dissipativity and the turnpike property, p. 16

Example 2: a macroeconomic model

The second example is a 1d macroeconomic model

[Brock/Mirman '72]

Minimise the finite horizon objective with

$$\ell(x,u) = -\ln(Ax^\alpha - u), \quad A = 5, \quad \alpha = 0.34$$

with dynamics $\quad x^+ = u$

on $\quad X = U = [0,10]$

Here the optimal trajectories are less obvious

UNIVERSITÄT
BAYREUTH

Example 2: optimal trajectories

Optimal trajectory for $N = 5$

Lars Grüne, On the relation between dissipativity and the turnpike property, p. 18

UNIVERSITÄT BAYREUTH

Example 2: optimal trajectories

Optimal trajectories for $N = 5, \ldots, 7$

Lars Grüne, On the relation between dissipativity and the turnpike property, p. 18

UNIVERSITÄT BAYREUTH

Example 2: optimal trajectories

Optimal trajectories for $N = 5, \ldots, 9$

Lars Grüne, On the relation between dissipativity and the turnpike property, p. 18

UNIVERSITÄT BAYREUTH

Example 2: optimal trajectories

Optimal trajectories for $N = 5, \ldots, 11$

Lars Grüne, On the relation between dissipativity and the turnpike property, p. 18

UNIVERSITÄT BAYREUTH

Example 2: optimal trajectories

Optimal trajectories for $N = 5, \ldots, 13$

Lars Grüne, On the relation between dissipativity and the turnpike property, p. 18

Example 2: optimal trajectories

Optimal trajectories for $N = 5, \ldots, 15$

Lars Grüne, On the relation between dissipativity and the turnpike property, p. 18

Example 2: optimal trajectories

Optimal trajectories for $N = 5, \ldots, 17$

Lars Grüne, On the relation between dissipativity and the turnpike property, p. 18

Example 2: optimal trajectories

Optimal trajectories for $N = 5, \ldots, 19$

Lars Grüne, On the relation between dissipativity and the turnpike property, p. 18

Example 2: optimal trajectories

Optimal trajectories for $N = 5, \ldots, 23$

Lars Grüne, On the relation between dissipativity and the turnpike property, p. 18

UNIVERSITÄT
BAYREUTH

How to formalize the turnpike property?

Lars Grüne, On the relation between dissipativity and the turnpike property, p. 19

UNIVERSITÄT
BAYREUTH

Example 2: optimal trajectories

Optimal trajectories for $N = 5, \ldots, 21$

Lars Grüne, On the relation between dissipativity and the turnpike property, p. 18

UNIVERSITÄT
BAYREUTH

Example 2: optimal trajectories

Optimal trajectories for $N = 5, \ldots, 25$

Lars Grüne, On the relation between dissipativity and the turnpike property, p. 18

UNIVERSITÄT
BAYREUTH

How to formalize the turnpike property?

Number of points outside the blue neighbourhood is bounded by a number independent of N (here: by 8)

UNIVERSITÄT BAYREUTH

The turnpike property: formal definitions

Let x^e be an equilibrium, i.e., $f(x^e, u^e) = x^e$

Define the optimal value function $V_N(x) := \inf_{\mathbf{u}} J_N(x, \mathbf{u})$

UNIVERSITÄT BAYREUTH

The turnpike property: formal definitions

Let x^e be an equilibrium, i.e., $f(x^e, u^e) = x^e$

Define the optimal value function $V_N(x) := \inf_{\mathbf{u}} J_N(x, \mathbf{u})$

Turnpike property: There is $C > 0$ and $\rho \in \mathcal{K}_\infty$ such that for all $x \in X$ and $N \in \mathbb{N}$, all optimal trajectories $x^\star$ with $x^\star(0) = x$ and all $\varepsilon > 0$, the number

$$Q_\varepsilon := \#\{k \in \{0, \ldots, N-1\} \mid \|x^\star(k) - x^e\| \geq \varepsilon\}$$

satisfies $Q_\varepsilon \leq C/\rho(\varepsilon)$

Near optimal turnpike property: There is $C > 0$ and $\rho \in \mathcal{K}_\infty$ such that for all $x \in X$, $N \in \mathbb{N}$ and $\delta > 0$, all trajectories $x_{\mathbf{u}}$ with $J_N(x, \mathbf{u}) \leq V_N(x) + \delta$ and all $\varepsilon > 0$, the number

$$Q_\varepsilon := \#\{k \in \{0, \ldots, N-1\} \mid \|x_{\mathbf{u}}(k) - x^e\| \geq \varepsilon\}$$

satisfies $Q_\varepsilon \leq (C + \delta)/\rho(\varepsilon)$

UNIVERSITÄT BAYREUTH

Lars Grüne, On the relation between dissipativity and the turnpike property, p. 20

History

- Apparently first described by [von Neumann 1945]

- Name "turnpike property" coined by [Dorfman/Samuelson/Solow 1957]

UNIVERSITÄT BAYREUTH

Lars Grüne, On the relation between dissipativity and the turnpike property, p. 21

History

- Apparently first described by [von Neumann 1945]
- Name "turnpike property" coined by [Dorfman/Samuelson/Solow 1957]
- Extensively studied in the 1970s in mathematical economy, cf. survey [McKenzie 1983]

Applications

Economists are interested in the turnpike property because it gives structural insight about optimal economic equilibria and the optimal trajectories' tendency to stay near them

History

- Apparently first described by [von Neumann 1945]
- Name "turnpike property" coined by [Dorfman/Samuelson/Solow 1957]

History

- Apparently first described by [von Neumann 1945]
- Name "turnpike property" coined by [Dorfman/Samuelson/Solow 1957]
- Extensively studied in the 1970s in mathematical economy, cf. survey [McKenzie 1983]
- Renewed interest in recent years [Zaslavski '14, Trélat/Zuazua '15, Faulwasser et al. '15, ...]

Applications

Economists are interested in the turnpike property because it gives structural insight about optimal economic equilibria and the optimal trajectories' tendency to stay near them

The finite horizon turnpike property at an equilibrium is also closely related to the convergence of infinite horizon optimal trajectories towards this equilibrium

Lars Grüne, On the relation between dissipativity and the turnpike property, p. 22

UNIVERSITÄT BAYREUTH

Applications

The turnpike property can be used for the synthesis of optimal trajectories on long time horizons

Lars Grüne, On the relation between dissipativity and the turnpike property, p. 23

UNIVERSITÄT BAYREUTH

Applications

The turnpike property can be used for the synthesis of optimal trajectories on long time horizons:

Knowing that the system has the turnpike property allows to reduce the computation task to computing the equilibrium and the best way to approach it and to leave it

Lars Grüne, On the relation between dissipativity and the turnpike property, p. 23

UNIVERSITÄT BAYREUTH

Applications

The turnpike property can be used for the synthesis of optimal trajectories on long time horizons:

Knowing that the system has the turnpike property allows to reduce the computation task to computing the equilibrium and the best way to approach it and to leave it

Ideas of this type can be found, e.g., in [Anderson/Kokotovic '87]

Lars Grüne, On the relation between dissipativity and the turnpike property, p. 23

UNIVERSITÄT BAYREUTH

Application: Model predictive control

Turnpike properties are also pivotal for analysing economic Model Predictive Control (MPC) schemes

MPC is a method in which an optimal control problem on an infinite horizon

$$\underset{\mathbf{u}}{\text{minimise }} J_\infty(x, \mathbf{u}) = \sum_{n=0}^{\infty} \ell(x_{\mathbf{u}}(n), \mathbf{u}(n))$$

is approximated by the iterative solution of finite horizon problems

$$\underset{\mathbf{u}}{\text{minimise }} J_N(x, \mathbf{u}) = \sum_{n=0}^{N-1} \ell(x_{\mathbf{u}}(k), \mathbf{u}(k))$$

with fixed $N \in \mathbb{N}$

UNIVERSITÄT
BAYREUTH

Lars Grüne, On the relation between dissipativity and the turnpike property, p. 24

MPC from the trajectory point of view
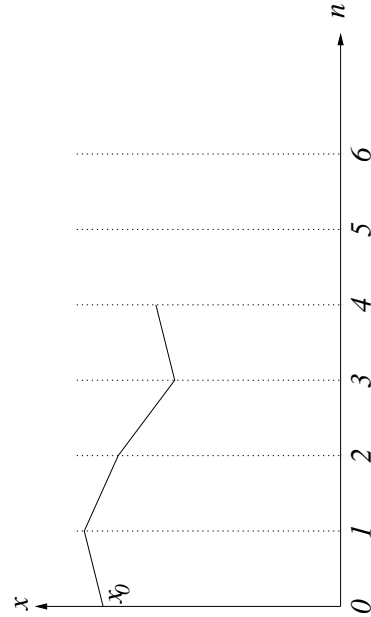
black = predictions (open loop optimization)

UNIVERSITÄT
BAYREUTH

Lars Grüne, On the relation between dissipativity and the turnpike property, p. 25

MPC from the trajectory point of view

black = predictions (open loop optimization)

red = MPC closed loop

Lars Grüne, On the relation between dissipativity and the turnpike property, p. 25

UNIVERSITÄT BAYREUTH

MPC from the trajectory point of view

black = predictions (open loop optimization)

red = MPC closed loop

Lars Grüne, On the relation between dissipativity and the turnpike property, p. 25

UNIVERSITÄT BAYREUTH

MPC from the trajectory point of view

black = predictions (open loop optimization)

red = MPC closed loop

Lars Grüne, On the relation between dissipativity and the turnpike property, p. 25

UNIVERSITÄT BAYREUTH

MPC from the trajectory point of view

black = predictions (open loop optimization)

red = MPC closed loop

Lars Grüne, On the relation between dissipativity and the turnpike property, p. 25

UNIVERSITÄT BAYREUTH

MPC from the trajectory point of view

black = predictions (open loop optimization)

red   = MPC closed loop

Lars Grüne, On the relation between dissipativity and the turnpike property, p. 25

UNIVERSITÄT
BAYREUTH

MPC from the trajectory point of view

black = predictions (open loop optimization)

red   = MPC closed loop

Lars Grüne, On the relation between dissipativity and the turnpike property, p. 25

UNIVERSITÄT
BAYREUTH

MPC from the trajectory point of view

black = predictions (open loop optimization)

red   = MPC closed loop

Lars Grüne, On the relation between dissipativity and the turnpike property, p. 25

UNIVERSITÄT
BAYREUTH

MPC from the trajectory point of view

black = predictions (open loop optimization)

red   = MPC closed loop

Lars Grüne, On the relation between dissipativity and the turnpike property, p. 25

UNIVERSITÄT
BAYREUTH

MPC from the trajectory point of view

black = predictions (open loop optimization)

red = MPC closed loop

Lars Grüne, On the relation between dissipativity and the turnpike property, p. 25

UNIVERSITÄT
BAYREUTH

MPC from the trajectory point of view

black = predictions (open loop optimization)

red = MPC closed loop

Lars Grüne, On the relation between dissipativity and the turnpike property, p. 25

UNIVERSITÄT
BAYREUTH

Approximation result for MPC

If the finite horizon problems have the turnpike property, then a rigorous approximation result can be proved

Lars Grüne, On the relation between dissipativity and the turnpike property, p. 26

UNIVERSITÄT
BAYREUTH

MPC from the trajectory point of view

black = predictions (open loop optimization)

red = MPC closed loop

Lars Grüne, On the relation between dissipativity and the turnpike property, p. 25

UNIVERSITÄT
BAYREUTH

Approximation result for MPC

If the finite horizon problems have the turnpike property, then a rigorous approximation result can be proved

The result exploits that the **red** closed loop trajectory approximately follows the first part of the **black** predictions up to the equilibrium

We illustrate this behaviour by our second example for $N = 10$

Lars Grüne, On the relation between dissipativity and the turnpike property, p. 26

UNIVERSITÄT
BAYREUTH

MPC for Example 2

Lars Grüne, On the relation between dissipativity and the turnpike property, p. 27

UNIVERSITÄT
BAYREUTH

Lars Grüne, On the relation between dissipativity and the turnpike property, p. 26

UNIVERSITÄT
BAYREUTH

MPC for Example 2

Lars Grüne, On the relation between dissipativity and the turnpike property, p. 27

UNIVERSITÄT
BAYREUTH

MPC for Example 2

Lars Grüne, On the relation between dissipativity and the turnpike property, p. 27

MPC for Example 2

Lars Grüne, On the relation between dissipativity and the turnpike property, p. 27

MPC for Example 2

Lars Grüne, On the relation between dissipativity and the turnpike property, p. 27

MPC for Example 2

Lars Grüne, On the relation between dissipativity and the turnpike property, p. 27

MPC for Example 2

Lars Grüne, On the relation between dissipativity and the turnpike property, p. 27

MPC for Example 2

Lars Grüne, On the relation between dissipativity and the turnpike property, p. 27

MPC for Example 2

Lars Grüne, On the relation between dissipativity and the turnpike property, p. 27

MPC for Example 2

Lars Grüne, On the relation between dissipativity and the turnpike property, p. 27

MPC for Example 2

Lars Grüne, On the relation between dissipativity and the turnpike property, p. 27

UNIVERSITÄT
BAYREUTH

MPC for Example 2

Lars Grüne, On the relation between dissipativity and the turnpike property, p. 27

UNIVERSITÄT
BAYREUTH

MPC for Example 2

Lars Grüne, On the relation between dissipativity and the turnpike property, p. 27

UNIVERSITÄT
BAYREUTH

MPC for Example 2

Lars Grüne, On the relation between dissipativity and the turnpike property, p. 27

UNIVERSITÄT
BAYREUTH

MPC for Example 2

Lars Grüne, On the relation between dissipativity and the turnpike property, p. 27

MPC for Example 2

Lars Grüne, On the relation between dissipativity and the turnpike property, p. 27

MPC for Example 2

Lars Grüne, On the relation between dissipativity and the turnpike property, p. 27

MPC for Example 2

Lars Grüne, On the relation between dissipativity and the turnpike property, p. 27

MPC for Example 2

Lars Grüne, On the relation between dissipativity and the turnpike property, p. 27

MPC for Example 2

Lars Grüne, On the relation between dissipativity and the turnpike property, p. 27

MPC for Example 2

Lars Grüne, On the relation between dissipativity and the turnpike property, p. 27

MPC for Example 2

Lars Grüne, On the relation between dissipativity and the turnpike property, p. 27

MPC for Example 2

Lars Grüne, On the relation between dissipativity and the turnpike property, p. 27

MPC for Example 2

Lars Grüne, On the relation between dissipativity and the turnpike property, p. 27

MPC for Example 2

Lars Grüne, On the relation between dissipativity and the turnpike property, p. 27

MPC for Example 2

Lars Grüne, On the relation between dissipativity and the turnpike property, p. 27

MPC for Example 2

Lars Grüne, On the relation between dissipativity and the turnpike property, p. 27

UNIVERSITÄT
BAYREUTH

MPC for Example 2

Lars Grüne, On the relation between dissipativity and the turnpike property, p. 27

UNIVERSITÄT
BAYREUTH

MPC for Example 2

Lars Grüne, On the relation between dissipativity and the turnpike property, p. 27

UNIVERSITÄT
BAYREUTH

MPC for Example 2

Lars Grüne, On the relation between dissipativity and the turnpike property, p. 27

UNIVERSITÄT
BAYREUTH

Known results

We say that x^e is cheaply reachable if there is $E > 0$ such that
$V_N(x) \leq N\ell(x^e, u^e) + E$ for all $x \in X$, $N \in \mathbb{N}$

UNIVERSITÄT
BAYREUTH

Known results

We say that x^e is cheaply reachable if there is $E > 0$ such that
$V_N(x) \leq N\ell(x^e, u^e) + E$ for all $x \in X$, $N \in \mathbb{N}$

Theorem [Gr. '13] If the system is strictly dissipative with
supply rate $s(x, u) = \ell(x, u) - \ell(x^e, u^e)$ and bounded storage
function λ and x^e is cheaply reachable, then the near optimal
turnpike property holds

(In fact, similar statements can be found in earlier papers and
monographs, e.g. in [Carlson/Haurie/Leizarowitz '91])

UNIVERSITÄT
BAYREUTH

Known results

Known results

We say that x^e is cheaply reachable if there is $E > 0$ such that
$V_N(x) \leq N\ell(x^e, u^e) + E$ for all $x \in X$, $N \in \mathbb{N}$

Theorem [Gr. '13] If the system is strictly dissipative with
supply rate $s(x, u) = \ell(x, u) - \ell(x^e, u^e)$ and bounded storage
function λ and x^e is cheaply reachable, then the near optimal
turnpike property holds

UNIVERSITÄT
BAYREUTH

302

Known results

We say that x^e is cheaply reachable if there is $E > 0$ such that
$V_N(x) \leq N\ell(x^e, u^e) + E$ for all $x \in X$, $N \in \mathbb{N}$

Theorem [Gr. '13] If the system is strictly dissipative with supply rate $s(x,u) = \ell(x,u) - \ell(x^e, u^e)$ and bounded storage function λ and x^e is cheaply reachable, then the near optimal turnpike property holds

Idea of proof: Near optimality and cheap reachability implies
$$J_N(x,u) \leq N\ell(x^e, u^e) + E + \delta$$

Strict dissipativity with bounded λ implies
$$J_N(x,u) \geq N\ell(x^e, u^e) - C + \sum_{k=0}^{N-1} \alpha(\|x_\mathbf{u}(k) - x^e\|)$$

UNIVERSITÄT BAYREUTH

Lars Grüne, On the relation between dissipativity and the turnpike property, p. 29

Known results

We say that x^e is cheaply reachable if there is $E > 0$ such that
$V_N(x) \leq N\ell(x^e, u^e) + E$ for all $x \in X$, $N \in \mathbb{N}$

Theorem [Gr. '13] If the system is strictly dissipative with supply rate $s(x,u) = \ell(x,u) - \ell(x^e, u^e)$ and bounded storage function λ and x^e is cheaply reachable, then the near optimal turnpike property holds

Note: Boundedness of λ is typically unrealistic to expect when X is unbounded.

UNIVERSITÄT BAYREUTH

Lars Grüne, On the relation between dissipativity and the turnpike property, p. 29

Known results

We say that x^e is cheaply reachable if there is $E > 0$ such that
$V_N(x) \leq N\ell(x^e, u^e) + E$ for all $x \in X$, $N \in \mathbb{N}$

Theorem [Gr. '13] If the system is strictly dissipative with supply rate $s(x,u) = \ell(x,u) - \ell(x^e, u^e)$ and bounded storage function λ and x^e is cheaply reachable, then the near optimal turnpike property holds

Idea of proof: Near optimality and cheap reachability implies
$$J_N(x,u) \leq N\ell(x^e, u^e) + E + \delta$$

Strict dissipativity with bounded λ implies
$$J_N(x,u) \geq N\ell(x^e, u^e) - C + \sum_{k=0}^{N-1} \alpha(\|x_\mathbf{u}(k) - x^e\|)$$

$\Rightarrow$ if $\|x_\mathbf{u}(k) - x^e\| \geq \varepsilon$ for K times $k \in \{0, \ldots, N-1\}$, then
$J_N(x,\mathbf{u}) - N\ell(x^e, u^e) \to \infty$ as $K, N \to \infty$, contradicting near optimality

UNIVERSITÄT BAYREUTH

Lars Grüne, On the relation between dissipativity and the turnpike property, p. 29

Known results

We say that x^e is cheaply reachable if there is $E > 0$ such that
$V_N(x) \leq N\ell(x^e, u^e) + E$ for all $x \in X$, $N \in \mathbb{N}$

Theorem [Gr. '13] If the system is strictly dissipative with supply rate $s(x,u) = \ell(x,u) - \ell(x^e, u^e)$ and bounded storage function λ and x^e is cheaply reachable, then the near optimal turnpike property holds

Idea of proof: Near optimality and cheap reachability implies
$$J_N(x,u) \leq N\ell(x^e, u^e) + E + \delta$$

Strict dissipativity with bounded λ implies
$$J_N(x,u) \geq N\ell(x^e, u^e) - C + \sum_{k=0}^{N-1} \alpha(\|x_\mathbf{u}(k) - x^e\|)$$

UNIVERSITÄT BAYREUTH

Lars Grüne, On the relation between dissipativity and the turnpike property, p. 29

Known results

We say that x^e is cheaply reachable if there is $E > 0$ such that $V_N(x) \leq N\ell(x^e, u^e) + E$ for all $x \in X$, $N \in \mathbb{N}$

Theorem [Gr. '13] If the system is strictly dissipative with supply rate $s(x,u) = \ell(x,u) - \ell(x^e, u^e)$ and bounded storage function λ and x^e is cheaply reachable, then the near optimal turnpike property holds

Note: Boundedness of λ is typically unrealistic to expect when X is unbounded. However, here we are only interested in the behaviour of the trajectories in a bounded region around x^e, where this assumption is reasonable.

Lars Grüne, On the relation between dissipativity and the turnpike property, p. 29

UNIVERSITÄT
BAYREUTH

Known results

We say that x^e is cheaply reachable if there is $E > 0$ such that $V_N(x) \leq N\ell(x^e, u^e) + E$ for all $x \in X$, $N \in \mathbb{N}$

Theorem [Gr. '13] If the system is strictly dissipative with supply rate $s(x,u) = \ell(x,u) - \ell(x^e, u^e)$ and bounded storage function λ and x^e is cheaply reachable, then the near optimal turnpike property holds

Note: Boundedness of λ is typically unrealistic to expect when X is unbounded. However, here we are only interested in the behaviour of the trajectories in a bounded region around x^e, where this assumption is reasonable. If desired, boundedness can be replaced by other assumptions, e.g., coercivity

Lars Grüne, On the relation between dissipativity and the turnpike property, p. 29

UNIVERSITÄT
BAYREUTH

Known results

We say that x^e is cheaply reachable if there is $E > 0$ such that $V_N(x) \leq N\ell(x^e, u^e) + E$ for all $x \in X$, $N \in \mathbb{N}$

Theorem [Gr. '13] If the system is strictly dissipative with supply rate $s(x,u) = \ell(x,u) - \ell(x^e, u^e)$ and bounded storage function λ and x^e is cheaply reachable, then the near optimal turnpike property holds

Question

Conclusion: Strict dissipativity can be used as a checkable condition for the turnpike property

Lars Grüne, On the relation between dissipativity and the turnpike property, p. 30

UNIVERSITÄT
BAYREUTH

Question

Conclusion: Strict dissipativity can be used as a checkable condition for the turnpike property

Question: How conservative is this condition, i.e., how much stronger is strict dissipativity than the turnpike property?

In fact, the theorem just presented relies on another theorem which does not require cheap reachability

Known results

Near equilibrium turnpike property: There is $C > 0$ and $\rho \in \mathcal{K}_\infty$ such that for all $x \in X$, $N \in \mathbb{N}$ and $\delta > 0$, all trajectories $x_\mathbf{u}$ with $J_N(x, \mathbf{u}) \leq N\ell(x^e, u^e) + \delta$ and all $\varepsilon > 0$, the number

$$Q_\varepsilon := \#\{k \in \{0,\ldots,N-1\} \,|\, \|x_\mathbf{u}(k) - x^e\| \geq \varepsilon\}$$

satisfies $Q_\varepsilon \leq (C+\delta)/\rho(\varepsilon)$

Theorem [Gr. '13] If the system is strictly dissipative with supply rate $s(x,u) = \ell(x,u) - \ell(x^e, u^e)$ and bounded storage function, then the near equilibrium turnpike property holds

Question

Conclusion: Strict dissipativity can be used as a checkable condition for the turnpike property

Question: How conservative is this condition, i.e., how much stronger is strict dissipativity than the turnpike property?

In fact, the theorem just presented relies on another theorem which does not require cheap reachability

Lars Grüne, On the relation between dissipativity and the turnpike property, p. 30

UNIVERSITÄT BAYREUTH

Known results

Near equilibrium turnpike property: There is $C > 0$ and $\rho \in \mathcal{K}_\infty$ such that for all $x \in X$, $N \in \mathbb{N}$ and $\delta > 0$, all trajectories $x_\mathbf{u}$ with $J_N(x, \mathbf{u}) \leq N\ell(x^e, u^e) + \delta$ and all $\varepsilon > 0$, the number

$$Q_\varepsilon := \#\{k \in \{0,\ldots,N-1\} \,|\, \|x_\mathbf{u}(k) - x^e\| \geq \varepsilon\}$$

satisfies $Q_\varepsilon \leq (C+\delta)/\rho(\varepsilon)$

Theorem [Gr. '13] If the system is strictly dissipative with supply rate $s(x,u) = \ell(x,u) - \ell(x^e, u^e)$ and bounded storage function, then the near equilibrium turnpike property holds

Lars Grüne, On the relation between dissipativity and the turnpike property, p. 31

UNIVERSITÄT BAYREUTH

Known results

Near equilibrium turnpike property: There is $C > 0$ and $\rho \in \mathcal{K}_\infty$ such that for all $x \in X$, $N \in \mathbb{N}$ and $\delta > 0$, all trajectories $x_\mathbf{u}$ with $J_N(x,\mathbf{u}) \leq N\ell(x^e, u^e) + \delta$ and all $\varepsilon > 0$, the number

$$Q_\varepsilon := \#\{k \in \{0, \ldots, N-1\} \mid \|x_\mathbf{u}(k) - x^e\| \geq \varepsilon\}$$

satisfies $Q_\varepsilon \leq (C+\delta)/\rho(\varepsilon)$

Theorem [Gr. '13] If the system is strictly dissipative with supply rate $s(x,u) = \ell(x,u) - \ell(x^e, u^e)$ and bounded storage function, then the near equilibrium turnpike property holds

Note: the turnpike properties only differ in the condition on J_N:

Turnpike property:	$J_N(x,\mathbf{u}) \leq$	$V_N(x)$
Near optimal turnpike property:	$J_N(x,\mathbf{u}) \leq$	$V_N(x) + \delta$
Near equilibrium turnpike property:	$J_N(x,\mathbf{u}) \leq$	$N\ell(x^e, u^e) + \delta$

Lars Grüne, On the relation between dissipativity and the turnpike property, p. 31

UNIVERSITÄT BAYREUTH

New results

New result I

Theorem: The following statements are equivalent

(a) The system is strictly dissipative with supply rate
$s(x,u) = \ell(x,u) - \ell(x^e,u^e)$ and bounded storage function

(b) The near equilibrium turnpike property holds and x^e is uniformly near optimal, i.e., there is $D > 0$ with $V_N(x) + D \geq N\ell(x^e,u^e)$ for all $x \in X$, $N \in \mathbb{N}$

Lars Grüne, On the relation between dissipativity and the turnpike property, p. 33

UNIVERSITÄT BAYREUTH

New result I

Theorem: The following statements are equivalent

(a) The system is strictly dissipative with supply rate
$s(x,u) = \ell(x,u) - \ell(x^e,u^e)$ and bounded storage function

Lars Grüne, On the relation between dissipativity and the turnpike property, p. 33

UNIVERSITÄT BAYREUTH

New result I

Theorem: The following statements are equivalent

(a) The system is strictly dissipative with supply rate
$s(x,u) = \ell(x,u) - \ell(x^e,u^e)$ and bounded storage function

(b) The near equilibrium turnpike property holds and x^e is uniformly near optimal, i.e., there is $D > 0$ with $V_N(x) + D \geq N\ell(x^e,u^e)$ for all $x \in X$, $N \in \mathbb{N}$

(c) The near equilibrium turnpike property holds and the system is dissipative with supply rate
$s(x,u) = \ell(x,u) - \ell(x^e,u^e)$ and bounded storage function

Lars Grüne, On the relation between dissipativity and the turnpike property, p. 33

UNIVERSITÄT BAYREUTH

New result I

Theorem: The following statements are equivalent

(a) The system is strictly dissipative with supply rate
$s(x, u) = \ell(x, u) - \ell(x^e, u^e)$ and bounded storage function

(b) The near equilibrium turnpike property holds and
x^e is uniformly near optimal, i.e., there is $D > 0$ with
$V_N(x) + D \geq N\ell(x^e, u^e)$ for all $x \in X$, $N \in \mathbb{N}$

(c) The near equilibrium turnpike property holds and
the system is dissipative with supply rate
$s(x, u) = \ell(x, u) - \ell(x^e, u^e)$ and bounded storage function

In other words, the near equilibrium turnpike property exactly closes the gap between dissipativity and strict dissipativity

Lars Grüne, On the relation between dissipativity and the turnpike property, p. 33

UNIVERSITÄT BAYREUTH

Proof idea

We need to prove the equivalences of

(a) strict dissipativity
(b) near equilibrium turnpike and uniform near optim. of x^e
(c) near equilibrium turnpike and dissipativity

(b) ⇔ (c) follows by straightforward computation using the available storage for "⇒"

Lars Grüne, On the relation between dissipativity and the turnpike property, p. 34

UNIVERSITÄT BAYREUTH

Proof idea

We need to prove the equivalences of

(a) strict dissipativity
(b) near equilibrium turnpike and uniform near optim. of x^e
(c) near equilibrium turnpike and dissipativity

(b) ⇔ (c) follows by straightforward computation using the available storage for "⇒"

(a) ⇒ (c) follows from the known result from [Gr. '13]

Lars Grüne, On the relation between dissipativity and the turnpike property, p. 34

UNIVERSITÄT BAYREUTH

Proof idea

We need to prove the equivalences of

(a) strict dissipativity
(b) near equilibrium turnpike and uniform near optim. of x^e
(c) near equilibrium turnpike and dissipativity

(b) ⇔ (c) follows by straightforward computation using the available storage for "⇒"

(a) ⇒ (c) follows from the known result from [Gr. '13]
(c) ⇒ (a) follows from a rather technical construction of α in the strict dissipativity condition, using the available storage

Question: Can we get rid of dissipativity in (c)?

New result II

Corollary: Assume X is closed and U is compact, ℓ is continuous and bounded from below, x^e is an equilibrium around which the system is locally controllable and

$$u^e \in \mathrm{argmin}\{\ell(x^e, u) \mid x^e \in X,\ f(x^e, u) = x^e\}$$

Proof idea

We need to prove the equivalences of

(a) strict dissipativity
(b) near equilibrium turnpike and uniform near optim. of x^e
(c) near equilibrium turnpike and dissipativity

(b) ⇔ (c) follows by straightforward computation using the available storage for "⇒"

(a) ⇒ (c) follows from the known result from [Gr. '13]
(c) ⇒ (a) follows from a rather technical construction of α in the strict dissipativity condition, using the available storage

Question: Can we get rid of dissipativity in (c)?

Proof idea

We need to prove the equivalences of

(a) strict dissipativity
(b) near equilibrium turnpike and uniform near optim. of x^e
(c) near equilibrium turnpike and dissipativity

(b) ⇔ (c) follows by straightforward computation using the available storage for "⇒"

(a) ⇒ (c) follows from the known result from [Gr. '13]
(c) ⇒ (a) follows from a rather technical construction of α in the strict dissipativity condition, using the available storage

Question: Can we get rid of dissipativity in (c)?

Yes, if we use that the near equilibrium turnpike property induces an averaged form of optimality of x^e which under additional conditions implies dissipativity

[Müller '14, Müller/Angeli/Allgöwer '13]

New result II

Corollary: Assume X is closed and U is compact, ℓ is continuous and bounded from below, x^e is an equilibrium around which the system is locally controllable and $u^e \in \arg\min\{\ell(x^e,u)\,|\,x^e \in X,\, f(x^e,u)=x^e\}$

Then the following statements are equivalent

(a) The system is strictly dissipative with supply rate $s(x,u)=\ell(x,u)-\ell(x^e,u^e)$ and bounded storage function

(b) The near equilibrium turnpike property holds

Question: Is local controllability really needed?

UNIVERSITÄT BAYREUTH

Example

$$x^+ = \frac{1}{2}x \qquad \text{and} \qquad \ell(x,u)=u^2+\frac{\log 2}{\log|x|}$$

The system has (all three kinds of) the turnpike property at $x^e=0$, because all solutions converge to 0

However, one computes that the available storage satisfies

$$\lambda(x) := \sup_{K,u}\sum_{k=0}^{K-1} -\big(\ell(x(k),u(k))-\ell(x^e,u^e)\big) = \infty,$$

because $\log|x| \to -\infty$ too slowly as $|x|\to 0$

UNIVERSITÄT BAYREUTH

Example

$$x^+ = \frac{1}{2}x \quad \text{and} \quad \ell(x,u) = u^2 + \frac{\log 2}{\log |x|}$$

The system has (all three kinds of) the turnpike property at $x^e = 0$, because all solutions converge to 0

However, one computes that the available storage satisfies

$$\lambda(x) := \sup_{K,u} \sum_{k=0}^{K-1} -\big(\ell(x(k),u(k)) - \ell(x^e,u^e)\big) = \infty,$$

because $\log |x| \to -\infty$ too slowly as $|x| \to 0$. Hence the system is not dissipative and thus also not strictly dissipative

Since all other assumptions of the previous corollary are satisfied, it is the lack of controllability which makes its statement fail

UNIVERSITÄT BAYREUTH

Towards new result III

Recall the first two equivalences in the first theorem:

Theorem: The following statements are equivalent

(a) The system is strictly dissipative with supply rate $s(x,u) = \ell(x,u) - \ell(x^e,u^e)$ and bounded storage function

(b) The near equilibrium turnpike property holds and the equilibrium is uniformly near optimal

Can we replace the near equilibrium turnpike property by the (more intuitive and "classical") near optimal turnpike property?

UNIVERSITÄT BAYREUTH

311

Towards new result III

Recall the first two equivalences in the first theorem:

Theorem: The following statements are equivalent

(a) The system is strictly dissipative with supply rate $s(x,u) = \ell(x,u) - \ell(x^e, u^e)$ and bounded storage function

(b) The near equilibrium turnpike property holds and the equilibrium is uniformly near optimal

Can we replace the near equilibrium turnpike property by the (more intuitive and "classical") near optimal turnpike property?

Yes, but again we need additional assumptions

New result III

Theorem: Assume ℓ is bounded and the system is locally controllable around x^e

Then the following statements are equivalent

(a) The system is strictly dissipative with supply rate $s(x,u) = \ell(x,u) - \ell(x^e, u^e)$ and bounded storage function and x^e is cheaply reachable

(b) The near optimal turnpike property holds and x^e is uniformly near optimal

New result III

Theorem: Assume ℓ is bounded and the system is locally controllable around x^e

Then the following statements are equivalent

(a) The system is strictly dissipative with supply rate $s(x,u) = \ell(x,u) - \ell(x^e, u^e)$ and bounded storage function and x^e is cheaply reachable

(b) The near optimal turnpike property holds and x^e is uniformly near optimal

New result III

Theorem: Assume ℓ is bounded and the system is locally controllable around x^e

Then the following statements are equivalent

(a) The system is strictly dissipative with supply rate $s(x,u) = \ell(x,u) - \ell(x^e, u^e)$ and bounded storage function and x^e is cheaply reachable

(b) The near optimal turnpike property holds and x^e is uniformly near optimal

Idea of proof: cheap reachability and uniform near optimality of x^e, respectively, allow to pass from the near equilibrium to the near optimal turnpike property and vice versa

Note: the implication "(b) $\Rightarrow$ strict dissipativity" also holds without assuming local controllability

UNIVERSITÄT BAYREUTH

Application: shape of turnpike trajectories

As usually defined, the turnpike property only limits the number of time instances at which the trajectory is outside an ε-neighbourhood of x^e

Hence, according to the definition, a turnpike trajectory could look like this

Lars Grüne, On the relation between dissipativity and the turnpike property, p. 39

UNIVERSITÄT BAYREUTH
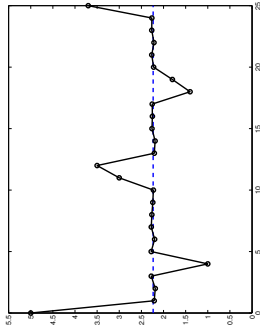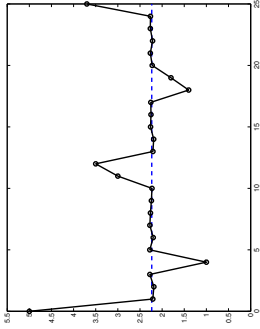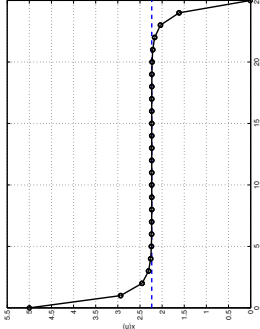
Application: shape of turnpike trajectories

As usually defined, the turnpike property only limits the number of time instances at which the trajectory is outside an ε-neighbourhood of x^e

Hence, according to the definition, a turnpike trajectory could look like this

Lars Grüne, On the relation between dissipativity and the turnpike property, p. 39

UNIVERSITÄT BAYREUTH

Application: shape of turnpike trajectories

As usually defined, the turnpike property only limits the number of time instances at which the trajectory is outside an ε-neighbourhood of x^e

However, in practice in many examples turnpike trajectories look like this

Lars Grüne, On the relation between dissipativity and the turnpike property, p. 39

UNIVERSITÄT BAYREUTH

Application: shape of turnpike trajectories

As usually defined, the turnpike property only limits the number of time instances at which the trajectory is outside an ε-neighbourhood of x^e

Lars Grüne, On the relation between dissipativity and the turnpike property, p. 40

UNIVERSITÄT BAYREUTH

Application: shape of turnpike trajectories

This is because under the stated conditions the turnpike property implies strict dissipativity, which in turn implies stability of the optimal trajectories, in the sense that if $x^\star(k) \approx x^e$ then $x^\star(k+p) \approx x^e$ for k, p sufficiently small relative to N [Gr. 13]

UNIVERSITÄT
BAYREUTH

Conclusions

- We have established equivalence relations between two classical properties from mathematical systems theory and optimal control, respectively

UNIVERSITÄT
BAYREUTH

Application: shape of turnpike trajectories

This is because under the stated conditions the turnpike property implies strict dissipativity, which in turn implies stability of the optimal trajectories, in the sense that if $x^\star(k) \approx x^e$ then $x^\star(k+p) \approx x^e$ for k, p sufficiently small relative to N [Gr. 13]

This excludes excursions from x^e except at the end of the optimal trajecory

UNIVERSITÄT
BAYREUTH

Conclusions

- We have established equivalence relations between two classical properties from mathematical systems theory and optimal control, respectively
- Under a local controllability condition, equivalence between strict dissipativity and the near equilibrium turnpike property holds

UNIVERSITÄT
BAYREUTH

Conclusions

- We have established equivalence relations between two classical properties from mathematical systems theory and optimal control, respectively
- Under a local controllability condition, equivalence between strict dissipativity and the near equilibrium turnpike property holds
- Under appropriate bounds on the value function (i.e., cheap reachability and uniform near optimality of x^e), this extends to the near optimal turnpike property
- The results precisely describe the gap between strict dissipativity and turnpike properties

UNIVERSITÄT BAYREUTH   Lars Grüne, On the relation between dissipativity and the turnpike property, p. 41

References

L. Grüne, M.A. Müller, *On the relation between strict dissipativity and turnpike properties*, Systems & Control Letters, 90, 45–53, 2016

M.A. Müller, *Distributed and economic model predictive control: beyond setpoint stabilization*, PhD thesis, Universität Stuttgart, Germany, 2014

M.A. Müller, D. Angeli, F. Allgöwer, *On convergence of averagely constrained economic MPC and necessity of dissipativity for optimal steady-state operation*, Proceedings of the ACC 2013, 3141–3146

L. Grüne, C.M. Kellett, S.R. Weller, *On a discounted notion of strict dissipativity*, submitted, 2016

UNIVERSITÄT BAYREUTH   Lars Grüne, On the relation between dissipativity and the turnpike property, p. 42

Conclusions

- We have established equivalence relations between two classical properties from mathematical systems theory and optimal control, respectively
- Under a local controllability condition, equivalence between strict dissipativity and the near equilibrium turnpike property holds
- Under appropriate bounds on the value function (i.e., cheap reachability and uniform near optimality of x^e), this extends to the near optimal turnpike property

UNIVERSITÄT BAYREUTH   Lars Grüne, On the relation between dissipativity and the turnpike property, p. 41

Conclusions

- We have established equivalence relations between two classical properties from mathematical systems theory and optimal control, respectively
- Under a local controllability condition, equivalence between strict dissipativity and the near equilibrium turnpike property holds
- Under appropriate bounds on the value function (i.e., cheap reachability and uniform near optimality of x^e), this extends to the near optimal turnpike property
- The results precisely describe the gap between strict dissipativity and turnpike properties
- As a consequence, assuming strict dissipativity for ensuring the turnpike property does not seem overly conservative

UNIVERSITÄT BAYREUTH   Lars Grüne, On the relation between dissipativity and the turnpike property, p. 41

Part 4

List of Participants

Thomas Abbate
University of Mons
Belgium
thomas.abbate@umons.ac.be

Francesco Acciani
University of Twente
The Netherlands
f.acciani@utwente.nl

Farid Alavi
Delft University of Technology
The Netherlands
f.alavi@tudelft.nl

Athanasios Antoulas
Rice University
USA
aca@rice.edu

Behnam Asadi Khashooei
Eindhoven University of Technology
The Netherlands
b.asadi.khashooei@tue.nl

Sanand Athalye
Université Catholique de Louvain
Belgium
sanand.athalye@uclouvain.be

Nikolaos Athanasopoulos
Université Catholique de Louvain
Belgium
nikolaos.athanasopoulos@uclouvain.be

Alrianes Bachnas
Eindhoven University of Technology
The Netherlands
a.a.bachnas@tue.nl

Xiaoshan Bai
University of Groningen
The Netherlands
xiaoshan.bai@rug.nl

Iris Ballesteros Tolosana
Renault-CentraleSupelec
Belgium
iris.ballesteros-tolosana@renault.com

Eamon Barrett
University of Twente
The Netherlands
e.barrett@utwente.nl

Henrik Beelen
Eindhoven University of Technology
The Netherlands
h.p.g.j.beelen@tue.nl

Ir. Ruud Beerens
Eindhoven University of Technology
The Netherlands
r.beerens@tue.nl

Michiel Beijen
Eindhoven University of Technology
The Netherlands
m.a.beijen@tue.nl

Lennart Blanken
Eindhoven University of Technology
The Netherlands
l.l.g.blanken@tue.nl

Thomas Blanken
Eindhoven University of Technology
The Netherlands
t.c.blanken@tue.nl

Ruxandra Bobiti
Eindhoven University of Technology
The Netherlands
r.v.bobiti@tue.nl

Niek Borgers
Eindhoven University of Technology
The Netherlands
d.p.borgers@tue.nl

Rully Tri Cahyono
University of Groningen
The Netherlands
r.tri.cahyono@rug.nl

Luis Cauto Mendoca
Université Libre de Bruxelles
Belgium
luis.daniel.couto.mendonca@ulb.ac.be

Xiaodong Cheng
University of Groningen
The Netherlands
x.cheng@rug.nl

Simon Cherlet
University of Ghent
Belgium
simon.cherlet@ugent.be

Pierre-Yves Chevalier
Université Catholique de Louvain
Belgium
pierre-yves.chevalier@uclouvain.be

Pepijn Cox
Eindhoven University of Technology
The Netherlands
p.b.cox@tue.nl

Pèter Zoltán Csurcsia
Vrije Universiteit Brussel
Belgium
pcsurcsi@vub.ac.be

Dmitri Danilov
Eindhoven University of Technology
The Netherlands
d.danilov@tue.nl

Mohamed Darwish
Eindhoven University of Technology
The Netherlands
m.a.h.darwish@tue.nl

Raffaella Carloni
University of Twente
The Netherlands
r.carloni@utwente.nl

Alexander De Cock
Vrije Universiteit Brussel
Belgium
adecock@vub.ac.be

Bram de Jager
Eindhoven University of Technology
The Netherlands
a.g.de.jager@tue.nl

Claudio De Persis
University of Groningen
The Netherlands
c.de.persis@rug.nl

Dimitri Jeltsema
Delft University of Technology
The Netherlands
D.Jeltsema@tudelft.nl

Matthijs de Jong
University of Groningen
The Netherlands
matthijs.de.jong@rug.nl

Massimo De Mauri
Katholieke Universiteit Leuven
Belgium
massimo.demauri@kuleuven.be

Andreas De Preter
Katholieke Universiteit Leuven
Belgium
adepreter@octinion.com

Robin de Rozario
Eindhoven University of Technology
The Netherlands
robinderozario@gmail.com

Jan Decuyper
Vrije Universiteit Brussel
Belgium
jan.decuyper@vub.ac.be

Jonathan Dehaye
University of Namur
Belgium
jonathan.dehaye@unamur.be

Kevin Dekemele
University of Ghent
Belgium
kevin.dekemele@ugent.be

Mamadou Aliou Diallo
Cheikh Anta Diop University
Senegal
mamadoualiou.diallo27@yahoo.com

Alina Doban
Eindhoven University of Technology
The Netherlands
a.i.doban@tue.nl

Victor Dolk
Eindhoven University of Technology
The Netherlands
v.s.dolk@tue.nl

Tijs Donkers
Eindhoven University of Technology
The Netherlands
m.c.f.donkers@tue.nl

Masoud Dorosti
Eindhoven University of Technology
The Netherlands
m.dorosti@tue.nl

Yanick Douven
Eindhoven University of Technology
The Netherlands
y.g.m.douven@tue.nl

Martijn Dresscher
University of Groningen
The Netherlands
m.dresscher@rug.nl

Jacob Engwerda
University of Tilburg
The Netherlands
engwerda@uvt.nl

Anneroos Everts
University of Groningen
The Netherlands
anneroos@gmail.com

Alireza Fakhrizadeh Esfahani
Vrije Universiteit Brussel
Belgium
afakhriz@vub.ac.be

Marc Favier
University of Kaiserslautern
Germany
marc-alexandre.favier@mv.uni-kl.de

Federico Felici
Eindhoven University of Technology
The Netherlands
f.felici@tue.nl

Shuai Feng
University of Groningen
The Netherlands
s.feng@rug.nl

Sofia Fernandes de Sousa
University of Mons
Belgium
sofia.afonsofernandes@umons.ac.be

C.G. Feudjio
University of Mons
Belgium
christian.feudjioletchindjio@umons.ac.be

Paolo Frasca
University of Twente
The Netherlands
p.frasca@utwente.nl

Debrouwere Frederik
Katholieke Universiteit Leuven
Belgium
frederik.debrouwere@kuleuven.be

Rolf Gaasbeek
Eindhoven University of Technology
The Netherlands
r.i.gaasbeek@tue.nl

Matthieu Genicot
Université Catholique de Louvain
Belgium
matthieu.genicot@uclouvain.be

François Gonze
Université Catholique de Louvain
Belgium
francois.gonze@uclouvain.be

Pierre-Yves Gousenbourger
Université Catholique de Louvain
Belgium
pierre-yves.gousenbourger@uclouvain.be

Alain Govaert
University of Groningen
The Netherlands
alain.govaert@gmail.com

Jonathan Grimard
University of Mons
Belgium
lars.gruene@uni-bayreuth.de

Lars Grüne
Bayreuth University
Germany
jonathan.grimard@umons.ac.be

Leonardo Gutierrez
Université Catholique de Louvain
Belgium
leonardo.gutierrez@uclouvain.be

Jurre Hanema
Eindhoven University of Technology
The Netherlands
j.hanema@tue.nl

Leroy Hazeleger
Eindhoven University of Technology
The Netherlands
l.hazeleger@tue.nl

Stefan Heijmans
Eindhoven University of Technology
The Netherlands
s.h.j.heijmans@tue.nl

Hans Hellendoorn
Delft University of Technology
The Netherlands
j.hellendoorn@tudelft.nl

Julien Hendrickx
Université Catholique de Louvain
Belgium
julien.hendrickx@uclouvain.be

Gabriel Hollander
Vrije Universiteit Brussel
Belgium
gabriel.hollander@vub.ac.be

Frans Hoogeboom
Eindhoven University of Technology
The Netherlands
f.n.hoogeboom@tue.nl

Lars Huijben
Eindhoven University of Technology
The Netherlands
l.i.huijben@student.tue.nl

Edwin Insuasty
Eindhoven University of Technology
The Netherlands
e.g.insuasty.moreno@tue.nl

Mariya Ishteva
Vrije Universiteit Brussel
Belgium
mishteva@vub.ac.be

M Jafarian
University of Groningen
The Netherlands
m.jafarian@rug.nl

Hildeberto Jardón Kojakhmetov
University of Groningen
The Netherlands
h.jardon.kojakhmetov@rug.nl

Bayu Jayawardhana
University of Groningen
The Netherlands
b.jayawardhana@rug.nl

Hidde-Jan Jongsma
University of Groningen
The Netherlands
h.jongsma@rug.nl

Monika Jozsa
University of Groningen
The Netherlands
m.jozsa@rug.nl

Mr. M Kanematsu
University of Tokyo
Japan
kanematsu@hflab.k.u-tokyo.ac.jp

Yuri Kapitanyuk
University of Groningen
The Netherlands
i.kapitaniuk@rug.nl

Y. Kasemsinsup
Eindhoven University of Technology
The Netherlands
y.kasemsinsup@tue.nl

Tamas Keviczky
Delft University of Technology
The Netherlands
t.keviczky@tudelft.nl

Khadija Khadija
Université Libre de Bruxelles
Belgium
kmhallem@ulb.ac.be

Dhruv Khandelwal
Eindhoven University of Technology
The Netherlands
d.khandelwal@tue.nl

Jens Kober
Delft University of Technology
The Netherlands
j.kober@tudelft.nl

Filip Koerts
University of Groningen
The Netherlands
filipjk@gmail.com

Sandor Kolumban
Eindhoven University of Technology
The Netherlands
s.kolumban@tue.nl

Nikolaos Kontaras
Eindhoven University of Technology
The Netherlands
n.kontaras@tue.nl

C Labar
Université Libre de Bruxelles
Belgium
pascale.lathouwers@ulb.ac.be

Erik Lambrechts
Katholieke Universiteit Leuven
Belgium
erik.lambrechts@kuleuven.be

François Lamoline
University of Namur
Belgium
francois.lamoline@unamur.be

Mircea
Eindhoven University of Technology
The Netherlands
m.lazar@tue.nl

Erjen Lefeber
Eindhoven University of Technology
The Netherlands
a.a.j.lefeber@tue.nl

Xiao Lin
Delft University of Technology
The Netherlands
x.lin@tudelft.nl

Xi Luo
Eindhoven University of Technology
The Netherlands
x.luo@tue.nl

Pieter Maelegheer
University of Ghent
Belgium
pieter.maelegheer@ugent.be

Bert Maljaars
Eindhoven University of Technology
The Netherlands
e.maljaars@tue.nl

Anna Marconato
Vrije Universiteit Brussel
Belgium
anna.marconato@vub.ac.be

Estelle Massart
Université Catholique de Louvain
Belgium
estelle.massart@uclouvain.be

Noorma Yulia Megawati
University of Groningen
The Netherlands
n.y.megawati@rug.nl

Tim Mercy
Katholieke Universiteit Leuven
Belgium
tim.mercy@kuleuven.be

Ruben Merks
Eindhoven University of Technology
The Netherlands
r.w.h.merks@tue.nl

Ir Khadija Mhallem Gziri
Université Libre de Bruxelles
Belgium
kmhallem@ulb.ac.be

Shi Mingming
University of Groningen
The Netherlands
m.shi@rug.nl

Rishi Mohan
Eindhoven University of Technology
The Netherlands
r.mohan@tue.nl

Pooya Monshizadeh
University of Groningen
The Netherlands
p.monshizadeh@rug.nl

Nima Monshizadeh
University of Groningen
The Netherlands
n.monshizadeh@rug.nl

Sikandar Moten
Katholieke Universiteit Leuven
Belgium
sikandar.moten@kuleuven.be

Bao Nguyen
University of Groningen
The Netherlands
d.b.nguyen@rug.nl

Tuan T. Nguyen
Eindhoven University of Technology
The Netherlands
t.t.nguyen@tue.nl

Marco M. Nicotra
Université Libre de Bruxelles
Belgium
marco.maria.nicotra@ulb.ac.be

Henk Nijmeijer
Eindhoven University of Technology
The Netherlands
h.nijmeijer@tue.nl

Leonidas Niyonkuru
Vrije Universiteit Brussels
Belgium
niyonkuru.leonidas@vub.ac.be

Tom Oomen
Eindhoven University of Technology
The Netherlands
t.a.e.oomen@tue.nl

Martha W. Otte
Delft University of Technology
The Netherlands
m.w.otte@tudelft.nl

Julian Oviedo
University of Mons
Belgium
julian.oviedosantana@umons.ac.be

Matthew M. Philippe
Université Catholique de Louvain
Belgium
matthew.m.philippe@gmail.com

Goele Pipeleers
Katholieke Universiteit Leuven
Belgium
goele.pipeleers@kuleuven.be

Marcella Porru
Eindhoven University of Technology
The Netherlands
m.porru@tue.nl

Ioannis Proimadis
Eindhoven University of Technology
The Netherlands
i.proimadis@tue.nl

Anton Proskurnikov
Universiity of Groningen
The Netherlands
avp1982@gmail.com

Yuzhen Qin
University of Groningen
The Netherlands
y.z.qin@rug.nl

Gustavo Quintana-Carapia
Vrije Universiteit Brussel
Belgium
gustavo.quintana-carapia@vub.ac.be

Pouria Ramazi
University of Groningen
The Netherlands
p.ramazi@gmail.com

Rishi Relan
Vrije Universiteit Brussel
Belgium
rishi.relan@vub.ac.be

Emilie Renard
Université Catholique de Louvain
Belgium
emilie.renard@uclouvain.be

M.Sc. Rodolfo Reyes-Báez
University of Groningen
The Netherlands
r.reyes-baez@rug.nl

James Riehl
University of Groningen
The Netherlands
j.r.riehl@rug.nl

Mark Rijnen
Eindhoven University of Technology
The Netherlands
m.w.l.m.rijnen@tue.nl

Luc Rocher
Université Catholique de Louvain
Belgium
luc.rocher@uclouvain.be

Raffaele Romagnoli
Université Libre de Bruxelles
Belgium
pascale.lathouwers@ulb.ac.be

Muhammad Zakiyullah Romdlony
University of Groningen
The Netherlands
m.z.romdlony@rug.nl

T.C.J. Romijn
Eindhoven University of Technology
The Netherlands
t.c.j.romijn@tue.nl

Wilbert Samuel Rossi
University of Twente
The Netherlands
w.s.rossi@utwente.nl

Alessandro Saccon
Eindhoven University of Technology
The Netherlands
a.saccon@tue.nl

Jacquelien Scherpen
University of Groningen
The Netherlands
j.m.a.scherpen@rug.nl

Tjardo Scholten
University of Groningen
The Netherlands
t.w.scholten@rug.nl

Julien Schorsch
Université Libre de Bruxelles
Belgium
pascale.lathouwers@ulb.ac.be

Johan Schoukens
Vrije Universiteit Brussel
Belgium
johan.schoukens@vub.ac.be

Danial Senejohnny
University of Groningen
The Netherlands
d.senejohnny@rug.nl

Arman Sharifi Kolarijani
Delft University of Technology
The Netherlands
a.sharifikolarijani@tudelft.nl

Andrea Simonetto
Université Catholique de Louvain
Belgium
a.simonetto@tudelft.nl

Muhammad Mohsin Siraj
Eindhoven University of Technology
The Netherlands
m.m.siraj@tue.nl

Konstantinos Smpoukis
Université Catholique de Louvain
Belgium
cosmoks@hotmail.gr

Veaceslav Spinu
Eindhoven University of Technology
The Netherlands
v.spinu@tue.nl

Tjerk Stegink
University of Groningen
The Netherlands
t.w.stegink@rug.nl

Maarten Steinbuch
Eindhoven University of Technoloyg
The Netherlands
m.steinbuch@tue.nl

Armin Steinhauser
Katholieke Universiteit Leuven
Belgium
armin.steinhauser@kuleuven.be

Zhiyong Sun
University of Groningen
The Netherlands
f.g.fokkens@rug.nl

Jan Swevers
Katholieke Universiteit Leuven
Belgium
jan.swevers@kuleuven.be

Hadi Taghvafard
University of Groningen
The Netherlands
taghvafard@gmail.com

Adrien Taylor
Université Catholique de Louvain
Belgium
adrien.taylor@uclouvain.be

Pietro Tesi
University of Groningen
The Netherlands
p.tesi@rug.nl

Pauline Themans
University of Namur
Belgium
pauline.themans@unamur.be

Bart Tiemersma
Eindhoven University of Technology
The Netherlands
b.j.m.tiemersma@student.tue.nl

Son Duy Son
Katholieke Universiteit Leuven
Belgium
tong.duyson@kuleuven.be

Sebastian Trip
University of Groningen
The Netherlands
s.trip@rug.nl

Dora Turk
Katholieke Universiteit Leuven
Belgium
dora.turk@kuleuven.be

Tobias Van Damme
University of Groningen
The Netherlands
t.van.damme@rug.nl

Paul Van den Hof
Eindhoven University of Technology
The Netherlands
p.m.j.vandenhof@tue.nl

Annemiek van der Maas
Eindhoven University of Technology
The Netherlands
a.v.d.maas@tue.nl

Arjan van der Schaft
University of Groningen
The Netherlands
a.j.van.der.schaft@rug.nl

Robert van der Weijst
Eindhoven University of Technology
The Netherlands
r.v.d.weijst@tue.nl

Paul van Dooren
Université Catholique de Louvain
Belgium
paul.vandooren@uclouvain.be

Niels van Duijkeren
Katholieke Universiteit Leuven
Belgium
niels.vanduijkeren@kuleuven.be

Eelco van Horssen
Eindhoven University of Technology
The Netherlands
e.p.v.horssen@tue.nl

Thijs van Keulen
DAF Trucks N.V. and Eindhoven University of Technology
The Netherlands
t.a.c.v.keulen@tue.nl

Simon van Mourik
Wageningen University
The Netherlands
simon.vanmourik@wur.nl

Ruben Van Parys
Katholieke Universiteit Leuven
Belgium
ruben.vanparys@kuleuven.be

Prof.em. J.H. van Schuppen
Delft University of Technology
The Netherlands
jan.h.van.schuppen@xs4all.nl

Jurgen van Zundert
Eindhoven University of Technology
The Netherlands
jurgenvanzundert@gmail.com

Jaime Vargas Delgado
University of Groningen
The Netherlands
j.a.vargas.delgado@gmail.com

Sandra Vasquez
Vrije Universiteit Brussel
Belgium
savasque@vub.ac.be

Maarten Verbandt
Katholieke Universiteit Leuven
Belgium
maarten.verbandt@kuleuven.be

Dieter Verbeke
Vrije Universiteit Brussel
Belgium
dieter.verbeke@vub.ac.be

Cees Verdier
Delft University of Technology
The Netherlands
c.f.Verdier@tudelft.nl

Benjamin Vincent
Université Catholique de Louvain
Belgium
benjamin.vincent@uclouvain.be

Harm Weerts
Eindhoven University of Technology
The Netherlands
h.h.m.weerts@tue.nl

Siep Weiland
Eindhoven University of Technology
The Netherlands
s.weiland@tue.nl

Erik Weitenberg
University of Groningen
The Netherlands
e.r.a.weitenberg@gmail.com

Professor Joseph Winkin
University of Namur
Belgium
joseph.winkin@unamur.be

Ir Han Wopereis
University of Twente
The Netherlands
h.w.wopereis@utwente.nl

Kaihua Xi
Delft University of Technology
The Netherlands
k.xi@tudelft.nl

Shuai Yuan
Delft University of Technology
The Netherlands
s.yuan-1@tudelft.nl

Hans Zwart
University of Twente
The Netherlands
h.j.zwart@utwente.nl

Part 5

Organizational Comments

I

Welcome

The Organizing Committee has the pleasure of welcoming you to the *35th Benelux Meeting on Systems and Control*, at Kontakt der Kontinenten in Soesterberg, The Netherlands.

Aim

The aim of the Benelux Meeting is to promote research activities and to enhance cooperation between researchers in Systems and Control. This is the thirty-fifth in a series of annual conferences that are held alternately in Belgium and The Netherlands.

Scientific Program Overview

1. Mini course by *Athanasios C. Antoulas* (Rice University, USA) on **Data-driven model reduction for large-scale dynamical systems**.

2. Plenary lectures by *Claudio De Persis* (University of Groningen, The Netherlands) on **A control theoretic framework for power grids**.

3. Plenary lectures by *Lars Grüne* (Bayreuth University, Germany) on:

   - **Receding horizon control**.
   - **Dissipativity and the turnpike property**.

4. Contributed short lectures. See the list of sessions for the titles and authors of these lectures.

Directions for speakers

For a contributed lecture, the available time is 25 minutes. Please leave a few minutes for discussion and room changes, and adhere to the indicated schedule. In each room overhead projectors are available. *When using a projector, you have to provide a notebook yourself and you have to start your lecture with the notebook up and running and the external video port switched on.*

Registration

The Benelux Meeting registration desk, located in the foyer, will be open on Tuesday, March 22, from 10:00 to 14:00. Late registrations can be made at the Benelux

Meeting registration desk, when space is still available. The on-site fee schedule is:

Arrangement	Price
single room	575
shared room	475
only meals (no dinners)	375
one day (no dinner)	275

The registration fee includes:

- Admission to all sessions.

- A copy of the Book of Abstracts.

- Coffee and tea during the breaks.

- In the case of an *accommodation* arrangement: lunch and dinner on Tuesday; breakfast, lunch, and dinner on Wednesday; and breakfast and lunch on Thursday.

- In the case of a *only meals (no dinner)* arrangement: lunch on Tuesday, Wednesday, and Thursday.

- In the case of a *one day (no dinner)* arrangement: lunch on Tuesday, or Wednesday, or Thursday.

- Free use of a wireless Internet connection (WiFi).

The registration fee does *not* include:

- Cost of phone calls.

- Special ordered drinks during lunch, dinner, in the evening, etc.

Organization

The Organizing Committee of the 35th Benelux Meeting consists of

Vincent Blondel
Universite Catholique de Louvain
E-mail: vincent.blondel@uclouvain.be

Ming Cao
University of Groningen
E-mail: m.cao@rug.nl

Raffaella Carloni
University of Twente
E-mail: r.carloni@utwente.nl

Claudio De Persis
University of Groningen
E-mail: c.de.persis@rug.nl

Sergio Grammatico
Eindhoven University of Technology
E-mail:s.grammatico@tue.nl

Maurice Heemels
Eindhoven University of Technology
E-mail: m.heemels@tue.nl

Paul M.J. van den Hof
Eindhoven University of Technology
E-mail: p.m.j.vandenhof@tue.nl

Clara M. Ionescu
University of Ghent
E-mail: claramihaela.ionescu@ugent.be

Dimitri Jeltsema
Delft University of Technology
E-mail: d.jeltsema@tudelft.nl

Raphael Jungers
Universite Catholique de Louvain
E-mail:raphael.jungers@uclouvain.be

Robain de Keyser
University of Ghent
E-mail: robain.dekeyser@ugent.be

Tamas Keviczky
Delft University of Technology
E-mail: t.keviczky@tudelft.nl

Mircea Lazar
Eindhoven University of Technology
E-mail: m.lazar@tue.nl

Sarthak Misra
University of Twente
E-mail: s.misra@utwente.nl

Rudy R. Negenborn
Delft University of Technology
E-mail:r.r.negenborn@tudelft.nl

Henk Nijmeijer
Eindhoven University of Technology
E-mail: h.nijmeijer@tue.nl

Arjan J. van der Schaft
University of Groningen
E-mail: a.j.van.der.schaft@math.rug.nl

Jacquelien M.A. Scherpen
University of Groningen
E-mail: j.m.a.scherpen@rug.nl

Bart de Schutter
Delft University of Technology
E-mail: b.deschutter@tudelft.nl

Hans Stigter
University of Wageningen
E-mail: hans.stigter@wur.nl

Stefano Stramigioli
University of Twente
E-mail: s.stramigioli@utwente.nl

Roland Toth
Eindhoven University of Technology
E-mail:r.toth@tue.nl

Hans J. Zwart
University of Twente
E-mail: h.j.zwart@utwente.nl

The meeting has been organized by Raffaella Carloni (University of Twente), Dimitri Jeltsema (Delft University of Technology), and Mircea Lazar (Eindhoven University of Technology).

Sponsor

The meeting is supported by the following organizations:

- Dutch Institute for Systems and Control (DISC).

- Netherlands Organization for Scientific Research (NWO).

Conference location

The lecture rooms of Kontakt der Kontinenten are situated on the ground floor. Consult the map at the end of this booklet to locate rooms. During the breaks, coffee and tea will be served in the foyer. Announcements and personal messages will be posted near the main conference room. Accommodation is provided in the conference center and in the cottages. Breakfast will be served between 7:00 and 8:30 AM. Room keys can be picked up at lunch time on the first day and need to be returned before 10:00 on the day of departure. Parking is free of charge.

The address of Kontakt der Kontinenten is

      Amersfoortsestraat 20
      3769 AS Soesterberg
      The Netherlands

Best junior presentation award

Continuing a tradition that started in 1996, the 35th Benelux Meeting will close with the announcement of the winner of the Best Junior Presentation Award. This award is given for the best presentation, given by a junior researcher, and it consists of a trophy that may be kept for one year and a certificate. The award is specifically given for quality of presentation rather than quality of research, which is judged in a different way. At the meeting, the chairs of sessions will ask three volunteers in the audience to fill out an evaluation form. After the session, the evaluation forms will be collected by the Prize Commissioners who will then compute a ranking. The winner will be announced on Thursday, March 24, in room **St. Janzaal**, at 16:40. The evaluation forms of each presentation will be returned to the junior researcher who gave the presentation. The Prize Commissioners are Bayu Jayawardhana (University of Groningen), Hans Zwart (University of Twente), and Julien Hendrickx (Université Catholique de Louvain).

The organizing committee counts on the cooperation of the participants to make this contest a success.

Website

An *electronic version* of the Book of Abstracts can be downloaded from the Benelux Meeting web site.

Meetings

The following meetings are scheduled:

- Board DISC on Tuesday, March 22, 19:30 – 21:00 (during dinner).

- Management Team DISC on Wednesday, March 23, room Angola, 21:00 – 22:30.

DISC certificates and best thesis award

The ceremony for the distribution of the DISC certificates and for the Best Thesis Award will be held on Thursday, March 24, room **St. Janzaal**, 16:20–16:40. The jury of the Best Thesis Award is formed by Hans Butler (Eindhoven University of Technology), André Ran (Vrije Universiteit Amsterdam), and Tamas Keviczky (Delft University of Technology).

Tuesday March 22, 2016

Time						
11:25 – 11:30	P0 – St. Janzaal _Welcome and Opening_					
11:30 – 12:30	P1 – St. Janzaal _Data-driven model reduction for large-scale dynamical systems_ Athanasios Antoulas					
12:30 – 13:45	Lunch					
13:45 – 14:45	P2 – St. Janzaal _Data-driven model reduction for large-scale dynamical systems_ Athanasios Antoulas					
14:45 – 15:10	Coffee Break					

Room TuE	St. Janzaal TuE01 _System Identification A_	Angola TuE02 _System Theory A_	Botswana TuE03 _Optimization A_	Congo TuE04 _Non-Linear Control A_	Ghana TuE05 _Distributed Parameter Systems_	Tanzania TuE06 _Model Reduction_
15:10 – 15:35	Csurcsia	Dolk	Ballesteros Tolosana	Spinu	Zwart	Li
15:35 – 16:00	Mauroy	Megawati	Mohsin Siraj	Heijmans	Dehaye	Cheng
16:00 – 16:25	De Cock	Everts	Duy Son	Lefeber	de Jong	Jardón
16:25 – 16:50	Vasquez	Jardón	Cahyono	Romdlony	Merks	Genicot
16:50 – 17:15	Hollander	Yuan	Lin	Scholten	Kontaras	Jongsma
17:15 – 17:40	-	-	-	-	Tiemersma	-

Time	
17:15 – 17:30	Break
18:00 – 19:00	Reception
19:30 – 21:00	Board DISC
19:30 – 21:00	Dinner

Wednesday March 23, 2016

Time						
8:30 – 9:30	P3 – St. Janzaal — *Data-driven model reduction for large-scale dynamical systems* — Athanasios Antoulas					
9:30 – 9:50	Break					
9:50 – 10:50	P4 – St. Janzaal — *A control theoretic framework for power grids* — Claudio De Persis					
10:50 – 11:20	Coffee Break					
11:20 – 12:20	E1 – Meet the Experts					
12:20 – 13:45	Lunch					

Room WeP	St. Janzaal WeP01 *System Identification B*	Angola WeP02 *Power Systems A*	Botswana WeP03 *Optimization B*	Congo WeP04 *Optimal Control*	Ghana WeP05 *Modeling for Control A*	Tanzania WeP06 *Robotics A*
13:45 – 14:10	Quintana-Carapia	Jafarian	Rostampour	Kapitanyuk	Dekemele	Rijnen
14:10 – 14:35	Marconato	Monshizadeh	Taylor	Asadi Khashooei	Moten	Wopereis
14:35 – 15:00	Relan	Koerts	Massart	Sharifi Kolarijani	Gonze	van Duijkeren
15:00 – 15:25	Huijben	Monshizadeh	Taghvaafrd	Van Parys	Maelegheer	Barrett
15:25 – 15:50	Verbeke	Weitenberg	Maljaars	Hanema	Dorosti	Cherlet
15:50 – 16:20	Coffee Break					

Room WeE	St. Janzaal WeE01 *System Identification C*	Angola WeE02 *Power Systems B*	Botswana WeE03 *Games and Agent-based Models A*	Congo WeE04 *Modeling for Control B*	Ghana WeE05 *Biochemical Engineering & System Biology*	Tanzania WeE06 *Observers*
16:20 – 16:45	Cox	Trip	Engwerda	Jetto	Fernandes de Sousa	Beelen
16:45 – 17:10	Jozsa	Alavi	Rossi	van Horssen	Oviedo	Feudjio
17:10 – 17:35	Turk	Bao Nguyen	Acciani	Mohan	Aliou Diallo	Porru
17:35 – 18:00	Darwish	Stegink	Riehl	Gonze	Vargas-Delgado	Vincent
18:00 – 18:25	Esfahani	Jeltsema	Ramazi	Dresscher	Abbate	Blanken
18:25 – 18:50	-	-	-	van Mourik	Mhallem Gziri	-

Time	
19:30 – 21:00	Dinner
21:00 – 22:30	Management Team DISC (room Angola)

333

Thursday March 24, 2016

Time						
8:30 – 9:30	P5 – St. Janzaal *Receding horizon control* Lars Grüne					
9:30 – 9:45	Break					
9:45 – 10:45	P6 – St. Janzaal *Receding horizon control* Lars Grüne					
10:45 – 11:00	Coffee Break					

Room ThM	St. Janzaal ThM01 *System Identification D*	Angola ThM02 *Optimal Control B*	Botswana ThM03 *Mechanical Engineering A*	Congo ThM04 *Non-linear Control B*	Ghana ThM05 *Medical Applications*	Tanzania ThM06 *Robotics B*
11:00 – 11:25	Weerts	Mercy	Kasemsinsup	Nicotra	Taghvaafrd	Steinhauser
11:25 – 11:50	Khandelwal	Blanken	Luo	Labar	van der Maas	Heck
11:50 – 12:15	de Rozario	De Preter	Blanken	Hazeleger	Renard	Bai
12:15 – 12:40	Grimard	Van Damme	van Zundert	Gaasbeek	Gousenbourger	Mac Thi
12:40 – 13:05	Decuyper	Bachnas	Borgers	Reyes-Báez	Douven	Sun

Time						
13:05 – 14:00	Lunch					

Room ThP	St. Janzaal ThP01 *System Theory*	Angola ThP02 *Games and Agent-based Models B*	Botswana ThP03 *Mechanical Engineering B*	Congo ThP04 *Electro-Mechanical Engineering*	Ghana	Tanzania
14:00 – 14:25	Feng	Chevalier	Beijen	Nguyen		
14:25 – 14:50	Niyonkuru	Senejohnny	Hoogeboom	Kanematsu		
14:50 – 15:15	Doban	Grammatico	van der Weijst	Proimadis		
15:15 – 15:40	Bobiti	de Montjoye	Couto	Schorsch		
15:40 – 16:05	Philippe	-	Verbandt	-		

Time						
16:05– 16:20	Break					
16:20 – 16:40	E2 – St. Janzaal *DISC Certificates & Best Thesis Award Ceremony*					
16:40 – 16:55	E3 – St. Janzaal *Best Junior Presentation Award Ceremony*					
16:55	E4 – St. Janzaal *Closure of the 35th Benelux Meeting*					

ProefLokaal De Wereld
Restaurant

Ghana

Congo

Kenia

Mozambique

Afrika

Botswana

Angola

Tanzania

Togo

Begane grond KdK

ProefLokaal De Wereld
Bar

St. Janzaal

Receptie

Lounge

031
030
029
027
025
023
021
019
017

Europa

028
026
024
022
020
018
016
015

014
013
012
011
010

001
002
003
004
005
006
007

Noord-Amerika

009
008